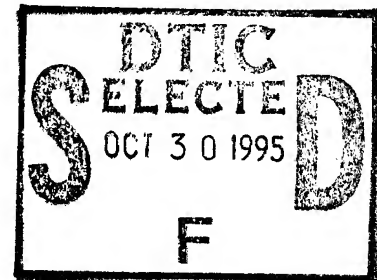
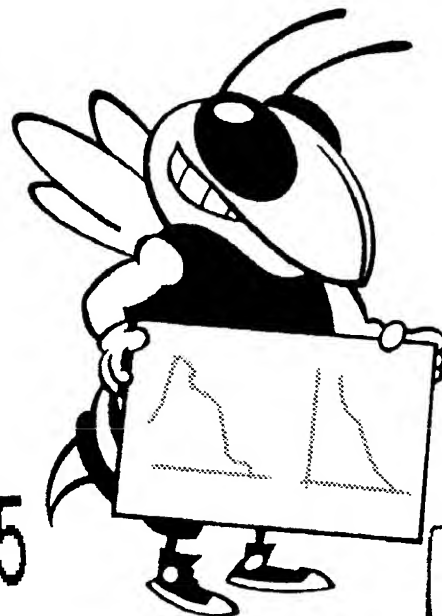


GEORGIA INSTITUTE OF TECHNOLOGY
School of Materials Science & Engineering

SHOCK SYNTHESIS OF MATERIALS



19951026 065

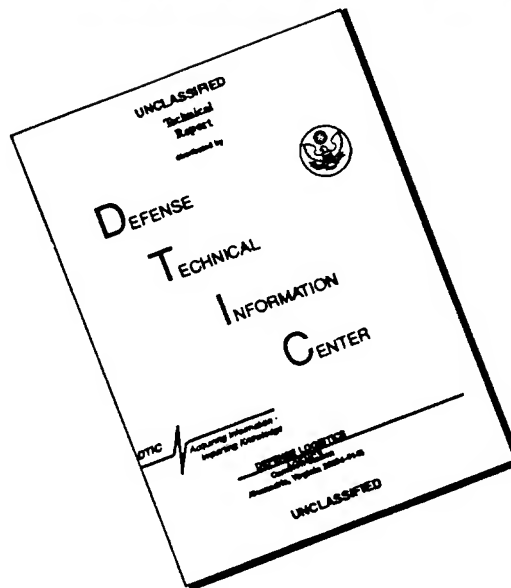
DISTRIBUTION STATEMENT A
 Approved for public release
 Distribution Unlimited

Workshop
 May 24 - 26, 1994

DTIC QUALITY INSPECTED 8

Sponsored by:
U.S. Army Research Office, Research Triangle Park
U.S. Army Research Office, (AMC) Far East
U.S. Army Research, Development & Standardization Group (UK)

DISCLAIMER NOTICE



THIS DOCUMENT IS BEST QUALITY AVAILABLE. THE COPY FURNISHED TO DTIC CONTAINED A SIGNIFICANT NUMBER OF PAGES WHICH DO NOT REPRODUCE LEGIBLY.

"The views, opinions, and/or findings contained in this report are those of the authors and should not be construed as an official Department of the Army position, policy, or decision, unless so designated by other documentation"

REPORT DOCUMENTATION PAGE

Form Approved
OMB No. 0704-0188

Public reporting burden for this collection of information is estimated to average 1 hour per response, including the time for reviewing instructions, searching existing data sources, gathering and maintaining the data needed, and completing and reviewing the collection of information. Send comments regarding this burden estimate or any other aspect of collection of information, including suggestions for reducing this burden, to Washington Headquarters Services, Directorate for Information Operations and Reports, 1215 Jefferson Davis Highway, Suite 1204, Arlington, VA 22202-4302, and to the Office of Management and Budget, Paperwork Reduction Project (0704-0188), Washington, DC 20503.

1. AGENCY USE ONLY (Leave blank)		2. REPORT DATE September 8, 1995		3. REPORT TYPE AND DATES COVERED Final Report - May 1, '94 to Jun 30, '95	
4. TITLE AND SUBTITLE SHOCK SYNTHESIS OF MATERIALS (WORKSHOP PROCEEDINGS)				5. FUNDING NUMBERS DAAH04-94-G-0192	
6. AUTHOR(S) Naresh Thadhani and Edward Chen					
7. PERFORMING ORGANIZATION NAME(S) AND ADDRESS(ES) School of Materials Science and Engineering Georgia Institute of Technology Atlanta, GA 30332-0245				8. PERFORMING ORGANIZATION REPORT NUMBER	
9. SPONSORING / MONITORING AGENCY NAME(S) AND ADDRESS(ES) U. S. Army Research Office P. O. Box 12211 Research Triangle Park, NC 27709-2211				10. SPONSORING / MONITORING AGENCY REPORT NUMBER ARO 33115.1-MS-CF	
11. SUPPLEMENTARY NOTES The view, opinions and/or findings contained in this report are those of the author(s) and should not be construed as an official Department of the Army position, policy, or decision, unless so designated by other documentation.					
12a. DISTRIBUTION / AVAILABILITY STATEMENT Approved for public release; distribution unlimited.				12b. DISTRIBUTION CODE	
13. ABSTRACT (Maximum 200 words) Synthesis of materials by shock-induced chemical reactions (shock chemistry) has in recent years, evolved from the stage of curiosity-driven and proof-of-concept experiments, to the need for developing a fundamental understanding of this unique process. The unusual combination of pressure and temperature states that produce the large plastic deformations, are only singularly possible during shock-compression. Shock chemistry can, thus, be applied for synthesis of metastable phases, non-stoichiometric compounds, and modified microstructures. The complex nature of the reaction process-mechanisms and kinetics, has however, been only recently realized. It is therefore essential to obtain a complete understanding of the fundamental mechanistic and kinetic aspects of processes responsible for shock-induced reaction chemistry. This proceedings includes abstracts and viewgraphs/papers of talks presented during the four topical sessions: Shock-compression Principles; Real-time In-situ Measurements; Mechanistic Issues Associated Processes; and Shock-Synthesis Applications and Process Mechanisms. Comments and remarks of session chairs are included at the beginning of each session. Questions targeted for discussions during the workshop, and highlights of issues presented and discussed, are presented as separate listings following the preface.					
14. SUBJECT TERMS shock chemistry; materials synthesis; reaction mechanisms and kinetics; real-time <i>in-situ</i> measurements; metastable phase and compounds				15. NUMBER OF PAGES 283 (double sided)	
17. SECURITY CLASSIFICATION OF REPORT UNCLASSIFIED				16. PRICE CODE	
18. SECURITY CLASSIFICATION OF THIS PAGE UNCLASSIFIED		19. SECURITY CLASSIFICATION OF ABSTRACT UNCLASSIFIED		20. LIMITATION OF ABSTRACT UL	

PREFACE

Synthesis of materials by shock-induced chemical reactions (shock chemistry) has in recent years, evolved from the stage of curiosity-driven and proof-of-concept experiments, to the need for developing a fundamental understanding of this unique but complex process. The unusual combination of pressure and temperature states that produce the large plastic deformations, are only singularly possible during shock-compression. Shock chemistry can, thus, be applied for synthesis of metastable phases, non-stoichiometric compounds, and modified microstructures. The complex nature of the reaction process-mechanisms and kinetics, has however, been only recently realized. It is therefore essential to obtain a complete understanding of the fundamental mechanistic and kinetic aspects of processes responsible for shock-induced reaction chemistry.

The workshop on "Shock Synthesis of Materials", held at Georgia Institute of Technology, brought together researchers having different backgrounds, with expertise in solid-state phase transformations, high-pressure chemistry, mechanical alloying, combustion synthesis, energetic materials, high-strain-rate deformation, and shock-wave physics. It was for the first time that such a group was assembled to review, discuss, and critique the current understanding of shock chemistry, and to provide different perspectives of the complex issues that need to be addressed. The workshop was attended by about 45 scientists, including five each from Japan and Russia. The specific focus highlighted for the workshop was to discuss about the "process mechanisms" and "reaction kinetics" associated with shock chemistry relevant to materials synthesis applications.

This proceedings includes abstracts and viewgraphs/papers of talks presented during the four topical sessions: Shock-compression Principles; Real-time In-situ Measurements; Mechanistic Issues Associated Processes; and Shock-Synthesis Applications and Process Mechanisms. The comments and remarks of session chairs are included at the beginning of each session. The final half-day included coordinator-led discussions on general issues related to "Modeling and Measurements" and "Mechanisms and Applications." The questions that were targeted for discussions during the workshop, and the highlights of issues presented and discussed, as well as other questions raised, during the various sessions and on the final day, are presented as separate listings following this preface.

The help of Ms. Ruth Book in coordinating the many things before and during the workshop, and in the compilation of this proceedings, is greatly appreciated.

Naresh Thadhani
Georgia Institute of Technology
Office

Edward Chen
U.S. Army Research

Availability Codes	
Dist	Avail and/or Special
A-1	

CONTENTS

PREFACE

QUESTIONS TARGETED

HIGHLIGHTS OF ISSUES DISCUSSED

WORKSHOP PROGRAM

SESSION 1: SHOCK-COMPRESSION PRINCIPLES

K. IYER, Session Chair Comments

Y. HORIE, "Kinetic Modeling of Shock Chemistry" and Discussion Comments

M.A. MEYERS, "Shock Synthesis: General Remarks and Recent Results" and Discussion Comments

S. PSAKHIE, "Modeling Powder Compaction by Element Dynamics"

N. AKHMADEEV, "Modeling Physical and Chemical Transformations"

SESSION 2: REAL-TIME IN-SITU MEASUREMENTS

D.P. DANDEKAR, Session Chair Comments

G. RAVICHANDRAN, "Dynamic Pore Collapse in Rate-Dependent Materials and their Implications in Shock Synthesis"

Y.M. GUPTA, "Real-time Spectroscopic Measurements in Shocked Materials"

S.S. BATSANOV, "Shock Chemistry: Real Time Measurements"

M. BOSLOUGH, "Real-time Temperature Measurements"

M.U. ANDERSON, "Nano-second Time-resolved Pressure Measurements"

SESSION 3: MECHANISTIC ISSUES IN ASSOCIATED PROCESSES

A.NILER, Session Chair Comments

Z. MUNIR, "The Mechanism of Activated Combustion Synthesis"

M. NICOL, "Chemistry at Static High Pressure Principles and Developments"

J.J. GILMAN, "Mechanism of Shock-Induced Mechanochemistry"

A.N. DREMIN, "Shock Chemistry Mechanisms, Kinetics and Applications"

M. BAER, "Modeling Shock-Compression of Porous Composite Materials and Correlation with Observed Behavior"

SESSION 4: SHOCK SYNTHESIS APPLICATIONS AND PROCESS MECHANISMS

R. YOUNG, Session Chair Comments

T. SEKINE, "Synthesis of Organic and Inorganic Materials"

V. NESTERENKO, "Shock Synthesis of Non-equilibrium Materials"

M. YOSHIDA, "Shock Synthesis of Diamond and C-B-N Materials"

T. SYONO, "Shock-induced Transformations in Oxides"

N.N. THADHANI, "Materials Synthesis by Shock-Induced and Shock-Assisted Chemical Reactions"

CONTENTS

PREFACE

QUESTIONS TARGETED

HIGHLIGHTS OF ISSUES DISCUSSED

WORKSHOP PROGRAM

SESSION 1: SHOCK-COMPRESSION PRINCIPLES

K. IYER, Session Chair Comments

Y. HORIE, "Kinetic Modeling of Shock Chemistry" and Discussion Comments

M.A. MEYERS, "Shock Synthesis: General Remarks and Recent Results" and Discussion Comments

S. PSAKHIE, "Modeling Powder Compaction by Element Dynamics"

N. AKHMADEEV, "Modeling Physical and Chemical Transformations"

SESSION 2: REAL-TIME IN-SITU MEASUREMENTS

D.P. DANDEKAR, Session Chair Comments

G. RAVICHANDRAN, "Dynamic Pore Collapse in Rate-Dependent Materials and their Implications in Shock Synthesis"

Y.M. GUPTA, "Real-time Spectroscopic Measurements in Shocked Materials"

S.S. BATZANOV, "Shock Chemistry: Real Time Measurements"

M. BOSLOUGH, "Real-time Temperature Measurements"

M.U. ANDERSON, "Nano-second Time-resolved Pressure Measurements"

SESSION 3: MECHANISTIC ISSUES IN ASSOCIATED PROCESSES

A. NIILER, Session Chair Comments

Z. MUNIR, "The Mechanism of Activated Combustion Synthesis"

M. NICOL, "Chemistry at Static High Pressure: Some General Principles and Recent Developments"

J.J. GILMAN, "Mechanism of Shock-Induced Mechanochemistry"

M. BAER, "Modeling Shock-Compression of Porous Composite Materials and Correlation with Observed Behavior"

SESSION 4: SHOCK SYNTHESIS APPLICATIONS AND PROCESS MECHANISMS

R. YOUNG, Session Chair Comments

T. SEKINE, "Synthesis of Organic and Inorganic Materials"

V. NESTERENKO, "Shock Synthesis of Non-equilibrium Materials"

M. YOSHIDA, "Shock Synthesis of Diamond and C-B-N Materials"

T. SYONO, "Shock-induced Transformations in Oxides"

N.N. THADHANI, "Materials Synthesis by Shock-Induced and Shock-Assisted Chemical Reactions"

QUESTIONS TARGETED

The following questions were emphasized for the workshop and targeted during the various presentations and discussions:

- (a) Has the initiation and completion of chemical reactions during shock compression of powder mixtures, been conclusively demonstrated?
- (b) Is it possible to establish the progress of reaction (fraction transformed with time) with available time-resolved measurement techniques?
- (c) What are the limitations of current time-resolved measurement techniques and what other novel in-situ measurement techniques need to be explored?
- (d) What is the current understanding of the process mechanisms and kinetics of chemical reactions occurring during shock compression of powders?
- (e) Can mechanisms of other types of chemical reaction and phase transformation processes, occurring in time scales ranging from 10^{-9} to 10^3 seconds, be used to develop mechanistic models of shock chemistry?
- (f) Can numerical models be developed to account for the influence of materials characteristics and shock compression conditions on configuration changes leading to chemical reactions during shock compression?
- (g) Can applications of shock chemistry be realized for synthesis of materials?

HIGHLIGHTS OF ISSUES

Some of the important issues presented by the speakers, or more extensively discussed during the respective and general discussion sessions are highlighted below:

- * Shock chemistry was first investigated almost fifty years ago, along with and at the same time as mechanical alloying of powders and sonar chemistry.
- * Do chemical reactions initiate during the "collapse of pores (voids)" or during plastic deformation as a consequence of collapse of voids? What is the extent of reaction in each stage?
- * Are mechanisms of shock chemistry analogous to those occurring during combustion synthesis or mechanical alloying of powders?
- * Once initiated, chemical reactions in exothermic ($\Delta H_R < 0$) powder mixture systems, should be self-sustained. If not, what stops the reactions or prevents them from being self-sustained?
- * Modeling of shock compression of powders with element dynamics shows local velocity increases, cracking of solid particles during compression (collapse), and rotations of particles (elements) in the vicinity of the cracks. Furthermore, smaller particles undergo more rotations than larger particles. Questions then arise about how would a liquid element behave in contrast to solid particle? Will it also show similar rotations, or will it act as a lubricant during element rotation.
- * Cylindrical implosion experiments on Mo-Si and Nb-Si powder mixtures show that chemical reactions in these systems occur in shear band regions.
- * What is the role of shear in reaction initiation? Shear will not enhance mass transport, but will promote plastic flow and cleansing of surfaces.
- * Initiation of chemical reactions can be correlated with regions of turbulent plastic flow and instabilities at interfaces.
- * Thermochemical modeling of shock-induced chemical reactions can be more correctly calculated from assumptions of constant pressure as a reference state rather than constant volume as the reference state.

- * Shock-induced chemical reactions occur by mechanisms involving solid- or liquid-state processes. Mixing in either state may be proposed by various types of conceptual models, but for complete chemical reaction to occur, need mixing at the molecular level.
- * Factors influencing pore collapse during shock compression of powders include inertial effects and strain-rate sensitivity effects. Both of these retard the collapse of pores.
- * Strain-rates during pore-collapse are of the order of $1.5 \times 10^5 \text{ s}^{-1}$.
- * There is convincing evidence that at the shock front, material is in a plasma state, and bonding electrons are free electrons. Therefore, transport numbers have to be similar to those for liquid-like and not solid-like systems. Furthermore, shock compression involves states that are far from equilibrium; thus, one has to be careful about how we define and distinguish between a liquid and a solid phase. Under shock loading, defect concentrations can be pumped up beyond saturation levels such that a solid is not easily distinguished from a liquid.
- * X-ray diffractions studied have been used for investigating sub-nanosecond resolution shock-wave effects in materials. Q. Johnson et al (1970-72) reported first such studies. Kondo also reported about some investigations in 1974. In more recent years J. Wark, R. Whitlock, and E. Zaretsky have used x-ray diffraction for investigations of sub-nanosecond effects.
- * In-situ Raman spectroscopy has been used to investigate symmetry changes in diamond in real time. It has also been used to investigate decomposition mechanisms in amine-sensitized nitromethane explosives, where the breaking of C-N bonds is clearly revealed.
- * Time resolved temperature (thermocouple) and pressure (manganin gauges) measurements have now been performed on Sn + S and Sn + Te systems, with a time resolution of better than 10^{-7} s . According to these measurements, shock-induced chemical reactions in Sn + S occur in 20 ns at 150 GPa, and in Sn + Te mixtures in 18 ns at 50 GPa threshold pressures.
- * Mechanisms of chemical reactions in Sn+S and Sn+Te involve processes of superfast diffusion.

- * The time-dependent loading response of powders is a function of particle morphology. Their crush strength is dominated by initial void volume and particle size. Shock-wave rise times in powders are of the order of several hundreds of nanoseconds, making them more like "dispersed" waves, thus use of jump conditions for such non-steady dispersed waves is limited.
- * A model (or so-called "homogeneous") system needs to be used for attaining a detailed understanding of shock-induced chemical reactions. Can layered structures be used to simulate or develop a model system? Layered structures may not be truly representative of a powder mixture system. Particle velocity changes are different in powders in contrast to layers.
- * Shock-compression is a means of producing very large strains at low/moderate temperatures. Since, solids sustain shear deformation at low temperature, the strain energy developed can be significantly greater than the thermal energy.
- * Bridgman's shear experiments are classic examples of the role of shear on chemical reaction. He measured reactions in a shear cell at 15 kbar static pressure, in time scales of $0.1 \mu\text{s}$, with the reaction wave propagating at velocities of 10^6 cm/s . But in these experiments, in the absence of gas, what does the work that causes an explosion. There is a large release of energy density and the product literally splits into particles.
- * Shear deformation has the largest effect and shear can also break symmetry. Thus, shear should have a greater contribution on bond breakage than the dilatational changes.
- * Combustion synthesis can be activated by the application of a magnetic field, mechanical force, and thermal means. Magnetic field introduces an excess thermal energy to the combustion synthesis process, thereby triggering self-sustained reactions in otherwise sluggish systems.
- * The chemical driving force ($\Delta\mu$) for static high pressure chemistry is the contribution due to $P\Delta V$. For example for teflon, the chemical potential increases from -1 to -100 kJ/mol, with pressure increase from 1 to 10 GPa, and volume change (ΔV) from -1 to -10 cm^3/mol .
- * From the applications point, effect of physical/chemical shock activation has proven successful in enhancing the sinterability of hard-to-bond powders.

- * Shock-compression has been used to synthesize β -phase modifications in mixtures of different rare-earth oxides ($\Delta H_R > 0$), in which the product appears to form upon rapid solidification of the eutectic.
- * Real-time (in situ) electrical conductivity measurements, in Sn + S powder mixtures shock-compressed at ≈ 10 GPa (much below pressures used/reported by Batsanov), show initiation of chemical reaction in millisecond time scales, while complete reaction occurs in 1 s.
- * For successful theoretical modeling work, more information is needed regarding the dispersive nature of multiphase waves, localized mechanics, nature of hot spots, chemical and thermal paths, and mixed phase behavior.
- * Present work on shock chemistry is only the beginning in the field of synthesis of metastable materials by shock compression.
- * Attempts to shock synthesize C-N compounds, from compounds such as $C_9H_3N_3$ result in crystalline graphite with trapped N ($C_{4.66}N$).
- * Control of shock temperature and pressure are both necessary for maximizing the yield of diamond formed by explosive shock synthesis.
- * Synthesis of high-pressure phases via phase transformations involve reaction paths that include diffusionless transformations followed by diffusional processes to lock in the high-pressure phase.
- * Precursors of B-C-N mixed with 96 mass % Cu and compacted to 70% TMD, forms B-N-C products containing a solid-solution of BN and C.
- * For shock-induced polymorphic phase transformations, the threshold pressure is a function of the crystal orientation.
- * Unusual shock-induced phase transitions are observed in rare earth materials in which the product phase density is lower than that of the initial state. Some of these systems include Tm_2Sm_3 ($\delta\rho = 7.27$ to 6.07), Nd_2O_3 ($\delta\rho = 7.42$ to 6.29), SmF_3 (6.93 to 6.64), HoF_3 ($\delta\rho = 7.83$ to 7.64), $GeSeTe$ (α to β phase). There are only 20 compounds that show such a behavior.
- * Model experiments and internal state variables need to be designed and identified to help model numerical simulations.

SHOCK SYNTHESIS WORKSHOP

Tuesday, May 24, 1994

7:45 a.m. Registration

8:15 a.m. Welcome, Introduction, and Remarks (*Ed Chen, Andrew Crowson, and Naresh Thadhani*)

SESSION I: SHOCK COMPRESSION PRINCIPLES

Session Chair: Kailasam Iyer, U.S. Army Research Office

8:35 a.m. Yuki Horie, North Carolina State University

"KINETIC MODELING OF SHOCK CHEMISTRY"

9:10 a.m. Marc A. Meyers, University of California-San Diego

"SHOCK SYNTHESIS: GENERAL REMARKS AND RECENT RESULTS"

10:00 a.m. S. Psakhie, North Carolina State University

"MODELING POWDER COMPACTION BY ELEMENT DYNAMICS"

10:35 a.m. N. Akhmadeev, North Carolina State University

"MODELING PHYSICAL AND CHEMICAL TRANSFORMATIONS"

11:10 a.m. General Discussion

SESSION II: REAL-TIME IN-SITU MEASUREMENTS

Session Chair: D.P. Dandekar, Army Materials Laboratory

1:00 p.m. G. Ravichandran, CalTech

"DYNAMIC PORE COLLAPSE IN RATE DEPENDENT MATERIALS AND THEIR IMPLICATIONS IN SHOCK SYNTHESIS"

1:35 p.m. Y.M. Gupta, Washington State University

"REAL-TIME SPECTROSCOPIC MEASUREMENTS IN SHOCKED MATERIALS"

2:10 p.m. S.S. Batsanov, University of California-San Diego

"SHOCK CHEMISTRY: REAL-TIME MEASUREMENTS"

3:00 p.m. Mark Boslough, Sandia National Laboratory

"REAL-TIME TEMPERATURE MEASUREMENTS"

3:35 p.m. Mark Anderson, Sandia National Laboratory

"NANOSECOND, TIME-RESOLVED PRESSURE MEASUREMENTS"

4:10 p.m. General Discussion

Wednesday, May 25, 1994

SESSION III: MECHANISTIC ISSUES IN ASSOCIATED PROCESSES

Session Chair: Andrus Nüiler, Army Research Laboratory

8:00 a.m. Zuhair Munir, University of California-Davis

"THE MECHANISM OF ACTIVATED COMBUSTION SYNTHESIS"

8:35 a.m. Malcolm Nicol, University of California-Los Angeles

"CHEMISTRY AT STATIC HIGH PRESSURE: SOME GENERAL PRINCIPLES AND RECENT DEVELOPMENTS"

9:10 a.m. J.J. Gilman, University of California-Los Angeles

"MECHANISM OF SHOCK-INDUCED MECHANOCHEMISTRY"

10:00 a.m. A.N. Dremin, Russian Academy of Sciences

"SHOCK CHEMISTRY MECHANISMS, KINETICS, AND APPLICATIONS"

10:35 a.m. Mel Baer, Sandia National Laboratory

"MODELING SHOCK-COMPRESSION OF POROUS COMPOSITE MATERIALS AND CORRELATION WITH OBSERVED BEHAVIOR"

11:10 a.m. General Discussion

SESSION IV: SHOCK SYNTHESIS APPLICATIONS & PROCESS MECHANISMS

Session Chair: Robert Young, Southwest Research Institute

1:00 p.m. T. Sekine, National Institute for Research in Inorganic Materials

"SYNTHESIS OF INORGANIC AND ORGANIC MATERIALS"

1:35 p.m. V. Nesterenko, University of California-San Diego

"SHOCK SYNTHESIS OF NON-EQUILIBRIUM MATERIALS"

2:10 p.m. M. Yoshida, National Institute of Materials and Chemical Research

"SHOCK SYNTHESIS OF DIAMOND AND C-B-N MATERIALS"

3:00 p.m. T. Syono, Tohoku University

"SHOCK-INDUCED TRANSFORMATIONS IN OXIDES"

3:35 p.m. Naresh Thadhani, Georgia Institute of Technology

"MATERIALS SYNTHESIS BY SHOCK-INDUCED AND SHOCK-ASSISTED SOLID-STATE CHEMICAL REACTIONS"

4:10 p.m. General Discussion

Thursday, May 26, 1994

SESSION V: GENERAL DISCUSSION AND FUTURE TRENDS

Session Chair: Ed Chen, U.S. Army Research Office

8:00 a.m. Yuki Horie, North Carolina State University

DISCUSSIONS ON MODELING AND MEASUREMENTS

9:00 a.m. Marc Meyers, University of California-San Diego

DISCUSSIONS ON MECHANISMS AND APPLICATIONS

10:15 a.m. A. Crowson, U.S. Army Research Office

FUTURE TRENDS AND DIRECTIONS OF RESEARCH IN SHOCK SYNTHESIS

12:00 p.m. Adjourn

1:30 p.m. Tour of GTRI / MSE Laboratory Facilities

SESSION - I

SHOCK-COMPRESSSION PRINCIPLES

SESSION I: SHOCK - COMPRESSION PRINCIPLES

K. Iyer, SESSION CHAIR COMMENTS

The subjects of shock synthesis and shock-induced reactions have been somewhat oversold in the past. Not really knowing what the "other side" was doing was enough of an inducement to get into any subject in the past. I hope, at least from now on, we can formulate directions for our research activities on well-thought out scientific reasons.

Conditions at or behind the shock front are severe and uniquely different from quasi-static loading conditions. There is reason to believe that many processes and phenomena (phase transformations, chemical reactions, material conditioning etc.,) are possible under such conditions; some of them may even turn out to be technologically significant.

The workshop was a first in the sense just about everybody who was either working in the field or interested in the field was a participant. For the first time workers from several countries could exchange ideas without having to guess at it. I think the workshop tried to cover too much and too many subjects. A much more focussed affair, say on chemical reactions, might have produced tangible conclusions and directions for future work. Many potential applications were mentioned and they were all based on wishful thinking.

From a scientific point of view, a lot of qualitative observations have been made. Many speculative models have been proposed. Knowledge from studies of SHS reactions, mechanical alloying, and equilibrium phase diagrams have been extended to understand an essentially non-equilibrium process. I see a need for unambiguous, reliable, and reproducible diagnostics; development of theory to interpret the measurements; and then development of models for predictive capability. Until questions such as when?, what?, and how much? are answered it is difficult to see much future for this kind of endeavor. I hope this is not viewed as a negative remark but as a strong suggestion for future direction.

Kinetic Modeling of Shock Chemistry

**Y. Horie
North Carolina State University**

**ARO Workshop
G.I.T.
May 24, 1994**

KINETIC MODELING OF SHOCK CHEMISTRY

Y. Horie
North Carolina State University

Abstract

There is increasing experimental evidence that significant fast chemical reactions occur at the shock front in inorganic powder mixtures. These observations are based on (1) anomalies in the Hugoniot of reactant mixtures, (2) pressure and temperature profile measurements, and (3) a combined analysis of recovered specimens and pressure measurements. It is thought that these fast reactions that occur on the order of one microsecond or less cannot be adequately described by conventional diffusion mechanisms, but at the present time there is very little understanding of the detailed mechanisms.

This paper describes the development and selected testings of the hydrodynamic constitutive models called VIR to analyze and interpret the observed fast chemical reactions in powder mixtures. The acronym VIR signifies the three most important ingredients of the model: Void, Inactive and Reactive species. The critical assumption of the VIR is that the latter two form separate thermodynamic sub-systems within a closed mixture system as a whole. Theoretically, this separation is intended to describe localized reactions, but is also based on recovery experiments. The most recent model, however, includes reactions even in the I sub-system.

Currently, there are two basic types of the VIR model. The difference is based on the assumptions we ascribe to the behavior of the subsystems. The first and most often used model is based on homobaric (mechanical equilibrium) and homokinetic (single particle velocity) assumptions. There is no mass transport between the two subsystems, but heat transport is permitted.

The major purpose of developing this model is to study the interaction of hydrodynamic flow of porous inorganic media with thermodynamic changes associated with chemical reactions. Recently, however, we found that the theoretical underpinning of this model is very closely related to that of Johnson, Tang, and Forester for solid explosives, and the Herrmann's formulation of reactive solid media.

Testing of this model has been successfully carried out with a variety of material combinations. They include Al/Ni, Al/Hematite, Ti/Si, and Si/C/diamond. But, it is important to note that these calculations are basically model calculations involving a variety of assumptions. They are for instance, hypothesized chemical reactions, estimated equations data, and crush-up behavior of the powder mixtures.

The second model is a heterogenous model and removes the homobaric and homokinetic assumptions. The resulting governing equations resemble basically those for two phase flow. But, our model which is based on the continuum mixture theory extensively used by Baer at Sandia for the study of solid explosives, contain an extra term that is controlled by the volume fractions of constituent species.

At the present time this model is only used to study the heterogenous flow in binary powder mixtures. Also, voids are treated not as a separate entity, but as a part of the equation of state of each constituent.

For application the model is used to demonstrate the existence of slip velocity in shock-loaded Ni/Al powder mixtures. Obviously, the result strongly depends on the inter-particle interactions we specify in the model, but a model with viscous shear produces the slip velocity on the order of several hundred meters per second under the symmetric impact of a Ni/Al mixture at 1 km/s. There is experimental evidence that the chemical initiation may be related to the question of how this large kinetic energy is dissipated under shock compression. That is, if it were dissipated "uniformly" among the powder grains, then there will be no significant chemical reactions. Under such circumstances, the powders maintain their starting neighbor configurations. However, if it were dissipated heterogeneously, the results are intense localized flow and may even cause global turbulent and chaotic motions. These localized intense shear motions and vorticity will then enhance mass mixing and initiate explosive chemical reactions because of elevated temperatures.

References

1. Y. Horie and A.B. Sawaoka, Shock Compression Chemistry of Materials, KTK Scientific Publishers, Tokyo, 1993.
2. Y. Horie, "Shock-Induced Chemical Reactions in Inorganic Powder Mixtures," in Shock Waves in Materials Science, ed. by A.B. Sawaoka, Springer, Tokyo, 1993, Chapt. 4.

CONTENTS

1. Introduction

2. NCSU Models and Model Calculations

- Lagrangian Model (single P & u)**
- Heterogeneous Flow Model**

3. Concluding Remarks

"Shock chemistry, as it now exists, is an exercise in old-fashioned chemistry: a science of end states in which substances were mixed and processed, and the reaction products were collected and analyzed."

George E. Duvall (1984)

Real-Time Measurements of Shock Initiation and Shock-Wave Profiles in Reactive Granular Mixtures

<u>Year</u>	<u>Team</u>	<u>Measurement</u>	<u>Threshold (GPa)</u>
1986	Batsanov et (Sn+S)	Shift in Hugoniot	15
1988	Boslough (Al+Fe ₂ O ₃)	Temperature	5
1990	Hardt (Al+Fe ₂ O ₃)	Pyrometer	12-15
1992	Bennett et al (Al+Ni)	Reflected Hugoniot	15
1992	Yoshida & Thadhani (Nb+Si)	C _s & Hugoniot	20
1993	Dunbar et al (Ti+Si)	Hugoniot	1-2
1990's	SNL	P & u	
1991	Grogulya et al S + (Mg, Al, Ti, Fe)	Pyrometer	24~31
1991	Batsanov et al Sm + TX	Hugoniot	~50
1991	Gryadunov et al Ti + C	Pyrometer	7~9

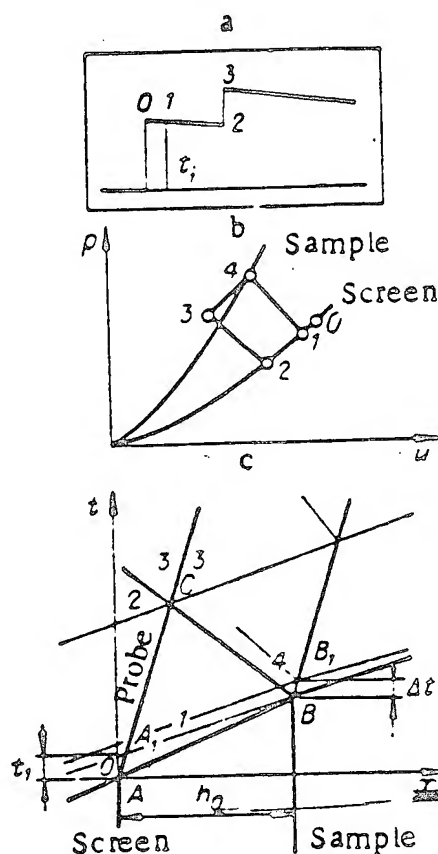
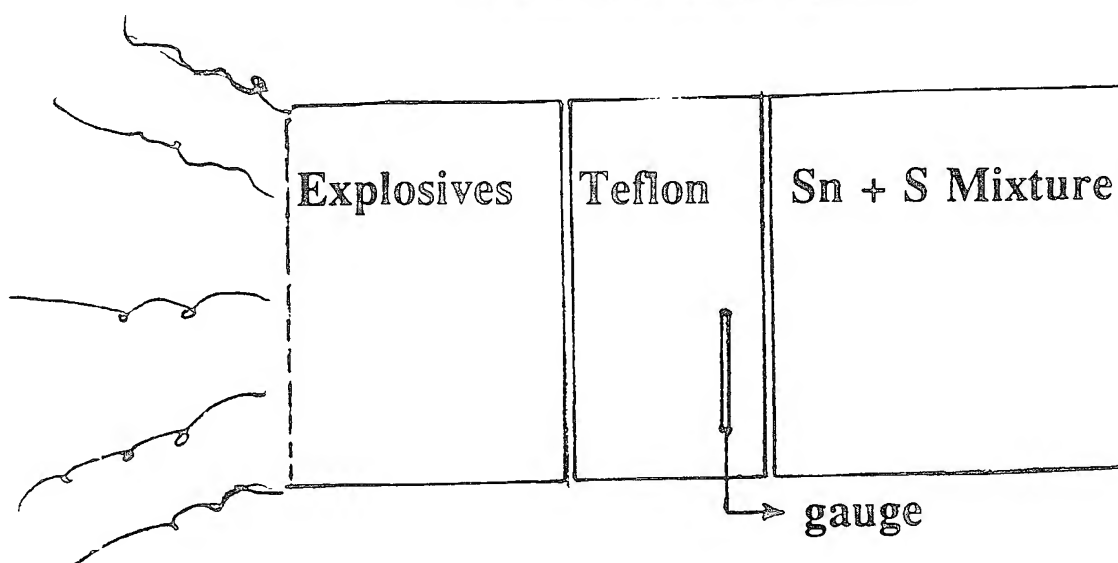


Fig. 1

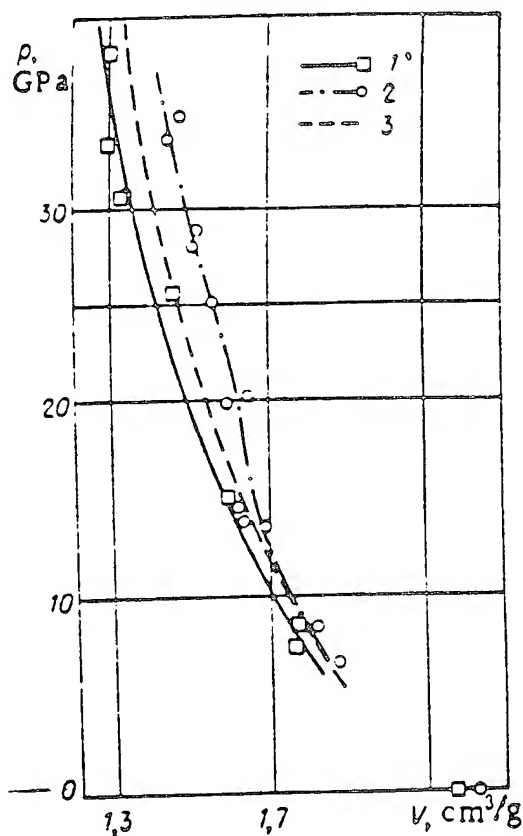


Fig. 2

Fig. 1. A typical $x-t$ oscilloscope trace and $p-u$ diagram for calculating the shock parameters in a test sample.

Fig. 2. The shock adiabat of tin sulfide (points 1) and of a stoichiometric mixture of Sn + S (points 2). (Points 3 denote the shock adiabat of an inert Sn + S mixture.)

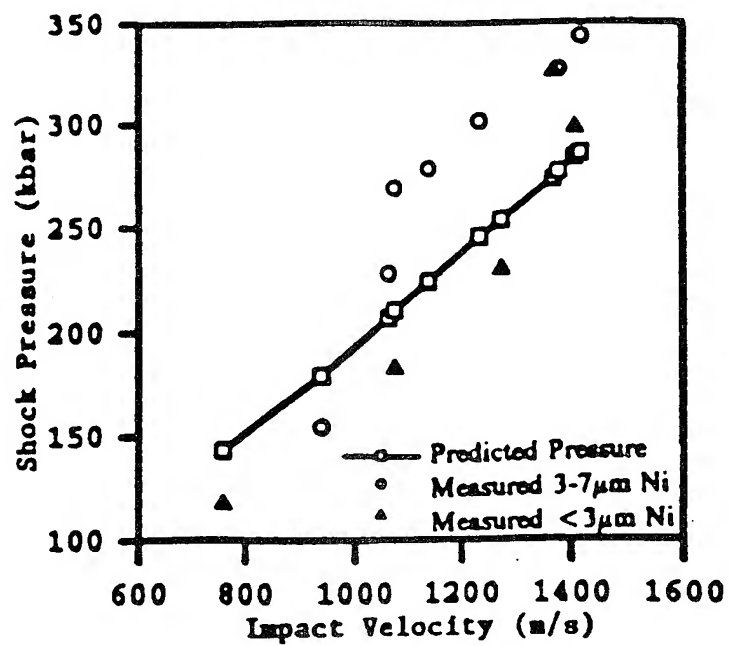
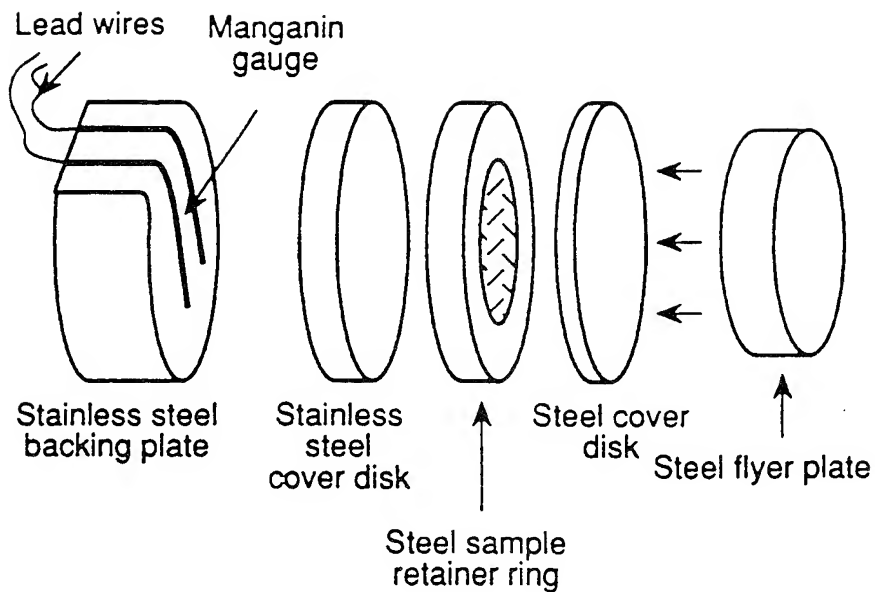


Figure 2. Measured reflected shock pressure vs impact velocity for two series of experiments.

Basic Issues

1. Initiation and Growth of Chemical Reactions

- Threshold conditions
- Mechanisms
- Microstructural effects
- Chemical paths
- Rates

2. Equation of State and Pore Compaction Data

- Properties of exotic liquid products
- Crush-up pressure
- Rate effect

3. Dynamics of Heterogenous Flow

- Fundamental theoretical problems associated with multiphase and multispecies systems.

4. Instabilities of Flow and Interfaces

5. Energetic v.s. Ballotechnic Reactions

6. Non-Hydrostatic Stress Components

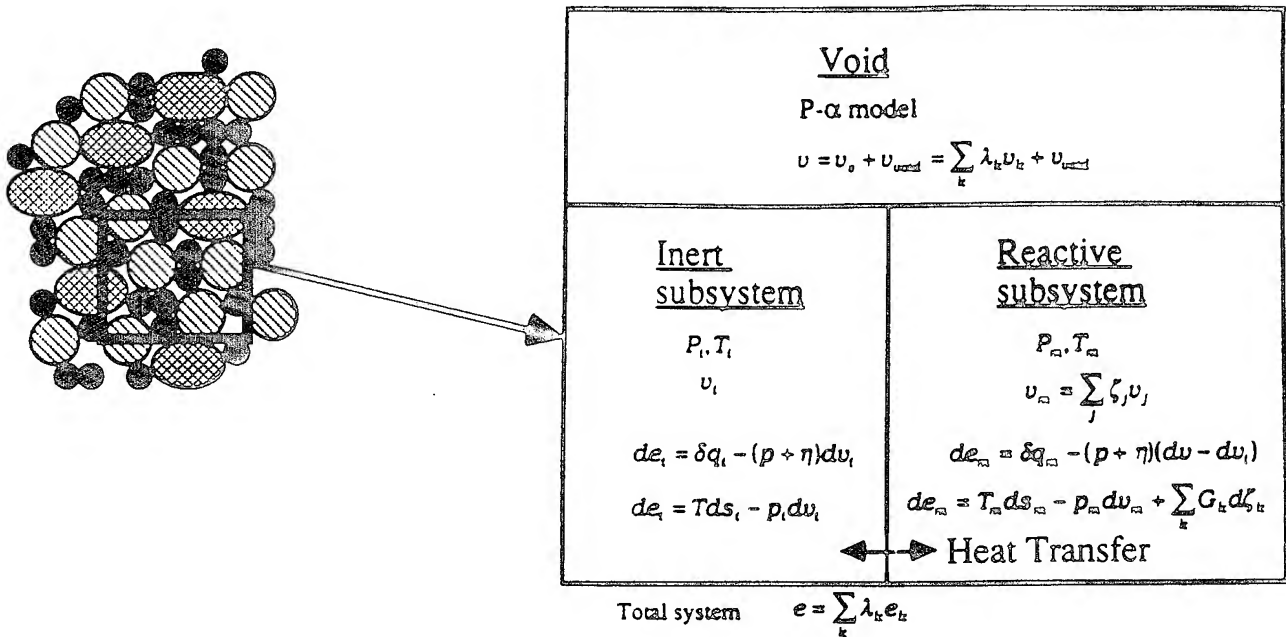
Focus of Theoretical Work at NCSU

- Interaction of complex material motion with the thermodynamic changes associated with chemical changes

Approach

- Numerical analysis of detailed simulation models

Philosophy of Basic VIR Model



Postulates:

- Three subsystems: one void and two materials
- Internal heat transfer (two T), but not mass
- Mechanical equilibrium; single p and u
- Multispecies

Rate Equations:

- Heat transfer
- Chemical kinetics
- Pore collapse

$$de = -(p + \eta)dv$$

MATHEMATICAL VIR MODEL

a) Specific internal energy equations:

$$dE = - (P+\eta) dv$$

i) Subsystem (a):

$$dE_a = \delta q_a - (P+\eta)dv_a$$

$$dE_a = T_a ds_a - P_a dv_a + \sum d\zeta_{ai} g_{ai}$$

ii) Subsystem (b):

$$dE_b = \delta q_b - (P+\eta)(dv_b + dv_{void}/\lambda_b)$$

$$dE_b = T_b ds_b - P_b dv_b + \sum d\zeta_{bi} g_{bi}$$

b) Extensive properties:

$$E_x = \sum \zeta_{xi} E_{xi}$$

$$s_x = \sum \zeta_{xi} s_{xi} \quad s_{xi} = s_{xi}(v_{xi}, T_{xi})$$

$$v_x = \sum \zeta_{xi} v_{xi} \quad v_{xi} = v_{xi}(P_{xi}, T_{xi})$$

where $x = a, b$ and the summation applies over the species i

c) Heat conduction between subsystems (a) and (b):

$$\dot{q}_a = A_s h_t (T_b - T_a)$$

$$\dot{q}_b = - (\lambda_a/\lambda_b) \dot{q}_a$$

where $h_t = \rho_0 C_v \delta / R_0$ (δ = thermal diffusivity, R_0 = mean particle radius)

d) Chemical reactions:

$$\dot{\xi}_x = \dot{\xi}_{ox} (1 - \xi_x) e^{-\epsilon_x / RT_x}, \quad \text{First order Arrhenius equation}$$

$$\text{Reactant: } \zeta_{xj} = (M_{xj} / \sum M_{xj}) (1 - \xi_x)$$

$$\text{Product: } \zeta_{xk} = (M_{xk} / \sum M_{xk}) \xi_x \quad \text{Initiation} = f(p, T, \dots)$$

e) Pore Collapse:

Polynomial P - α model

f) Volumetric compatibility equation:

$$\dot{v} = \dot{\alpha} v_d + \alpha (\lambda_a \dot{v}_a + \lambda_b \dot{v}_b) \quad \text{where } v_d = \lambda_a v_a + \lambda_b v_b$$

g) Equation of state:

$$P_{xi}(v_{xi}, T_{xi}) = (\beta_{To}/n)_{xi} [(v_{xi}/v_{xio})^{-n} - 1] + C_{vxi} (\Gamma/v)_{xi} (T_{xi} - T_{xio})$$

h) Mechanical equilibrium:

$$P_a = P_b$$

VIR MODEL

$$\left[\begin{array}{c} \frac{P_b - (P + \eta)}{C_{va}} - T_a \frac{\Gamma_a}{v_a} \\ \frac{P_b}{C_{vb}} - T_b \frac{\Gamma_b}{v_b} + \frac{\lambda_a}{\lambda_b} \frac{P + \eta \beta_{Tb}}{C_{vb} \beta_{Ta}} \frac{v_a}{v_b} \\ \frac{\lambda_a}{\lambda_b} \frac{v_a}{\beta_{Ta}} + \frac{v_b}{\beta_{Tb}} \end{array} \right] \left[\begin{array}{c} 0 \\ \beta_{sb} - P_b \frac{\Gamma_b}{v_b} \\ -\frac{C_{vb}}{\beta_{Tb}} \Gamma_b \end{array} \right] \left[\begin{array}{c} \frac{\beta_{sa}}{v_a} - \frac{\Gamma_a}{v_a} [P_b - (P + \eta)] \\ -\frac{\lambda_a}{\lambda_b} \frac{P + \eta \beta_{Tb}}{C_{vb} \beta_{Ta}} \frac{C_{va}}{v_b} \Gamma_a \\ -\frac{\lambda_a}{\lambda_b} \frac{C_{va}}{\beta_{Ta}} \Gamma_a \end{array} \right] \left[\begin{array}{c} \dot{P}_b \\ \dot{T}_b \\ \dot{T}_a \end{array} \right] =$$

$$\left\{ \begin{array}{l} \frac{\beta_{Ta}}{C_{va} v_a} (\dot{q}_a + H_{0a} \dot{\xi}_a) \\ \frac{\beta_{Tb}}{C_{vb} v_b} \left[-\frac{P + \eta}{\lambda_b} (\dot{v} - \lambda_a \sum_i \dot{\xi}_i v_i) + \dot{q}_b + H_{0b} \dot{\xi}_b \right] \\ \left(\frac{\lambda_a}{\lambda_b} \sum_i \dot{\xi}_i v_i + \sum_j \dot{\xi}_j v_j \right) - \frac{1}{\alpha \lambda_b} (\dot{v} - \alpha v_d) \end{array} \right\}$$

REDUCED VIR MODEL

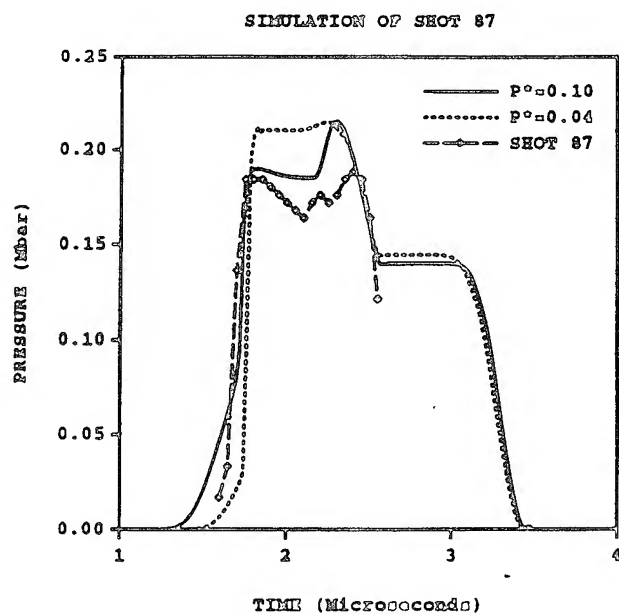
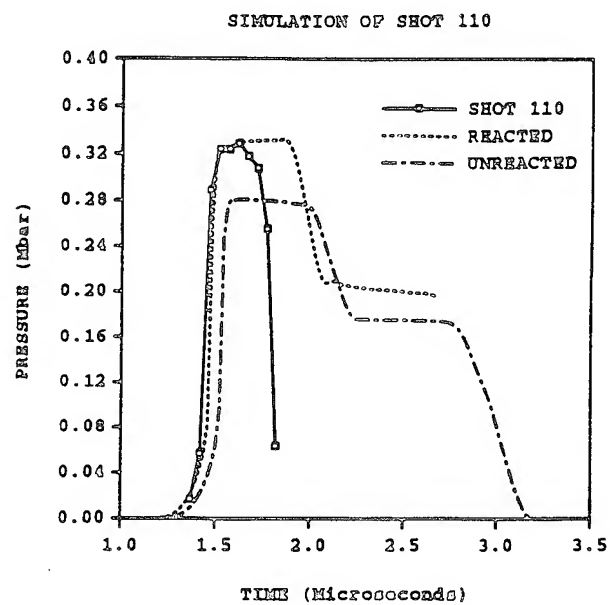
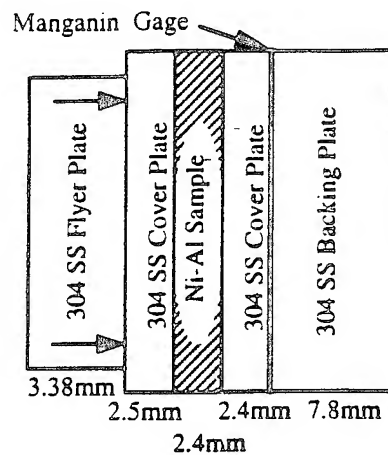
Pressure and Temperature for a Single Reactive Mixture

$$\blacklozenge \dot{P} = (H_0 \dot{\xi} - P \dot{v}_{ch}) \frac{\Gamma}{v} - (\dot{v} - \dot{v}_{ch}) \frac{\beta_s}{v}$$

$$\blacklozenge \dot{T} = (H_0 \dot{\xi} - P \dot{v}_{ch}) \frac{1}{C_v} - (\dot{v} - \dot{v}_{ch}) T \frac{\Gamma}{v}$$

where $H_0 \dot{\xi}$ = Internal Energy Change due to Reaction

$$\text{and } \dot{v}_{ch} = \sum_j \dot{\xi}_j v_j.$$



Model Simulation of $\text{Al-Fe}_2\text{O}_3$ Experiment (Boslough)

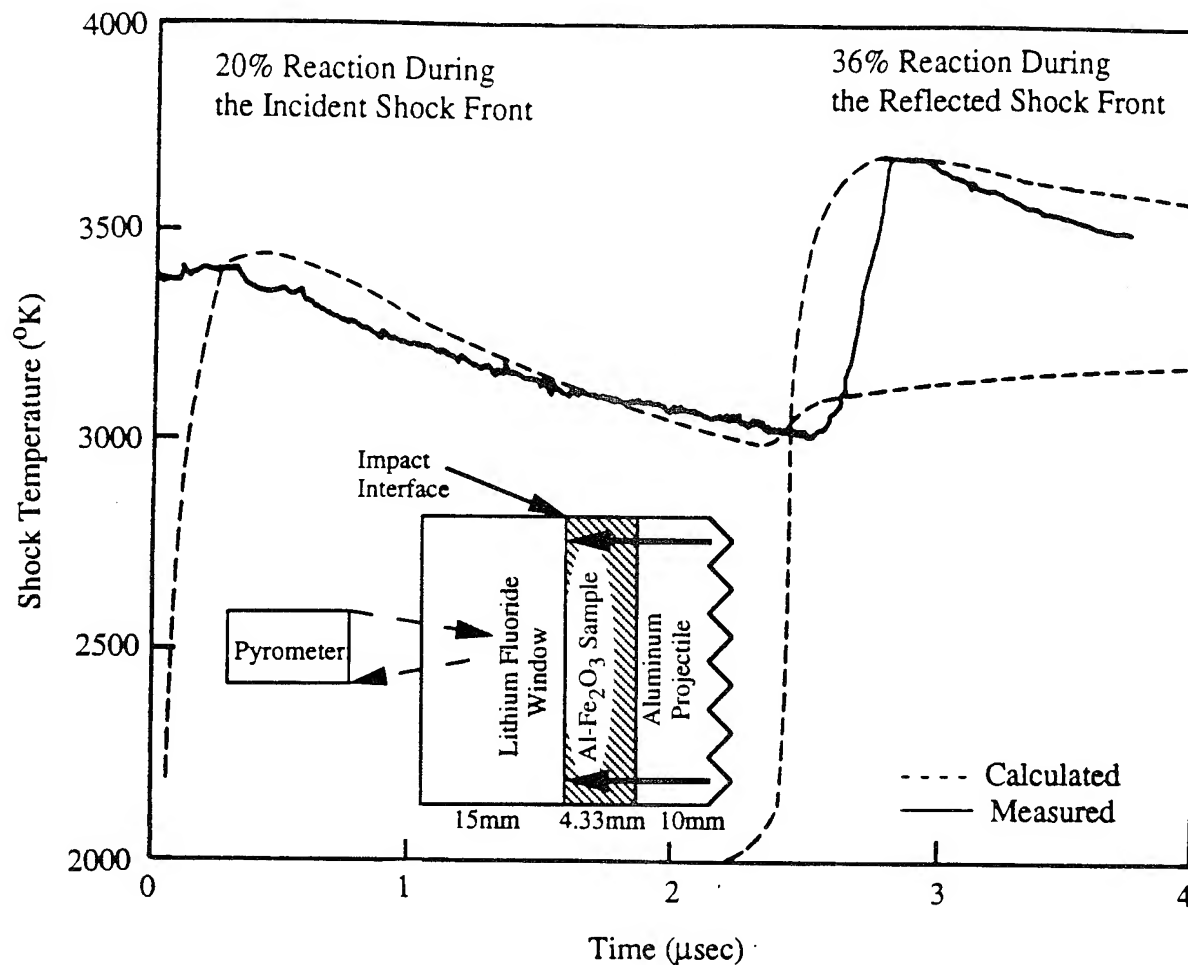
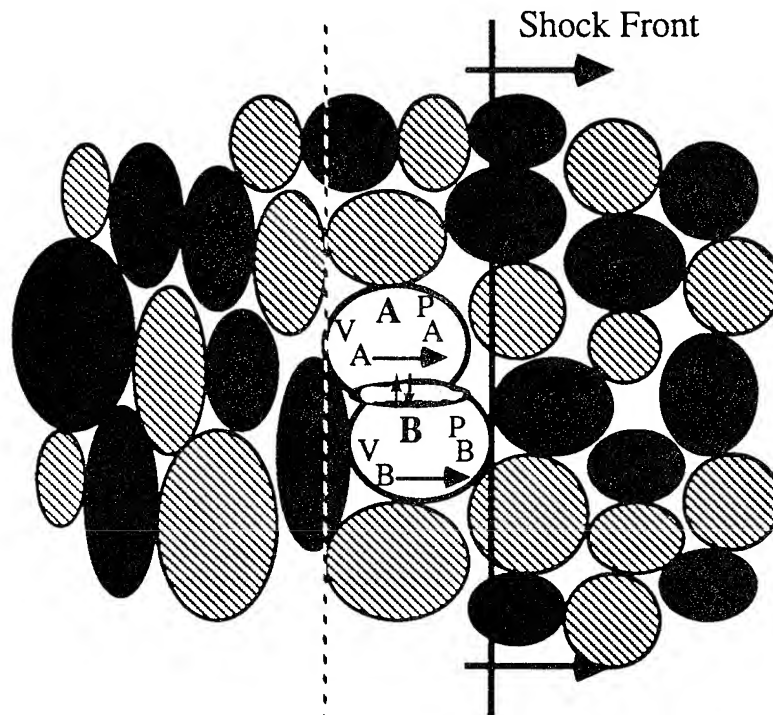


Figure 3. Experimental and numerically computed incident and reflected shock temperature profiles for an $\text{Al-Fe}_2\text{O}_3$ powder mixture. The experimental arrangement is illustrated in the insert. Disagreement between the arrival time of the measured and calculated reflected shocks is most likely caused by inaccuracies in the material properties.

Features of Shock-Induced Inorganic Reactions (Computational Observations)

- Reaction Rate Constant: $0.5 \sim 2 \mu\text{sec}$.
- Initiation Threshold: 800 -1,200 K,
sensitive to p and u ,
initiation in the shock front.
- Incubation time: $0 \sim 1.4 \mu\text{sec}$.
- Key Parameters: Heat of reaction, β_s , and specific
volumes of products.

Shock-Induced Heterogeneous Flow in a Powder Mixture



Continuum Mixture

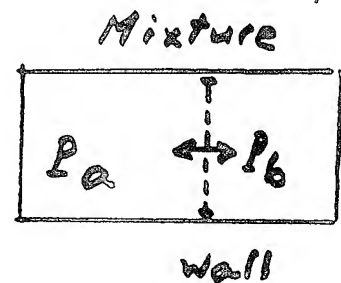
<u>Void</u>	
<u>Material A</u>	<u>Material B</u>
V_A P_A	V_B P_B
<div style="display: flex; align-items: center; justify-content: center;"> <div style="margin-right: 10px;">←</div> <div style="text-align: center;">Momentum Transfer</div> <div style="margin-left: 10px;">→</div> </div>	
<div style="display: flex; align-items: center; justify-content: center;"> <div style="margin-right: 10px;">T_A</div> <div style="text-align: center;">Heat Transfer</div> <div style="margin-left: 10px;">→</div> </div>	

EQUATION OF MOTION FOR A BINARY MIXTURE

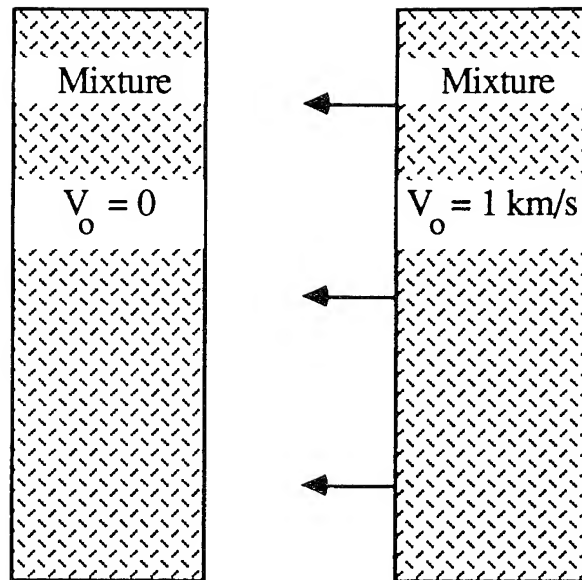
$$\rho_a \left(\frac{\partial v_a}{\partial t} + v_a \frac{\partial v_a}{\partial x} \right) = -\alpha_a \frac{\partial P_a}{\partial x} - \underbrace{\delta(v_a - v_b)}_{\text{slip vel.}} + \underbrace{(P_b - P_a)}_{\text{Vol. Fraction}} \frac{\partial \alpha_a}{\partial x}$$

slip vel. *Vol. Fraction*

$$\frac{\partial \alpha_a}{\partial t} + v_a \frac{\partial \alpha_a}{\partial x} = \frac{1}{\mu} (P_a - P_b)$$



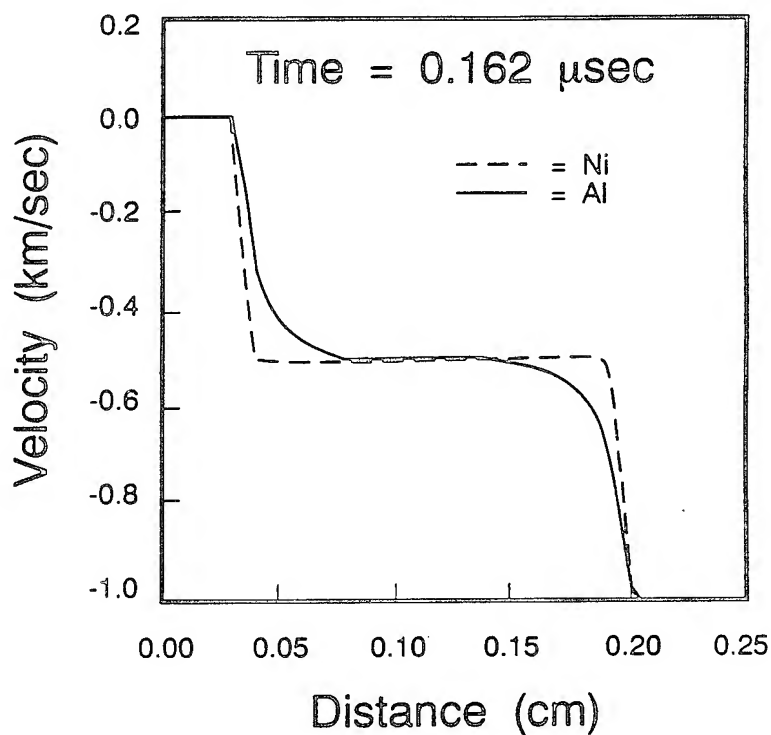
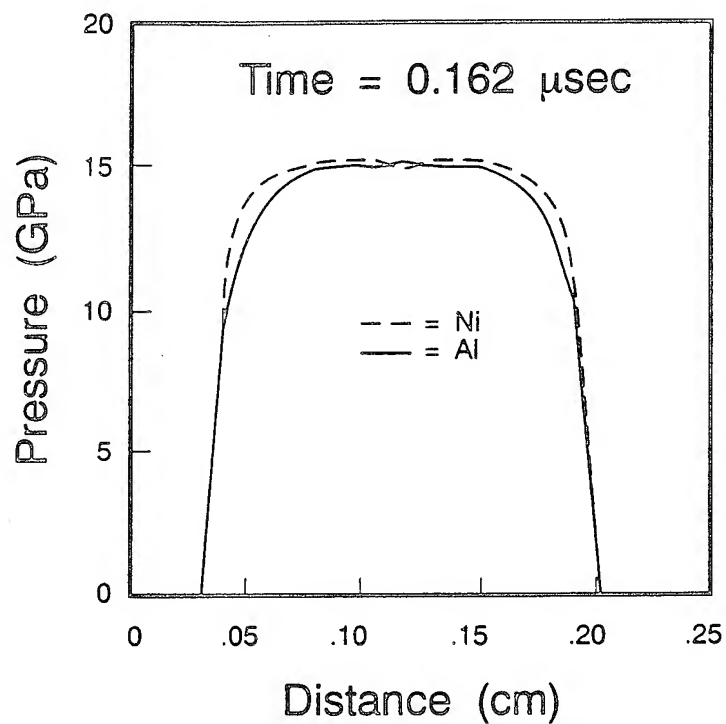
M. Baer,



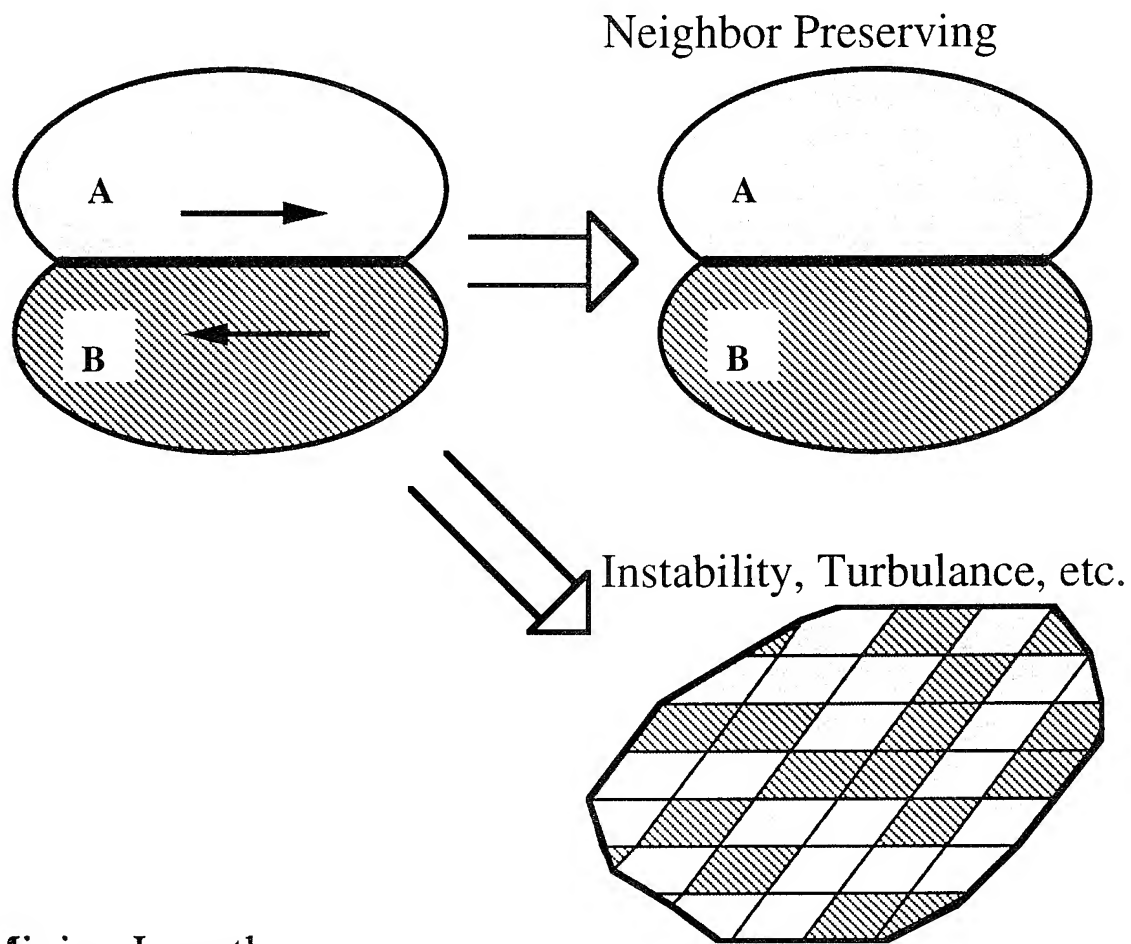
Impact of a Ni - 50% wt. Al Mixture.

SIMULATION OF SHOCK-INDUCED HETEROGENOUS FLOW IN 50/50 wt % Ni-Al MIXTURE

(Symmetric Impact)



Transformation of Kinetic Energy to Surface Energy



Mixing Length:

$$l = \frac{6 \sigma}{\varepsilon \rho u^2}$$

Typical Metals:

$$\left. \begin{array}{l} \sigma = 1 \text{ joule/m}^2 \\ u = 200 \text{ m/s} \end{array} \right\} \rightarrow l \cong 0.1 \text{ micrometer}$$

Concluding Remarks

More Light

- More material data
- Experiments to test model assumptions
- New Models

Comments by Y. Horie

My comments will be made in the form of replies to the questions raised in the preamble of the Workshop.

(a) Has the initiation and completion of chemical reactions during shock compression of powder mixtures, been conclusively demonstrated?

There are strong experimental indications (pressure measurements) that can only be explained by the initiation of chemical reactions at the shock front. It is not fruitful to argue whether they are conclusive or not, because short of spectroscopic measurements the term can connote different things to different people. What is more important at the present time is to demonstrate the reproducibility of the observed phenomena. There is nothing more stimulating in science than a repeatable phenomenon that cannot be explained by existing theories.

To my knowledge there has been no experiment that showed the completion of reactions during shock compression. Like phase transitions, this question could be settled by measuring Hugoniot.

(b) Is it possible to establish the progress of reaction (fraction transformed with time) with available time-resolved measurement techniques?

I believe so. The techniques such as VISAR and PVDF gauge have the time resolution of a few nanoseconds. This should be fast enough to resolve the progress of hypothesized reactions in real time. The problem is how to design experiments so that data from the probes will provide the information we are seeking. It is conceivable that there is no single configuration that will yield all the information we need. We may have to design a combination of experiments. But whatever we do, it is likely that the results will not be conclusive on the microscopic level, because the question of reaction paths will remain near impossibility for many years to come.

Design and engineering of starting microstructures need to be tried to control the reaction rate. Also recovery experiments should not be abandoned. Rapid quenching techniques is still a viable technique to obtain information (obviously limited, but useful) on the progress of reaction.

(c) What are the limitations of current time-resolved measurement techniques and what other novel in-situ measurement techniques need to be explored?

The problem as I see it is not the limitations of measurement techniques, but often the question of how to use them as I indicated in (b). For instance, VISAR has been a workhorse

in shock physics and its limitations are well documented, but so far as I am aware of, there has been no systematic use of it to investigate shock-induced reactions in inorganic materials? Before we try a novel, expensive technique, there is plenty we can do with existing techniques. I am not, however, denying the significance of any new technique that are superior to the existing ones.

Obviously there is no one technique that solves all the questions. We need a variety of techniques. In this regard I believe that it is more important to try techniques that probe electro-magnetic properties of materials than the development of new techniques for in-situ measurements (though they are not mutually exclusive). It is also conceivable that such non-mechanical measurements may show unique properties produced by shock loading.

(d) What is the current understanding of the process mechanisms and kinetics of chemical reactions occurring during shock compression of powders?

There is increasing experimental evidence of chemical initiation, but there is not enough data to clearly articulate the mechanisms as well as kinetics. There are lots of proposals for mechanisms, but I am not certain that there is a consensus about any of them and how widely these models are studied beyond the small circles of the authors' inner group. Time has come that we begin to think about conducting experiments to test model assumptions and competing models. Without well integrated programs, shock compression chemistry, particularly as it relates to materials synthesis, will remain "just exploratory, old-fashioned chemical experiments."

Proof of uniqueness of any sort is difficult to get, but sometimes there exists a qualitative test that can be used to test models. One such example is the onset of instability. Hwang, for instance, has shown numerically (1993) that even with chemical reaction, there is splitting of a plane shock as that with phase transition in solids. The testing of a prediction like this can be easily accomplished without advanced instrumentation.

(e) Can mechanisms of other types of chemical reaction and phase transformation processes, occurring in time scales ranging from 10^{-9} to 10^3 seconds, be used to develop mechanistic models of shock chemistry?

May be. In view of the status of (d) above, however, this question remains a moot point.

(f) Can numerical models be developed to account for the influence of materials characteristics and shock compression conditions on configuration changes leading to chemical reactions during shock compression?

Definitely yes. But again, the question is "how we test the model? What experiments?"

Probably we need new models to deal with heterogeneity inherent in powder mixtures. There is also a question of scales (time, space, etc) associated with such media. All in all, the question is not something we can solve in a short time.

(g) Can applications of shock chemistry be realized for synthesis of materials?

Obviously, yes. But, again time has come that we conduct experiments based on some theoretical predictions and model calculations. There is still a lot of art in materials science, but, without theorizing about why and what we are doing, progress is totally a chance event. It is my belief that there is enough "theoretical machineries" around to tackle shock chemistry and put it on a firm scientific ground. The questions is how to build a comprehensive model using those theories and test it experimentally.

At the moment the community is too "in-grown." We need people from outside to build a robust community of diverse ideas.

Ten years ago, Duvall in his NMAB report concluded that there are substantial grounds for believing that the novel physical and chemical processes involved may ultimately serve as the basis for useful technologies, but that many of the questions that need to be answered are not addressed by work now in progress.

Since then some of the questions have been answered and there is increasing evidence for a unique sequence of shock-induced chemical reactions, but an overwhelming portion of the questions still remain unanswered. I will cite two outstanding problems that remain unanswered.

1. Understanding of physical processes in mixed powders under shock loading.
2. Theory, either fundamental or empirical, that gives even semiquantitative insight to the final products.

Reference

Hwang, M.D., Ph.D thesis, North Carolina State University, 1993.

SHOCK SYNTHESIS: GENERAL REMARKS AND RECENT RESULTS

M.A. Meyers, K. S. Vecchio and A. Strutt
U. of California, San Diego
La Jolla, CA 92093

Shock-induced chemical reactions have been actively studied since the 1960's. A brief review of the principal studies is presented. These reactions have been classified into polymorphic phase transformations, chemical decomposition processes, and chemical synthesis processes. The effects of pressure and shear strains/stresses imparted by the propagation of shock waves through dense and porous materials is discussed. There are essentially two schools of thought regarding shock-induced synthesis processes: solid-state and solid-liquid reactions. These two mechanisms will be discussed in light of the unique stress, strain, and of the high density of defects (point, line, interfacial defects, microcracks) generated.

Experiments carried out by the authors and collaborators over the past eight years will be described. Five experimental configurations have been used, enabling a good understanding of the reaction mechanism in the Nb-Si system. These configurations, as well as the principal results obtained, are described:

- a) Sawaoka shock compression fixtures (collaboration with N. N. Thadhani and L. H. Yu)
- b) Sandia Bear fixtures (collaboration with R. A. Graham) - This fixture was used for Ni-Al reaction investigation [5].
- c) Cal Tech gas gun experiments (collaboration with G. Ravichandran and W. Tong)
- d) LLNL gas gun experiments (collaboration with W. Nellis) [6].
- e) Novosibirsk TWC (thick-wall cylinder) experiments (collaboration with V. F. Nesterenko, M. Bondar, and B. Chen) [7].

The effects of particle size, initial temperature, and shock compression pressure on the chemical reaction Nb+Si between elemental powders were established. These experiments enable the identification of the principal reaction mechanism for the Nb-Si system. The effect of shock compression is to produce a large plastic deformation, leading to melting of Si and to a reaction between liquid silicon and solid niobium. The niobium silicide layer (Nb Si₂) formed a liquid layer surrounding the Nb particles. This layer separates into small spherulles (~ 1-2 μ m) which float into the silicon, ensuring the maintenance of a fresh reaction interface and a high reaction rate.

Recent experiments in which intense plastic deformation and shear localization were created yielded enhanced reaction in these regions, indicating that plastic deformation energy, in addition to shock deformation energy, helps the reaction. Two different experimental configurations using the cylindrical implosion method were used to produce controlled shear bands in porous mixtures: MoSi₂ + SiC + Mo + Si and Nb + Si. The thick-wall cylinder (TWC) method [7] and a simple cylindrical configuration in which the powders were placed in a tube loaded by explosives in an implosion mode. Localization of plastic deformation with localized reaction was observed. The configurations used enabled the measurement of the average strain and strain rate of the shear process. The shear localization regions had high plastic

macrostrain ($\gamma \sim 5-10$) and strain rate (10^6s^{-1}); particle fracture and melting resulting in reaction were observed. The structure of the shear bands included rotations and microshear bands within the particles and was dependent on porosity.

These observations were the basis into a mechanism that incorporates the thermodynamics and kinetics of shock-induced chemical synthesis of (Nb, Mo, Ti) silicides.

This work was supported by the National Science Foundation Grant MSS 90-21671, by the U.S. Army Research Office Contract DAA 1104-93-6-0261, and by Sandra National Laboratories Contract No. 12-9490.

REFERENCES

1. L. H. Yu and M. A. Meyers, *J. Mater. Sci.* 26 (1991) 601.
2. L. H. Yu, M. A. Meyers, and K. S. Vecchio, in "Proc. Intl. Symp. on Intense Dynamic Loading and its Effects", Chengdu, China, June 9-12, 1992, p. 741.
3. K. S. Vecchio, L. H. Yu, and M. A. Meyers, *Acta Met. Mat.* 42 (1994) 701.
4. M. A. Meyers, L. H. Yu, and K. S. Vecchio, *Acta Met. Mat.*, 42 (1994) 715.
5. A. J. Strutt, K. S. Vecchio, L. H. Yu, M. A. Meyers, and R. A. Graham, in "Shock Compression of Condensed Matter - 1993", A.P.S., in press (1994).
6. L. H. Yu, W. J. Nellis, M. A. Meyers and K. S. Vecchio, in "Shock Compression of Condensed Matter - 1993", A.P.S., in press (1994).
7. V. F. Nesterenko, M. A. Meyers, M. Bondar and B. Chen, manuscript in preparation, 1994.

**SHOCK SYNTHESIS: GENERAL
REMARKS
AND RECENT RESULTS**

M. A. Meyers, K. S. Vecchio, and
A. J. Strutt

**WORKSHOP ON SHOCK SYNTHESIS OF
MATERIALS**

Georgia Institute of Technology
May 24, 25, 26, 1994

Research Supported by:
U.S. Army Research Office Contract
National Science Foundation
Sandia National Laboratories

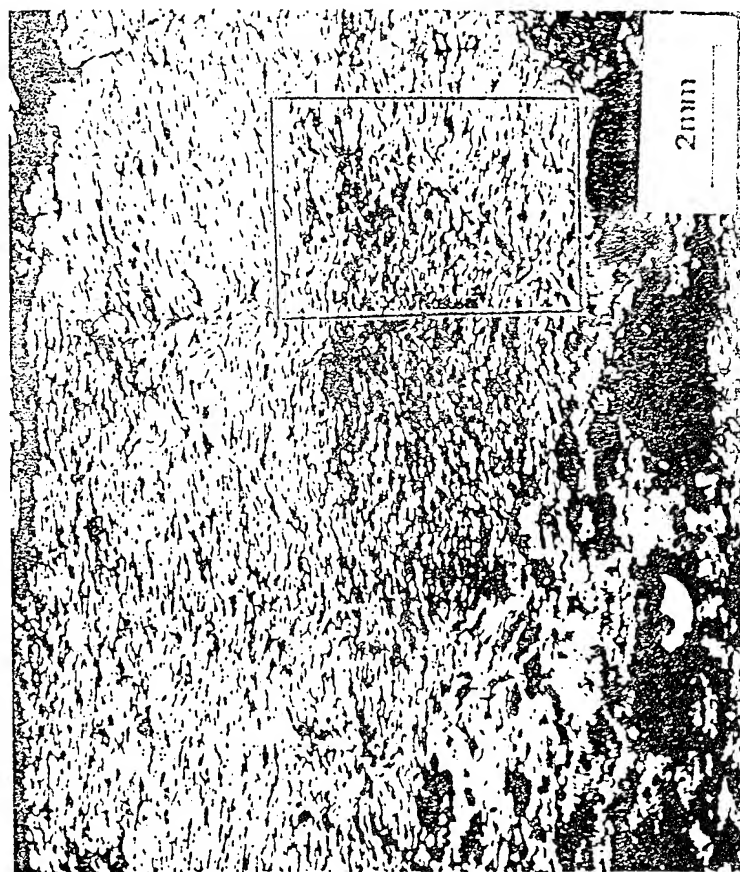
EXPERIMENTAL METHODS

- 1 Sawaoka shock compression fixtures (collaboration with N. N. Thadhani and L. H. Yu)
- 2 Sandia Bear fixtures (collaboration with R. A. Graham) - This fixture was used for Ni-Al reaction investigation [5].
- 3 Cal Tech gas gun experiments (collaboration with G. Ravichandran and W. Tong)
- 4 LLNL gas gun experiments (collaboration with W. Nellis) [6].
- 5 Novosibirsk TWC (thick-wall cylinder) experiments (collaboration with V. F. Nesterenko, M. Bondar, and B. Chen) [7].

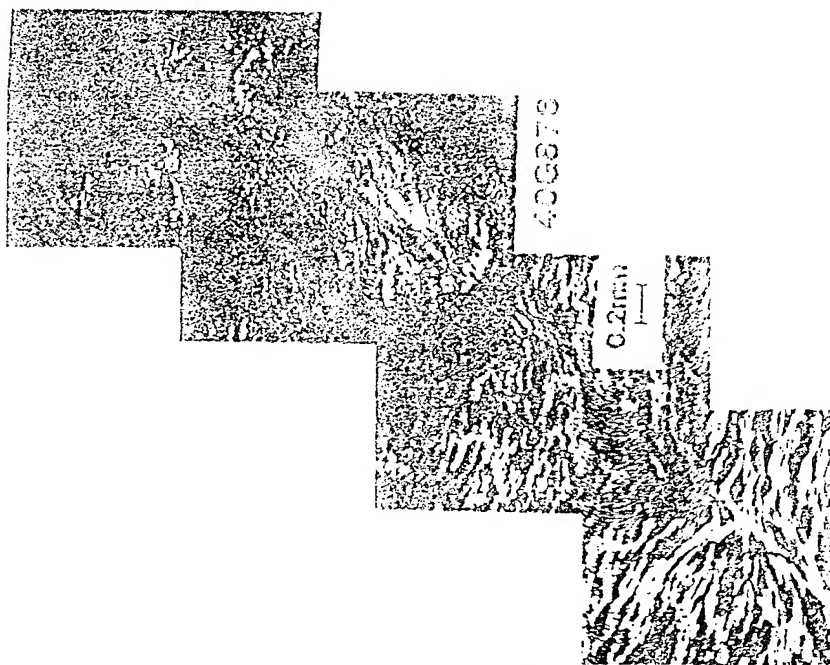
REACTION MECHANISMS

- 1968 Dremin and Breusov - ROLLER MODEL
- 1986 Batsanov, Doronon, et al
 ULTRA-RAPID SOLID-STATE DIFFUSION
 $\Delta U_{p12} = U_{p1} - U_{p2}$
- 1988 Horie + Kipp - VIR COMPUTER MODEL
- 1989 Graham - CONMAH MODEL
- 1990 Boslough and Yu et al.
 $E - E_0 = (1/2) P (V_0 - V) + \Delta Q$
- 1991 Krueger and Vreeland - THRESHOLD ENERGY

N. N. Thadhani *et al.*: Shock-induced reaction synthesis (SRS) of nickel aluminides

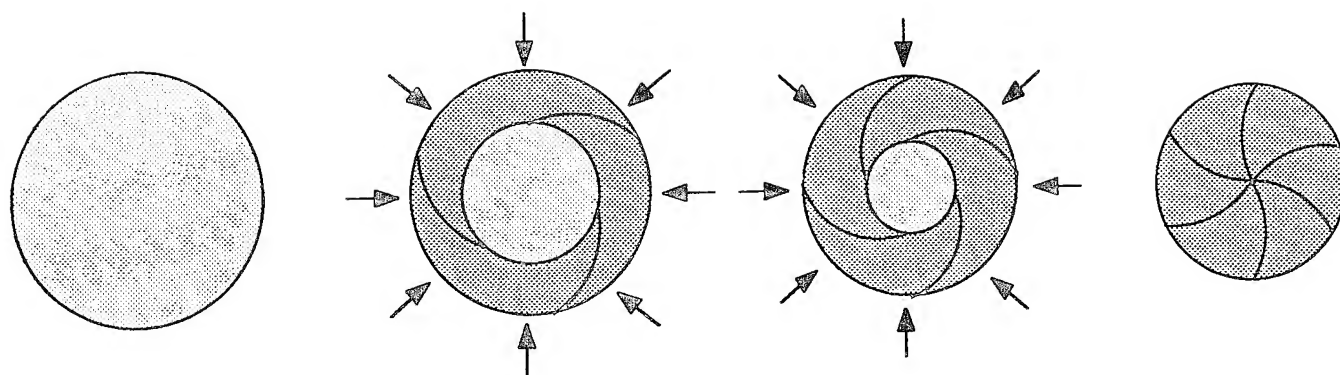


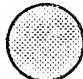
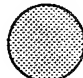
(a)



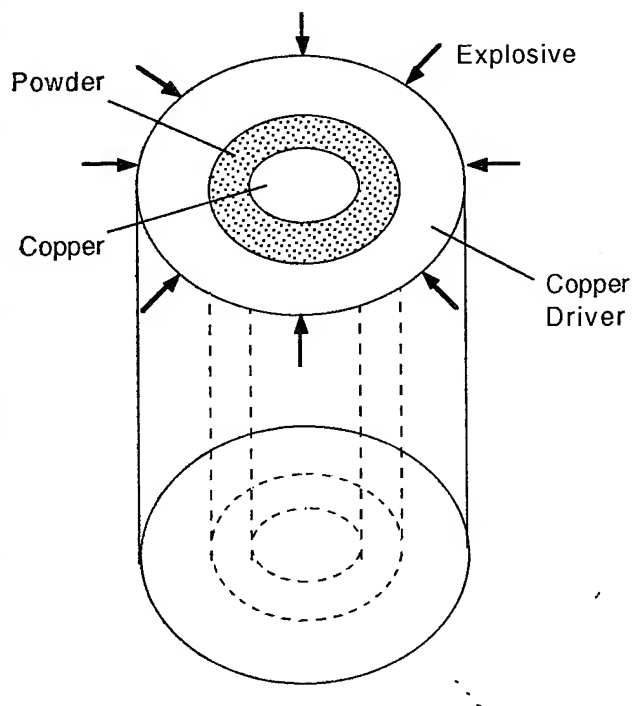
(b)

FIG. 6. (a) Optical micrograph showing regions of shear instabilities formed due to nonplanar loading (sample #40G876); (b) high mag-

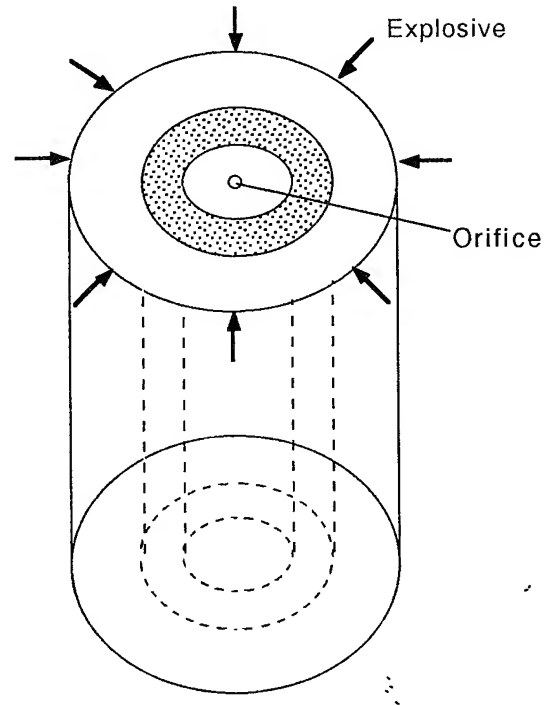


-  - Powder material
-  - Compacted material

Thick-Walled Cylinder Method

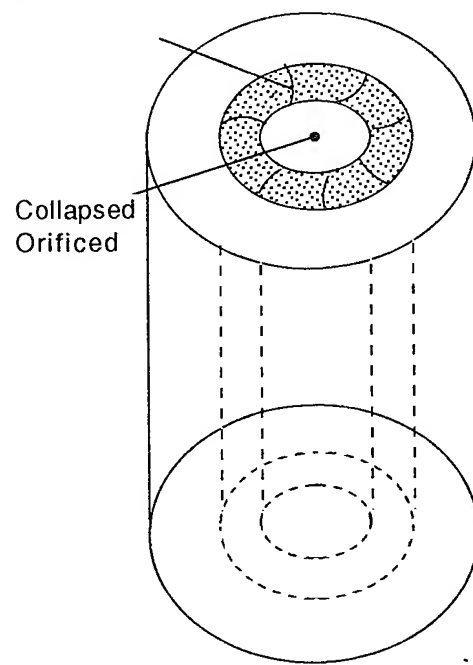


(a)

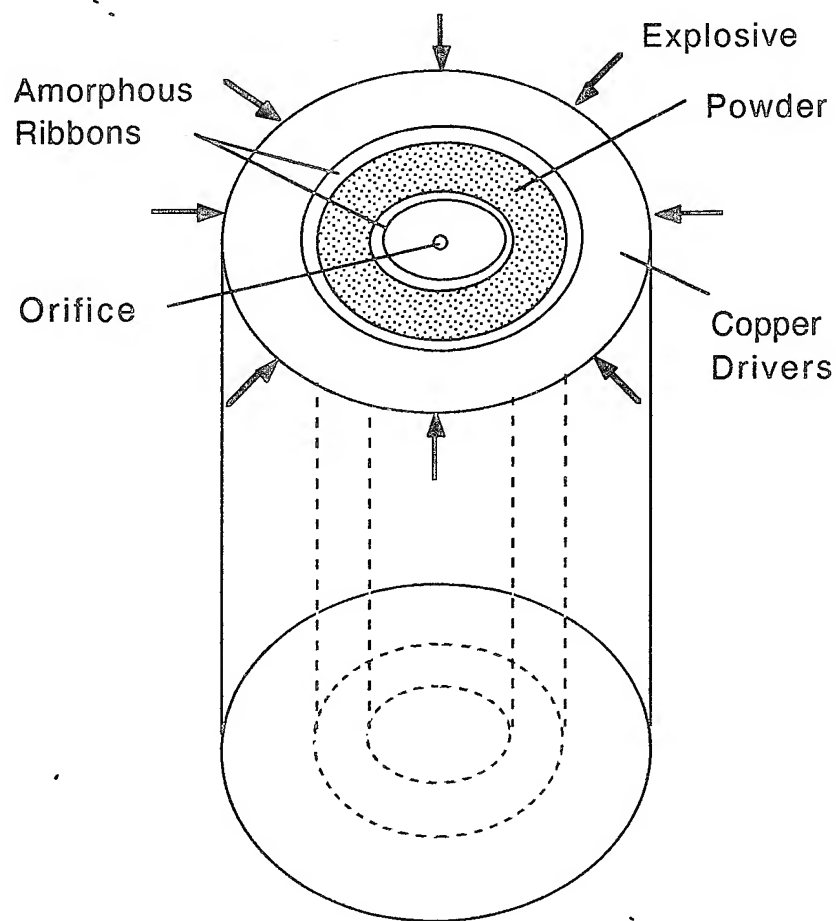


(b)

Shear Bands



(c)



CONCLUSIONS - GENERAL

- 1) Shock synthesis is an extremely complex physico-chemical process.
- 2) Both solid state and liquid-solid reactions seem to occur.
- 3) Initiation of reaction under shock compression. These seem to be different cases: (a) continuation and termination after shock pulse passage; (b) completion during shock-wave passage; (c) interruption of reaction after shock pulse passage.
- 4) For silicide systems, there seems to be a threshold energy level for shock synthesis, in accordance with Kruegar and Vreeland's proposal.
- 5) There are strong indications from literature that shear stresses/strains can have a significant effect on reactions.

- 7) Controlled experiments with a high shear strain concentration indicate that the reaction can be influenced by localization of plastic deformation.
- 8) Post-shock thermal effects are important.

CONCLUSIONS - OUR RESEARCH

- 1) Different experimental configurations are needed to fully understand the shock chemistry.

Sawaoka - wide range of shock energy conditions in each capsule - high pressures.

Graham-Bear - wide range of shock energy conditions in each capsule - low pressures.

Nellis-LLNL - rapid cooling after shock-wave passage.

Cal Tech - recovery of intact specimens and post-shock thermal effects.

TNL - effect of plastic deformation/shear localization.

- 2) In Nb-Si system, reaction occurs by the melting of silicon, formation of a NbSi₂ layer (liquid) on the Nb particles (solid), their separation from the interface by the formation of spherules, and the confirmation of reaction.
- 3) Consistently with energy threshold model, the reaction is initiated for a fraction of molten silicon of approximately 30pct.
- 4) The thermal energy can be added to the shock energy, as shown by experiments on pre-heated powders.
- 5) A kinetic mechanism was proposed for the reaction and is combined with thermodynamic considerations to explain the extraordinarily high reaction rate obtained.
- 6) The kinetics of the Nb-Si reaction is accelerated by the reduction in powder size.



SHOCK SYNTHESIS OF SILICIDES—II. THERMODYNAMICS AND KINETICS

M. A. MEYERS, LI-HSING YU and K. S. VECCHIO

Department of Applied Mechanics and Engineering Sciences, University of California, San Diego, La Jolla, CA 92093-0411, U.S.A.

(Received 16 September 1992; in revised form 23 July 1993)

Abstract—A thermodynamic and kinetic analysis of shock-induced reactions in the (Nb or Mo)–Si systems provides a framework for the extraordinarily high reaction rates and a quantitative interpretation of the experimental results obtained in Part I. The thermodynamic analysis is conducted by adding the heat of reaction to the shock energy; increases in shock pressure, temperature, and velocity are predicted. At the particle level, melting at the silicon–metal interface is found to be a necessary condition for the initiation of reaction; heat conduction calculations enable the prediction of a critical molten (Si) region size for which the heat generated through the reaction exceeds the heat lost to the unreacted regions. The calculation of melt fraction (of Si) as a function of shock energy coupled with critical melt pool sizes enables the determination of a minimum shock energy for the initiation of shock-induced reaction. At the local level, the reaction kinetics can be rationalized through the production of a liquid-phase reaction product (NbSi_2), the formation of spherical nodules ($\sim 2 \mu\text{m}$ diameter) of this product through interfacial tension and their subsequent solidification (in times of 1–5 ns). The heat generated by the reaction is sufficient to melt niobium along the interface which facilitates both the expulsion of the NbSi_2 nodules into the liquid Si, and the generation of fresh Nb interface for further reaction. In addition, the dissolved Nb enriches the surrounding Si liquid, promoting more NbSi_2 reaction and formation.

1. INTRODUCTION

Shock-wave propagation through materials generates significant structural changes; these effects have been the object of extensive studies, that were initiated with the Manhattan project in the early 1940's and continue to this day. Analytical investigations coupled with experimental studies have yielded mechanisms rationalizing the production of dislocations and point defects due to shock-wave passage through solid materials. The first mechanism was proposed by Smith [1], followed by Hornbogen [2] and later modified by Meyers [3] and Weertman [4]. This work is reviewed by Mogilevski [5], who also applied molecular dynamics to explain the generation of defects at the shock front [6]. Weak shock-wave effects have been modeled by Weertman and Follansbee [7, 8]. The effects of shock-wave passage through porous (powder) materials are considerably more complex, because intense and non-uniform plastic deformation is coupled with the shock-wave effects. Thus, the particle interiors experience primarily the effects of shock waves, while the surfaces undergo intense plastic deformation which can result in melting. This localized melting leads to the bonding of the powder, and this gave rise to the research field of shock-wave compaction. A theoretical framework predicting a minimum shock energy and shock pulse duration to create and solidify an interparticle melting layer has been developed by Gourdin [9] and Schwarz *et al.* [10]. This framework has recently been

extended by Potter and Ahrens [11] to ultrahard materials incorporating material strength effects through a Carroll–Holt model. When potentially reactive powder mixtures are used, the shock pulse may trigger these reactions and synthesize new materials. The energy of reaction has to be incorporated into the computations, and efforts by Horie and Kipp [12], Boslough [13], and Yu and Meyers [14] are noteworthy. Recently, Krueger *et al.* [15] and Krueger and Vreeland [16] proposed models that address, in a predictive manner, shock-induced reactions, with the postulation of a threshold energy (provided by the shock wave) for the initiation of reaction.

In this paper, a rational and quantitative analysis is provided for the results reported by Vecchio *et al.* [17], consistent with the threshold energy concept proposed by Krueger and Vreeland [16].

The introduction of exothermic reactions in concurrence with the physical processes under shock compression of porous materials requires special analyses, at the following levels:

- (i) continuum—thermodynamic;
- (ii) local—particle level;
- (iii) local—sub-particle (interface) level.

It will be shown that the extraordinarily high reaction rates encountered under shock conditions can be rationalized and quantified. The experimentally obtained regions where shock-induced reactions

occur are compared with computational predictions in Section 2. An analytical framework that enables a mechanistic understanding of shock synthesis of silicides will be developed in Section 3–5. Through this framework it will be possible to develop quantitative expressions that predict the major effects of shock synthesis.

2. COMPUTED SHOCK PRESSURES AND ENERGIES

In order to rationalize the experimental results of the companion paper (Part I) [17], computed predictions of shock pressures and energies within the capsules are important. The contours of partially and fully reacted regions of Fig. 2 of Part I [17] can be correlated to the pressure and energy levels experienced by the powders within the capsules. A strictly one-dimensional strain computation using the equation of state for the Nb–Si mixture developed according to the method described in Section 2 is shown in Fig. 1. These plots were obtained in a simple hydrodynamic code MYIDL, developed by Yoshida [18]. The first pressure pulse, which carries

most of the energy and travels through the porous powder, compacting it, has pressures of ~ 7 and 15 GPa, for the 1.2 and 1.9 km/s impact velocities (these are the impact velocities used in [17]). A second, higher amplitude pulse is initiated at the back surface of the capsule (~ 15 and 30 GPa, respectively) and travels through the compacted material. The tri-dimensional effects introduced by the finite lateral dimensions of the capsule are very significant and produce large deviations of pressure and temperature from the values of Fig. 1. The pressure and energy contours predicted using an advanced, two-dimensional CSQ code by Norwood and Graham [19] are shown in Fig. 2. These simulations were conducted using rutile at $\sim 60\%$ theoretical density as a model material. The pressure levels are at a time of $1.95 \mu\text{s}$ after the shock wave enters the capsule, and the energy levels are at a time of $5 \mu\text{s}$ after the shock wave enters the capsule. A spike is seen at the center, along the axis of the disk. This central pressure/energy spike is due to the convergence of the shock from the sides (the shock wave travels faster in the capsule than in the powder, creating a “pincer” action). The energy was obtained from Norwood and Graham’s [19] bulk temperature contours by proper

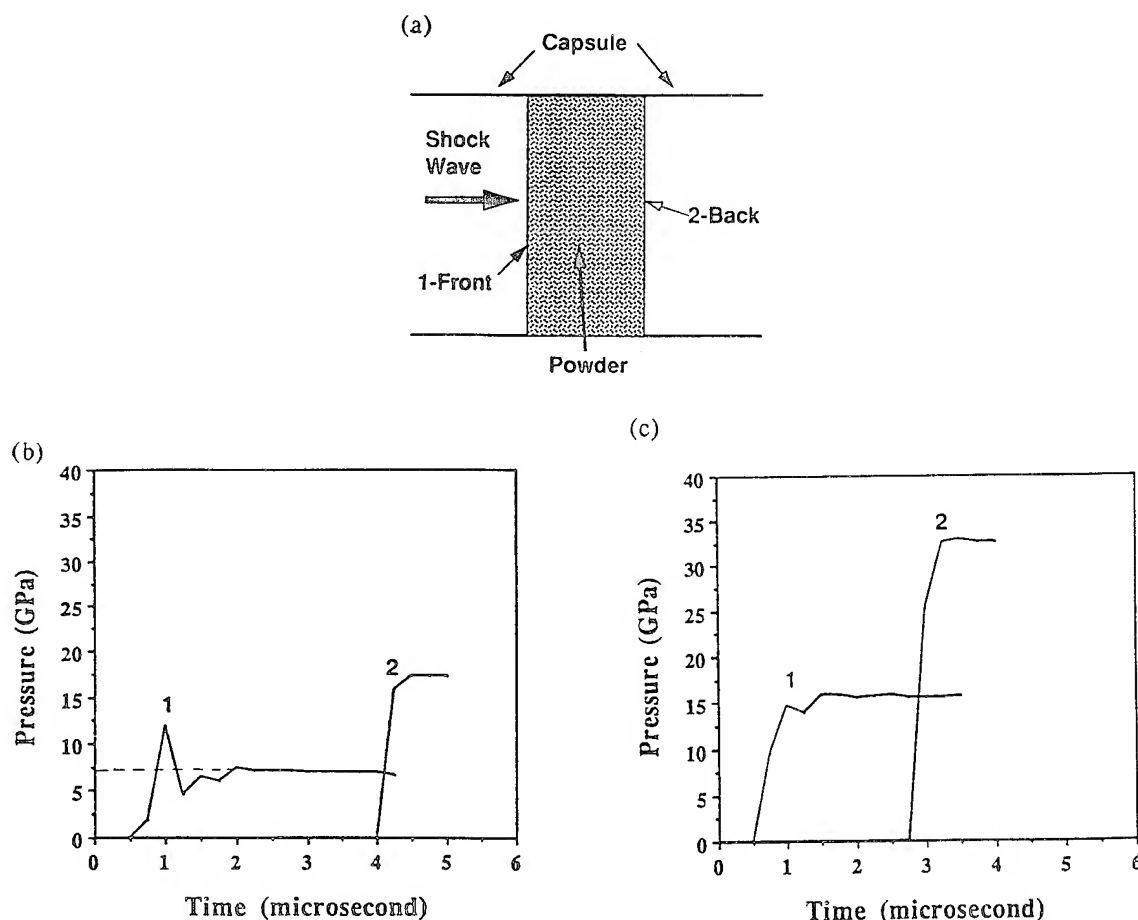


Fig. 1. One dimensional computed pressure as a function of time at front (1) and rear (2) surfaces of the shock capsule; pressure at the front represents amplitude of the first wave, whereas pressure at the back represents amplitude of the reflected pulse (a) computational configuration, (b) profiles for 1.2 km/s impact, and (c) profiles for 1.9 km/s impact.

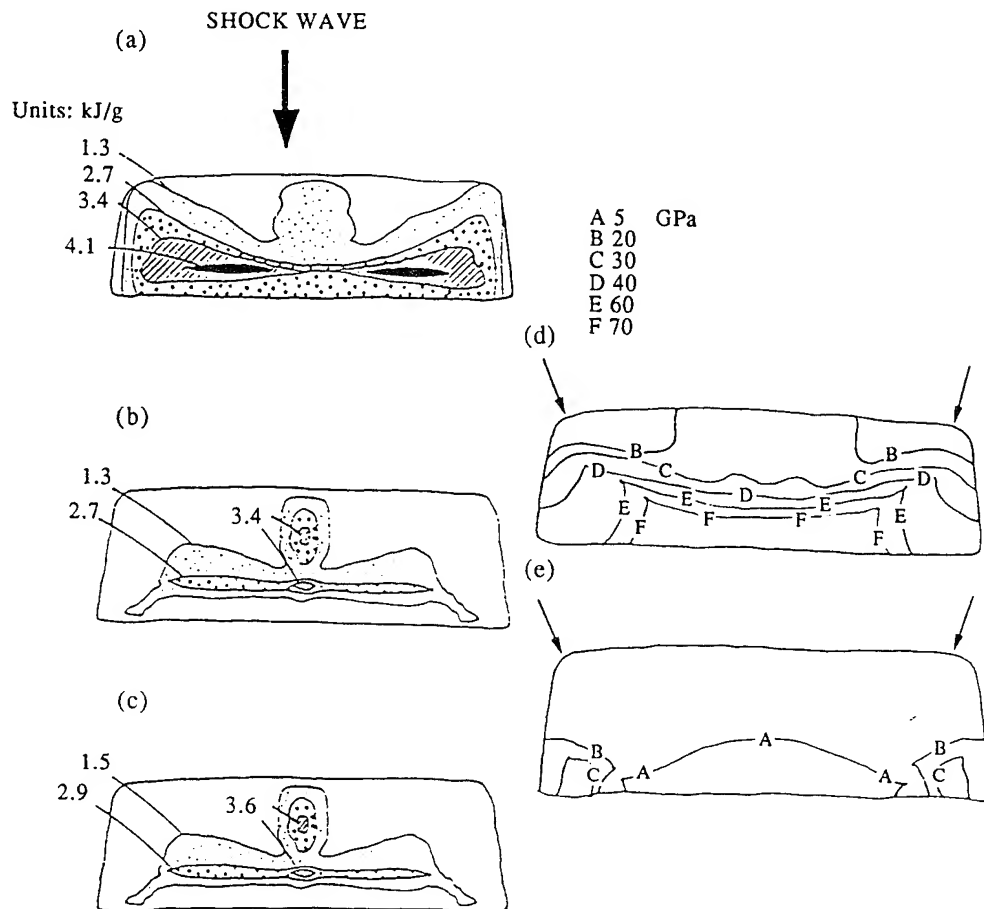


Fig. 2. The summaries of energy contours at a time of $5 \mu\text{s}$ after shock wave enters capsule for impact velocities: (a) 1.9 km/s at room temperature, (b) 1.3 km/s at room temperature, (c) 1.3 km/s at 500°C , and pressure contours at a time of $1.95 \mu\text{s}$ after shock wave enters capsule for impact velocities of (d) 1.9 km/s, and (e) 1.3 km/s.

conversion, using a heat capacity that is the mass average

$$E = \int_{T_0}^T C_v dT. \quad (2)$$

For the 500°C experiment, the thermal energy of the specimen prior to shocking was added to the shock energy: $E_{\text{th}} = C_v \Delta T = 220 \text{ J/g}$. Throughout this paper we will use C_p and C_v interchangeably since the volume changes are not appreciable. Thus, the values of the energies are increased by this amount on the curves for the 500°C experiment; this is a relatively minor change in the level. Figure 2 shows that the top of the capsule undergoes pressures of ~ 7 and 15 GPa , for the 1.3 and 1.9 km/s impact velocities, respectively. This is consistent with the one-dimensional computations. However, the pressure and energy levels at other regions are considerably higher, due to the three-dimensional effects. Although a quantitative assessment is not possible, the following observations can be made:

- (a) The partially and fully reacted regions follow more closely the energy contours than the pressure contours. The pressure, at

times earlier than shown in Fig. 2(d,e) reaches very high values at the upper edges of the capsule (marked by arrows), where no reaction was seen to occur. The fully-reacted region is concentrated on the bottom/central portions of the capsule, corresponding to the maximum energies.

- (b) By comparing Fig. 3 of Part I [17] with Fig. 2, it can be seen that a threshold energy of $600\text{--}800 \text{ J/g}$ is necessary to initiate the reaction for the room temperature experiments in the Nb-Si system. For the 500°C experiment, this energy seems to be somewhat lower. This threshold energy concept was proposed by Krueger *et al.* [15, 16].

A possible complicating factor not considered in the above comparison between observed and computed reaction profiles is the possibility that reactions can continue after the passage of the shock pulse. The reaction, initiated during the passage of the shock pulse, can continue to completion. This complicates the interpretation of recovery specimens, and has not been addressed quantitatively in the present or past studies.

3. THERMODYNAMICS OF SHOCK SYNTHESIS OF SILICIDES

In this section, it will be seen how the threshold energy can be correlated to the state of the sample. The thermodynamics of shock-wave passage through porous materials has traditionally been treated by using the Mie-Grüneisen equation of state (EOS) for a constant volume [20, 21]. Krueger *et al.* [15] developed a theory for the propagation of shock waves through powder mixtures. The treatment used here will be the simple Mie-Grüneisen approach, since accuracy in the equation of state is not essential to the development. The "Mixture" program developed by Yoshida [22] was used in the computation of the equation of state; it is based on the simple mixing of the constituents in the isothermal compression curve, as proposed by McQueen and Marsh [21].

First, the equations of state for the porous Nb-Si and Mo-Si powder mixtures will be calculated under shock compression, assuming that they are inert (no reaction). Secondly, the reaction energy will be added to them. Thirdly, the melting of the components as a function of shock energy will be established.

3.1. Equation of state for porous mixtures

Two components, A and B (Nb and Si or Mo and Si) are considered, and the mass fractions are m_A and m_B . The specific volume, V , internal energy, E , and heat capacity, C_v , of the mixture is taken as

$$\begin{aligned} V &= m_A V_A + m_B V_B \\ E &= m_A E_A + m_B E_B \\ C_v &= m_A C_{vA} + m_B C_{vB}. \end{aligned} \quad (3)$$

Similarly, the Mie-Grüneisen parameter (at ambient pressure), γ_0 , of the mixture is obtained from the mass average

$$\frac{\gamma_0}{V_0} = m_A \frac{\gamma_{A0}}{V_{A0}} + m_B \frac{\gamma_{B0}}{V_{B0}}. \quad (4)$$

The procedure followed in the calculation is to obtain the isothermal compression curve for the mixture from the isothermal compression curves for the components. From the isothermal states (E_T, P_T, V_T) one obtains the Hugoniot states (E_H, P_H, V_H) for the mixture by applying the Mie-Grüneisen equation, which relates one state to the other state by the equation

$$E_H - E_T = \frac{\gamma}{V_{H,T}} (P_H - P_T). \quad (5)$$

The conversion from the reference state (isothermal) to the shock state (Hugoniot) is made at a constant volume ($V_H = V_T$), in the Mie-Grüneisen treatment. The shock temperature can be obtained from the reference temperature by

$$E_H - E_T = \int_{T_{298}}^{T_H} C_v dT. \quad (6)$$

The internal energy is defined as (from the conservation of energy equation)

$$E_H - E_0 = \frac{1}{2}(P + P_0)(V_0 - V). \quad (7)$$

For the porous material the initial specific volume of the solid material is simply replaced by the specific volume of the porous material, V_{00} ($P_0 \sim 0$)

$$E_P - E_{00} = \frac{1}{2}P(V_{00} - V_H). \quad (8)$$

If the porous mixture reacts during the passage of the shock wave, the internal energy equation can be expressed simply as

$$E_{HR} - E_{00} = \frac{1}{2}P(V_{00} - V_{HR}) + mE_R. \quad (9)$$

m is the mass fraction reacted, and E_R the energy of reaction; this approach was introduced by Boslough [13] and Yu and Meyers [14].

These calculations were conducted for the Nb-Si and Mo-Si powder mixtures, at an initial porosity of 40% ($V_{00} = 1.4V_0$), which corresponds to the initial packing of the powders; the results are shown in Fig. 3. If the reaction takes place at the shock front one expects an increase in pressure and shock velocity; these have been predicted by Boslough [13] and Yu and Meyers [14]. The threshold energy for reaction, assumed to be ~ 700 J/g for Nb-Si and Mo-Si

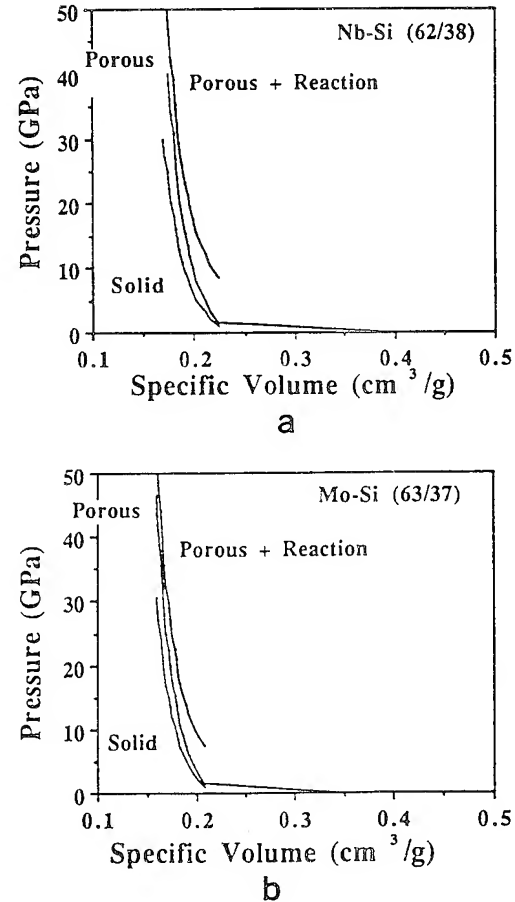


Fig. 3. Equation of state for powder mixtures at 60% of the theoretical density and for mixtures after reaction; (a) Nb-Si; (b) Mo-Si.

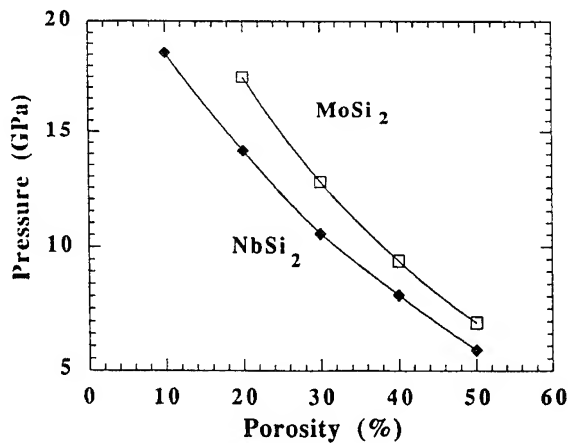


Fig. 4. Predicted (one-dimensional) pressure required to initiate reaction in Nb-Si and Mo-Si systems, as a function of initial porosity.

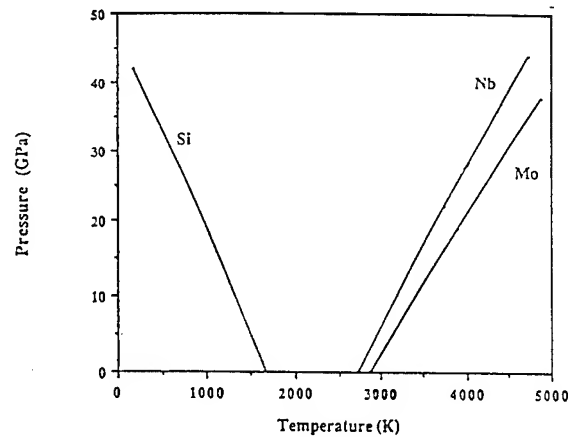


Fig. 5. The effect of shock pressure on the melting points of Nb, Mo and Si.

will be used to calculate a threshold pressure as a function of porosity. This is simply done by solving simultaneously equations (5) and (8). Figure 4 shows the predicted threshold pressures. Higher pressures are required as the porosity of the powder mixture is decreased. This analysis is in agreement with experimental results by Song [23].

3.2. Melting as a function of shock energy

The melting of the components is not considered in the EOS graphically expressed in Fig. 3. It is important to determine what the threshold energies correspond to, in physical terms. The shock energy is deposited in the two components. The melting points of the components are determined, as a function of pressure, by the Clapeyron equation

$$\frac{dP}{dT} = \frac{\Delta H}{T_m \Delta V} \quad (10)$$

where T_m is the melting point, ΔV is the volume change in melting, and ΔH is the enthalpy of fusion. The effect of pressure is expressed as

$$\begin{aligned} \text{Si: } T &= 1685 + \Delta P \left(-35.7 \frac{\text{K}}{\text{GPa}} \right) \\ \text{Nb: } T &= 2740 + \Delta P \left(45.7 \frac{\text{K}}{\text{GPa}} \right) \\ \text{Mo: } T &= 2890 + \Delta P \left(52.93 \frac{\text{K}}{\text{GPa}} \right). \end{aligned} \quad (11)$$

The melting points of the elemental constituents as a function of pressure are plotted in Fig. 5. Silicon has the lowest melting point; additionally, its melting point decreases with pressure because there is a volume decrease associated with its melting. At the one-dimensional pressures of 7 and 15 GPa (Fig. 1), the melting points for silicon are

$$MP_{\text{Si}}^{7 \text{ GPa}} = 1460 \text{ K}$$

$$MP_{\text{Si}}^{15 \text{ GPa}} = 1100 \text{ K}.$$

The distribution of the energy deposition between Si and (Mo or Nb) components will establish the energy level at which melting is initiated

$$E = x \left(\int_T^{T_{m1}} C_p dT + \lambda L_f \right)_{\text{Si}} + (1-x) \left(\int_T^{T_{m2}} C_p dT \right)_{\text{Nb}} \quad (12)$$

T_{m1} is the melting point of Si at the energy level E . L_f is the enthalpy of fusion, λ is the fraction of silicon that is molten, x is the fraction of energy deposited in Si, and $(1-x)$ is the fraction of energy deposited in the (Nb, Mo) powder. It is assumed, to a first approximation, that the temperatures in the two components are the same (after Krueger *et al.* [15]). By using the quadratic expressions for the heat

Table 1. Physical and thermodynamic data of Nb-Si, Mo-Si systems

Property	Niobium	Materials Molybdenum	Silicon
Melting temperature (K)	2740	2890	1685
Latent heat of fusion (kJ/mol)	26.79	27.47	39.62
Thermal conductivity (W/cm-K)	0.54	1.38	1.49
Heat capacity (C_p)	$a = 24.63$	$a = 24.18$	$a = 23.94$
$a + b \times 10^{-3} T + c \times 10^5 T^{-2}$	$b = 3.39$	$b = 1.17$	$b = 2.47$
(J/°C-mol)	$c = 9.21$	$c = 0$	$c = 4.14$
Compressive strength (MPa)	200-400	300	90
Main reaction product with Si	NbSi ₂	MoSi ₂	—
Melting temperature of product (K)	2420	2300	—
Heat of reaction to form product (kJ/mol)	138	129.6	—

capacity from Table 1. and equations (11) and (12), one arrives at, for the Nb-Si system

$$\begin{aligned} \frac{1}{2}P(V_{00} - V) = & x[0.295 \times 10^{-3}(1685 - 35.7P)^2 \\ & + 5.72(1685 - 35.7P) + 0.99 \\ & \times 10^5(1685 - 35.7P)^{-1} - 2.06 \times 10^3 \\ & + \lambda 430] + (1-x)[0.405 \\ & \times 10^{-3}(1685 - 35.7P)^2 \\ & + 5.885(1685 - 35.7P) + 2.2 \\ & \times 10^5(1685 - 35.7P)^{-1} - 2.53 \times 10^3]. \end{aligned} \quad (13)$$

The equation of state from Fig. 4(a) can be expressed as

$$V_{(s)} - V = -\frac{1}{46.04} \ln\left(\frac{P + 0.0029}{0.0029}\right) \quad (\text{in GPa}). \quad (14)$$

By substituting equation (14) into equation (13), one obtains the melting fraction, λ , as a function of shock pressure, P , or shock energy, E . The results are plotted in Fig. 6(a) for two values of x : 1 and 0.38. When $x = 1$, the energy is entirely absorbed by Si. For $x = 0.38$, it is uniformly distributed among the two phases in proportion to their mass ratios. Melting of Si starts at an energy of ~ 400 J/g for $x = 1$ and ~ 600 J/g for $x = 0.38$. Melting of Si is complete ($\lambda = 1$) for

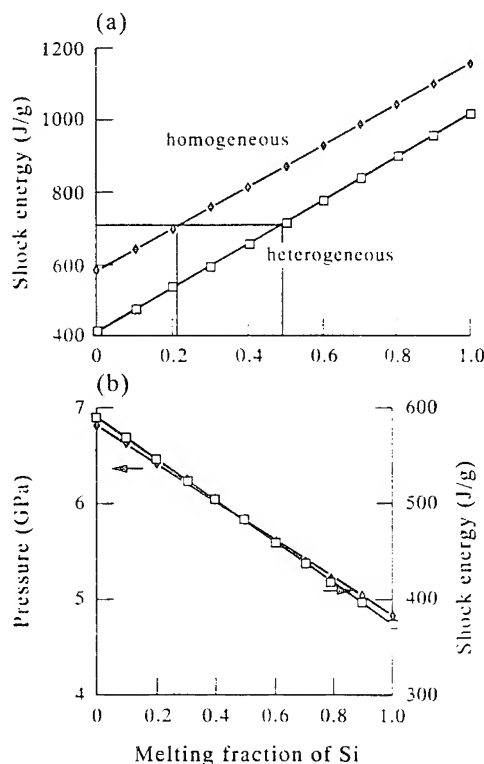


Fig. 6. (a) Melting fraction of Si as a function of shock energy for homogeneous (equally, in Nb and Si) and heterogeneous energy distribution (completely into Si), and (b) melting fraction when energy of reaction is added to shock energy.

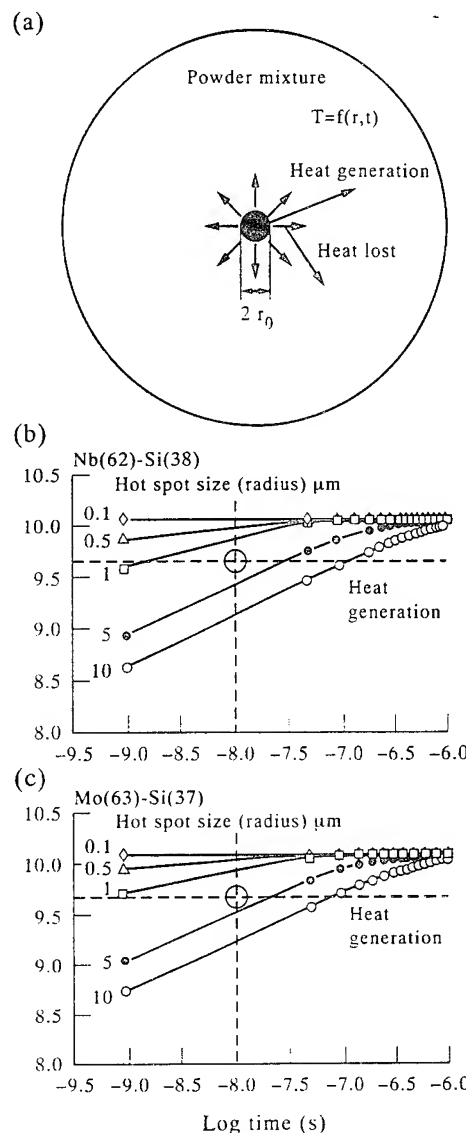


Fig. 7. (a) Molten region with radius r_0 at t_0 ; heat is conducted to the environment, in which the temperature is function of position and time. Calculated heat losses from "hot spots" for different hot spot radii r_0 (0.1, 0.5, 1, 5 and 10 μm) and heat generation (instantaneous) from shock synthesis of (b) Nb-Si and (c) Mo-Si powder mixtures; heat generation time is 10^{-8} s.

~ 1000 J/g ($x = 1$) and ~ 1150 J/g ($x = 0.38$). The threshold energy level of 700 J/g corresponds to a melting fraction, of Si, λ , between 0.2 and 0.5. This analysis is in accord with the experimental results of Section 2, which indicate that melting of Si is a precondition for reaction. By considering that the molten silicon reacts integrally, and by computing the energy of reaction, the plot of Fig. 6(b) is obtained (for $x = 0.38$). It shows the energy required to propagate the reaction is lower than the energy required to initiate it, and therefore the reaction tends to be self-sustaining.

There is, however, a remaining question: Why is a minimum fraction of molten silicon necessary to initiate the reaction? In order to address this question, a model is proposed below that is based on

the following assumptions. (consistent with the observations of Part I [17]):

- (a) melting of silicon is required for the initiation of reaction; and
- (b) a minimum size of reacted materials is required for the propagation of reaction.

Consider an idealized molten pool [Fig. 7(a)] of radius $2r_0$, at T_{ml} and surrounded by material at a temperature T_0 . The reaction of this molten Si with the surrounding solid (Nb or Mo) will generate heat, that is transferred to the surrounding. A general equation that addresses both the heat generation (along the solid-liquid interface, with a surface equal to $4\pi r_0^2$) and heat extraction from this central core, in spherical coordinates, is

$$4\pi r_0^2 \dot{Q} + \rho C_p \frac{\partial T}{\partial t} = k \left(\frac{\partial^2 T}{\partial r^2} + \frac{2}{r} \frac{\partial T}{\partial r} \right) \quad (15)$$

$$\dot{Q} = H_f e^{-\Delta H/RT} H(T - T_{ml}) \quad (16)$$

where ρ is the density, k is the thermal conductivity, \dot{Q} is the heat generation rate, H_f is the enthalpy of reaction, ΔH the activation energy for reaction, $H(T - T_{ml})$ is a Heaviside function (reaction rate = 0 at $T < T_{ml}$, where T_{ml} is the melting point at the shock pressure). Equation (16) has an implicit assumption: that the reaction stops when the temperature is below the melting point of silicon.

Rideal and Robertson [24] proposed a simpler formalism for the detonation of explosives. They assumed that the heat was instantaneously generated at a hot spot. They calculated the heat extracted from the reacted region as a function of time by using equation (17) (this is the Fourier equation in spherical coordinates)

$$\frac{\rho C_p \partial T}{k \partial t} = \frac{\partial^2 T}{\partial r^2} + \frac{2}{r} \frac{\partial T}{\partial r} \quad (17)$$

The heat gained by the environment is equal to the heat lost by the hot spot. At a time t , the heat gained by a spherical shell of radius r ($r > r_0$) and thickness dr is

$$dQ = (4\pi r^2 dr) \rho C_p T. \quad (18)$$

By integrating from r_0 to infinity, one obtains the total heat gained by the surrounding (or lost by the hot spot)

$$Q = \int_{r_0}^{\infty} 4\pi r^2 \rho C_p T dr. \quad (19)$$

Figure 7 shows the heat generated and heat lost to environment as a function of time for different "hot spots" sizes; calculations were made for the Nb-Si [Fig. 7(b)] and Mo-Si [Fig. 7(c)] systems. The curves for different hot spot sizes converge to the total value of the heat contained in the hot spot for times on the order 1 ms. Hot spot radii of 0.1, 0.5, 1, 5 and 10 μm

were considered. As the hot spot size increases, the time required for the heat to be extracted increases. The heat generated is plotted as a horizontal (dashed) line for the three cases. The heat is actually not instantaneously generated, but over a period that can be approximated as the transit time of the shock wave over a particle. An approximate shock-wave velocity can be obtained from Fig. 1; the capsule thickness is 10 mm, yielding a shock velocity of $\sim 3 \text{ mm}/\mu\text{s}$. For a particle diameter of 40 μm , a shock transit time of $\sim 10^{-8} \text{ s}$ is obtained. The circles on Fig. 7(b,c) correspond to the critical "hot spot" radii for the two materials. These critical "hot spot" sizes for reaction to be initiated are equal to 3 and 4 μm for Nb-Si and Mo-Si systems, respectively. These predictions are in agreement with our experimental results. The critical sizes of these "hot spots" are consistent with the thermodynamic predictions.

4. MODELING SHOCK-INDUCED REACTIONS AT THE PARTICLE LEVEL

An attempt to rationalize the acceleration of reaction kinetics observed in shock compression can be made by analyzing the various terms of an Arrhenius equation, in which both forward and reverse reaction terms are considered. Figure 8 shows the activation barrier necessary to be overcome to react A and B to produce A_xB_y . ΔG is the difference in free energy between products and reactants, while ΔQ is the activation energy (enthalpy) for the reaction. Under shock compression, the equation that expresses the rate of reaction has to be modified to incorporate various effects. Figure 8(a) shows three principal effects:

(a) The reactants are in a highly excited state due to the shock passage. High defect densities characterize this state. Panin *et al.* [25] have proposed that under these conditions the material is in a more energetic state.

(b) The activation energy for reaction is decreased because of a "reaction strain" term. If the product (e.g. NbSi_2) has a lower specific volume than the reactants (Nb and Si), there is an energetic gain with the process, due to local reduction in strain energy. Figure 8(b) shows this effect schematically. Product A_xB_y occupies a smaller volume than reactants A and B. By a hypothetical procedure devised by Eshelby [26], it is possible to estimate this energy. For purely dilatational strains, Eshelby's equation simplifies itself to

$$E = \frac{1}{2} P \epsilon_v V \quad (20)$$

where V is the volume transformed, ϵ_v the volumetric strain associated with the reaction, and P is the applied pressure.

(c) The effect of pressure on the thermodynamic equilibrium of the phases. The free energy difference

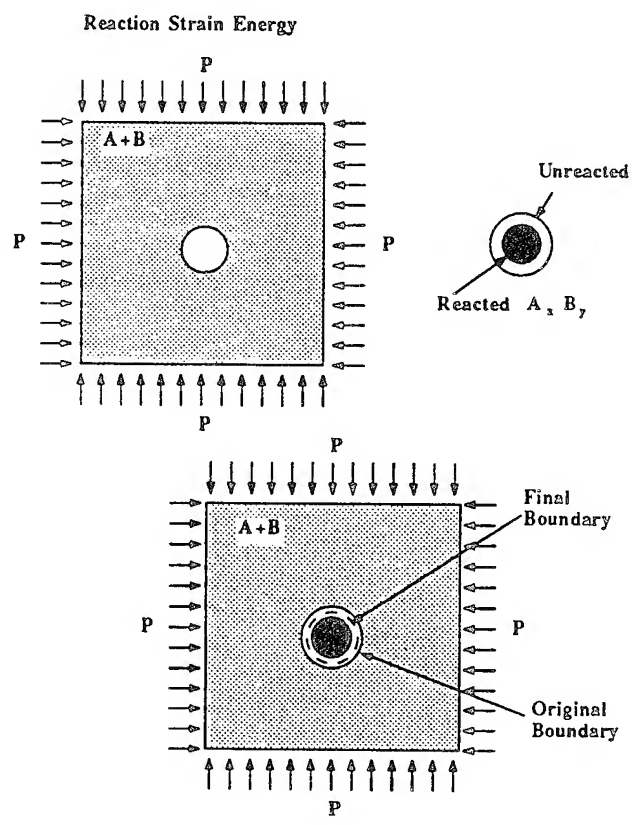
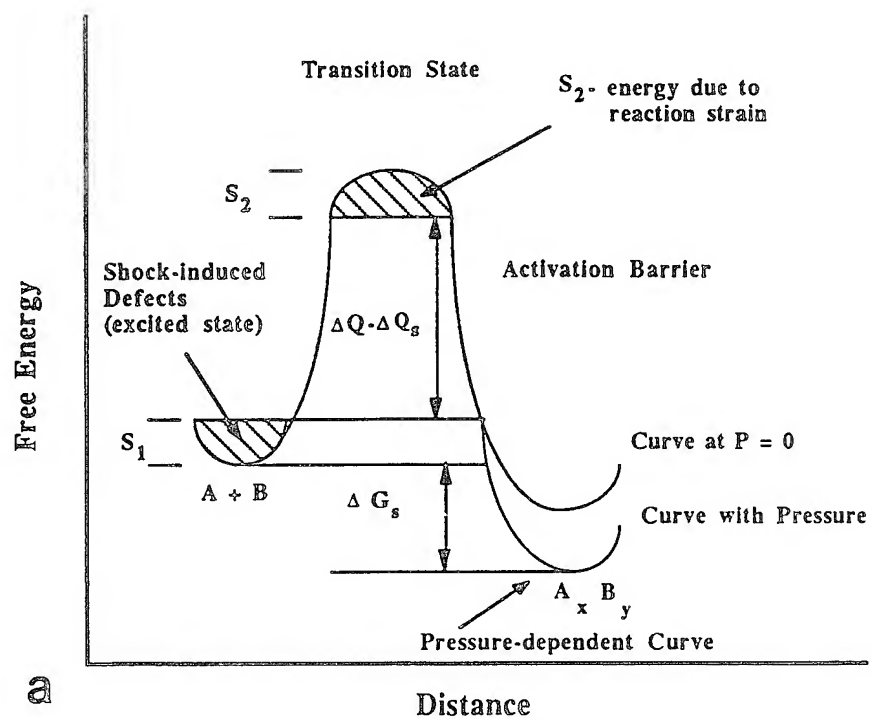


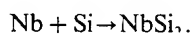
Fig. 8. (a) Activation energy curve for reaction $xA + yB \rightarrow A_x B_y$ and effect of shock wave on parameters. (b) Reaction strain as schematically illustrated by Eshelby's "cut and paste" method [26].

between products and compounds, ΔG , is dependent on the superimposed pressure.

Thus, the Arrhenius rate equation, under shock compression processing (that incorporates both forward and reverse reactions) can be expressed as

$$r = A \exp \frac{-(\Delta Q - \Delta Q_s)}{RT} \left[1 - \exp \frac{-(\Delta G + \Delta G_s)}{RT} \right]. \quad (21)$$

The terms ΔQ and ΔG are the activation energy for the reaction and the free energy difference between reactants and products, respectively. The terms ΔQ_s and ΔG_s results from shock modification, as schematically indicated in Fig. 8(a). A is a pre-exponential factor related to the attempt frequency. Normalized reaction rates are calculated in the absence and presence of shock compression, for the reaction



The reaction strain (or volumetric contraction) accompanying the conversion of the Nb and Si to NbSi_2 is 0.29; this corresponds to a reaction strain of 0.11. Considering an applied stress of 14 GPa, one obtains an energy of 178 J/g. The defect energy can be estimated from a dislocation density generated by shock. Assuming a dislocation density of $5 \times 10^{10}/\text{cm}^2$ (typical of materials shocked to high pressures), one obtains an energy of 9 J/g. This yields: $\Delta Q_s = 187 \text{ J/g}$. The free energy of reaction can be taken as $\Delta G = 926 \text{ J/g}$. The change in free energy with pressure can be obtained directly from the Clapeyron equation [equation (10)]. It was found to be: $\Delta G_s = 2477 \text{ J/g}$.

The activation energy for the formation of MoSi_2 from elemental Mo and Si has been calculated by Kumar *et al.* [27] and found to be equal to 99.7 kJ/mol. Since the activation energy is not known exactly, a range of values from 100 to 400 kJ/mol was used in the calculations. The pre-exponential factor, A , is not known and only the ratios r/A were calculated. The results are shown in Fig. 9(a) for the forward reaction only, and Fig. 9(b) for both forward and reverse reactions. Although shock compression enhances the rate r/A , the changes are not dramatic. For the forward reaction only, the increase is $\sim 10\%$, while considering both forward and reverse rates, the increase is fourfold. These increases are much inferior to the ones observed between the rates of reaction in quasi-static and shock experiments; in the latter, these rates are compared in Section 3 of the companion paper [17]. The shock-induced reaction rate was found to be $\sim 10^8$ times higher than the solid state, diffusion governed rate. Thus, unless the pre-exponential factor A is radically different in the two processes, the Arrhenius rate equation shows that the acceleration of the reaction cannot be ascribed to the shock effects above, and has to be indicative

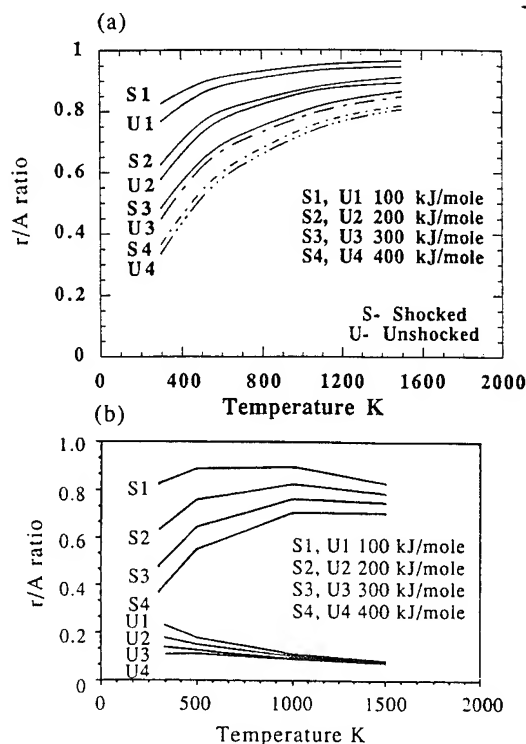


Fig. 9. Reaction rate/pre-exponential parameter ratio as a function of temperature under unshocked and shock conditions; (a) forward reaction only; (b) forward and reverse reactions.

of another mechanism operating. The specific aspects of this new mechanism will be described in Section 5.

It is possible to calculate the overall fraction reacted as a function of time for shock-induced reactions. These global reaction kinetics, as opposed to the local reaction kinetics discussed earlier, are determined by the density of initiation sites, and by the mass reacted per individual event as a function of time. A general formulation will be presented that captures the essential phenomena of the process.

It will be assumed that the initiation sites for reaction will be at particle-particle junctions. The justification for this is that molten pools are observed at particle triple points, in shock consolidation (planar sections). As the particles are accelerated against each other, the molten material is ejected and captured at these regions that are, in a tri-dimensional view, centers of tetrahedra. A tri-dimensional view of a tetrahedral arrangement of spheres is shown in Fig. 10(a). A small sphere in the center indicates the possible initiation site. The initiation sites are the regions where the greatest gaps exist, and where, as a consequence, shock energy is preferentially deposited. The initial density of powders for the silicides was 60% of the theoretical density (TD). This justifies the selection of an idealized body-centered cubic arrangement for the (spherical) particles, with a density of 68% TD. It is assumed that there are n tetrahedral sites per atom. The mean distance between these sites with respect to a b.c.c. cell, if

the sites are equidistant, is d . After the consolidation of the unit cell by the shock pressure, the cell size will be reduced from $2.3 S$ to $2 S$ (S is the particle radius). Thus

$$nd^3 = a^3 = 2^3 S^3. \quad (22)$$

There are 24 tetrahedral sites per unit cell, each being shared by two adjacent cells in a b.c.c. arrangement. Thus, one has six initiation sites per particle. For $n = 6$, the mean distance between initiation sites is $1.1 S$.

If all sites are simultaneously initiated at a time τ_0 (equal to an incubation time), the fraction transformed at a time τ can be estimated by separating the reaction into two stages [Fig. 10(b)]:

- (a) independent reaction events [$\tau_0 < t < \tau_1$; Fig. 10(b) (i, ii)];
- (b) interpenetrating reaction fronts [$t > \tau_1$; Fig. 10(b) (iii, iv)].

The fraction transformed, f , can be estimated as a function of reaction front advance, r . If n_1 is the number of initiation sites per unit volume, we have, for $r_0 < r < d/2$

$$df = n_1 dV = n_1 4\pi r^2 dr. \quad (23)$$

Equation (23) assumes that the reaction is occurring at the surface of a spherical reaction region. Integrating from r_0 to r_1 yields the fraction transformed as

$$f = \frac{4\pi n_1}{3} (r_1^3 - r_0^3). \quad (24)$$

For $r > d/2$ we have to subtract the overlap volumes of spherical segments V_0 shown in Fig. 10(b, iv). If each initiation site has n_2 nearest neighbors, we have (each overlap volume is shared between two reaction regions)

$$f = n_1 \left[\frac{4\pi}{3} (r_1^3 - r_0^3) - \frac{n_2}{2} V_0 \right]. \quad (25)$$

But the volume of two juxtaposed spherical caps is

$$V_0 = \frac{2\pi}{3} \left(r - \frac{d}{2} \right)^2 \left(2r + \frac{d}{2} \right). \quad (26)$$

Thus:

$$f = n_1 \left[\frac{4\pi}{3} (r_1^3 - r_0^3) - n_2 \frac{\pi}{3} \left(r - \frac{d}{2} \right)^2 \left(2r + \frac{d}{2} \right) \right]. \quad (27)$$

We can use a Heaviside function, $H(r - d/2)$, to generalize the above expression

$$f = \frac{4\pi n_1}{3} \left[(r_1^3 - r_0^3) - H\left(r - \frac{d}{2}\right) \frac{n_2}{12} \times \left(r - \frac{d}{2} \right)^2 \left(2r + \frac{d}{2} \right) \right]. \quad (28)$$

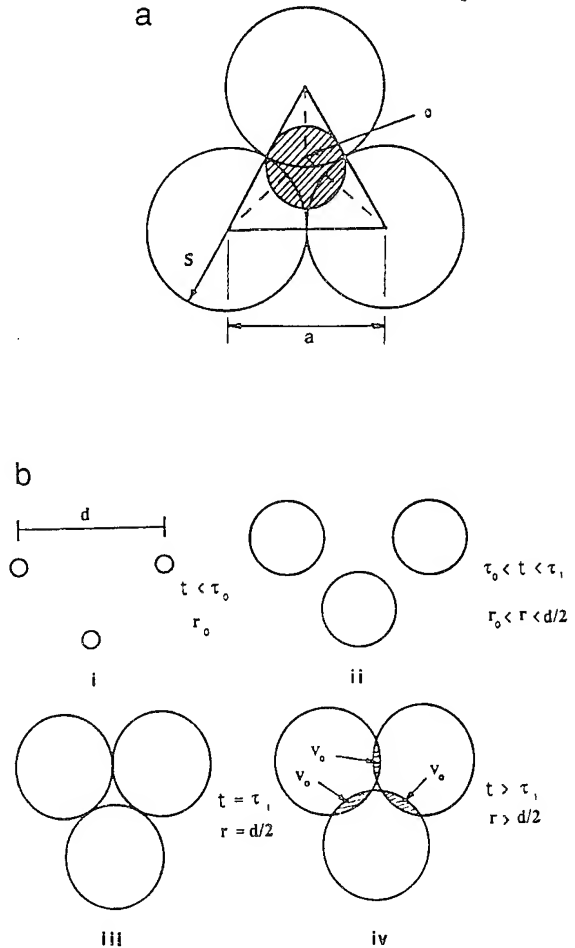


Fig. 10. (a) Tetrahedron formed by spherical particles and center 0. (b) Reacted regions as a function of time: (i) at initiation; (ii) and (iii) during propagation; (iv) during superposition/interaction stage.

The maximum value of r_1 can be estimated as the distance from the center to the vertices of a tetrahedron; or $0.61 d$.

The reaction rate, ξ , is defined as mass reacted per unit area of products/reactants interface. By assuming a constant reaction rate, ξ , we can obtain a fraction reacted vs time relationship

$$\xi = \frac{1}{A} \frac{dm}{dt} = \frac{1}{A} \rho \frac{dV}{dt} = \rho \frac{dr}{dt} \quad (29)$$

$$r - r_0 = \frac{\xi}{\rho} (t - \tau_0) \quad (30)$$

here again ρ is the density of the material. Substituting equation (30) into equation (27) (assuming, to a first approximation, $r_0 = \tau_0 = 0$) gives

$$f = \frac{4\pi}{3} n_1 \left(\frac{\xi}{\rho} \right)^3 \left[t^3 - \frac{n_2}{12} H(t - \tau_1) \times (t - \tau_1)^2 (2t + \tau_1) \right]. \quad (31)$$

The maximum value of t is

$$t_{\max} = \frac{\rho}{\zeta} r_{\max} = \frac{0.61\rho d}{\zeta}.$$

The number of initiation sites per unit volume, n_i , can be expressed as (six initiation sites per particle): $n_i = d^{-3} = (1.1S)^{-3}$. If one considers that each reaction region will overlap with six neighboring regions, then

$$f \cong 3.15 \left(\frac{\zeta}{S\rho} \right)^3 [t^3 - \frac{1}{2}H(t - \tau_1)(t - \tau_1)^2(2t + \tau_1)]. \quad (32)$$

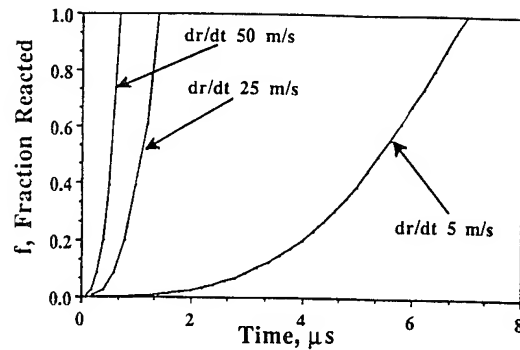
Figure 11 shows plots of the fraction synthesized, f , as a function of time for different reaction rates, ζ , and particle sizes, d . In Fig. 11(a) the reaction rates are varied for a constant particle size (50 μm), while in Fig. 11(b) the particle sizes are varied (10, 50, 500 μm) at a constant reaction rate. These plots are only illustrative since the reaction rates were varied arbitrarily. The reaction rates were assumed consistent with synthesis within the time frames of shock-wave passage. This corresponds dr/dt values of 5–50 m/s. The particle sizes were varied between 10 and 500 μm . The reaction rates, ζ , are obtained from

$$\zeta = \rho \frac{dr}{dt}. \quad (33)$$

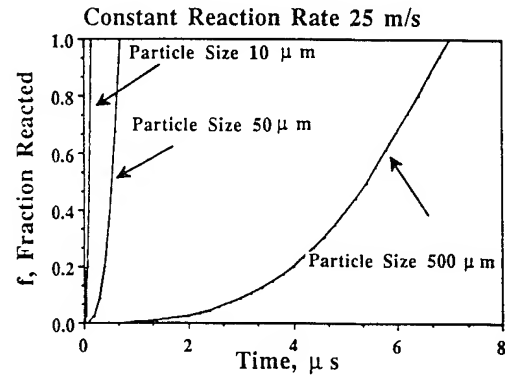
These results show conclusively that the kinetics of synthesis are highly dependent upon both of these parameters. The fraction transformed increases initially with t^3 , and for $t > \tau_1$, with $At^3 - B(t - \tau_1)^2(2t + \tau_1)$, reaching saturation at $f = 1$. Beyond τ_1 the reaction rate slows down sensibly; this is the sphere overlap region $0.5d < r < 0.61d$. Depending on the reaction rate and particle size, the reaction may or may not reach completion during the passage of the shock pulse. These results rationalize the results obtained in Part I [17] (partially and fully reacted regions).

5. REACTION MECHANISM

The analysis of the partially reacted regions in the Nb–Si shock experiments revealed the detailed nature of the reaction sequence and mechanisms. There are clear indications that a threshold energy level exists above which the reaction occurs. This is the confirmation of the Krueger–Vreeland [16] suggestion: for the Nb–Si and Mo–Si systems this threshold energy is the level that results in the melting of the pre-established fraction of silicon. The preponderance of small NbSi₂ particles surrounded by silicon, as well as the existence of NbSi₂ particles attached to the niobium particles (Figs 3 and 4 of Part I [17]) are evidence for a reaction mechanism in which the NbSi₂ particles are continuously being generated at the interface and



a



b

Fig. 11. Fraction reacted as a function of time for (a) different reaction rates (constant particle size of 50 μm) and (b) different particle sizes (constant interface advance rate of 25 m/s).

ejected into the (molten) silicon. Thus, a permanent diffusion barrier (i.e. an interphase layer) that would slow down the reaction process is not formed, and reaction can proceed at a constant rate until the entire niobium or silicon are consumed. The simple calculation below shows that the temperature rise due to the reaction leads to a temperature (locally) higher than the melting point of NbSi₂. Figure 12 shows the sequence of events envisaged to occur. NbSi₂ will form at a Si–Nb interface, where silicon is molten and niobium solid. Assuming an adiabatic reaction, the temperature is

$$T = T_{\text{MP}}^{\text{Si}} + \frac{\Delta H_r}{C_p}. \quad (34)$$

The enthalpy of reaction of NbSi₂ is (at $P = 0$) equal to 926 J/g. The heat capacity of NbSi₂ was estimated by interpolation between those of Nb and Si on a mass basis (m^{Si} and m^{Nb} are mass fractions of Si and Nb)

$$C_p = m^{\text{Si}}C_p^{\text{Si}} + m^{\text{Nb}}C_p^{\text{Nb}}. \quad (35)$$

This gives a value of 0.58 J/gK for NbSi₂. Thus, assuming that the pressure exerted by the shock wave

corresponds to the threshold energy, at 40% porosity, the melting point of silicon is 1400 K (see Figs 4 and 5). This leads to: $T \approx 3000$ K.

This temperature is considerably higher than the melting point of NbSi_2 (2420 K at $P = 0$): It is therefore likely that the sequence shown in Fig. 12 takes place. The suggestion was made by Glassman [28] that interfacial energy plays an important role in the kinetics of shock synthesis, which led to the development of the following mechanistic model.

Following Fig. 12, the reaction is initiated at (a), along the Nb–Si interface. After reaction has proceeded to a certain extent (c), surface (interfacial) forces become dominant, and the liquid reaction product agglomerates, forming a spherule (e). At this point, reaction kinetics are drastically decreased, because of the reduction of the Nb–Si interfacial area, and solidification of the sphere starts (e). As the sphere solidifies, new nuclei form along the Nb–Si interface (f). They grow, agglomerate into spheres when they reach a critical size, and form neighboring spheres (g). These neighboring regions are constrained and exert forces on the first sphere, expelling it (h) and thus exposing fresh surfaces. This reaction process can continue until the reactants are consumed. As such, no diffusion barrier is formed. The cooling rate of the NbSi_2 spherules can be calculated, and equation (36) shows the effect of time, t , and distance r , on temperature, T , for a spherical particle (spherical coordinates)

$$\frac{\partial T}{\partial t} = \frac{k}{\rho C_p} \left(\frac{\partial^2 T}{\partial r^2} + \frac{2}{r} \frac{\partial T}{\partial r} \right) \quad (36)$$

where k , ρ , and C are the thermal conductivity, density, and heat capacity, respectively. The initial conditions are

$$T = 3200 \text{ K at } t = 0 \text{ for } r < a, \text{ and}$$

$$T = 1600 \text{ K at } t = 0 \text{ for } r > a,$$

where a is the radius of the nodule, which can be obtained from measurements in Figs 4, 5, and 10 of part I [17]. An average value of $2.5 \mu\text{m}$ was taken in the calculations, and values for k , ρ , and C were averaged from Nb and Si for NbSi_2 . Figure 13 shows the results of the computations using equation (37). The solidification heat is not incorporated into the calculations. Nevertheless, it is clearly seen that solidification can be initiated 2–5 ns after the spherule is formed. Thus, the solidification time is a small fraction ($\sim 1/1000$) of the shock pulse duration time. It is therefore easy to see how successive generations of nodules can be formed, solidified, and ejected from the reaction interface.

The forces that can be exerted by the liquid NbSi_2 on the solid NbSi_2 spherule can be calculated in an approximate manner. These forces are due to the interfacial energy between liquid NbSi_2 and liquid Si as a result of the liquid NbSi_2 attempting to become spherical. A liquid sphere can be flattened into a prolate spheroid by a force F , as shown in Fig. 14(a). It is possible to calculate this force F , due exclusively to interfacial energy, γ_s

$$F = \frac{dE}{dy} = \gamma_s \frac{dS}{dy}. \quad (37)$$

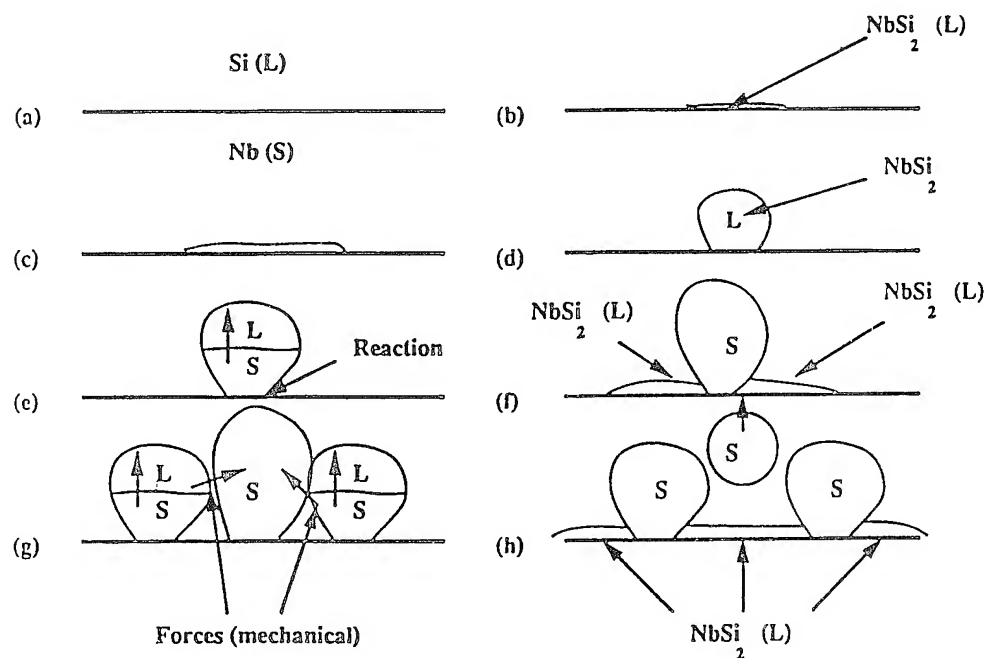


Fig. 12. Sequence of events in the synthesis of NbSi_2 spherules at Nb(solid)–Si(liquid) interface under shock loading; (a–c) nucleation and growth of thin layer; (d) interfacial energy produces spheroidization; (e) solidification and reduced reaction; (f) adjacent reaction regions form in newly exposed interface; (g) spheroidization and solidification of adjacent reaction region; (h) expulsion of spherule.

S is the surface area of the spheroid, equal to

$$S = 2\pi b^2 + \frac{2\pi ab}{\epsilon} \sin^{-1} \epsilon. \quad (38)$$

Here a and b are the major and minor axes of the spheroid and ϵ is the eccentricity, defined as

$$\epsilon = \left(1 - \frac{b^2}{a^2}\right)^{1/2} = \left(1 - \frac{y^2}{x^2}\right)^{1/2}. \quad (39)$$

The volume of the spheroid is constant and equal to $(4/3)\pi a^2 b$. By substituting equations (38) and (39) into (37) and eliminating the variable a , one arrives at

$$F = \gamma_s \left\{ 4\pi y - \frac{3\pi k}{(1 - k^{-2}y^3)^{1/2}y^{1.2}} + \left[\frac{\pi k y^{-1/2} + 2\pi k^{-1}y^{5/2}}{(1 - k^{-2}y^3)^{3/2}} \right] \sin^{-1}(1 - k^{-2}y^3)^{1/2} \right\} \quad (40)$$

where $k = r^{1/2}$ and r is the initial spherule radius.

The interfacial energy for the NbSi_2 is not known but the surface energy of liquid NbSi_2 can be estimated from the values of Nb and Si, by interpolation. These values are given by Murr [29]: $\gamma_s^{\text{Nb}} = 1.9 \text{ J/m}^2$ at 2473°C ; $\gamma_s^{\text{Si}} = 0.73 \text{ J/m}^2$. By interpolation on a mass fraction basis, one obtains: $\gamma_s^{\text{NbSi}_2} = 1.46 \text{ J/m}^2$. Close inspection of Table 3.6 from Murr [29] shows that $\gamma \sim (0.8-1.2) \times 10^{-3} T_m$ for a large number of metals. Since the melting point of NbSi_2 (2420 K) substan-

tially exceeds that of Si (1685 K) and is close to the melting point of Nb (2740 K), the above estimate is realistic.

Figure 14(b) shows the variation of F with distance, y , for a spherical particle with radius equal to $1 \mu\text{m}$ ($V = 4/3\pi \mu\text{m}^3$). Note that the value of F_r between $y = 0.9$ and $y = 1 \mu\text{m}$ is shown by a dashed line. The formulation breaks down at high values of y . The force exerted by a prolate spheroid of $r = 1 \mu\text{m}$ is approximately equal to $1.5 \times 10^{-5} \gamma_s$.

From this value it is possible to estimate the total force exerted on a spherule; Fig. 14(c) shows a solid spherule surrounded by liquid prolate spheroids. One can assume that n spheroids surround one spherule. Thus, the total force is: $F_T \cong nF$. The stress exerted by these spherules is approximately equal to

$$\sigma = \frac{nF}{4\pi r_1^2} = \frac{1.5 \times 10^{-5} n \gamma_s}{4\pi r_1^2} \quad (41)$$

where r_1 is the contact area radius, determined by the relative interfacial energies [see Fig. 14(c)]. It is possible to estimate the stresses produced in solid spherules by these surface (interfacial) tensions. An average value of $2 \times 10^{-5} \sigma_s$ is assumed for F ; r_1 is assumed to be equal to $r/2$; and one considers that each spherule is surrounded by four prolate spheroids of liquid silicide. Thus, $\sigma = 28 \text{ MPa}$.

This stress is of the order of the strength of the silicide. Thus, the stresses can conceivably eject

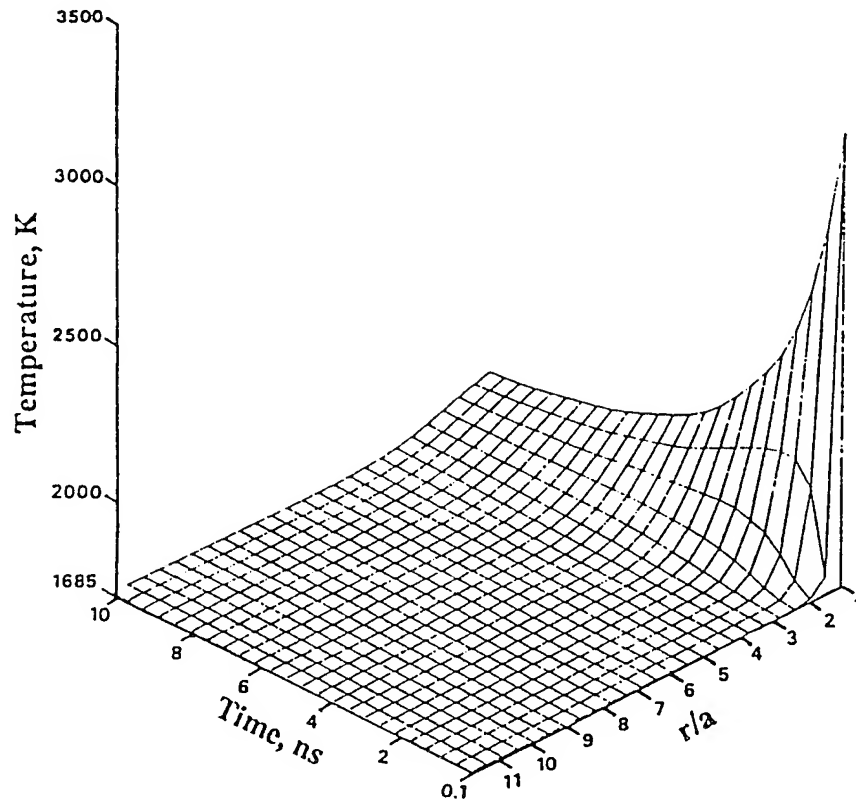


Fig. 13. Heat extraction from spherule with initial temperature of 3200 K while surroundings are at 1600 K .

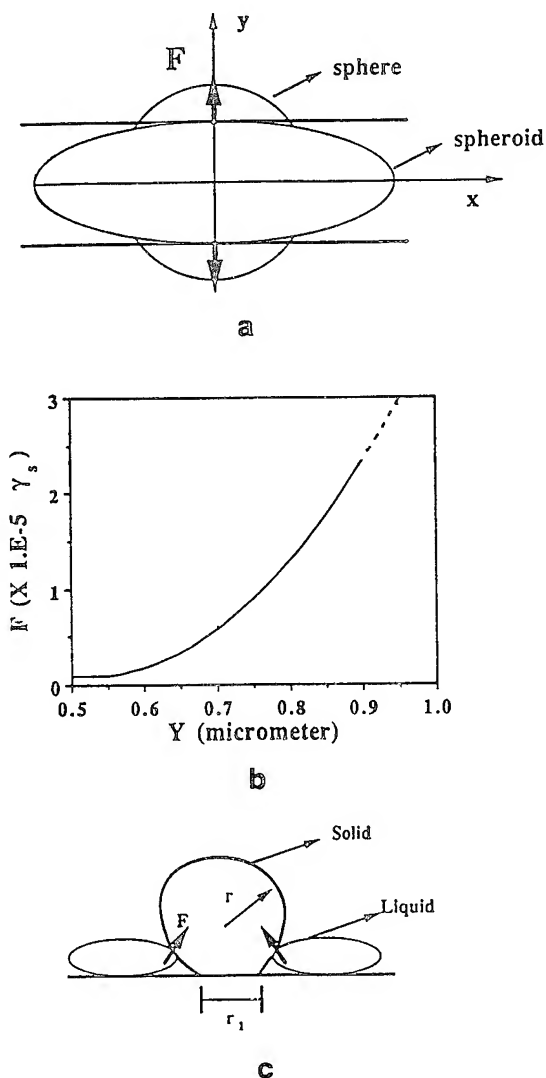


Fig. 14. (a) Prolate spheroid and force F exerted by surface energy as it is deformed. (b) force, F , as a function of distance y , for spherical radius $r = 1 \mu\text{m}$. (c) forces, F , exerted by liquid spheroids on solid spherule.

the solid spherule, and the mechanism proposed is realistic.

Turbulent flow of liquid silicon under shock can also contribute to the detachment of the spherules from the interface; however this mechanism is difficult to quantify. Undoubtedly the drag exerted by the liquid silicon also plays a role, as well as thermal stresses and stress concentrations at the spherule-substrate (Nb) interface. None of these effects have been considered in this analysis; however, they all contribute to more rapid detachment of the NbSi_2 spherules from the solid Nb interface, thereby making new solid-liquid interface available for subsequent reaction.

6. CONCLUSIONS

1. The thermodynamics of shock synthesis was analyzed by considering an equation of state for the porous inert and reactive mixtures. The application

of a threshold energy concept below which no reaction takes place enabled the determination of the critical pressure for reaction as a function of powder density.

2. The fraction of silicon melted as a function of shock energy was calculated and it is found that the threshold energy corresponds to a molten fraction in the range 0.2–0.5 for the Nb–Si system.

3. Heat transfer calculations were conducted in an effort to establish a critical molten region size for which the heat generated by the reaction exceeds the energy dissipated to the environment. Assuming sphericity, these critical radii were found to be equal to 3 and $4 \mu\text{m}$ for the Nb–Si and Mo–Si systems, respectively. These sizes are qualitatively consistent with observations; the smaller critical shock energy for reaction occurs in the system with the larger heat of reaction and lower thermal conductivity.

4. Reaction kinetics calculations were performed using an Arrhenius equation with forward and reverse rates and modified to incorporate the effects of shock compression. The reaction rate increase that could conceivably be produced by shock compression processing (assuming the same mechanism) is much lower than the one observed in actual experiments, leading to the conclusion that shock compression induces different reaction mechanisms.

5. The global reaction kinetics were calculated by considering a number of initiation sites per unit volume that is a function of powder size. This formulation enables the prediction of the fraction transformed as a function of time and particle size.

6. A reaction mechanism occurring at the (Nb or Mo)–Si interface is proposed. This reaction mechanism involves the dissolution of (Nb or Mo) into molten Si, the reaction producing a molten intermetallic, its spheroidization, solidification, and subsequent expulsion into the liquid silicon melt. In this reaction mechanism a fresh solid (Nb or Mo)–liquid (Si) interface is continuously maintained, enabling a high reaction rate.

Acknowledgements—This research was supported by National Science Foundation Grant DMR 8713258 (Materials Processing Initiative), and by McDonnell-Douglas Research Laboratory. We thank the support provided by Dr B. McDonald (NSF) and by Drs C. Whitsett and P. Meschter (MDRL). Discussions with Professor I. Glassman, Princeton University, were extremely helpful in arriving at the mechanism for spherule formation and solidification. The interaction with Dr R. A. Graham, Sandia National Laboratories, through several discussions has provided motivation for this work and contributed significantly to its approach.

REFERENCES

1. C. S. Smith, *Trans. Metall. Soc. AIME* **212**, 574 (1958).
2. E. Hornbogen, *Acta metall.* **10**, 978 (1962).
3. M. A. Meyers, *Scripta metall.* **12**, 21 (1978).

4. J. Weertman, in *Shock Waves and High-Strain-Rate Phenomena in Metals* (edited by M. A. Meyers and L. E. Murr), p. 469. Plenum Press, New York.
5. M. A. Mogilevski, *Phys. Rep.* **S7**, 359 (1983).
6. M. A. Mogilevski, in *Shock Waves and High-Strain-Rate Phenomena in Metals* (edited by M. A. Meyers and L. E. Murr), p. 531. Plenum Press, New York.
7. J. Weertman and P. S. Follansbee, *Mech. Mater.* **2**, 265 (1983).
8. P. S. Follansbee and J. Weertman, *Mech. Mater.* **1**, 345 (1982).
9. W. Gourdin, *J. appl. Phys.* **55**, 172 (1984).
10. R. B. Schwarz, P. Kasiraj, T. Vreeland Jr and T. J. Ahrens, *Acta metall.* **32**, 1243 (1984).
11. D. K. Potter and T. J. Ahrens, *J. appl. Phys.* **63**, 910 (1988).
12. Y. Horie and M. J. Kipp, *J. appl. Phys.* **63**, 5718 (1988).
13. M. B. Boslough, *J. chem. Phys.* **92**, 1839 (1990).
14. L. H. Yu and M. A. Meyers, *J. Mater. Sci.* **26**, 601 (1991).
15. B. R. Krueger, A. H. Mutz and T. Vreeland Jr, *J. appl. Phys.* **70**, 5362 (1991).
16. B. Krueger and T. Vreeland Jr, in *Shock-Wave and High-Strain-Rate Phenomena in Materials* (edited by M. A. Meyers, L. E. Murr and K. P. Staudhammer), p. 241. Marcel Dekker, New York (1992).
17. K. S. Vecchio, L. H. Yu and M. A. Meyers, *Acta metall. mater.* **42**, 701 (1994).
18. M. Yoshida, Program MY 1DL One-Dimensional Lagrangian Hydrodynamic Code, CETR. New Mexico Institute of Mining and Technology, Socorro, N.M. (1986).
19. F. R. Norwood and R. A. Graham, in *Shock-Wave and High-Strain-Rate Phenomena in Materials* (edited by M. A. Meyers, L. E. Murr and K. P. Staudhammer), p. 989. Marcel Dekker, New York (1992).
20. L. V. Alt'schuler, *Sov. Phys.—USPEKHI* **8**, 2 (1965).
21. R. G. McQueen and S. P. Marsh, in *Behavior of Dense Media Under High Dynamic Pressures*, p. 207. Gordon & Beach, New York (1968).
22. M. Yoshida, Mixture Program, Report. Center for Explosives Technology Research, New Mexico Institute of Mining and Technology, Socorro, N.M. (1986).
23. I. Song, Ph.D. thesis, New Mexico Institute of Mining and Technology, Socorro, N.M. (1991).
24. E. K. Rideal and A. J. B. Robertson, *Proc. R. Soc.* **195**, 135 (1948).
25. V. E. Panin, Yu V. Grinvaev, V. E. Egorushkin, I. L. Buehinder and S. N. Kul'kov, Translation from *Izv. vyssh. Zaved. Fiz.* **1**, 34 (1987).
26. J. D. Eshelby, *Proc. R. Soc.* **9A**, 376 (1957).
27. S. Kumar, J. A. Puszynski and V. Hlavacek, in *Combustion and Plasma Synthesis of High Temperature Materials* (edited by Z. A. Munir and J. B. Holt), Chap. 27, p. 273. VCH Publishers, New York.
28. I. Glassman, Princeton Univ., private communication (1991).
29. L. E. Murr, *Interfacial Phenomena in Metals and Alloys*, p. 131. Addison-Wesley (1975).



SHOCK SYNTHESIS OF SILICIDES—I. EXPERIMENTATION AND MICROSTRUCTURAL EVOLUTION

K. S. VECCHIO, LI-HSING YU and M. A. MEYERS

Department of Applied Mechanics and Engineering Sciences, University of California, San Diego,
La Jolla, CA 92093-0411, U.S.A.

(Received 16 September 1992; in revised form 23 July 1993)

Abstract—Niobium and molybdenum silicides were synthesized by the passage of high-amplitude shock waves through elemental powder mixtures. These shock waves were generated by planar parallel impact of explosively-accelerated flyer plates on momentum-trapped capsules containing the powders. Recovery of the specimens revealed unreacted, partially-reacted, and fully-reacted regions, in accord with shock energy levels experienced by the powder. Electron microscopy was employed to characterize the partially- and fully-reacted regions for the Mo-Si and Nb-Si systems, and revealed only equilibrium phases. Selected-area and convergent beam electron diffraction combined with X-ray microanalysis verified the crystal structure and compositions of the reacted products. Diffusion couples between Nb and Si were fabricated for the purpose of measuring static diffusion rates and determining the phases produced under non-shock condition. Comparison of these non-shock diffusion results with the shock synthesis results indicates that a new mechanism is responsible for the production of the NbSi₂ and MoSi₂ phases under shock compression. At the local level the reaction can be rationalized, for example, in the Nb-Si system under shock compression, through the production of a liquid-phase reaction product (NbSi₂) at the Nb-particle/Si-liquid interface, the formation of spherical nodules (~2 μm diameter) of this product through interfacial tension, and their subsequent solidification.

1. INTRODUCTION

Shock-induced reactions (or shock synthesis) have been studied since the 1960s but are still poorly understood, partly due to the fact that the reaction kinetics are very fast making experimental analysis of the reaction difficult. Shock-induced reactions are quite distinct from shock-induced phase transformations, such as the synthesis of diamond from graphite which is a diffusionless phase transformation. Shock-induced reactions also differ from detonations because only condensed products are formed, in the former. Shock synthesis is closely related to combustion synthesis, and occurs in the same systems that undergo exothermic gasless combustion reactions. The thermite reaction ($\text{Fe}_2\text{O}_3 + 2\text{Al} \rightarrow 2\text{Fe} + \text{Al}_2\text{O}_3$) is prototypical of this class of reactions. The first report of these shock-induced reactions is due to Batsanov *et al.* [1]. This initial discovery was followed by activity in Japan [2, 3] and the USSR [4-8]. In the U.S., the pioneering work of Graham and co-workers [9-11] was followed by investigations by Vreeland and co-workers [12, 13], Horie *et al.* [14, 15], Boslough [16], Thadhani and co-workers [17, 18], and Yu *et al.* [19, 20].

Shock-wave propagation through materials generates significant structural changes; these effects have been the object of extensive studies, that were initiated with the Manhattan project in the 1940's and continue to this day. Analytical investigations

coupled with experimental studies have yielded mechanisms rationalizing the production of dislocations and point defects due to shock-wave passage through solid materials. The first mechanism was proposed by Smith [21], followed by Hornbogen [22] and later modified by Meyers [23], and Weertman [24]. The effects of shock-wave passage through porous (powder) materials are considerably more complex, because intense and non-uniform plastic deformation is coupled with the shock-wave effects. Thus, the particle interiors experience primarily the effects of shock waves, while the surfaces undergo intense plastic deformation which can often result in interfacial melting. This localized melting leads to the bonding of the powder, and this gave rise to the research field of shock-wave compaction. Quantitative, predictive models have been developed by Gourdin [25] and Schwarz *et al.* [26].

Shock synthesis of compounds from powders is triggered by the extraordinarily high energy deposition rate at the surfaces of the powders, thereby changing their configuration, forcing them in close contact, activating them by introducing large densities of defects, and heating them close to or even above their melting temperatures [8-11]. Some fundamental questions regarding these reactions remain unanswered. Prominent among them are the following: (1) How can the extraordinarily high reaction rates encountered in shock compression be explained?

(2) Are the phases formed under shock-synthesis conditions unique and/or non-equilibrium?

This paper (in conjunction with its companion paper [27]) presents experimental results coupled with characterization and analysis of two metal silicides formed by shock synthesis directed at providing an answer to these questions. It is shown that the mechanism of shock-induced reaction is quite different than conventional solid-state reaction mechanisms for the silicides. The high thermal gradients imparted by the effect of shock compression, combined with the high pressures and material flux, enable a reaction mechanism unique to shock compression; however, only equilibrium phases and structures were found for the systems investigated.

2. EXPERIMENTAL PROCEDURES

Two elemental powder mixtures were used in this investigation: Nb-Si and Mo-Si. The powders, produced by CERAC, had irregular shapes, and sizes smaller than $44\text{ }\mu\text{m}$ (-325 mesh). The purity levels were 99.9% for Nb, Mo and Si. The powders were mixed in the proportions to provide, upon reaction, the intermetallic compounds NbSi_2 and MoSi_2 , for each system respectively. These powders were encapsulated under controlled argon atmosphere in stainless steel capsules (internal dimensions of 15 mm diameter and 5 mm height). These capsules were subjected to shock compression in a Sawaoka fixture; this fixture is described in detail elsewhere [e.g. 28]; the system (cross-section) is shown in Fig. 1. Each system contains 12 capsules; four sectioned capsules are shown in this figure. A flyer plate is accelerated downwards by an explosive system consisting of a main charge (PBX 9404 explosive) initiated simultaneously along its top surface by an explosive lens consisting of two explosives with different detonation velocities. Impact velocities of 1.2 and 1.9 km/s were achieved by varying the quantity and type of explosive accelerating the flyer plate. Shock experiments were conducted on capsules at room temperature and others preheated to 773 K.

The high-temperature shock fixture is shown in Fig. 1(b). The capsules and momentum traps are heated in a discardable furnace, with the explosive system at a safe distance. When the temperature reaches the desired value, the furnace top is removed and the explosive assembly, together with the flyer plate, roll down a 4° inclined ramp until they are properly positioned above the capsules; the system is then electrically detonated. Solenoid 1 ensured remote activation and enabled the flyer plate/explosive system to roll down at the desired time. In case of misfire or any other unexpected event, the explosive system could be withdrawn from above the furnace by the activation of solenoid 2.

After shock processing, the specimen capsules were sectioned and analyzed by scanning and transmission electron microscopy. Scanning electron microscopy

(SEM) was conducted on a Cambridge S360 electron microscope equipped with a LINK Analytical energy dispersive X-ray spectrometer (EDS). Compositional measurements of individual phases were conducted using the ZAF correction procedure with unreacted powder regions used for standards. Since the shock experiment is very rapid, and the resultant thermal excursion short lived, the unreacted powder regions were considered chemically unchanged and subsequently used as pure elemental standards. Standardless quantification was also conducted on both the unreacted powders, and the reaction products,

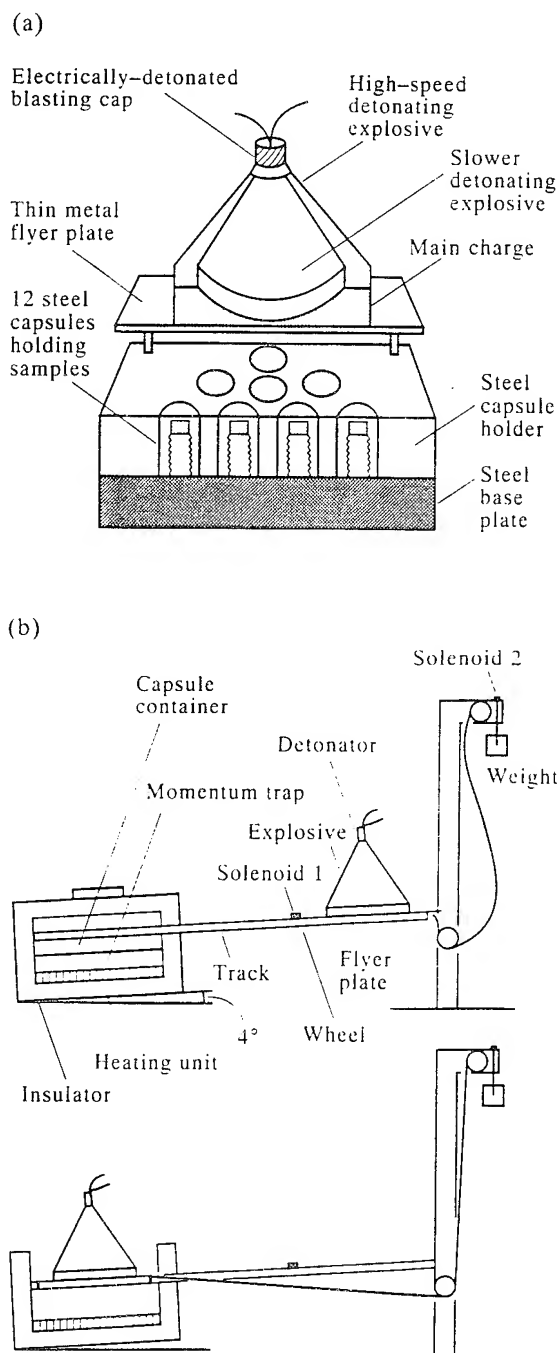


Fig. 1. Schematic illustration of planar impact (Sawaoka) system: (a) room temperature fixture. (b) elevated temperature shock fixture.

and the results were consistent with the standards-based quantification results.

Static reaction experiments (i.e. non-shock experiments) were conducted by annealing Nb-Si diffusion couples for different times at 1200°C and recovering the specimens for observation. The identification of reaction products and their thicknesses in these diffusion couples was established by SEM and quantitative EDS X-ray microanalysis using the specimen regions well away from the interface as pure elemental standards.

Transmission electron microscopy (TEM) was carried out in a Philips CM30 electron microscope equipped with a LINK Analytical AN1085 ultra-thin window (UTW) energy dispersive X-ray spectrometer (EDS) system. The TEM work was conducted at an accelerating voltage of 300 kV, with the exception of both the X-ray microanalysis and convergent beam electron diffraction work which were each conducted at 100 kV.

The pressure and temperatures induced by shock waves in the capsules were obtained from computer

simulations, conducted by Norwood and Graham [29]. Two-dimensional effects are very important since the shock waves travel faster in the capsule than in the powder. Thus, the shock waves enter the capsules laterally, as well as at their top surface, generating highly inhomogeneous pressure and temperature regimes. This inhomogeneity in both pressures and temperatures was readily apparent within the recovered capsules, and was actually a highly useful effect since it enabled the analysis of unreacted, partially-reacted, and fully-reacted regions within the same specimen.

3. EXPERIMENTAL RESULTS AND DISCUSSION

3.1. Shock recovery experiments

Figure 2 shows reaction maps of the cross-sections for the recovered capsules for the Nb-Si and Mo-Si samples; fully-reacted, partially-reacted, and unreacted regions are evident. Upon recovery, the specimens were considerably cracked, and portions of the specimens were lost during sectioning.

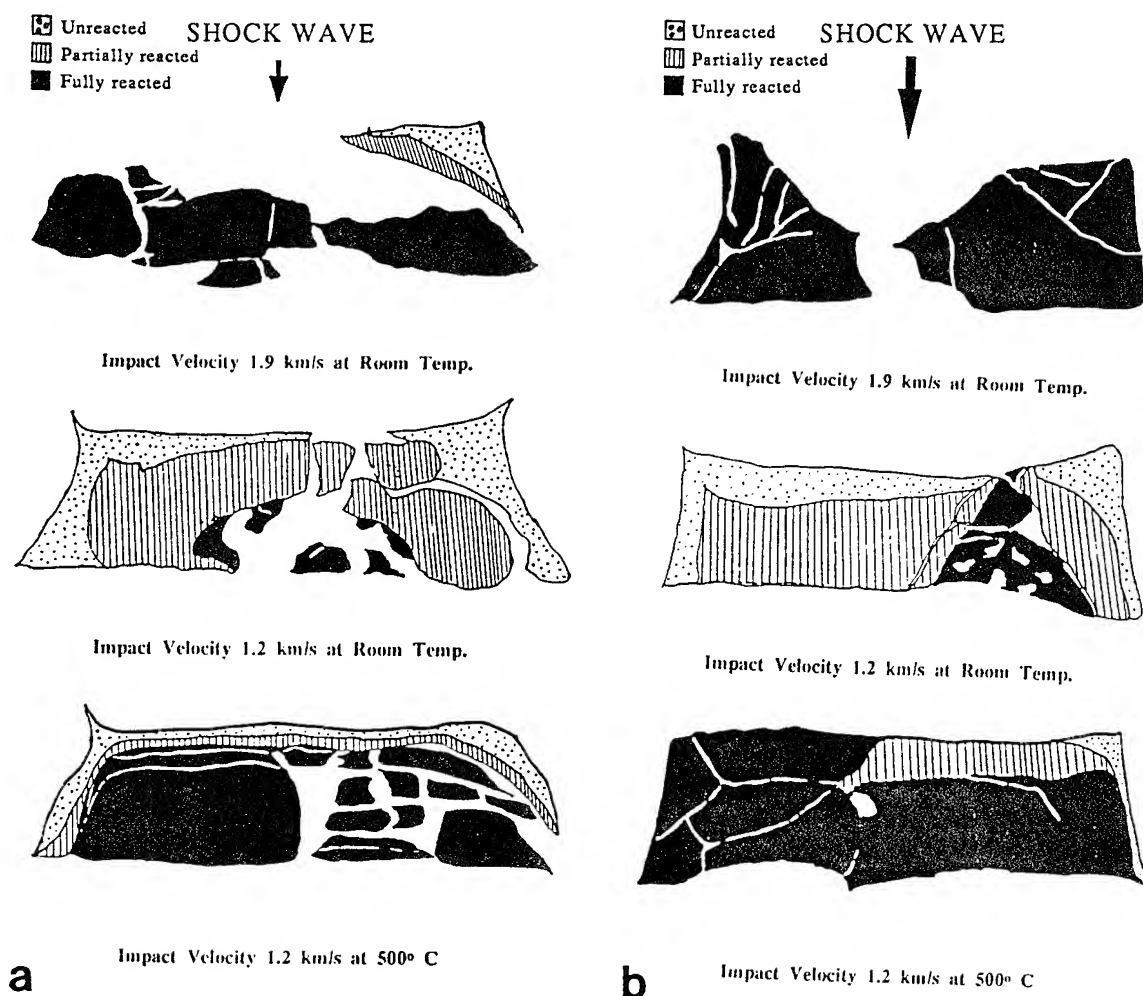


Fig. 2. Maps showing fully-reacted, partially-reacted, and unreacted regions for (a) Nb-Si system and (b) Mo-Si system. Impact velocity and temperature marked below each plot. Black regions represent fully-reacted, hatched regions-partially-reacted, dotted region-unreacted, and white represents voids and/or cracks.

3.1.1. Scanning electron microscopy and microanalysis. Backscattered electron micrographs of a polished section of the Nb-Si sample shocked at room temperature and low velocity (1.2 km/s) are shown in Fig. 3. Figure 3(a) shows the unreacted but compacted region taken from near the top of the capsule. Figure 3(b) shows the transition region between unreacted and partially-reacted material, with the reacted material being the small gray nodules identified as NbSi₂ (Nb-38 wt% Si via X-ray micro-

analysis); the identification of the crystal structure of this phase will be discussed in detail later. Figure 3(c) shows the partially-reacted region which made up the majority of the sample and consisted of Nb particles surrounded by a reaction layer of NbSi₂ nodules and embedded within a two-phase matrix of NbSi₂ nodules and silicon. Figure 3(d) shows the transition region from the partially-reacted to fully-reacted material located near the bottom of the capsule. Within this transition region an additional interfacial

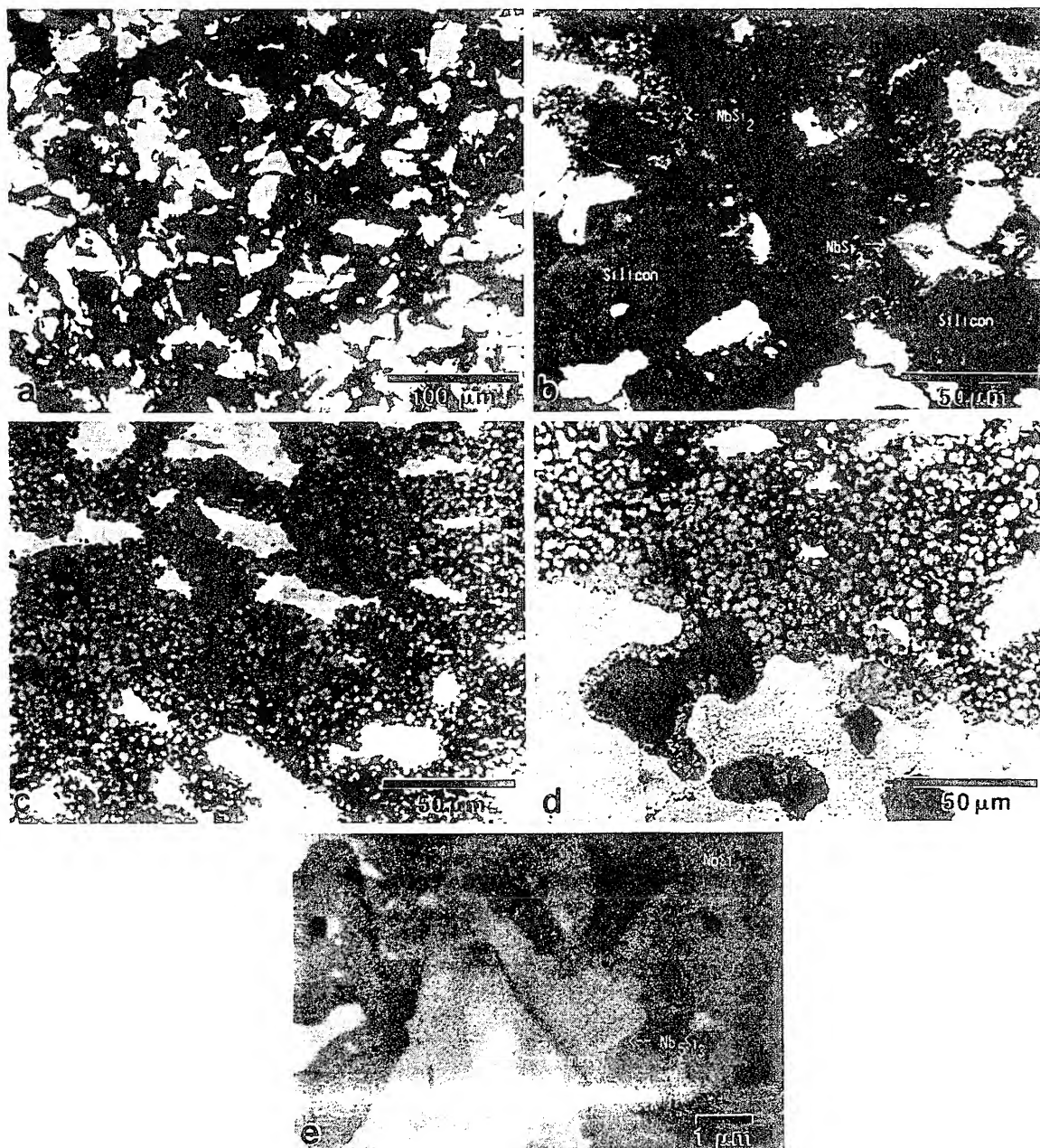


Fig. 3. Backscattered electron micrographs of (a) the unreacted but compacted region taken from near the top of the capsule, (b) the transition region between unreacted and partially-reacted material, with the reacted material being the small gray nodules identified as NbSi₂, (c) the partially-reacted region which makes up the majority of the sample and consists of Nb particles surrounded by a reaction layer of NbSi₂ nodules and embedded within a two-phase matrix of NbSi₂ nodules and silicon, (d) the transition region from the partially-reacted to fully-reacted material located near the bottom of the capsule: within this transition region an additional interfacial reaction product could be observed as shown in (e) which was identified by X-ray microanalysis as Nb₅Si₃.

reaction product could be observed as shown in Fig. 3(e) which was identified by X-ray microanalysis as Nb_5Si_3 (Nb-15 wt% Si). Some Nb_5Si_3 reaction product could be found between the NbSi_2 phase and the Nb particles within the partially-reacted region; however, the thickness of the Nb_5Si_3 layer, in this region, never exceeded 100 nm. In the transition region, the Nb_5Si_3 layer exceeded 1 μm in thickness. In the unreacted region, the niobium particles retain their original powder configuration (i.e. undeformed, irregularly shaped particles), whereas the silicon particles have been deformed and compacted around the

niobium particles. Figure 4(a) shows a backscattered electron micrograph of the microstructure of the partially-reacted region in the low velocity (1.2 km/s) and elevated temperature (773 K) shock experiment. The most notable feature that differentiates this sample from the room temperature, low velocity experiment is the significantly increased amount of reacted product NbSi_2 . Comparison between Fig. 3(c) and Fig. 4(a) indicates that a greater volume fraction of NbSi_2 was formed as a result of capsule preheating. This is expected since a higher temperature will be achieved in the capsule as a result of the shock, plus preheating, and the capsule will remain hotter for a longer time following the shock since the shock fixture is no longer an efficient quenching medium.

Figure 4(b, c) show the partially-reacted region of the specimen shocked at higher velocity (1.9 km/s) and room temperature. In this sample less nodular NbSi_2 was observed; however, a significant amount of NbSi_2 was also found present as a lamellar eutectic structure within the silicon rich matrix, as shown in Fig. 4(c). Under these shock conditions, the molten silicon matrix becomes enriched with niobium, and subsequently solidifies at 1300°C via a eutectic reaction between Si and NbSi_2 . A small amount of this eutectic reaction was evident in the other two Nb-Si samples; however, in those samples the volume fraction was very insignificant compared to the amount of nodular NbSi_2 that was found.

This result suggests that the temperature throughout the molten Si exceeded the melting temperature of the NbSi_2 phase ($\sim 1940^\circ\text{C}$) causing the nodular NbSi_2 to dissolve in Si and to subsequently resolidify through the eutectic reaction. Incontrovertible proof that silicon was molten in the partially-reacted region of even the low velocity, room temperature experiment is provided by the observation of a fine eutectic structure of lamellar NbSi_2 and Si. This eutectic structure formed last as the molten, Nb-enriched silicon solidified. The higher shock energies achieved in the 1.9 km/s sample result in significantly higher temperatures within the powders. A greater fraction of this shock energy is deposited in the silicon powder compared to the Nb powder as evidenced by the considerable plastic deformation of the silicon particles in the unreacted region, and the extremely high temperature achieved in the molten silicon in the partially-reacted region. In addition, the higher shock energy is likely to result in increased turbulence in the molten Si which will aid in homogenizing the melt (i.e. dissolve the NbSi_2 nodules) through a stirring action. Clearly, the reaction mechanism associated with the formation of the nodular NbSi_2 is distinct from the eutectic reaction observed in Fig. 4(b, c).

Comparison of the low velocity (1.2 km/s), elevated temperature (773 K) experiment with the room temperature, high velocity (1.9 km/s) experiment reveals several interesting observations regarding the nature and extent of the shock reaction. First, the extent of reaction (i.e. the amount of reaction product formed)

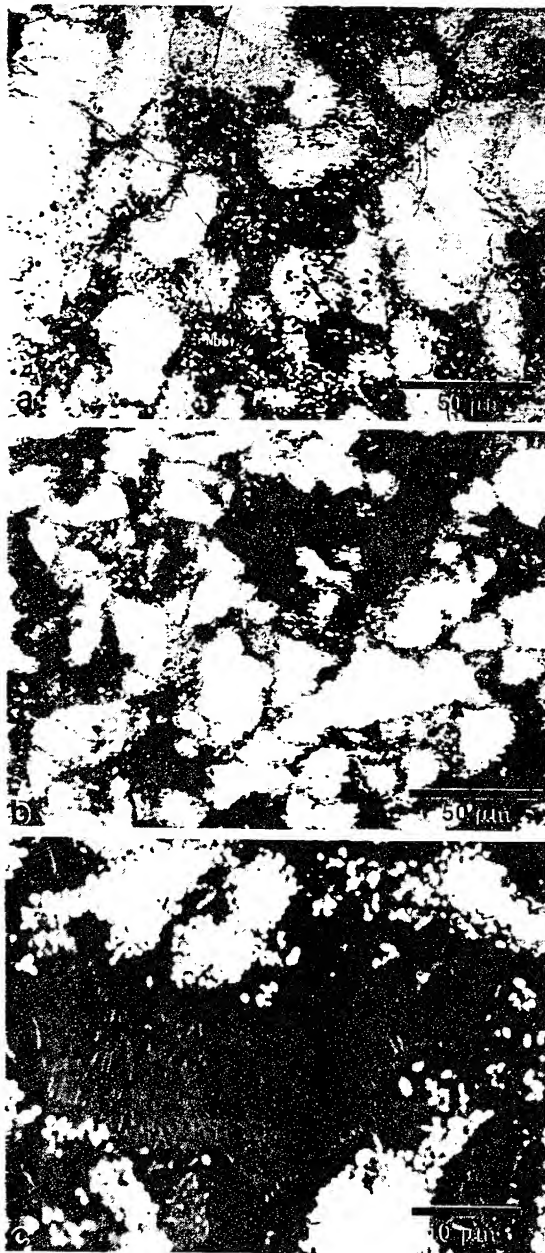


Fig. 4. Backscattered electron micrographs of the microstructure of (a) the partially-reacted region in the low velocity (1.2 km/s) and elevated temperature (773 K) shock experiment, (b, c) the partially-reacted region of the specimen shocked at higher velocity (1.9 km/s) and room temperature.

was greater for the low velocity (1.2 km/s), elevated temperature experiment than the high velocity (1.9 km/s) experiment, even though the high velocity experiment creates a higher temperature within the capsule compared to the low velocity, elevated temperature experiment after the preheat temperature is added to the calculated temperatures (as based on the calculations of Norwood and Graham [29] also shown as Fig. 2 in the companion paper to this work [27]). The preheating is more effective for promoting the reaction because the temperature is uniform throughout the powders, heating up both the Nb and Si particles relatively evenly, whereas the shock energy (i.e. heat) is preferentially deposited in the softer Si particles. As such, a larger fraction of shock energy can contribute to the reaction in the preheated sample, rather than heating of the powders in the high velocity experiment. Secondly, the morphology of the NbSi₂ phase differs between the high velocity experiment and the elevated temperature experiment. In the high velocity experiment the NbSi₂ exists both as a lamellar eutectic structure within the Si regions, as well as nodules along the Nb-Si interface. In contrast, the NbSi₂ phase exists as nodules

surrounding a thick layer of NbSi₂, which encapsulates the Nb particles, as shown in Fig. 4(a). Since the preheating raises the temperature of both the powders and the whole fixture itself, the cooling rate in this experiment is considerably lower than in either of the other two (low velocity-room temperature and high velocity-room temperature) experiments. The morphology of the thick NbSi₂ reaction layer surrounding the Nb particles suggests that this layer: (1) forms through solid-state diffusion, (2) occurs subsequent to the nodule reaction mechanism, and (3) is not directly associated with shock-wave passage.

Backscattered electron micrographs of a polished section of the Mo-Si sample shocked at room temperature and low velocity (1.2 km/s) are shown in Fig. 5. Analysis of the other two Mo-Si samples will not be presented here, but examination of these samples revealed structures similar to the corresponding Nb-Si samples. Figure 5(a) shows the unreacted but compacted region taken from near the top of the capsule. Figure 5(b) shows the transition region between unreacted and partially-reacted material, with the reacted material being the small gray nodules

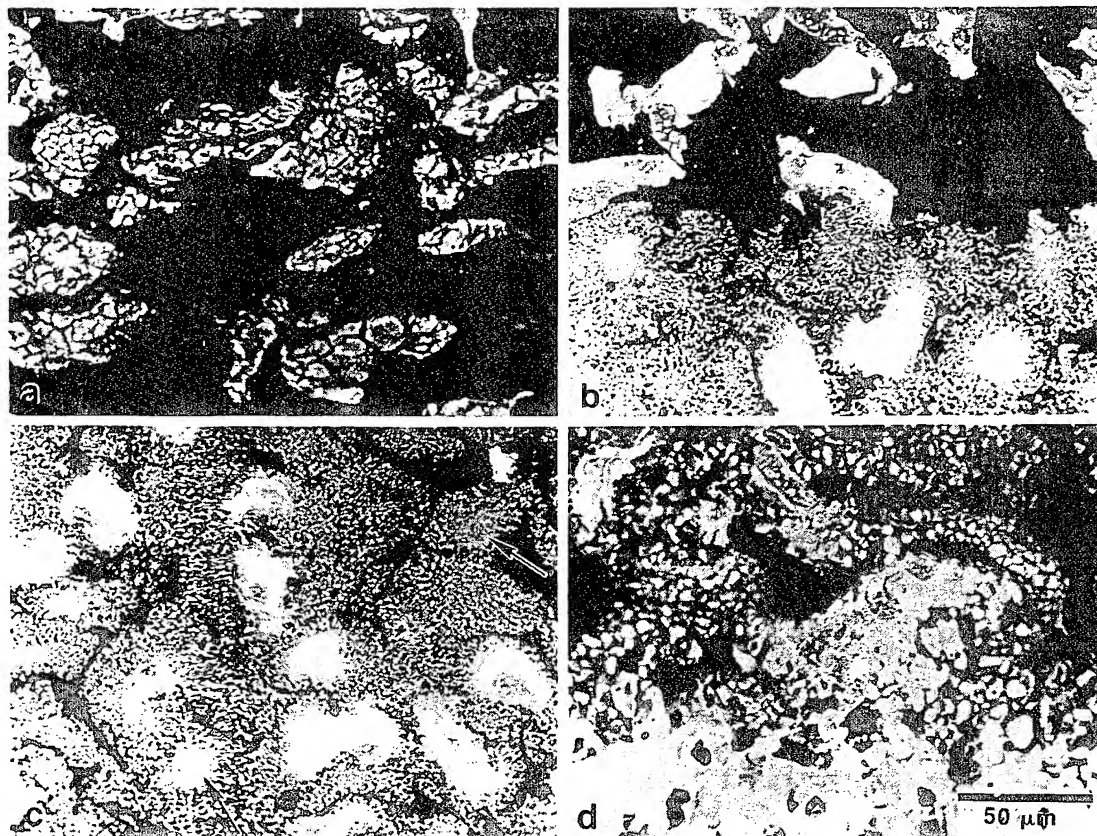


Fig. 5. Backscattered electron micrographs of a polished section of the Mo-Si sample shocked at room temperature and low velocity (1.2 km/s), (a) the unreacted but compacted region taken from near the top of the capsule, (b) the transition region between unreacted and partially-reacted material, with the reacted material being the small gray nodules identified as MoSi₂, (c) the partially-reacted region which made up the majority of the sample and consisted of Mo particles surrounded by a reaction layer of MoSi₂ nodules and embedded within a two-phase matrix of MoSi₂ nodules and silicon; in many instances, the entire Mo particle has been reacted to form the MoSi₂ phase, as indicated by an arrow in (c); (d) shows the transition region from the partially-reacted to fully-reacted material located near the bottom of the capsule.

identified as MoSi_2 (Mo-37 wt% Si via X-ray microanalysis); the identification of the crystal structure of this phase will be presented later. Figure 5(c) shows the partially-reacted region which made up the majority of the sample and consisted of Mo particles surrounded by a reaction layer of MoSi_2 nodules and embedded within a two-phase matrix of MoSi_2 nodules and silicon. In many instances, the entire Mo particle has been reacted to form the MoSi_2 phase, as indicated by an arrow in Fig. 5(c). Figure 5(d) shows the transition region from the partially-reacted to fully-reacted material located near the bottom of the capsule. No additional interfacial reaction product could be observed in this sample, unlike the Nb-Si samples. In the unreacted region, the Mo particles appear to fragment along grain boundaries within the particles, while the silicon particles seem to have undergone intense plastic deformation.

The fully-reacted regions for the Nb-Si and Mo-Si samples were essentially identical in term of macroscopic morphology. Voids were present throughout, resulting from either solidification shrinkage, gases evolved during the reaction, or tensile stresses imposed on the compact prior to solidification. The presence of spherical voids, as well as dendritic structures observed are evidence of melting and

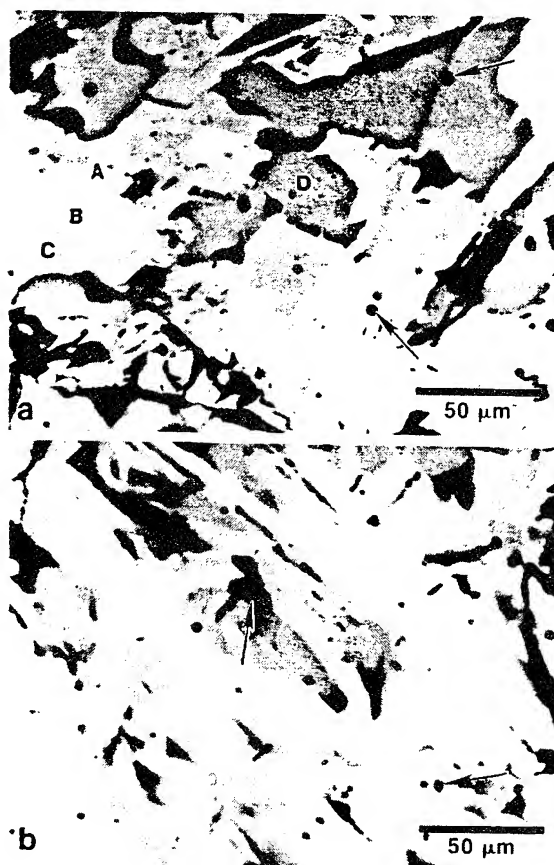


Fig. 6. Backscattered electron micrographs of fully-reacted regions of the Nb-Si capsules tested at (a) elevated temperature (773 K) and (b) high velocity (1.9 km/s) and room temperature. Microvoids are marked by arrows and several different phases are present marked A, B, C and D in (a).

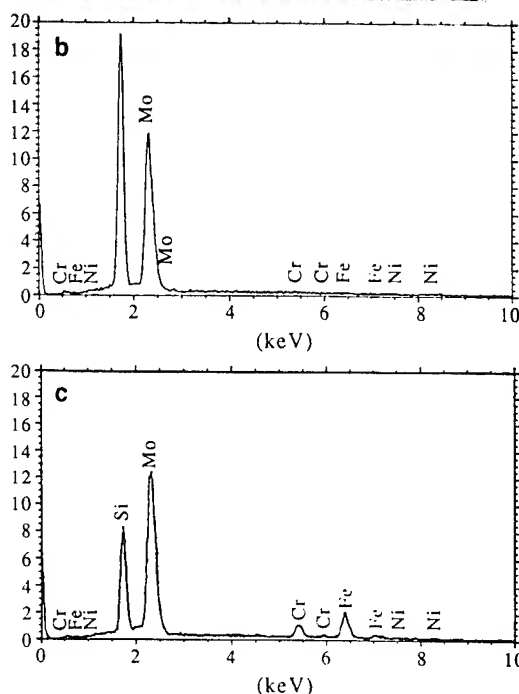
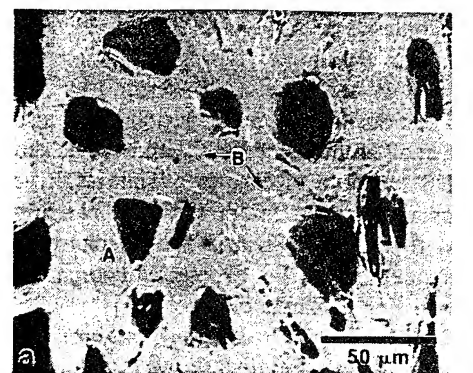


Fig. 7. (a) Backscattered electron micrograph of the fully-reacted region of the Mo-Si capsule which contains primarily MoSi_2 [labeled A in this figure]; (b) shows a typical EDS spectrum from this phase. A second phase [labeled B in (a)] had a composition close to Mo_5Si_3 , but also contained small amounts of Fe, Cr and Ni, as shown in the EDS spectrum of (c).

re-solidification. Figure 6(a) and (b) show the microstructure in the fully-reacted regions of the Nb-Si capsules tested at elevated temperature (773 K) and high velocity (1.9 km/s), respectively; the microvoids are marked by arrows and several different phases are present. Energy dispersive X-ray analysis of these distinct phases [marked A, B, C and D in Fig. 6(a) for example] reveals Fe, Ni and Cr peaks, in addition to differences in the relative intensities of the much larger Nb and Si peaks. The presence of Fe, Ni and Cr is evidence for melting of the capsule (which is stainless steel) and subsequent contamination of specimen. This is a post-shock effect, since there would be no time for diffusion of these elements during shock-wave passage. The phases which contained the Fe, Cr and Ni to varying amounts also had an overall Nb-Si ratio close to the composition of Nb_5Si_3 . Figure 7(a) shows the fully-reacted region of the Mo-Si capsule

which contains primarily MoSi_2 [labeled A in this figure]; Fig. 7(b) shows a typical EDS spectrum from this phase. A second phase [labeled B in Fig. 7(a)] had a composition close to Mo_5Si_3 , but also contained small amounts of Fe, Cr and Ni, as shown in the EDS spectrum of Fig. 7(c). This result, in conjunction with similar findings for the Nb-Si system suggest that the Nb_5Si_3 and Mo_5Si_3 phases have a greater solubility for Fe, Cr, and Ni compared to the corresponding disilicide phases.

3.1.2. Transmission electron microscopy and diffraction analysis. Figure 8 shows transmission electron micrographs of the partially-reacted region of the low impact velocity, room temperature Nb-Si

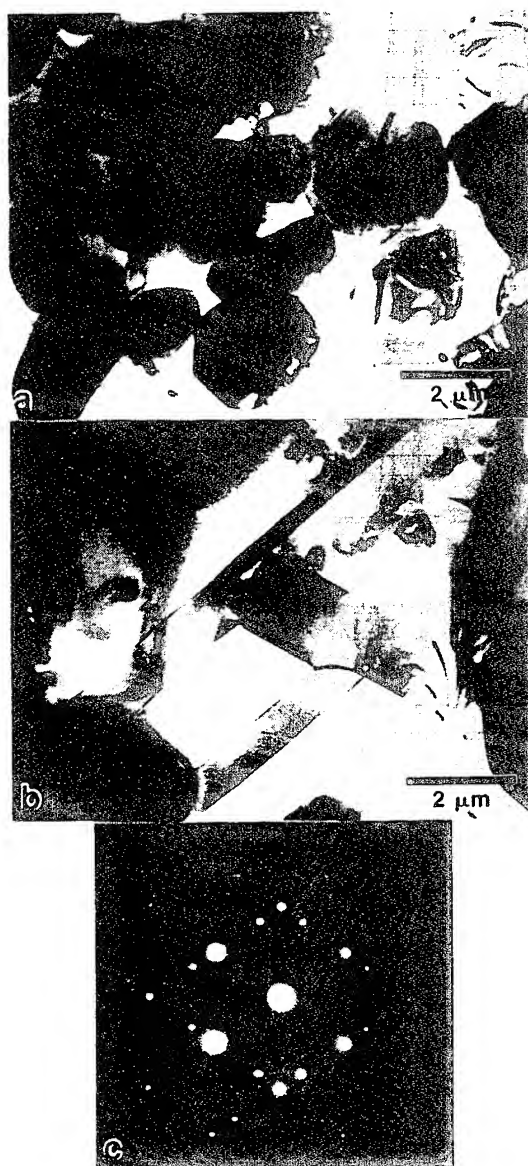


Fig. 8. Transmission electron micrographs of the partially-reacted region of the low velocity, room temperature Nb-Si sample. (a, b) reveal the structure of the nodules and of the surrounding silicon matrix. The silicon surrounding these reacted regions generally shows an annealed structure with a profusion of annealing twins. (c) Electron diffraction pattern from twins in (b).

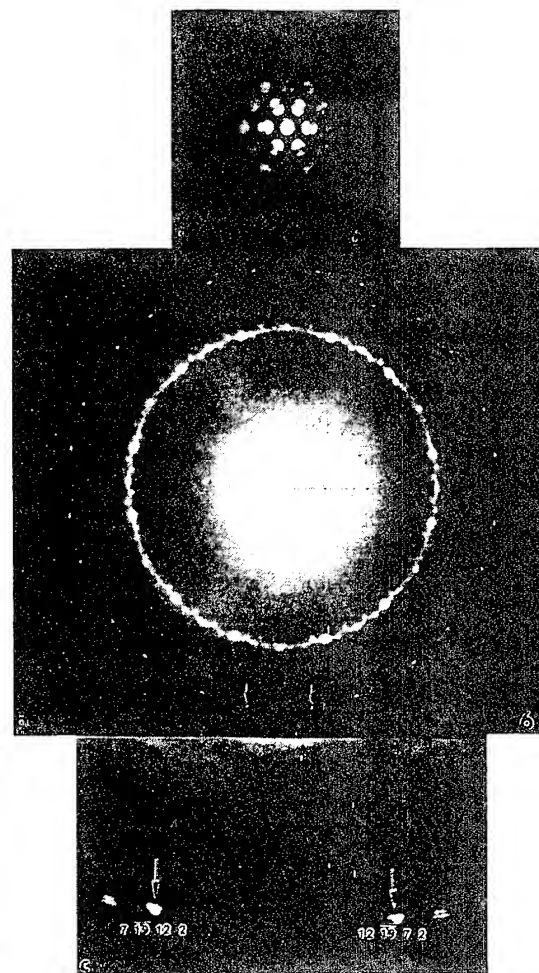


Fig. 9. [0001] zone axis CBED pattern obtained from the NbSi_2 nodules. (a) shows the zero-order Laue layer pattern which possesses 6mm projection diffraction symmetry. (b) shows the whole pattern revealing only 6-fold rotational symmetry; no mirror planes exist in this pattern, and (c) shows an enlarged view of the black rectangle outlining a small portion of the second-order Laue ring in (b).

sample. Figure 8(a) and (b) reveal the structure of the nodules and of the surrounding silicon matrix. The NbSi_2 nodules are monocrystalline, approx. 1–2 μm in diameter, and have facets. They do not show any marked internal structure, such as dislocations, stacking faults, or twins. The silicon surrounding these reacted regions generally shows an annealed structure with a profusion of annealing twins, as shown in Fig. 8(b). A few silicon regions exhibit a microcrystalline structure. These regions were either subjected to intense plastic deformation and recrystallized (statically or dynamically) or were molten and rapidly re-solidified. This microstructure is in stark contrast with the previous silicon regions [Fig. 8(b)] which suggested melting followed by slow re-solidification.

The crystal structure of the NbSi_2 nodules was determined by convergent beam electron diffraction (CBED) analysis. Figure 9 shows the [0001] zone axis CBED pattern obtained from the NbSi_2 nodules. Figure 9(a) shows the zero-order Laue layer pattern



Fig. 10. Transmission electron micrographs of the partially-reacted region of the low velocity, room temperature Mo-Si sample. (a) and (b) reveal the structure of the MoSi_2 nodules and the surrounding silicon matrix, respectively. The silicon surrounding these reacted regions generally shows an annealed structure with a profusion of annealing twins.

which possesses $6mm$ projection-diffraction† symmetry. Figure 9(b) shows the whole pattern† revealing only 6-fold rotational symmetry; no mirror planes exist in this pattern. Figure 9(c) shows an enlarged view of the black rectangle outlining a small portion of the second-order Laue ring in Fig. 9(b). Careful examination of Fig. 9(c) reveals that the reflections indicated by the arrows [$7\ 19\ 12\ 2$] and [$12\ 19\ 7\ 2$] do not mirror to each other. This lack of mirror symmetry reduces the whole pattern symmetry from $6mm$ to 6 in the $[0001]$ zone axis orientation. As such, the diffraction group for this symmetry is $6m_1m_1$ and the point group is 622. CBED analysis of both the $\langle 1120 \rangle$ and $\langle 1100 \rangle$ type orientations, not shown

†The terms projection-diffraction symmetry and whole pattern symmetry have the same meanings as in Buxton *et al.* [31]. Projection-diffraction symmetry corresponds to the symmetry of the diffraction disks and diffuse intensity within diffraction disks of the zero-order Laue layer. Whole pattern symmetry refers to the symmetry of the higher-order Laue zone (HOLZ) reflections and HOLZ Kikuchi lines seen in low camera length patterns such as Fig. 9(b).

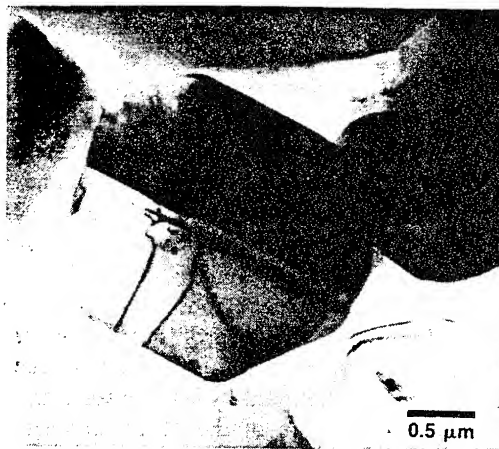


Fig. 11. Transmission electron micrograph of the partially-reacted region of the low velocity, room temperature Mo-Si sample revealing the internal structure of the MoSi_2 nodules including dislocations and twins.

here, displayed only 2-fold whole-pattern symmetry consistent with the point group 622. The established crystal structure for the NbSi_2 phase is the $C40$ hexagonal structure (space group $P6_322$ and point group 622) [30]. No attempt was made here to determine the space group of this phase; however there is no reason to suspect any other space group.

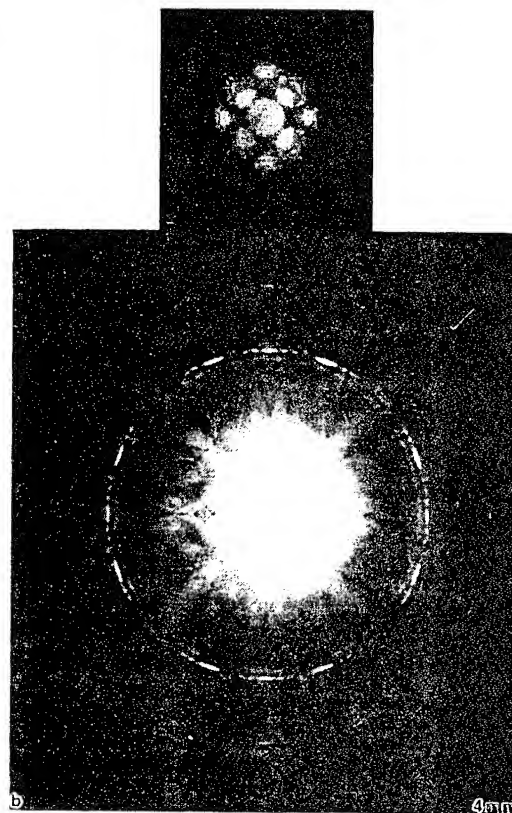


Fig. 12. $[001]$ zone axis CBED pattern obtained from the MoSi_2 nodules. (a) shows the zero-order Laue layer pattern which possesses $4mm$ projection-diffraction symmetry, and (b) shows the whole-pattern symmetry revealing $4mm$ symmetry as well.

Figures 10 and 11 show transmission electron micrographs of the partially-reacted region of the low impact velocity, room temperature Mo-Si sample. Figure 10(a) and (b) reveal the structure of the MoSi_2 nodules and the surrounding silicon matrix, respectively. The MoSi_2 nodules are monocrystalline, approx. $1\text{--}2\text{ }\mu\text{m}$ in diameter, and have facets. They show significant internal structure, including dislocations and twins, as shown in Figure 11. The silicon surrounding these reacted regions generally shows an annealed structure with a profusion of annealing twins, as shown in Fig. 10(b). This microstructure suggested melting followed by slow re-solidification.

The crystal structure of the MoSi_2 nodules was determined by CBED analysis. Figure 12 shows the $[001]$ zone axis CBED pattern obtained from the

MoSi_2 nodules. Figure 12(a) shows the zero-order Laue layer pattern which possesses $4mm$ projection-diffraction symmetry; Fig. 12(b) shows the whole-pattern symmetry revealing $4mm$ symmetry as well. Examination of both the $[100]$ and $[110]$ orientations, not shown here, displayed $2mm$ whole-pattern symmetries. These symmetries, in conjunction with the $4mm$ symmetry of the $[001]$ orientation, are consistent with a point group of $4/mmm$. From the whole pattern shown in Fig. 12(b) the centering of the structure was determined to be body-centered (I). Since no dynamical absences could be located in any orientations, the space group was determined to be $I4/mmm$. MoSi_2 has been reported to exist as two different crystal structures, $C40$ hexagonal ($\beta\text{-MoSi}_2$) above 1900°C and as $C11_b$ (body-centered tetragonal

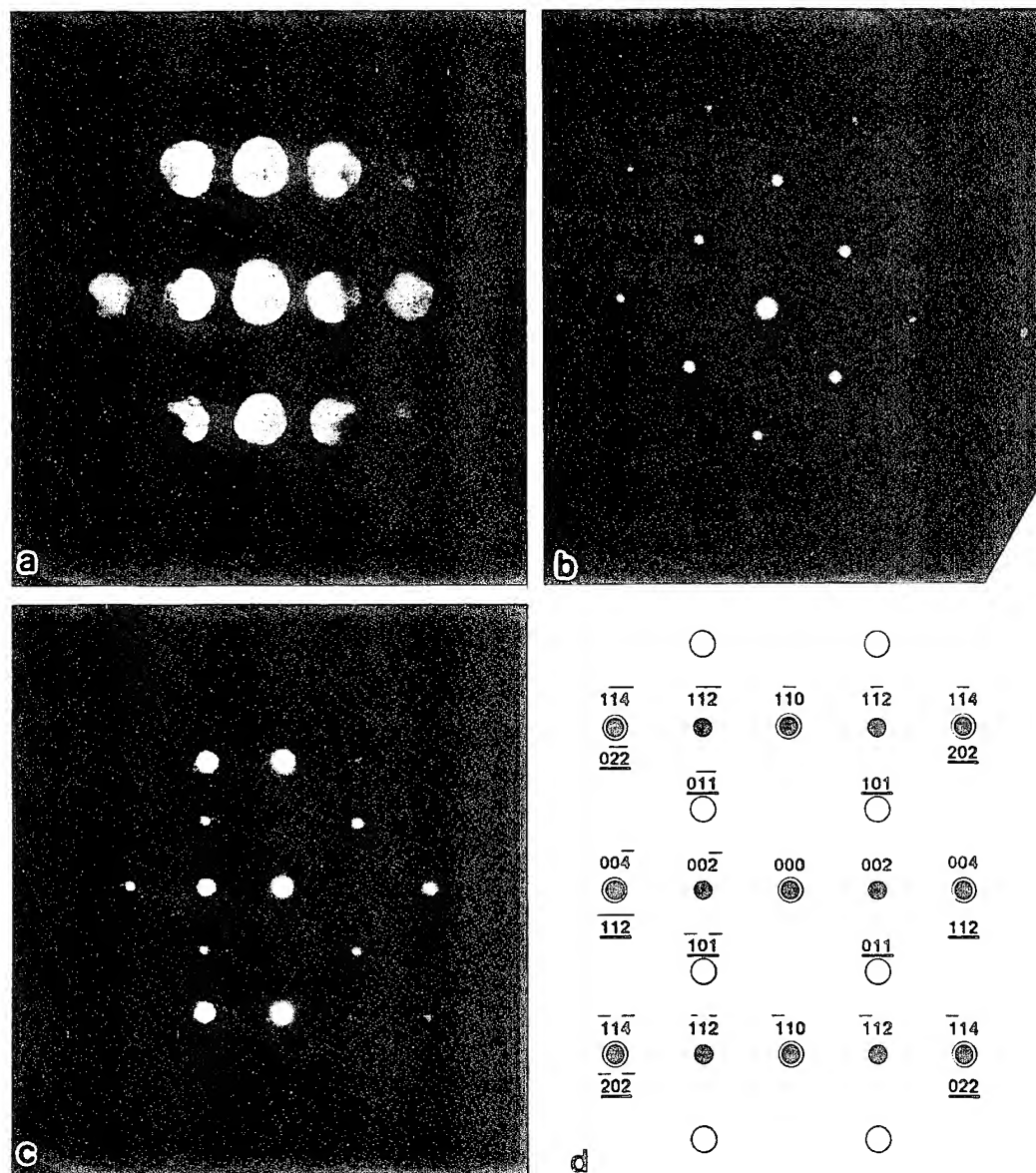


Fig. 13. (a) $[110]$ microdiffraction pattern from one side of the twin plane in a MoSi_2 nodule and (b) shows a $[111]$ selected area diffraction pattern (SADP) from the other side. (c) shows a composite SADP across both sides of the twin, and (d) shows the indexing of the composite pattern. The solid circles indicate the first variant pattern shown in (a), the open circles represent the reflections from the second variant shown in (b), and a solid circle inside an open circle indicates overlapping reflections.

α - MoSi_2) below 1900°C [32]. Boettinger *et al.* [33] have reported that pure MoSi_2 exists only as the C11_b structure, and that the C40 is only metastable at high temperatures as a result of other solutes stabilizing this phase. In addition, they point out that in rapid liquid quenching operations, such as plasma-spraying, and we propose here for the conditions of this reaction mechanism, that "the formation of a metastable MoSi_2 C40 phase can occur directly from the melt if the undercooling takes the melt below the metastable melting point of the C40 phase. This melting point may be only a few degrees Celsius below the melting point of the C11_b phase." The MoSi_2 phase observed here is consistent with the low temperature tetragonal phase (C11_b) suggesting that either this phase formed via solid-state below 1900°C ,

in contradiction to the mechanism being proposed herein, or was formed from the liquid state (consistent with the mechanism proposed here) first as the high-temperature C40 structure which subsequently transformed during cooling to the low-temperature C11_b phase.

Mitchell *et al.* [34] have examined the (C40) hexagonal-to-(C11_b) tetragonal transformation of MoSi_2 in plasma-sprayed processing in which the MoSi_2 phase starts to form in the liquid state. Their results indicate that a hexagonal-to-tetragonal phase transformation does occur in their experiments even for the very rapid solidification rates of the plasma-spray processing. During the transformation the stacking is changed from ABC in the hexagonal phase to AB in the tetragonal phase, and three different stacking

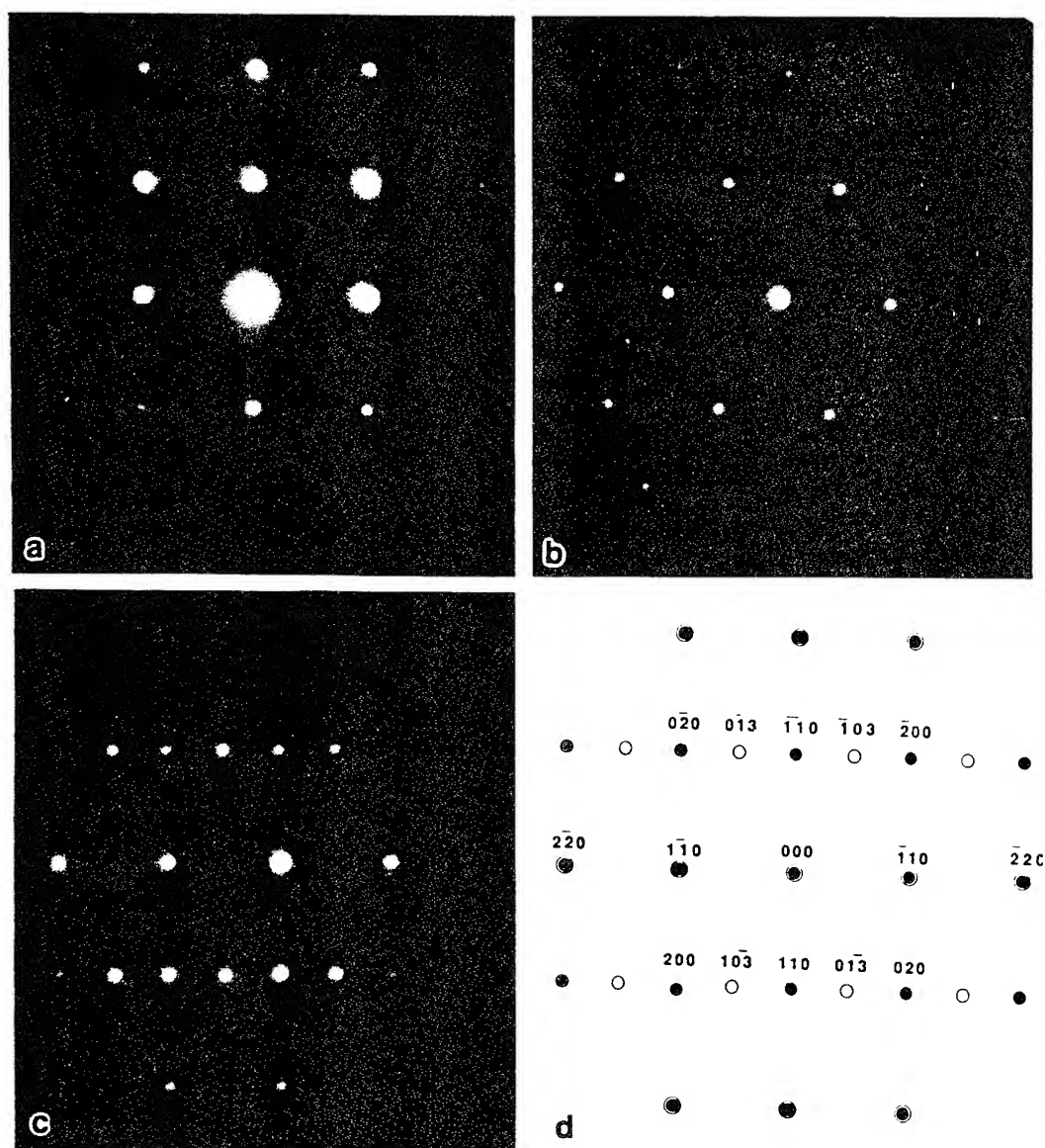


Fig. 14. (a) $[001]$ selected area diffraction pattern from one side of the twin plane in a MoSi_2 nodule and (b) shows a $[331]$ selected area diffraction pattern from the other side. (c) shows a composite SADP across both sides of the twin, and (d) shows the indexing of the composite pattern. The solid circles indicate the first variant pattern shown in (a), the open circles represent the reflections from the second variant shown in (b), and a solid circle inside an open circle indicates overlapping reflections.

variants are possible within a given hexagonal grain: AB, BC and CA. If two different variants form within a given grain they will possess a twin relationship with each other. Mitchell *et al.* [34] suggest that their observation of $\{110\}$ twins in the tetragonal MoSi_2 phase is a direct consequence of the hexagonal-to-tetragonal phase transformation. Figure 11 shows a nodule of MoSi_2 containing a twin; each MoSi_2 nodule examined, when suitably oriented, displayed twins. Figure 13(a) shows a $[110]$ microdiffraction pattern from one side of the twin plane and Fig. 13(b) shows a $[111]$ selected area diffraction pattern (SADP) from the other side. Figure 13(c) shows a composite SADP across both sides of the twin, and Fig. 13(d) shows the indexing of the composite pattern; the twin boundary is parallel to $(1\bar{1}0)$ which is common to both sides of the twin, and the (004) plane of one variant is parallel to the (112) plane of the other. The crystallographic nature of the twin was further analyzed by tilting one variant into the $[001]$ orientation, shown in Fig. 14(a), and the other variant was oriented along the $[331]$ axis [Fig. 14(b)]. Figure 14(c) shows the combined SADP taken across the twin in this orientation, and Fig. 14(d) shows the indexing of Fig. 14(c). The twin boundary is still parallel to (110) and common to both variants, while (130) of one variant is parallel to (013) of the other. These results are consistent with the analysis of Mitchell *et al.* [34] and suggest here that the nodules of MoSi_2 were formed from the liquid state, solidified as hexagonal. β - MoSi_2 , which subsequently transformed to the low-temperature, tetragonal, α - MoSi_2 . In addition, these results are consistent with the phase equilibria discussed by Boettinger *et al.* [33] for MoSi_2 , particularly with regard to the C40 to C11_b polymorphic transformation.

3.2. Static synthesis (diffusion couple) experiments

The morphologies of the partially-reacted regions in the Nb–Si and Mo–Si systems have unique features that are indicative of the mechanisms operating. The profuse presence of NbSi_2 and MoSi_2 nodules at the Nb–Si and Mo–Si interfaces, and, more importantly, interspersed in the silicon are a unique aspect of shock-induced chemical reactions. In order to both compare reaction mechanisms and assess the kinetics of reaction under conventional heat treatment, in the solid state, pieces of niobium and silicon were polished flat, clamped together, and then encapsulated. These diffusion couples were annealed at 1200°C for different times, sectioned, and analyzed. Figure 15(a) shows typical reaction layers that formed as a result of solid-state diffusion (in this example the couple was annealed at 1200°C for 2 h). The interdiffusion resulted in the formation of a thick layer of NbSi_2 , adjacent to the silicon sample, followed by a lamellar eutectic structure of Nb_5Si_3 in NbSi_2 , growing from a layer of Nb_5Si_3 adjacent to the pure Nb sample. These reaction products and morphologies are consistent and predictable from the Nb–Si phase diagram. The

thicknesses of the product layers (excluding the eutectic region) as a function of time for each of the diffusion couples fabricated are plotted in Fig. 15(b). The data can be easily rationalized in terms of a simple diffusion equation

$$x = k\sqrt{Dt} \quad (1)$$

where x is the thickness of the reaction layer, D is the diffusion coefficient, t is the time, and k is a parameter that is a function of the geometry, phases formed, etc. The activation energy for diffusion for these materials varies from 200 to 400 kJ/mol. Taking a weighted average (among the available data) between the activation energies for self-diffusion of silicon and niobium, a value of 350 kJ/mol is obtained. Hence

$$x = KD_0^{1/2}(e^{-\Delta Q/RT})^{1/2}t^{1/2} \quad (2)$$

By grouping the two unknown parameters k and $D_0^{1/2}$ and fitting equation (2) to the experimental results of Fig. 15(b), it is possible to predict reaction layer thicknesses as a function of time for both Nb_5Si_3 and NbSi_2 . These predicted thicknesses, for a range of temperatures below the melting point of silicon, are plotted in Fig. 15(c). The effect of temperature on the product layer thickness is very small, in the scale of Fig. 15(c). The usefulness of this plot is that it enables comparison of the amount of expected reaction product on the time scale of the shock experiments. The predicted reaction layer thicknesses, for a time of $5\mu\text{s}$ (maximum duration of stress pulse within shocked specimens) and a temperature of 1673 K [the maximum admissible temperature for solid-state process (the melting temperature of silicon = 1687 K)] are 10^{-7} and $10^{-9}\mu\text{m}$ for NbSi_2 and Nb_5Si_3 , respectively. Under shock compression, the reaction front advances by a dimension on the order of the radius of the nodules ($\sim 1\mu\text{m}$) within this same time span ($5\mu\text{s}$). Thus, the reaction rates under shock compression are 10^7 – 10^9 times higher than under static, solid-solid conditions.

3.3. Proposed reaction mechanism

The analysis of the partially-reacted regions in the Nb–Si and Mo–Si shock experiments revealed the detailed nature of the reaction sequence and mechanisms (for the sake of brevity only the Nb–Si system will be discussed below, however this analysis applies equally well to the Mo–Si system). A thermodynamic treatment of the reaction mechanism proposed below is given in a companion paper [27]. The preponderance of small NbSi_2 particles surrounded by silicon, as well as the existence of NbSi_2 particles attached to the niobium particles (Figs 3 and 4) are evidence for a reaction mechanism in which the NbSi_2 or MoSi_2 particles are continuously being generated at the interface and ejected into the (molten) silicon. Thus, no permanent diffusion barrier that would slow down the reaction process is formed, and reaction can proceed at a constant rate until the entire metal

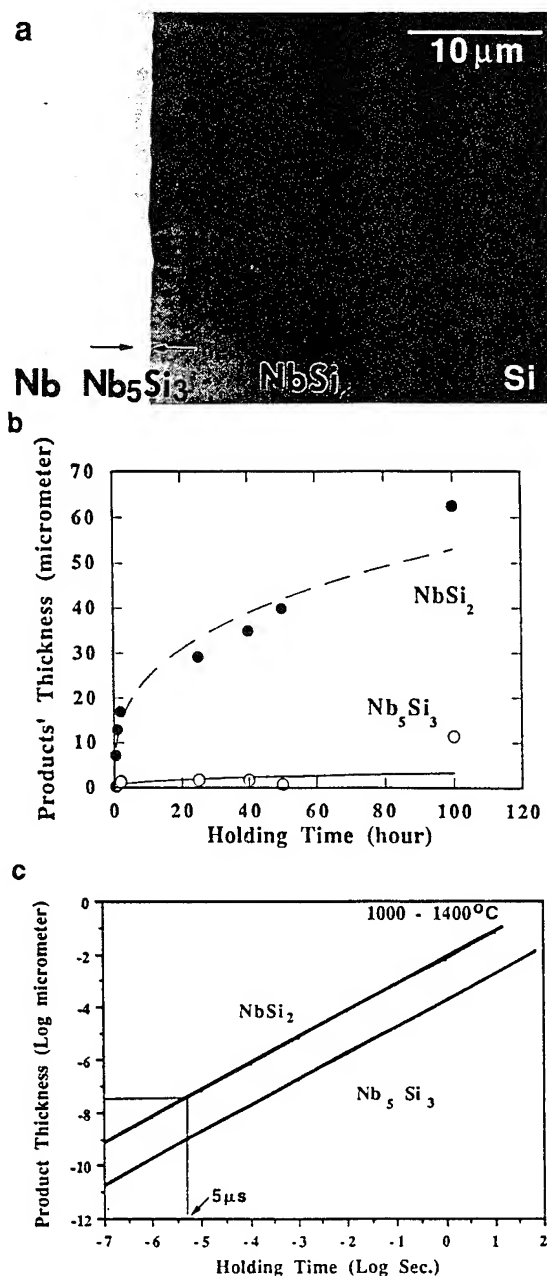


Fig. 15. (a) Backscattered electron micrograph of typical reaction layers that formed as a result of solid-state diffusion (in this example the couple was annealed at 1200°C for 2 h). The interdiffusion resulted in the formation of a thick layer of NbSi₂, adjacent to the silicon sample, followed by a lamellar eutectic structure of Nb₅Si₃ in NbSi₂, growing from a layer of Nb₅Si₃ adjacent to the pure Nb sample. (b) a plot of the measured thicknesses of the product layers (excluding the eutectic region) as a function of time for each of the diffusion couples fabricated, the dashed and solid lines represent best fit curves. (c) is a plot of the predicted thicknesses, based on equation (2), for a range of temperatures below the melting point of silicon.

(Nb or Mo) or silicon is consumed. The shock-induced reaction is initiated along the solid metal-molten Si interface. After reaction has proceeded to a certain extent, surface (interfacial) forces become dominant, and the liquid reaction product agglomerates, forming a spherule. At this point,

reaction kinetics are drastically decreased, due to the reduction in the Nb-Si interfacial area, and solidification of the disilicide sphere starts. As the sphere solidifies, new nuclei form along the Nb-Si interface. The new nuclei grow, agglomerate into spheres when they reach a critical size, and thereby form neighboring spheres. As these neighboring spheres solidify, they exert forces on the first sphere, expelling it into the molten silicon, and thus exposing fresh surfaces. This reaction process can continue unimpeded, until the reactants are consumed. In addition, turbulent flow of the liquid silicon under shock can also contribute to the detachment of the spherules from the interface. The companion paper (Part II; [27]) presents this mechanism in detail.

4. CONCLUSIONS

1. It was possible to successfully initiate and propagate shock-induced reactions for the two systems investigated (Nb-Si and Mo-Si), and the extent of reaction was found to increase with shock energy, shock temperature, and the energy of reaction.

2. The following qualitative statements can be made: (a) as the heat of reaction increases, the shock pressure/temperature necessary for full reaction decreases, and (b) the extent of shock-induced reaction increases with shock energy, at a constant temperature, and with temperature, at a constant shock energy.

3. Electron microscopy observations reveal that the main reaction product in the partially-reacted regions is the disilicide formed from the molten state as spherules with radii of approx. 1–2 μm. These spherules are formed at the metal-Si interface and are expelled into the silicon.

4. There is clear indication that silicon melting is a prerequisite for shock-induced reactions.

5. The kinetics in static solid-state reactions were established and found to be lower, by $\sim 10^8$ compared to the kinetics in shock compression.

6. A reaction mechanism under shock compression for the metal-Si interface is proposed involving the dissolution of Nb or Mo into molten Si, producing the molten intermetallic, with its subsequent spheroidization, solidification, and expulsion into the surrounding liquid silicon melt. In this reaction mechanism a fresh solid (Nb or Mo)-liquid (Si) interface is continuously maintained, enabling a high reaction rate.

Acknowledgements—This research was supported by National Science Foundation Grant DMR 8713258 (Materials Processing Initiative), and by McDonnell-Douglas Research Laboratory. We thank the support provided by Dr B. McDonald (NSF) and by Drs C. Whitsett and P. Meschter (MDRL). The help of Dr N. N. Thadhani and of the Center of Explosives Technology Research (New Mexico Institute of Mining and Technology) Field Laboratory technicians in the execution of the experiments is gratefully acknowledged.

REFERENCES

1. S. S. Batsanov, A. A. Deribas, E. V. Dulepov, M. G. Ermakov, and V. M. Kudinov, *Combust. Explos. Shock Waves (USSR)* **1**, 47 (1965).
2. Y. Horiguchi and Y. Nomura, *Carbon* **2**, 436 (1965).
3. Y. Horiguchi and Y. Nomura, *Chem. Inds., Lond.*, p. 1791 (1965).
4. G. A. Adadurov, V. I. Gold'anskii, and P. A. Yampol'skii, *Mandeleev Chem. J.* **18**, 92 (1973).
5. G. A. Adadurov, and V. I. Gold'anskii, *Russ. chem. Revs* **50**, 948 (1981).
6. A. N. Dremin and O. N. Breusov, *Russ. chem. Revs* **37**, 392 (1968).
7. S. S. Batsanov, *Russ. chem. Revs* **37**, 197 (1968).
8. S. S. Batsanov, G. S. Doronin, S. V. Klochdov and A. I. Tent, *Combust. Explos. Shock Waves (USSR)* **22**, 765 (1986).
9. R. Graham, B. Morosin, E. L. Venturini and M. J. Carr, *Ann. Rev. Mater. Sci.* **16**, 315 (1986).
10. W. F. Hammett, R. A. Graham, B. Morosin, and Y. Horie, in *Shock Waves in Condensed Matter* (edited by S. C. Schmidt and N. C. Holmes), p. 431. Elsevier Science, Amsterdam (1988).
11. B. Morosin, R. A. Graham, E. L. Venturini, M. J. Carr and D. L. Williamson, in *Shock Waves in Condensed Matter* (edited by S. C. Schmidt and N. C. Holmes), p. 435. Elsevier Science, Amsterdam (1988).
12. B. R. Krueger and T. Vreeland Jr, in *Shock-Wave and High-Strain-Rate Phenomena in Materials* (edited by M. A. Meyers, L. E. Murr and K. P. Staudhammer), p. 245. Marcel Dekker, New York (1992).
13. B. Krueger, A. Mutz and T. Vreeland Jr, *Metall. Trans.* **23A**, 55 (1991).
14. Y. Horie, R. A. Graham, and I. K. Simonsen, *Mater. Lett.* **3**, 354 (1985).
15. Y. Horie and M. J. Kipp, *J. appl. Phys.* **63**, 5718 (1988).
16. M. B. Boslough, *J. chem. Phys.* **92**, 1839 (1990).
17. Z. Iqbal, N. N. Thadhani, N. Chawla, B. L. Ramakrishna, R. Sharma, S. Skumeyev, F. Reidinger and H. Eckhardt, *Appl. Phys. Lett.* **55**, 2339 (1989).
18. N. N. Thadhani, A. Advani, I. Song, E. Dunbar, A. Grebe and R. A. Graham, in *Shock-Wave and High-Strain-Rate Phenomena in Materials* (edited by M. A. Meyers, L. E. Murr and K. P. Staudhammer), p. 271. Marcel Dekker, New York (1992).
19. L. H. Yu and M. A. Meyers, *J. Mater. Sci.* **26**, 601 (1991).
20. M. A. Meyers, L. H. Yu and K. S. Vecchio, in *Shock Compression of Condensed Matter—1991*, (edited by S. C. Schmidt, R. D. Dick, J. W. Forbes and D. G. Tasker), p. 629. North Holland, Amsterdam (1992).
21. C. S. Smith, *Trans. Am. Inst. Min. Engrs* **212**, 574 (1958).
22. E. Hornbogen, *Trans. Am. Inst. Min. Engrs* **221**, 721 (1961).
23. M. A. Meyers, *Scripta metall.* **12**, 21 (1978).
24. J. Weertman, in *Shock-Wave and High-Strain-Rate Phenomena in Metals* (edited by M. A. Meyers and L. E. Murr), p. 469. Plenum Press, New York (1981).
25. W. Gourdin, *J. appl. Phys.* **55**, 172 (1984).
26. R. B. Schwarz, P. Kasiraj, T. Vreeland Jr, and T. J. Ahrens, *Acta Metall.* **32**, 1243 (1984).
27. M. A. Meyers, L.-H. Yu and K. S. Vecchio, *Acta metall. mater.* **42**, 715 (1994).
28. A. B. Sawaoka and T. Akashi, U. S. Patent 4655830 (1987).
29. F. R. Norwood and R. A. Graham, in *Shock-Wave and High-Strain-Rate Phenomena in Materials*, p. 989. Marcel Dekker, New York (1992).
30. R. P. Elliot and F. A. Shunk (contributing editors), *Bull. Alloy Phase Diagr.* **2**, (1981).
31. B. F. Buxton, J. A. Eades, J. W. Steeds and G. M. Rackman, *Phil. Trans. R. Soc.* **281**, A1301, 171 (1976).
32. P. Villars, *Pearson's Handbook of Crystallographic Data for Intermetallic Phases* (edited by P. Villars and L. D. Calvert), Am. Soc. Metals, Metals Park, Ohio (1985).
33. W. J. Boettinger, J. H. Perepezko and P. S. Frankwicz, *Mater. Sci. Eng.* **A155**, 33 (1992).
34. T. E. Mitchell, R. G. Castro and M. M. Chadwick, *Phil. Mag.* **A65**, 1339 (1992).

Modeling Powder Compaction by Element Dynamics.

S.Psakhie*

North Carolina State University, Raleigh, NC

Shock wave loading is widely used a way to create chemical synthesis in powder mixtures [1-3]. A great number of local active centers or hot spots, here chemical reaction occurs, are generated due to the shock compression. Such effects are closely connected with nonhomogeneous structure of the powder mixture. The last leads to localization of the deformation and fracture on the different structural levels [4-8] and in its turn to arising of the hot spots on micro- and mezo- levels.

The problem of hot spot initiation has been studied extensively by both theoretical and experimental methods [6].

Computer simulation methods are very usefull for understanding of the specific mechanisms of hot spots initiation. This approach allow to test influence of the different conditions of the loading and different initial structures on the behaviour of the nonhomogeneous medium. The molecular dynamics method (MDM) is common for modeling on micro-level [4-6,8,9]. But we do not commonly accepted method to simulate behaviour of the nonhomogeneous media on macro- and mezo- levels.

In this paper Element Dynamics Method (EDM) [5,8] is described as method to simulate nonhomogenous media on macro- and mezo-levels.

Typically one of the most aims of computer simulation to study the temporal - spatial evolution of the investigated object. In our case, if we use Element Dynamics Method, the object (non-homogenous medium) is represented as a system of particles or elements. Each element has ability to move as whole (translational mode) and rotate around its own center (rotational mode).

Each element has its own size - factor, mass and tensor of the moment of inertia.

In order to describe state and behaviour for each element at different time we use spatial coordinates, rotation angles, translation velocity and angle velocity.

* On leave from Russian Materials Science Center, Tomsk, Russia.

One of the most assumption of the EDM is description of the normal interparticles forces in framework of interparticle pair potential approach.

It should be noted that EDM is usable as MDM. To do this would require only to exclude the rotational equations of motion.

The influence of macro-defects, for example pores, on the energy spatial distribution are discussed. The results of the simulation for shock compression of the particles with microcrack showed that such defects produce localization of the deformation on the mezo - level and arise the mezo - hot spots.

References

- [1] M.B.Boslough and R.A.Graham, Chem.Phys.Lett. 1985, v.121, p.446.
- [2] Y.Horie and A.B.Sawaoka, Shock compression chemistry of materials. 1993, KTK Scientific Publishers, Tokyo.
- [3] S.S.Batsanov, Russian Chemical Reviews, 1986,v.55,p.297.
- [4] V.Yu.Klimenko, M.A.Iakovenctev, A.N.Dremin, Chem.Phys. (Russia) 1993,v.12,p.671.
- [5] V.E.Panin,V.A.Klimenov,S.G.Psakhie, New materials and technologies, 1992, Nauka, Novosibirsk.
- [6] D.H.Tsai, J.Chem.Phys.1991, v.95,p.7497.
- [7] S.I.Negreskul,S.G.Psakhie,S.Yu.Korostelev, in Shock Compression of Condensed matter, Ed.S.C.Schmidt, J.N.Johnson,L.W.Davison,1990,Elsevier Science Publisher B.V.,N.Y.
- [8] S.G.Psakhie,S.Yu.Korostelev,S.I.Negreskul etal., Phys.Stat.Sol. 1993, v.176b, p.k41.
- [9] U.Landman, in Computer Simulation Studies in Condensed Matter Physics:Recent Developments, Ed.D.P.Landau, K.K.Mon and H.B.Schuttler, 1988, p.108.

Modeling Physical and Chemical Transformations

N. Akhmadeev*

North Carolina State University, Raleigh, NC

This report is devoted to theoretical studies of mechanical and physical-chemical processes taking place under shock waves in condensed media. Shock waves may trigger phase transitions and chemical reactions in solids. These transformations may also have a very strong influence upon shock waves propagation. For analyses of these processes the mathematical model was developed by methods of the mechanics of multiphase (heterogeneous) medium. Traditional activities with explosions and high-speed impact and creation of new technological processes are related to these investigations.

A model is presented for two phase solids that takes into account of possible physical and chemical transformations under shock loading when the effects of strength of solid are still important. One-dimensional, non-stationary numerical code is considered with application to plane collision of two plates, initiation and propagation of a condensed explosive detonation, and interaction between detonation wave and metal in the contact explosion. Significant parameters pertinent to the development of flow field are evaluated. On the basis of these results a theoretical method of research is proposed for the study of the kinetics of phase transition and chemical reaction.

The report has been selected from the investigations of shock-waves processes in solid with phase transitions, chemical reactions and structural transformations at Institute of Mechanics of Moscow University and Institute of Mechanics at Ufa Branch of Russian Academy of Science by academician R. Nigmatulin and myself some times ago.

* On leave from the Institute of Mechanics at Ufa Branch of Russian Academy of Science, Ufa, Russia

Nail Akhmadeev
Professor, Dr. Sci. (Phys. & Math.)

Modeling

Physical and Chemical Transformations

1. Introduction

2. Equations of Model

3. Applications

3.1. Numerical Modeling of the Initiation of an Explosive Charge Detonation and Interaction between Detonation Wave and Solid in the Contact Explosion

3.2. Phase Transitions in Iron under Shock Waves

3.2.1. Numerical Analysis of the Pressure-Measurement Results Based on the Manganin-Technique

3.2.2. Numerical Analysis of Experiments Based on Use of the Laser Interferometr for Measurement of the Free-Surface Velocity at the Time

3.2.3. Numerical Analysis of the Residual Effects of Post Shock Iron and Low Carbon Steel Samples

4. Conclusion

Mixture Representation

$$\rho = \sum \rho_i = \sum \rho_i^0 \alpha_i ,$$

$$\rho_i^0 = \frac{m_i}{V_i} ,$$

$$\alpha_i = \frac{V_i}{V_{\text{total}}} .$$

m_i , v_i - mass and volume of i-th phase.

Conservation Equations

Equations of mass
in the first and second phases

$$(C. 1) \quad \frac{\rho_0}{\rho} \frac{\partial \rho_1}{\partial t} + \rho_1 \frac{\partial v}{\partial r} + \frac{\rho_0}{\rho} J_{12} = 0,$$

$$(C. 2) \quad \frac{\rho_0}{\rho} \frac{\partial \rho_2}{\partial t} + \rho_2 \frac{\partial v}{\partial r} - \frac{\rho_0}{\rho} J_{12} = 0,$$

Equation of momentum for the entire mixture

$$(C. 3) \quad \rho_0 \frac{\partial v}{\partial t} = \frac{\partial \sigma^{11}}{\partial r},$$

Equation of energy for entire mixture

$$(C. 4) \quad \frac{\rho_0}{\rho} \left[\rho_1 \frac{\partial e_1}{\partial t} + \rho_2 \frac{\partial e_2}{\partial t} + (e_2 - e_1) J_{12} \right] = \sigma^{11} \frac{\partial v}{\partial r}.$$

Additional Relations

Euler stress

$$(A. 1) \quad \sigma^{11} = -p + \tau^{11}.$$

Condition of phase joint deformation

$$(A. 2) \quad p = p_1(\rho_1^0, T) = p_2(\rho_2^0, T) .$$

Hook's Law

$$(A. 3) \quad \frac{d\tau^{11}}{dt} = \frac{4}{3} \mu \frac{\rho_0}{\rho} \frac{\partial v}{\partial r}, \quad \tau^{11} < \tau^*$$

μ, τ^* - shear modules and elastic limit

Kinetic Relations

$$(A.4) \quad J_{12} = j_{12} - j_{21} \quad .$$

1. Chemistry (irreversible)

$$(A.41) \quad j_{12} = \frac{p_{10}}{\tau_{12}} \quad , \quad j_{21} = 0; \quad \tau_{12} - \text{time constant.}$$

2. Phase Change (Quasi - Reversible)

$$(A.42) \quad j_{12} = \alpha_1 j_{12}^0 \left\{ 1 - \exp \left[- \left(\frac{p - p_s}{\Delta_{12}} \right)^{n_{12}} \right] \right\} ,$$

$$j_{21} = \alpha_2 j_{21}^0 \left\{ 1 - \exp \left[- \left(\frac{p_s - p}{\Delta_{21}} \right)^{n_{21}} \right] \right\} ,$$

p_s - phase change pressure (on the phase equilibrium curve) ,

j_{21}^0 , n_{21} , Δ_{21} - kinetic constants.

Equations of State

$$(A.5) \quad e = e_p(\rho^0) + e_T(T) ,$$

$$p = p_p(\rho^0) + p_T(\rho^0, T) .$$

Elastic parts

$$(A.51) \quad e_p = 3A(b\rho_0^0)^{-1} \exp[b(1 - x^{1/3})] - 3K(\rho_0^0)^{-1} x^{-1/3} ,$$

$$p_p = - \frac{de_p}{dx} ; \quad x = \frac{\rho_0^0}{\rho^0} .$$

Thermal parts

$$(A.52) \quad e_T = c_v T ,$$

$$p_T = \gamma(\rho^0) \rho^0 e_T .$$

3. Applications

The model was use for a numerical description a detonation in charges of crystalline and porous hexogene, interaction between detonation wave and solid in the contact explosion and phase transitions in Armko-iron under shock wave, initiating by impact of projectile or impact of detonation wave.

4. Conclusion

The numerical study of the detonation waves and the shock-wave motion with phase transitions, and comparison with experimental data, prove that the model of two phase condensed continuous medium enables the shock-wave phenomena with physical-chemical transformations to be described in exactly the same manner.

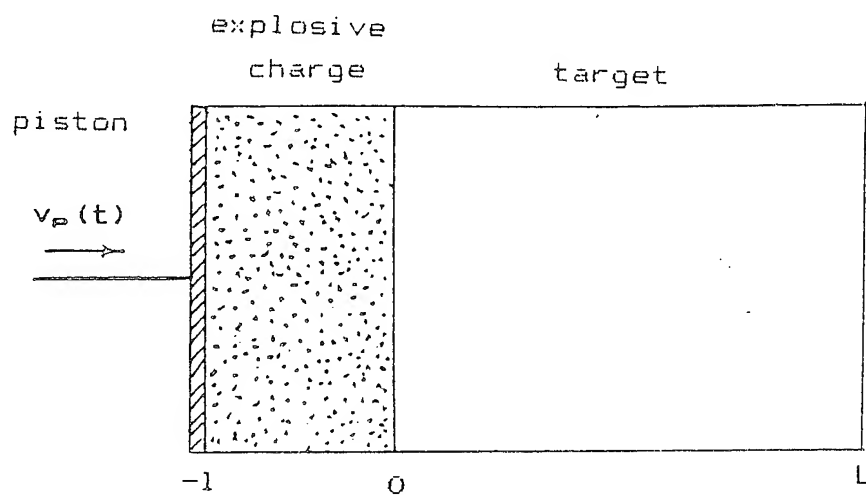


Figure 1 . Schematic of initiation of detonation in explosive charge by piston and impact of detonation wave against a solid.

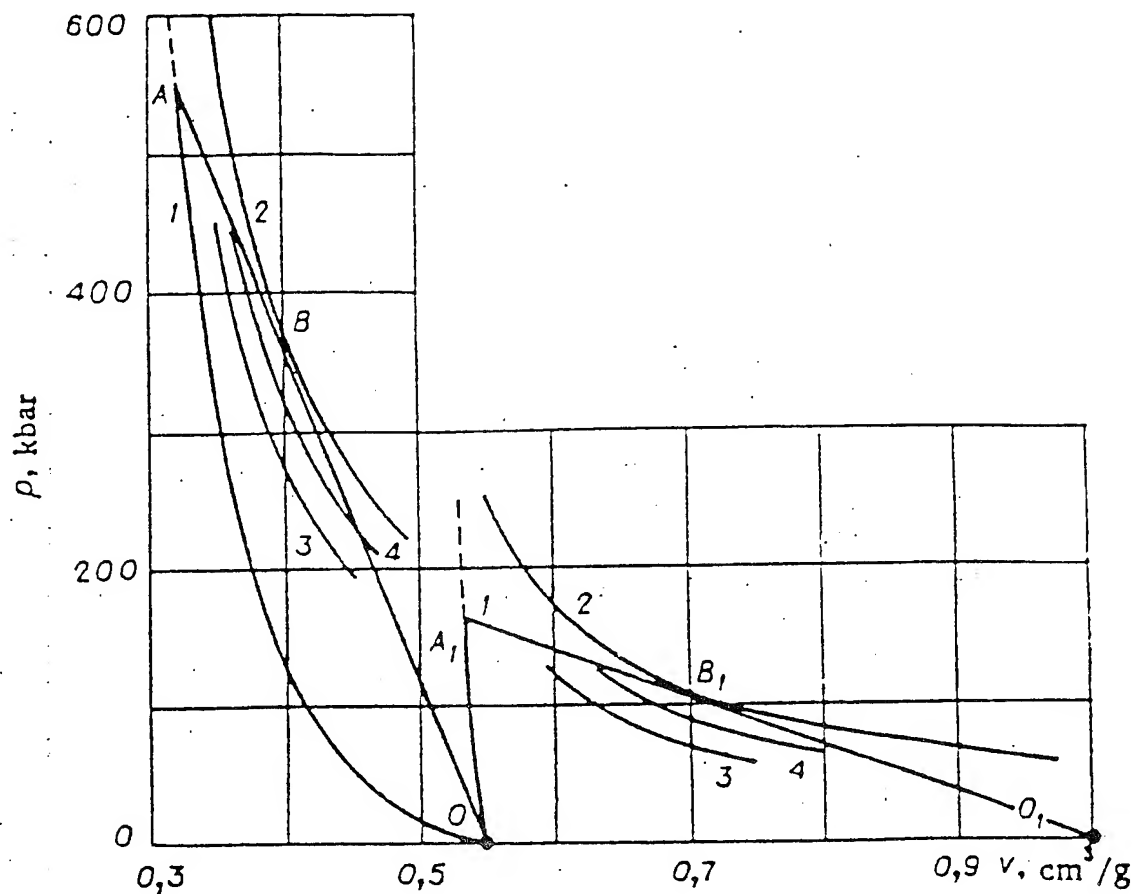


Fig. 2. The p-V diagrams for the detonation of crystalline and porous ($m=1.82$) forms of hexogene: 1) shock-wave adiabat for unreacted hexogene; 2) detonation adiabat for the products of hexogene on complete release of the explosion energy $Q_f(\rho_{10}, T_0)$; 3 and 4) intermediate detonation adiabats for the products with 50 and 75% release of $Q_f(\rho_{10}, T_0)$; OBA) Michelson line.

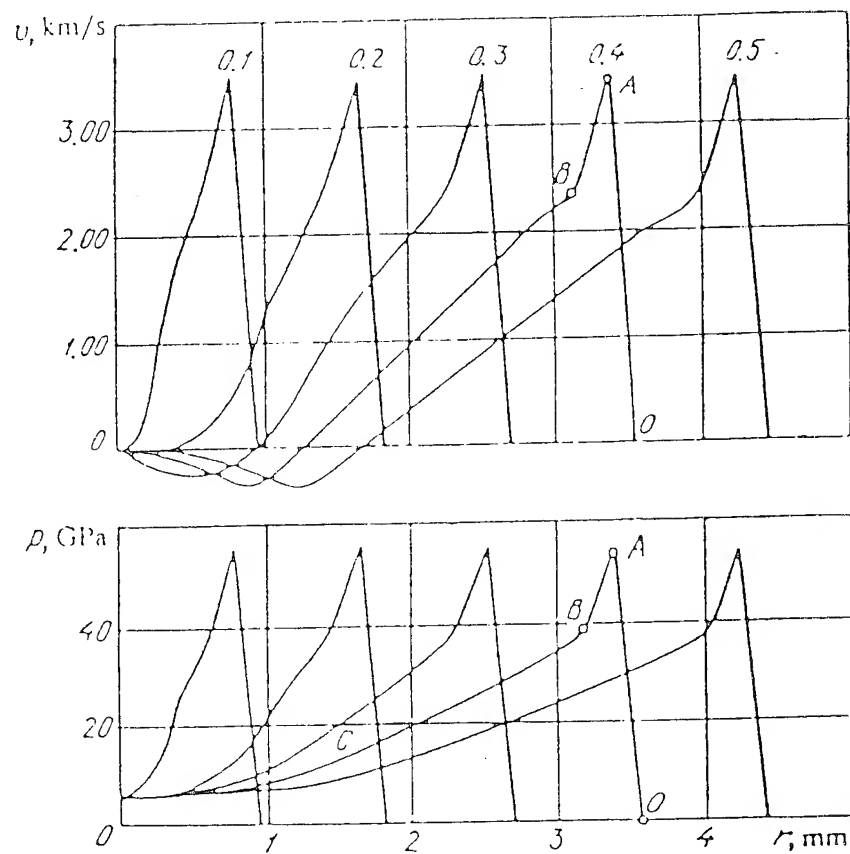


Fig. The substance bulk velocity v diagrams, and the pressure p diagrams in the detonation wave induced by a solid ($m_0 = 0$) hexogen ($\rho_0 = 1820$ kg/m) charge and propagating from a stationary wall, at different points in time t , in microseconds (indicated on the graphs).

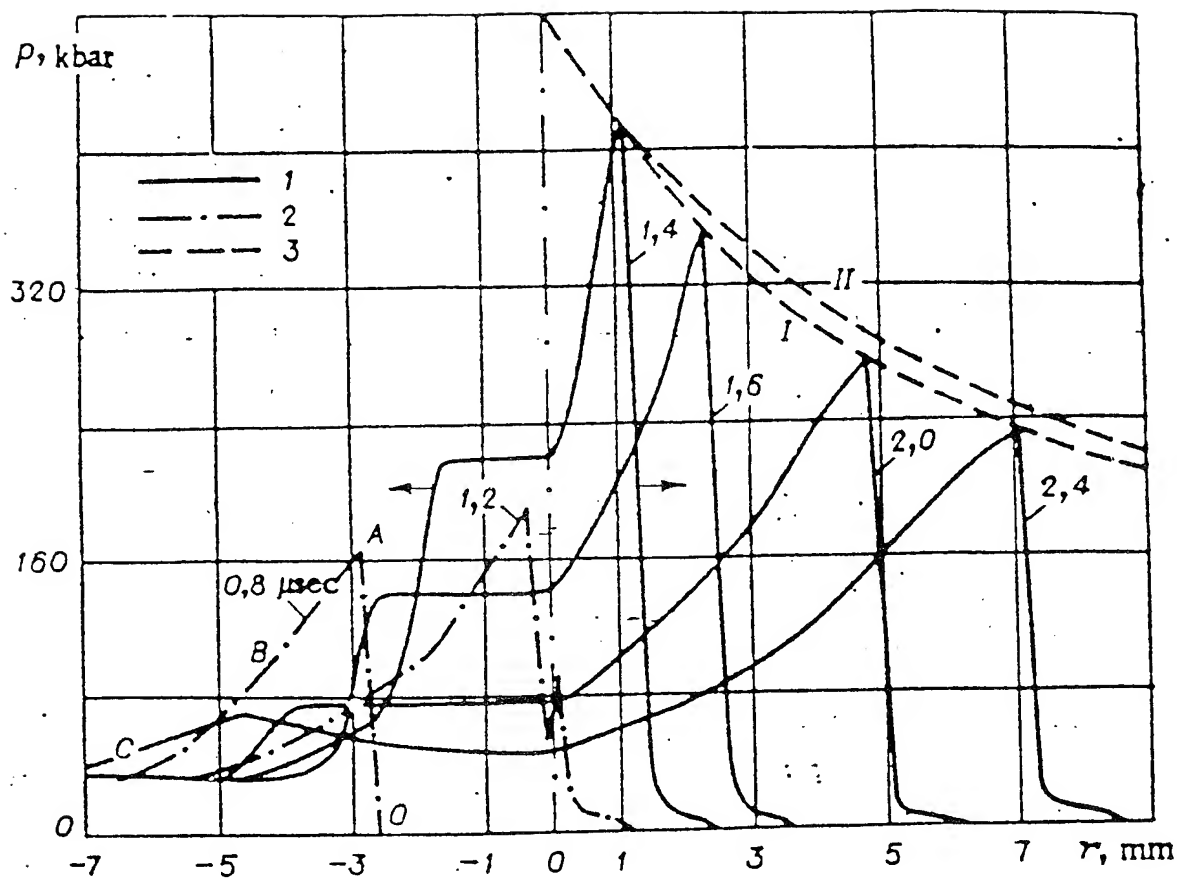


Fig. 4. Waveforms of pressure p arising from the detonation of a surface charge of hexogene ($m=1.82$, $l=7$ mm) on a specimen of nickel at various instants: 1) shock waves in the detonation products from hexogene and nickel; 2) detonation wave propagating through explosive (from left to right); 3) decay of shock wave with depth in specimen.

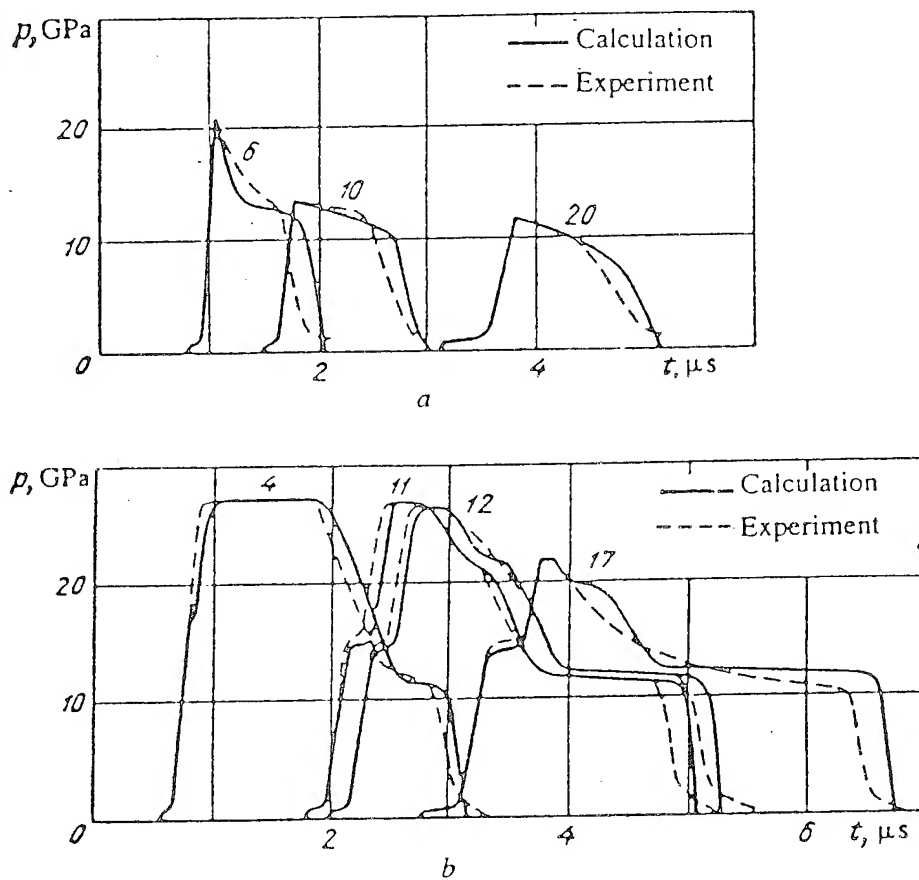


Figure 5. The analytical and experimental pressure oscillograms at various depths in an iron specimen during a flat shock with a velocity v_0 by an aluminum plate of thickness l . The figures denoting the curves correspond to depths in mm; a is for $v_0 = 3.5$ km/s, b is for $v_0 = 2.1$ km/s, $l = 7$ mm.

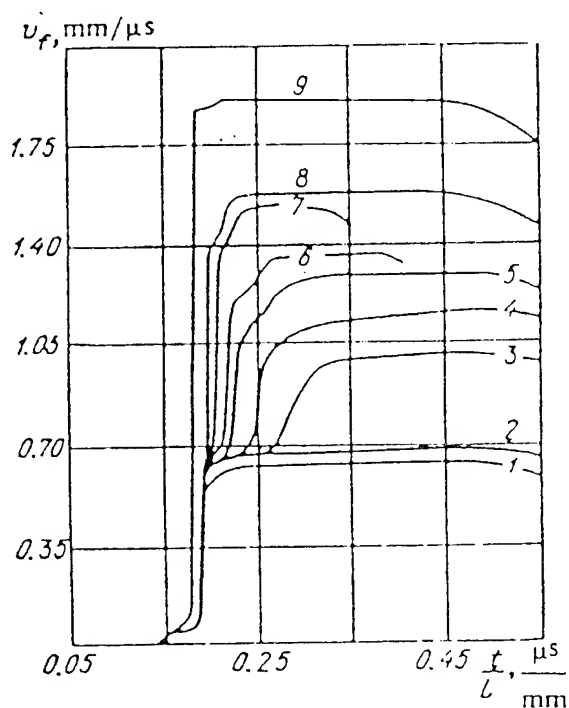


Figure 6. The analytical and experimental oscillograms of the variation of the velocity of the iron target free surface (which is opposite to the surface of contact with the iron striker) which reveal a satisfactory agreement. The numerical indicators relate to the following values of the striker velocity and target thickness (v_0 in km/s ; L in mm): 1) (0.612; 6.37), 2) (0.671; 6.38), 3) (0.992; 6.32), 4) (1.15; 6.31), 5) (1.29; 6.31), 6) (1.40; 15.8), 7) (1.56; 19.8), 8) (1.57; 6.37), 9) (1.90; 6.35).

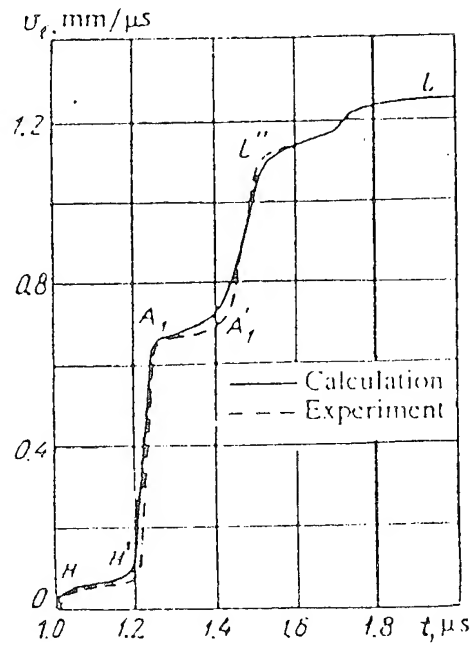


Figure 7 . Analytical and experimental oscillograms of the free-surface velocity variation for conditions related to line 5 in Fig. ($v_0 = 1.29 \text{ km/s}$, $L = 6.31 \text{ mm}$).

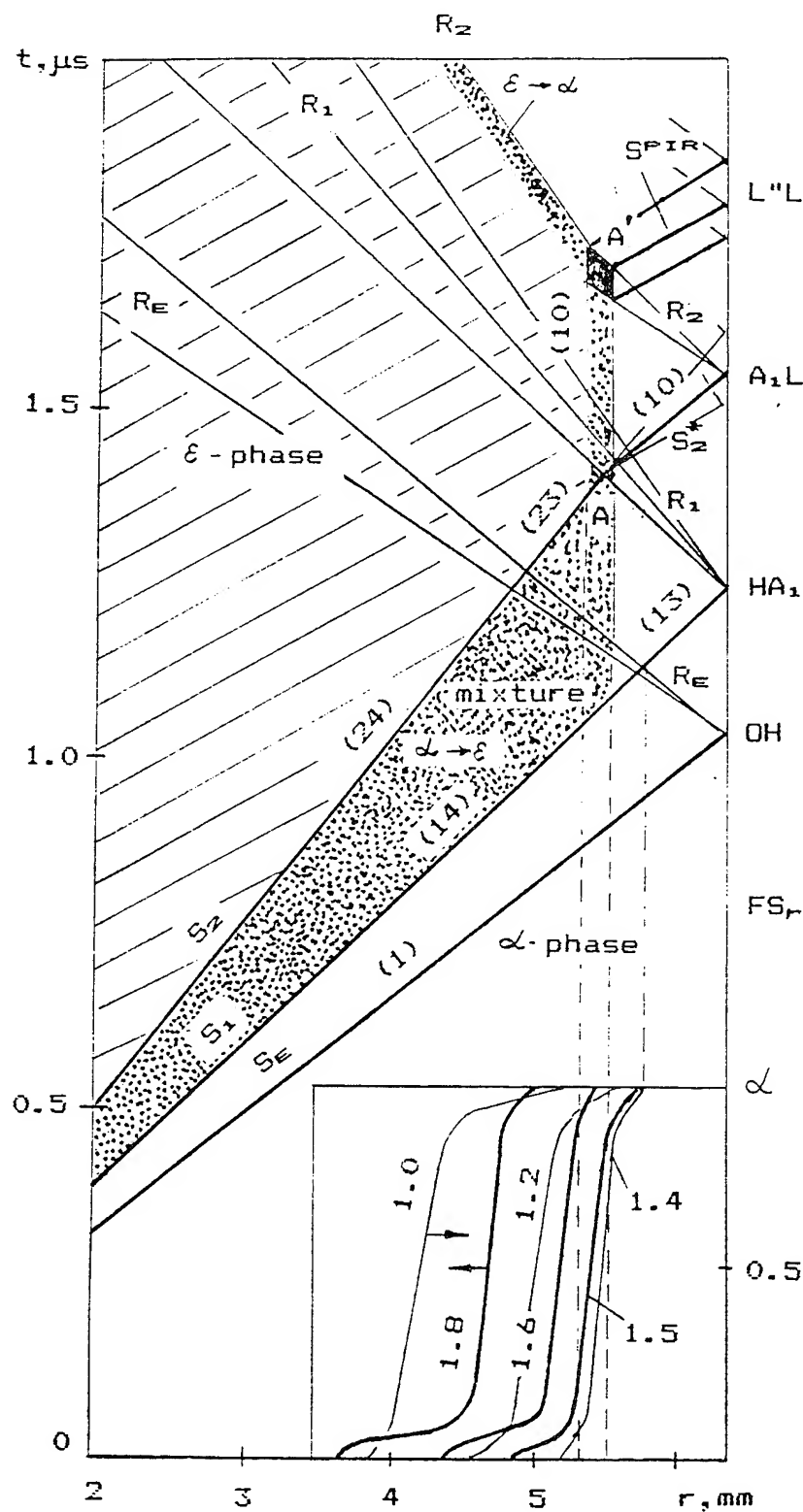


Figure 8. r - t scheme of wave propagation in iron target for the 5-th (see Fig.) experiment. White zone is δ -phase of iron, striped zone is ϵ -phase, dotted zone is a zone of δ and ϵ phases mixture. Waves S_E , R_E , S_1 , R_1 and S_2 , R_2 are corresponds elastic, first plastic and second plastic (phase transition) compression and rarefaction waves. Wave S_2^* is the part of the wave S_2 after unloaded by wave R_1 . Figures in brackets are the pressure of waves in GPa. Wave SP_{IR} is the part of wave R_2 which is reflected back from "softer" layer AA' near the point A' . Point OH corresponds to the reflection of the S_E wave from free surface FS_r , HA_1 corresponds to the reflection of the S_1 wave, A_1L'' corresponds to the reflection of the S_2^* wave, $L''L$ is the result of reflected back (to FS_r) part of R_2 wave from "softer" layer. The diagrams of volume concentration of the δ -phase of iron are represented below (at the right corner) at the different points in time (in μs).

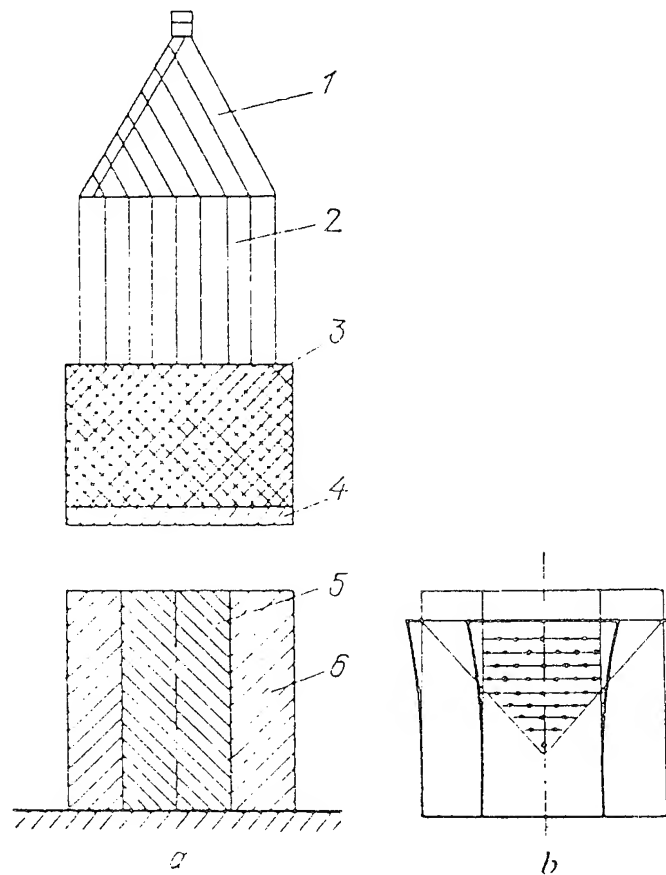


Figure 6 Schematic of the experiment (a) on the hardening of a specimen by a flat impact by a plate accelerated by an explosion; schematic of the hardness measurement (b) in the longitudinal section of the treated specimen; 1) linear wave generator, 2) plane wave generator, 3) explosive charge; 4) accelerated plate (striker), 5) specimen subjected to hardening (target), 6) casing designed for protection against the lateral unloading.

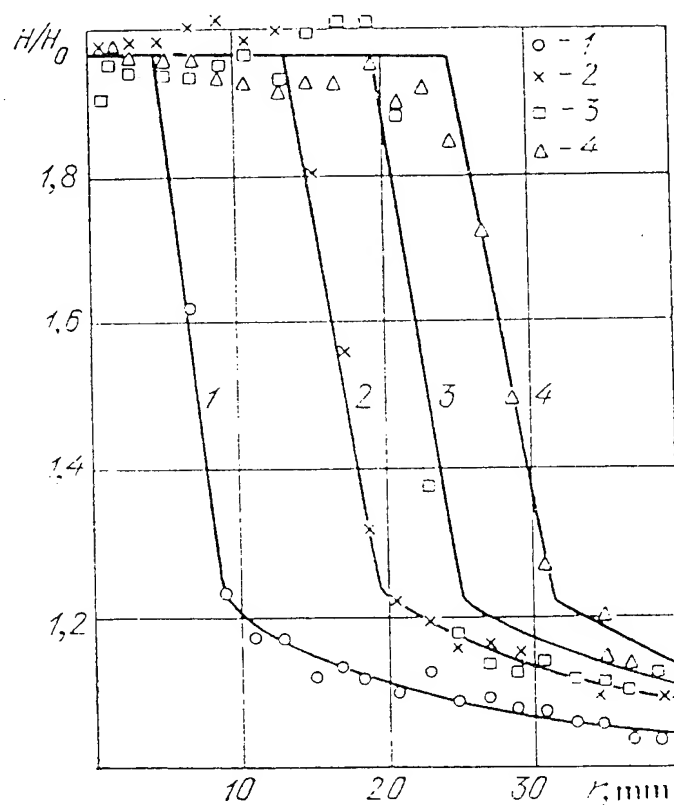


Figure 10 Hardness variation with specimen depth: the specimen (made of Armeo iron) is hardened by a striking plate (made of the same material) of thickness 3 mm, and moving with speeds: $v_n = 1.45$ km/s (curve 1), 1.95 km/s (curve 2), 2.4 km/s (curve 3), and 2.8 km/s (curve 4).

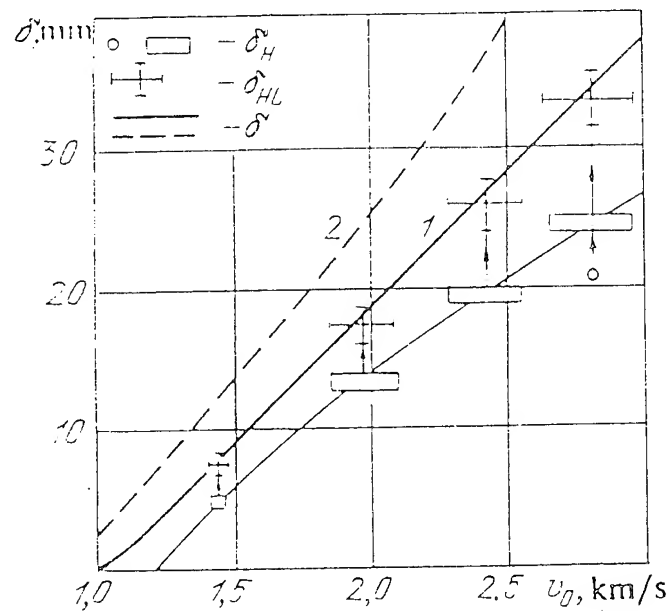


Figure 1. Relationship between the estimated depth δ of the complete-phase-transition zone (curves 1 and 2) in the target made of Armcro iron and the velocity of mutual collision v_0 (striker-iron plate of thickness 3 mm, and diameters of 90 and 130 mm); dependence of the experimental depth δ_H of the permanent-hardening zone (rectangles), and the Lagrangian depth δ_{HL} of the last zone (crosses) on the velocity v_0 . The size of rectangles and crosses reflects possible measurement errors. The circles indicate the experimental result with a smaller target diameter (90 mm) when, at the shock velocity $v_0 = 2.8$ km/s, the effect of the side unloading upon the phase transition process $\alpha \rightarrow \epsilon$ becomes noticeable in the center portion of the specimen (see Fig. 3.5.5). Line 1 corresponds to the evaluation based on the phase transition $\alpha \rightarrow \epsilon$ kinetics, the dashed line 2 corresponds to the evaluation based on the linear kinetics.

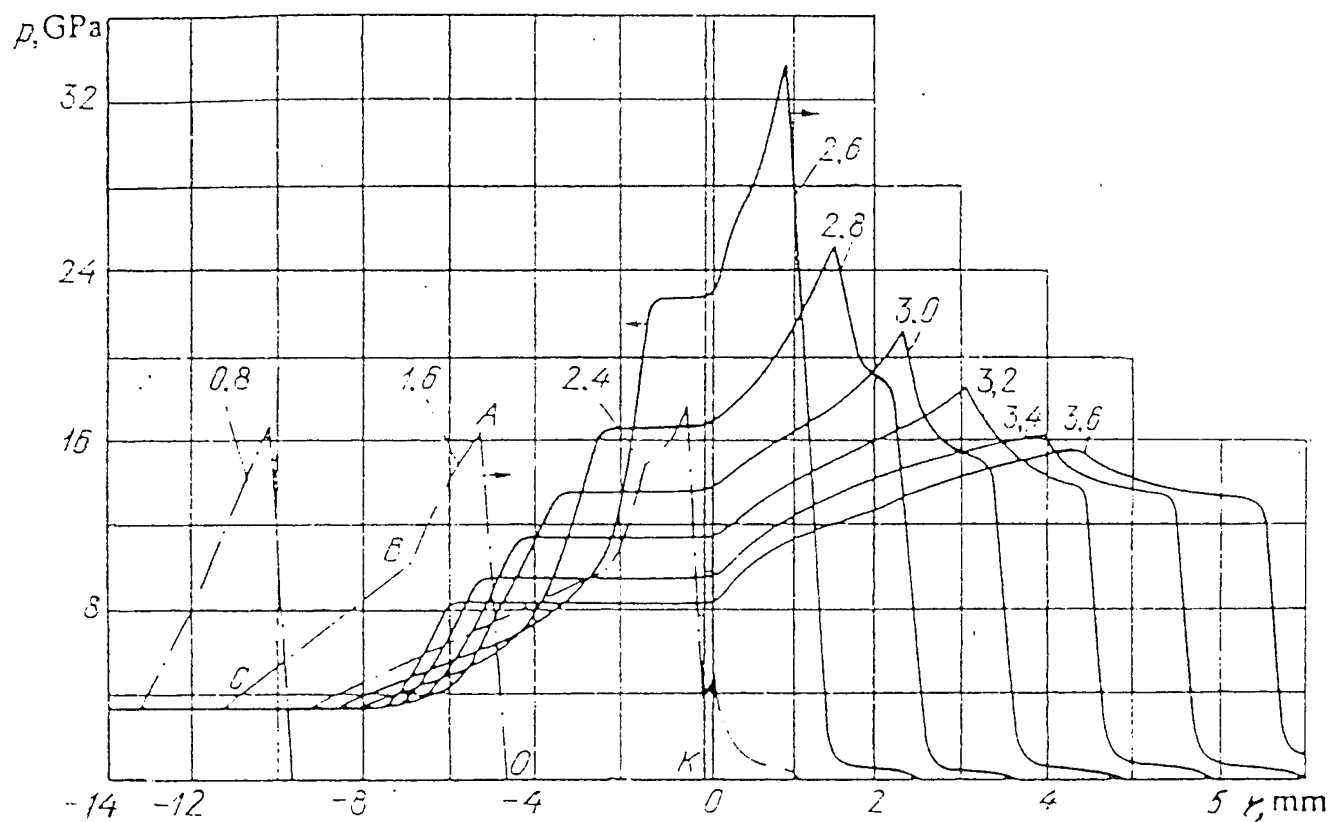


Figure 10. The pressure p diagrams resulting from detonation of the pressure charge (hexogen, $\rho_0 = 1000 \text{ kg/m}^3$, $l = 14 \text{ mm}$) applied to an iron specimen ($r > 0$) at different points in time t , which are identified by figures (in μs) on the curves. The detonation wave propagating through the explosive substance is shown by dashed lines. The shock waves in the detonation products of hexogen and in iron are represented by solid lines.

a - depth of complete $\alpha \rightleftharpoons \varepsilon$ phase change

b - zone of incomplete $\alpha \rightleftharpoons \varepsilon$ phase change

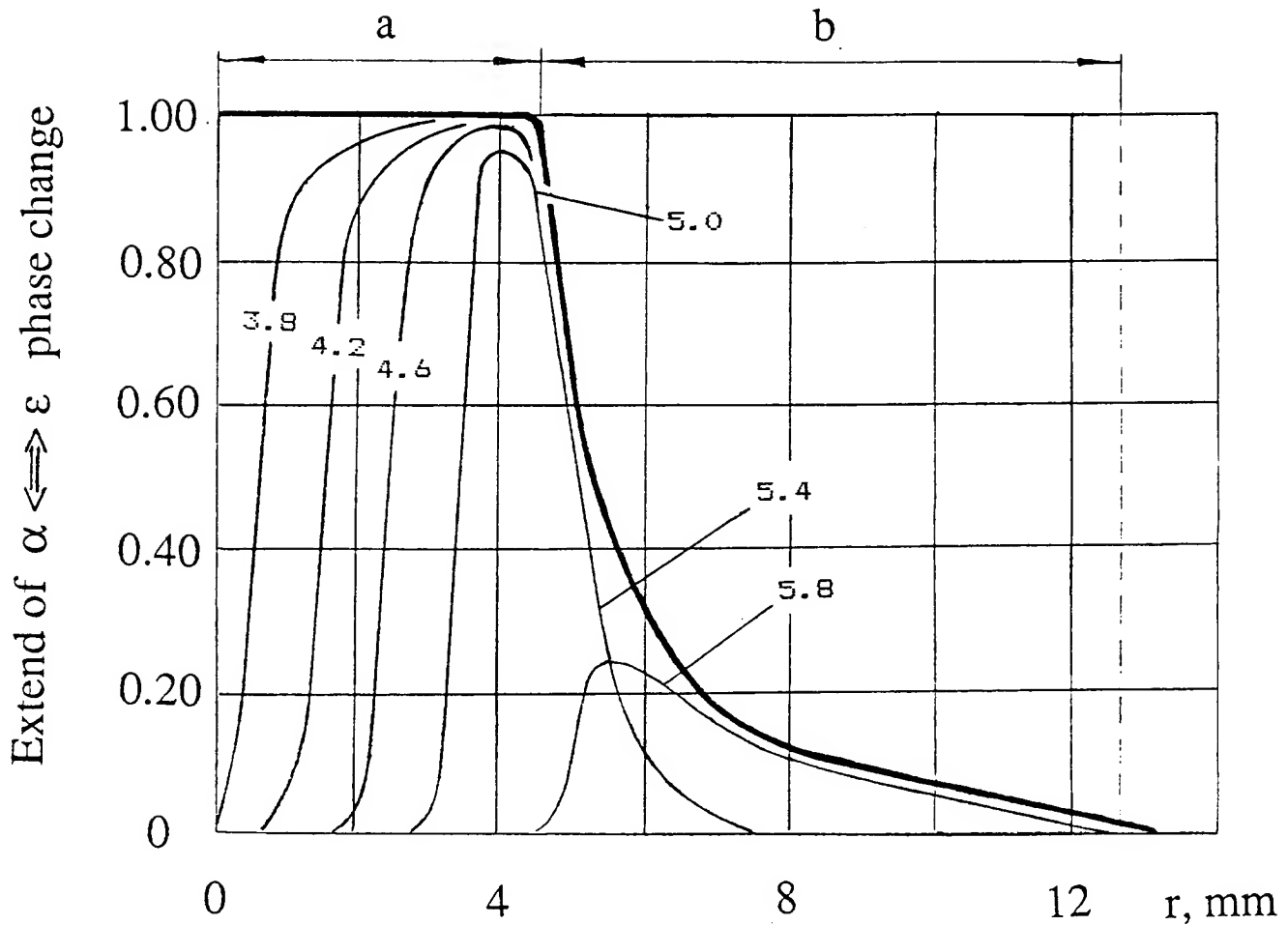


Figure 13. The diagrams of the extend $\alpha \rightleftharpoons \varepsilon$ phase change at different points in time (in μs) during the detonation of a pressure charge of porous (1.00 g/cm^3) hexogene with length $l_e = 14 \text{ mm}$.

SESSION - II

REAL-TIME IN-SITU MEASUREMENTS

SESSION II: REAL-TIME IN-SITU MEASUREMENTS

D.P. Dandekar: SESSION CHAIR COMMENTS

Shock processing and synthesis of materials can involve very rapid shock-induced chemical reactions. It, is therefore, imperative to develop time resolved measurements of parameters which influence such reactions. The deliberations and discussions that took place during the workshop on the Shock Synthesis of Materials brought out one very important point which has a direct bearing on in-situ measurements. Shock induced chemical reactions occurring in a material system are inherently heterogeneous both spatially and temporally. The net effect of this observation is that real time in-situ measurements like (i) measurement of temperature by means of optical pyrometer, (ii) time resolved optical spectroscopy and x-ray diffraction measurements which provide direct observation of atomic/molecular mechanisms governing the chemical state in the shock environment and rate of chemical reactions made in a single location/region of reacting system may not be representative of the whole system. These measurements are absolutely essential to improve our understanding of the fundamentals of shock induced chemical reactions. The challenge is to make them useful to investigate the variation in the kinetics of shock induced reaction in a chemical system in material and time coordinate.

The investigators who presented their work in the session on "Real-Time In-situ Measurements" were all well aware of the problem. For example, existence of rate dependency of chemical and mechanical equilibration, multiplicity of reaction products in various reacting systems, and non-uniformity of temperature in the reacting system were common themes that Anderson, Boslough, Gupta addressed in their talks. Boslough was probably the most candid about his own pioneer work dealing with the pitfalls of obtaining reliable measurements of temperature in a system that can be confidently used for either calculations or understanding the reactions taking place in a material medium. It appears to this reviewer that a measurable improvement in the status of the real time in-situ measurement technique will come about only if the reacting system chosen is a simple one which does not produce a multitude of products under the spatially and temporally varying pressure and temperature present in the reacting system. In absence of such a strategically evolved set of measurements, we will have to await a breakthrough or a novel and very attractive material due to serendipitous circumstances. But in the latter case we will have a hard time justifying such an approach to develop a better understanding of the shock induced chemical synthesis. It seems odd that infrared spectroscopy which is relatively easy to use and can be used in opaque material systems has not been so far used to probe shock induced chemical reactions.

DYNAMIC PORE COLLAPSE IN RATE DEPENDENT MATERIALS AND THEIR IMPLICATIONS IN SHOCK SYNTHESIS

G. Ravichandran

Graduate Aeronautical Laboratories
California Institute of Technology
Pasadena, CA 91125

A model for shock consolidation of porous powders is presented and their implication on shock synthesis of materials is discussed. Dynamic pore collapse in porous materials is studied by analyzing the finite deformation of an elastic/viscoplastic spherical shell under impulsive pressure loading. Effects of dynamic loading rate, pore size, initial porosity, strain-rate sensitivity, strain hardening, thermal softening and mass density of the matrix material on the pore collapse process are examined and results are compared with those from quasi-static analyses of both rate-independent and rate-dependent matrix materials. Dynamic (inertial) effects are found to be significant or even dominant in certain shock wave consolidation conditions. An approximate method is proposed to incorporate dynamic effects into quasi-static pore-collapse relations of viscoplastic matrix materials. Implications of results of current study are discussed in terms of understanding the processes of shock wave consolidation of powders (Tong and Ravichandran, 1993).

The rise time of a strong shock wave propagating through a highly porous material is related to the pore collapse time of powders. The analysis explains the relatively large rise times observed during consolidation of powders. The shock rise time is shown to decrease with increasing pressure and becomes relatively constant at high shock pressures. The rise time is found to have a weak dependence on the initial temperature of the powder. Our pore collapse analysis is contrasted with existing models and the results are compared with existing experimental data (Tong and Ravichandran, 1994).

Scaling laws are developed for quantities such as pore collapse time and temperature distribution (reaction zone size) in relation to the initial pore and powder size. The role of heat conduction on pore collapse and temperature distribution is also critically examined. The limitations and validity of existing pore collapse models to model shock wave consolidation of powders are discussed. Recent full-scale finite element computations are presented and they confirm the essential predictions of our pore collapse model.

On the basis of our dynamic pore collapse model, it appears that a key factor in shock induced synthesis is the maximum critical temperature attained during pore collapse, which initiates the chemical reaction. It will be shown that the understanding of mechanics of pore collapse is essential in analyzing shock induced reactions. It will be also shown that the reactions could be initiated within the rise time (a fraction of a μ s) of the shock wave and the reactions may continue long after the passage of the shock wave (a few ms). The kinetics of shock synthesis is outlined based on melt diffusion and solid state diffusivity processes. On the basis of the bulk diffusivities of matter, solid state reactions during shock synthesis are ruled out and the observed reaction layer thicknesses are related to diffusion of species within the super cooled melt layer.

Experimental evidence for our proposed model for shock synthesis is shown from controlled one-dimensional experiments performed on Ti/Si, Ti/SiC and constantan/Si systems (Kruger, et al., 1992, Mutz and Vreeland, 1992 and Tong, et al., 1994). Results from detailed finite element computations reveal that the shock induced reactions are influenced by the bulk thermal quenching of the fixture and corroborative experimental evidence is presented from recent experiments performed on a Nb/Si system. Factors influencing shock induced reactions are summarized and suggestions for enhancing reactivity in powders are made.

REFERENCES

- Kruger, B. R., Mutz, A. H., and Vreeland, T. (1992) "Shock Induced and Self Propagating High Temperature Synthesis Reactions in 2 Powder Mixtures-5-3 Atomic Ratio Ti/Si and 1-1 Atomic Ratio Ni/Si," *Metallurgical Transactions-A*, 23, 55-58.
- Mutz, A. H., and Vreeland, T. (1992) "Several Techniques for One-Dimensional Strain Shock Consolidation of Multiple Cavities," in: *Shock Wave and High-Strain-Rate Phenomena in Materials*, Editors: M. A. Meyers, L. E. Murr, and K. P. Staudhammer, Marcel Dekker, New York, 425-434.
- Tong, W., and Ravichandran, G., (1993) "Dynamic Pore Collapse in Viscoplastic Materials," *Journal of Applied Physics*, 74, 2425-2435.
- Tong, W., and Ravichandran, G., (1994) "Rise Time in Shock Consolidation of Rate Dependent Powders," submitted to the *Journal of Applied Physics Letters*.
- Tong, W., Ravichandran, G., Christman, T. A., and Vreeland, T. (1994) "Processing SiC-Particulate Reinforced Titanium-based Metal Matrix Composites by Shock Wave Consolidation," to appear in *Acta Metallurgica et Materialia*.

Dynamic pore collapse in viscoplastic materials

W. Tong and G. Ravichandran

Division of Engineering and Applied Science, California Institute of Technology, Pasadena, California 91125

(Received 23 January 1993; accepted for publication 29 April 1993)

Dynamic pore collapse in porous materials is studied by analyzing the finite deformation of an elastic/viscoplastic spherical shell under impulsive pressure loading. Effects of dynamic loading rate, pore size, initial porosity, strain-rate sensitivity, strain hardening, thermal softening, and mass density of the matrix material on the pore collapse process are examined and results are compared with those from quasistatic analyses of both rate-independent and rate-dependent matrix materials. Dynamic (inertia) effects are found to be significant or even dominant in certain shock wave consolidation conditions. An approximate method is proposed to incorporate dynamic effects into quasistatic pore-collapse relations of viscoplastic matrix materials. Implications of results of current study are discussed in terms of understanding the processes of shock wave consolidation of powders.

1. INTRODUCTION

Dynamic consolidation of metallic and ceramic powders provides an alternate approach for processing materials with unique microstructures and, hence, properties.¹⁻⁶ This process holds to be a promising new technology for consolidating advanced materials such as nanophase intermetallics and composites. However, several major difficulties hinder its practical application and remain to be overcome, such as criteria for optimization of processing parameters (shock pressure, shock duration, etc.) and the cracking of compacts that occurs during shock release to ambient pressure. Researchers have continued to improve dynamic compaction fixtures, the use of cleaner powders, postconsolidation annealing or isostatic hot pressing, and other means to address these problems. However, the determination of shock consolidation processing parameters and prevention of cracking depends upon the detailed understanding of the dynamic consolidation process at both continuum and microstructural levels.

The densification and bonding of particles are accomplished by the passage of a strong shock wave through an initially porous material. During the densification most of the energy is deposited near the particle surfaces and the resulting heating produces melting of the particle surfaces that solidify rapidly via heat conduction into the interior of the particles before release of shock pressure.² The physical phenomena of such a dynamic consolidation process at the particle level are very complex and remain poorly understood. Localized energy depositions at interparticle surfaces are thought to be due to local plastic deformation and frictional sliding and contribute largely to the particle-particle bonding. Berry and Williamson⁷ presented a computer simulation of the shock wave compaction of stainless-steel cylinders by considering plastic deformation at the particle level and predicted indeed highly localized plastic deformation and large temperature rises occur at particle boundaries during consolidation. Their numerical results have been qualitatively confirmed by experimental observations.^{8,9} Several estimates of the shock wave pressure required for obtaining good compact of metallic pow-

ders (fully densified with good mechanical strength) have been proposed by Schwarz *et al.*² and Gourdin³ using an energy partition and balance approach. Ferreira and Meyers¹⁰ also used a similar energy balance approach by including the effect of the matrix material strength on the required compaction pressure for various materials. The lower bound on the shock duration is also given by Schwarz *et al.*² by requiring the duration of shock compaction pulse to exceed the time for the melt to solidify. In all of these analyses, the total energy input during shock consolidation is determined through the equation of state of porous materials, such as the one first described by Herrmann¹¹ and modified by Carroll and Holt¹² and Swegle.¹³ In these porous material models, the volume change due to pore collapse is separated from that due to volume change of the matrix material. It is assumed that the form of the function that relates pressure to specific volume and specific internal energy of porous material is the same as that of the fully densified matrix material. To complete the model, a pore-collapse relation that relates pressure p to the distention of the porous material α is needed and has generally been assumed to be an algebraic relation between pressure and distention, $\alpha = g(p)$. The matrix material is essentially treated to be elastic/perfectly plastic, rate independent, and dynamic effects are neglected. This type of equation of state of porous materials has also been commonly used in computer simulation of shock consolidation experiments.⁸

Both high-pressure loading rates and high rates of deformation are encountered in the consolidation process of powders by the passage of a shock wave. Shock pressures of 1–10 GPa or higher are commonly used and typical shock rise times are of the order of 100–1000 ns;^{14,15} thus, the typical pressure rate is 1–100 MPa/ns or higher. The initial relative density of powders used in shock wave consolidation is usually around 0.5–0.75 and hence the inelastic volumetric strain is about 0.3–0.7 after consolidation. The overall strain rate can be estimated to be of the order of 10^5 – 10^7 per second within the shock wave front (dividing the volumetric strain by the shock wave rise time).

Carroll and Holt¹⁶ showed that there is a significant difference between the static and dynamic pore-collapse relations for perfectly plastic and rate-independent matrix materials under these pressure rates of shock wave loading. It should be also noted that the matrix material model used in the dynamic analyses by both Berry and Williamson⁷ and Carroll and Holt¹⁶ is perfectly plastic and rate independent. There is increasing experimental evidence that indicates that some metals become strongly rate dependent at very high strain rates.¹⁷⁻¹⁹ While there have been some empirical and analytical formulations on the densification process of viscoplastic porous materials under quasistatic conditions,²⁰⁻²⁵ there are relatively few on the dynamic pore collapse of such matrix materials.^{8,26} The inertial effect combined with strain rate, strain-hardening, and thermal softening effects on dynamic consolidation of powders remains unclear and thus have not been included in the determination of consolidation process parameters. The applicability of relatively simple results of viscoplastic porous matrix materials under quasistatic conditions to dynamic loading conditions is also not known.

Analogous to the work by Carroll and Holt¹⁶ on the dynamic pore collapse of perfectly plastic, rate-independent materials, here the collapse of an elastic/viscoplastic spherical shell under an external impulsive pressure loading is studied. The thermal softening effect is also included by considering adiabatic heating of the matrix material due to accumulated plastic work. The collapse of a spherical shell is an idealization of the consolidation process and does not consider other effects such as the shape and distribution of pores, but it does provide a basis in terms of simple analytical and/or numerical solutions which can be readily obtained, and the effect of dynamic loading, rate-dependent, and temperature-dependent behavior of the matrix material on pore-collapse process can be directly assessed. Our results indicate that parameters characterizing strain rate sensitivity, strain hardening, thermal softening, mass density of matrix material, dynamic loading rate, pore size, and initial relative density of the porous material play a significant role on the pore collapse under impulsive pressure loading, such as the characteristic time of densification. For viscoplastic matrix materials, rate sensitivity, dynamic effects, and others should be assessed carefully in formulating a realistic p - α relation for a given material under a particular loading condition. For rate-dependent matrix materials, the densification process is significantly slowed down at high loading rates.

In the following section a complete formulation of finite elastic/viscoplastic deformation of a spherical shell is presented. In Sec. III results of a series of numerical simulations of dynamic pore collapse process are presented. Finally, discussions and conclusions of the present study are given in Sec. IV.

II. FINITE DEFORMATION FORMULATION

Following the approach used by Carroll and Holt¹⁶ and Wilkinson and Ashby,²⁰ we study the consolidation of porous materials by considering the collapse of a spherical

shell under a given external pressure loading $p(t)$. The current inner and outer radii r of the spherical shell are a and b , respectively, at the time $t > 0$. The initial inner and outer radii R are A and B , respectively (i.e., $t = 0$). The initial f_0 and current f volume fractions of porosity in the material are thus given by

$$f_0 = (A/B)^3, \quad f = (a/b)^3, \quad 0 < f_0 < 1, \quad 0 < f \leq 1, \quad (1)$$

the initial α_0 and current α distortions of the porous material are given by

$$\alpha_0 = \frac{1}{1 - (A/B)^3}, \quad \alpha = \frac{1}{1 - (a/b)^3}, \quad 1 < \alpha_0, \quad 1 \leq \alpha, \quad (2)$$

and the initial $\bar{\rho}_0$ and current $\bar{\rho}$ relative densities are given by

$$\bar{\rho}_0 = 1 - (A/B)^3, \quad \bar{\rho} = 1 - (a/b)^3, \quad 0 < \bar{\rho}_0 < 1, \quad 0 < \bar{\rho} \leq 1. \quad (3)$$

Because we are interested in the whole pore-collapse process as the final relative density of the porous material approaching unity, it warrants a finite deformation analysis. In this section we outline the finite deformation formulation for stress wave propagation in elastic/viscoplastic materials applied to a spherical shell. The elastic deformation and an appropriate constitutive model are also included in our analysis. Tong and co-workers¹⁹ have presented the corresponding finite deformation formulation for elastic/viscoplastic materials in plane strain.

A. Kinematics

For a spherical shell, let \mathbf{x} represent a material element in the current configuration (i.e., the spherical coordinates at time $t > 0$) that was initially at \mathbf{X} in the reference configuration (i.e., the spherical coordinates at time $t = 0$). The deformation of the spherical shell under a pressure loading can be represented by

$$\mathbf{x} = \hat{\mathbf{x}}(\mathbf{X}, t) = r(R, t) \mathbf{e}_R, \quad (4)$$

where $\mathbf{X} = R \mathbf{e}_R$, R is the radial coordinate in the reference configuration ($A \leq R \leq B$), r is the radial coordinate in the current configuration [$a(t) \leq r(R, t) \leq b(t)$], \mathbf{e}_R is the unit basis vector in the radial direction.

The deformation gradient \mathbf{F} is then given by²⁷

$$\mathbf{F} = \frac{\partial \mathbf{x}}{\partial \mathbf{X}} = \begin{bmatrix} \frac{\partial r}{\partial R} & 0 & 0 \\ 0 & \frac{r}{R} & 0 \\ 0 & 0 & \frac{r}{R} \end{bmatrix} = \begin{bmatrix} \frac{\eta R^2}{r^2} & 0 & 0 \\ 0 & \frac{r}{R} & 0 \\ 0 & 0 & \frac{r}{R} \end{bmatrix}. \quad (5)$$

Here η is the ratio of the current volume to the reference volume of the matrix material, i.e., $\det \mathbf{F} = \eta(R, t)$.

The rate of change of the deformation gradient \mathbf{F} is

$$\dot{\mathbf{F}} = \begin{bmatrix} \frac{\partial}{\partial t} \left(\frac{\partial r}{\partial R} \right) & 0 & 0 \\ 0 & \frac{1}{R} \frac{\partial r}{\partial t} & 0 \\ 0 & 0 & \frac{1}{R} \frac{\partial r}{\partial t} \end{bmatrix}$$

$$= \begin{bmatrix} \frac{\eta R^2}{r^2} - \frac{2\eta R^2 u}{r^3} & 0 & 0 \\ 0 & \frac{u}{R} & 0 \\ 0 & 0 & \frac{u}{R} \end{bmatrix} = \begin{bmatrix} \frac{\partial u}{\partial R} & 0 & 0 \\ 0 & \frac{u}{R} & 0 \\ 0 & 0 & \frac{u}{R} \end{bmatrix}, \quad (6)$$

where the radial particle velocity u is defined as $u(R, t) = \partial r(R, t) / \partial t$. The corresponding spatial velocity gradient is

$$\mathbf{L} = \mathbf{D} + \mathbf{W} = \dot{\mathbf{F}}\mathbf{F}^{-1} = \begin{bmatrix} \frac{r^2}{\eta R^2} \frac{\partial u}{\partial R} & 0 & 0 \\ 0 & \frac{u}{r} & 0 \\ 0 & 0 & \frac{u}{r} \end{bmatrix}, \quad (7)$$

where $\mathbf{D} = (\mathbf{L} + \mathbf{L}^T) / 2$ is the rate of deformation tensor and $\mathbf{W} = (\mathbf{L} - \mathbf{L}^T) / 2$ is the spin rate tensor. However, for the axisymmetric deformations considered here, $\mathbf{W} = \mathbf{0}$ and thus $\mathbf{D} = \mathbf{L}$.

B. Momentum balance and constitutive relation

The balance of linear momentum in a spherical coordinates is given as²⁷

$$\frac{\partial T_R}{\partial R} + \frac{2}{R} (T_R - T_\theta) = \rho_0 \frac{\partial u}{\partial t}, \quad (8)$$

where T_R and T_θ are the radial and transverse components of the first Piola-Kirchhoff stress tensor \mathbf{T} , and ρ_0 is the mass density of the matrix material in the reference configuration. The matrix material is considered to be an elastic/viscoplastic solid as the one considered by Tong and co-workers.¹⁹ The material is assumed to be homogeneous, isotropic, and incompressible in plastic deformation, and its elastic moduli remains constant during plastic deformation and under moderately high pressures. The rate form of constitutive relation for such a solid is (see Tong and co-workers¹⁹ with $\mathbf{W} = \mathbf{0}$ in this case):

$$\dot{\bar{\mathbf{T}}} - (\mathbf{D} - \mathbf{D}^p) \bar{\mathbf{T}} + \bar{\mathbf{T}} (\mathbf{D}^p - \mathbf{D}) = \mathbf{C}^e : (\mathbf{D} - \mathbf{D}^p), \quad (9)$$

where \mathbf{C}^e is the elastic moduli tensor of the matrix material and takes the familiar form in Cartesian coordinates as

$$C_{ijkl} = \lambda^e \delta_{ij} \delta_{kl} + \mu^e (\delta_{ik} \delta_{jl} + \delta_{il} \delta_{jk}), \quad (10)$$

where λ^e and μ^e are the Lamé constants.

The weighted Cauchy stress $\bar{\mathbf{T}}$ is defined as

$$\bar{\mathbf{T}} = \mathbf{F} \mathbf{T}^T = \begin{bmatrix} \frac{\eta R^2}{r^2} T_R & 0 & 0 \\ 0 & \frac{r}{R} T_\theta & 0 \\ 0 & 0 & \frac{r}{R} T_\theta \end{bmatrix}, \quad (11)$$

and the rate of plastic deformation tensor \mathbf{D}^p is determined from the J_2 flow rule

$$\mathbf{D}^p = \dot{\gamma} \frac{\mathbf{S}}{2\tau_e}, \quad \text{where } \mathbf{S} = \bar{\mathbf{T}} - \frac{1}{3} \text{tr}(\bar{\mathbf{T}}) \mathbf{I}, \quad \tau_e^2 = \frac{1}{2} S_{ij} S_{ij}, \quad (12)$$

where τ_e is the effective shear stress. The plastic shear strain rate $\dot{\gamma}$ is in general a function of applied stress, temperature, and internal state variables.^{28,29} The specific form of the plastic shear strain rate function used here is chosen to be a power law given by Klopp and co-workers,¹⁷

$$\dot{\gamma} = \dot{\gamma}_0 \left(\frac{\tau}{\tau_r} \right)^{1/m}, \quad \tau_r = \tau_0 \left(\frac{\gamma}{\gamma_0} \right)^n \left(\frac{\theta}{\theta_0} \right)^v, \quad (13)$$

where $\dot{\gamma}_0$, τ_0 , γ_0 , and θ_0 are reference strain rate, flow stress, plastic strain, and temperature, τ , γ , and θ are current flow stress, plastic strain, and temperature, m is the rate sensitivity, n is the strain-hardening exponent, and v is the thermal softening exponent.

C. Spherical wave analysis

For wave analysis it is advantageous to rewrite the rate form of elastic/viscoplastic constitutive relation given above in terms of the first Piola-Kirchhoff stress tensor \mathbf{T} (noting only the diagonal components of \mathbf{T} , \mathbf{F} , \mathbf{D} , and \mathbf{D}^p are nonzero):

$$\dot{\mathbf{T}} = \mathbf{T} \mathbf{D} + \mathbf{F}^{-1} (\mathbf{C}^e : \mathbf{D}) - 2\mathbf{T} \mathbf{D}^p - \mathbf{F}^{-1} (\mathbf{C}^e : \mathbf{D}^p), \quad (14)$$

or, in the component form, as

$$\frac{\partial T_R}{\partial t} = A_1(R, t) \frac{\partial u}{\partial R} - B_1(R, t), \quad (15a)$$

$$\frac{\partial T_\theta}{\partial t} = A_2(R, t) \frac{\partial u}{\partial R} - B_2(R, t), \quad (15b)$$

in which the coefficients A_1 , B_1 , A_2 , and B_2 are

$$A_1 = \frac{r^2}{\eta R^2} T_R + (\lambda^e + 2\mu^e) \frac{r^4}{\eta^2 R^4}, \quad (16a)$$

$$B_1 = \left(2T_R - \frac{2r^2}{\eta R^2} \mu^e \right) D_R^p - \frac{2r\lambda^e}{\eta R^2} u, \quad (16b)$$

$$A_2 = (r/\eta R) \lambda^e, \quad (16c)$$

$$B_2 = 2 \left(T_\theta + \frac{R}{r} \mu^e \right) D_\theta^p - \frac{T_\theta}{r} u - 2(\lambda^e + \mu^e) \frac{R}{r^2} u. \quad (16d)$$

The rate form of constitutive equations combining with the balance equation of linear momentum, and the compatibility condition comprise a system of quasilinear, hyperbolic, partial differential equations for T_R , T_θ , u , and η ,

$$\frac{\partial T_R}{\partial t} = A_1(R, t) \frac{\partial u}{\partial R} - B_1(R, t), \quad (17a)$$

$$\frac{\partial T_\theta}{\partial t} = A_2(R, t) \frac{\partial u}{\partial R} - B_2(R, t), \quad (17b)$$

$$\frac{\partial T_R}{\partial R} + \frac{2}{R} (T_R - T_\theta) = \rho_0 \frac{\partial u}{\partial t}, \quad (17c)$$

$$\frac{\partial \eta}{\partial t} = \frac{r^2}{R^2} \frac{\partial u}{\partial R} + \frac{2\eta u}{r}. \quad (17d)$$

This system can be written in terms of relations along characteristics

$$dT_R = \pm \rho_0 c \, du - B_1 \, dt \mp \frac{2}{R} (T_R - T_\theta) c \, dt,$$

$$\frac{dR}{dt} = \pm c = \pm \left(\frac{A_1}{\rho_0} \right)^{1/2}, \quad (18a)$$

$$dT_\theta = \frac{A_2}{A_1} (dT_R + B_1 \, dt) - B_2 \, dt, \quad \frac{dR}{dt} = 0, \quad (18b)$$

$$d\eta = \frac{r^2}{R^2 A_1} (dT_R + B_1 \, dt) + \frac{2\eta u}{r} \, dt, \quad \frac{dR}{dt} = 0. \quad (18c)$$

For infinitesimal deformations we have

$$\eta \rightarrow 1, \quad r/R \rightarrow 1, \quad T_R/\mu^e \rightarrow 0, \quad \text{and} \quad T_\theta/\mu^e \rightarrow 0, \quad (19)$$

so the above finite difference equations can be easily reduced to a simpler form (for example, see Hopkins³⁰).

This system of characteristic relations Eq. (18) written in the form of a finite difference equations is solved by using a second-order accurate integration method,³¹ except, where large oscillations exist, a first-order accurate scheme is used.³² Because the material wave speed c is strongly dependent on r/R , an updated nonuniform meshing scheme is adopted such that the accuracy of computation is maintained while the stability condition $c\Delta t/\Delta R = \zeta \leq 1$ is satisfied for all nodes at each time step. For each time step, the current radius r and the temperature θ are updated by

$$dr = u \, dt \quad \text{and} \quad d\theta = (\beta \tau \dot{\gamma} / c_p \rho_0) dt, \quad (20)$$

where the adiabatic condition is assumed for the spherical shell under dynamic loading by shock waves, and c_p is the heat capacity of the matrix material and β the fraction of the plastic work converted to heat. In general β may depend on plastic strain and strain rate.³³ In our present analysis we are interested in the consolidation of powders by shock wave propagation in which the rate of deformation of the bulk matrix material during pore collapse could be as high as 10^7 per second. Due to the lack of experimental data on β in the very high strain rate range (10^5 – 10^7 per second), β is set to be a constant 0.9 in our calculations. In the following section, a detailed computational analysis of dynamic collapse of a viscoplastic spherical shell under external pressure is presented.

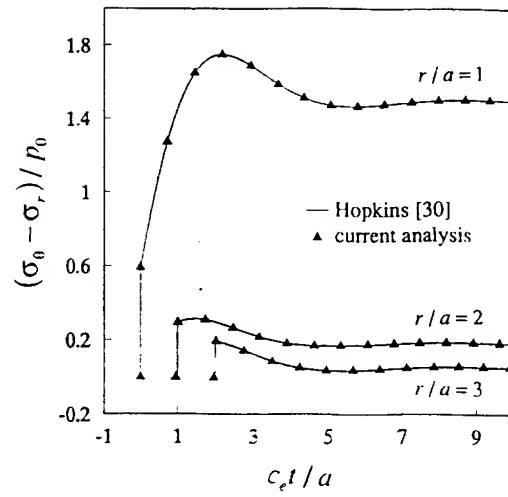


FIG. 1. Variation of shear stress $(\sigma_\theta - \sigma_r)/\rho_0$ with time $c_e t/a$ at various locations: $r/a=1$ (cavity surface), 2, and 3. ρ_0 is the applied pressure, c_e the elastic spherical wave speed, a the cavity radius, and Poisson's ratio $\nu=0.29$.

III. COMPUTATIONAL ANALYSIS AND RESULTS

A numerical scheme for studying collapse of a spherical shell is implemented using the finite elastic/viscoplastic deformation formulation described above. To verify the numerical scheme and to demonstrate the effectiveness of the current formulation presented here, several simple examples of spherical wave propagation are at first simulated and compared with those reported in the literature. The first example is the expansion of a cavity in an infinite elastic media when a pressure is applied suddenly on the interior surface of the cavity. The numerical result as well as the result from the analytical solution (see the review by Hopkins³⁰) is given in Fig. 1. The numerical solution agrees with the analytical solution extremely well. The second example is the expansion of a cavity in an infinite elastic/perfectly plastic rate-independent media when a time-dependent pressure is applied on the interior surface of the cavity.³⁴ In our formulation, we use a very small $m=0.005$ along with $n=\nu=0$ in our material model to represent a perfectly plastic, nearly rate-independent material. To avoid using a prohibitively small time step in our calculation, a maximum cutoff strain rate of 10^9 per second is used. The numerical result is given in Fig. 2 along with the result by Friedman and co-workers.³⁴ Once again, the agreement is excellent. Finally, we simulated the dynamic collapse of an aluminum spherical shell of elastic/perfectly plastic rate-independent behavior when the outer surface of the spherical shell under a linearly increasing pressure loading and the inner surface of the shell is stress free. In particular, we simulated the case considered by Carroll and Holt¹⁶ as shown in their Fig. 5. Our numerical simulation gives essentially the same result (Fig. 3). The slight difference between the two results is due to the fact that we use $m=0.005$ (as opposed to $m=0$ for the rate-independent case) to approximate a rate-independent material. Thus, results of the dynamic analysis presented in

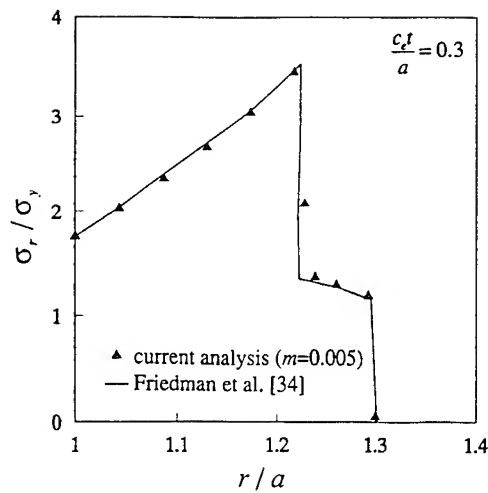


FIG. 2. Variation of radial stress σ_r/σ_y with distance at the time $c_e t/a=0.3$. σ_y is the yield stress of the material, a the cavity radius, c_e the elastic spherical wave speed, the applied pressure on the cavity surface is $p(t) = -5\sigma_y \exp(-3.5c_e t/a)$, and Poisson's ratio $\nu=0.25$.

the following with $m=0.005$ for the matrix material can be regarded as a good approximation for a rate-independent material.

In the following we present the results of systematic parametric studies through a series of numerical simulation to illustrate the effect of various factors on the collapse of a spherical shell, including strain-rate sensitivity, inertia, and transient wave propagation, strain hardening, thermal softening, impulsive loading rate, pore size, and initial porosity. The matrix material is assumed to be pure aluminum in most of the calculations. We also include some of the results for pure iron and copper for comparison purposes. Relevant material parameters for these materials are listed in Tables I and II. Some computations of large problems have been carried out on a Cray supercomputer at

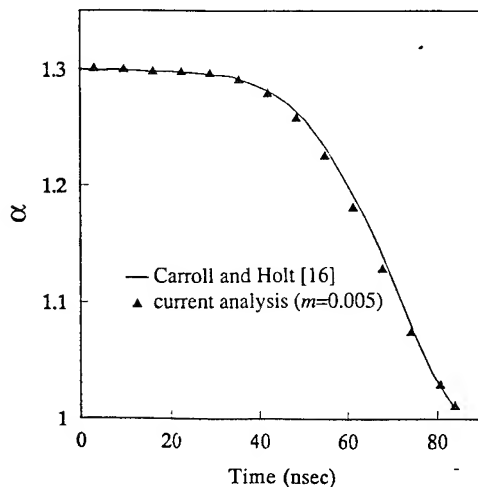


FIG. 3. Dynamic pore collapse of an aluminum hollow sphere of initial pore radius $a_0=20 \mu\text{m}$ and initial relative density $\bar{\rho}_0=0.769$ (i.e. initial distention $\alpha_0=1.3$), with an applied external pressure rate $\dot{p}=10 \text{ MPa/ns}$.

TABLE I. Selected thermal-mechanical properties of matrix materials.

Material	Density (kg/m^3)	μ_c (GPa)	λ_c (GPa)	c_p (J/kg/K)	θ_m (K)
Aluminum	2700	26	56	893	920
Iron	7800	81	112	500	1530
Copper	8940	44	117	383	1356

San Diego Supercomputer Center and smaller problems are solved on an Ultrix DEC 3100 workstation. One of the important variables is the densification time at which the porous material is nearly fully densified. Because of the asymptotic nature of pore-collapse process as $\bar{\rho} \rightarrow 1$, the pore-collapse time or densification time t_c is chosen to be the time when $\bar{\rho}_c=0.98$ for illustrative purposes.

Figure 4(a) shows the effects of strain rate sensitivity of the matrix materials and dynamic loading on the collapse process of a spherical shell under a linearly increasing loading with $\dot{p}=10 \text{ MPa/ns}$. For simplicity as well as for direct comparison with the results of quasistatic analyses by Carroll and Holt¹⁶ for a rigid, perfectly plastic, rate-independent material and by Wilkinson and Ashby²⁰ for a rigid, perfectly plastic, rate-dependent material under the same loading condition, effects of strain hardening and thermal softening are at first not included [i.e., $n=\nu=0$ in our model, Eq. (13)]. The result of the quasistatic analysis given by Carroll and Holt¹⁶ is

$$\bar{\rho} = \begin{cases} \bar{\rho}_0 & (0 < p < p_c) \\ 1 - e^{-\sqrt{3}p/2\tau_0} & (p \leq p_c) \end{cases}$$

$$\text{where } p_c = (2\tau_0/\sqrt{3}) \ln[1/(1-\bar{\rho}_0)], \quad (21)$$

and the result by Wilkinson and Ashby²⁰ is

$$\dot{\bar{\rho}} = \frac{\sqrt{3}}{2} \dot{\gamma}_0 \frac{\bar{\rho}(1-\bar{\rho})}{[1-(1-\bar{\rho})^m]^{1/m}} \left(\frac{\sqrt{3}m}{2} \frac{p}{\tau_0} \right)^{1/m}. \quad (22)$$

The time in Fig. 4(a) is normalized by t_0 which corresponds to the time when the applied pressure equals the yield stress in a perfectly plastic, rate-independent material, i.e., $p(t_0)=\sqrt{3}\tau_0$. The time t_0 can be regarded as a characteristic time of pore collapse for such a material in the quasistatic situation and hence is used as a reference time scale. Clearly in both quasistatic and dynamic analyses, a strong rate sensitivity retards the pore collapse. The pore collapse obtained from the present dynamic solution in all cases is faster than that predicted by static analysis initially but becomes slower at later times. Thus, the dynamic results by Carroll and Holt¹⁶ will give a much shorter densification time for rate-sensitive materials. Un-

TABLE II. Viscoplastic parameters for matrix materials.

Material	τ_0 (MPa)	$\dot{\gamma}_0$ (10^5 s^{-1})	m	γ_0	n	θ_0 (K)	ν
Aluminum	125	1.53	0.254	0.05	0.04	295	-0.4
Iron	420	4.0	0.20	0.15	0.085	295	-0.6
Copper	270	5.0	0.20

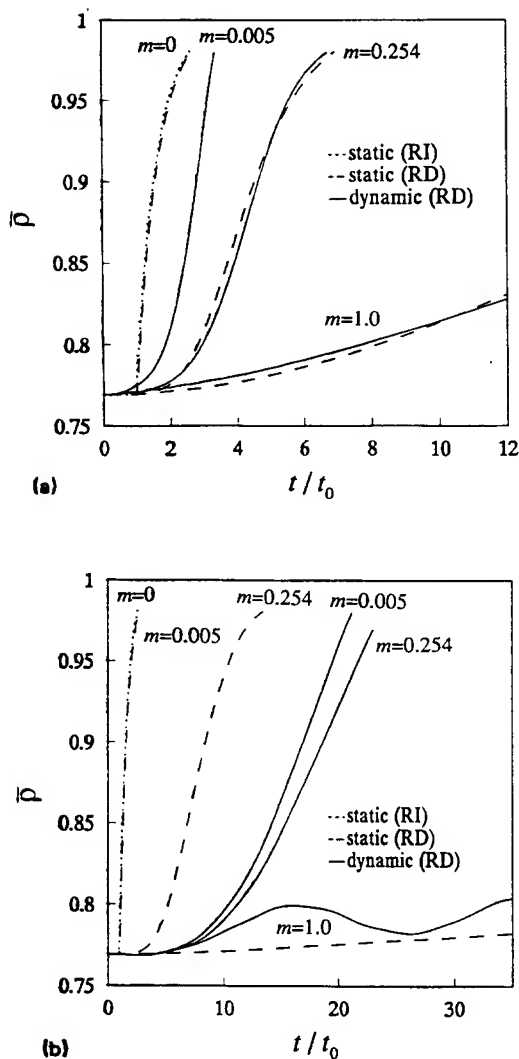


FIG. 4. Comparison of static and dynamic pore collapse of an elastic/viscoplastic aluminum spherical shell of initial pore radius $a_0 = 20 \mu\text{m}$ and initial relative density $\bar{p}_0 = 0.769$. The material model for plastic deformation in the current dynamic analysis is given as $\tau = \tau_0(\dot{\gamma}/\dot{\gamma}_0)^m$: (a) With an applied external pressure rate $\dot{p} = 10$ MPa/ns, $t_0 = 21.65$ ns; (b) with an applied external pressure rate $\dot{p} = 250$ MPa/ns and $t_0 = 0.866$ ns.

der this particular loading rate (relatively slow), the quasistatic and dynamic results are somewhat quite similar to each other when $m=0.254$ (for pure aluminum) or $m=1.0$ (the Newtonian viscous material). However, there is a large difference between static and dynamic analyses for $m=0.005$ (nearly rate independent) which indicates a strong dynamic effect in very weakly rate-sensitive materials even under relatively slow loading rate.

Variations of plastic strain rate, plastic shear strain, and temperature within the spherical shell are given in Figs. 5(a)–5(c), respectively, for pure aluminum. The plastic strain rate is indeed of the order 10^5 – 10^7 per second (note $\dot{\gamma}_0 = 1.53 \times 10^5$ per second). Initially the plastic strain rate is relatively uniform across the cross section. As the pore collapses, the plastic strain rate in the innermost region of the shell ($R/a_0 \rightarrow 1$) increases dramatically while the plastic strain rate reduces gradually in the outer region. The accumulated plastic shear strain also becomes nonuniform at the later stage of pore collapse, Fig. 5(b). Large-

shear strain, as high as 2.86, can be found near the inner surface of the shell at the time $t/t_0 = 4.78$ (at which $\bar{p} = 0.909$). At the same time, the temperature increases in that region due to adiabatic heating by plastic work to as high as 815 K (88% of the melting temperature of the matrix material) while the temperature at the outer surface of the shell remains relatively low (about 321 K).

The influence of large plastic strain and temperature rise on dynamic pore collapse is examined by incorporating strain hardening and thermal softening into the viscoplastic model and the results are given in Fig. 6 for $m=0.254$. As expected, strain hardening slows down pore collapse (see the case with $n=0.25$, $v=0$) and thermal softening accelerates the process (see the case with $n=0$, $v=-1.0$). The result of dynamic pore collapse of pure aluminum using parameters given by Klopp and co-workers¹⁷ (see Table II) is found to be almost identical to the result using $m=0.254$ and $n=v=0$. The effect of strain hardening appears to annul the effect of thermal softening on dynamic pore collapse for pure aluminum. Because of this fact, only the simple viscoplastic model ($m=0.254$, $n=v=0$) is used in the following calculations which can also be directly compared with the results of quasistatic analyses by Carroll and Holt¹⁶ and by Wilkinson and Ashby.²⁰

So far, we have investigated the dynamic pore collapse of an aluminum spherical shell under a relatively low pressure rate of $\dot{p} = 10$ MPa/ns. Figure 4(b) presents the results using the same material parameters as in Fig. 4(a) but under a relatively high pressure rate of $\dot{p} = 250$ MPa/ns. In contrast to the results in Fig. 4(a), there is large difference between quasistatic and dynamic analyses for all cases: $m=0.005$, 0.254 , and 1.0 . The difference between the dynamic results with $m=0.005$ and $m=0.254$ in Fig. 4(b) is somewhat smaller than in Fig. 4(a). For $m=1.0$, the dynamic analysis actually predicts a faster pore-collapse rate than that of static analysis for quite a while.

Figures 7(a) and 7(b) show the effect of pore size on dynamic pore collapse of the viscoplastic aluminum spherical shell ($m=0.254$) under a low pressure rate of $\dot{p} = 10$ MPa/ns and a high pressure rate of $\dot{p} = 250$ MPa/ns. For $\dot{p} = 10$ MPa/ns, the results by dynamic analysis are very similar to those by static analysis for $a_0 = 2$ and $20 \mu\text{m}$. For $a_0 = 100 \mu\text{m}$ and larger, there is a strong dynamic effect even under a relatively slow pressure rate. For $a_0 = 50 \mu\text{m}$, the dynamic pore collapse is evidently slower than static one but the densification time is shorter. For $\dot{p} = 250$ MPa/ns, the dynamic results for $a_0 = 20 \mu\text{m}$ deviate largely from static ones. The dynamic effect becomes more dominant for larger pores of given initial relative density. The “critical” pore size under which both dynamic and static results are similar reduces as the applied pressure rate increases. There is no effect of pore size in quasistatic analysis. It is also interesting to note that the relative density of large pore sizes decreases by a large amount initially in our dynamic analysis as shown in Fig. 7(b), which is due to transient wave propagation and elastic deformation. Because the relative density is measured by $\bar{p} = 1 - (a/b)^3$, the rate of reduction in b can be faster than that of a during the initial collapse stage, thus it leads to a decrease in \bar{p} .

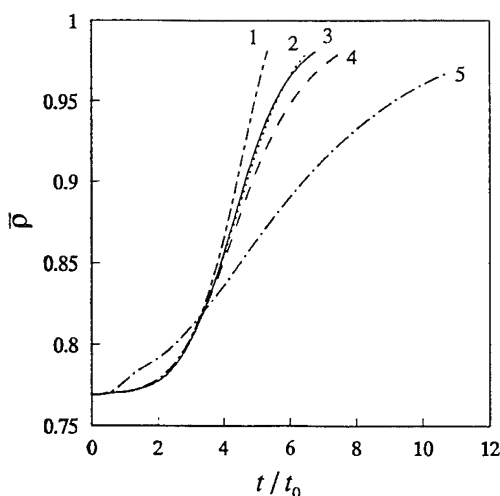
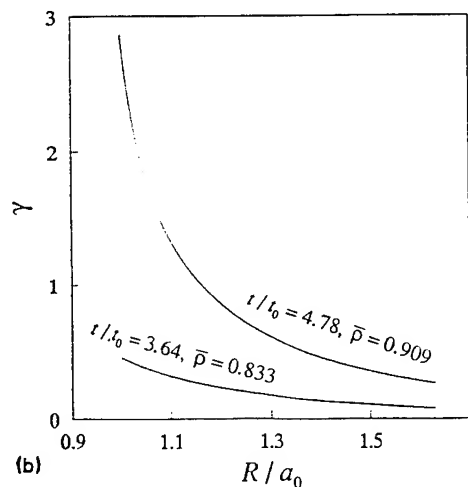
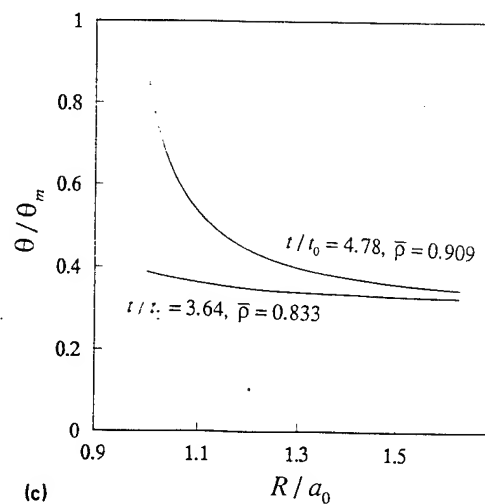
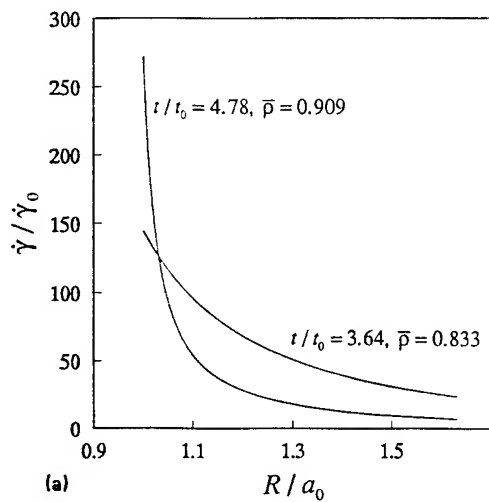


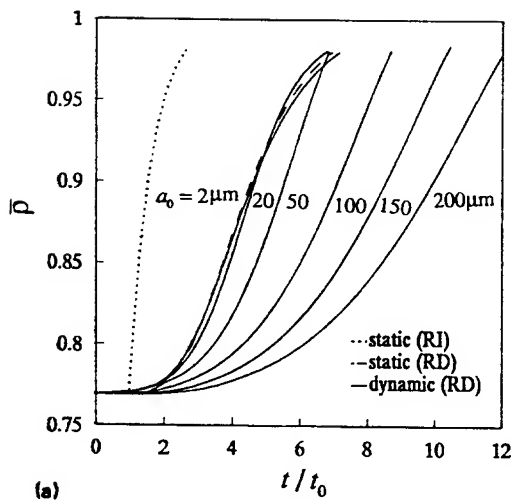
FIG. 6. Effect of strain hardening and thermal softening on dynamic pore collapse of an elastic/viscoplastic aluminum spherical shell: $a_0=20\text{ }\mu\text{m}$, $\bar{p}_0=0.769$, $\dot{p}=10\text{ MPa/ns}$, $\tau=\tau_0(\dot{\gamma}/\dot{\gamma}_0)^m(\gamma/\gamma_0)^n(\theta/\theta_0)^v$, and $t_0=21.65\text{ ns}$: (1) $n=0$, $v=-1.0$; (2) $n=0.04$, $v=-0.4$; (3) $n=v=0$; (4) $n=0.04$, $v=0$; (5) $n=0.25$, $v=0$.

FIG. 5. Variations of (a) plastic shear strain rate, (b) plastic shear strain, and (c) temperature rise due to adiabatic heating of plastic work within the spherical shell at times $t/t_0=3.64$ ($\bar{p}=0.833$) and $t/t_0=4.78$ ($\bar{p}=0.909$): $a_0=20\text{ }\mu\text{m}$, $\bar{p}_0=0.769$, $\dot{p}=10\text{ MPa/ns}$, $\tau=\tau_0(\dot{\gamma}/\dot{\gamma}_0)^m$, and $t_0=21.65\text{ ns}$. $R/a_0=1$ corresponds to the inner surface of the shell, and $R/a_0=1.603$ corresponds to the outer surface of the shell.

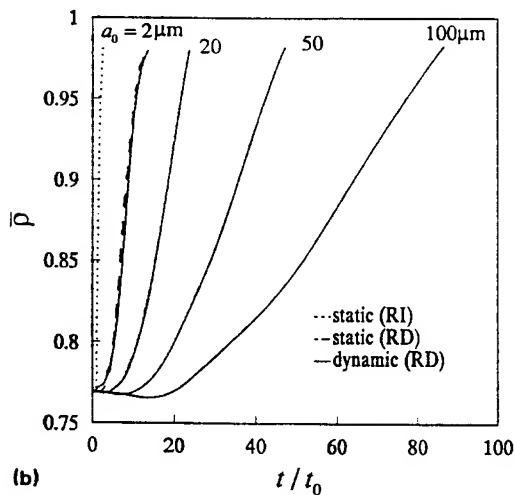
This transient phenomenon occurs in all dynamic analyses presented here and is more evident for larger pores and at higher loading rates.

The effect of initial relative density on static and dynamic pore collapse of an aluminum spherical shell with the same pore size is also studied for both slow and fast pressure loading rates and results are given in Figs. 8(a) and 8(b). The difference between static and dynamic analysis results is small for $\dot{p}=10\text{ MPa/ns}$ but becomes quite significant for $\dot{p}=250\text{ MPa/ns}$, with $\bar{p}_0=0.555$, 0.769 , and 0.909 . The retardation of the collapse process due to dynamic effect is evident for all three different initial relative densities. According to our dynamic analysis, the lower the initial relative density, the faster the pore collapses completely, which is in contrast to the results of quasistatic analysis.

In order to examine the effect of the strength and/or mass density-of-matrix materials on dynamic pore collapse, numerical simulations for pure aluminum, iron, and copper are carried out and results are presented in Fig. 9(a) under the same applied pressure history and in Fig. 9(b) with the same static, rate-dependent pore-collapse response. The order of the densification times for aluminum, iron, and copper in dynamic analysis in terms of their respective static pore-collapse characteristic time is just opposite to that in static analysis, Fig. 9(a). This behavior

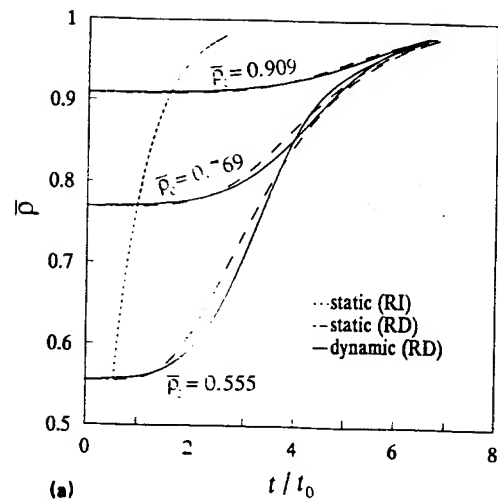


(a)

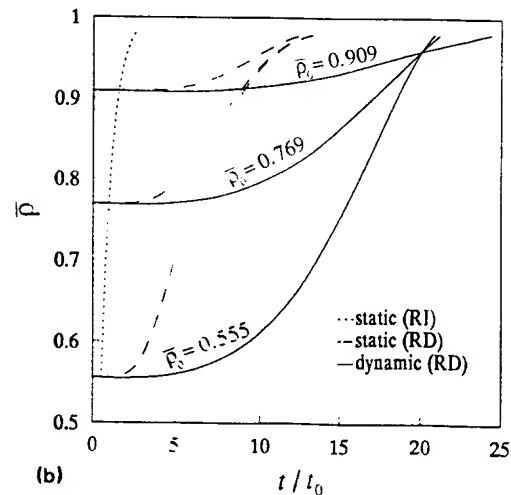


(b)

FIG. 7. Effect of pore size on static and dynamic pore collapse of an elastic/viscoplastic aluminum spherical shell: $\bar{\rho}_0 = 0.769$, $\tau = \tau_0(\dot{\gamma}/\dot{\gamma}_0)^m$, $\tau_0 = 125$ MPa, $\dot{\gamma}_0 = 1.53 \times 10^5$ ℓ/s , $m = 0.254$: (a) $a_0 = 2, 20, 50, 100, 150$, and 200 μm , with an applied external pressure rate $\dot{p} = 10$ MPa/ns, $t_0 = 21.65$ ns; (b) $a_0 = 2, 20, 50$, and 100 μm , with an applied external pressure rate $\dot{p} = 250$ MPa/ns and $t_0 = 0.866$ ns.



(a)



(b)

FIG. 8. Effect of initial relative density on static and dynamic pore collapse of an elastic/viscoplastic aluminum spherical shell: $a_0 = 20$ μm , $\bar{\rho}_0 = 0.555, 0.769$, and 0.909 . $\tau = \tau_0(\dot{\gamma}/\dot{\gamma}_0)^m$: (a) with an applied external pressure rate $\dot{p} = 10$ MPa/ns, $t_0 = 21.65$ ns; (b) with an applied external pressure rate $\dot{p} = 250$ MPa/ns and $t_0 = 0.866$ ns.

should be expected because the dynamic effect is more dominant if the applied load is higher in comparison to the strength of the matrix material. In Fig. 9(b) the pressure rate is adjusted for each matrix material such that the quasistatic rate-dependent pore collapse is the same for all three matrix materials. The results from dynamic analysis are quite different from those of static analysis. The order of the densification times for aluminum, iron, and copper seems to correspond to the order of ρ_0/\dot{p} for each matrix material, i.e., the higher the density of the matrix material, the larger the dynamic effect.

IV. CONCLUSIONS AND DISCUSSIONS

The dynamic consolidation is accomplished by the passage of a shock wave through the powder. Major physical processes (rearrangement, deformation, and heating) occur during the densification process, i.e., during the shock rise time or within the shock front region. According to

our computational analysis, the combined effects of inertia and strain-rate sensitivity strongly retard the densification of porous materials under impulsive loading, Figs. 4(a) and 4(b). For a given loading rate, the viscous effect is more important when the matrix material becomes strongly rate sensitive ($m \rightarrow 1$). The dynamic effect (inertia) is significant in weakly rate-sensitive matrix materials under all typical shock wave loading rates. For three typical elastic/viscoplastic materials studied here with $m \approx 0.2-0.25$, the difference in the densification time predicted by quasistatic and rate-independent analysis is very large. Even though the dynamic and rate-independent analysis reduces the difference to some degree its predicted densification time is still significantly smaller than that from the present dynamic and rate-dependent analysis, especially when the loading rate is moderately high. Under the condition given in Fig. 4(a), dynamic effects are small, thus the results by quasistatic and rate-dependent analysis are applicable to shock wave consolidation of alu-

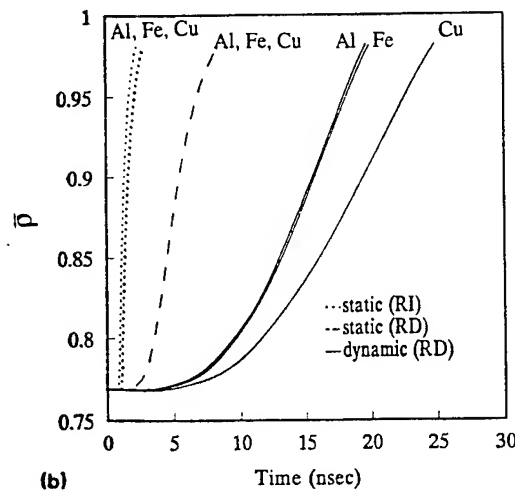
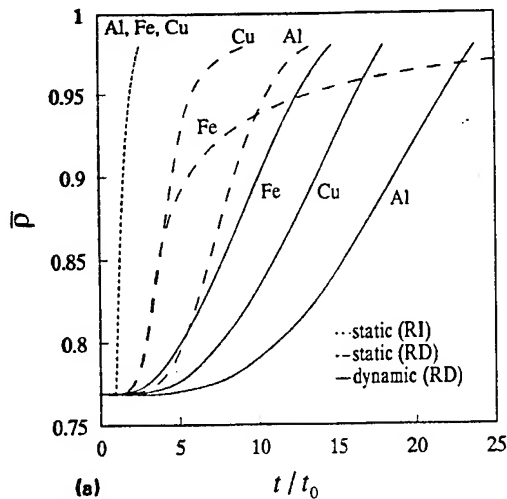


FIG. 9. (a) Comparison of static and dynamic pore collapse for aluminum, iron, and copper spherical shells with the same applied external pressure rate $\dot{p}=250$ MPa/ns; $a_0=20$ μm , $\bar{\rho}_0=0.769$, $\tau=\tau_0(\dot{\gamma}/\dot{\gamma}_0)^m$. Aluminum: $\tau_0=125$ MPa, $\dot{\gamma}_0=1.53 \times 10^5$ ℓ/s , $m=0.254$, $t_0=0.866$ ns; iron: $\tau_0=420$ MPa, $\dot{\gamma}_0=4.0 \times 10^5$ ℓ/s , $m=0.20$, $t_0=2.910$ ns; copper: $\tau_0=270$ MPa, $\dot{\gamma}_0=5.0 \times 10^5$ ℓ/s , $m=0.20$, $t_0=1.871$ ns. (b) Comparison of dynamic pore collapse for aluminum, iron, and copper spherical shells with the same static rate-dependent pore collapse: $a_0=20$ μm , $\bar{\rho}_0=0.769$, $\tau=\tau_0(\dot{\gamma}/\dot{\gamma}_0)^m$. Aluminum: $\tau_0=125$ MPa, $\dot{\gamma}_0=1.53 \times 10^5$ ℓ/s , $m=0.20$, $\dot{p}=250$ MPa/ns, $\rho_0/\dot{p}=10.8 \times 10^3$ s/m^2 ; iron: $\tau_0=420$ MPa, $\dot{\gamma}_0=4.0 \times 10^5$ ℓ/s , $m=0.20$, $\dot{p}=693$ MPa/ns, $\rho_0/\dot{p}=11.3 \times 10^3$ s/m^2 ; copper: $\tau_0=270$ MPa, $\dot{\gamma}_0=5.0 \times 10^5$ ℓ/s , $m=0.20$, $\dot{p}=426$ MPa/ns, $\rho_0/\dot{p}=20.9 \times 10^3$ s/m^2 .

minum powders. Under a higher loading rate [Fig. 4(b)] or when the pore size is larger [Figs. 7(a) and 7(b)], dynamic effects become significant or even dominant. For Newtonian viscous fluid like solids ($m=1$), dynamic effects are insignificant in most cases and results of quasistatic and rate-dependent analysis are applicable to dynamic consolidation process. The same conclusion has been reached for void growth in Newtonian viscous solids by Johnson.³⁵

For simplicity, the pore-collapse time or densification time t_c under a linearly increasing pressure loading (i.e., constant \dot{p}) can be written as

$$t_c = (\sqrt{3}\tau_0/\dot{p})g(\dot{p}, \tau, \rho_0, a_0, \bar{\rho}_0). \quad (23)$$

The pore-collapse time to a good approximation can be regarded to be independent of initial porosity or initial relative density [see Figs. 8(a) and 8(b)]. For quasistatic loading and rate-independent matrix materials, $g \approx 1$. When dynamic effects are insignificant (for example, $m \approx 1$, or a small pore size or a low pressure rate), $g \approx g_R$ for rate-dependent matrix material, where g_R is a normalized quasistatic and rate-dependent pore-collapse time and can be computed by using the results for relative density rate from quasistatic analysis of rate-dependent, strain-hardening, and thermal softening matrix materials. For power-law perfectly viscoplastic materials (Wilkinson and Ashby²⁰), g_R can be obtained as [see Eq. (22)]

$$g_R = \left(\frac{G}{F} \right)^{m/(1+m)},$$

where

$$G = \int_{\bar{\rho}_c}^{\bar{\rho}} \frac{[1 - (1 - \bar{\rho})^m]^{1/m}}{\bar{\rho}(1 - \bar{\rho})} d\bar{\rho},$$

$$F = \frac{m}{1+m} \left(\frac{3m}{2} \right)^{(1+m)/m} \frac{\tau_0 \dot{\gamma}_0}{\dot{p}}. \quad (24)$$

For strain-hardening viscoplastic materials, the results such as the one by Haghi and Anand²⁵ may be used to evaluate g_R . Finally, when dynamic effects are not negligible (the pressure loading rate is high for a given matrix material and pore size), $g \approx g_R g_D$, where g_D is a nondimensional parameter, a measure of dynamic effects (≥ 1). The dynamic parameter g_D may be in general dependent on pressure loading rate, viscoplastic properties of matrix materials, and initial pore size. For a given matrix material, g_D may be tabulated for different loading rates or different pore sizes. Furthermore, g_D can also be used as a criterion in determining whether the pressure loading rate is low or high for a given matrix material and pore size: The pressure loading rate is low when $g_D \approx 1$ and the pressure loading rate is high when $g_D \gg 1$.

Schwarz and co-workers¹⁴ reported measurements on the temperature rise time of about 60–70 ns during shock wave consolidation of copper-constantan powders (60 μm in diameter) for shock pressures between 1.3 and 9.4 GPa. The maximum temperature can be regarded to be due to the shock wave heating as the powder is being fully densified and hence the temperature rise time is a good measure of the densification time by shock wave. The relatively large rise time is in itself an indicator of dynamic and strain-rate effects on consolidation process. The finite rise time is commonly attributed to the time for the shock wave passing through 1–2 or 3–5 powder particles.^{2,15} However, the temperature rise times measured for two tests no. 801 and no. 802 are 67 and 63 ns, respectively while the shock velocities in copper powder for these two tests are 0.75 and 2.03 km/s.¹⁴ The times for these two shock waves passing through 1.5 particles (90 μm) are about 120 and 44 ns, respectively. Such a big difference in rise time is not observed in the experimental measurements, rather, the measured temperature rise times are almost identical. The ex-

perimental observation could be partly explained in terms of the dynamic effects on pore collapse. The shock pressures in these two experiments are 1.3 and 9.4 GPa, respectively, and thus the pressure loading rates \dot{p} are 19.4 and 149.2 MPa/ns, respectively. The dynamic effects will be stronger in the later test (higher-pressure loading rate) and thus retard the densification process.

As mentioned in Sec. I, constitutive relations of porous materials, especially such as the one proposed by Herrmann,¹¹ are commonly used in computer simulation of dynamic consolidation by shock wave propagation. The crush curve (i.e., the p - α relation), however, is often taken to be that determined from quasistatic tests and without the inclusion of rate effects.^{11,15,36} Acceptable for certain rate-insensitive materials under slow (low rate) loading conditions,³⁷ the quasistatic rate-independent p - α relation cannot be assumed to be valid in general applications of shock wave consolidation without careful examination of effects of inertia and strain rate. If the quasistatic rate-independent p - α relation is used in modeling shock consolidation, the finite rise time of the shock wave (the finite width of the shock front) can only be artificially imposed (say, by numerical viscosity). On the other hand, from our present analysis, it can be seen that the finite rise time is the natural consequence of a rate-dependent and dynamic pore-collapse process during the passage of the consolidation shock wave. Thus, a rate-dependent and dynamic p - α relation will improve the modeling of physical processes during shock wave consolidation. As pointed out by Carroll and Holt,¹⁶ even for perfectly plastic and rate-independent materials, a dynamic pore-collapse relation becomes extremely complex (a second-order nonlinear ordinary differential equation). However, approximate dynamic p - α relations may be obtained for some simple loading cases. As a first approximation, quasistatic but rate-dependent pore-collapse relations such as the one proposed by Wilkinson and Ashby²⁰ [Eq. (22)] should be used for $m \approx 1$, or a small pore size, or a low pressure rate (i.e., when $g_D \approx 1$). For a given loading condition in which dynamic effects are not negligible ($g_D > 1$), a modified quasistatic and rate-dependent relation may be used instead. For example, Eq. (22) may be modified as

$$\dot{p} = D^* \frac{\sqrt{3}}{2} \dot{\gamma}_0 \frac{\bar{p}(1-\bar{p})}{[1-(1-\bar{p})^m]^{1/m}} \left(\frac{\sqrt{3}m}{2} \frac{p}{\tau_0} \right)^{1/m}, \quad (25)$$

where D^* (≤ 1) is a nondimensional coefficient to account for dynamic effects. Again, for a given matrix material, D^* can be tabulated for different loading rates or different pore sizes.

The localized melting near particle surfaces is another important aspect of shock consolidation. Large temperature rises in pore interior surface are predicted by our dynamic pore collapse analysis [Fig. 5(c)]. Heat conduction is neglected here (although it can easily be incorporated into our current analysis) because the times required for densification process are very short (≈ 100 ns). For some low-pressure loading rate cases or if the matrix material is very strongly rate sensitive (say, a Newtonian viscous solid with $m=1$), the time for complete consolidation of pow-

ders may be longer (1 μ s or more) and an adiabatic condition will be no longer valid. While large plastic deformation, frictional sliding, and other processes contribute to the localized heating, frictional sliding between particles has commonly been regarded to be the dominant factor,^{9,38} however, the conclusion may not be completely justified. The estimate of frictional work using a Coulomb friction model (constant coefficient of friction) is questionable for very high-pressure contact between particles encountered in shock wave loading.³⁹⁻⁴¹ The sliding friction stress is essentially limited by the shear strength of matrix material under high pressure.^{39,40} For closely or near closely packed powders, the relative sliding distance between particles is very small (of the order of several micrometers or less). Due to surface oxide layer and other contaminations, the sliding friction between dry surfaces is also strongly dependent on the sliding distance such that the friction stress during the initial sliding stage is relatively much smaller than that in the steady-state stage.^{40,41} Interparticle surfaces will soften and melt due to the heating by frictional sliding and will not transmit any significant friction stress afterward. Thus, the frictional working would be much smaller than that estimated by simple dry Coulomb friction law.

The plastic work of the viscoplastic matrix material during consolidation may be underestimated by assuming homogenous deformation of perfectly plastic and rate-independent material. The deformation of a spherical shell under pressure loading [Fig. 5(b)] is quite nonuniform and the plastic work done upon the pore collapse of porous materials can be quite large. Finally, a recent experimental study and analysis by Mutz⁴² on the fraction of the melt after shock wave consolidation concludes that the assumption of all heat flowing into the particle surface (such as by frictional sliding) gives an overestimate of the melt fraction and even predicts the possibility of vaporization of the particle surface layer which is unrealistic. He found that a 70% bulk and 30% surface layer partition of heat flow from shock energy input (which is similar to viscoplastic pore collapse) provides the best agreement with the experimental data. From available experimental results we conclude that the present dynamic pore-collapse analysis describes not only the densification process but also to a significant degree the surface melting of particles through adiabatic heating due to plastic work.

One of the implications of our computational results is that the dynamic pore collapse of a spherical shell can be used to study material response under very large strain and strain rates. In particular, because of the strong strain-rate and dynamic effects for matrix materials with large m (say, 0.2-1), the combined experimental and computational investigation can be carried out to evaluate such as the rate sensitivity of materials at very high strain rates. This may also provide a sensitive method to rigorously examine the hypothesis whether the behavior of Newtonian viscous fluids ($m=1$) prevails at strain rates higher than 10^4 per second.

While most efforts have been directed toward the understanding of the consolidation process by shock wave,^{2,4}

much less attention has been paid to problems of cracking in near fully densified compacts due to release tensile waves. Our current analysis can be easily extended to more complicated loading paths such as compressive-tensile loading and to include more complex viscoplastic models, especially those with strain-rate history effects.^{19,43} The effect of dynamic loading and viscoplastic properties of matrix materials on void growth (and eventually cracking) in compacts can be assessed. Furthermore, there is an increasing application of continuum, phenomenological constitutive relations of porous material to dynamic ductile fracture,⁴⁴ and spallation.⁴⁵ The flow potentials of porous materials used in these analyses are based on quasistatic results. The correction due to dynamic effects on void growth using those flow potentials can also be examined using our analysis.

ACKNOWLEDGMENTS

The authors would like to acknowledge the support of this research by the Division of Materials Research of the National Science Foundation through Grant No. DMR-9116570. G.R. acknowledges the support of a NSF Presidential Young Investigator award, Grant No. MSS-9157846. Discussions with Professor T. Vreeland, Jr. and Professor T. Christman on shock wave consolidation are gratefully acknowledged. The computations were performed on a Cray Y-MP at the San Diego Supercomputer Center (SDSC).

¹V. D. Linse, *Dynamic Compaction of Metal and Ceramic Powders*, NMAB-394, (National Academy Press, Washington, DC, 1983).

²R. B. Schwarz, P. Kasiraj, T. Vreeland, Jr., and T. J. Ahrens, *Acta Metall.* **32**, 1243 (1984).

³W. H. Gourdin, *Prog. Mater. Sci.* **30**, 39 (1986).

⁴Y. Horie, R. A. Graham, and I. K. Simonsen, *Mater. Lett.* **3**, 354 (1985).

⁵N. N. Thadhani, *Adv. Mater. Manufac. Proc.* **3**, 493 (1988).

⁶T. Christman, K. Heady, and T. Vreeland, Jr., *Scr. Metall.* **25**, 631 (1991).

⁷R. A. Berry and R. L. Williamson, in *Shock Waves in Condensed Matter*, edited by Y. M. Gupta (Plenum, New York, 1986), p. 337.

⁸J. E. Flinn, R. L. Williamson, R. A. Berry, R. N. Wright, Y. M. Gupta, and M. Williams, *J. Appl. Phys.* **64**, 1446 (1988).

⁹J. Gao, B. Shao, and K. Zhang, *J. Appl. Phys.* **69**, 7547 (1991).

¹⁰A. Ferreira and M. A. Meyers, in *Shock-Wave and High-Strain-Rate Phenomena in Materials*, edited by M. A. Meyers, L. E. Murr, and K. P. Staudhammer (Marcel Dekker, New York, 1992), p. 361.

¹¹W. Herrmann, *J. Appl. Phys.* **40**, 2490 (1969).

¹²M. M. Carroll and A. C. Holt, *J. Appl. Phys.* **43**, 759 (1972).

¹³J. W. Swegle, *J. Appl. Phys.* **51**, 2574 (1980).

¹⁴R. B. Schwarz, P. Kasiraj, and T. Vreeland, Jr., in *Metallurgical Applications of Shock Waves and High-Strain-Rate Phenomena*, edited by L. E. Murr, M. A. Meyers, and K. P. Staudhammer (Marcel Dekker, New York, 1986), p. 313.

¹⁵D. Raybould and T. Z. Blazynski, in *Materials at High Strain Rates*, edited by T. Z. Blazynski (Elsevier, New York, 1987), p. 71.

¹⁶M. M. Carroll and A. C. Holt, *J. Appl. Phys.* **43**, 1626 (1972).

¹⁷R. W. Klopp, R. J. Clifton, and T. G. Shawki, *Mech. Mater.* **4**, 375 (1985).

¹⁸R. J. Clifton, *Appl. Mech. Rev.*, **43**, s9 (1990).

¹⁹W. Tong, R. J. Clifton, and S. Huang, *J. Mech. Phys. Solids* **40**, 1251 (1992).

²⁰D. S. Wilkinson and M. F. Ashby, *Acta Metall.* **23**, 1277 (1975).

²¹B. Budiansky, J. W. Hutchinson, and S. Slutsky, in *Mechanics of Solids, The Rodney Hill 60th Anniversary Volume*, edited by H. G. Hopkins and M. J. Sewell (Pergamon, New York, 1982), p. 13.

²²M. M. Carroll, *Metall. Trans. A* **17**, 1977 (1986).

²³K. T. Kim and M. M. Carroll, *Int. J. Plasticity* **3**, 67 (1987).

²⁴M. Hori and S. Nemat-Nasser, *J. Appl. Phys.* **64**, 856 (1988).

²⁵M. Haghi and L. Anand, *Int. J. Plasticity* **7**, 123 (1991).

²⁶L. Seaman, R. E. Tokheim, and D. R. Curran, Stanford Research Institute Report PYU-2407, 1974.

²⁷L. E. Malvern, *Introduction to the Mechanics of a Continuous Medium* (Prentice-Hall, New Jersey, 1969), p. 670.

²⁸J. R. Rice, *J. Appl. Mech. Trans. ASME* **37**, 728 (1970).

²⁹R. J. Clifton, *J. Appl. Mech. Trans. ASME* **50**, 941 (1983).

³⁰H. G. Hopkins, in *Progress in Solid Mechanics*, edited by I. N. Sneddon and R. Hill (Wiley-Interscience, New York, 1960), Vol. 1, p. 85.

³¹S. Ranganath and R. J. Clifton, *Comp. Meth. Mech. Eng.* **1**, 173 (1972).

³²W. Tong, Ph.D. thesis, Brown University, Providence, RI, 1991.

³³J. J. Mason, A. J. Rosakis, and G. Ravichandran, to appear in *Mechanics of Materials: Special Volume on Shear Instabilities and Viscoplasticity Theories Dedicated to the Memory of J. Duffy*, edited by R. W. Armstrong, R. C. Batra, M. A. Meyers, and T. W. Wright (Press, City, in press).

³⁴M. B. Friedman, H. H. Bieich, and R. J. Parnes, *J. Eng. Mech. Proc. ASCE EM3*, 189 (1965).

³⁵J. N. Johnson, *J. Appl. Phys.* **52**, 2812 (1981).

³⁶R. K. Linde, L. Seaman, and D. N. Schmidt, *J. Appl. Phys.* **43**, 3367 (1972).

³⁷M. da Silva and K. T. Ramesh, *J. Phys. IV Colloq.* **1**, C3-909 (1991).

³⁸T. J. Ahrens, G. M. Bond, W. Yang, and G. Liu, in *Shock-Wave and High-Strain-Rate Phenomena in Materials*, edited by M. A. Meyers, L. E. Murr, and K. P. Staudhammer (Marcel Dekker, New York, 1992), p. 339.

³⁹W. Tong, L. Anand, D. M. Parks, A. C. Pisoni, and L. Cheng (unpublished).

⁴⁰T. Wanheim, *Wear* **25**, 225 (1973).

⁴¹V. Prakash and R. J. Clifton, in *Proceedings of the VII International Congress on Experimental Mechanics* (Society for Experimental Mechanics, Bethel, CT, 1992), p. 556.

⁴²A. Mutz, Ph.D. thesis, California Institute of Technology, Pasadena, CA, 1992.

⁴³P. S. Follansbee and U. F. Kocks, *Acta Metall.* **36**, 81 (1988).

⁴⁴A. Needleman and V. Tvergaard, *Int. J. Fract.* **49**, 41 (1991).

⁴⁵J. Eftis and J. A. Nemes, *Int. J. Plasticity* **7**, 275 (1991).

Real-Time Spectroscopic Measurements in Shocked Materials

Y.M. Gupta
Shock Dynamics Center and Department of Physics
Washington State University
Pullman, Washington 99164-2814

Extended Abstract

The use of plane shock wave experiments to examine high stress and high strain-rate response of materials is now over forty years old. Because of the unique combination of large compression, high temperature, nonhydrostatic deformation, and short times attained in these experiments, a wide variety of structural and chemical changes have been observed in shocked materials. A mechanistic understanding of these changes is important for addressing fundamental issues in materials physics and chemistry, and for applications involving shock synthesis of novel materials.

Time-resolved optical spectroscopy and x-ray diffraction measurements in shock wave experiments, though inherently difficult, are important for obtaining mechanistic understanding for the following reasons: (a) they can provide direct insight into atomic/molecular mechanisms governing the shocked state, and (b) the fast time-scales in these experiments permit real time examination of processes governing structural and chemical changes.

Three recent studies on time - resolved spectroscopy (electronic and vibrational) in shocked materials are summarized. First, changes in the luminescence spectra of embedded chromium ions are related to microscopic aspects of shock induced elastic and inelastic deformation in sapphire crystals. Second, shock induced symmetry changes in diamond are determined from Raman measurements. Third, results of an ongoing study on a condensed explosive (liquid nitromethane) are summarized to demonstrate the use of time - resolved Raman measurements to determine molecular changes associated with the onset of shock induced chemical reactions in pure and sensitized nitromethane.

The advantages and limitations of the spectroscopic methods for monitoring structural and chemical changes will be outlined. To address the scientific issues relevant to this workshop, the above experimental developments need to be combined with time -

resolved continuum measurements and carefully controlled recovery experiments. In particular, the determination of reaction mechanisms and the extent of the reaction is a difficult problem. Future plans to address mechanistic and kinetic issues will be indicated.

Acknowledgments: The following individuals are gratefully acknowledged for their contribution to the work reported here: ruby work (P.D. Horn, S.M. Sharma, and X.A. Shen), diamond work (J.M. Boteler), nitromethane work (G.I. Pangilinan, C.P. Constantinou, J.M. Winey, and G.E. Duvall).

Relevant Publications:

1. Y.M. Gupta, "Progress in Understanding Shock Deformation in Condensed Materials at the Atomic/Molecular Level: Recent Experimental Developments," *Shock Compression of Condensed Matter-1991*, edited by S.C. Schmidt, R. Dick, J.W. Forbes (North-Holland, 1992).
2. Y.M. Gupta, "Time-Resolved Spectroscopy Under Shock Loading: Electronic and Chemical Changes in Liquid Carbon Disulfide," *High Pressure Research*, **10**, 717 (1992).
3. C.S. Yoo and Y.M. Gupta, "Time-Resolved Absorption Changes of Thin CS₂ Samples Under Shock Compression: Electronic and Chemical Implications," *J. Phys. Chem.* **94**, 2857 (1990).
4. S.M. Sharma and Y.M. Gupta, "Theoretical Analysis of R-Line Shifts of Ruby Subjected to Different Deformation Conditions," *Phys. Rev. B.*, **43**, 879 (1991).
5. X.A. Shen and Y.M. Gupta, "Effect of Crystal Orientation on Ruby R-Line Shifts Under Shock Compression and Tension," *Phys. Rev B*, **48**, 2929 (1993).
6. J.M. Boteler and Y.M. Gupta, "Shock Induced Splitting of the Triply Degenerate Raman Line in Diamond", *Phy. Rev. Lett.* **71**, 3497 (1993).
7. G.I. Pangilinan and Y.M. Gupta, "Time-Resolved Raman Measurements in Nitromethane Shocked to 140 Kbar," *J. of Phys. Chem.* (April 1994).
8. Y.M. Gupta, C.P. Constantinou, G.I. Pangilinan, and J.M. Winey, "Optical Spectroscopy to Understand Shock Induced Chemical Changes in Pure and Sensitized Nitromethane," Zel'dovich Memorial International Conference on Combustion, Moscow Region, Russia (September, 1994).

REAL-TIME SPECTROSCOPIC MEASUREMENTS IN SHOCKED MATERIALS

**Y.M. Gupta
Shock Dynamics Center
Washington State University
Pullman, Washington 99164-2814**

ACKNOWLEDGMENTS

**Work supported by O.N.R. and D.N.A.
The following individuals are thanked for their
contributions to the work described here.**

**Ruby Luminescence: S.M. Sharma,
X.A. Shen, J.K. Hyun**

Diamond Raman: J.M. Boteler

**Liquid
Nitromethane: G.I. Pangilinan,
J.M. Winey, and
C.P. Constantinou**

**Presented at the ARO Workshop on
Shock Synthesis of Materials
held at the Georgia Institute of Technology
May 24, 1994**

OUTLINE

- Background and Scientific Issues Related to Shock Synthesis of Materials
- Real Time Examination of Microscopic Changes in Shocked Materials
 1. X-Ray Diffraction (Q. Johnson, et. al., J. Wark, et. al.; E. Zaretsky, et. al.).
 2. Elastic and Inelastic Deformation in Ruby.
 3. Symmetry Changes in Diamond. *Only this work is presented in the proceedings*
 4. Chemical Reactions in Liquid Nitromethane.
- Relevance to Shock Synthesis; Workshop Questions; Future Direction.

Caution: The term "shock wave" is not strictly valid and the term "stress wave" or "dynamic loading" may be more appropriate for discussing material synthesis.

SHOCK SYNTHESIS OF MATERIALS

Established Results

- 1. Shock wave loading of powder mixtures has been used to synthesize a broad range of materials.**
- 2. Large number of recovery experiments have been carried out in the Soviet Union, United States, and Japan which clearly demonstrate the potential for using shock wave methods for materials synthesis and consolidation.**
- 3. Role of material variables has been examined to a limited degree.**

Unresolved Issues

- 1. Characteristic time scales associated with chemical reactions (or extent of reaction) in powder mixtures are not well known. Difficult problem!**
- 2. Mechanisms responsible for chemical reactions in powder mixtures are not well understood. Is rapid mass transport essential?**
- 3. What is the state of the material prior to the onset of the reaction? Is solid state reaction the right term?**



X-RAY DIFFRACTION IN SHOCKED MATERIALS

1. Q. Johnson, et.al. (1970-72): Carried out the first measurements; demonstrated crystal structure behind the shock front.
2. J. Wark, R. Whitlock, et.al. (1987-1991): First sub-nanosecond measurements; measurements on the shock input side. *Detailed analyses to simulate the x-ray diffraction data.*
3. E. Zaretsky, et. al. (1991): x-ray diffraction measurements using a gas gun; examined the intermediate step in the KCl phase transition (NaCl \rightarrow CsCl structure).
4. Research collaboration between Washington State University and Ben-Gurion University (E. Zaretsky) is underway to routinely carry out x-ray diffraction measurements in gas-gun experiments using commercially available equipment (1994 - ?).

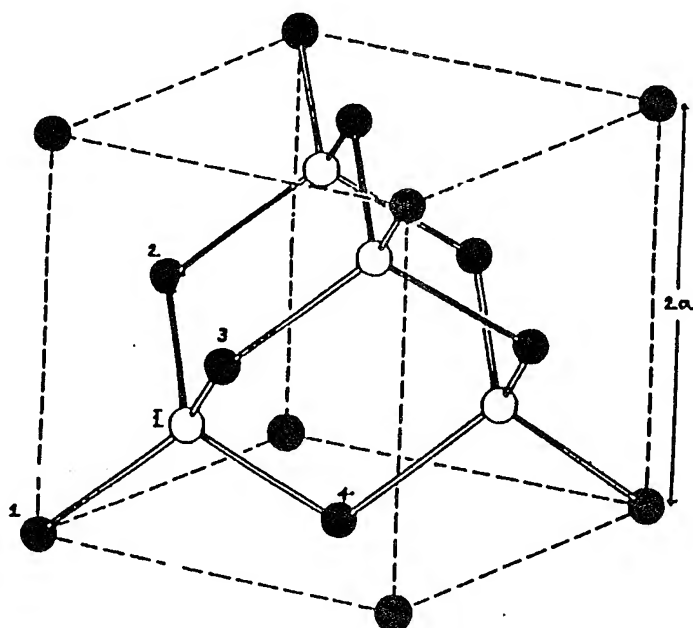
Note: Kondo, et. al. also reported some results in impacted LiF (1977).

TIME - RESOLVED RAMAN MEASUREMENTS IN SHOCKED DIAMOND

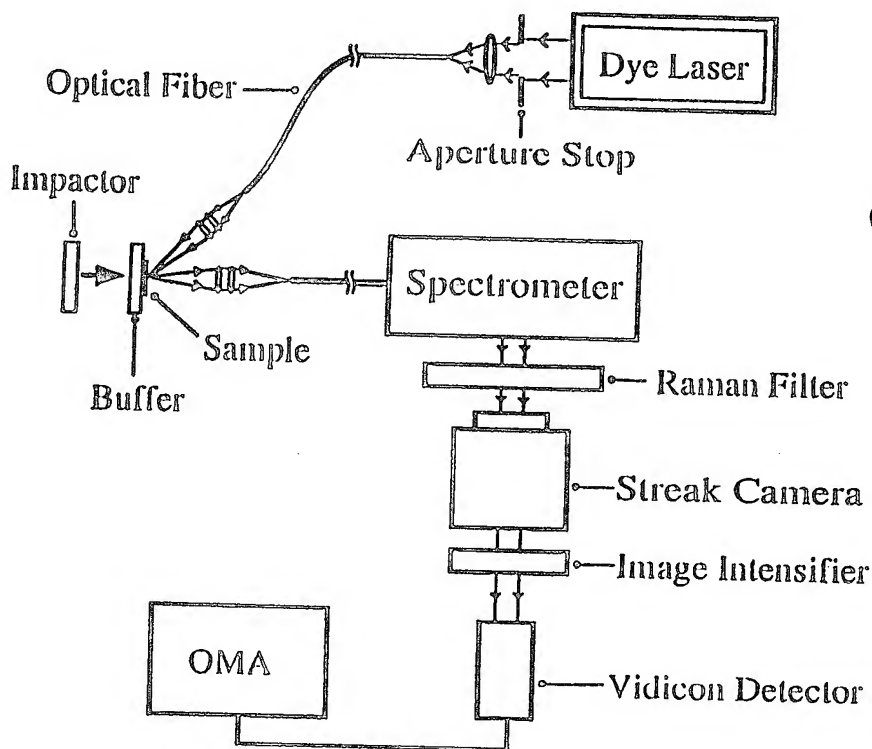
(Representative Example)

OBJECTIVES

1. Obtain fast time-resolved (10 ns resolution) Raman Spectra in shocked diamond.
2. Investigate symmetry (structural) changes in shocked diamond.
3. Theoretical developments to analyze Raman data at large stresses and for arbitrary deformation.

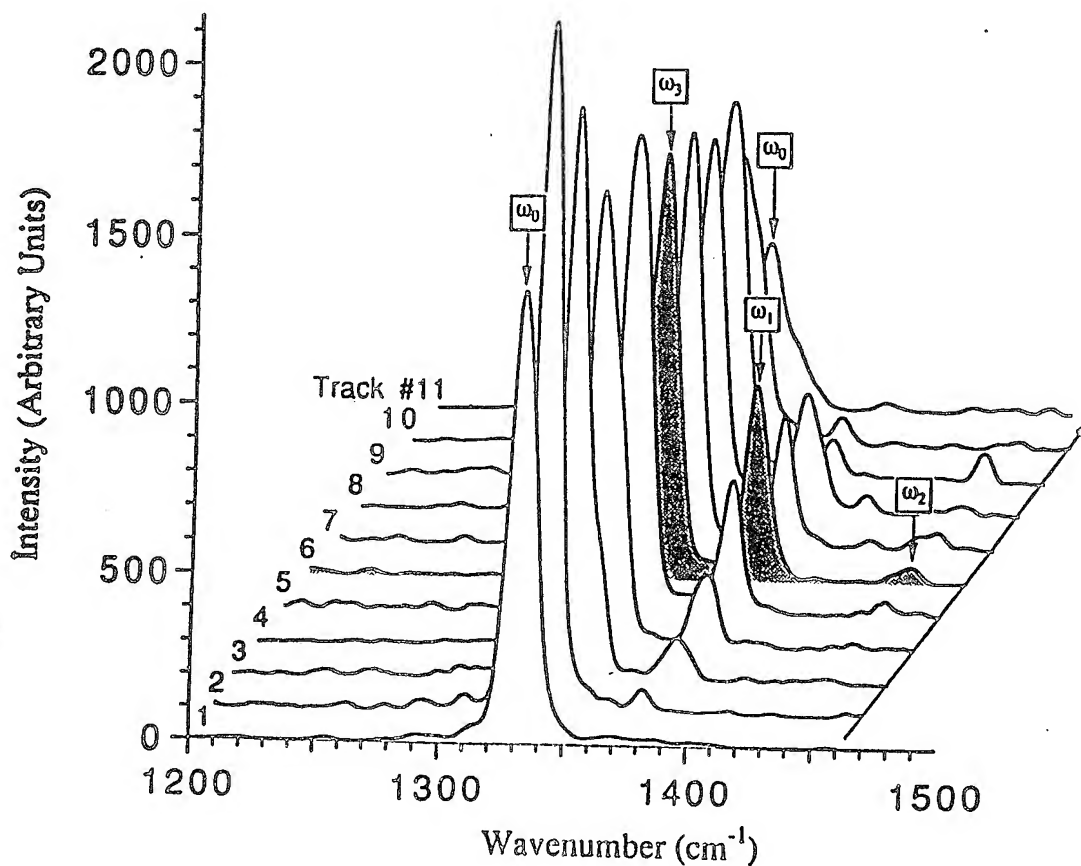


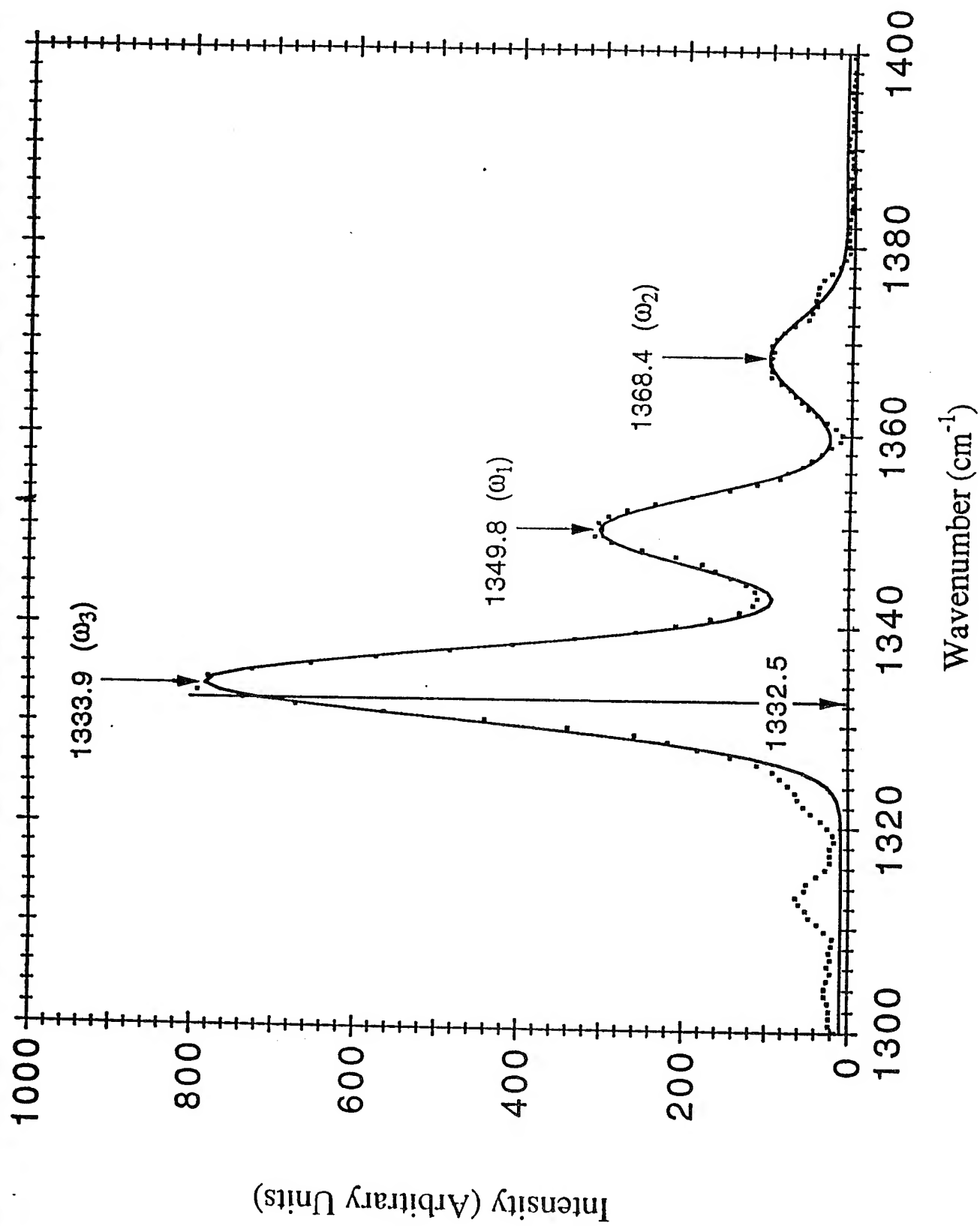
DIAMOND LATTICE

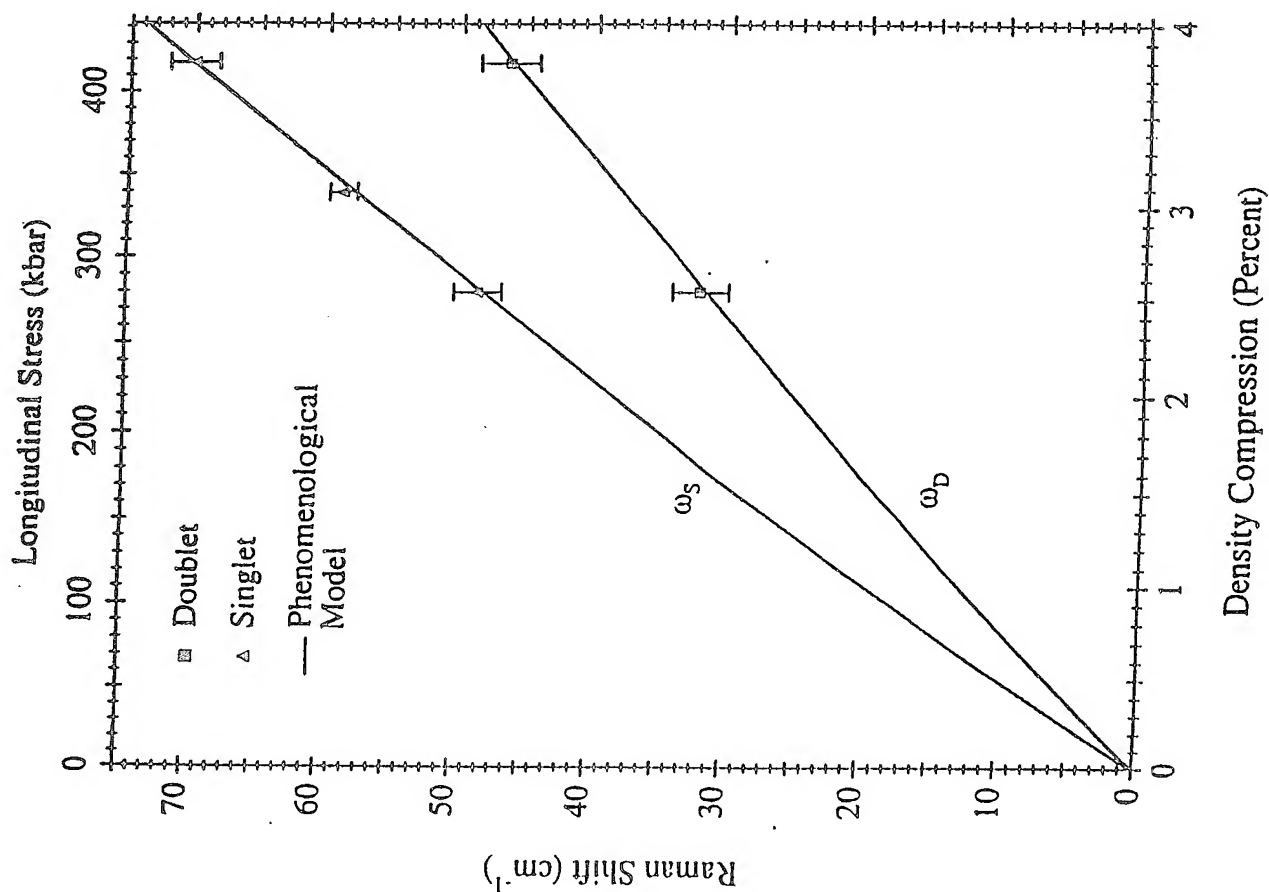
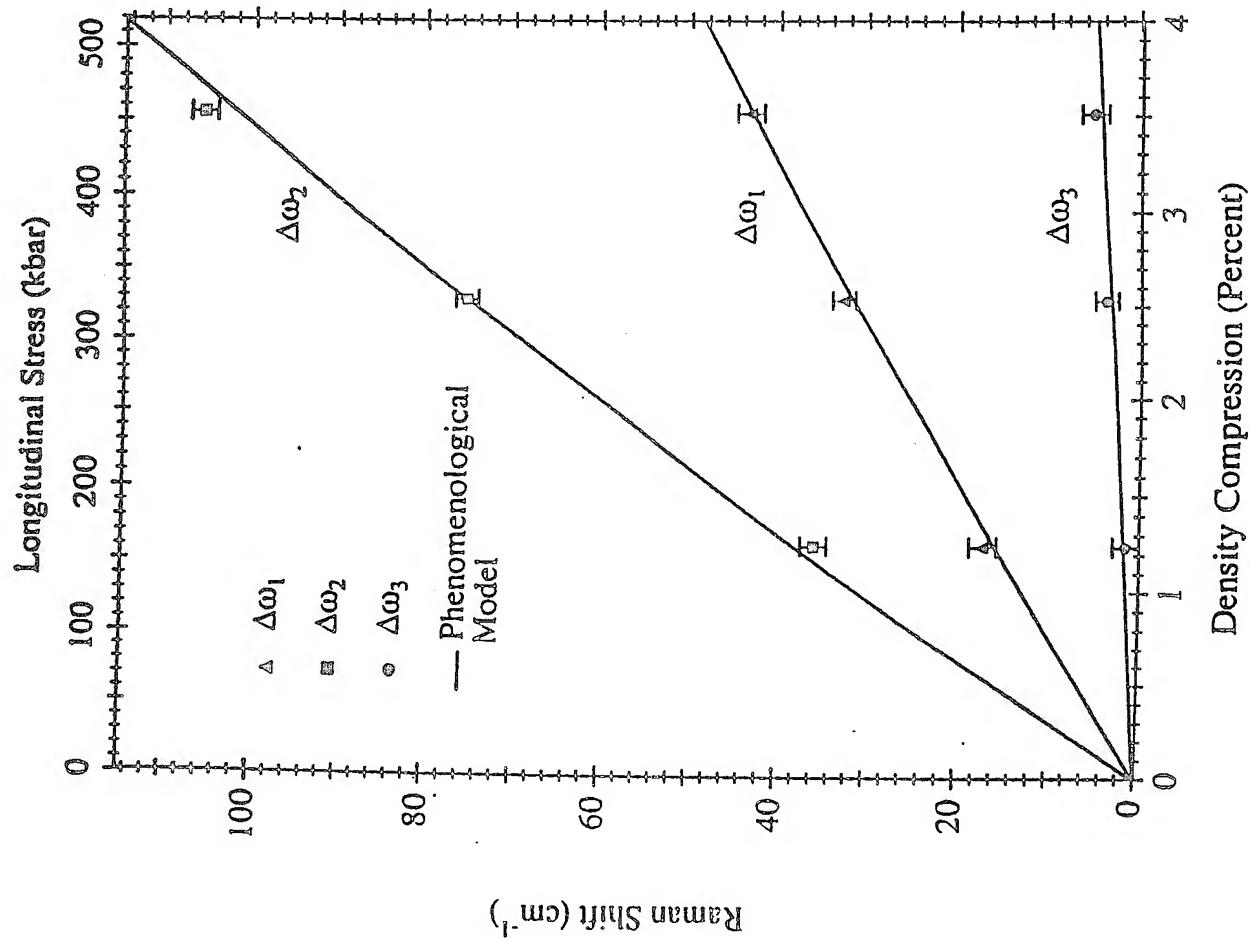


① Diamond Samples:
3-4 mm in diameter
& 0.75-1 mm thick

② 1-D Strain
 ≈ 80 ns







SUMMARY AND CONCLUSIONS

(Diamond Work)

- Time-resolved Raman spectroscopy (10 ns resolution) in shock compressed diamond has been demonstrated for longitudinal stresses to 500 kbar.
- Strain-induced splitting of the degenerate Raman line was observed for the first time during shock compression; direct evidence of shock-induced symmetry changes.
- The diamond mechanical response is elastic for the stresses considered in this work.
- Phenomenological model parameters can be obtained uniquely from the {110} data; subsequent {100} predictions show excellent agreement with experimental measurements.

RELEVANCE OF REAL TIME MICROSCOPIC MEASUREMENTS (TO DATE) TO SHOCK SYNTHESIS

1. Very little at first or even second glance.
2. The ability to examine shock induced changes at the microscopic level has been demonstrated.

3. For particular scientific problems,

ruby (elastic and inelastic deformation in a brittle solid)

diamond (symmetry changes and relationship to in-material stresses)

nitromethane (chemical reaction in an explosive),

new and useful results have been obtained after a sustained effort.

4. X-ray diffraction measurements (at appropriate time scales) on carefully selected materials have considerable potential to address mechanistic and kinetic questions for shock synthesis applications.

ns- μ s



WORKSHOP QUESTIONS

- (A) Has the initiation and completion of chemical reactions, during shock compression of powder mixtures, been conclusively demonstrated?

NO

- (B) Is it possible to establish the progress of reaction (fraction transformed with time) with available time-resolved measurement techniques? NOT SURE; MODEL DEPENDENT

WHAT IF ΔP_x or Δu IS VERY SMALL

- (C) What are the limitations of current time-resolved measurement techniques and what other novel in-situ measurement techniques need to be explored? VERY MINIMAL WORK

TO DATE

SEVERAL, BUT THEY ARE DIFFICULT

- (D) What is the current understanding of the process mechanisms and kinetics of chemical reactions occurring during shock compression of powders? CONJECTURES; OFTEN INCONSISTENT

WITH ONE ANOTHER

- (E) Can applications of shock chemistry be realized for synthesis of materials? YES

Cannot comment regarding cost effectiveness or practical applications.

FUTURE DIRECTIONS

If understanding of mechanisms and extent of reaction (as a function of time) are important needs, then the following tasks are recommended:

1. Careful material characterization of starting materials.
2. Well controlled recovery experiments with carefully defined stress histories. Instrumented recovery experiments?
3. Time-resolved continuum measurements using a variety of methods and careful analyses of these data. What is a characteristic signature of a reaction?
4. Need for other probes (thermal, electrical, etc.). Interpretation of these data is very difficult.
5. Analyses of experimental data (particularly the determination of extent of reaction) require considerable computational modeling. How to develop realistic material models? *Incorporation of mesoscopic scale is important.*
6. Microscopic measurements (x-ray diffraction) have the best potential for determining fundamental mechanisms. Further development and idealized experiments are needed.

SHOCK CHEMISTRY -- REAL-TIME MEASUREMENTS

S.S. Batsanov
Center for High Dynamic Pressures,
Mendeleevo, Moscow Region, 141570, RUSSIA

(presently at the University of California at San Diego, La Jolla, California)

The enthalpy changes of phase transformations have values about 10^{-3} to 10^{-4} times the energies atomization (E_a), while the thermal effects of chemical reactions may reach $2/3 E_a$. In result of the thermal extension of products of the exothermal reactions, the total changes of the volume may be 0. It means that on the curve of compressibility of reacting mixtures must be the corresponding change. The experimental Hugoniot investigations of synthesis reactions were carried out on examples of mixtures of Sn+S and Sn+Te, and for the dissociation reactions on examples of systems $\text{CuCl} = \text{Cu} + \text{CuCl}_2$ and $\text{CuI} = \text{Cu} + \text{CuI}_2$. The interaction Sn+S was investigated also by the optical pyrometer method. In that case a bell-like dependence of temperature and pressure was established. The optical measurements were carried out on 10 mm and therefore may be coupled with the thermocouple measurements which have time to $< 10^{-4}$.

The mechanism of superfast diffusion based on the difference of the particle velocities is discussed. It is supposed that for the chemical interactions in heterogeneous mixture the particles of reagents, must be fractured to sizes of $\sim 100\text{\AA}$. Then the chemical reactions on surfaces of that domains in the process of the mutual passage of particles may provide the transformation rate about 20% that was established in experiments.

ON THE POSSIBILITY OF CHEMICAL REACTIONS AT HIGH DYNAMIC PRESSURES

S.S. BATSANOV

All-Union Research Institute for Physicotechnical and Radiotechnical Measurements, Mendeleevo

(Received January 12, 1987)

The papers devoted to estimation of the reaction time in detonation waves propagating in charges of composite explosives and behind shock waves in hetero- and homogeneous mixtures of various components are analyzed. Based on the studies of detonation parameters or compositions of the products formed after shock compression it is suggested that the reaction may be completed within 10^{-6} - 10^{-5} s. A direct experiment on determination of shock Hugoniot of reacting mixtures is discussed and ideas concerning a new mechanism of superfast forced diffusion in mixtures of materials of different hardness pressurized dynamically are suggested.

Since the kinetics of solid-phase chemical reactions is controlled by the diffusion velocity, which ranges between ~ 0.1 and 1.0 mm/s at normal pressures, the diffusion layer formed within $\sim 10^{-6}$ s amounts to $1 - 10$ Å, i.e. only a monomolecular layer of the contacting particles in the mixture may react. These simple considerations underlay the conclusion about the low probability of solid-phase chemical reactions in any appreciable volume within the shock compression time, the more so at high pressures at which the diffusion velocity is small.

In heterogeneous reactions the diffusion time reduces

by 1 or 2 orders of magnitude compared to the reactants. However, the reaction path to become powder particles. The theory does not allow a reaction will be in the zone.

At the same time, which a more or less reaction of the reaction present work is experimental papers on

DETONATION OF COMPOSITE

The first chemical completion within investigations of materials with surroundings). Taking into pressure zone for 10^{-7} s, the characteristic expansion is 10^{-6} high-pressure characteristics of the walls and (expansion layers) are not interaction of explosion product

Below (Table devoted to investigation of detonation products. Investigations of processes in composite

by 1 or 2 orders owing to the gas or liquid state of one of the reactants. However this is insufficient for the diffusion path to become commensurate with the normal size of powder particles. Thus in this case the classical diffusion theory does not allow one to expect that the chemical reaction will be completed in the dynamic high-pressure zone.

At the same time there are many papers published in which a more or less substantiated conclusion about completion of the reaction within $10^{-5} - 10^{-6}$ s is made. The present work is devoted to a critical analysis of the experimental papers on this topic available in the literature.

DETONATION OF COMPOSITE EXPLOSIVES

The first chemical evidence of the feasibility of reaction completion within $\tau \leq 10^{-5}$ s was furnished by experimental investigations of detonation in mixtures of solid energetic materials with some additives (simple species and compounds). Taking into account that the duration of the high pressure zone in a detonation wave ranges from 10^{-6} to 10^{-7} s, the characteristic time of the detonation-product expansion is $10^{-5} - 10^{-6}$ s, depending on the size of the high-pressure chamber, and that the materials deposited on the walls and cooled there (within $10^{-5} - 10^{-6}$ s for thin layers) are not reactive, one can believe that the chemical interaction of the additives with each other or with the explosion products occurs within $\tau \leq 10^{-5}$ s.

Below (Table 1) we present the chronology of the works devoted to investigations of the chemical composition of the detonation products for various mixtures.

Investigations into the dynamics of detonation processes in composite explosives can also provide some informati-

TABLE 1

Additives	Zn, SiO ₂	Be, Mg, B, Al, Zr	B	Zn, S, Se, Te
Reaction Product	Zn ₂ SiO ₄	M _m N _n	B ₂ O ₃ , BN B ₄ C ₃	ZnS, ZnSe, ZnTe
Year	1938	1958	1972	1982
Reference	[1]	[2]	[3]	[4]

on about the rates of the chemical reactions. Although studies performed during many years (see the review paper [5]) have revealed no increase in the detonation velocity when such substances as Al are added to the energetic material (this increase would be an unequivocal evidence in favor of reaction completion within the high-pressure zone), more precise measurements of some detonation parameters allow determination of the time of chemical interaction of Al with the energetic material. The reaction time estimates made by various authors based on the studies of the dynamics of detonation-product expansion or from the second maximum on the $u(\tau)$ versus $P(\tau)$ dependence seem to be most convincing. The results of such experimental estimates of the Al + O₂ interaction time are listed in Table 2.

TABLE 2

$\tau \cdot 10^{-6}$, s	~20	~14	~4	2-3	10-30	500
year	1968	1970	1976	1978	1981	1985
Reference	[6]	[7]	[8]	[9]	[10]	[11]

It is obvious that in the majority of experiments the time of Al - energetic material interaction is about 10^{-6} s. The spread of the results obtained in different experiments may be due both to the different sensitivity of the measurement techniques employed and dissimilar sizes of the aluminum particles. Thus, as shown in [12], the burning time

of metal particles 10.6, 118, and 1180 μ m diameter, respectively, are of the same order of magnitude. It is expected that the reaction time

At the same time, the experiments show that the sizes of about 10 μ m particles of detonation wave temperatures below 1000 K, the temperature of the reagent, and the diffusion.

SHOCK PRESSURE

In experiments, the recovery of the material after cooling even minutes after the reaction in the detonation wave is solely on the structure, or compared with the mic pressurization.

Thus, the KBr solid state thermally synthesized standard value of alkali metal, the presence of the reaction with the stoichiometric [14], which is

of metal particles strongly depends on their size, e.g. $\tau = 10.6, 118, \text{ and } 326 \cdot 10^{-6} \text{ s}$ for particles 1, 5, and 10 μm in diameter, respectively. Since this is a spread of the particle sizes typical of conventional powders, one may naturally expect the respective scatter in the reaction times.

At the same time the above mentioned two types of experiments yield consistent results, namely, solid particles of about 10 μm in diameter react completely behind detonation waves within $\tau \sim 10^{-6} \text{ s}$. Inasmuch as the temperatures behind detonation waves are 2000 - 5000 K, the high-temperature gas- or liquid-phase state of at least one of the reagents may be considered as a reason for high-velocity diffusion.

SHOCK PRESSURIZATION OF MATERIALS IN RECOVERY AMPOULES.

In experiments on shock pressurization of materials in recovery ampoules analysis of the results is more complex since cooling of the expanded material lasts seconds and even minutes. Therefore a conclusion about completion of the reaction in the course of shock pressurization may be drawn solely on the basis of essential changes in the composition, structure, or properties of the compounds synthesized, as compared with those of the materials produced without dynamic pressurizing.

Thus in 1967 the authors of Ref. [13] obtained KCl - KBr solid solutions with a higher density than that of thermally synthesized specimens, which dropped to the standard value after annealing. An unusual feature of formation of alkali metal haloid - ammonium solutions is the dependence of the product composition on the shock wave intensity, with the stoichiometry of the initial mixture being constant [14], which is not observed in experiments with thermal

Zn, S, Se, Te

ZnS, ZnSe,

ZnTe

1982

[4]

ons. Although

review paper

tion velocity

the energetic

l evidence in

essure zone),

on parameters

interaction of

time estimates

the dynamics

second maximum

most convin-

es of the Al +

30 500

31 1985

31 [11]

xperiments the

about 10^{-6} s .

at experiments

f the measur-

sizes of the

burning time

synthesis. However this may also be attributed to a high residual static pressure in the recovery ampoule because of evaporation of the ammonium salts in a closed volume.

A specific composition of the shock - pressurizing product was observed for Nd_2O_3 where the $\text{Nd}_2\text{O}_3 \cdot n\text{SiO}_2$ compound was detected [15]. The SiO_2 presumably formed from the silicon contained in the ampoule walls and was introduced into the ampoule volume due to microspalling, which was confirmed later on by a direct experiment [16]. It is notable that Si, SiO, or SiO_2 deliberately added to Nd_2O_3 did not produce compounds with the same structure as in specimens in which Nd_2O_3 interacted with silicon spalled from the walls. The reason is probably a great difference between the thermodynamic parameters of the material in the jets and pressurized powder.

The material from the walls is ejected nonuniformly over the ampoule and its concentration exceeds the possible diffusion contamination [17-30]. The dependence of the contamination degree on the physicochemical conversions and fineness of the powdered material [21] indicates that the major contaminants are introduced into the material and react with it in the course of shock pressurization. Thus, with LiH pressurized by HMX detonation in a standard cylindrical recovery ampoule (0.5 cm i.d. and 4 cm long) about 1% of the iron is introduced in the material, which yields about 10 mg per 1 cm^2 of the internal ampoule surface [21]. According to [22] traversing of a shock wave across the free surface of the ampoule is accompanied by a microjet ejection of up to 100 mg of the material per 1 cm^2 , depending on the roughness of the surface.

Shock-induced interaction of Ln_2O_3 with TiO_2 , ZrO_2 , and HfO_2 was shown to produce materials whose composition and

crystalline structure synthesized by parameters of specimens re-heating. Although structural changes after shock synthesis induced

The product water behind a 26]. Since the metals more so molecules, the shock compression occurred liquid nitrogen unstable compounds of low-temperature be considered reaction can since the amp pressure and the detonation

To understand with H_2) was supplementary during deposition ZrO_2 modification analysis of the synthesis was

The experimental investigation

crystalline structure differed from those of the thermally synthesized material [23,24]. It is noteworthy that the parameters of the elementary cells of "shock pressurized" specimens relax to their equilibrium "thermal" values upon heating. Although the authors of these works attribute the structural discrepancies to rapid freezing of the melts after shock compression, these facts may also be due to the synthesis induced by high dynamic pressures.

The products of chemical interaction of metals with water behind shock waves were investigated in the works [25, 26]. Since water behaves as an acid at high pressures, metals more active than hydrogen must displace it in H_2O molecules, provided the reaction is completed during the shock compression. Experiment confirmed this, and the reaction occurred even when the specimen was precooled to the liquid nitrogen temperature. Formation of such thermally unstable compounds as ZnO_2 also indirectly confirms the fact of low-temperature reaction. However these results can not be considered as an exhaustive chemical verification of reaction completion in the zone of high dynamic pressures since the ampoule serves as an autoclave with a high static pressure and temperature exceeding $100^\circ C$ after expansion of the detonation products.

To unequivocally resolve the problem, a reaction of Zr with H_2 was conducted in an ampoule connected with a large supplementary volume into which the water or vapor expanded during depressurization. This experiment yielded a cubic ZrO_2 modification, which is a high-pressure phase. An analysis of the experimental conditions showed that the synthesis was completed within $\tau \sim 10^{-5}$ s [27].

The examples considered above are synthesis reactions. Investigations into decomposition reactions in shocked mate-

rials are also available. Decomposition of CdCO_3 into CdO and CO_2 is affected by the diameter of the charge of pressurizing energetic material, i.e. by the duration of the shock pressure pulse, despite the fact that the residual temperature is the same, the shock pressure being constant [28]. This is an argument in favor of the occurrence of the reaction in the high-pressure zone, however it is not of principal importance for the problem being discussed since no diffusion processes are needed for carbonate decomposition (the decomposition is of the intramolecular nature, while removal of the gas is not kinetically hindered).

Shock-induced decomposition of bromates and nitrates of alkali metals [29] and potassium persulfate [30] resembles radiolysis processes, i.e. it is not due to the residual heat. The shock Hugoniot of CO and CH_4 can be described satisfactorily only if pressure-induced decomposition of the molecules is assumed to occur at $p > 20$ GPa [31].

Decomposition of shock-pressurised Al_2SiO_5 into Al_2O_3 and SiO_2 is of greater interest from the methodological point of view since the decomposition products are amorphous, which points to a high rate and nonthermal nature of the process. At high pressures Al_2SiO_5 decomposes into corundum and stishovite, which is direct evidence of the baric nature of the reaction [32, 33]. Similarly the authors of Ref. [34] observed partial decomposition of ZnBaGeO_4 into ZnO and BaGeO_3 at $p > 41$ GPa. The shock compression curve of forsterite at $80 < p < 180$ GPa agrees with the calculated Hugoniot of mixtures $\text{MgO} + \text{SiO}_2$ (stishovite) and $\text{MgO} + \text{MgSiO}_3$ (perovskite) [35]. Finally, it was found quite recently [36] that the compression of powder and monocrystalline ZrSiO_4 by shock waves with amplitudes of 53 and 94 GPa, respectively, yielded the tetragonal ZrO_2 phase.

Experimental data indicate that the shock pressure pulse pressure exceeded that of the transport bulk nature, equal to the time, it is possible in solid assumption that are equal for state is that can never be new diffuser in the solid.

PHYSICAL MECHANISMS

When studying the process of shock wave propagation into air and decelerated decelerated slightly and by the reaction minimum is aluminum part and velocity is 10 km/s at period and path lengths $13 \cdot 10^{-6}$ s, the oxidation state

From the

Experiments [37] showed that diffusion in iron subjected to plastic deformation was enhanced most strongly upon pulse pressurization (in which case the diffusion rate exceeded that for the liquid state). It should be noted that the transport of atoms during pulse pressurization is of the bulk nature, with the atom mobility being approximately equal to the plastic-deformation velocity [38]. At the same time, it is pointed out in [39] that the diffusion velocities in solids turn out to be anomalously high due to the assumption that the diffusion and shock-compression times are equal and that the diffusion velocity in the liquid state is the physical limit for the condensed state, which can never be reached in solids. In what follows we discuss a new diffusion mechanism that may ensure a diffusion velocity in the solid state which is higher than that in liquids.

PHYSICAL MEASUREMENTS DURING AND AFTER SHOCK PRESSURIZATION

When studying high-velocity projection of aluminum powder into air and inert gases [40] it was found that the powder decelerated in air more rapidly; in 30% of the runs it decelerated sharply at 60 mm from the free surface and then slightly accelerated. These observations are accounted for by the reaction of Al with oxygen. Here the additional aluminum is due to ablation and further burning of the aluminum particles accompanied by an increase in their mass and velocity. Taking into account that the particle velocity is 10 km/s at the beginning of the anomalous-deceleration period and 6 km/s at the minimum, and that the respective path lengths are 60 and 80 mm, we obtain $6 \cdot 10^{-6}$ s and $13 \cdot 10^{-6}$ s, respectively, for the times at which ablation and oxidation start.

From the dynamic-pressure records in a Cu + CBr₄ system

the authors of the paper [41] inferred that CuBr formed within $(1.2 - 3.4) \cdot 10^{-6}$ s. However, because of the lack of the pressure profiles in inert CuBr or CBr₄ specimens under identical conditions of pressurization by semispherical shaped charges the specific shape of the oscillographic traces can not be attributed to the combination reaction only.

In the work [42] the brightness temperature in Al + Ni mixtures pressurized by plane shock waves was measured. Optical pyrometric measurements with computer-aided processing revealed hot spots in the shocked mixture that were brighter than the average background and had a temperature of $T > 650$ and 875°C . The appearance of these hot spots was explained by exothermic interaction of the metals. However, taking into account the possibility of local heating of the mixture due to plastic deformations and surface phenomena [43, 44] and also the lack of reference measurements on the product of the Al + Ni reaction under the same conditions, the conclusion about the completion of the Al + Ni reaction within several microseconds made by the authors of the above mentioned paper can not be considered properly substantiated.

Thus, although the times reported in Refs. [41, 42] seem to be realistic, they should be treated not more than theoretical estimates because of the absence of rigorous experimental verification.

In 1985 at the Conference of the American Physical Society on shock waves, where the paper [42] was presented, we reported the results of our studies on electrical conductivity in systems metal + sulfur under conditions of pulse pressurization [45]. The full text of the paper was published later [46]. It was shown there that 30-50 μs after the

electrical static pressure (σ) vs. temperature characteristic of the reaction of the time interval monotonic increase plastic defects in further reaction

The compressed mixture where the temperature $10^{-4} - 10^{-3}$ cal/cm² defect concentration structure alone are concerned measurement metal half several cycles phase transition of the data assessing the

The mixture with a Sn-S mixture the explosive metal SnS, and exothermic

electrical explosion of the metal powder in sulfur under a static pressure of several GPa the sign of the conductivity (σ) vs. temperature dependence changed from that characteristic of metal to the semiconductor-type one. Hence formation of the semiconductor compound is completed within this time interval. Measurements on prepared compounds showed a monotonic $\sigma(T)$ dependence. It may be anticipated that intense plastic flows and the high density of the shock-induced defects in the conditions of explosion experiment will further reduce the reaction time.

The change of the electrical conductivity in shock compressed Sn + S mixtures was studied in the work [47], where the reaction was found to be completed within about $10^{-4} - 10^{-3}$ s. It should however be noted that the electrical conductivity is strongly dependent on the temperature, defect concentration, and other parameters of the real structure, therefore electrical conductivity measurements alone are insufficient for making unequivocal conclusions concerning chemical reactions. For example, conductivity measurements in a number of powders of crystalline alkaline-metal halides revealed that σ changed with pressure by several orders of magnitude, growing drastically in the phase transition area [48]. Difficulties in interpretation of the data on σ made us use temperature measurements when assessing the reaction time in shocked solid materials.

The first investigation on this subject was performed with a Sn + S mixture in 1969 [19]. The temperature of the mixture was measured with thermocouples 0.05 - 0.1 s after the explosion. The residual temperature in identical experimental conditions was 110, 122, 131, and 1140°C for Sn, S, SnS, and Sn + S, respectively, which is associated with the exothermic nature of the combination reaction (the estimate

of the residual temperature in the Sn + S mixture using the standard thermochemical data is 1400°C). In the work [49] the rise time of the temperature measurements was reduced to 10^{-4} s by employing thin foils, and in [50] it was even lower, 10^{-5} s. It turned out that the reaction of SnS formation was completed within the shortest of the time intervals indicated above.

Generally speaking, since the effect of the explosion on the mixture of the components shifts the beginning of the reaction only insignificantly (just by several percent, see [51]), it can be inferred from a comparison of the residual temperature of the components of the system ($110 - 122^{\circ}\text{C}$) and the temperature at which the Sn + S reaction starts in the absence of pressure (measured by a Kurnakov pyrometer [19] and equal to 250°C) that reaction begins in the shock wave.

The problem was solved completely in the work [52] where the Hugoniot for SnS and a Sn + S mixture were measured. The experiments showed that starting from $p > 15$ GPa the compressibility curve for the mixture deviates from the monotonic dependence, practically coinciding with the Hugoniot of the prepared compound, towards greater specific volumes, which is due to heat release in the combination reaction. The pressure profiles for the compound and reactive mixture also differ due to the additional thermal pressure in the mixture. An analysis of the experimental data demonstrates that about 25% of the mixture reacted within $0.05 \cdot 10^{-6}$ s.

What is the mechanism of superfast diffusion in shock-pressurized solid materials? The author of Ref. [53] suggests that the plastic flows are responsible for fast diffusion, whereas in [13] a quasiliquid state of the pressurized

material
ment.

in mater
[54].

56], whe

preced
gents)

to the
paper

cal for
ensured

The gro
reduc

multipl

ture
the pos

ent to

pressur
52)

solids

the

effect

mech

from 2

diffus

occu

diffus

cles,

the

of th

material was assumed to be the cause of diffusion enhancement. A concrete mechanism of diffusion with high velocities in materials undergoing plastic deformations is proposed in [54]. Another mechanism was suggested in the papers [55, 56], where it was assumed that the chemical interaction was preceded by phase transition (at least in one of the reagents) drastically increasing the mobility of the atoms due to the breakdown of the chemical bonds. Finally, in the paper [57] a special case of ion crystals in which electrical forces responsible for polarization of the material ensure great diffusion velocities of the ions is considered. The growth of the contact surface between the particles, the reduction of the activation energy caused by generation of multiple defects, and the heterogeneous heating of the mixture components [58, 55] accelerate solid state reactions in the post-shock regime.

At present the aforesaid reasons seem to be insufficient to account for all the reactions occurring under shock pressurization of solid materials. In our recent works [59, 52] we suggested a new diffusion mechanism in reactive solids. It is the discrepancy in the particle velocities of the reagents which causes (like in the wellknown Kirkendall effect) forced diffusion with velocity Δu . Depending on the mechanical properties of the mixture components Δu may vary from zero to several km/s, which explains both the superhigh diffusion velocity and the threshold nature of the processes occurring behind shock waves.

In conclusion we discuss a terminological question. The diffusion time is a function of the size of reacting particles, while reaction detection depends on the sensitivity of the technique employed. For this reason a strict definition of the reaction time implies specification of the particle

size and chemical-conversion degree [46], otherwise one may obtain any result. It seems to be reasonable to use the time to reaction completion or the time required for the conversion degree to change within an order of magnitude, e.g. from 10 to 100%, as the normal criterion.

Thus, the results of numerous investigations considered above allow a definite conclusion to be made, namely, that hetero- and solid-phase reactions in shock-compressed materials may be completed within 10^{-6} - 10^{-5} s. Superhigh diffusion velocities are due to the high temperatures and low activation energies in hetero-phase systems and to the difference in the particle velocities of the mixture components leading to forced diffusion with velocity Δu in systems with solid phase reactions. Hence, the reaction may be completed in the high-pressure zone or in the expanded material, depending on the experimental conditions and properties of the materials.

REFERENCES

1. A. Mishel-Leuy and J. Wyart, *Compt. Rend.* 206, 261 (1936).
2. A.Ya. Apin, Yu.A. Lebedev, and O.I. Nefedova, *Zhurn. Fiz. Khimii* 32, 819 (1958) (in Russian).
3. V.I. Pepekin, M.I. Makhov, and A.Ya. Apin, *Fizika Goreniya i Vzryva* 8, 135 (1972) (in Russian).
4. S.S. Batsanov, L.I. Kopaneva, E.V. Lazareva, et al. *Zhurn. Neorg. Khimii* 27, 2135 (1982) (in Russian).
5. A.I. Aniskin, *Materialy VIII Vsesoyuzn. simpoziuma po goreniyu* (Materials of the VIII USSR symposium on combustion) (IKhF AN SSSR, Chernogolovka, 1986) p. 26 (in Russian).
6. V. Strauss, *AIAA J.* 6, 159 (1968).
7. M. Finger, H. Hornig, E. Lee, and J. Kury, *V Symp. on Detonation* (Naval Surface Weapons Center, White Oak, 1970) p. 55.
8. G. Bjarnholt, *VI Symp. on Detonation* (Naval Surface Weapons Center, White Oak, 1976) p. 510.
9. H. Moulard, Lonbard, p. 293.
10. A.I. Aniskin, *detonatsiya* (detonation) (in Russian).
11. B. Veyssier, *Detonatsiya*.
12. A.F. Belyaev, *Goreniya i Vzryva*.
13. S.S. Batsanov, (Russian).
14. S.S. Batsanov, *Vsesoyuzn. simpozium po goreniyu* (VNIIFTRI, presented).
15. S.S. Batsanov, (Paris, 1972).
16. D.L. Gurzhanov, *Goreniya i Vzryva*.
17. S.S. Batsanov, *Goreniya i Vzryva*.
18. S.S. Batsanov, *Fizika Goreniya i Vzryva*.
19. S.S. Batsanov, *Dokl. Akad. Nauk SSSR*.
20. S.S. Batsanov, *Fizika Goreniya i Vzryva* (in Russian).
21. V.M. Pyatkov, *simpozium po goreniyu i vzryvu* (the I USSR symposium on combustion) (Moscow, 1972).
22. P. Chapoy, (New York, 1972).
23. A.V. Kiselev, *Dokl. Akad. Nauk SSSR* (in Russian).
24. A.V. Kiselev, *Vsesoyuzn. simpozium po goreniyu i vzryvu* (VIII USSR symposium on combustion) (SSSR, 1972).
25. S.S. Batsanov, *Vysokikiye Davleniya*.
26. S.S. Batsanov, *Fizika Goreniya i Vzryva*.

9. H. Moulard, C. Fauquignon, M. Lichtenberger, and J. Lonbard, *Sympos. on High Dynamic Pressures* (Paris, 1978) p. 293.
10. A.I. Aniskin, *Mater. II Vsesoyuzn. soveshch. po detonatsii* (Materials of the II USSR conference on detonation) (IKhF AN SSSR, Chernogolovka, 1981) p. 39 (in Russian).
11. B. Veyssiere, *Dynamics of Shock Waves. Explosions and Detonations* 94 (AIAA, New York, 1985) p. 264.
12. A.F. Belyaev, Yu.V. Frolov, and A.I. Korotkov, *Fizika Goreniya i Vzryva* 4, 323 (1968) (in Russian).
13. S.S. Batsanov, *Izv. SO AN SSSR*, No. 14, 22 (1967) (in Russian).
14. S.S. Batsanov, L.I. Kopaneva, and E.V. Lazareva, *Dokl. I Vsesoyuzn. simpoz. po impul'snym davleniyam*, 2 (Papers presented at the I USSR sympos. on dynamic pressures) (VNIIFTRI, Moscow, 1974) (in Russian).
15. S.S. Batsanov, *Symposium on High Dynamic Pressures* (Paris, 1968) p. 371.
16. D.L. Gur'ev, E.V. Lazareva, and L.I. Kopaneva, *Fizika i Goreniya i Vzryva* 19, No. 2, 110 (1983) (in Russian).
17. S.S. Batsanov, S.S. Derbeneva, and A.A. Deribas, *Fizika Goreniya i Vzryva* 2, 110 (1966) (in Russian).
18. S.S. Batsanov, V.M. Nigmatullina, and I.G. Yudelevich, *Fizika Goreniya i Vzryva* 4, 422 (1968) (in Russian).
19. S.S. Batsanov, N.A. Shestakova, V.P. Stupnikov, et al., *Dokl. Akad. Nauk SSSR* 185, 330 (1969) (in Russian).
20. S.S. Batsanov, I.A. Ovsyanikova, and N.A. Shestakova, *Fizika i Khimiya Obrabotki Materialov*, No. 1, 166 (1974) (in Russian).
21. V.M. Pyatak and S.S. Batsanov, *Dokl. I Vsesoyuzn. simpoz. po impul'snym davleniyam* (Papers presented at the I USSR sympos. on dynamic pressures) (VNIIFTRI, Moscow, 1974) p. 101 (in Russian).
22. P. Chapron and P. Elias, *Shock Waves in Condensed Matter* (New York, 1986) p. 645.
23. A.V. Kolesnikov, L.G. Shcherbakova, and O.N. Breusov, *Dokl. Akad. Nauk SSSR* 251, 142 (1980); 256, 113 (1981) (in Russian).
24. A.V. Kolesnikov and L.G. Shcherbakova, *Mater. VIII Vsesoyuzn. simpoz. po goreniyu i vzryvu* (Mater. of the VIII USSR sympos. on combustion and explosion) (IKhF AN SSSR, Chernogolovka, 1986) p. 57 (in Russian).
25. S.S. Batsanov, E.V. Lazareva, and L.I. Kopaneva, *Khimiya Vysokikh Energii* 16, 184 (1982) (in Russian).
26. S.S. Batsanov, E.V. Lazareva, and L.I. Kopaneva, *Khim. Fizika* 3, 905 (1984) (in Russian).

27. S.S. Batsanov, D.L. Gur'ev, and L.I. Kopaneva, *Fizika Goreniya i Vzryva* 23, No. 5, (1987) (in Russian).
28. S.S. Batsanov, V.A. Bakhmutskaia, A.A. Deribas, and E.N. Zalivina, *Fizika Goreniya i Vzryva* 3, 148 (1967) (in Russian).
29. V.V. Boldyrev, E.E. Zarko, and A.A. Deribas, *Khimiya Vysokikh Energii* 1, 177 (1967) (in Russian).
30. A.I. Lapshina, V.E. Borodaevskii, and S.S. Batsanov, *Khimiya Vysokikh Energii* 4, 154 (1970) (in Russian).
31. W. Nellis, F. Ree, M. van Thiel, and A. Michell, *J. Chem. Phys.* 75, 3055 (1981).
32. H. Schneider, W. Klee, and U. Hornemann, *J. Mater. Sci.* 15, 154 (1980).
33. H. Schneider and U. Hornemann, *J. Mater. Sci.* 16, 45 (1981).
34. H. Takei, Y. Syono, T. Goto, and M. Kikuchi, *Phys. Chem. Miner.* 10, 16 (1983).
35. J. Watt and T. Ahrens, *J. Geophys. Res.* B88, 9500 (1983).
36. K. Kusaba, Y. Syono, M. Kikuchi, and K. Fukuoka, *Earth Planet. Sci. Lett.* 72, 433 (1985).
37. L.N. Larikov, V.M. Fal'chenko, V.F. Mazanko, et al., *Dokl. Akad. Nauk SSSR* 221, 1073 (1975) (in Russian).
38. V.M. Fal'chenko, *Metallofizika*, No. 76, 21 (1979) (in Russian).
39. Yu.L. Krasulin, *Fizika i Khimiya Obrab. Materialov*, No. 4, 133 (1981) (in Russian).
40. S.S. Batsanov, A.A. Nerchenko, V.V. Roman'kov, et al., *Inzh.-phys. Zhurn.* 24, 354 (1973) (in Russian).
41. R. Heimann, J. Kleimann, and N. Salansky, *J. Cryst. Growth.* 67, 213 (1984) (in Russian).
42. M. Boslough, R. Graham, and D. Webb, *Shock Waves in Condensed Matter* (New York, 1986) p. 767.
43. G.V. Belyakov, V.N. Rodionov, and V.P. Samosadnyi, *Fizika Goreniya i Vzryva* 13, 614 (1977) (in Russian).
44. K. Kondo and T. Ahrens, *Phys. Chem. Miner.* 9, 173 (1983).
45. S.S. Batsanov and A.V. Parshukov, *Bull. Amer. Phys. Soc.* 30, 1319 (1985).
46. S.S. Batsanov and A.V. Parshukov, *Khim. Fizika* 5, 1545 (1986) (in Russian).
47. S.O. Subitidze, S.S. Nabatov, V.V. Yakushev, and D.A. Mogilyanskii, *Mater. VIII Vsesoyuzn. simpoz. po goreniyu i vzryvu*. (Materials of VIII USSR sympos. on combustion and explosion) (IKhF AN SSSR, Chernogolovka, 1986) p. 19 (in Russian).
48. A.V. Parshukov, V.S. Petrov, and S.S. Batsanov, *Izv. Akad. Nauk SSSR. Neorganich. Materialy* 21, 1981 (1985)

- (in Russian)
49. D.L. Gur'ev, *Fizika Goreniya i Vzryva* 30, 1320 (1987)
50. S.S. Batsanov, *Fizika Goreniya i Vzryva* 23, No. 2, (1987)
51. R. Graham, *Matter* (1986)
52. S.S. Batsanov, *Fizika Goreniya i Vzryva* (in Russian)
53. B. Alder, *J. Chem. Phys.* 38, 385 (1962)
54. A.N. Dremin, *Fizika Goreniya i Vzryva* (1968)
55. S.S. Batsanov, *Fizika Goreniya i Vzryva* (Detonation versions Chernogolovka)
56. S.S. Batsanov, *Fizika Goreniya i Vzryva* (in Russian)
57. V.S. Trofimov, *Fizika Goreniya i Vzryva* (Detonation versions Chernogolovka)
58. S.S. Batsanov, *Fizika Goreniya i Vzryva* (Preprints) (Mir Publ.)
59. S.S. Batsanov, *Fizika Goreniya i Vzryva* (Russian)

(in Russian).

va, *Fizika*

an).

s, and E.M.

(1967) (in

Khimiya

Batsanov,

Russian).

Hill, J.

Water. Sci.

1. 16, 45

Phys. Chem.

, 9500

ka, Earth

et al.,

Russian).

(1979) (in

ialov, No.

ov, et al.,

).

Cryst.

ves in

sadnyi,

Russian).

9 173

r. Phys. Soc.

a 5, 1545

and D.A.

po goreniiya

n combustion

, 1986) p. 19

v, Izv.

1981 (1985)

11. D.L. Gur'ev and S.S. Batsanov, *Bull. Amer. Phys. Soc.* 30, 1320 (1985).

10. S.S. Batsanov and D.L. Gur'ev, *Fizika Goreniya i Vzryva* 23, No. 2, 137 (1987) (in Russian).

11. R. Graham, Y. Horie, et al., *Shock Waves in Condensed Matter* (New York, 1986) p.693.

12. S.S. Batsanov, G.S. Doronin, S.V. Klochkov, and A.I. Teut, *Fizika Goreniya i Vzryva* 22, No. 6, 134 (1986) (in Russian).

13. B. Alder, *Solids under Pressure*, (New York, 1963) p. 385.

14. A.N. Dremine and O.N. Breusov, *Uspekhi Khimii* 37, 898 (1968) (in Russian).

15. S.S. Batsanov, *Detonatsiya. Kriticheskie yavleniya. Fiziko-khimicheskie prevrashcheniya v udarnykh volnakh.* (Detonation. Critical phenomena. Physico-chemical conversions behind shock waves) (IKhF AN SSSR, Chernogolovka, 1978) p. 126 (in Russian).

16. S.S. Batsanov, *Zhurn. Neorgan. Khimii* 27, 1903 (1982) (in Russian).

17. V.S. Trofimov, *Detonatsiya. Kriticheskie yavleniya. Fiziko-khimicheskie prevrashcheniya v udarnykh volnakh.* (Detonation. Critical phenomena. Physico-chemical conversions behind shock waves) (IKhF AN SSSR, Chernogolovka, 1978) p. 11 (in Russian).

18. S.S. Batsanov, *Preparativnye metody v khimii tverdogo tela* (Preparative methods in the chemistry of solids) (Mir Publ., Moscow, 1976) p. 157 (in Russian).

19. S.S. Batsanov, *Uspekhi Khimii* 55, 579 (1986) (in Russian).

"Real-Time Temperature Measurements"

Mark Boslough
Experimental Impact Physics Department
Sandia National Laboratories, MS-0821
Albuquerque, NM 87123-0821

Methods for shock processing and synthesis of materials can involve very rapid, exothermic, shock-induced chemical reactions. To fully understand these reactions, time-resolved measurements of their progress must be made during a shock experiment. Unless the products of the reactions include vapor, the thermodynamic state variable that is most sensitive to the extent of reaction is the temperature. Time-resolved temperatures can be determined directly from pyrometer measurements of thermal radiation emitted from shocked material. However, radiation pyrometer measurements are dominated by the highest temperatures present in a sample. Application to nonuniform materials like powders will always be complicated by the fact that the temperature distribution is heterogeneous for a period of time after the shock wave arrives at the region where the measurement is made. Until temperature equilibrium is achieved, the measured temperature will be that of local heterogeneities, and not that of the bulk material. The measured temperature will be a function of parameters such as particle size and morphology, pore space, thermal diffusivity, heat capacity and other mechanical and physical properties that have nothing to do with chemical reactions. If the relaxation time for temperature equilibration is greater than the shock duration, then true shock temperatures cannot be measured and the progress of any chemical reaction cannot be determined. For powders with particle sizes of greater than a few microns, the relaxation time is greater than the microsecond-scale duration of gun experiments. Thus micron and submicron particle-size powders are required for real-time shock temperature measurements. Even in this case the time resolution of the temperature measurement is limited by the temperature equilibration time. Despite this limitation, temperature measurements have strengthened the evidence for sub-microsecond shock-induced chemical reactions in micron-scale powders of nickel-aluminum and of hematite-aluminum (thermite). Because of the complications associated with shock compaction of powder mixtures, control experiments need to be performed on pure compacts of each component to characterize the effects of the physical and mechanical (but not chemical) properties. Any conclusion based on experiments without the requisite control experiments should be suspect.

1. Boslough, M. B. (1992) Thermochemistry of shock-induced exothermic reactions in selected porous mixtures. In M.A. Meyers, L.E. Murr, and K.P. Staudhammer, Eds., *Proceedings of Explomet '90 International Conference on Shock-Wave and High-Strain-Rate Phenomena in Materials*, Marcel Dekker, New York, 253-260.
2. Boslough, M. B., (1992) Postshock spectral radiance measurements in nickel and nickel/aluminum powders. In S. C. Schmidt et al., Eds., *Shock Compression of Condensed Matter - 1991*, North-Holland, Amsterdam, 617-620.
3. Boslough, M. B. (1991) A thermochemical model for shock-induced chemical

- reactions in porous solids: analogs and contrasts to detonation. Proc. 9th Symposium (International) on Detonation, Vol. II, Office of the Chief of Naval Research, 1199-1209.
4. Boslough, M. B. (1991) Thermochemical model for shock-induced chemical reactions in porous thermite: the heat detonation model. Shock Waves in Condensed Matter 1989, 671-674.
 5. Boslough, M. B. (1990) A thermochemical model for shock-induced reactions (heat detonations) in solids. J. Chem. Phys., 92, 1839-1848.
 6. Boslough, M. B. (1989) Shock-induced chemical reactions in nickel-aluminum powder mixtures: radiation pyrometer measurements. Chem. Phys. Lett., 160, 618-622.
 7. Boslough, M. B. and Ahrens, T. J. (1989) A sensitive time-resolved radiation pyrometer for shock-temperature measurements above 1500 K. Rev. Sci. Instrum., 60, 3711-3716.
 8. Boslough, M. B. (1988) Post-shock temperatures in silica. J. Geophys. Res., 93, 6477-6484. Taylor, P. A., Boslough, M. B. and Horie, Y. (1988) Modeling of shock-induced chemistry in nickel-aluminum systems. Shock Waves in Condensed Matter 1987, 395-398.
 9. Boslough, M. B. (1987) Shock-induced solid state chemical reactivity studies using time-resolved radiation pyrometry Internat. J. Impact Eng., 5, 173- 180.
 10. Boslough, M. B., Graham, R. A. and Webb, D. M. (1986) Optical measurements of shock-induced chemical reactions in mixed aluminum-nickel powder. Shock Waves in Condensed Matter--1985, 767-772.
 11. Graham, R. A., Morosin, B., Horie, Y., Venturini, E. L., Boslough, M., Carr, M. J. and Williamson, D. L. (1986) Chemical Synthesis under shock compression. Shock Waves in Condensed Matter--1985, 693-711.
 12. Boslough, M. B., Ahrens, T. J., and Mitchell, A. C. (1986) Shock temperatures in anorthite glass. Geophys. J. R. Astr. Soc., 84, 475-489.
 13. Boslough, M. B. and Graham R. A. (1985) Submicrosecond shock-induced chemical reactions in solids: first real-time observations. Chem.. Phys. Lett., 121, 446-452.
 14. Boslough, M. B. (1985) A model for time dependence in shock-induced thermal radiation of light. J. Appl. Phys., 58, 3394-3399. Boslough, M. B., Ahrens, T. J., and Mitchell, A. C. (1984) Shock temperatures in CaO. J. Geophys. Res., 89, 7845-7851.

(This work was supported by the United States Department of Energy under Contract DE-AC04-94AL85000)

POSTSHOCK SPECTRAL RADIANCE MEASUREMENTS IN NICKEL AND NICKEL/ALUMINUM POWDERS

M. B. BOSLOUGH

Sandia National Laboratories, Albuquerque, NM 87185

Because of complications associated with temperature heterogeneities in shocked metal powders, time-resolved radiation pyrometer measurements of shock temperatures in powders with particle sizes greater than a few tens of microns cannot be made under normal laboratory conditions with uniaxial loading durations limited to about one microsecond. Fortunately, for highly porous, reactive powders, the difference between shock and postshock temperature is negligible. For loading conditions similar to those that have yielded reaction products in recovery experiments, there is no evidence of any chemical reaction in a coarse (-325 mesh) nickel/aluminum powder mixture within the first 6 μ s of shock arrival, based on constraints on postshock temperatures provided by thermal radiation measurements. This result is in contrast to that for a micron-sized nickel/aluminum mixture, for which there is evidence of significant reaction on a time scale of 100 ns under similar shock loading conditions.

1. INTRODUCTION

There are a number of complications associated with the radiative measurement of shock temperatures in powders. Foremost is the fact that radiation pyrometer measurements are dominated by the highest temperatures present in a sample. When a heterogeneous medium such as a powder is shocked, the temperature distribution immediately behind the shock front is not uniform because of pore collapse and differential plastic deformation of powder grains. The intensity of thermal radiation emitted from a material is dictated by the Planck function, so it is a very strong function of temperature. Most of the measured visible and near infrared light from a heterogeneously heated material is emitted from the hotter regions. Until sufficient time has elapsed for thermal diffusion to cause the temperature to become uniform, it is the highest localized temperature of a shocked powder sample that dominates the measurement, not its equilibrium, or "mean-bulk" shock temperature,¹ and the initial color temperature can be from two to ten times higher than that calculated assuming homogeneous heating.²

It is reasonable to expect the spatial scale of temperature heterogeneity to be determined by the scale of physical heterogeneity of the initial powder; the temperature should vary over distances on the order of

particle size. This expectation has been borne out by measuring thermal radiation emitted from shocked powders with different particle sizes. When nickel powder with a particle size distribution in the range between 44 and 74 μ m is shocked,³ it takes significantly longer for thermal radiation (presumably from cooling heterogeneities) to decay than when nickel with a 2 μ m typical particle size is shocked under similar conditions.^{4,5} Spectral radiance histories for shocked nickel powders with two different mean particle sizes are plotted in Fig. 1.

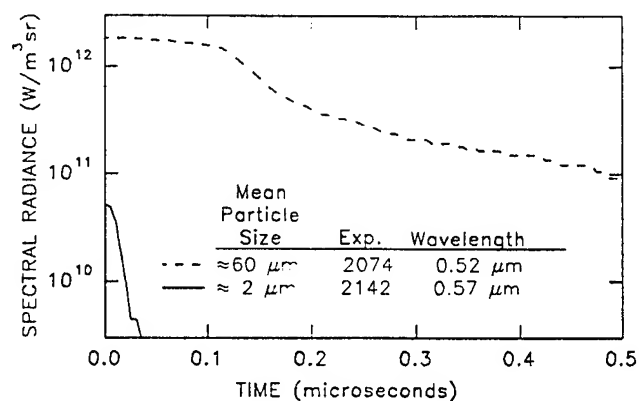


FIGURE 1
Time-resolved spectral radiances for nickel powders with different particle size distributions under uniaxial shock loading.

For experiments on Sandia's 63-mm bore compressed gas gun, shock durations and uniaxial strain conditions cannot be sustained for much more than one microsecond under the target geometries required for forward ballistic shock temperature measurements in powders for which light is collected from a 19-mm diameter area. For shocked metal powders with mean particle sizes in the ten μm range, the approach to thermal equilibrium is not complete on this time scale, so radiation pyrometry cannot be used to make direct measurements of equilibrium shock temperatures without extending the shock duration. The coarser powders that have been used in shock recovery experiments^{6,7} (in which product phases have been found in the recovered samples) are thus not amenable to time-resolved shock temperature measurements. However, for highly porous powders that react exothermically when shocked, the post-shock temperature does not differ significantly from the shock temperature.⁸ In addition, Horie and Kipp⁹ have suggested extending temperature measurements to cover a time period from a few μs to as long as 10 μs in order to further constrain kinetic parameters associated with chemical reactivity. The present work represents the first attempt to measure the post-shock temperature of a reactive powder by extending the time interval of spectral radiance measurements.

2. EXPERIMENTAL

Postshock spectral radiance experiments were carried out on two different samples: 1) flaky nickel of -325 mesh size (AESAR 13788), and 2) a mechanical mixture of this nickel with rounded -325 mesh aluminum (AESAR 11067). The mixture had a molar ratio of 3 Ni to 1 Al, which corresponds to the stoichiometry of the Ni_3Al compound that has been shock-synthesized. The mixture is identical to that used in recent recovery experiments⁷ in which shock-induced reactions were observed. The pure nickel powder provided a control experiment; because it is inert its shock temperature cannot include a chemical energy contribution.

The powder compacts were pressed into modified "Momma Bear" recovery fixtures to provide conditions approximating those achieved in recovered samples.¹⁰ The compact densities were kept as low as possible in an attempt to maximize the conditions that would lead to shock-initiation of a reaction. The center portion of the rear plug of the copper fixture was replaced by a 19 mm diameter sapphire window to allow time-resolved measurement of thermal radiation at four wavelengths in the visible and near infrared.¹ These fixtures were directly impacted by copper flyer plates launched at velocities of about 1.2 km/sec from a gas gun.

The present target configuration (Fig. 2) differs significantly from those used in conventional shock compression experiments in that no attempt was made to achieve uniaxial strain conditions. Like the recovery fixtures whose loading conditions it was designed to simulate,¹⁰ the loading and unloading are dominated by radial flow. However, the postshock temperature depends primarily on the initial porosity, the strength of the initial shock wave, and the amount of reaction, not on the direction or path of unloading. Because the principal purpose of these experiments was to determine whether the powder had reacted on the time scale of the measurements, the variation in conditions across the sample were of secondary importance. A qualitative picture of the compression process has been obtained from a numerical simulation that was carried out for a target of similar design that was used in previous optical measurements of shocked nickel/aluminum compacts.¹¹

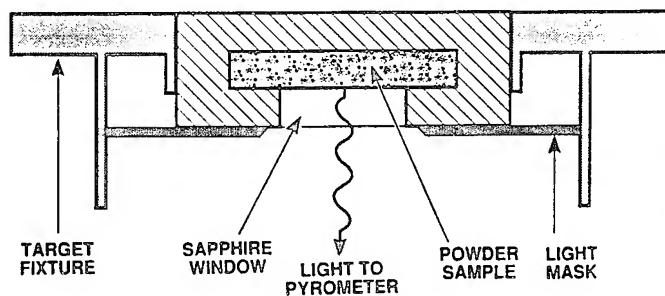


FIGURE 2
Experimental configuration; light radiated from the powder-sapphire interface is measured at four wavelengths.

3. RESULTS AND DISCUSSION

Fig. 3 presents the time-resolved spectral radiance data from one experiment on each type of powder. The time is referenced to the time at which light was first detected (when the earliest shock arrives at the powder-sapphire interface). Gaps in the data indicate off-scale or below-scale signals (because of the strong dependence of spectral radiance on shock temperature, the values can change by up to four orders of magnitude in less than a microsecond). Only the data for the first 6 μ s are presented; after that time there may be a significant contribution from spurious light that can be indirectly scattered into the optical system from other parts of the target. In both experiments, all four spectral radiances rapidly dropped to nearly constant values within 5 μ s. This observation is consistent with an asymptotic approach of temperature heterogeneities to the mean bulk temperature through thermal transport processes, so the measured radiances can be taken as an upper bound to that which would be radiated after equilibrium has been reached. Unlike spectral radiance measurements of micron-sized powders under uniaxial strain conditions (Fig 4), there is no significant difference between the nickel and nickel/aluminum experiments.

Temperature and effective emissivity histories determined from a least squares fit to a graybody distribution function¹ are plotted in Figs. 5 and 6.

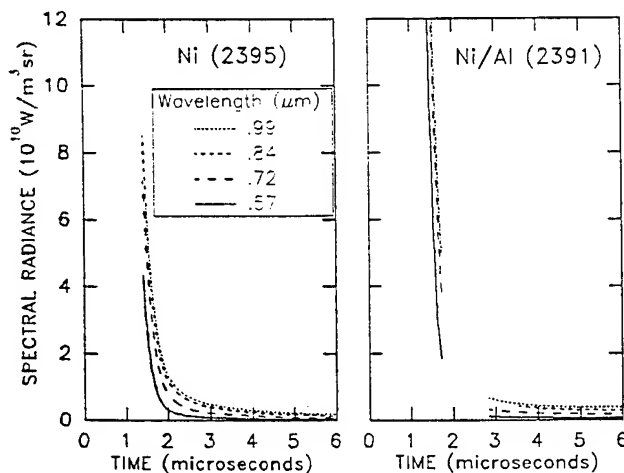


FIGURE 3
Time-resolved spectral radiances from -325 mesh nickel and nickel/aluminum mixture, shocked using configuration in Fig. 2

These histories are remarkably similar; the graybody temperatures rapidly drop to a nearly constant value in the 2300 to 2400 K range. However, the effective emissivities remain very low in both cases, indicating either that: 1) the samples are radiating at this temperature from only a small fraction of the observed area, or 2) the spectral radiances from the samples drop to values below a weak background level of scattered light. The first possibility is consistent with streak camera records under similar conditions showing a concentration of hotter shocked material on the axis of symmetry¹¹. In either case, the spectral radiances lie below the values associated with temperatures and emissivities consistent with a significant degree of reaction.

The present results are in apparent contrast to the results of recovery experiments by Song and Thadhani⁷, who detected significant quantities of intermetallic nickel/aluminum alloys in recovered specimens. This discrepancy may be due to the differences between the two experiments in details of shock loading. It is also possible that the temperatures associated with the reaction are lower than expected, because the high temperature thermochemical data on nickel/aluminum alloys are limited.¹² Another interpretation is that the reaction takes place, but on a much longer time scale.

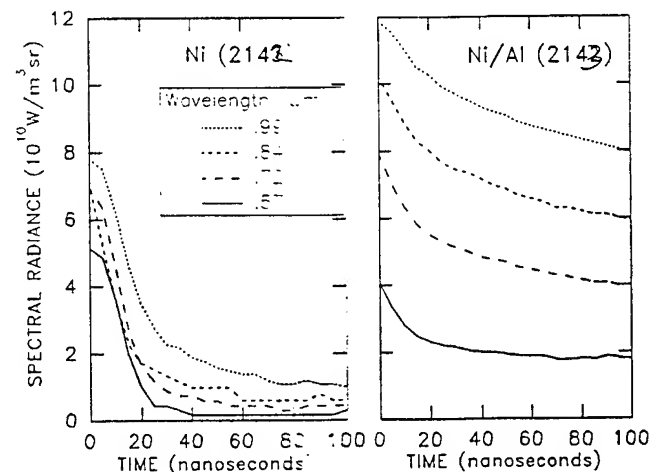


FIGURE 4
Time-resolved spectral radiances from powders with typical particle sizes of 1 to 2 μm under uniaxial shock loading

4. CONCLUSIONS.

There is no evidence from spectral radiance measurements that a -325 mesh mixture of nickel and aluminum powder exhibits significant reaction during or within 6 μ s of shock compression--even under the most favorable gas gun loading conditions attainable. Shock temperature measurements have previously indicated that a partial reaction takes place within 100 ns of uniaxial shock-loading of a powder with a much smaller particle size⁵. For the nickel/aluminum system, particle size appears to be an important parameter controlling the rate and/or sensitivity of shock-induced chemical reactions, with finer-grained powders reacting more readily than coarser powders.

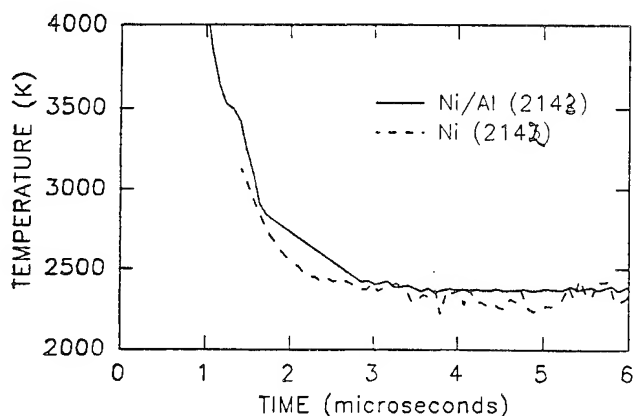


FIGURE 5
Time-resolved graybody temperatures
for shocked nickel/aluminum and nickel.

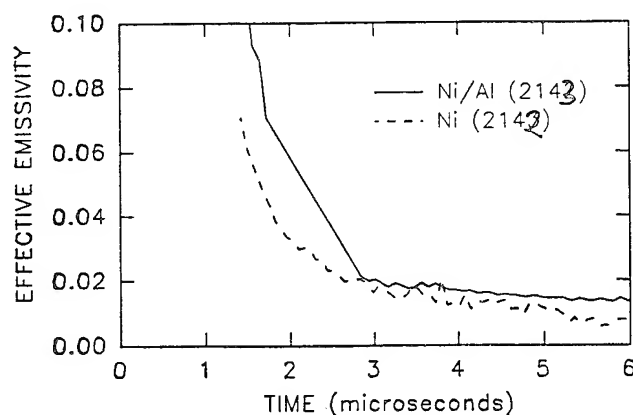


FIGURE 6
Time-resolved effective emissivities
for shocked nickel/aluminum and nickel.

Because of low levels of spurious light that can interfere with spectral radiance measurements at times greater than a few microseconds after impact, it may be more appropriate to use this method to investigate reactive powders with much larger heats of reaction, such as aluminum/metal oxide thermites, for which thermal spectral radiances would be much larger than those reported here, even for small amounts of reaction.

ACKNOWLEDGMENTS

This work was performed at Sandia National Laboratories supported by DOE contract DE-AC04-76DP00789 with partial funding from DARPA. Sample material was kindly provided by I. Song and N.N. Thadhani of New Mexico Tech.

REFERENCES

1. M. B. Boslough and T. J. Ahrens, *Rev. Sci. Instrum.* 60 (1989) 3711.
2. N. F. Masharov and S. S. Batsanov, *Combustion, Explosion, and Shock Waves* 25 (1989) 256.
3. M. B. Boslough, *Int. J. Impact Eng.* 5 (1987) 173.
4. P. A. Taylor, M. B. Boslough and Y. Horie, in: *Shock Waves in Condensed Matter-1987*, ed. S.C. Schmitt and N.C. Holmes (North Holland, Amsterdam, 1988), pp. 395-398.
5. M. B. Boslough, *Chem. Phys. Lett.*, 160 (1989) 618.
6. Y. Horie, R. A. Graham and I. K. Simonsen, *Mat. Letters* 3 (1985) 354.
7. I. Song and N. N. Thadhani, *Met. Transactions* (in press).
8. M. B. Boslough, *Expiomet '90*, (in press)
9. Y. Horie and M. E. Kipp, *J. Appl. Phys.* 63 (1988) 5718.
10. R. A. Graham and D. M. Webb, in: *Shock Waves in Condensed Matter-1983*, eds. J. R. Asay, R. A. Graham and G. K. Staub (North Holland, Amsterdam, 1984) pp. 211-214.
11. M. B. Boslough, R. A. Graham and D. M. Webb, in *Shock Waves in Condensed Matter*, ed. Y. M. Gupta (Plenum, New York, 1986), pp. 767-772.
12. P. D. Desai, *J. Chem. Phys. Ref. Data* 16 (1987) 109.

SHOCK-INDUCED CHEMICAL REACTIONS IN NICKEL-ALUMINUM POWDER MIXTURES: RADIATION PYROMETER MEASUREMENTS

Mark B. BOSLOUGH

Sandia National Laboratories, Albuquerque, NM 87185, USA

Received 18 May 1989

Time-resolved emission of visible and near-infrared thermal radiation has been measured from powders of pure nickel and mixed nickel-aluminum shocked to peak pressures of 14 GPa. Temperatures determined from the measurements indicate that the Ni-Al mixture has a source of heat in addition to that supplied by shock compression. The extra heat, produced on a time scale of 100 ns, is inferred to come from an exothermic reaction between the two metals forming a binary alloy. If the alloy is Ni_3Al , the measured temperatures are consistent with prompt shock-induced reaction of at least 45% of the reactants.

1. Introduction

Observations of shock-induced chemical reactions in solids are numerous [1,2]. One such reaction is the subject of the present research. It was discovered by Horie et al. [3] who used explosive-loading techniques to shock nickel-aluminum powder compacts. According to analysis of the shocked material, the major end-product was ordered Ni_3Al , with a shock temperature of about 500°C required for initiation. Other products included NiAl , Ni_2Al_3 , and NiAl_3 . While such shock-recovery experiments can determine many features of shock-controlled chemical reactions, they cannot provide direct data on rates and mechanisms. To attain this information, shock-temperature experiments are required.

For highly exothermic synthesis reactions the most sensitive variable is temperature. For many such reactions there are no large volume or pressure changes that would give significant differences in pressure-volume shock states (Hugoniot). For example, Hugoniot measurements were used to demonstrate that reactions forming tin sulfide from its components can take place under shock [4], but the relative error in determining reaction completeness was as much as 30% owing to uncertainties in the measured Hugoniot and its relative insensitivity to differences between the equations of state of the reactants and products. By contrast, precise measurements of shock

temperatures of reactive powders can be compared to calculated (or measured) temperatures for shocked inert powders to more accurately determine the amount of reaction. Radiation pyrometry was one of the approaches [5,6], used to measure thermal radiation from Ni-Al powders in a configuration designed to simulate earlier recovery experiments [3]. A brief emission of light consistent with the presence of temperatures as high as 5000 K was observed [6], and was taken to be evidence for shock-induced chemical reactions on a submicrosecond time scale. Similar measurements of infrared radiation emitted from shocked $\text{Al}/\text{Fe}_2\text{O}_3$ powders by Hornig et al. [7], led to the same conclusion. In both cases, extremely high temperatures exist only briefly, and low emissivity values are associated with them. This suggests that the shock energy in the powders is localized, resulting in temperature heterogeneities.

The present experiments were performed to isolate the early light emission from that due to a homogeneous, equilibrium temperature increase associated with shock compression and chemical reaction. The nickel-aluminum system was studied because: (1) recovery experiments have demonstrated shock-induced reactions and identified the products [3], (2) it has been theoretically modelled [8,9], (3) the large heat of reaction leads to a measurable temperature increase for partial reactions, (4) reactants and products are all metals, and therefore

graybody emitters (a requirement for radiation pyrometry) and (5) the alloys have useful applications, and are candidates for industrial shock processing.

2. Experimental

Spectral radiance of visible and near-infrared light radiated from the shocked sample is measured simultaneously at four different wavelengths with a radiation pyrometer [10]. A least-squares fit to these data determines a time-resolved temperature and effective emissivity. The target consists of a thin (about 0.5 mm) powder layer sandwiched between a copper driver and a lithium fluoride window. The thickness/diameter ratio of the powder layer is small, so the strain experienced by the center portion of the sample remains uniaxial, and the shock pulse quickly reverberates the powder up to the peak pressure (14 GPa). A mask obscures the sample edge, where rarefactions enter and disrupt the uniaxial flow. Impact of a 63 mm diameter projectile launched from a gas gun [11] generates the shock wave. Impact velocities of 1.18 km/s were employed, and the projectiles carried copper impactors. The target chamber was evacuated to eliminate air shocks, and the samples were in contact with vacuum, to minimize residual air in the pore space.

Two powders were investigated: an inert powder of 99.9% pure nickel (CERAC N-1089) with a 2 μ m mean particle size, and a stoichiometric mixture (87% Ni, 13% Al by weight) of the same nickel with 99.5% pure aluminum powder (CERAC A-1183) of 1 μ m mean particle size. The reactive mixture consists of only 13% aluminum by weight, so pure nickel

was chosen to represent the inert powder. It has similar density, compressibility, and mechanical properties, and should therefore have a similar shock-compression response. Moreover, the similarity of spectral emissivity is important for a comparative study based on optical measurements. The details of the two experiments are summarized in table 1.

3. Results

Spectral radiance histories are shown in figs. 1 and 2. The origins of the time axes coincide with arrival of the initial shock wave at the powder-window interface. In both cases, the radiance history consists of an initial pulse at all four wavelengths, followed

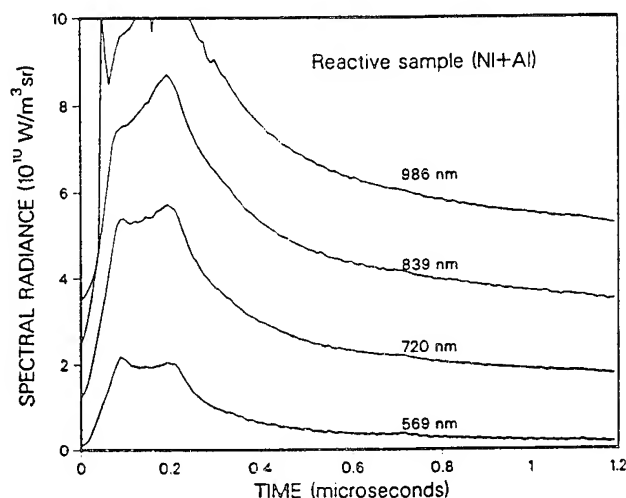


Fig. 1. Time-resolved spectral radiances for Ni-Al experiment 2208. Shock reaches powder/window interface at $t=0$. Data for each wavelength is vertically offset by 10^{10} W/m² sr above the next-shorter wavelength. Shortest wavelength data is not offset.

Table 1
Summary of experiments

Experiment number	Powder type	Initial density		Window material	Velocity (km/s)
		(g/cm ³)	(% of solid)		
2208	Ni-Al ^{a)}	2.96	43	LiF	1.183
2209	Ni	3.36	38	LiF	1.184

^{a)} 87% Ni, 13% Al by weight.

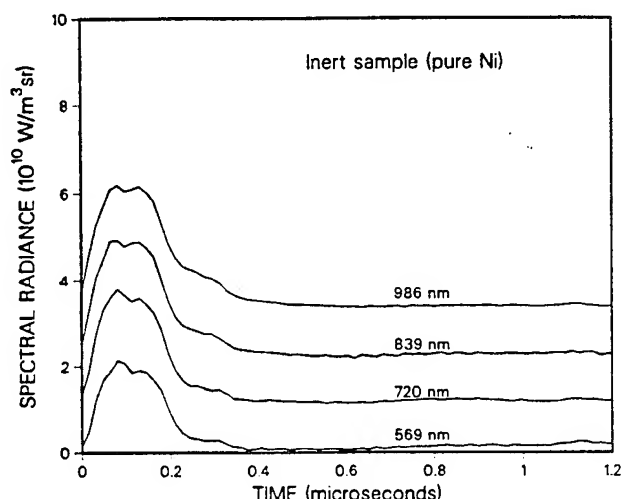


Fig. 2. Time-resolved spectral radiances for Ni experiment 2209, plotted in same manner as data in fig. 1.

by a decay. The initial pulses have double peaks; one corresponds to the initial shock wave, and the other is due to a twice-reflected shock that has completed one round trip through the thin sample layer, as illustrated by the $x-t$ and $P-u$ diagrams in figs. 3 and 4, respectively.

Ideally, the initial pulse would be sharply defined, with a nearly instantaneous rise time. However, any deviation from parallelism between the plane of the shock front and the sample-window interface will prevent simultaneous arrival. Instead, the intersection of the two planes forms a line that sweeps across

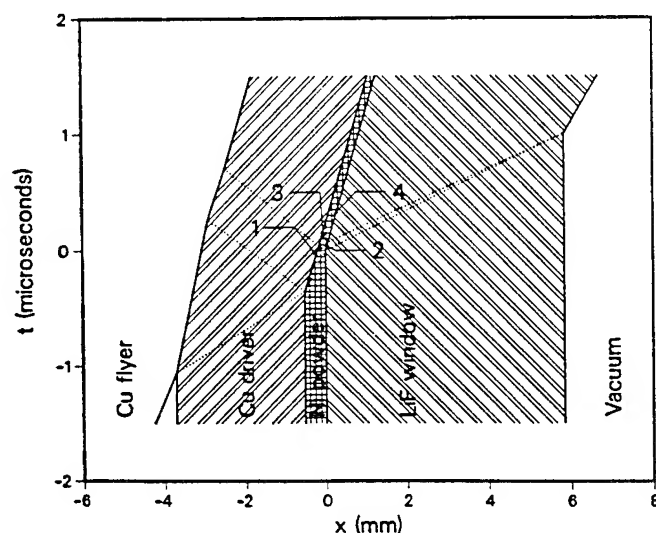


Fig. 3. Distance-time diagram for powder experiments. Shocks and rarefaction waves are represented by dotted lines. Numbers refer to states in nickel.

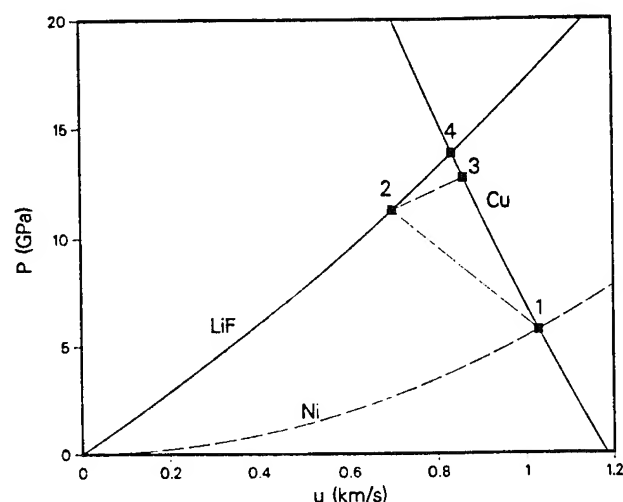


Fig. 4. Pressure-particle velocity diagram for powder experiments. Numbered states correspond to those in fig. 3.

the field of view. The time required to complete the sweep is proportional to the aperture diameter (19 mm), and inversely proportional to the shock velocity (less than 2 km/s). Angles between the surfaces of the powder pellets were as great as 0.001 rad, contributing further to shock wave tilt. Other factors include possible non-planarity of the shock wave due to lack of uniformity in the initial density of the powder, and non-zero rise time of the shock.

There are obvious differences in the data displayed in figs. 1 and 2. In addition to the greater intensities exhibited by the mixed powder, the decay rate is longer, and the spectral radiance ratios for different wavelengths are different than for the nickel. These data can be expressed in more useful terms by fitting them to the graybody distribution function,

$$N(\lambda) = \alpha \epsilon C_1 \lambda^{-5} [\exp(C_2/\lambda T - 1)]^{-1}, \quad (1)$$

where α is the fraction of the area within the pyrometer field of view that is radiating light at temperature T , ϵ is the emissivity of the radiating surface, $N(\lambda)$ is the measured spectral radiance at wavelength λ , and C_1 and C_2 are known constants. Because $N(\lambda)$ is measured at four different wavelengths, there are four equations with two unknowns, and time-resolved values for ϵ and T can be determined. Since α and ϵ cannot be independently determined, their product is defined as the "effective emissivity". For uniformly heated material, 100% of the surface within the field of view is at the same temperature, and the effective emissivity is equal to

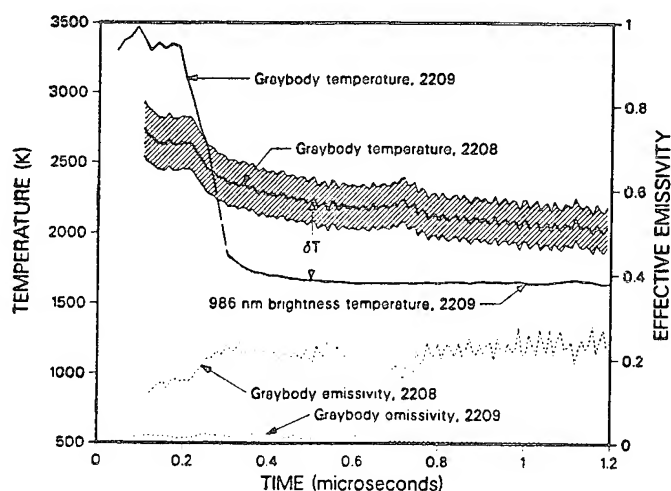


Fig. 5. Time-resolved temperature and emissivities, calculated from data in figs. 1 and 2. Numbers refer to experiments in table 1. Hatched band indicates uncertainties from least-squares fit.

the true emissivity of the surface. However, if the sample is heterogeneously heated, only some fraction of the area radiates at high temperature, and the effective emissivity is reduced from the true emissivity by the fractional area α .

The time-resolved temperature of the mixed powder is shown in fig. 5. The initial light pulse corresponds to a temperature of nearly 2800 K, with an effective emissivity of about 0.1. After approximately 500 ns, the temperature drops to about 2250 K, and the emissivity reaches a relatively stable value. This rapid cooling is consistent with heat conduction eliminating temperature heterogeneities. Any non-uniformity accompanying pore collapse and local plastic deformation is likely to have spatial variation on the same scale as the powder particle size. Temperature heterogeneities on the order of 1 μm disappear in less than 500 ns leaving a uniformly radiating surface with an effective emissivity equal to its true emissivity. The final value of 0.24 is consistent with for nickel emissivities, which vary between 0.12 and 0.37 depending on temperature and surface quality.

The time-resolved temperature for the pure nickel powder is also shown in fig. 5. It is initially higher than that of the mixed powder, presumably due to the slight differences in thermomechanical properties that lead to energy localization, and also drops rapidly in the first two or three hundred nanoseconds. Unlike the mixed powder, however, the effective emissivity starts much lower and does not in-

crease. Pure nickel should have a slightly higher emissivity than the mixed powder; an admixture of aluminum into nickel would tend to lower the emissivity of the pellet surface (the pure pellets are darker in appearance than the mixed pellets – corresponding to higher emissivity). After 400 ns, the measured temperature begins to increase, while the emissivity drops to extremely low values. This happens when the spectral radiance from the sample drops below background levels; other experiments have shown that light can be weakly scattered from outside the direct field of view of the pyrometer (the scattering has subsequently been eliminated by a minor modification of the target design). This scattered light has a spectral radiance below about $10^9 \text{ W/m}^2 \text{ sr}$, and is negligible unless the light radiated from the sample is just as weak. Nevertheless, an upper bound can be calculated for the bulk temperature by assuming an effective emissivity of 0.24 ($\epsilon = 0.24$, $\alpha = 1.0$) and using the longest wavelength (least likely to be affected by scattered radiation) to determine the brightness temperature from eq. (1). The brightness temperature assumes that all the light of a given wavelength is thermal radiation coming from a uniformly heated surface with an emissivity of 0.24. Since some fraction of the measured light is actually scattered from another source, this brightness temperature (which remains less than about 1700 K, see fig. 5), is an upper bound. The brightness temperature is not plotted for the first few hundred nanoseconds, when the temperature distribution is known to be heterogeneous.

6. Discussion

The temperature of the shocked nickel–aluminum powder mixture is about 2250 K when thermal equilibrium is reached. At the equivalent time in the pure nickel sample, an experimental upper bound for the temperature is about 1650 K. The shock temperature of the mixed powder is thus at least $\delta T = 600 \text{ K}$ higher than that of the nickel powder. For low density, porous metals, the snowplow model (a special case of the P - α model [12]) is used to estimate equilibrium shock temperatures. It assumes that the first shock wave increases the initial density of the powder (ρ_{00}), to its full density (ρ_0). Reflected shocks increase the pressure of the crushed-up pow-

der, but increase the density by only a negligible amount. The Hugoniot of the powder for the first shock is given simply by

$$P = u^2 \rho_0 \rho_{00} / (\rho_0 - \rho_{00}), \quad (2)$$

where P is the shock pressure and u is the particle velocity. The porous Hugoniot of nickel powder is plotted in fig. 4. Impedance matching this Hugoniot to the inverted Hugoniot for copper centered on the impact velocity of 1.18 km/s gives an initial shock pressure of about 6 GPa. The net increase in internal energy is given by the Rankine-Hugoniot equation

$$\Delta E = \frac{1}{2} P (1/\rho_{00} - 1/\rho_0), \quad (3)$$

and the increase in temperature is approximated by $\Delta T = \Delta E / C_p$ where $C_p = 520$ J/gK is used to approximate the specific heat of the nickel. In the snowplow model, no further energy is acquired by the nickel in reverberating to the peak pressure of 14 GPa. In reality, there is a small volume change after the initial shock, but it is so small compared to the volume change on crushing that it can be ignored. The estimated temperature increase is about 1100 K, and when added to the initial temperature gives a calculated shock temperature of about 1400 K, somewhat less than the experimental upper bound. If the crush strength of the powder is significant, the snowplow assumptions are no longer valid, and the actual temperature would be lower.

The shock component of temperature increase will be somewhat less for the mixed powder, because of slightly different thermomechanical properties. According to ref. [13], the energy released by the reaction $3\text{Ni} + \text{Al} \rightarrow \text{Ni}_3\text{Al}$ is about 40 kJ/mol of Ni_3Al at standard conditions, which is sufficient to raise the adiabatic temperature by about 1300 K. The measured temperature difference of at least 600 K is, therefore, equivalent to prompt shock-induced reaction of at least 45% of the material.

5. Conclusions

Radiation pyrometry measurements have been used to demonstrate the existence, time scale and completeness of prompt shock-induced chemical reactions in the Ni-Al system. By varying the shock pressure and porosity of starting materials, such experiments can determine the conditions required for

shock initiation of these reactions. Other highly reactive solids are candidates for shock-temperature measurements to determine the thresholds, rates and energetics of their reactions under shock, with time resolution limited by the equilibration time for temperature heterogeneities in powders. With these measurements, the underlying mechanisms controlling shock-induced chemical reactions in solids can be studied.

Acknowledgement

This work was performed at Sandia National Laboratories supported by the US Department of Energy under contract #DE-AC04-76DP00789. M.U. Anderson, M.R. Lewis and D.E. Wackerbarth provided expert technical assistance.

References

- [1] G.A. Adadurov, V.I. Gol'danskii and P.A. Yampolskii, *Mendeleev Chem. J.* 18 (1973) 92.
- [2] R.A. Graham, in: *Shock waves in condensed matter 1987*, eds. S.C. Schmidt and N.C. Holmes (North-Holland, Amsterdam, 1988) p. 11.
- [3] Y. Horie, R.A. Graham and I.K. Simonsen, *Mater. Letters* 3 (1985) 354.
- [4] S.S. Batsanov, G.S. Doronin, S.V. Klochkov and A.I. Teut, *Combust. Explos. Shock Waves* 22 (1986) 134.
- [5] M.B. Boslough and R.A. Graham, *Chem. Phys. Letters* 121 (1985) 446.
- [6] M.B. Boslough, R.A. Graham and D.M. Webb, in: *Shock waves in condensed matter*, ed. Y.M. Gupta (Plenum Press, New York, 1986) p. 755.
- [7] H.C. Hornig, J.W. Kury, R.L. Simpson, F.H. Helm and W.G. Von Holle, *Proceedings of the Eleventh International Pyrotechnics Seminar* (IIT Research Institute, Chicago, 1986) p. 699.
- [8] Y. Horie and M.E. Kipp, *J. Appl. Phys.* 63 (1988) 5718.
- [9] P.A. Taylor, M.B. Boslough and Y. Horie, in: *Shock waves in condensed matter 1987*, eds. S.C. Schmidt and N.C. Holmes (North-Holland, Amsterdam, 1988) p. 395.
- [10] M.B. Boslough and T.J. Ahrens, *Rev. Sci. Instr.* submitted for publication (1989).
- [11] R.E. Setchell, in: *Shock waves in condensed matter 1981*, eds. W.J. Nellis, L. Seaman and R.A. Graham (AIP, New York, 1982) p. 657.
- [12] W. Herrmann, *J. Appl. Phys.* 40 (1969) 2490.
- [13] P.D. Desai, *J. Phys. Chem. Ref. Data* 16 (1987) p. 109.

A sensitive time-resolved radiation pyrometer for shock-temperature measurements above 1500 K

Mark B. Boslough

Sandia National Laboratories, Albuquerque, New Mexico 87185

Thomas J. Ahrens

Seismological Laboratory, California Institute of Technology, Pasadena, California 91125

(Received 31 March 1989; accepted for publication 7 August 1989)

An optical system has been developed which can determine time-resolved temperatures in shocked materials by measuring the spectral radiance of light emitted from shocked solid samples in the visible and near-infrared wavelength range ($0.5\text{--}1.0\ \mu\text{m}$). It can measure temperatures as low as 1500 K and has been successfully used to observe shock-induced chemical reactions in powder samples. The high sensitivity of this radiation pyrometer can be attributed to the large angular aperture ($0.06\ \text{sr}$), the large bandwidth per channel (up to $0.1\ \mu\text{m}$), the large photodiode detection areas ($1.0\ \text{cm}^2$), and the small number of calibrated channels (4) among which light is divided. Improved calibration techniques, as well as the layout of the instrument, eliminate certain sources of error encountered in previous shock-temperature experiments. Errors in the measured spectral radiance were reduced by: (1) recalibration before every experiment to account for changes in optical components; (2) direct calibration of voltage recorded at each digitizer to prevent transfer error by an intermediate step; (3) use of a spectral irradiance calibration lamp to exclude errors due to spatial inhomogeneities associated with spectral radiance sources; and (4) obtaining a large spatial average of light at each wavelength from the same portion of the sample to eliminate errors from possible inhomogeneities in the sample. The magnitude each of these errors could previously contribute was 1%–2% of the total signal. Absolute temperature uncertainties, determined from the standard deviation of the measured spectral radiances from the least-squares-fit values, are typically about 5%. Emissivities are poorly constrained by spectral radiance data because of a weak functional dependence, and uncertainties can easily exceed 50% for temperatures of around 2000 K.

INTRODUCTION

Time-resolved radiation pyrometry has proven to be a useful tool in the study of condensed matter in the shocked state. It has been applied to problems in condensed matter physics and chemistry, high explosives, and high-pressure geophysics. In many ways it complements other optical experimental methods such as spectroscopy and high speed framing and streak photography. Not only can shock temperatures be measured but, in some cases, the optical properties of the shocked state can be determined from the time dependence of the radiated light.¹ The method has been used to constrain high pressure equations of state, detect and quantify phase transformations, and study shock-induced chemical reactions.

The first application of pyrometry to study shocked materials was by Kormer *et al.*,^{2,3} who measured light emitted from initially transparent solids at two different wavelengths and were able to determine color temperatures. Subsequently, various types of pyrometers have been used by Raikes and Ahrens⁴ to measure residual temperatures of shocked minerals, by Von Holle⁵ in studies of reacting high explosives, by Lyzenga and others^{6–9} and Ahrens *et al.*¹⁰ to determine high pressure thermal equations of state, and by Radousky and co-workers^{11,12} for studies of shocked fluids. A similar device

has been used by Brannon *et al.*¹³ to measure shock-induced nonthermal light radiated from solids.

The present system was designed to be more sensitive to spectral radiance (and therefore to lower temperatures) than previous pyrometers, while at the same time providing a high degree of precision and time resolution. High sensitivity was achieved in part by increasing the spectral bandwidths and photodetector area beyond what had previously been used. The corresponding reductions in spectral resolution and time response did not significantly reduce the quality of the data.

The generic design of the present pyrometer was initially implemented by Boslough¹⁴ on the Caltech two-stage light-gas gun,¹⁵ which launches 25 mm diam projectiles that strike specimens at speeds of 4–7 km/s. Shock pressures in the 50–200 GPa range are generated during the propagation time of the shock wave through the sample. This original instrument has been applied mostly to problems in high pressure geophysics (e.g., Boslough *et al.*¹⁶) and was used in conjunction with other techniques by Williams *et al.*¹⁷ to estimate the temperature of the Earth's core. A more sensitive system, which is described in the present article, was designed to be used with Sandia's 25-m single-stage gas-gun,¹⁸ which launches 63 mm diam projectiles at speeds up to 1.2 km/s and achieves shock pressures up to 25 GPa in

samples of interest. This newer pyrometer has been used primarily for studies of shock-induced chemical reactions in powders.¹⁹

I. EXPERIMENT DESIGN

The description of the newer radiation pyrometer (Fig. 1) will proceed in the direction of light propagation, beginning with the target assembly. A number of types of targets have been used. Of current interest are measurements of light radiated from shocked powders. These experiments are performed in one of two ways. One method makes use of a target consisting of a transparent solid, usually lithium fluoride, which is struck directly by an impactor containing a powder pellet carried on the face of a projectile. In these "reverse impact" experiments, the initial shock state in the pellet is viewed by the pyrometer. The other type of target consists of a powder pellet with an attached transparent window (or anvil), again usually lithium fluoride. In these "direct impact" experiments, the first state observed by the pyrometer is actually the second (reflected) shock state. A version of this target is depicted in Fig. 2. In either case, two coaxial shorting pins are mounted on either side of the sample to provide triggering pulses before impact.

To observe a single, well-defined state the sample edge must be masked, because the field of view of the pyrometer is greater than the portion of the sample in which one-dimensional wave motion occurs during times of interest. Edge effects (two-dimensional flow) occur at only the outer edges of the sample. For this reason an aluminum edge-mask (anodized black) is attached to the free surface of the transparent window. The mask contains a central hole which provides the only path for light from the sample to enter the

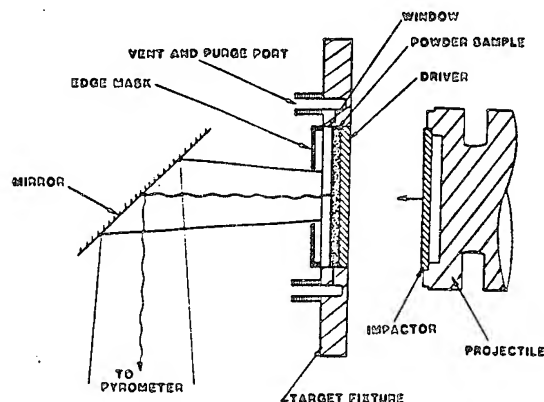


FIG. 2. An example of a powder target assembly. This configuration was designed for direct impact experiments.

pyrometer. A large set of experiments²⁰ has demonstrated that, for a properly designed target, there are no other sources of light which can contaminate the signal, a problem that had been experienced previously.²¹

The circular aperture varies in diameter from 6 to 25 mm depending on the particular target design. The light radiated by the sample is reflected by an aluminized mirror, turning it toward the radiation pyrometer port in the target chamber. This port is covered with a protective Pyrex window that separates the target chamber from the objective lenses, which are two crown glass plano-convex lenses, with focal lengths of 50 cm and clear apertures of 14 cm. The target is near the focal point of the first lens. The collected light is separated into four legs by three reflective-coated pellicle beamsplitters. Each of the four resulting beams falls upon a detector assembly, which consists of an interference filter, a focusing lens, and a photodiode with a bias circuit. The bandpass filters are 50 mm in diameter and have peak wavelengths in the visible or near-infrared within the effective bandwidth range of the silicon photodiodes. The filters have half-height bandwidths of 0.1 μm or less.

The detectors used were RCA C30810 N-type silicon pin photodiodes, with an active area of 1.0 cm^2 . Germanium photodiodes have also been used to extend the wavelength range further into the infrared, but the poorer frequency response of germanium complicates the data reduction. To ensure that the image of the sample (and calibration lamp filament) falls entirely within the photodiode active area, a 52-mm-diameter, 32-mm focal length aspheric glass focusing lens is positioned between the filter and photodiode. This demagnifies the image by a factor of about 0.3. The detector assemblies are mounted on three-axis translation stages to allow for alignment and focus adjustments. The focusing lens and filter holder can be moved independently to permit separate adjustment of focus and demagnification.

This optical configuration ensures that each detector views precisely the same area of the target. Thus, when radiation is heterogeneously emitted, as is the case when shear bands or hot spots develop (e.g., Kondo and Ahrens²²), the average brightness is measured by each detector. This eliminates the possibility of an erroneous temperature measurement due to different detectors viewing different target areas

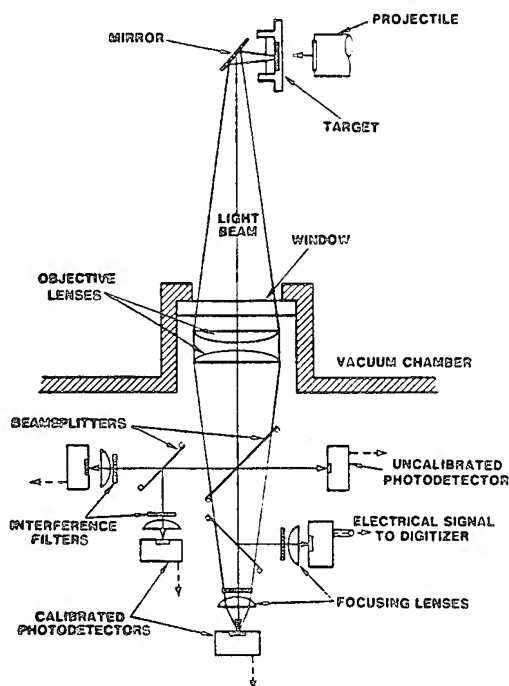


FIG. 1. Schematic diagram of radiation pyrometer, showing its relation to gas-gun impact chamber.

which may not have the same temperature distribution. Also, by viewing the entire unmasked portion of the target, the sensitivity of the instrument is increased. Because the image is demagnified there is sufficient tolerance in alignment and focusing, as long as the entire image falls within the active area of the detector.

The silicon photodiode circuit supplies a 45 V reverse bias from a dc power supply to the photodiode. Signals are transmitted by terminated 50- Ω cables, and recorded by an array of LeCroy 6880 and Tektronix 7612 digitizers. There is also an optional unfiltered, uncalibrated fifth channel which consists of an RCA C30872 silicon avalanche photodiode. It has a nominal rise time of 2 ns, and provides fast time response to ensure that any high-frequency component of the light is recorded. This photodiode is positioned where it receives stray light reflected from one of the optical filters. Its output can be recorded by a high frequency digital oscilloscope, but is not used in the temperature calculation.

II. CALIBRATION PROCEDURE

Unlike previous shock pyrometers which used a spectral radiance source for calibration, the present system uses a spectral irradiance source. A spectral radiance source typically consists of a tungsten ribbon which can have a nonuniform temperature distribution over its surface. During calibration the possibility exists that different photodetectors measure light from different parts of the ribbon, leading to calibration error. By contrast, a spectral irradiance source is usually a tungsten filament. During calibration, the image of the entire source filament falls entirely within the active area of each photodetector. All detectors therefore view exactly the same light source, thereby reducing the calibration error.

The standard of spectral irradiance is placed in the position of the target in the impact chamber and the pyrometer is aligned. The spectral irradiance is given in units of $\mu\text{W}/\text{cm}^2\text{nm}$ at a distance of 50 cm (a surface 50 cm from the lamp receives the given spectral irradiance). At this distance, 1 cm^2 of area subtends a solid angle of 0.0004 sr, so the spectral radiant intensity (power per unit solid angle per unit wavelength) of the lamp is equal to its spectral irradiance divided by 0.0004 sr/ cm^2 . Since the entire lamp filament is imaged onto the photodiodes, its spectral radiant intensity is equivalent to that of a point source. The standard source used is a commercial General Electric type Q6.6A/T4Q/5CL 200 W tungsten coil filament quartz-halogen lamp calibrated by Optronics Laboratories, Inc. by transfer from a National Bureau of Standards source. Use of this lamp as a standard is described by Schneider and Goebel.²³ The lamp is mounted on a target assembly and aligned in the same manner as a real target, using the same mirror and window as are used in the actual experiment. It is driven by 6.50 A from an Optronics Laboratories, Inc., model 83DS precision dc constant current power supply. The use of dc current avoids the 120-Hz ripple in light intensity associated with calibration lamps powered by ac current, thereby eliminating another source of error that has been experienced in the past.

For calibration of the pyrometer with the Tektronix 7612 digitizers, the light beam incident on the pyrometer is

mechanically chopped at approximately 250 Hz, and the resulting square wave is recorded for each detector. The voltage amplitude of the square wave, as recorded on each channel, is divided into the spectral radiant intensity of the lamp at the mean effective wavelength of its corresponding filter, resulting in a calibration factor. The appropriate spectral irradiance for calibration is found by interpolating between values given by a table supplied by Optronics Laboratories for the quartz halogen lamp. The pyrometer is calibrated with the LeCroy 6880 digitizers similarly, but because of the short sampling window of these digitizers (about 7 μs maximum), the light source cannot be physically chopped fast enough. Instead, a number of measurements are made with the lamp both on and off, and averaged to compensate for baseline drift and other effects normally accounted for by using the mechanical chopper. The resulting calibration factors are multiplied by the amplitude of the experimental waveform to get a time-resolved spectral radiant intensity for the shocked material. To determine the spectral radiance from which the temperature is calculated, spectral radiant intensity is divided by the area of the aperture in the edge mask. The actual solid angle subtended by the objective lens need not be known, as long as the calibration lamp is used in the same position as the target. This procedure is carried out prior to every experiment, to account for differences between the expendable components (the mirror and window), and minor differences in experimental configuration, cleanliness of optics, etc. It is not necessary to carry out a voltage calibration on the recording digitizers because for each channel the same digitizer is used for both calibration and experiment. This procedure takes a potentially error-compounding step out of the calibration process.

Because of the large (up to 0.1 μm) half-height bandwidths of the filters used with this pyrometer, it is necessary to calculate the mean effective wavelength of each filter, which depends on the spectral dependence of the other optical components, and on the temperature of the source. The other optical components have only a weak wavelength dependence relative to the filters, and this does not change greatly from experiment to experiment as components are replaced. It is thus possible to use nominal values published in component specifications, and representative values for the expendable components (the mirror and window) without greatly affecting the results. The wavelength-dependent parameters of the various optical components (Fig. 3) are defined in Table I. All are functions of λ , the wavelength in vacuum.

The spectral reduction factors for each pyrometer station, $r_i(\lambda)$ are given by

$$r_1(\lambda) = R_M T_W T_L^2 T_{B_1} T_{B_2} T_I T_1 R_d, \quad (1)$$

$$r_2(\lambda) = R_M T_W T_L^2 T_{B_1} R_{B_2} T_I T_2 R_d, \quad (2)$$

$$r_3(\lambda) = R_M T_W T_L^2 R_{B_1} R_{B_2} T_I T_3 R_d, \quad (3)$$

$$r_4(\lambda) = R_M T_W T_L^2 R_{B_1} T_{B_2} T_I T_4 R_d. \quad (4)$$

These factors are multiplied by T_p , the transmittance of the anvil, for every experiment except those in which light is measured directly from the free surface of the target.

The mean wavelength of channel i is therefore

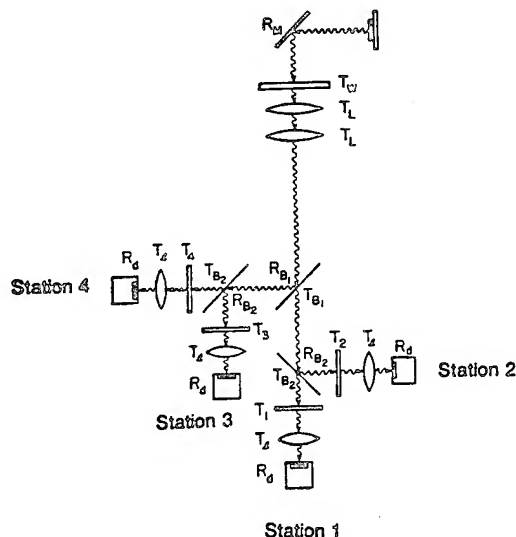


FIG. 3. Expanded diagram of radiation pyrometer. Components are labeled with symbols defined in Table I.

$$\bar{\lambda}_i = \left(\int_0^\infty r_i(\lambda) \lambda d\lambda \right) / \left(\int_0^\infty r_i(\lambda) d\lambda \right). \quad (5)$$

There will also be a shift in effective wavelength as a function of temperature of the source, and this should be included. To calculate the shift, we must assume *a priori* that the source radiates with a spectral distribution described by the Planck function. In most of the experiments to date, the results indicate that this assumption is indeed valid.

The mean effective wavelength $\bar{\lambda}_i(T)$ is defined to be the temperature dependent wavelength such that

$$f[T, \bar{\lambda}_i(T)] = \frac{\int_0^\infty r_i(\lambda) f(T, \lambda) d\lambda}{\int_0^\infty r_i(\lambda) d\lambda}, \quad (6)$$

where $f(T, \lambda)$ is the Planck function

$$f(T, \lambda) \sim \lambda^{-5} [\exp(hc/k_b \lambda T) - 1]^{-1}, \quad (7)$$

and h , c , and k_b are Planck's constant, the speed of light and Boltzman's constant, respectively. $\bar{\lambda}_i(T)$ can be found by numerically evaluating Eq. (6). The mean effective wavelengths are weak functions of temperature for the pyrometer station-filter combinations which have been used to date, except at temperatures for which Wien's Law places the

maximum of the Planck function near the mean wavelength of the filter. Two examples are plotted in Fig. 4.

III. TEMPERATURE DETERMINATION

Once the values of spectral radiance N_λ are determined at each of the four wavelengths, a two-parameter least-squares (graybody) calculation can be carried out to find the temperature T and effective emissivity ϵ . It is important to note here that in general there is not a single temperature associated with the shocked material, but a range of temperatures, as in the case of hot spots, shear band heating, or inhomogeneous chemical reaction. Because spectral radiance is such a strong function of temperature, the least-squares method is highly skewed in favor of the highest temperature present. Depending on the true temperature distribution, this temperature calculation may or may not give a precise measure of the highest temperature present in the sample. For example, a bimodal temperature distribution, in which the high temperature region is much hotter than the rest of the sample, will give rise to a precise measurement, whereas a broad temperature distribution (many temperatures present) may not. The precision of the measurement can be found by the quality of the fit of the graybody distribution function to the data.

The graybody distribution function is the Planck function [Eq. (7)] which can be written in the form

$$N_\lambda = \epsilon C_1 \lambda^{-5} (e^{C_2/\lambda T} - 1)^{-1}, \quad (8)$$

where C_1 and C_2 are constants equal to 1.191×10^{-16} and 1.439×10^{-2} , respectively, in mks units. The effective emissivity is $\epsilon = \epsilon_0 \alpha$, where ϵ_0 is the actual emissivity of the radiating material, and α is the fraction of the observed area that is radiating light. To carry out the least-squares fit, we make initial guesses for temperature (T^0) and effective emissivity (ϵ^0) and determine the calculated spectral radiance (N_λ^0) from Eq. (8). We compute $\Delta T = T - T^0$ and $\Delta \epsilon = \epsilon - \epsilon^0$ from the equation

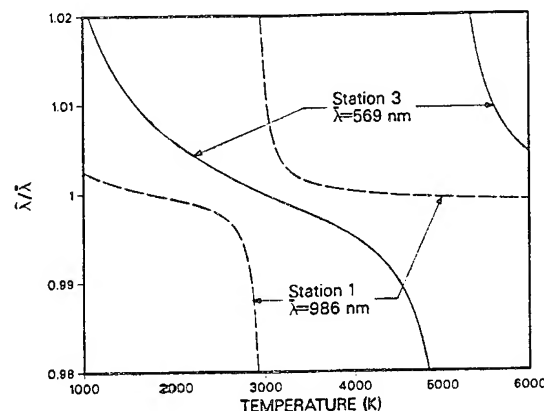


FIG. 4. Mean effective wavelength $\bar{\lambda}$, as defined by Eq. (6), of two pyrometer station-filter combinations, normalized to filter mean wavelength $\bar{\lambda}_0$. The mean effective wavelength is the wavelength a bandpass filter would have to have in the limit of zero bandwidth in order to pass the same amount of light from a Planck source as the actual filter. At temperatures away from those at which the filter wavelength is at the Wien's Law maximum, the corrections are small. At the maximum, the corrections are large but unnecessary.

TABLE I. Definitions of optical parameters.

Parameter	Definition
R_M	Reflectance of turning mirror
T_W	Transmittance of glass window
T_L	Transmittance of objective lens
T_{B_1}	Transmittance of primary beamsplitter
R_{B_1}	Reflectance of primary beamsplitter
T_{B_2}	Transmittance of secondary beamsplitter
R_{B_2}	Reflectance of secondary beamsplitter
T_f	Transmittance of focusing lens
$T_{1,2,3,4}$	Transmittance of optical bandpass filters
R_d	Responsivity of photodetector

$$N_{\lambda} - N_{\lambda}^0 = \frac{\partial N_{\lambda}}{\partial T} \Delta T + \frac{\partial N_{\lambda}}{\partial \epsilon} \Delta \epsilon. \quad (9)$$

It is a simple matter to determine the partial derivatives analytically from Eq. (8). By using ΔT and $\Delta \epsilon$ to obtain new trial values for T and ϵ , we can iterate until convergence is reached. In order to get time-resolved temperatures, this entire procedure is carried out for each time step. It is useful to use the final values for T and ϵ at a given time step for the initial guesses for the following step, as these parameters are generally smooth functions of time.

It is important to recall here that the mean effective wavelengths of the pyrometer channels are functions of temperature (Fig. 4), due to the large bandwidths. Carrying out the least-squares procedure as outlined above, using fixed wavelengths, is not sufficient to get the best answer. The effective pyrometer wavelengths can be recalculated based on the temperature being measured. This process can be carried out iteratively, and tends to converge rapidly, giving rise to a minor correction. In practice, for the filter bandwidths we have used, this correction is smaller than the temperature uncertainty, and is therefore unnecessary.

Uncertainties in temperature and emissivity were determined systematically by the equations

$$\delta T = \sigma_N / \left(\frac{\partial N_{\lambda}}{\partial T} \right)_{\epsilon, \lambda = \langle \lambda \rangle}, \quad (10)$$

$$\delta \epsilon = \sigma_N / \left(\frac{\partial N_{\lambda}}{\partial \epsilon} \right)_{T, \lambda = \langle \lambda \rangle}, \quad (11)$$

where σ_N is the standard deviation in spectral radiance, and the partial derivatives are evaluated at $\langle \lambda \rangle$, i.e., the average wavelength of all the pyrometer channels.

IV. RESULTS AND DISCUSSION

The present system has been used primarily to measure light emission from inert and reactive powder mixtures. Time-resolved spectral radiance data from one experiment are shown in Fig. 5. The target consisted of a thin (about 0.5 mm) powder layer sandwiched between a copper driver plate and a lithium fluoride window, similar to Fig. 2. In this

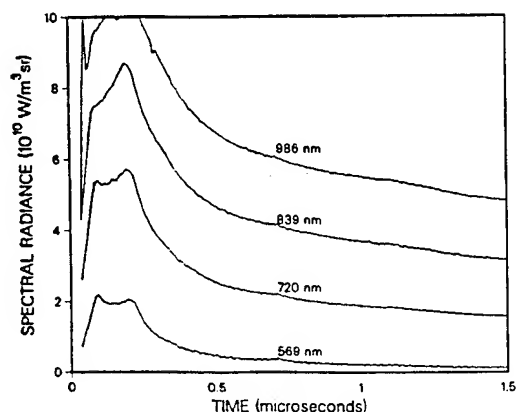


FIG. 5. Time-resolved data from nickel-aluminum powder mixture shocked to about 14 GPa. Origin of time axis corresponds to shock arrival at powder-window interface. Each curve is offset vertically from the curve below it by $10^{10} \text{ W/m}^2 \text{ sr}$ for display purposes. The lowest curve is not offset.

experiment, the powder was a mixture of 2- μm particle-size nickel and 1- μm particle-size aluminum in a 87%/13% ratio by weight, with an initial porosity of 57%. Shock-recovery²⁴ experiments have shown that this composition chemically reacts under shock. The target was struck by a copper impactor traveling at 1.18 km/s, achieving a peak shock pressure of about 14 GPa in the powder sample.

The time-resolved temperature and emissivity histories computed by the least-squares method are illustrated in Fig. 6. The measured temperature drops from about 2700 to 2000 K in the first microsecond after shock arrival. The initial high temperature is due to heterogeneous distribution of the shock energy. The total radiant energy is dominated by light emitted from the fraction of the observed area that is hotter than the rest, until thermal equilibrium is established. As thermal equilibrium is achieved, the highest observed temperature rapidly decreases to the mean bulk shock temperature, with an associated increase in effective emissivity as the fractional area of radiating sample increases to unity. At this time, the temperature continues to decrease more slowly by conduction of heat into the lithium fluoride window by a process modelled by Grover and Urtiew.²⁵ It should also be noted that the double peak at early times is due to a reflected shock in the thin powder layer.

The quality of the least-squares fit is shown by Fig. 7. The plot shows four measured spectral radiances from the experiment, 1 μs after arrival of the shock wave. The curve represents the best-fitting graybody function, with $T = 2100 \pm 150 \text{ K}$ and $\epsilon = 0.205 \pm 0.128$, where the uncertainties are determined by Eqs. (10) and (11). Emissivities are typically poorly constrained by visible spectral radiance data for temperatures in this range, due to the weak dependence of spectral radiance on emissivity in Eq. (8). However, the strong dependence of spectral radiance on temperature leads to relatively small uncertainties in temperature. In this case the temperature is well enough constrained to conclude that heat has been released from the chemical reaction initiated by the shock wave. The measured shock temperature exceeds the theoretical shock temperature, calculated assuming there is no chemical reaction, by more than 600 K.²⁶

Radiation pyrometry is extremely useful in measuring properties of the shock state, but other methods should also

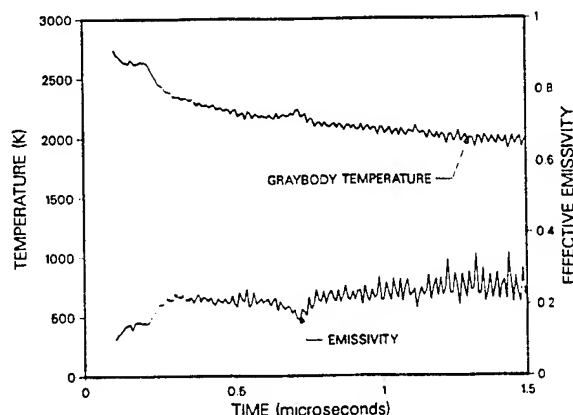


FIG. 6. Time-resolved temperature and emissivity data calculated from spectral radiance data in Fig. 5.

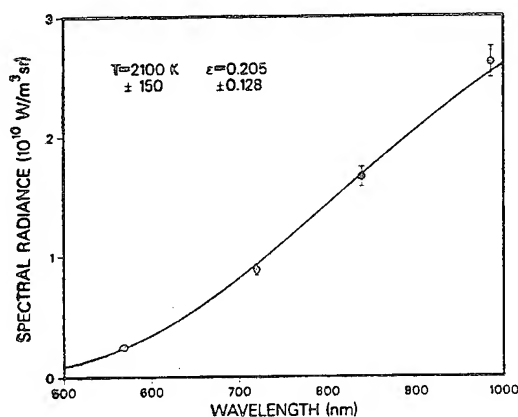


FIG. 7. Spectral radiances from Fig. 5 plotted for the time step $t = 1 \mu\text{s}$, with the best fitting graybody curve corresponding to $T = 2100 \text{ K}$ and $\epsilon = 0.205$.

be employed in order for an experimental program to be more complete. There are three principal variables to deal with when making measurements of shock-induced emission of radiation: wavelength, position, and time. These can be envisioned to define a three-dimensional space. Radiation pyrometry averages over the spatial dimension, obtains data discretely in the spectral dimension and continuously in the temporal dimension. Complimentary methods define "orthogonal" planes in variable space. Fast framing photography provides spatial resolution, discrete temporal information, and no spectral information. Streak photography provides continuous temporal data, spatial resolution in one direction, but again no spectral information. Gated spectroscopy provides the spectral resolution at discrete times, but no spatial resolution. There has been recent work in combining spectroscopy with streak photography,²⁷ which results in continuous data in the wavelength-time plane; however, it is not possible to get precise values of spectral radiance with this method. It is clear that no single experimental method can obtain a complete picture, and that radiation pyrometry is only one of several complementary experimental techniques which can be employed to study shock-induced light emission.

ACKNOWLEDGMENTS

We are grateful for the advice and assistance of M. Anderson, G. Lyzenga, D. Schmitt, and R. Setchell. This work

was performed at Sandia National Laboratories by DOE contract No. DE-ACO4-76DP00789. It was supported at the California Institute of Technology under NASA Grant No. NGL-05-002-105 and NSF Grant No. EAR86-08249, Contribution No. 4073, Division of Geological and Planetary Sciences. California Institute of Technology.

- ¹M. B. Boslough, *J. Appl. Phys.* **58**, 3394 (1985).
- ²S. B. Kormer, M. V. Sinitsyn, G. A. Kirillov, and V. D. Urtin, *Sov. Phys. JETP* **21**, 689 (1965).
- ³S. B. Kormer, *Sov. Phys. Usp. Engl. Transl.* **11**, 229 (1968).
- ⁴S. A. Raikes and T. J. Ahrens, *Geophys. J. R. Astr. Soc.* **58**, 717 (1979).
- ⁵W. G. Von Holler, *Fast Reactions in Energetic Systems*, edited by C. Capellos and R. F. Walker (Kluwer, Boston 1981), p. 485.
- ⁶G. A. Lyzenga and T. J. Ahrens, *Rev. Sci. Instrum.* **50**, 1421 (1979).
- ⁷G. A. Lyzenga and T. J. Ahrens, *Geophys. Res. Lett.* **7**, 141 (1980).
- ⁸G. A. Lyzenga, T. J. Ahrens, and A. C. Mitchell, *J. Geophys. Res.* **88**, 2431 (1983).
- ⁹G. A. Lyzenga, T. J. Ahrens, W. J. Nellis, and A. C. Mitchell, *J. Chem. Phys.* **76**, 6282 (1982).
- ¹⁰T. J. Ahrens, G. A. Lyzenga, and A. C. Mitchell, *High-Pressure Research in Geophysics*, edited by S. Akimoto and M. H. Manghnani (Reidel, Boston, 1982), p. 5-9.
- ¹¹H. B. Radousky, W. J. Nellis, M. Ross, D. C. Hamilton, and A. C. Mitchell, *Phys. Rev. Lett.* **57**, 2419 (1986).
- ¹²H. B. Radousky and M. Ross, *Phys. Lett. A* **129**, 43 (1988).
- ¹³P. J. Brannon, C. H. Konrad, R. W. Morris, E. D. Jones, and J. R. Asay, *J. Appl. Phys.* **54**, 6374 (1983).
- ¹⁴M. B. Boslough, Ph.D. thesis, California Institute of Technology, 1983.
- ¹⁵R. Jeanloz and T. J. Ahrens, *High-Pressure Research-Applications in Geophysics*, edited by M. H. Manghnani and S. Akimoto (Academic, New York, 1977), p. 439.
- ¹⁶M. B. Boslough, T. J. Ahrens, and A. C. Mitchell, *Geophys. J. R. Astr. Soc.* **84**, 475 (1986).
- ¹⁷Q. Williams, R. Jeanloz, J. Bass, B. Svendsen, and T. J. Ahrens, *Science* **236**, 181 (1987).
- ¹⁸R. E. Setchell, *Shock Waves in Condensed Matter 1981*, edited by W. J. Nellis, L. Seaman, and R. A. Graham (American Institute of Physics, New York, 1982), p. 657.
- ¹⁹M. B. Boslough, *Int. J. Impact Eng.* **5**, 173 (1987).
- ²⁰M. B. Boslough, R. E. Setchell, M. U. Anderson, M. R. Lewis, and D. E. Wackerbarth, *Sandia Report SAND88-2768*, 1989 (unpublished).
- ²¹M. Nicol, S. W. Johnson, and N. C. Holmes, *Shock Waves in Condensed Matter 1987*, edited by S. C. Schmidt and N. C. Holmes (North-Holland, Amsterdam, 1988), p. 471.
- ²²K. Kondo and T. J. Ahrens, *Phys. Chem. Minerals* **9**, 173 (1983).
- ²³W. E. Schneider and D. G. Goebel, *Light Measurement '81*, *Proc. SPIE* **262**, 74 (1981).
- ²⁴Y. Horie, R. A. Graham, and I. K. Simonsen, *Mater. Lett.* **3**, 354 (1985).
- ²⁵R. Grover and P. A. Urtiew, *J. Appl. Phys.* **45**, 146 (1974).
- ²⁶M. B. Boslough, *Chem. Phys. Lett.* **160**, 618 (1989).
- ²⁷R. E. Setchell, *AIAA Progress in Astronautics and Aeronautics* **106**, 607 (1986).

Abstract for the ARO-sponsored "Shock Synthesis of Materials" Workshop
Georgia Institute of Technology
Atlanta, Georgia, May 24 - 26, 1994

Nanosecond, Time-Resolved Pressure Measurements:
Sandia's Advanced Materials Department Program in
Shock-Induced Solid State Chemistry*

M. U. Anderson, R. A. Graham, M. R. Baer, and G. T. Holman

Our group at Sandia initiated a scientific program in shock-induced solid state chemistry in late 1979. Our current effort has evolved continuously from that time and has maintained a broad and deep emphasis in a well coordinated effort in materials science, solid state physics and shock-compression science.

Knowledge of the behavior of highly porous materials under shock compression is a fundamental aspect underlying shock-compression synthesis and processing. Although there is considerable data available based on sample preservation and subsequent analysis, there has previously been limited time-resolved pressure data available that observed highly porous materials under impulsive loading. The objective of the present work was to study the shock compression behavior of highly porous materials (45 - 65% dense) under impulsive loading (0.03 - 6.0 GPa) on a few nanosecond resolution scale. The data are necessary to provide a basis for modeling the consolidation, deformation, and chemical reaction processes of a range of solids. The observed process mechanisms show that typical "Hugoniot" descriptions typically used to describe solid state shock mechanics in full density or near full density states are not capable of describing the behavior of highly porous materials under shock compression.

A program is in place to routinely measure the material response of samples under impulsive loading using the PVDF piezoelectric polymer stress-rate gauge. The method of approach was to develop and qualify a time-resolved, shock-compression technique in order to develop an understanding of the process mechanisms that dominate highly porous material behavior under impulsive loading. In addition to the time-resolved PVDF pressure capability, we are in the early stages of developing a capability for nanosecond, time-resolved particle velocity measurements either in as an independent measure or in conjunction with PVDF measurements.

We have used the PVDF technique to study a range of highly porous solids including inert (TiO_2 , $2\text{Al} + \text{Fe}_2\text{O}_3$), and reactive ($5\text{Ti} + 3\text{Si}$; and the high explosive HMX) samples. The experimental technique uses a copper capsule to contain the sample which has PVDF gauge packages in direct contact with the front and rear surfaces. A precise measure (0.5%) is made of the compressive stress wave velocity through the sample, as well as the input and propagated shock stresses which are determined to an accuracy of 3%. The initial density is known from the sample preparation process to an accuracy of 3%. The wave speed through the sample is a sensitive indicator of crush strength, and compaction. The inert material rutile (TiO_2) was studied to develop an understanding of a

* Supported by the U. S. Department of Energy under contract number DE-AC04-76DP00789.

highly porous material under impulsive loading, and to fully qualify the time-resolved, shock-compression technique.

All impulsively-loaded samples that we have studied exhibit behavior during the shock processes that are strongly rate dependent, and this rate dependence is strongly dependent on morphology, and density for a specific material. The rate dependencies are observed upon entrance of the loading wave into the sample as the material is consolidated toward a higher density. The observed rate dependence at the input surface would be expected to lead to nonunique behaviors as the porous materials will be influenced by the shock impedance of the driver plate material. The propagated wave speed shows evidence in some cases for energy release in the reactive samples. The structure of the propagated waves in all cases shows very long risetimes (50 to 500 nsec) with complex waveshapes. It is clear from the data that rate dependent descriptions of dynamic deformation of highly porous solids are required to describe the processes. Further, these strongly rate dependent processes are specific to particular materials, density and morphology. It appears that any attempt to describe the processes with typical Hugoniot approaches can lead to qualitatively incorrect descriptions of the critical processes. The processes occurring in shock-loaded highly porous powder mixtures are perhaps the most complex ever countered under shock compression.

Selected publications:

1. SOLIDS UNDER HIGH-PRESSURE SHOCK COMPRESSION; Mechanics, Physics, and Chemistry, R. A. Graham, Springer Verlag, 1993.
2. R. A. Graham, B. Morosin, Y. Horie, E. L. Venturini, M. Boslough, M. J. Carr, and D. L. Williamson, in SHOCK WAVES IN CONDENSED MATTER, edited by Y. M. Gupta (Plenum, New York, 1986) pp. 693 - 711.
3. R. A. Graham, B. Morosin, E. L. Venturini, M. J. Carr, Annual Review of Materials Science, Volume 16, pp. 315 - 341 (1986).
4. PRESSURE MEASUREMENTS IN CHEMICALLY REACTING POWDER MIXTURES WITH THE BAUER PIEZOELECTRIC POLYMER GAUGE, R. A. Graham, M. U. Anderson, Y. Horie, S-K. You, G. T. Holman, Shock Waves (1993) Volume 3 pp. 79-82.
5. TIME-RESOLVED SHOCK COMPRESSION OF POROUS RUTILE: WAVE DISPERSION IN POROUS SOLIDS, M. U. Anderson, R. A. Graham, G. T. Holman, Joint AIRAPT/APS Conference, June 28-July 2, 1993, in press.
6. TIME-RESOLVED PRESSURE MEASUREMENTS IN CHEMICALLY REACTING POWDER MIXTURES, E. Dunbar, R. A. Graham, G. T. Holman, M. U. Anderson, N. N. Thadhani, Joint AIRAPT/APS Conference, June 28-July 2, 1993, in press.
7. SHOCK RESPONSE OF POROUS $2Al + Fe_2O_3$ MIXTURES, G. T. Holman, R. A. Graham, M. U. Anderson, Joint AIRAPT/APS Conference, June 28-July 2, 1993, in press.

NANOSECOND, TIME-RESOLVED
PRESSURE MEASUREMENTS
IN
HIGHLY POROUS SOLIDS:
SANDIA'S ADVANCED MATERIALS
PHYSICS PROGRAM
IN
SHOCK-INDUCED SOLID STATE
CHEMISTRY

M. U. Anderson, R. A. Graham,

M. R. Baer and G. T. Holman

Sandia National Laboratories, Albuquerque, NM

OBJECTIVE

REPORT OUT LATEST WORK ON NANOSECOND,
TIME-RESOLVED PRESSURE MEASUREMENTS IN
HIGHLY POROUS POWDERS

PROVIDE INTERPRETATIONS OF THE
SIGNIFICANCE OF OUR NANOSECOND, TIME-
RESOLVED WORK

PROVIDE BACKGROUND ON OUR PROGRAM
FROM WHICH THE PRESENT WORK HAS
EVOLVED

THE OVERALL OBJECTIVE
OF OUR
SHOCK-INDUCED SOLID STATE
CHEMISTRY PROGRAM
IS TO
PROVIDE SCIENTIFIC DESCRIPTION
TO THE
SOLID PROCESSES INFLUENCING
SYNTHESIS AND PROCESSING

OUTLINE

INTRODUCTION

BACKGROUND

Historical
Technical

SHOCK-COMPRESSION MECHANICS

Highly Porous Solids

EXPERIMENTAL ARRANGEMENTS

BEHAVIOR OF HIGHLY POROUS SOLIDS

Materials: HMX, TiO_2 , $\text{Al} + \text{Fe}_2\text{O}_3$, $\text{Ni} + \text{Al}$
 $5\text{Ti} + 3\text{Si}$

CONCLUSIONS

SANDIA ADVANCED MATERIALS PHYSICS

OUR VIEW

The technological influence of materials synthesis and processing studies under high pressure shock compression has historically largely been a disappointment.---

This situation has resulted from a *failure*

of *materials scientists* to recognize the
complexity

of the

shock-compression science issues

and,

of *shock-compression scientists* to recognize the
complexity

of the

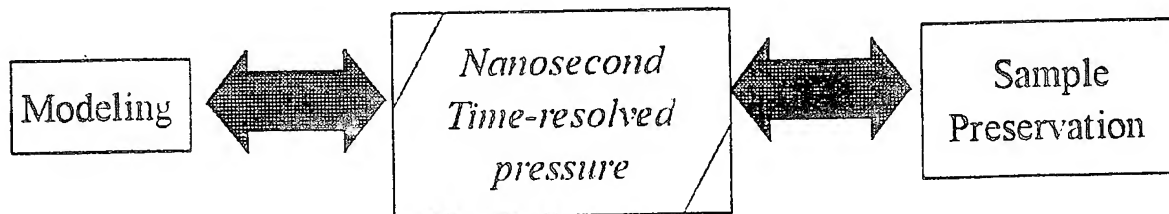
materials science issues.

Current Program

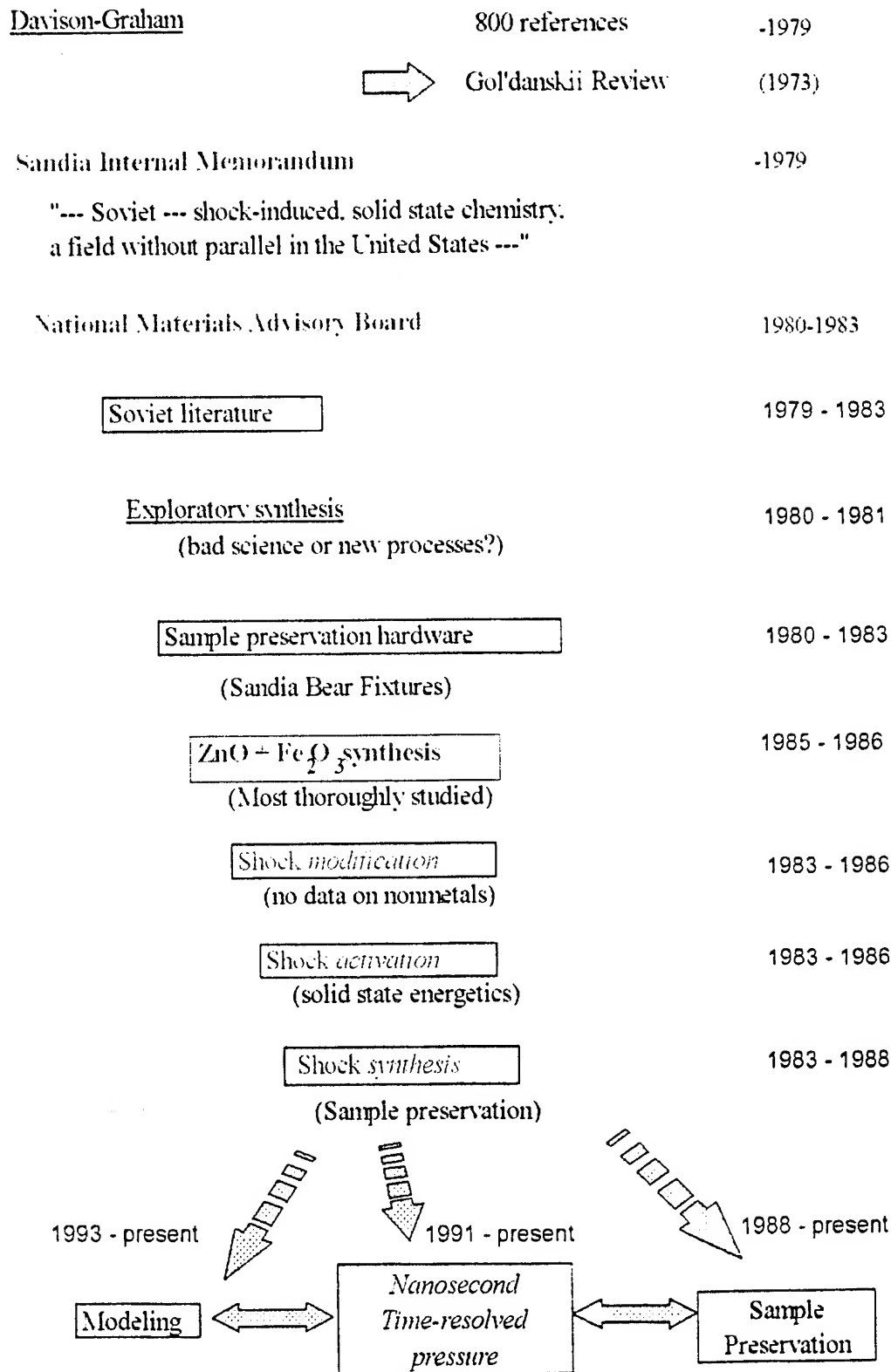
1993 - present

1991 - present

1988 - present



SANDIA ADVANCED MATERIALS
- Shock-induced Solid State Chemistry



SANDIA SHOCK-INDUCED SOLID STATE CHEMISTRY

Collaborators (coauthors of publications: 1979-1994)

Sandia	University	Other Laboratories
R. A. Graham	N. Thadhani, NMT, GaT	S. Pollak, Pit.
G. T. Holman	Y. Horie, NCSU	
M. U. Anderson	I. K. Simonsen, NCSU	
B. Morosin	F. Williams, UNM	
E. L. Venturini	M. Meyers, NMT, UCSD	
B. Dodson	K. Vecchio, UCSD	
M. J. Carr	D. Williamson, CSM	
W. J. Hammetter	M. White, UT	
D. Webb	*Golden, UNM	
F. Norwood	*Lee, UNM	
L. Davison	*Work, NMT	
E. Beauchamp	*Dunbar, NMT	
R. E. Loehman	*Joshi, NMT	
J. R. Hellman	*Zhang, Md	
D. L. Hankey		
M. Boslough		
D. S. Ginley		
J. E. Smuggeresky		
T. T. McCabe		
M. R. Baer		
M. L. Hobbs		

* graduate thesis

SIGNIFICANCE OF RESOLUTION: RESOLUTION FORCES CHANGE IN PARADIGMS

MATERIALS SCIENCE: great strides have resulted from
probing with qualitatively different spacial scales

Atomic, mesoscopic and microscopic spatial resolution

SHOCK-COMPRESSION SCIENCE: great strides have
resulted from probing with qualitatively different time scales

Manhattan project HE >>very high pressure science

Quartz gauge >>viscoplasticity, dynamic
yielding

VISAR >>viscoelasticity in polymers

PVDF >>viscoplasticity in powders

Nanosecond, time-resolved pressure measurements force
recognition of the dominance of heterogeneous, microstructural,
intraparticle and interparticle viscoplastic deformation.

For compatibility with materials science spacial scales, nanosecond
resolution of shock processes is required

PRIOR TIME-RESOLVED MEASUREMENTS

--SHOCK-INDUCED CHEMICAL REACTION--

Batsanov, Doronin, Klochkov, Teut (Sn+S , 26 kcal/m) M 1986

Gao, Jing (2Al + Fe₂O₃, 200) M 1991

Batsanov, Gogulya, Brazhnikov, Lazareva, Doronin
Klochkov, Banzhikova, Fedorov, Simakov (Sn+Te, 15)
(Sn + S, 26)
M,T 1991

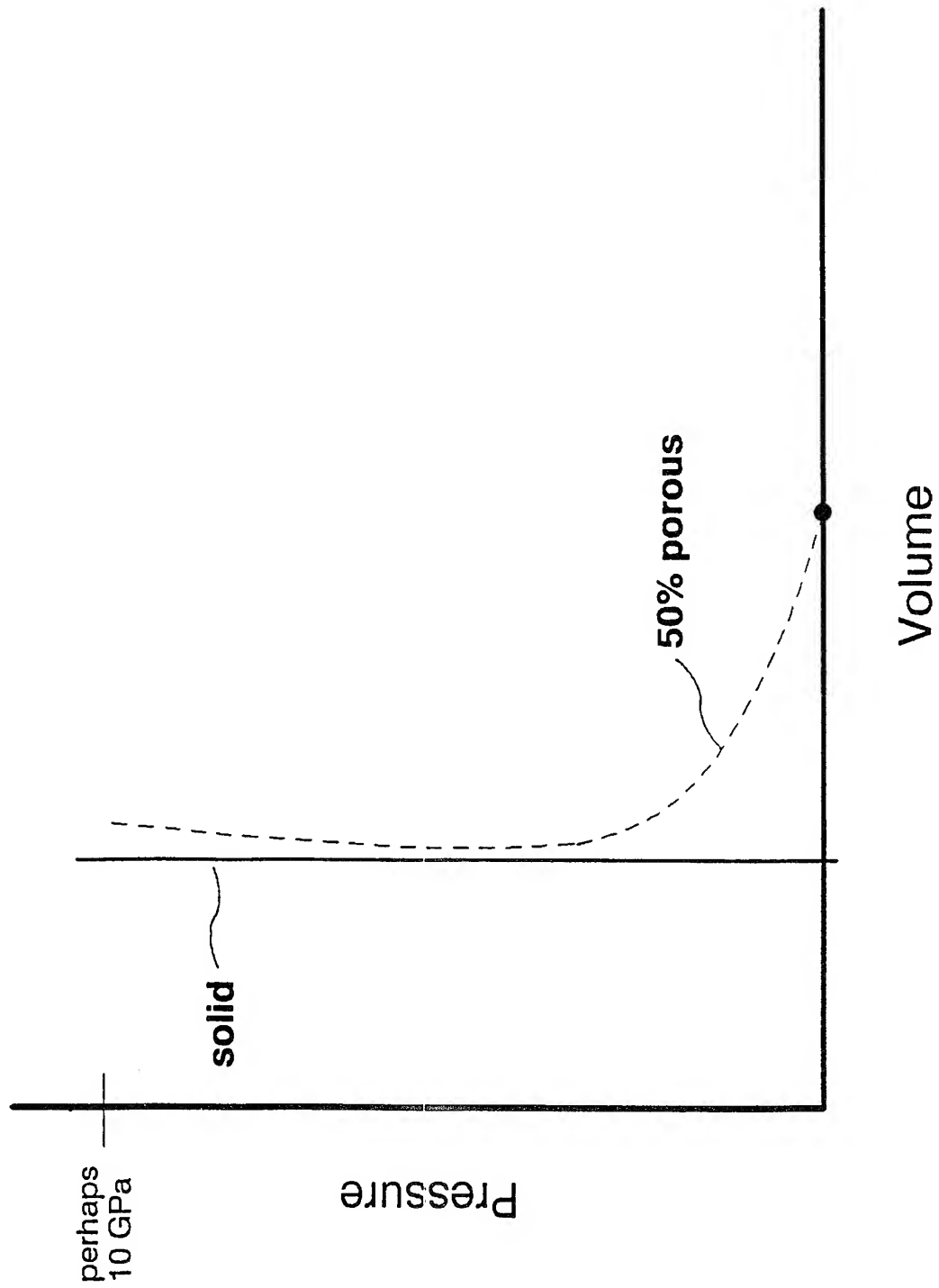
Gogulya, Voskoboynikov, Dogloborodov, Dorochoy, Brazhnikov,
(Al+S, 170)
Optical P, T 1992

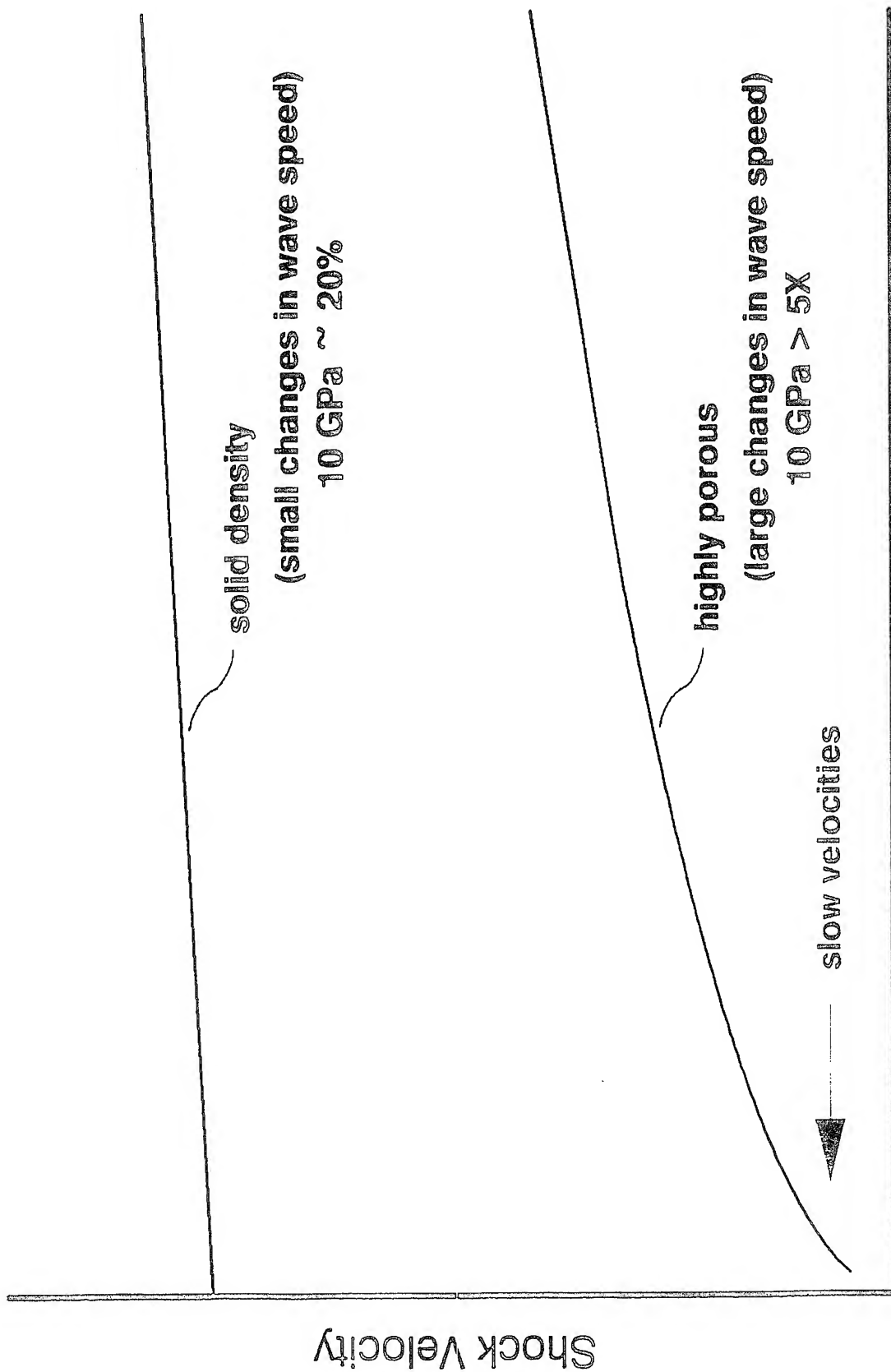
Manganin; T=temperature
(time resolution about 100 nsec)

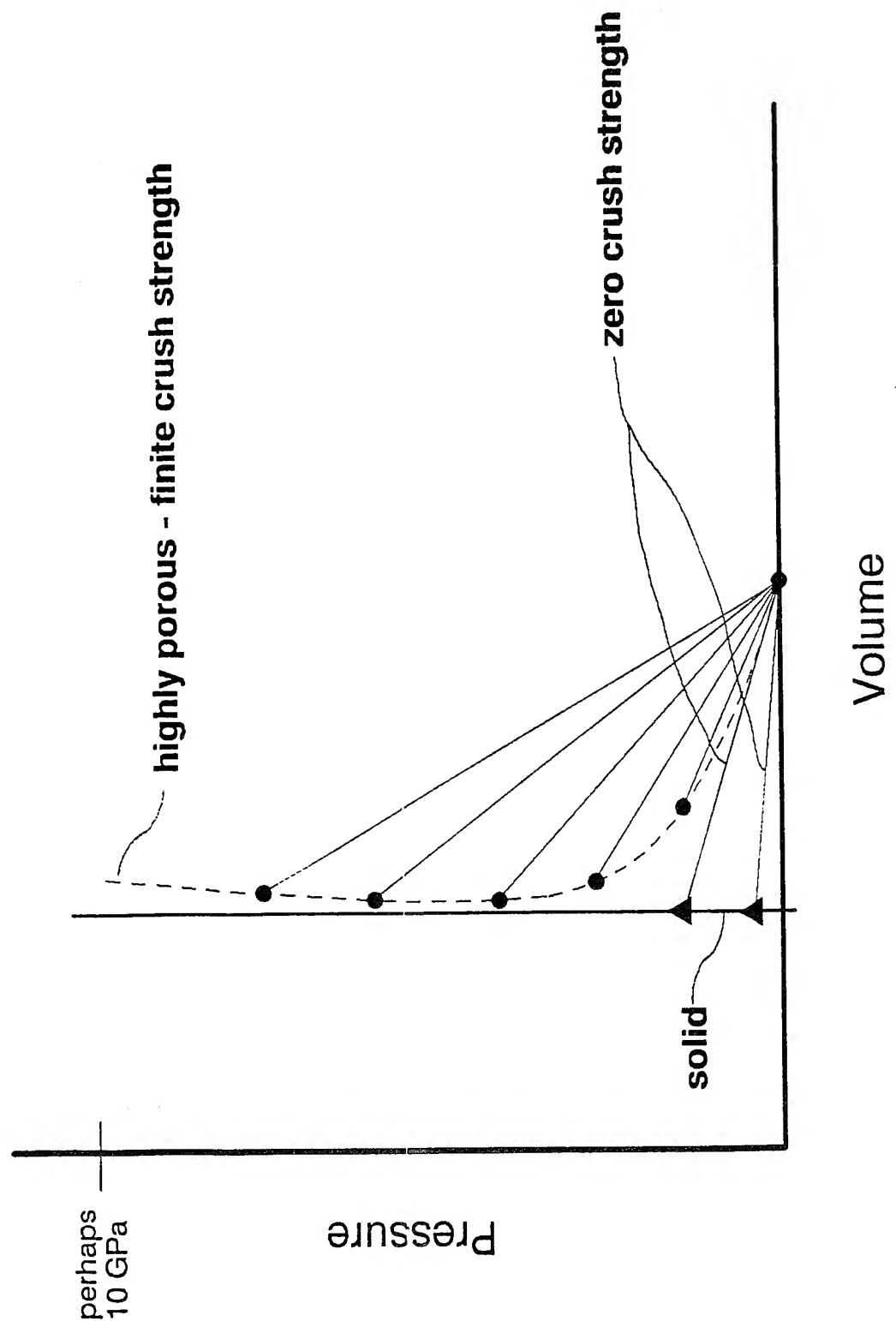
"HUGONIOT" SHOCK MEASUREMENTS

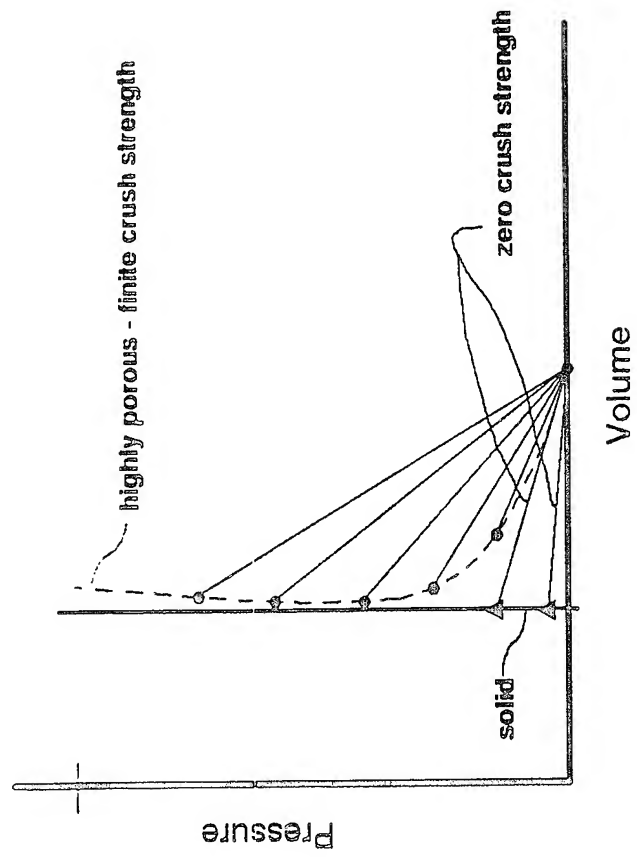
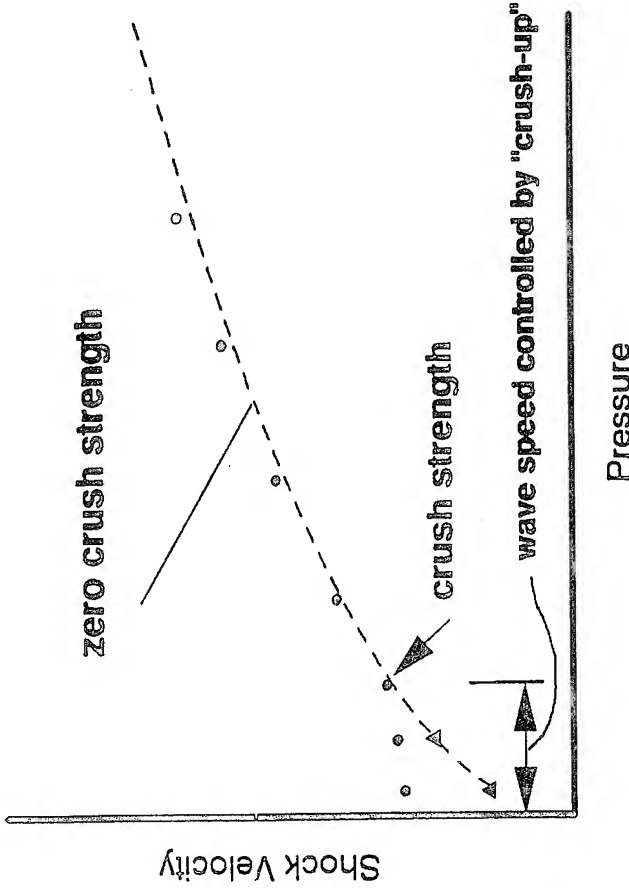
Yoshida, Thadhani (Nb+Si, 33) 1991

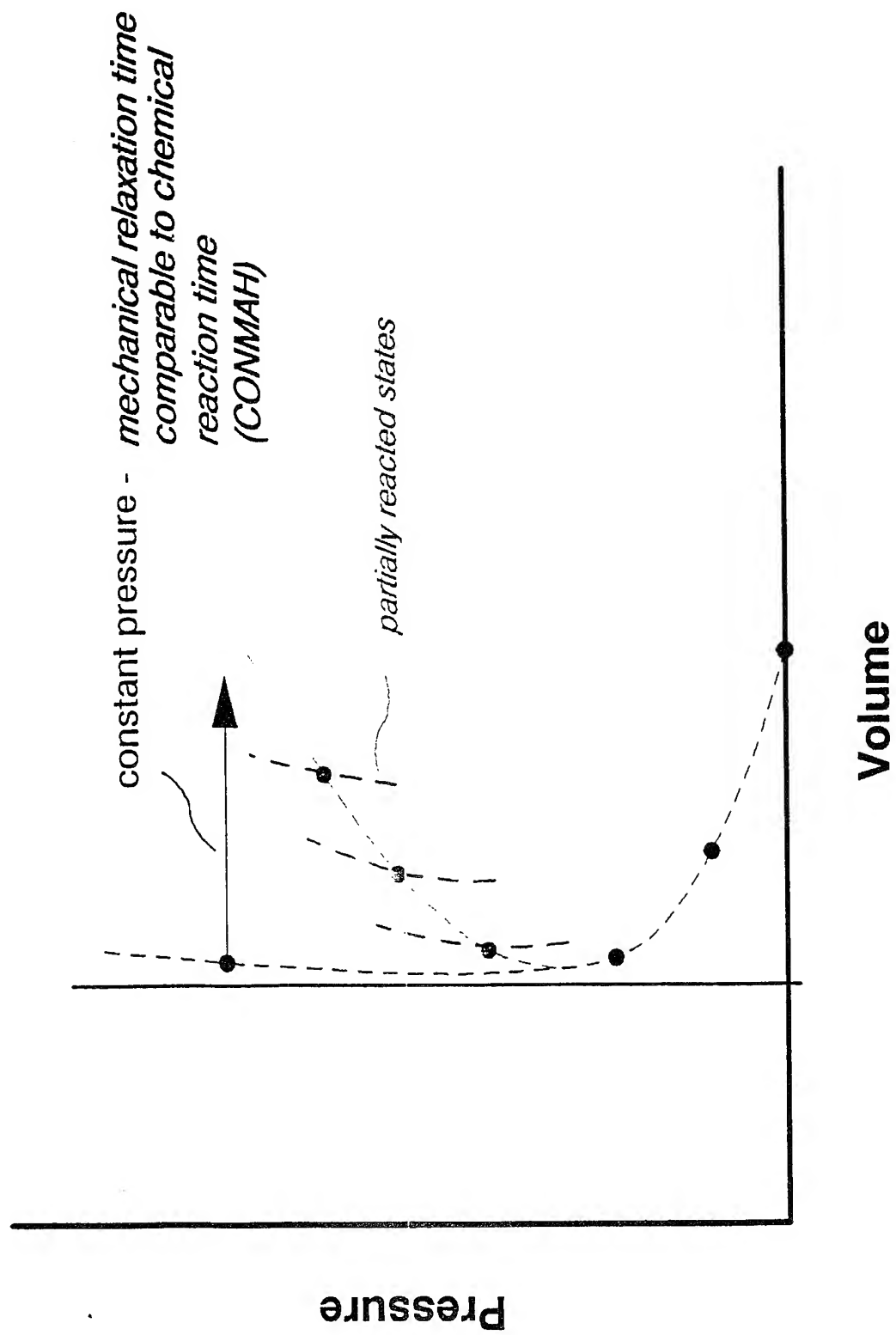
Chen, Jin, Yang (BaCO₃+TiO₂) 1989

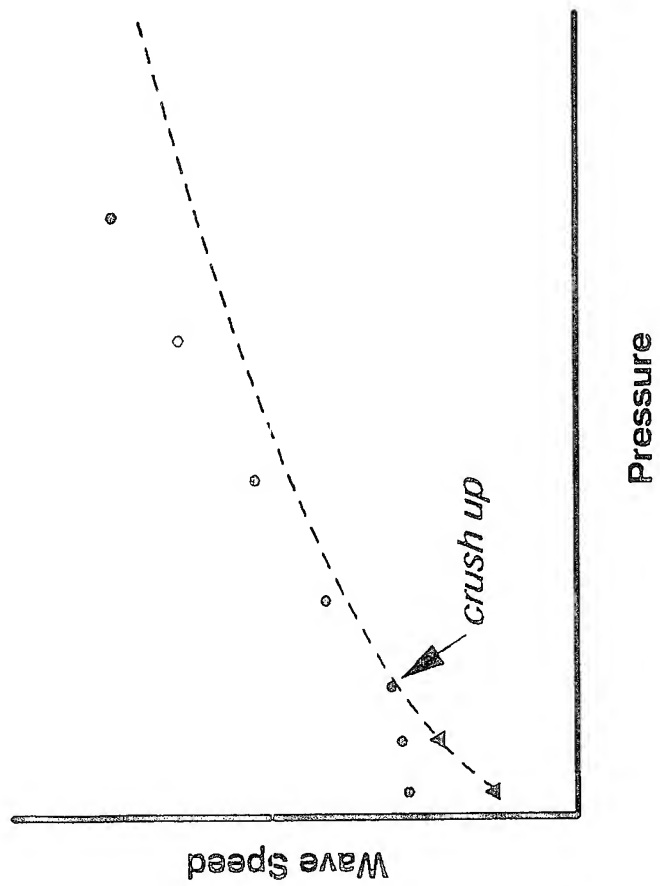
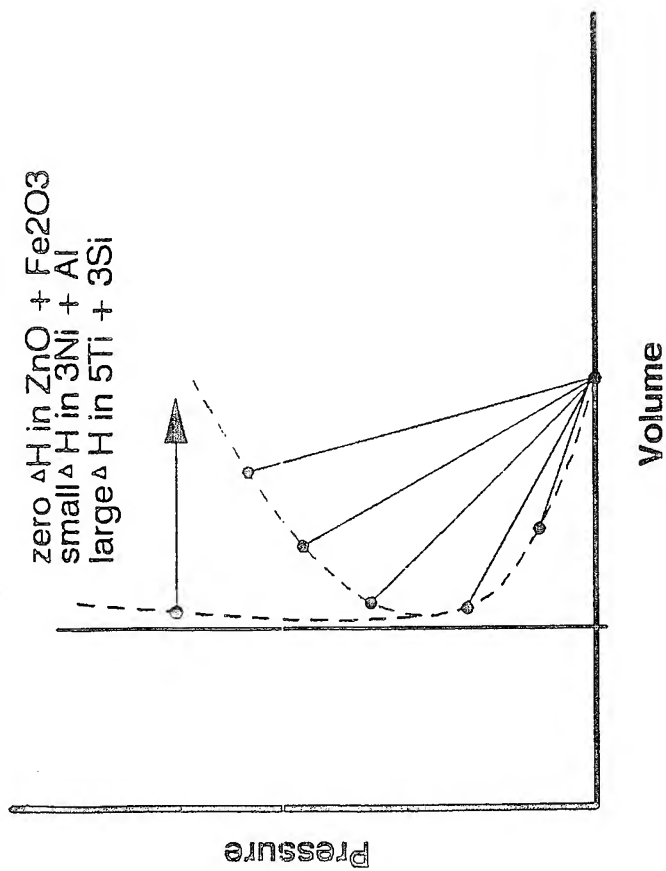




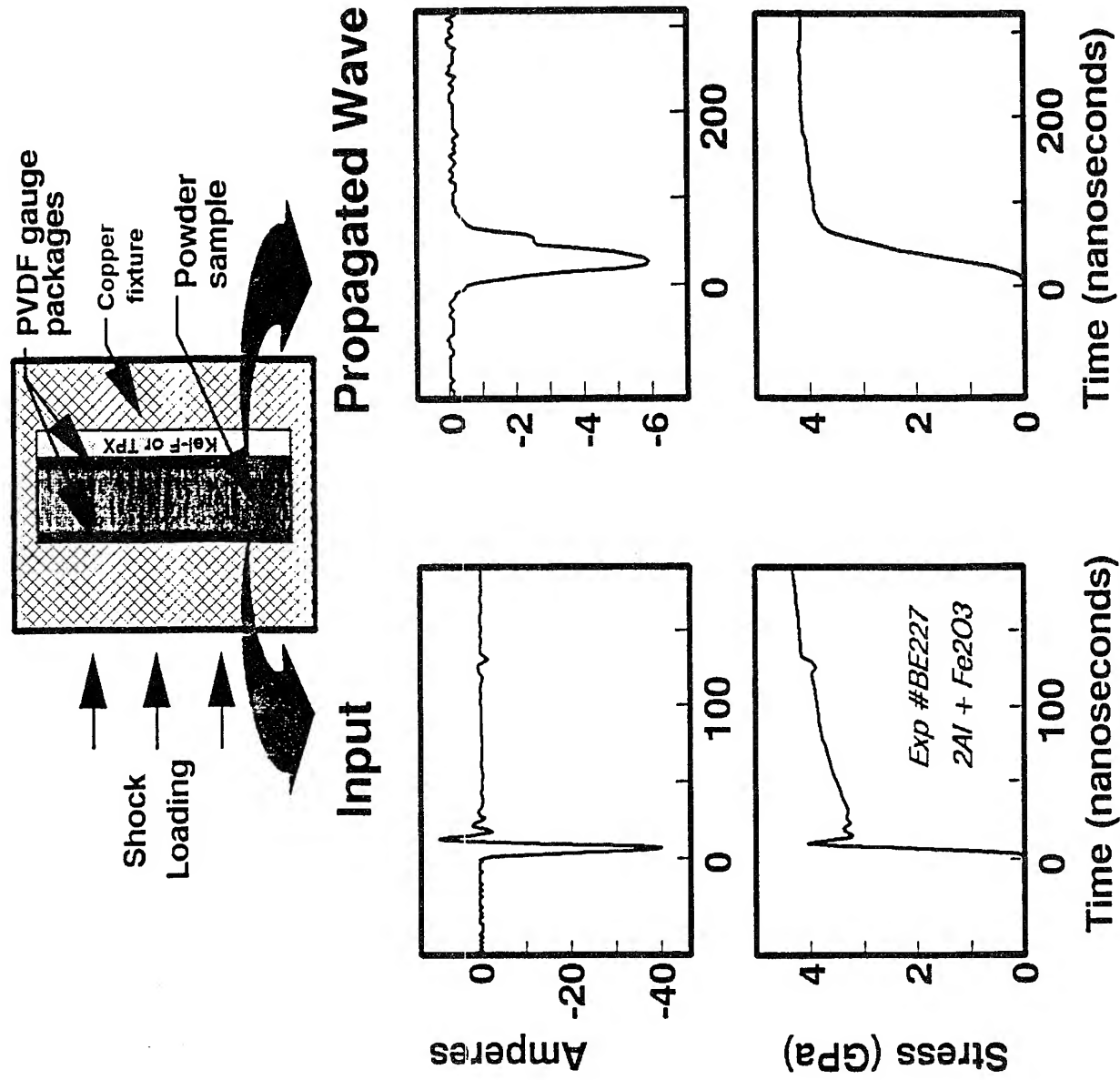




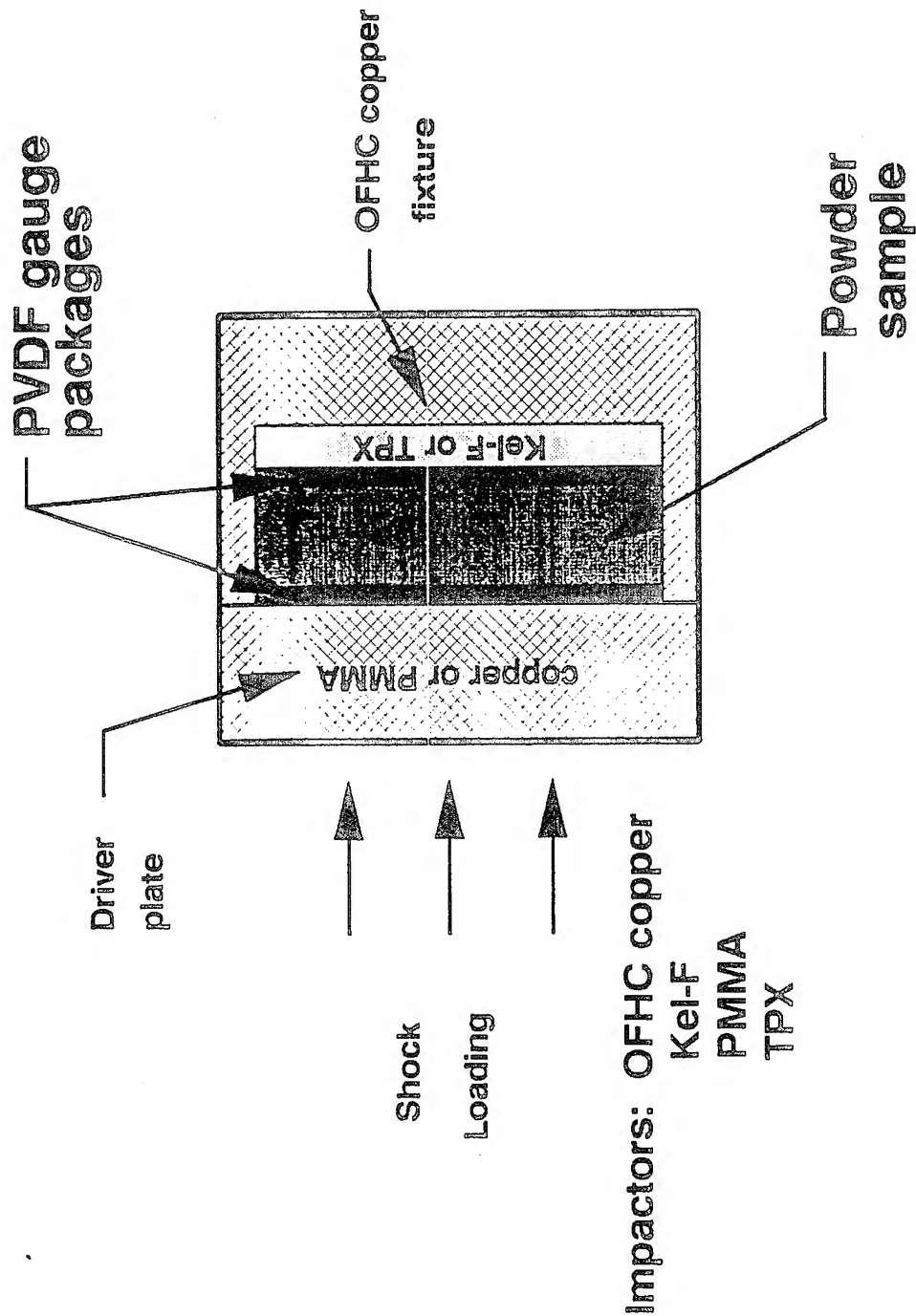




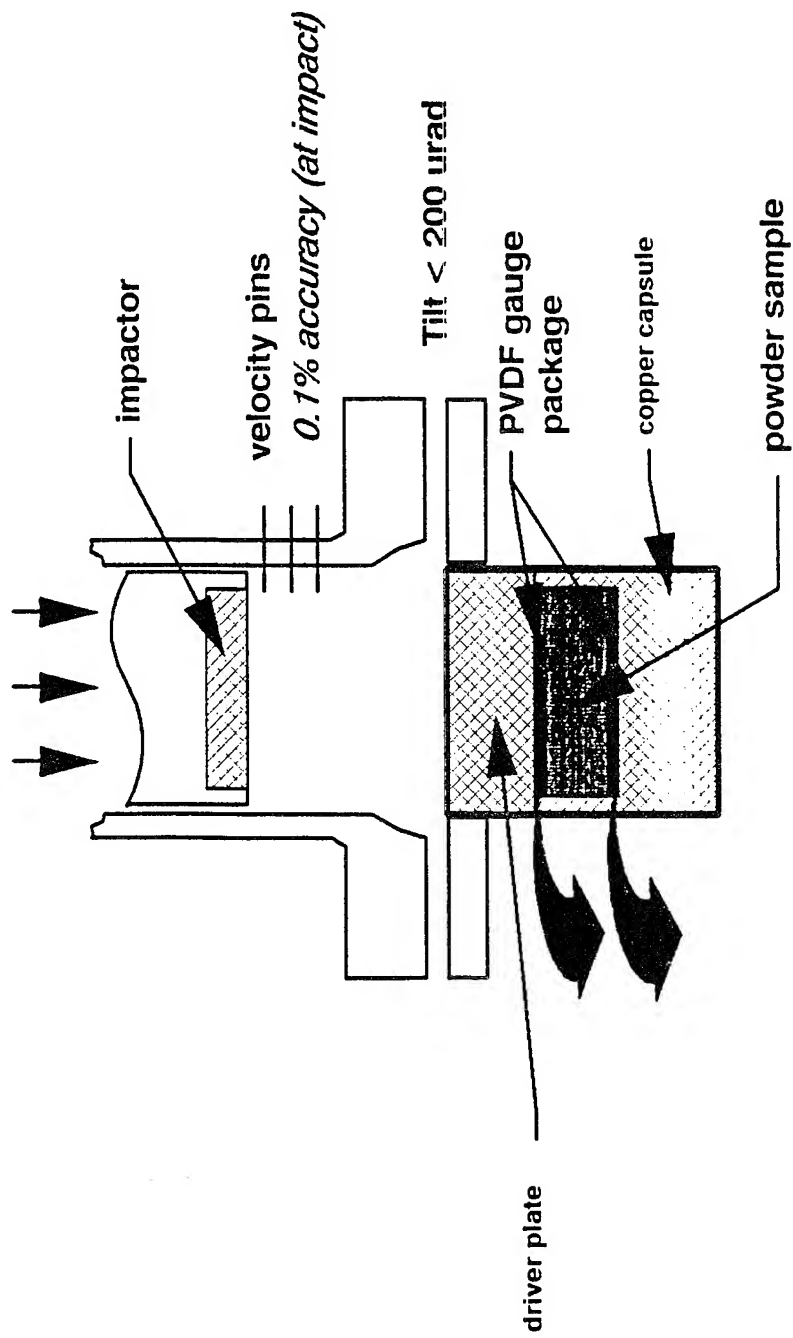
Stress-Rate Dependent Measurements



Sample Capsule Arrangement

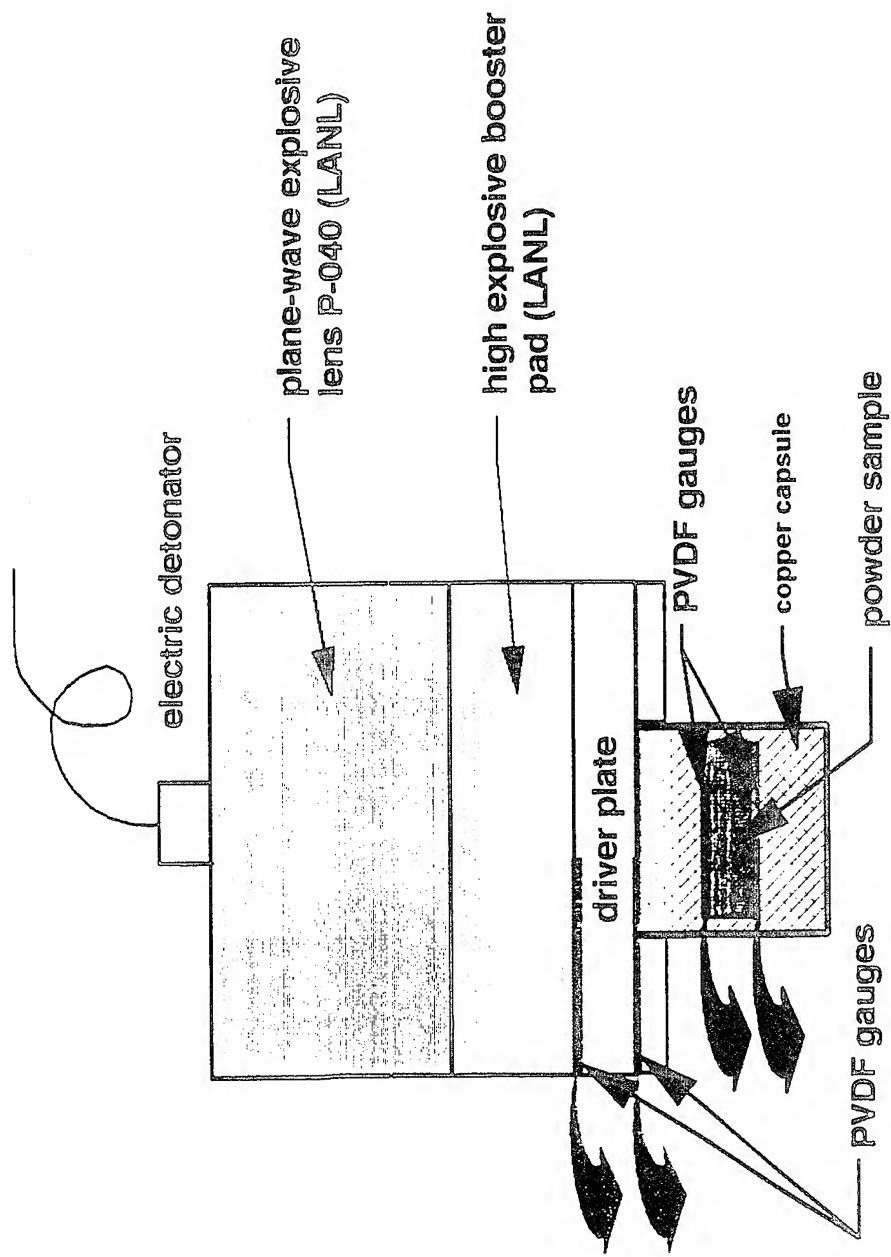


Impact Loading



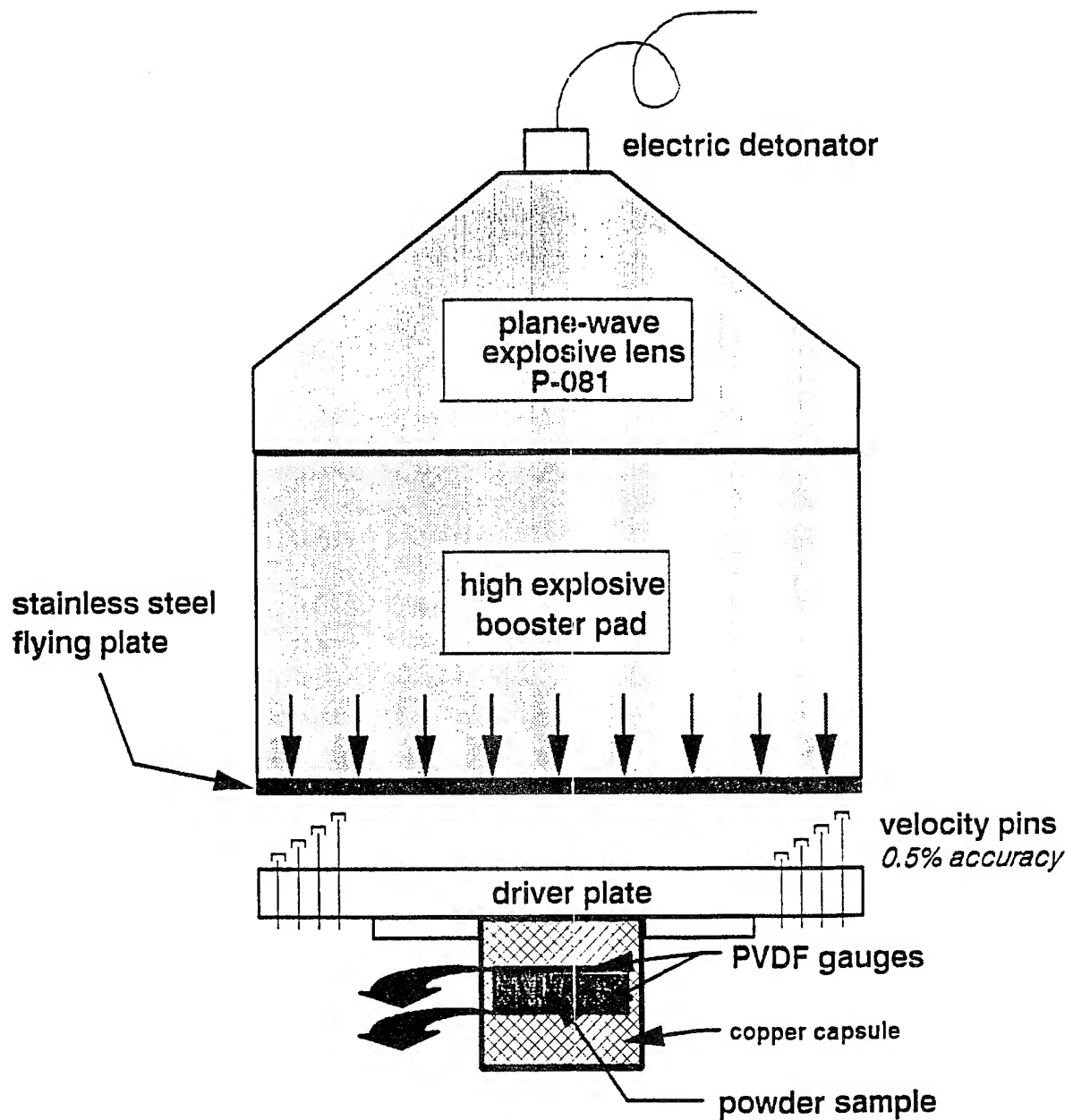
BT FIG 1 OF 1 DRW

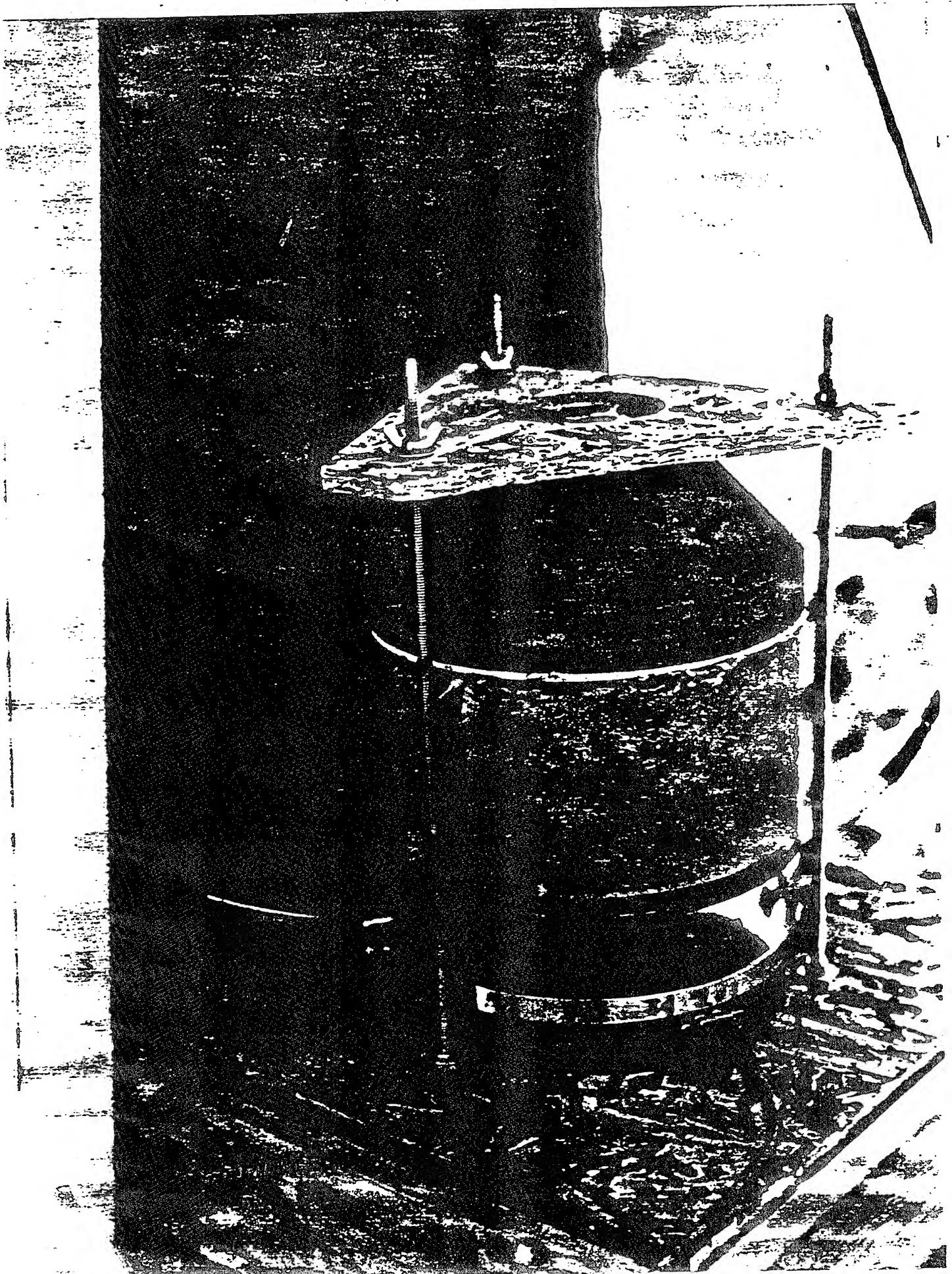
Direct Contact Explosive Loading



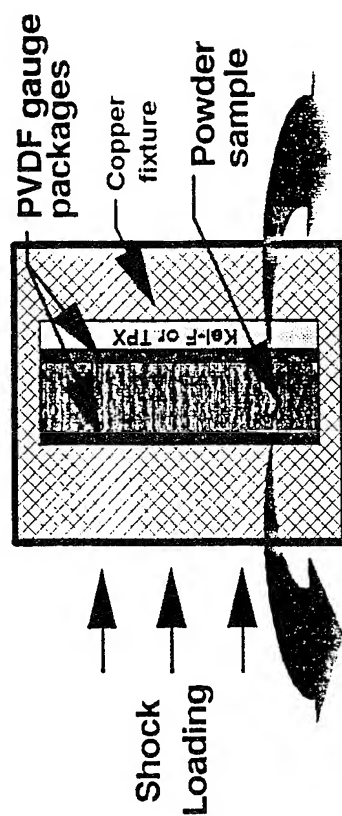
brfig10q.drw

Explosively-Driven Flying Plate



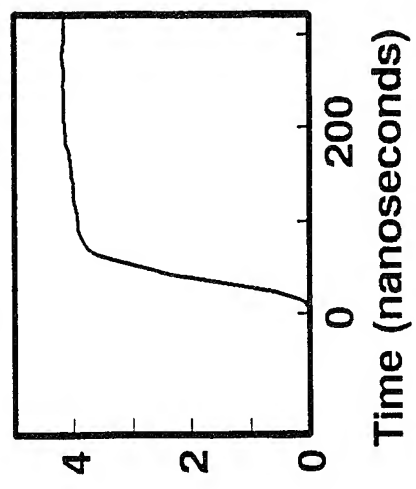
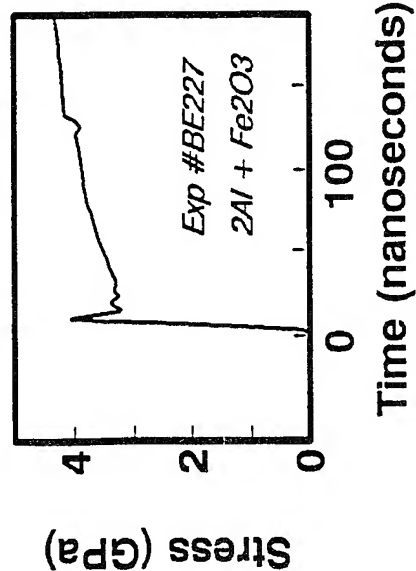
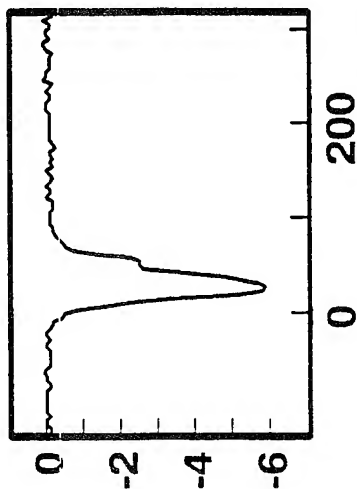
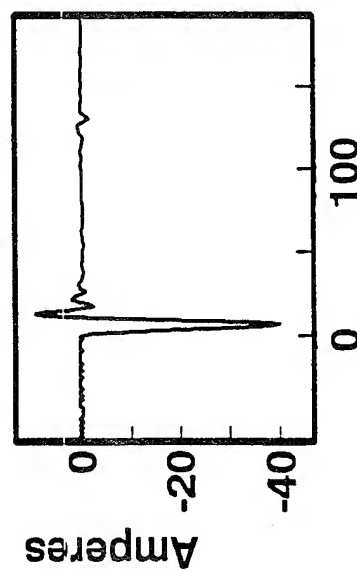


Stress-Rate Dependent Measurements



Input

Propagated Wave



Sample Materials:

HMX high explosive @ 64% dense

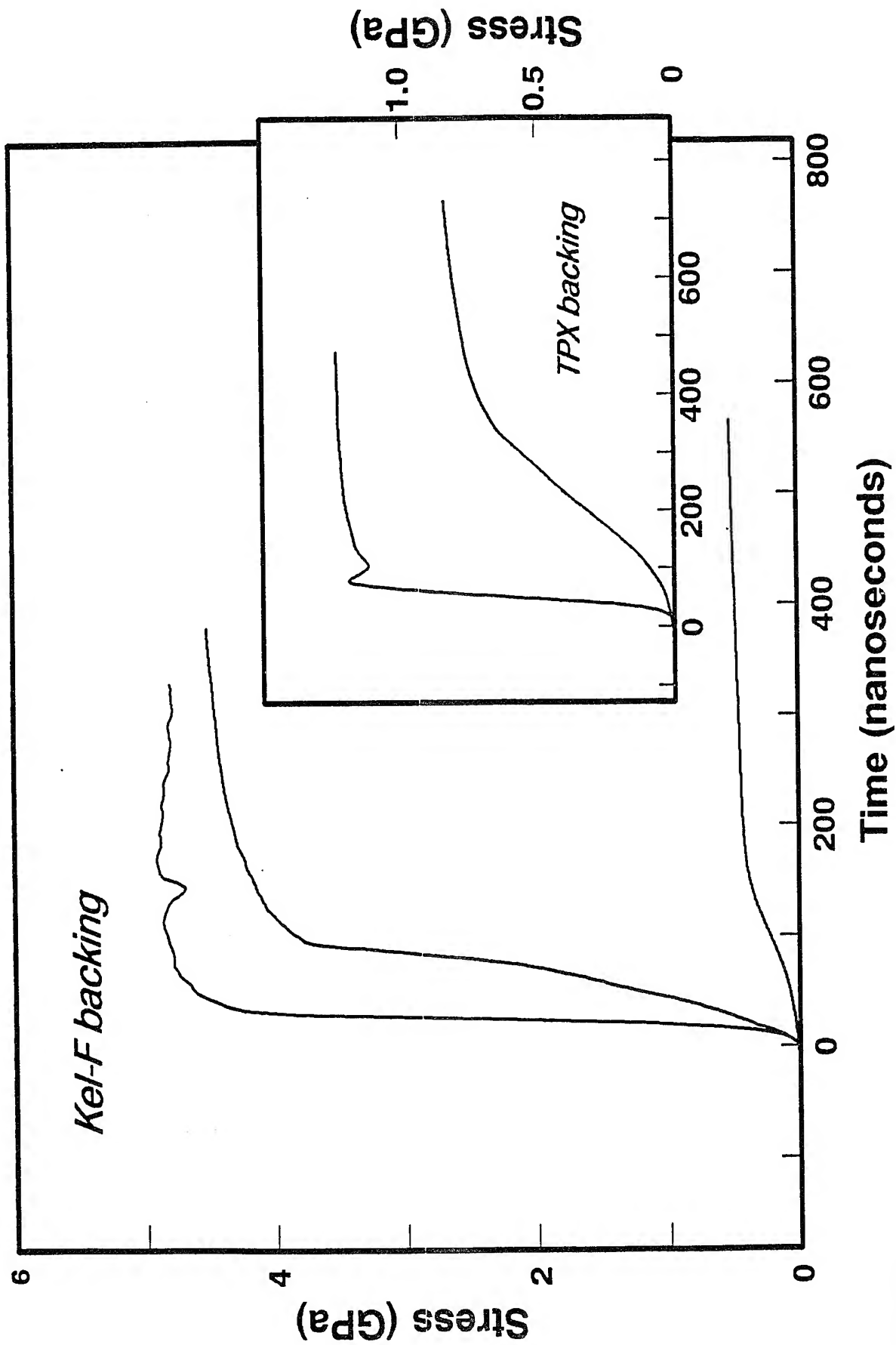
TiO₂ @ 60% dense

Al + Fe₂O₃ @ 53% dense

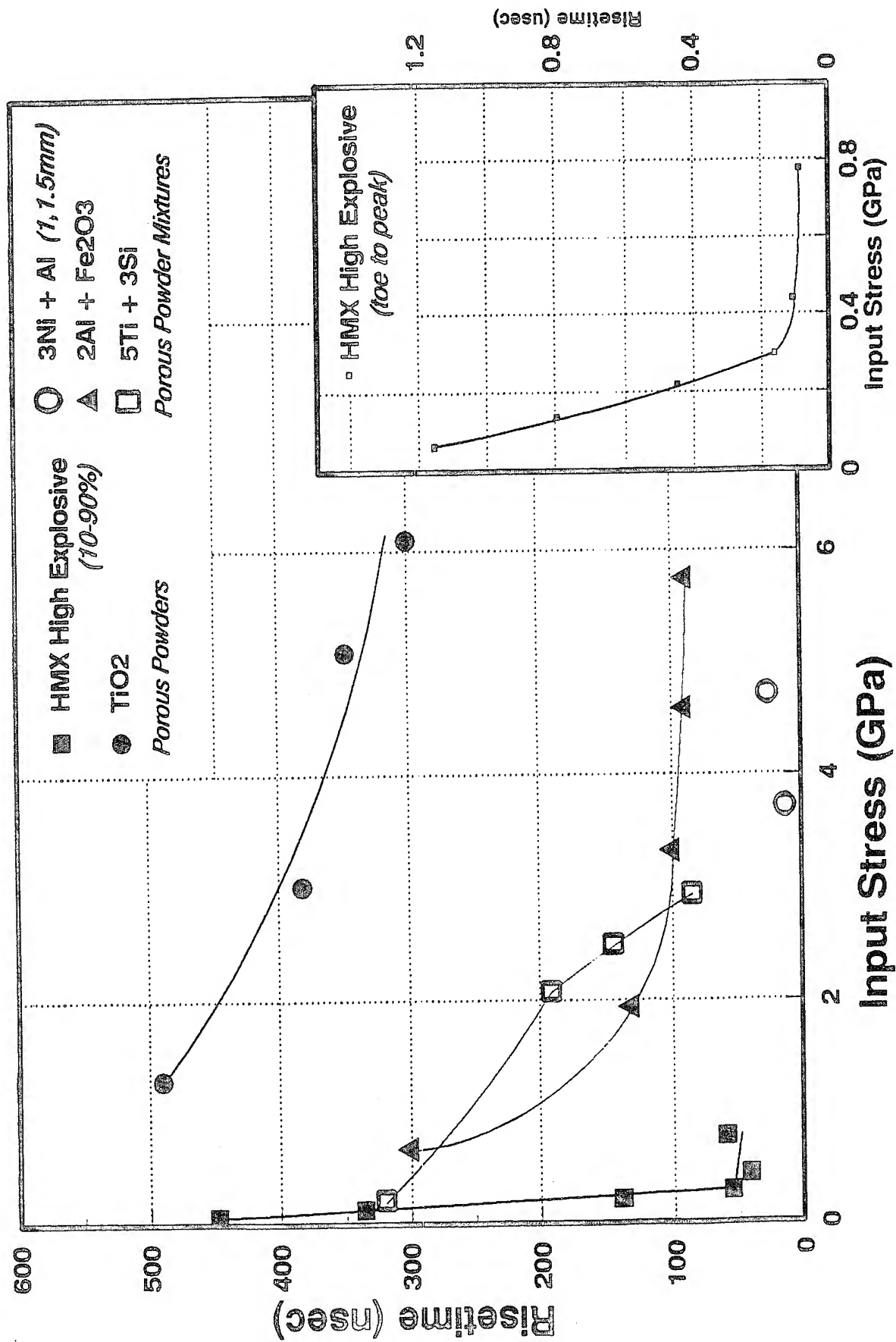
3Ni + Al @ 40% dense

5Ti + 3Si @ 53% dense

5Ti + 3Si Propagated Wave (4mm)

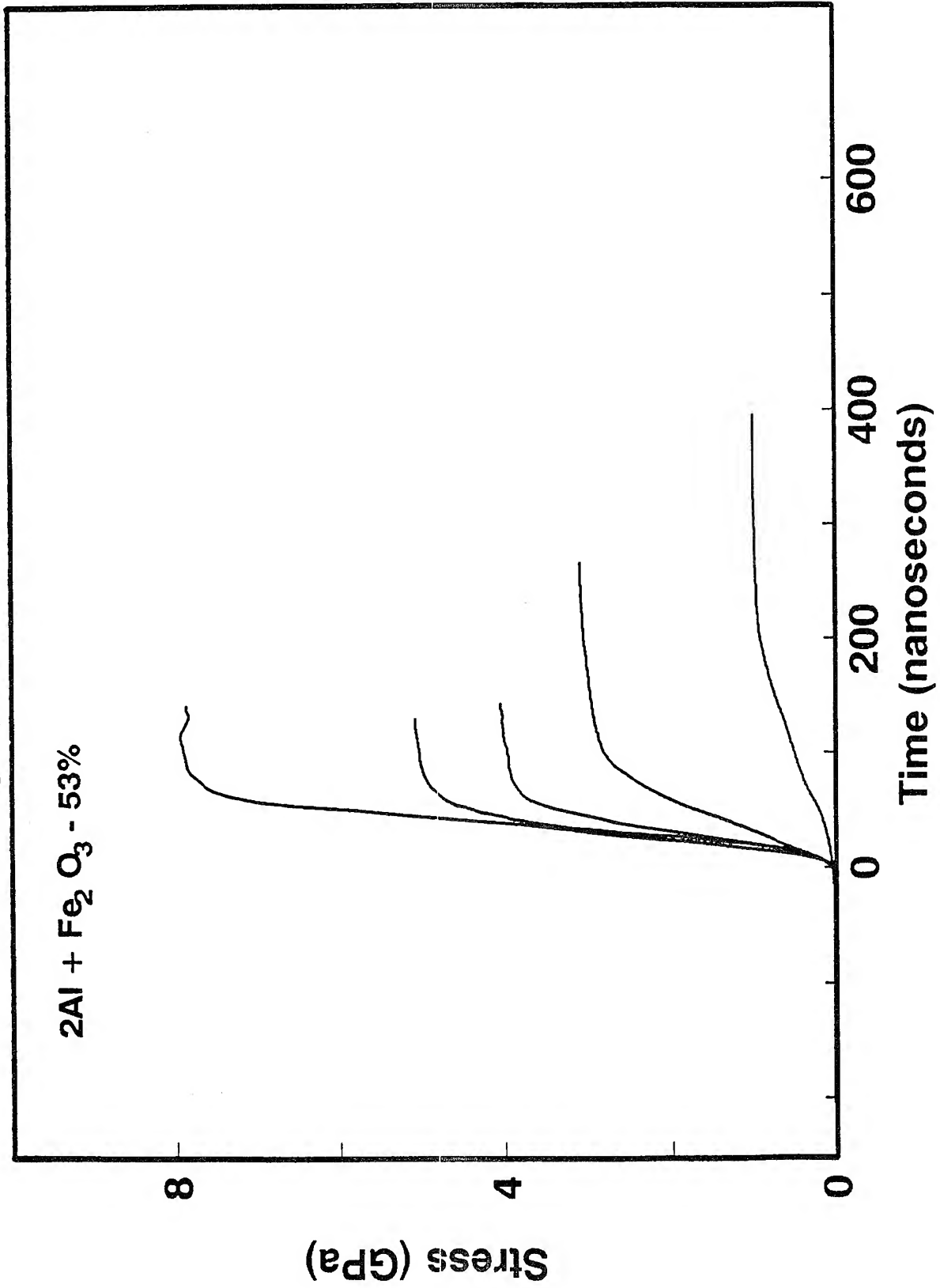


PROPAGATED WAVE (4mm) RISETIMES



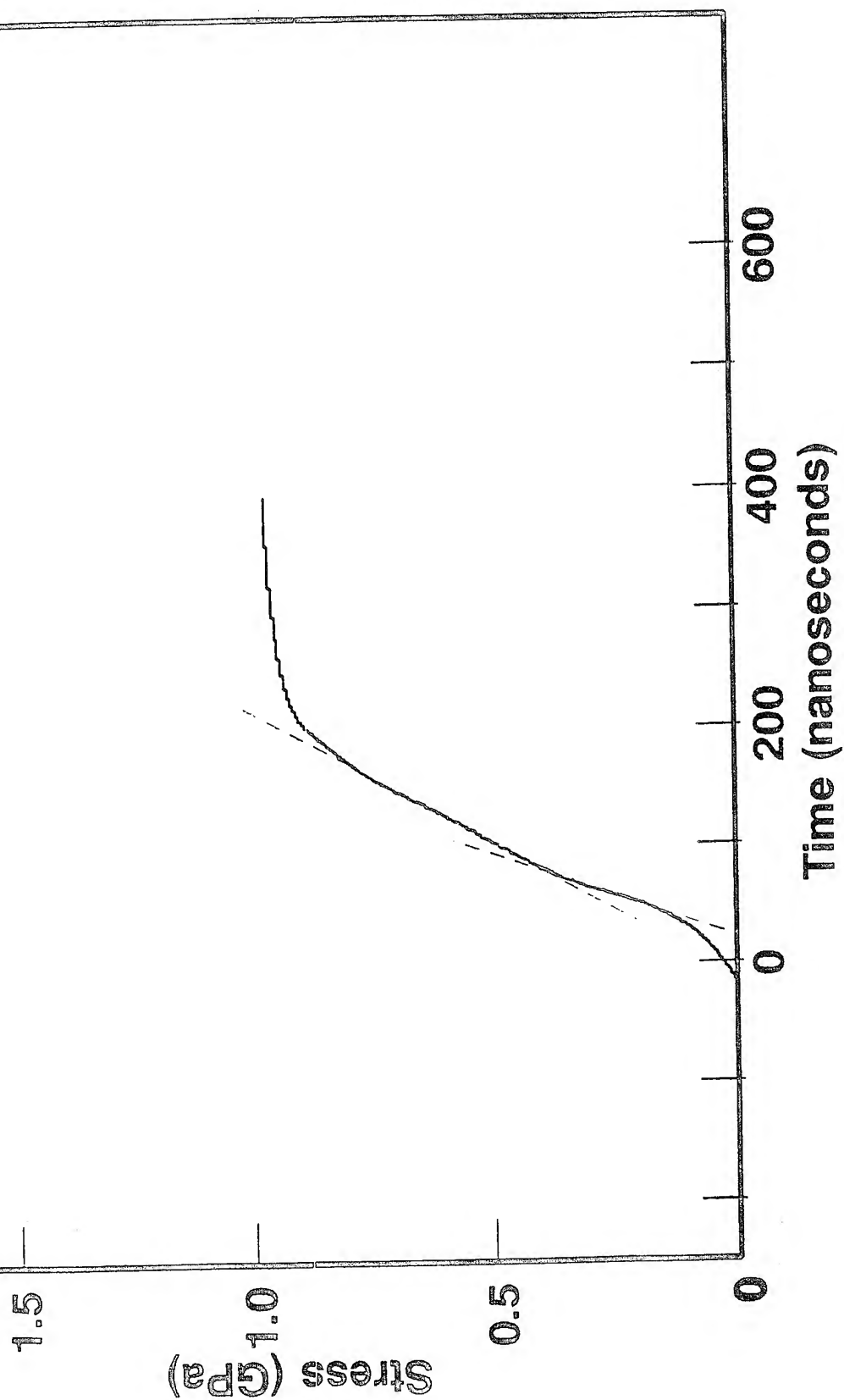
Propagated Wave (4mm)

2Al + Fe₂O₃ - 53%

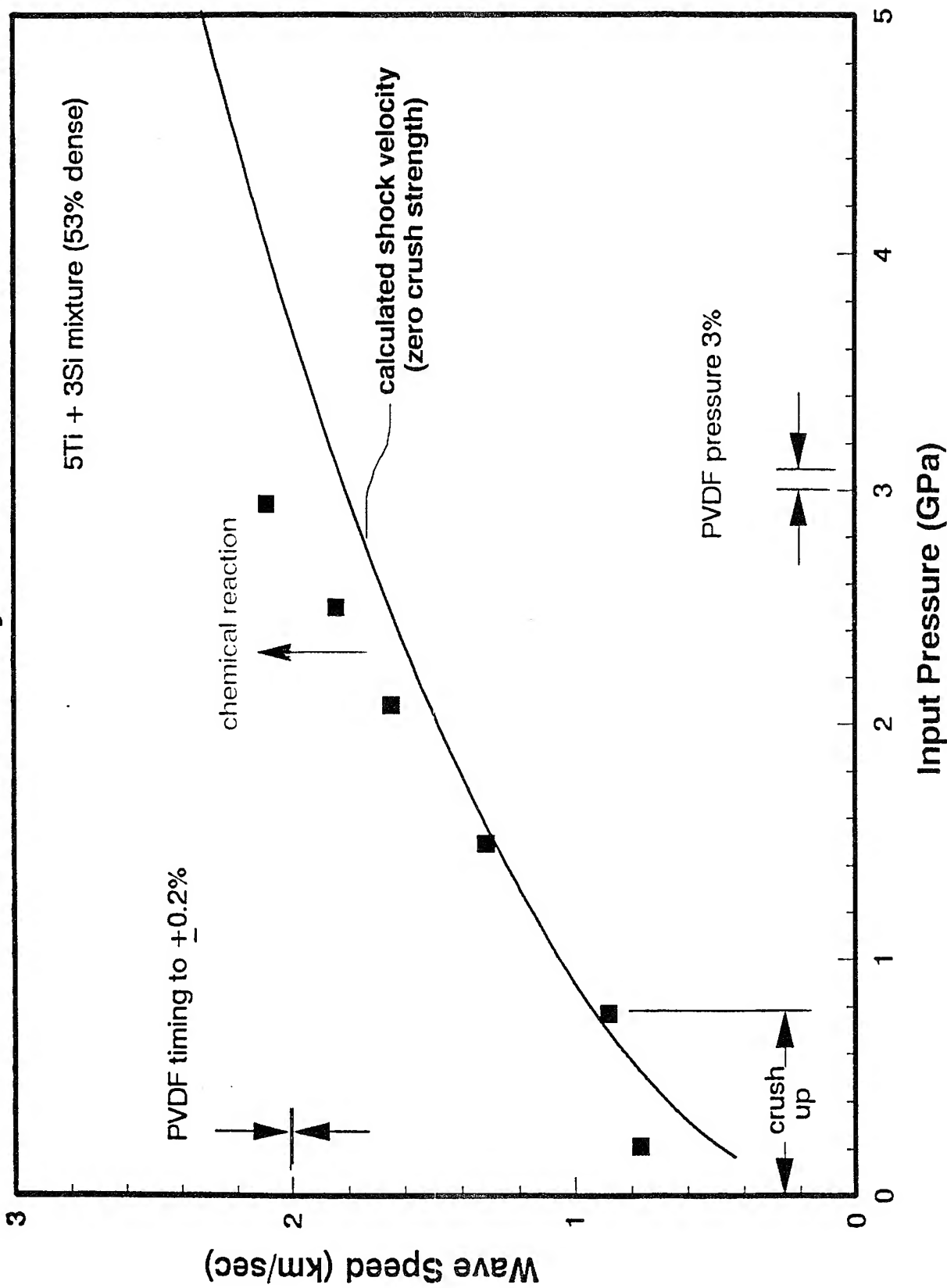


Propagated Wave (4mm)

2Al + Fe₂O₃ - 53%



Wave Velocity - Pressure



NANOSECOND TIME-RESOLVED PRESSURE MEASUREMENTS IN HIGHLY POROUS SOLIDS

---0.1 TO 10 GPa---

OBSERVED BEHAVIORS

GENERAL

OVERALL FEATURES FOLLOW EXPECTATIONS, BUT
ARE DOMINATED BY VISCOPLASTIC DEFORMATION

DOMINANT BEHAVIORS

TIME-DEPENDENT INPUT STRESSES

LONG RISE-TIME PROPAGATED WAVES

STRONG MORPHOLOGICAL EFFECTS

RATES (INPUT AND PROPAGATED)

CRUSH STRENGTHS

NANOSECOND TIME-RESOLVED PRESSURE MEASUREMENTS IN HIGHLY POROUS SOLIDS

----0.1 TO 10 GPa----

CONCLUSIONS

DEFORMATION OF HIGHLY POROUS
SOLIDS NOT DESCRIBED BY
HOMOGENEOUS, STEADY BEHAVIOR,
EQUILIBRIUM THERMODYNAMICS
(HUGONIOT)

"SHOCK-WAVE" ANALYSES ARE NOT
DESCRIPTIVE FOR DEFORMATION AND
THERMAL PREDICTION.

"SHOCK-WAVE" ANALYSES OF
RECOVERY CAPSULES ARE SUSPECT

CRUSH STRENGTH IS DENSITY AND
MORPHOLOGY DEPENDENT (NOT
MATERIALS STRENGTH ALONE)

STRONG EVIDENCE FOR CHEMICAL
ENERGY RELEASE IN Ti-Si SAMPLES

WHERE DO WE GO FROM HERE ??

THE PRESENT SITUATION IS ANALOGOUS TO EARLIER SITUATIONS WHEN TIME-RESOLVED MEASUREMENTS WERE FIRST TAKEN WITH SANDIA QUARTZ GAUGES AND WITH VISAR.

QUARTZ GAUGE REVEALED VISCOUS DEFORMATIONS ASSOCIATED WITH DYNAMIC YIELDING. NEW PHYSICAL AND NUMERICAL MODELS HAD TO BE DEVELOPED.

VISAR REVEALED STRONG VISCOELASTIC, VISCOPLASTIC DEFORMATIONS IN POLYMERS. NEW PHYSICAL AND NUMERICAL MODELS HAD TO BE DEVELOPED.

THE PRESENT WORK IS ONLY A BEGINNING..NEW PHYSICAL AND NUMERICAL MODELS INVOLVING REALISTIC DESCRIPTION OF VISCOPLASTIC, HETEROGENEOUS DERORMATIONS AT THE PARTICLE LEVEL ARE REQUIRED.

THE PRESENT STATUS OF KNOWLEDGE WITH DYNAMIC DEFORMATION IN HIGHLY POROUS SOLIDS IS ANALOGOUS TO THE HISTORICAL STATUS OF THE JONES, BENEDICK AND NEILSON PAPER ON DYNAMIC YIELDING PUBLISHED IN 1962.

MATERIALS MODIFICATION AND SYNTHESIS UNDER HIGH PRESSURE SHOCK COMPRESSION¹

*R. A. Graham, B. Morosin, E. L. Venturini, and
M. J. Carr*

Sandia National Laboratories, Albuquerque, New Mexico 87185

INTRODUCTION

There is currently a surge of interest in the use of high pressure shock compression to synthesize materials or to modify microstructure to achieve unique properties. This new thrust has developed from well-established knowledge of the physical and mechanical effects associated with shock compression, from new programs underway to study chemistry under shock compression, and from successful examples of industrial shock processing. Work in this area may prove technologically significant; but whether or not any significant material applications result, it is certain that the work will extend our knowledge of material responses and material properties into regimes not previously explored.

The high pressure, rapid material motion, intense plastic deformation (even in conventionally brittle materials), high temperature, and short duration of the shock event force matter through a unique process. To the extent that synthesis can occur in the microsecond duration of the high pressure pulse, chemical processing can be carried out in large volumes at extraordinarily high pressure. High pressure processing not only opens the door to new reactions but provides the opportunity to involve dense-phase polymorphs in reactions. Quenching of pressure and temperature from transient states permits formation of metastable states. High concen-

¹ The US Government has the right to retain a nonexclusive, royalty-free license in and to any copyright covering this paper.

trations of defects can promote metastability and can lead to small crystallite sizes, either through generation of large concentrations of nucleation sites or through primary recrystallization. Intense shock-induced plastic deformation of powder particles removes surface impurities such as oxides, activates them with defects, and mixes them with extraordinary efficiency.

Given the conditions of the process, there is little doubt that unusual materials can be produced. The question remains, however, as to whether such a complex, energetic, and intense process can be understood and controlled. Prior experience with the industrial processes of diamond synthesis, cubic boron nitride synthesis, explosive cladding, explosive metal working, and dynamic compaction of powders demonstrates that industrial scale processes are entirely feasible. However, the products must have a high value. Unique performance characteristics yield high value, and the thrust of much of current materials technology is to develop high value materials.

This report provides a perspective on the rapidly changing field of material synthesis with shock compression processes. As there are earlier summaries of findings on shock-induced structural changes, we emphasize chemical synthesis and modification of microstructural features of inorganic materials. We summarize the early work in the field and review certain contemporary work. Finally, a brief retrospective look at the field closes the report.

Several prior reviews are relevant to the content of this report. The review of Duvall & Graham (1) gives a comprehensive summary of research on structural phase transitions through about 1975. The recent review of Syono (2) on the same subject has brought that area up to date. The review of Davison & Graham (3) gives a comprehensive account of the overall area of shock compression of solids and summarizes the work on diamond and cubic boron nitride synthesis. There is no comprehensive review of chemical synthesis under shock compression, but the bibliography by Graham et al (4) contains over 400 references. The two reviews by Adadurov and Gol'danskii (5, 6) are revealing but contain a limited number of references. The most up-to-date reviews are those of Dodson & Graham (7) and Morosin & Graham (8). The early review of Dremine & Breusov (9) provides an incisive view of research on the shock process prior to 1970, and the nontechnical article by those same authors (10) on early chemical synthesis is also very revealing. The most recent account is that of Graham and coworkers on chemical synthesis (11).

THE EARLY WORK

Research on materials synthesis under high pressure shock compression stemmed from worldwide recognition in the period from 1956 to 1966 that

controlled shock compression of condensed matter presented an opportunity to subject matter to a hitherto unexplored process. This awareness was in part a result of the publication of a comprehensive review from Los Alamos in 1958 on use of shock compression to carry out scientific studies of solids under conditions of high stress and rapid deformation (12). Based on scientific principles quantified in the Los Alamos work, it became possible to define pressure and temperature and the behavior of solids under a variety of conditions. With this knowledge came the opportunity to control the synthesis of materials.

As shown in Table 1, Riabinin of the Soviet Union was the first to use modern shock-compression processes to affect chemical changes in condensed matter. This work and similar studies at the Lawrence Livermore Laboratory (15) were limited in scope. Although there is earlier work, the most crucial was that of DeCarli and his coworkers. In a dramatic experiment, they synthesized diamond from graphite. This early success was followed by later synthesis of the mineral maskelynite and a high pressure form of quartz, stishovite.

With DeCarli's success as an example, researchers in Japan and the Soviet Union proceeded to explore various aspects of shock-induced chemical synthesis. From work centered at the Japanese Defense Academy, Y. Kimura, Y. Horiguchi, and Y. Nomura demonstrated compound synthesis from elements, enhanced catalytic activity, and shock activation of carbon for carbide synthesis (see Table 1). Additional work was reported through 1969 but apparently was not pursued further (24).

At the Institute of Hydrodynamics at Novosibirsk, S. S. Batsanov started exploratory work in 1965 with A. A. Deribas and others, and he has continued this work to the present with over 70 publications in the area. His recent work is being carried out at the State Committee of

Table 1 Early shock synthesis studies

Author	Date	Synthesis	Remarks
Parsons (13)	1920	Graphite to diamond	Unsuccessful
Riabinin (14)	1956	Sublimation, dissociation	
Grover et al (15)	1958	Sublimation, dissociation	Abstract
DeCarli & Jamieson (16)	1961	Graphite to diamond	The key work
Milton & DeCarli (17)	1963	Maskelynite	Mineral synthesis
Kimura (18)	1963	TiC	From mixed powders
Adadurov et al (19)	1965	Polymerization	Acrylamide, trioxane
Batsanov et al (20)	1965	Potassium nitrate	
Horiguchi & Nomura (21)	1965	Catalytic activity	Carbon
Horiguchi & Nomura (22)	1965	Shock activation	WC
Bergmann & Barrington (23)	1966	Shock activation	Ceramics

Standards in Moscow. At the time of the Novosibirsk effort, a group at the Institute of Chemical Physics and the Institute of New Chemical Problems at Chernogolovka (near Moscow) started intensive research on chemical synthesis under shock compression. A. Dremin, G. A. Adadurov, O. N. Breusov, and others have carried out extensive investigations, which have continued to the present. More recently, G. A. Adadurov began work with V. Gol'danskii at the Institute of Chemical Physics in Moscow.

The early phase of materials synthesis was rounded out by the comprehensive study of Bergmann and coworkers, who reported the results of the use of shock compression of inorganic powders to activate them for subsequent, more conventional processing. The patent issued to this group in 1968 (25) is very comprehensive and may have inhibited others from further commercial exploratory work. This same group has a major industrial effort in the synthesis of diamond powder from graphite; this powder is currently used to polish components in numerous high technology products. This group is also responsible for much activity in industrial explosive metal bonding.

The early period of shock synthesis demonstrated its many potential uses. Numerous laboratories were able to demonstrate significant effects, some with the crudest of facilities. The range of material effects demonstrated included virtually all those of interest today. Why then were there so few impacts on materials technology? Why did interest wane only to be revived twenty years later? The situations were quite different in Japan, the US and the Soviet Union.

First, there were significant material applications even though they have not been widely recognized. The present successful diamond synthesis activity at DuPont stems directly from those early exploratory investigations. The explosive metal-cladding, metal-hardening, and metal-forming industries of today also originate from research of the early period. But the need for a high value product and for a concentration of significant resources apparently required focusing on specific materials problems with specific explosive loading capabilities. Shock-synthesized products are so different from those of other processes that it has required considerable time to identify commercial markets. Indeed, it has taken over ten years for a significant market to develop for shock-synthesized diamond in the US. Outside the Soviet Union, shock synthesis in the period 1965-1980 was directed at the most obvious and lucrative markets.

In the Soviet Union, chemical synthesis moved smoothly from early exploration to broader studies to industrial development, and research continues at a steady pace. The work is well integrated into the mainstream of shock-compression scientific activity. Apparently, shock-synthesized diamond and boron nitride have found significant markets within the

country, and patents have been issued worldwide. Nevertheless, these and other shock-synthesized materials have not been used extensively outside the USSR, and there has been no opportunity for outside materials scientists to study these materials. To what extent other significant materials developments have resulted is unknown; it is known that shock synthesis is used as a routine scientific tool for studies of phase stability and lattice parameters. Recent reports of synthesis of rare earth titanates, zirconates, and hafnates, for example, showed the results of what is estimated to be hundreds of experiments (26-28).

A measure of the broad nature of the Russian efforts is given in Table 2, which summarizes the range of different reactions studied and indicates the number of materials studied. The size of the overall program is quite remarkable.

In the US, the period beginning in about 1965 was marked by the development of the industrial synthesis facilities mentioned above and summarized by Davison & Graham (3). The principal industrial activity involved various aspects of processing metals with explosives, and a very considerable literature on metals developed (3). Except for work involving geophysical problems (29), research involving chemical changes was almost nonexistent until about 1980. Scientific research in shock-compression processes was and continues to be very active, but the area has been considered one of physics with a strong component of solid mechanics.

The lack of research interest in the US no doubt resulted from skepticism concerning many early results. Because of poorly defined shock conditions, it was not possible to determine if the products were the result of solid-solid, solid-liquid, liquid or even plasma or gas phase states. Issues of contamination could not be addressed. There was little basis on which to

Table 2 Shock-induced chemical changes*

Process	Typical reaction	Number of observations
Decomposition	$\text{NiO} \rightarrow \text{Ni} + \text{O}$	85
Oxidation reduction	$\text{Cr} + \text{Cr}_2\text{O}_3 \rightarrow \text{Cr}_2\text{O}_4$	16
Solid solution	$\text{Al}_2\text{O}_3 + \text{SiC} \rightarrow \text{Al}_2\text{O}_3$ structure	18
Reactions		
elements	$\text{Ti} + \text{C} \rightarrow \text{TiC}$	14
superconductors	$\text{Sn} + 3\text{Nb} \rightarrow \text{Nb}_3\text{Sn}$	10
oxides	$\text{Al}_2\text{O}_3 + \text{SiO}_2 \rightarrow \text{Al}_2\text{SiO}_5$	11
rare earths	$\text{RE}_2\text{O}_3 + \text{ZrO}_2 \rightarrow \text{various}$	12

* See references in Morosin & Graham (8).

determine whether observed chemical changes occurred during loading, release of pressure, or after the shock event. Too little was known of physical and mechanical processes in the mid 1960s to provide quantitative characterization of the shock conditions, and the strong commitment to develop high value materials technology consumed the available resources.

SHOCK-ENHANCED REACTIVITY

Background

The present vitality of research in materials synthesis under shock compression stems from a number of different sources. The Japanese began to develop a materials synthesis program in about 1975. Their interest led to the development of modern shock compression facilities at the Tokyo Institute of Technology and at Tohoku University, under the leadership of A. Sawaoka and Y. Syono, respectively. Research is currently very active in Japan, and significant materials developments are underway to supplement their existing program in industrial processing of cubic boron nitride. Shock processing is one of the approaches being investigated in their national "fine ceramics" program.

In the US, beginning in about 1979, a number of different factors focused attention on this area. These included a proposal to describe electrically generated signals in shock-loaded polymers in terms of a mechanically induced bond scission model (30). A follow-up study of the literature on stress-induced effects in polymers led to in depth study of the Soviet shock-induced chemistry literature and recognition of its substantial progress. That literature raised questions concerning the chemical nature of the shock process. The lack of chemical studies in the US, in spite of a considerable research effort in shock-compression science, was clearly a major oversight.

Recognition of this oversight led to the formation of the National Materials Advisory Board Committee on Shock Compression Chemistry in Materials Processing and Synthesis (31). The Committee's report, several workshops and special interest sessions at American Physical Society Topical Conferences on Shock Compression of Condensed Matter have increased awareness of chemical issues within the shock-compression community (32-34).

Coincident with the interest in the shock-compression science community, interest was developing in the materials science community in new processing methods for consolidation of rapidly solidified powders. One technique investigated for such solidification was dynamic compaction with explosives, which has been used successfully in common metals (35). This materials interest came at a time when the fast-reaction chemistry

community was interested in the use of fast spectroscopic probes to study energetic materials. Interest in energetic materials also led to the study of possible decomposition products under conventional shock-compression conditions (36). In 1981 the potential of the shock process for synthesis of unusual materials was dramatically demonstrated by Olinger & Newkirk of Los Alamos, who synthesized the A15 structure of the superconductor Nb_3Si (37, 38).

Solid-State Reactivity

Sample recovery fixtures must provide quantitative and reproducible conditions, and they must allow variation of the shock conditions over a wide range. Such fixtures have been designed (39–41), and they provide the basis for most of the work to be described in the present article.

Elementary principles of chemical processes in solids (42–44) show the first-order importance of defects in controlling reactivity. Deformation of solids under shock loading proceeds with extensive plastic deformation and formation of large concentrations of defects. Thus it is immediately important to relate shock-enhanced solid-state reactivity to defect structures and to provide quantitative descriptions of solid-state reactivity of shock-modified materials.

HYDRATION OF NEODYMIUM OXIDE Adadurov and coworkers (45) carried out shock-modification experiments on 99.97%-pure neodymium oxide and measured the hydration of unmodified and shock-modified powders. Hydration was measured by the increase in weight of 500 mg samples kept in a desiccator over water at temperatures between 22 and 23.5°C. Specimen compacts prepared by calcining at 1200°C with subsequent comminution showed an incubation period of about 60 hr, while a similar sample cooled in a desiccator over phosphorus pentoxide showed an incubation period for detectable hydration of about 20 hr. A similar shock-modified sample showed no incubation period and a rapid increase in weight; it reached a water content of 3 mol in about 100 hr. The shock-modified and starting powders were determined to have about the same powder-specific surface area. Although many details are not fully documented, it is clear that relatively unsophisticated experiments indicate that shock-modified neodymium oxide shows an extraordinary increase in reactivity, leading to greatly enhanced hydration rates.

REACTIVITY OF ZIRCONIA An increase in the solid-state reactivity of shock-modified zirconia in reaction with lead oxide has been reported by Hankey and coworkers (46) as part of a larger study on the influence of the reactivity of zirconia powders on the properties of lead zirconate (47). A zirconia powder of modest specific surface (8.5 m²/g) was subjected to

shock loading that is now known to produce peak shock pressures of 20 and 27 GPa and was preserved for study and reaction with lead oxide to form lead zirconate.

The powders were reacted with lead oxide and the reaction was followed with differential thermal analysis (DTA) measurements. The reaction temperature of the shock-modified zirconia was lowered significantly, and the change in reaction temperature was strongly dependent on the shock pressure. The DTA signature also suggests enhanced reaction rates. When compared with the reaction of another zirconia powder with a specific surface twice as large as the other powders, the shock-modified powders show a reaction characteristic of the higher specific surface powder even though the specific surface was not modified by the shock.

Further detailed studies were carried out to determine the source of the enhanced reactivity of the zirconia. X-ray diffraction was used to determine the extent of residual strain and reduction in crystallite size as revealed by line-broadening measurements (48). These same measurements determined structural changes. It was found that the residual strain and crystallite size reduction "washed out" high-angle diffraction lines. Crystallite sizes of about 30 nm and strains of about 3×10^{-3} were indicated. In addition, the starting monoclinic phase was partially converted to the tetragonal phase. A conversion of about 10% was seen at 20 GPa, and a conversion of about 20% was seen at 27 GPa. Transmission electron microscopy (TEM) revealed that the shock-modified powders were so heavily decorated with dislocations that individual details could not be resolved (49). The lower pressure sample showed localized particle size reduction, while the higher pressure sample showed strain-free tetragonal phase particles that had been recrystallized to a small grain size (30 nm). Whereas the heavily strained monoclinic particles showed recrystallization under the heating of the electron beam, the tetragonal particles were resistant to further recrystallization.

Differential thermal analysis measurements carried out while the shock-modified and starting powder were taken through the temperature-induced monoclinic-to-tetragonal transition at 1200 °C showed a significant reduction in transformation temperature for samples shock-modified above pressures of 16 GPa (50). This pressure corresponds to that at which the tetragonal phase is retained and the crystallite size is refined. The various properties of the shock-modified powders indicate that the most likely sources of the enhanced reactivity of zirconia with lead oxide are shock-induced crystallite size reduction and formation of tetragonal-phase particles and nuclei.

DISSOLUTION OF SILICON NITRIDE Silicon nitride is one of the most promising ceramic materials for high-temperature applications such as ceramic

engines or turbines. Its high-temperature strength is excellent, but powders are difficult to sinter to high density. The addition of a sintering aid such as magnesium oxide allows sintering to a high density, but the resulting oxides exhibit reduced strength at high temperature. It is generally believed that sintering occurs by mass transport through a grain boundary phase. Oxide additives combine with silicon dioxide present as a surface oxide layer to form a grain boundary phase that is liquid at the processing temperature. A solution-precipitation process that leads to densification is always associated with a crystallographic change from either the amorphous or the crystalline α -phase to the β -phase.

High-temperature chemical conversion studies on shock-modified silicon nitride show large changes in the dissolution-precipitation process required to affect the change to the β -form. Beauchamp and coworkers (51) have reported shock-modification and elevated-temperature conversion experiments on a commercial silicon nitride powder (GTE Sylvania SN502). This powder is of mixed phase with a nominal composition of 57% α -phase, 3% β -phase, and the balance amorphous. Conversion from α - to β -phase was determined after high-temperature treatment for powders shock-modified at peak shock pressures, now known to be 20 and 27 GPa. The powders were found not to be activated sufficiently to undergo the crystallographic transformation in the absence of liquid-phase transport. When the powders were mixed with 5% magnesium oxide and held at 1500–1700°C for periods up to 2 hr, a major change in the α -to- β conversion was observed compared to control specimens. At 1500°C, 10% conversion was observed after 2 hr in the shock-modified powders, while none was observed in the control specimens. At higher temperatures the effect of shock modification was even more dramatic. After 2 hr at 1700°C the most strongly shocked sample showed a conversion of 95%, while the starting powder showed a conversion of 55%. For the less strongly shocked powder, there was a large effect on conversion but it was less dramatic. The results indicate that the shock-modified powder showed a major increase in dissolution rate in the high-temperature oxides. The extent of the effect was found to be directly controlled by the shock conditions.

Defect and microstructural studies of the shock-modified powders were carried out to seek to identify the source of the enhanced dissolution rate. X-ray diffraction line broadening showed that shock treatment produced residual strains of about 10^{-3} and reductions of crystallite size from 200 nm to 120–160 nm. Electron spin resonance studies of shock-modified silicon nitride are described later in this review. It was determined that the shock process resulted in only a modest increase in specific surface area (52). This result was rather surprising as the particle morphology was drastically changed. Scanning electron microscopy (SEM) showed the starting powders to be in the shape of a small bundle of needle-like crystals

connected to a rounded, irregularly shaped base. After shock modification, no trace of the needle-like structures was observed. The change in particle morphology was also apparent in the powder flow characteristics; the starting material was excessively "fluffy," apparently due to the needle-like structure, while the shock-modified powder was free-flowing and achieved a much greater tap density than the starting material. This characteristic, in itself, makes the material much easier to process. The various characterizations reported above, combined with neutron activation analysis to identify oxide content before and after shock loading, show that the increased dissolution rate is a result of shock-induced defects.

CATALYTIC ACTIVITY OF RUTILE Early work on shock modification of inorganic powders showed that the catalytic activity of carbon black could be greatly enhanced (21). Batsanov, Boreskov and coworkers in the Soviet Union (53, 54) followed the first demonstration of the effect with a study of a number of semiconductor oxides in an attempt to identify the source of the increased catalytic activity. Their conclusion was that the enhanced activity was due to the introduction of point defects. A recent study (55) confirms the greatly enhanced catalytic activity of shock-modified rutile, but shows it is not associated with point defects. Recent work by Batsanov and coworkers has shown that specificity of reaction can be controlled by shock modification (56) and that the modification of catalytic support materials (57) can also strongly influence the reactions.

Williams and coworkers (55, 58) have carried out an extensive study of enhanced catalytic activity of shock-modified rutile powder. Shock-modification experiments have been carried out on high-purity rutile powders at peak pressures from 4.5 to 27 GPa. By varying the starting density of the sample powder compacts, a range of temperatures can be achieved independent of the shock-induced increase in pressure.

Catalytic activity of rutile was studied for the oxidation of carbon monoxide in a flow reactor (58). Depending on the shock modification conditions, the catalytic activity was observed to increase by up to five orders of magnitude. After removing an initial large transient change in reactivity by an initial thermal pretreatment, the catalytic activity remained constant for many hours. SEM and specific surface area determinations showed there were only modest changes in particle morphologies.

X-ray diffraction studies were particularly detailed (59, 60). No structural changes were observed as a result of the loading. Unlike in most other inorganics studied, the residual strain was somewhat reduced at the highest pressure, which indicates that annealing behavior accompanies higher shock-induced increases in temperature. Consistent with this behavior, lower density starting powder compacts with their larger increases in

shock-induced temperatures showed less residual strain than at somewhat lower pressures. Because of the tetragonal symmetry of the material, residual strain was significantly anisotropic. In the most extreme case, the strain might differ by 50% in various crystallographic directions. Differences in apparent crystallite size with crystallographic direction were also observed. Annealing studies showed reduction in residual strain at temperatures as low as 325°C, but detectable residual strain was not removed upon annealing until a temperature of 1100°C. The X-ray diffraction study showed that defect configurations responsible for the residual strain were present at 450°C, the temperature used to determine catalytic activity. However, paramagnetic defects in the shock-modified powders were substantially reduced in concentration at the temperatures at which catalytic activity was measured.

Electron spin resonance studies at liquid helium temperature were particularly revealing as to unique features of defects in shock-modified powders and their relation to enhanced catalytic activity (55, 61, 62). The starting powder showed no paramagnetic resonances and was white. After shock compression the color changed to a dark grey whose darkness depended directly upon the shock conditions both in various experiments and within the shock recovery sample fixture for a given experiment. (Upon annealing in air at 500–600°C, the powders return to their original white color.) Two paramagnetic resonances were produced by the shock process: an isotropic resonance with a g factor of 2.0029 (3) and an anisotropic defect with g factors of 1.969 (5) and 1.937 (3) for the 20 GPa shock modifications. From prior work these defects can be identified as free electrons trapped at vacancies and as the reduction of the valence of interstitial titanium to three, respectively. Concentrations were large: $3 \times 10^{16} \text{ cm}^{-3}$ and $3 \times 10^{15} \text{ cm}^{-3}$, respectively. At the higher shock pressure the axial defect is present in the same concentration as at lower pressure, but a strong dispersion is observed in the line shape, which indicates a relatively low microwave frequency resistivity of about $1 \times 10^{-4} \text{ ohm-cm}$.

The large concentrations of defects and low resistivity are clear indications of the unique nature of shock-induced defects in this material. Defects in rutile produced by chemical means or by elevated-temperature vacuum treatment have been studied extensively. Titanium interstitial concentrations greater than 10^{15} cm^{-3} have never been reported, nor have resistivities this low been observed. The rapid mechanical formation of these defects leads to configurations in which the individual defects are stable at much higher concentrations than in prior processes in which the defects are formed more slowly. The combination of high point defect concentrations and saturation density concentrations of dislocations is

also unique to the shock configuration. Similar effects are noted on a shock-modified single crystal.

Annealing studies on the shock-modified samples showed that the concentrations of both paramagnetic defects were reduced by two orders of magnitude at a temperature of 475°C. Because the point defects are readily annealed at temperatures at which catalytic activity is persistent, they are not the source of the enhanced catalytic activity.

Transmission electron microscopy studies of shock-induced microstructural features were also carried out (62, 63). Samples were shock modified at seven peak pressures from 5 to 22 GPa. Shock-induced microstructural features were so concentrated that it was possible to resolve individual details only at the lowest pressures. At pressures greater than 8 GPa, concentrations were so great that defect images overlapped and details could not be resolved. Deformation processes produced different residual microstructural features in different grains. Cleavage, twins, and high concentrations of dislocations were observed. Slip on {100} planes was not apparent in conventional deformation but was observed on these shock-modified powders. For samples subjected to higher pressure and temperature, defect-free recrystallized grains were observed. Clearly these defect-free grains were formed from shock-deformed grains that were subsequently recrystallized as no such features were observed at lower shock pressures.

Although there is some similarity between shock-deformed rutile and conventionally deformed rutile, the shocked powders show much higher deformation. The deformation features are uniformly distributed within the grains. Particular slip features are observed that have not been seen in conventionally deformed rutile. Microstructural features caused by the deformation are quite different within different grains. Crystallographic shear defects, features characteristic of conventional deformation and chemical treatment, are absent in the shock-deformed powders. The observed recrystallization process is particularly interesting as it results from so brief an exposure to elevated temperature. The recrystallization process is apparently enhanced by the high degree of stored energy.

The studies above are sufficient to rule out interstitial titanium defects and vacancies as the source of enhanced catalytic activity for shock-modified rutile, but it is not possible to identify the particular microstructural defects responsible for the effect. Detailed surface chemical studies in conjunction with microstructural studies would be required for a detailed description. Unfortunately, little is known about surface chemical processes in such heavily defective materials. A first set of surface desorption measurements has been carried out on a shock-modified rutile

(64). Williams and coworkers have recently extended their catalysis work to methanation with a shock-modified zinc oxide (65).

SHOCK-INDUCED MODIFICATION OF INORGANIC POWDERS

From the information presented above, the need for detailed studies of defect states of shock-modified materials is apparent, particularly in the area of shock-induced changes in chemical properties of solids and shock-induced chemical synthesis. There is a significant literature characterizing shock-modified metals (3), but there is little detailed literature on inorganic refractory materials, which are the focus of much of the contemporary chemical synthesis work. There are also little data on the characteristics of shock-modified powders compared with those of the same powders in the fully dense state. Our group has attempted to characterize the effects of shock-compression processes on inorganic powders. It is the objective of the program to develop a data base describing shock-modified powders to serve as a basis for modeling shock-induced chemical effects. The results of this effort are too extensive to be reported in the present work, and many of the measurements have been summarized elsewhere; hence, this section summarizes overall features of the observations and provides a set of references for further study. All the shock-modification work summarized here was carried out in powder compacts whose initial densities ranged from about 35 to 75% of solid density.

Specific Surface Area

It has been suggested that the observed enhanced reactivity of shock-modified powders is merely the result of comminution of the starting powders to a high specific surface state. Without detailed knowledge of the shock-compression process of powders, such a mechanism is entirely credible. Williams and coworkers have carried out detailed specific surface evaluations with the BET method on many shock-modified inorganic powders, including silicon nitride, rutile, titanium diboride, titanium carbide, alumina, zinc oxide, hematite, magnetite, manganese dioxide, and aluminum nitride (52, 66, 67).

Although each material has its own characteristic response, the overall result is that shock-induced changes in specific surface area are modest. The changes are typically a factor of two or less and may be due more to particle morphology changes than to comminution. In alumina, for example, at low pressure a modest increase in specific surface is observed with increasing pressure. At a pressure of about 16 GPa the trend reverses

and higher pressures reduce the specific surface from the maximum observed at lower pressure. This behavior is characteristic of a modest comminution process or morphological changes at low pressure followed by particle bonding at higher pressure. A soft material, such as zinc oxide, shows a continuous decrease in specific surface area with increasing shock pressure, in a manner characteristic of interparticle bonding.

The powders used in the specific surface measurements are typically given thermal pretreatments. One of the interesting results of the pretreatment is that the surfaces of the shock-modified powders are more chemically active than starting powders and they tend to collect impurities from exposure to ambient air.

X-Ray Diffraction Line Broadening

X-ray diffraction line broadening is a well-established tool for the study of residual strain and change in coherent domain (crystallite) size. Nevertheless, highly deformed refractories with refinement in grain size are rarely encountered, and the problems in interpreting line broadening in these materials are significant. Morosin and coworkers (59, 68-71) have carried out extensive, detailed studies that describe the unusual states of plastic deformation in these materials. A recent summary provides considerable detail on a range of materials (71) and detailed descriptions of analytical techniques (59). This work stands out as the most extensive study ever carried out on shock-modified materials, either metallic or inorganic, and the data on inorganics is unique.

Special problems are presented in the study of shock-modified materials with X-ray diffraction. Essentially all aspects of the diffraction process can be altered by the shock process; structure, strain, and crystallite size can all change, and the changes can be substantial. Thus, analysis of diffraction patterns is more complex than in situations in which only one feature is altered. Severe line broadening, a common finding, makes precise determination of d spacings difficult and limits the determination of quantities of multiphase systems. With severe line broadening due to both strain and crystallite size, it is difficult to simultaneously quantify both effects. In less severe cases such difficulties are compounded by anisotropy in both residual strain and crystallite size. Even though such anisotropy is frequently ignored, its characterization provides important data on deformation. As the degree of interaction is strongly influenced by the intensity of the shock process, meaningful study requires a series of experiments over a wide range of known shock conditions.

X-ray diffraction studies have been carried out on rutile (59), anatase (72), alumina (59), titanium carbide (73), titanium diboride (69), aluminum

nitride (69), and hematite (71). The work on rutile, alumina, titanium carbide, and hematite is particularly detailed. The particulars of their behavior are quite different, but their overall features are clear. Even at the lowest pressure of 4 GPa, which is modest for shock compression, there is detectable residual strain in all materials with the exception of titanium diboride and titanium carbide. In most cases it is thought that the critical stress level to achieve mechanical yielding under the one-dimensional strain condition of shock loading of solid density samples is greater than the threshold for observation of residual strain. Low pressure mechanical yielding is direct evidence that the states of stress and the stress history conditions achieved in low density powder compacts are considerably more conducive to plastic deformation than those achieved in solid density samples. With this observation, it is particularly significant to observe that titanium diboride has a threshold pressure for detectable residual strain of about 15 GPa.

A second feature determined from line broadening is that plastic strain is readily introduced in these refractories, which are considered to be brittle and only rarely can be made to deform plastically. This observation suggests that deformation processes in ceramics could be used routinely to refine the microstructure of metals. For example, plastic deformation may be useful in hot pressing of aluminum nitride, in which the shock-modified powders not only show significantly enhanced pressing rates but also show a unique microstructure due to dynamic recrystallization (74). Small grain size materials thought to undergo shock-induced primary recrystallization include highly deformed zirconia, rutile, and shock-synthesized zinc ferrite, which show the potential for microstructural modification with shock deformation.

With the exceptions of titanium diboride and titanium carbide, a characteristic feature of shock-induced residual strain is that a "saturation level" is achieved that varies significantly for different materials. Titanium carbide appears to approach saturation at a peak shock pressure of 27 GPa, but higher pressure data are not available to confirm the observation. At 27 GPa titanium diboride shows significant residual strain but appears to be far from saturation.

The influence of the shock-induced increase in mean bulk temperature (which is controlled by the density of the powder compact prior to shock treatment) differs significantly from material to material. In titanium carbide higher temperature (lower compact density) causes larger residual strain. In rutile at 20 GPa the same influence is observed, while higher pressure and temperature result in lower residual strain as the material is annealed in either the shock state or in the immediate-post-shock state in

the recovery fixtures. As mentioned above, such plastic strain is retained at high temperatures, as shown in studies on rutile that was subsequently annealed to 1100°C and on silicon nitride annealed to 1500°C.

Anisotropy in residual strain in different crystallographic directions is pronounced and differs considerably among different materials. Such behavior can be very important in controlling microstructural processes. In titanium carbide the degree of anisotropy is significantly different than that observed due to heavy ball milling (73).

The extent to which coherent domain size is reduced in shock-modified inorganics is strongly dependent on the material. The tendency is for increasing shock pressure up to 27 GPa to reduce size (71). Such an observation indicates the size is controlled by the deformation process rather than by relatively slow cooling in the post-shock state.

X-ray diffraction has proven to be a particularly important tool in characterizing shock modification of inorganic powders. The picture emerging from this work is one of extensive plastic deformation of normally brittle refractory materials.

Electron Spin Resonance

Prior study of shock-induced defects in metals has shown evidence for extraordinarily high concentrations of point defects, especially vacancies (3). The high concentrations are thought to be the result of the high-speed motion of dislocations. Because refractory inorganic materials are insulating, they provide an opportunity to study paramagnetic defects in a more direct and detailed manner than in metals. There has been little work on paramagnetic defects induced by plastic deformation in these brittle materials; thus the results are especially revealing, but there is little supporting independent work from which to build a more detailed interpretation based on modern solid-state physics. (The detailed work on rutile reported earlier in this article is not limited in that regard.) Investigations summarized in this section are largely unpublished; the materials studied include shock-modified silicon nitride, titanium carbide, titanium diboride, and aluminum nitride. The experiments were all conducted at liquid helium temperature and at a frequency of 9.8 GHz.

The silicon nitride studied was GTE SN502 powder, described earlier in this report. Two paramagnetic defects are observed, both with isotropic g factors. A resonance with a narrow line width and a g factor equal to 2.0028 (3) is not present in the starting powder. A resonance with a broader line width and a g factor of 2.0038 (5) is present in the starting material. Its concentration increases by a factor of 50 at 20 GPa and a factor of 100

at 27 GPa. This defect is thought to be due to a silicon dangling bond. The concentration of the latter defect is about $1 \times 10^{18} \text{ cm}^{-3}$ at the higher pressure.

Although the increase in concentration of the broad line width defect from the starting material was only by a factor of 100 and the concentration is an order of magnitude lower than that of the interstitial trivalent titanium in shock-modified rutile, it has a number of interesting features. Whereas the defect concentration in rutile is reduced to background at 775 K, a significant reduction in concentration is not observed in silicon nitride until temperatures greater than 1200 K are achieved. At still higher temperatures the character of the resonance signature changes, indicating the formation of a new chemical defect in significant concentrations. Because of the thermal stability of the paramagnetic defects in this material, high-temperature processing can be carried out in their presence. Their thermal stability is also reflected in the shock-modification process in which it is observed that higher pressures and temperatures yield higher concentrations. More strongly modified powders can apparently be obtained at pressures higher than those used in the present work.

The titanium carbide powder was obtained commercially, and chemical analysis indicated that it was 98.8% titanium carbide and 1.16% titanium dioxide. Mean particle size was $3.9 \mu\text{m}$, and scanning electron microscopy showed the agglomerate nature of the particles. To avoid further contamination with oxygen, this powder (and those discussed later) was handled in argon throughout the shock sample preparation and explosive capsule-opening process. The starting powder had a narrow line width (9 Oe), isotropic resonance with a g factor of 2.0022, and its concentration was about $3 \times 10^{15} \text{ cm}^{-3}$. The free-electron-like g factor suggests the defect is an electron trapped at a vacancy. The effect of shock loading depended on the specific shock conditions of pressure and temperature, but ranged from little, if any, increase in defect concentration to about one order of magnitude increase at the most extreme peak shock pressure of 27 GPa. No new resonances were introduced by the shock loading.

When spin concentration is investigated as a function of the peak shock pressure and the density of the starting sample, the concentration is not increased by shock compression up to a peak pressure of 20 GPa. Up to a peak pressure of 27 GPa and a compact density of 45% there is also no increase in concentration. For the higher density compact, for which the shock-induced mean bulk temperature is lower, there is up to an order of magnitude increase in spin concentration at the maximum peak pressure. This behavior is consistent with the annealing behavior of point defects in titanium carbide at higher temperatures.

The titanium diboride powder we investigated was of a commercial grade, and chemical analysis indicated it was composed of 99.3% titanium diboride and 0.66% titania. The mean particle size was $14.6\text{ }\mu\text{m}$, and SEM showed the powder to be composed of equiaxed particles that were relatively agglomerate free. The spectra of the starting powder had two distinct resonances, a small isotropic absorption and larger absorption with a characteristic axial symmetry. The two resonances correspond to a free-electron-like isotropic absorption centered near 2.0029 and a larger absorption with anisotropic symmetry and lower g factors corresponding to the trivalent titanium ion interstitial, previously studied in detail in rutile. Thus these resonances arise from the rutile impurity. After shock modification the two resonances remain and a third broader resonance is produced whose source has not been identified. The shock-induced broad resonance has a concentration of about $3 \times 10^{18}\text{ cm}^{-3}$ and does not change significantly between 17 and 27 GPa. Lower density samples (which have higher shock-induced increases in temperature) were found to have a slightly lower defect concentration, independent of pressure.

The aluminum nitride studied was a commercial powder of 93.4% aluminum nitride and 6.6% aluminum oxide. Mean particle size was $37.6\text{ }\mu\text{m}$, and the powders were polymodal with a fine fraction around $10\text{ }\mu\text{m}$ and a coarse fraction exceeding $40\text{ }\mu\text{m}$. The starting powder was found to have a weak resonance at a g factor of 2.0052. Upon shock loading the concentration of this defect increased from 2×10^{16} to $3 \times 10^{18}\text{ cm}^{-3}$. The line width remained about 50 Oe. Studies of the pressure dependence of the defect concentration show that the highest concentrations are observed at the lowest pressures. The effect of increased shock temperature is also to lower the concentration. This behavior indicates annealing due to high temperatures.

Although the point defects observed in these impure powders have not been interpreted in terms of detailed models, their characteristics, taken in conjunction with the more detailed work on rutile, show that the shock process results in the formation of significant concentrations of such defects and that their concentrations are quite sensitive to the shock conditions. Their sensitivity to temperature, except in the case of silicon nitride defects, provides an indication of shock-induced increases in temperature.

Transmission Electron Microscopy

Microstructural studies with TEM on rutile and zirconia were described above. Limited studies have also been carried out on aluminum nitride (74), aluminum oxide (75), titanium carbide (76), and titanium diboride (76). The commercial-grade aluminum nitride starting powder (Starck Type

E) was found to contain low concentrations of dislocations ($< 10^6 \text{ cm}^{-2}$), while samples subjected to 16 and 22 GPa peak shock pressures contained such high concentrations of dislocations that only a lower bound ($< 5 \times 10^{11} \text{ cm}^{-2}$) could be established.

A spherical alumina powder (Linde ST-228P) of about 30- μm particle size was subjected to a mean peak pressure of 20 GPa and a shock-induced increase in temperature of about 400°C. TEM examination (75) showed that less than 40% of the starting particles were primarily α -alumina. The remainder were in metastable phases. After shock treatment, TEM study showed that no phase transformations had occurred; however, considerable deformation was found in all grains. The monoclinic phase contained a very high density of dislocations, many fine twins, and finely distributed cleavage cracks. The α -alumina grains also exhibited very high concentrations of dislocations but contained no twins and no cleavage. The dislocation densities were found to be comparable with those found in severely cold-worked metals. No evidence was found for localized deformation at particle surfaces, but a large degree of anisotropy in deformation was evident between particles and within a given particle.

The titanium carbide and titanium diboride powders described above were subjected to peak shock pressures of 22 GPa and studied after dispersion in methyl alcohol and placement on "holey" carbon film (76). The as-received titanium carbide powder was found to contain dislocations, planar defects, and low-angle grain boundaries in low concentrations. The shock-modified sample was found to be heavily defective with "arched" reflections in the selected area diffraction pattern. Dislocation pile-up could clearly be seen, and some particles appeared to have escaped significant deformation. The titanium diboride starting powder showed a high density of dislocations and some planar defects. After shock modification the powder showed heavily deformed microstructures similar to those observed on aluminum nitride and zirconia. The selected area diffraction patterns showed arched reflections, evidence of heavy deformation.

Although little detail was obtained from TEM studies of shock-modified alumina, aluminum nitride, titanium carbide, and titanium diboride powders, the ubiquity of heavily deformed microstructures in these brittle refractories provides explicit evidence of the ability of shock compression to create heavily cold-worked microstructures in even the most brittle powders. This unique aspect of shock modification confirms the observations from X-ray diffraction line broadening, but provides considerably more information as to the distribution of deformation within particles and the details of the deformation microstructure.

Other Probes

Other material probes that have been used less extensively to characterize shock-modified powders include scanning electron microscopy, magnetization, and Mössbauer effect studies on magnetic powders. SEM studies have been carried out on almost all the powders reported on here. Except in cases in which the starting powder particles had a distinctive morphology, little was revealed concerning the influence of shock compression. In two cases, silicon nitride and spherical alumina, SEM provided insight into the shock deformation process. The change from needle-like particles to smooth agglomerates after shock compression of silicon nitride was reported earlier. The recent study of spherical alumina powder under controlled shock compression with SEM (75) provided explicit evidence for plastic deformation of alumina much like that seen in metals. The spherical particles were found to have been plastically deformed to fill voids. There was no evidence for strongly localized deformation at particle interfaces.

Recently studies have been carried out on ferrite powders to determine the effect of shock compression on magnetic properties. These investigations are revealing as to shock-induced modification at the atomic level. Ferrites have been well studied in prior work, and solid-state theory and experiment are well joined. Hematite (α -Fe₂O₃) powder is currently being studied over a wide range of shock conditions. It was recently reported (11) that the low-temperature magnetization increased by two orders of magnitude after shock treatment. This material is an antiferromagnet at low temperature as iron magnetic moments are ferromagnetically coupled within a (111) sheet and are perpendicular to the sheet. In successive atomic layers the moments are antiparallel. In this configuration any disorder that is not homogeneous between sheets will have a strong influence on magnetization, as has been observed. Mössbauer measurements on these same samples also provide more information on local iron environments (77). Magnetization and Mössbauer measurements on ferrite powders showed shock-induced changes due to residual strain and defects.

CHEMICAL SYNTHESIS UNDER SHOCK COMPRESSION

As is briefly summarized in Table 2, there are numerous reports of shock-induced chemical synthesis. Unfortunately, most of these reports are limited to situations in which the shock conditions are not quantitative or the shock conditions of temperature and pressure are limited to a narrow

range. One cannot formulate predictive models based on the probable mechanisms of the observed chemical changes or models to use in comparing shock synthesis to more conventional processes with such limited data. Two recent chemical synthesis programs have provided considerable information on the relation between shock-compression conditions and chemical changes in mixed powders. Detailed synthesis studies have been reported on a zinc ferrite synthesized from mechanically blended powders of zinc oxide and hematite in stoichiometric ratios and intermetallic synthesis from starting powders of aluminum and nickel (either mechanically blended or in composite powder form), as well as from mechanically blended powders of aluminum and titanium.

Synthesis of Zinc Ferrite

In recent reports (11, 78-83) the synthesis of a zinc ferrite was studied over a range of peak shock pressures from 7.5 to 27 GPa and shock-induced mean bulk temperatures from 125 to about 1100°C. Details of the shock conditions were described by Morosin et al (80). Starting materials and shock products were characterized with X-ray diffraction, magnetization, Mössbauer effect, and TEM measurements. This materials system is a particularly interesting one in that the starting powders and the synthesized products are readily discernible. Furthermore, the solid-state reactions have been studied thoroughly, and it is a system with little exothermic energy release. Several features stand out in the data from these synthesis studies. It was found that a zinc-deficient ferrite was readily synthesized and that the degree of synthesis could be readily controlled by changing the shock conditions. It was also found that characterization of the synthesized products with different probes revealed significantly different but complementary descriptions.

X-ray diffraction measurements provided direct evidence for the formation of the zinc ferrite in the spinel structure phase and showed evidence for the residual strain and crystallite size in both the unreacted powders and the chemical products (80). A peak shock pressure of 16 GPa was necessary to produce detectable yields and, in this case, spinel ferrite was only produced at temperatures greater than about 500 C. At 20 GPa temperatures as low as 175 C resulted in detectable product yield. At 22 GPa and higher, easily detectable yield was obtained under all conditions, and the yield was strongly influenced by shock temperature. At 27 GPa and 1100 C the yield of spinel ferrite was 85%. At the higher yields there is sufficient resolution to show that less zinc oxide is consumed relative to hematite, such that formation of a zinc-deficient zinc ferrite is suggested.

The unreacted products were found to have broadened diffraction lines, indicating large residual strain and reduced crystallite size. There was a

dramatic sharpening of the spinel-phase diffraction lines in the high-yield sample obtained under the highest pressure and temperature. Under all other conditions the lines of the spinel product were significantly broadened, but there is insufficient data to separate line broadening due to compositional variation from that due to strain and crystallite size.

For the high-yield sample, in which very sharp lines were obtained, the d spacing values can be analyzed to give a composition value. Based on compositional data in the literature, a composition with a zinc deficiency of 8% is found.

Because of its greater sensitivity, magnetization measurements reveal a quite different, but consistent, picture of the shock synthesis process (81). Even at the lowest pressure and temperature, detectable changes in magnetization associated with zinc ferrite formation were observed. The changes far exceed those observed for similar shock conditions on hematite powders. This observation is evidence of the importance of the mechanical nature of the synthesis process, which involves the formation of defects and the mechanical mixing of substituents. For the same loading system and sample configuration, systematic increases in magnetization were observed with increasing mean bulk temperature. Except for the samples with low yield, the magnetization measurements were consistent with the X-ray diffraction measurements. Based on the magnetization and magnetic susceptibility, the synthesized product appeared to be of the same composition independent of shock condition. Increasing shock pressure and temperature led to larger yields, not changes in composition. Based on magnetization versus composition data obtained on conventionally synthesized material, as reported in the literature, the magnetization study indicates a composition with a zinc deficiency of about 50%.

Mössbauer effect measurements provide a direct probe of the local iron environment, which gives direct information on magnetic structure and relaxation and occupation of iron on octahedral and tetrahedral sites. The data on shock-synthesized ferrite are particularly revealing (82). They appear to show two spinel-phase components, one magnetic and the other paramagnetic. The total yield of these two components is in agreement with the X-ray diffraction spinel yield determinations. The favored interpretation for the origin of the paramagnetic phase is that it has the same composition as the magnetic phase but is composed of such small crystallites (< 50 nm) that superparamagnetic relaxation is exhibited. Based on literature values for Mössbauer spectra parameters, determined at various compositions obtained from conventionally synthesized zinc ferrites, the indicated composition has a zinc deficiency of 15%.

The transmission electron microscopy study of the shock-synthesized zinc ferrite (83) was limited to the starting powder mixture, a mildly reacted

sample, and the most strongly shocked sample with the highest yield. At the grain level the starting sample was found to be an intimate mixture of well-annealed particles. The mildly reacted sample showed no evidence of reaction products, but the powders were heavily dislocated, macroscopically deformed, and unbonded. X-ray energy-dispersive spectroscopy (EDS) across regions between grains showed zinc (as zinc oxide) mainly concentrated between hematite grains, although most hematite grains were found to contain some zinc. As much as 5 wt% zinc was found in hematite grains. The strongly reacted sample was found to contain ferrite as well as unreacted zinc oxide and hematite. The ferrite grains were strain and defect free, with a recrystallized microstructure. EDS data showed the ferrite to be zinc deficient by 9%. There was no evidence of compositional gradients across ferrite grains.

In this study of chemical synthesis, each material probe provided a somewhat different picture of the product, which illustrates the importance of using multiple probes to characterize these unusual materials. The discrepancies in the composition found using various probes are based on comparison with conventionally synthesized materials, and they suggest that the present material may be considerably different than those prepared by other methods.

Synthesis of Nickel and Titanium Aluminides

Intermetallic alloys or compounds are a particularly interesting class of materials; they are currently under study with a variety of synthesis techniques. It has recently been demonstrated that nickel aluminides can be readily synthesized under shock compression (11, 84-88) and that titanium-aluminum mixtures yield an unusual composition after shock treatment (89).

Synthesis of the aluminides was carried out on mechanically mixed powders of aluminum and nickel or aluminum and titanium in ratios appropriate to form stoichiometric Ni_3Al or Ti_3Al . Limited work was also carried out on a composite nickel-aluminum particle configuration in which nickel was deposited on spherical aluminum particles. These composite particles have a nominal composition of 80 wt% nickel.

The mechanically blended aluminum nickel mixtures were studied over a wide range of shock pressures and temperatures. Nickel aluminide products were found to be readily synthesized and controlled by the shock conditions. Large yields of Ni_3Al were produced, and the material had a hardness like a cold-worked Ni_3Al , even though TEM analysis showed the material to be free of dislocations. The data currently available suggest that the hardness is due to an unusually small crystallite size of about 5 nm. Under certain conditions the products NiAl , Ni_2Al , Ni_2Al_3 , and NiAl_3

are formed. The two latter compositions are not obtained in fast quenching of ion-implanted layers. There is also no evidence of amorphous material in the shock-synthesized products. The shock-modified composite particles show no large-scale reaction regions as in the mixed powders, but show many localized regions of nickel aluminides.

Titanium-aluminum powder mixtures are observed to react far less strongly, and yields are so limited that the products are difficult to identify. It appears that a TiAl_3 structure-type product is formed that is difficult to distinguish from the ordered superstructures $\text{Ti}_9\text{Al}_{23}$ and $\text{Ti}_8\text{Al}_{24}$.

CONCLUSION

The summary presented here shows that materials synthesis and modification under high pressure shock loading is an emerging area with important new results appearing continually. Such synthesis may have a significant impact on materials technology; however, the shock process is complex and will require persistent research efforts to reach its potential. The available evidence indicates that the shock-induced chemical process is perhaps best described as an unusually intense, microsecond-duration, mechanochemical event that takes place at high pressure and modestly elevated temperature. The mechanical aspects of plastic deformation and high-speed material flow are critical to the solid-state reactions and are intimately involved in determining the microsecond time scale of the shock event. Upon melting, solid-liquid reactions and reactions in the liquid state are encountered. Modeling of these processes will require an understanding of the melt process in a highly defective solid at high pressure subjected to high-speed material motion. Predictive modeling of solid-state reactions will require considerable research on the details of shock-induced defect processes and the relationships between defects and shock-enhanced solid-state reactivity.

The shock process is unique. It enables us to synthesize a range of metastable states, including some ordinarily stable only at high pressure. Reaction at high pressure allows the synthesis of new structural forms with distinctive chemical properties. The recent work on synthesis of nickel aluminides demonstrates a strong influence of exothermic energy release. Exothermic energy releases can be expected to play a role in interparticle bonding in dynamic compaction, and additives that induce exothermic energy release may produce strong bonding in dynamic compaction of refractory ceramics. The recent direct observation (90, 91) of a rise in temperature associated with exothermic energy release in the aluminum-nickel mixture shows the potential for direct monitoring of such processes.

Clearly, shock-deformation processes in powders involve effects not

encountered in shock deformation of solid density materials. Very considerable work will have to be done to develop a scientific understanding of deformation of powders. Such work will necessarily involve a description of the process in the "catastrophic shock concept" (30, 92) based on descriptions of matter in a defect state appropriate for the shock conditions, rather than a "benign shock concept" based on perfect lattice descriptions.

Residual microstructures of shock-modified, normally brittle inorganic materials bear a marked resemblance to those of wrought ductile metallic materials. Shock-deformed inorganic powders appear to respond to thermomechanical treatment in a manner analogous to more familiar metallic materials. These controllable structural modifications offer the possibility of achieving property improvements in ceramic materials that would parallel the differences between cast and wrought metals.

Shock compression science is a significant enterprise in itself. The incorporation of chemical effects into the mainstream of this research, which has traditionally been considered a field of physics, presents a significant challenge. Certainly a major influence of synthesis and shock-induced chemical studies will be to provide a much more realistic, fundamentally sound basis for understanding shock-compression processes.

Literature Cited

1. Duvall, G. E., Graham, R. A. 1977. *Rev. Mod. Phys.* 49: 523-79.
2. Syono, Y. 1984. In *Materials Science of the Earth's Interior*, ed. I. Sunagawa, pp. 395-414. Tokyo: Terra Scientific.
3. Davison, L., Graham, R. A. 1979. *Phys. Rep.* 55: 255-379.
4. Graham, R. A., Morosin, B., Dodson, B. 1983. *The Chemistry of Shock Compression: A Bibliography*. Sandia Nat. Labs. Rep. SAND83-1887.
5. Adadurov, G. A., Gol'danskii, V. I., Yampol'skii, P. A. 1973. *Mendeleev Chem. J.* 18: 92-103.
6. Adadurov, G. A., Gol'danskii, V. I. 1981. *Russ. Chem. Rev.* 50: 948-57.
7. Dodson, B. W., Graham, R. A. 1982. In *Shock Waves in Condensed Matter—1981*, ed. W. J. Nellis, L. Seaman, R. A. Graham, pp. 42-51. New York: Am. Inst. Phys.
8. Morosin, B., Graham, R. A. 1982. See Ref. 7, pp. 4-13.
9. Dremmin, A. N., Breusov, O. N. 1968. *Russ. Chem. Rev.* 37: 392-402.
10. Dremmin, A. N., Breusov, O. N. 1971. *Priroda Moscow* 12: 10-17 (In Russian); 1980. Translation in Sandia National Laboratories Report SAND80-6003.
11. Graham, R. A., Morosin, B., Horie, Y., Venturini, E. L., Boslough, M., et al. 1986. In *Proc. 1985 Am. Physical Soc. Topical Conf. on Shock Waves in Condensed Matter, Spokane, Wash., July 22-25, 1985*, ed. Y. Gupta. In press.
12. Rice, M. H., McQueen, R. G., Walsh, J. M. 1958. In *Solid State Physics*, ed. F. Seitz, D. Turnbull, 6: 1-63. New York: Academic.
13. Parsons, C. A. 1920. *Philos. Trans. R. Soc. London A* 220: 67.
14. Riabinin, Iu. N., 1956. *Sov. Phys. Dokl.* 1: 424-26.
15. Grover, R., Christian, R. H., Alder, B. J. 1958. *Bull. Am. Phys. Soc.* 3: 230 (Abstr.)
16. DeCarli, P. S., Jamieson, J. C. 1961. *Science* 133: 821-22.
17. Milton, D. J., DeCarli, P. S. 1963. *Science* 140: 670-71.
18. Kimura, Y. 1963. *Jpn. J. Appl. Phys.* 2: 312.
19. Adadurov, G. A., Barkalov, I. M., Gol'danskii, V. I., Dremmin, A. N., Ignatovich, T. N., et al. 1965. *Polymer Sci. USSR* 7: 196-97.

20. Batsanov, S. S., Deribas, A. A., Dulepov, E. V., Ermakov, M. G., Kudinov, V. M. 1965. *Combust. Explos. Shock Waves USSR* 1: 47-49
21. Horiguchi, Y., Nomura, Y. 1965. *Carbon* 2: 436-37
22. Horiguchi, Y., Nomura, Y. 1965. *Chem. Industry London*: Oct: 1791-92
23. Bergmann, O. R., Barrington, J. 1966. *J. Am. Ceram. Soc.* 49: 502-7
24. Suzuki, H., Yoshida, H., Kimura, Y. 1969. *Yogyo Kōkai Shi* 77: 36-44 (In Japanese); Translation in Sandia National Laboratories Report RS3140:81/169
25. Barrington, J., Bergmann, O. R. 1968. *US Patent No. 3,367,766*
26. Shcherbakova, L. G., Kolesnikov, A. V., Breusov, O. N. 1979. *Inorganic Mater. USSR* 15: 1724-29
27. Kolesnikov, A. V., Shcherbakova, L. G., Breusov, O. N. 1980. *Proc. Acad. Sci. USSR Sect. Phys. Chem.* 251: 172-73
28. Kolesnikov, A. V., Shcherbakova, L. G., Breusov, O. N. 1981. *Proc. Acad. Sci. USSR Sect. Phys. Chem.* 256: 7-11
29. Jeanloz, R. 1980. *J. Geophys. Res.* 85: 3163-66
30. Graham, R. A. 1979. *J. Phys. Chem.* 83: 3048-56
31. Duvall, G. E. 1984. *Shock Compression Chemistry in Materials Synthesis and Processing*, Natl. Mater. Advisory Board, Natl. Res. Council, Natl. Acad. Sci. Rep. NMAB-414. Washington, DC: National Academy
32. Nellis, W. J., Seaman, L., Graham, R. A., eds. 1982. *Shock Waves in Condensed Matter—1981*. New York: Am. Inst. Phys.
33. Asay, J. R., Graham, R. A., Straub, G. K., eds. 1984. *Shock Waves in Condensed Matter—1983*. New York: North Holland
34. Gupta, Y., ed. 1986. *Shock Waves in Condensed Matter—1985*. In press
35. Gourdin, W. H. 1986. *Prog. Mater. Sci.* In press
36. Nellis, W. J., Ree, F. H., van Thiel, M., Mitchell, A. C. 1981. *J. Chem. Phys.* 75: 3055-63
37. Olinger, B., Newkirk, L. R. 1981. *Solid State Commun.* 37: 613-17
38. Stewart, G. R., Olinger, B., Newkirk, L. R. 1981. *Solid State Commun.* 39: 5-9
39. Davison, L., Webb, D. M., Graham, R. A. 1982. See Ref. 32, pp. 67-71
40. Graham, R. A., Webb, D. M. 1984. See Ref. 33, pp. 27-34
41. Graham, R. A., Webb, D. M. 1986. See Ref. 34, In press
42. West, A. R. 1984. *Solid State Chemistry and Its Applications*, New York: Wiley. 734 pp.
43. Schmalzried, H. 1981. *Solid State Reactions*, Weinheim: Verlag Chemie. 254 pp.
44. Hedvall, J. A. 1966. *Solid State Chemistry: Whence, Where and Whither*, Amsterdam: Elsevier. 100 pp.
45. Adadurov, G. A., Breusov, O. N., Dremmin, A. N., Drobyshev, V. N. 1971. *Russ. J. Inorganic Chem.* 16: 1073-74
46. Hankey, D. L., Graham, R. A., Hammetter, W. F., Morosin, B. 1982. *J. Mater. Sci. Lett.* 445-47
47. Hammetter, W. F., Hankey, D. L., Dosch, R. G. 1986. *J. Am. Ceram. Soc.* Submitted for publication
48. Morosin, B., Graham, R. A., Hellmann, J. R. 1984. See Ref. 33, pp. 383-86
49. Hellmann, J. R., Kuroda, K., Heuer, A. H., Graham, R. A. 1984. See Ref. 33, pp. 387-90
50. Hammetter, W. F., Hellmann, J. R., Graham, R. A., Morosin, B. 1984. See Ref. 33, pp. 391-94
51. Beauchamp, E. K., Loehman, R. E., Graham, R. A., Morosin, B., Venturini, E. L. 1984. In *Emergent Process Methods for High-Technology Ceramics*, ed. R. F. Davis, H. Palmour III, R. L. Porter, pp. 735-48. New York: Plenum
52. Lee, Y. K., Williams, F. L., Graham, R. A., Morosin, B. 1985. *J. Mater. Sci.* 20: 2488-96
53. Batsanov, S. S., Borekov, G. K., Gridasova, G. V., Keier, N. P., Kefeli, L. M., et al. 1967. *Kinet. Catal. USSR* 8: 1140-46
54. Borekov, G., Sazonova, I., Keyer, N., Kjudinov, V., Gridasova, G., et al. 1968. In *Behavior of Dense Media Under High Dynamic Pressures*, ed. J. Berger, pp. 389-96. New York: Gordon and Breach
55. Venturini, E. L., Morosin, B., Graham, R. A. 1982. See Ref. 32, pp. 77-81
56. Batsanov, S. S., Bokarev, V. P., Kostenchuk, I. A., Mardashev, Yu. S., Temnitskii, I. N. 1982. *React. Kinet. Catal. Lett.* 20: 43-45
57. Bokarev, V. P., Bondarev, Yu. M., Temnitskii, I. N., Kozlova, N. E., Shustaeva, A. I., et al. 1985. *React. Kinet. Catal. Lett.* 27: 181-84
58. Golden, J. 1982. MS thesis, University of New Mexico, Albuquerque. 75 pp.
59. Morosin, B., Graham, R. A. 1984. *Mater. Sci. Engr.* 66: 73-87
60. Morosin, B., Graeber, E. J., Graham, R. A. 1984. In *Advances in X-Ray Analysis*, ed. J. B. Cohen, J. C. Russ, D. E. Leyden, C. S. Barrett, P. K. Predecki, pp. 369-78. New York: Plenum
61. Venturini, E. L., Graham, R. A. 1984. In *Defect Properties and Processing of*

- High Technology Nonmetallic Materials*, ed. J. H. Crawford Jr., Y. Chen, W. A. Sibley, pp. 383-89. New York: North Holland
62. Carr, M. J., Graham, R. A., Morosin, B., Venturini, E. L. 1984. See Ref. 61, pp. 343-49
 63. Carr, M. J., Graham, R. A. 1986. In *Proc. Int. Conf. Metallur. Appl. Shock-Wave and High-Strain-Rate Phenomena*, Portland, Ore., July 28-Aug. 1, 1985. In press
 64. Chen, H., White, J. M., Graham, R. A. 1986. Submitted for publication
 65. Williams, F. L., Lee, Y. K., Morosin, B., Graham, R. A. 1986. See Ref. 34
 66. Lee, Y. K., Williams, F. L., Graham, R. A., Morosin, B. 1984. See Ref. 33, pp. 399-402
 67. Williams, F. L., Morosin, B., Graham, R. A. 1986. See Ref. 63
 68. Morosin, B., Graham, R. A. 1984. See Ref. 33, pp. 355-62
 69. Morosin, B., Graham, R. A. 1984. See Ref. 61, pp. 335-41
 70. Morosin, B., Graeber, E. J., Graham, R. A. 1984. See Ref. 60, pp. 369-78
 71. Morosin, B., Graham, R. A. 1986. See Ref. 63
 72. Morosin, B., Graham, R. A., White, J. M., Beck, D. D. 1984. *Chem. Phys. Lett.* 112: 555-58
 73. Morosin, B., Graham, R. A. 1985. *Mater. Lett.* 3: 119-23
 74. Beauchamp, E. K., Carr, M. J., Graham, R. A. 1986. *J. Am. Ceram. Soc.* Submitted for publication
 75. Beauchamp, E. K., Carr, M. J., Graham, R. A. 1985. *J. Am. Ceram. Soc.* 68: 686-89
 76. Kuroda, D., Heuer, A. H. 1983. In *2nd Progr. Rep. DARPA Dynamic Synthesis and Consolidation Progr.*, ed. C. F. Cline, pp. 260-309. Lawrence Livermore Laboratory Report UCID-19663-83-1
 77. Williamson, D. L., Morosin, B., Venturini, E. L., Graham, R. A. 1985. *Bull. Am. Phys. Soc.* 30: 477 (Abstr.)
 78. Venturini, E. L., Morosin, B., Graham, R. A. 1985. *J. Appl. Phys.* 57: 3814-16
 79. Venturini, E. L., Morosin, B., Graham, R. A. 1985. *Mater. Lett.* 3: 349-53
 80. Morosin, B., Venturini, E. L., Graham, R. A. 1986. See Ref. 34
 81. Venturini, E. L., Morosin, B., Graham, R. A. 1986. See Ref. 34
 82. Williamson, D. L., Morosin, B., Venturini, E. L., Graham, R. A. 1986. See Ref. 34
 83. Carr, M. J., Graham, R. A. 1986. See Ref. 34
 84. Horie, Y., Graham, R. A., Simonsen, I. K. 1985. *Mater. Lett.* 3: 354-59
 85. Horie, Y., Graham, R. A., Simonsen, I. K. 1986. See Ref. 63
 86. Simonsen, I. K., Horie, Y., Graham, R. A. 1986. See Ref. 34
 87. Mayers, S. A., Koch, C. C., Horie, Y., Graham, R. A. 1986. See Ref. 34
 88. Pak, H.-R., Horie, Y., Graham, R. A. 1986. See Ref. 34
 89. Horie, Y., Hoy, D. E. P., Simonsen, I., Graham, R. A., Morosin, B. 1986. See Ref. 34
 90. Boslough, M. B., Graham, R. A. 1985. *Phys. Chem. Lett.* In press
 91. Boslough, M. B., Graham, R. A. 1986. See Ref. 34
 92. Graham, R. A. 1980. *Bull. Am. Soc.* 25: 495

SESSION - III

MECHANISTIC ISSUES IN ASSOCIATED PROCESSES

SESSION III: MECHANISTIC ISSUES IN ASSOCIATED PROCESSES

A. Niiler: SESSION CHAIR COMMENTS

'The Mechanism of Activated Combustion Synthesis' by Zuhair Munir, UC Davis Activated Combustion Synthesis is another way of saying Joule heating assisted combustion synthesis. By applying a voltage across a sample, thus passing a current in a direction parallel to the reaction front, a system that is not energetic enough for self-propagation can be made to react. When the current 'assist' is removed, the reaction quenches. This method has made possible combustion reactions between Si+C to SiC, W+C to WC, B+C to B₄C as well as ceramic-ceramic composites with ratios between the components easily adjusted. Another benefit of this activated combustion synthesis is the ability to 'quench' the reaction at any point. This allows analysis of the partially reacted sample with a very good view of the area in the combustion front region, both just before the reaction and immediately post-reaction. It may be useful to study these regions for evidence for meta-stable state formations.

There is a good analogy between this activated combustion synthesis and shock synthesis, since both are methods of providing reaction initiation and sustaining heat energy. It is very possible that activated combustion, being a much easier to control process, could be used to study the same reactions as would be done with shock synthesis to gain understanding of details which may be beyond the capability of experimental techniques in the highly stressing environments present in shocks. Clearly, any aspect of shock synthesis which depends on the very high rate mixing of component materials could not be studied with the activated combustion technique.

Some basic modeling of what actually occurs during the current flow and concomitant heating of very localized regions of the sample in activated combustion should be done. That is, it seems that the very localized heated areas that must be responsible for melting of one component thus initiating the local reaction, should be theoretically described in detail. Such a description will, no doubt, show a very important dependence on things like powder morphologies, coatings, and perhaps less dependence on bulk properties of the material such as thermal or electrical conductivities. Detailed experimental studies of 'quenched' reaction zones should be able to reveal whether any reaction ever takes place in the absence of liquid formation. Or, to state it another way, this would be a way to study non-self-sustaining solid-solid reactions. The fact that the reaction stops when current is stopped probably indicates that the reaction itself is highly localized. Can an experiment or theoretical treatment be done which reveals a critical size of reacting volume necessary? Or is there even such a thing as a minimum critical volume? It may also be interesting to combine high pressure, whether shock or static, and Joule heating since the application of pressure will alter the electrical conductivity of a powder mix material.

'Chemistry at Static High Pressure: Some General Principles and Recent Developments' by Malcolm Nicol, UCLA This was a talk that was rather difficult for me to follow due to the large amount of chemistry jargon used. I am afraid that you will need someone else's perspective on

this topic. It was clearly relevant to shock chemistry, but my knowledge of chemistry is so limited that I really should not try to comment on any of the specific high pressure reactions, transformations and other mechanisms that Professor Nicol discussed. Sorry!

'Mechanism of Shock-Induced Mechanochemistry' by J.J. Gilman, UCLA. Chemical reactions driven by large mechanical strains are athermal. In effect, these strains, if caused by a compressive shear tensor, cause bending of covalent bonds and thus affect the electronic structure of the solid. Because the electronic structure rearrangement can occur very rapidly, it is a mechanism that can easily keep up with the speed of sharp shock fronts. This is a much simplified but hopefully almost correct reinterpretation of Professor Gilman's description of the high rate chemical reactions observed in shock chemistry. It is very elegantly appealing in that it describes at the molecular level a very complex mechanism. Specific examples of shock induced reactions like the polymerization of benzene, the decomposition of the azide ions, and the effect of shear strain on the ammonium ion were used to describe the influence of reductions of the LUMO-HOMO energy gap in these molecules.

A shock front which nominally produces uniaxial compression is really a combination of shear and isotropic compression. The role of shear strains in activating or driving high pressure reactions was very strongly emphasized. One of the paragraphs in Professor Gilman's abstract bears repeating in this summary: Shear effects are expected to be more important in most cases than the effects of isotropic compression for the following reasons: a) they cause the major part of the heating if the material is porous; b) covalent bonds have smaller bending force constants than compression force constants; c) shear strains cause larger changes in the electronic structures of materials than isotropic compressions, because they reduce the symmetry of the molecular structure; and d) shear strains cause shape changes and this is consistent with the molecular shape changes that occur during chemical reactions.

A very strong effort should be made by modelers to include these shear effects in calculations of shock chemistry and/or shock modification of materials.

'Shock Chemistry Mechanisms, Kinetics, and Applications' by A.N. Dremin. Professor Dremin began with a general discussion of a variety of investigations he and his department have pursued in the areas of basic shock induced events like chemical reactions, polymorphic transformations, changes in electrical, optical or mechanical properties of materials and relaxation phenomena. Additionally, he mentioned various applications of shock energy like metal treatments and super-hard materials synthesis. He then described the differences in the effects of the very large loading rates in the Shock Discontinuity Zone (SDZ) between molecular and ionic crystals where bond mechanisms differ substantially.

When discussing inorganic materials under shock loading, besides verifying results from many other research groups such as defect formation and enhancement of chemical activity, he presented interesting results on the formation of compounds of elements which are totally immiscible under normal conditions. Another point made by Prof. Dremin was that very high rate adiabatic cooling occurs during the unloading of the shock wave thus providing the opportunity for the formation of super-cooled liquid. Finally, he made a strong case for monitoring a shocked sample continuously during the time immediately following the application

of the shock in order to track the kinetics of phenomena such as metastable compound formation.

He stated that his group had developed an electrical conductivity measurement technique to satisfy this need. Professor Dremine's work appears to be very relevant to the subject of shock synthesis and it is recommended that ARO find some specific aspect of it for future collaboration/funding.

'Modeling Shock-Compression of Porous Composite Materials and Correlation with Observed Behavior' by Mel Baer. As in the case of Malcolm Nicol's paper, I feel very inadequate to summarize this talk as it concerns modeling concepts with which I have little familiarity. Baer did state that the work is only beginning so one must have patience with the fact that even in the highly reactive thermite reaction scenario, the current model did not include chemistry. Also, ignoring the relative flow effects under shock loading of disparate powders seems too important a factor to ignore, even in a simple calculation. At this point I would be very skeptical about drawing conclusions about comparisons of this model to experiment.

GENERAL IMPRESSIONS OF WORKSHOP

In attempting to answer the proposed target questions a) through g) here are my opinions.

a) Clearly initiation of chemical reactions can be accomplished in the shock wave but there was no evidence presented which unequivocally demonstrated that such reactions proceeded to completion during the shock. On the contrary, some evidence from Marc Meyers plots of the locations in the samples where there was incomplete reaction under very complicated shock conditions may demonstrate that shock may even quench initiated reactions.

b) Definitely no. I did not see any technique describe which could do this, especially in a bulk sample. However, I would like to see more of Dremine's idea of following electrical properties in samples in real time.

c) Limitations are high speed and a clear demonstration of a probe that can provide information in real time without affecting the progress of the reactions.

d) In most areas I think that good progress is being made. However, a lot more needs to be done to quantify the question of how mass is transported from individual material particles either through or around the compound formed from them. Liquid flow is of course the best candidate, but even here, quantification of flow rates in specific systems I think is lacking.

e) Yes. See my discussion under Munir's paper.

f) I don't know.

g) Possibly. The caveats here are that IF a given material can be made in the absence of shock (say only at high static pressure or high temperature) then forget shock. It will only serve as a scientific research tool but not commercially viable production technique. Another point is that if shock is the ONLY way to achieve a given material form, then determine if there is a commercial or other use for THAT material.

THE MECHANISM OF ACTIVATED COMBUSTION SYNTHESIS

Z.A. Munir

Department of Chemical Engineering and Materials Science
University of California
Davis, CA 95616

Abstract

The concept of activated combustion synthesis involves the simultaneous action of the chemical heat of the reaction and an additional energy imposed through the application of an electromagnetic field, gravitational field, or a force field. The use of an electric field to activate self-propagating high-temperature synthesis (SHS) reactions has been recently investigated. Such a process has been used successfully to synthesize a variety of ceramic and composite materials which cannot otherwise be prepared by conventional SHS. Examples of these include the carbides SiC, WC, B₄C, and the composites MoSi₂ -x SiC and y B₄C - TiB₂ with $0 \leq x \leq 1.0$ and $1.0 \leq y \leq 8.0$. Experimentally the process of activated synthesis is accomplished by igniting the reactants while they are under the influence of an electric field. A self-propagating wave is initiated and maintained as long as the applied voltage is above a minimum (threshold) value. The synthesis of materials by SHS has the advantage of higher heating rates ($10^3 - 10^6 \text{ K.s}^{-1}$) a circumstance which does not favor the formation of intermediate or undesired phases. This has been demonstrated in such cases as the synthesis of MoSi₂ and B₄C - TiB₂ composites.

Stoichiometric mixtures of Si and C (graphite) will not ignite (by a lungsten coil) unless a voltage of approximately 10 volts is imposed across them. It was found that at such a voltage, the combustion wave propagated in a non-steady (pulsating) mode. However, as the voltage is increased, the wave propagated in a steady-state fashion with its velocity being linearly proportional to the applied voltage. An investigation of the mechanistic role of the field on the combustion synthesis of β -SiC revealed a highly localized effect. Microstructural and analytical examinations of quenched combustion fronts led to the conclusion that the field produces a highly localized current confined to the area just ahead of the wave. The presence of a liquid phase (Si) promotes conduction in this zone and a subsequent heat input due to Joule heating. Thus the manner in which combustion synthesis is activated is through the incorporation of Joule heat into the combustion process. This then modifies the Fourier heat balance equation into the following:

$$\rho C_p \frac{\partial T}{\partial t} = \kappa \frac{\partial^2 T}{\partial x^2} + Q \frac{\partial \eta}{\partial t} + \sigma E^2$$

where the term on the left-hand side of the equation is the heat accumulation term, the first term on the right-hand side is the heat conduction term, the second term is the chemical heat generation term (due to the combustion reaction), and the last term is the electrical heat generation term. It is this last term (with σ being the conductivity and E is the field) which activates the process. Theoretical studies were also made to model this process with the results showing qualitative agreement with all of the experimental observations.

The practical aspect of the concept field-activated combustion synthesis can be seen by examining the cases of the composites $\text{MoSi}_2 - x \text{ SiC}$ and $y \text{ B}_4\text{C} - \text{TiB}_2$. The former is normally made by the synthesis of the separate phases and the subsequent processing of the mixture to achieve the desired composite. The field-activated process can product the composite from elemental reactants in one step for any value of x between zero and one. The second composite $y \text{ B}_4\text{C} - \text{TiB}_2$, extensively studied as potential armor material, can only be formed by normal SHS for $y = 0.5$. Higher values are desirable to provide lighter and harder materials but materials with $y \geq 1.0$ cannot be synthesize without the requirement of preheating the reactants. Although preheating can in may cases achieve the desired goal, in this case it leads to the formation of TiC and TiB as extraneous phases. Through field activated synthesis, composites of B_4C and TiB_2 have been made with y up to 8 without the presence of additional phases.

Relevant Publications:

1. Z.A. Munir, et., "Field-Assisted Combustion Synthesis", U.S. Patent, pending.
2. A. Feng and Z.A. Munir, "Field-Assisted Self-Propagating Synthesis of $\beta\text{-SiC}$ ", *J. Appl. Phys.*, in press (1994).
3. S. Gedevisanishvili and Z.A. Munir, "Field-Assisted Combustion Synthesis of $\text{MoSi}_2 - \text{SiC}$ Composites", *Scripta Met. et Mater.*, in press (1994).
4. A. Feng and Z.A. Munir, "The Effect of an Electric Field on Self-Sustaining Combustion Synthesis, Part I: Modeling Studies", *Met. Trans.*, submitted, 1994.
5. A. Feng and Z.A. Munir, "The Effect of an Electric Field on Self-Sustaining Combustion Synthesis, Part II: Field-Assisted Synthesis of $\beta\text{-SiC}$ ", *Met. Trans.*, submitted, 1994.

MECHANISMS OF COMBUSTION SYNTHESIS REACTIONS:
FIELD-ACTIVATED PROCESSES*

Z. A. Munir
Department of Chemical Engineering and Materials Science
University of California
Davis, California 95616
USA

Presented at: The ARO Workshop on Shock Synthesis of Materials
Georgia Institute of Technology
May 25, 1994

* Work supported by the National Science Foundation.

OUTLINE

1. Introduction: The Concept of Activated SHS
 2. Field-Activated Combustion Synthesis
 3. Mechanistic and Modeling Analysis for the Activated Synthesis of β -SiC
 4. Other Examples of Field-Activation: Composite Materials
-

ELECTROMAGNETIC FIELD ACTIVATION:

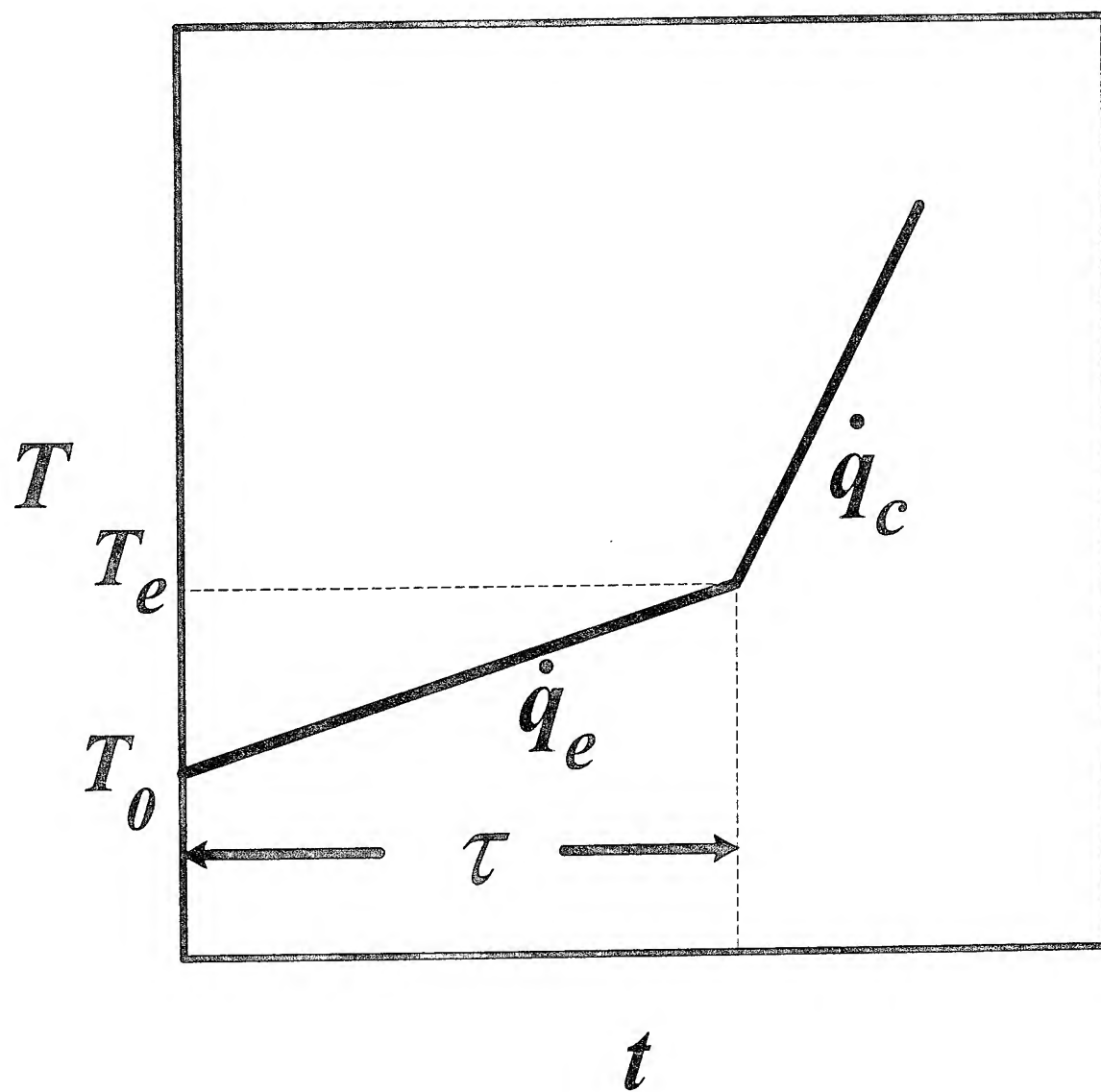
- Magnetic Field

Effect on Capillary Flow of Ferromagnetic Liquid

- Electric Field:

Prior Work: "Electrothermal Explosion"

Yamada, et al. on SiC
Shteinberg, et al. on TaC, TiC



SIMPLIFIED FORM OF FOURIER'S EQUATION:

$$C_p \frac{dT}{dt} = \dot{q}_c + \dot{q}_e$$

PRIOR TO IGNITION, $\dot{q}_c \sim 0$

$$T_e = T_o + \frac{V^2}{C_p Rm} \cdot \tau$$

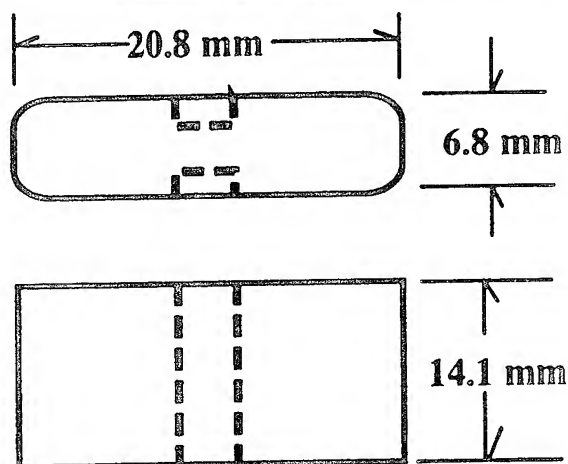
LIMITATIONS OF "ELECTROTHERMAL EXPLOSION"

- Restricted to low resistance materials
 - Subject to non-uniformity
 - Limited by reactant particle size
-

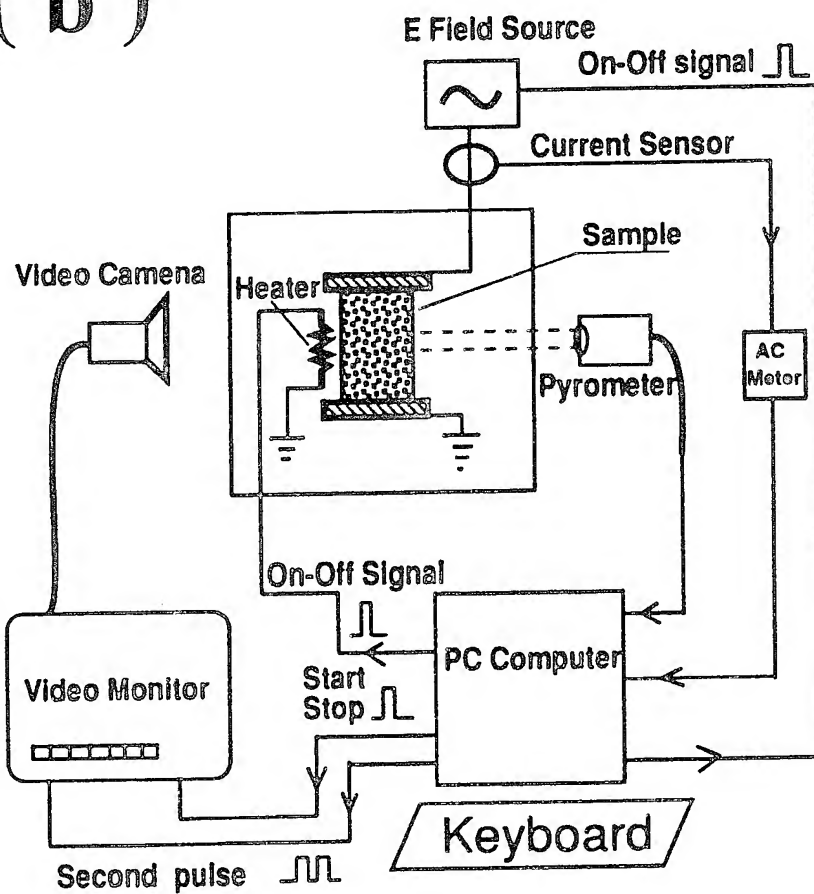
FIELD-ACTIVATED SHS:

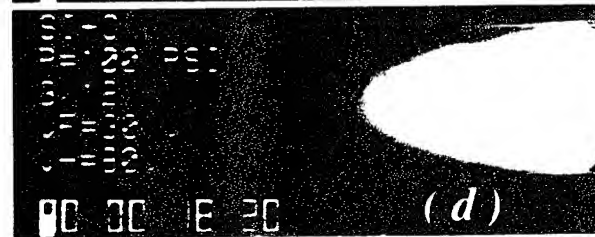
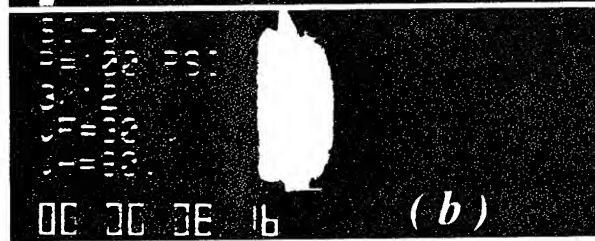
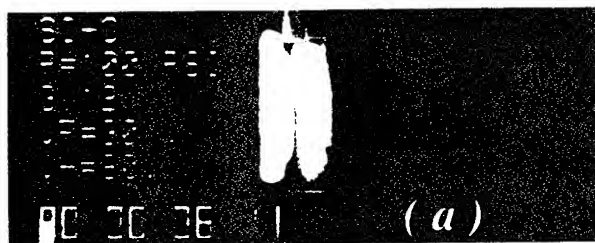
- Work on SiC
Experimental
Modeling
 - Work on Composites
 MoSi_2 - $x\text{SiC}$
 $y\text{B}_4\text{C}$ - TiB_2
 MoSi_2 - $y\text{Nb}$
 MoSi_2 - $y\text{ZrO}_2$
-

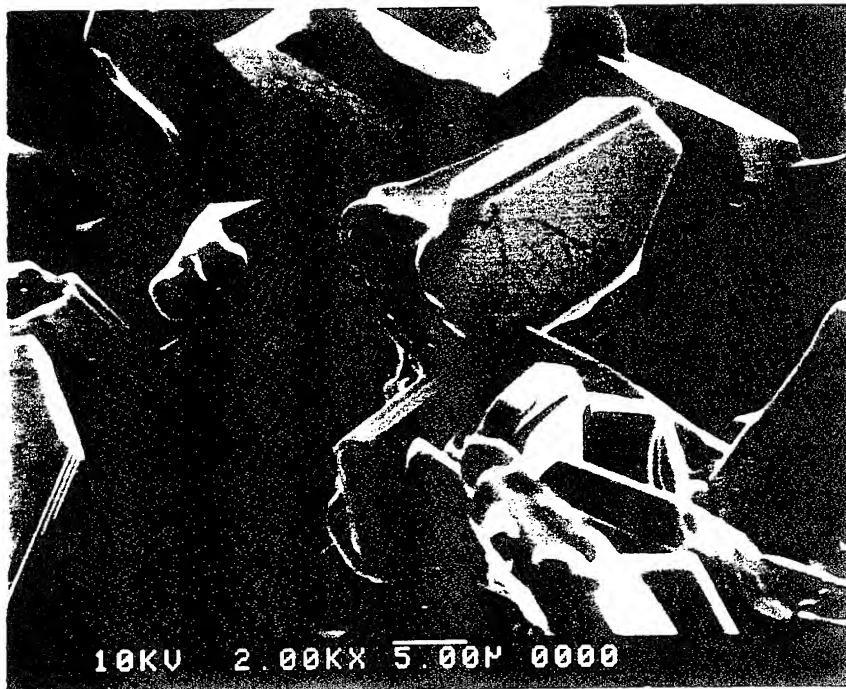
(a)



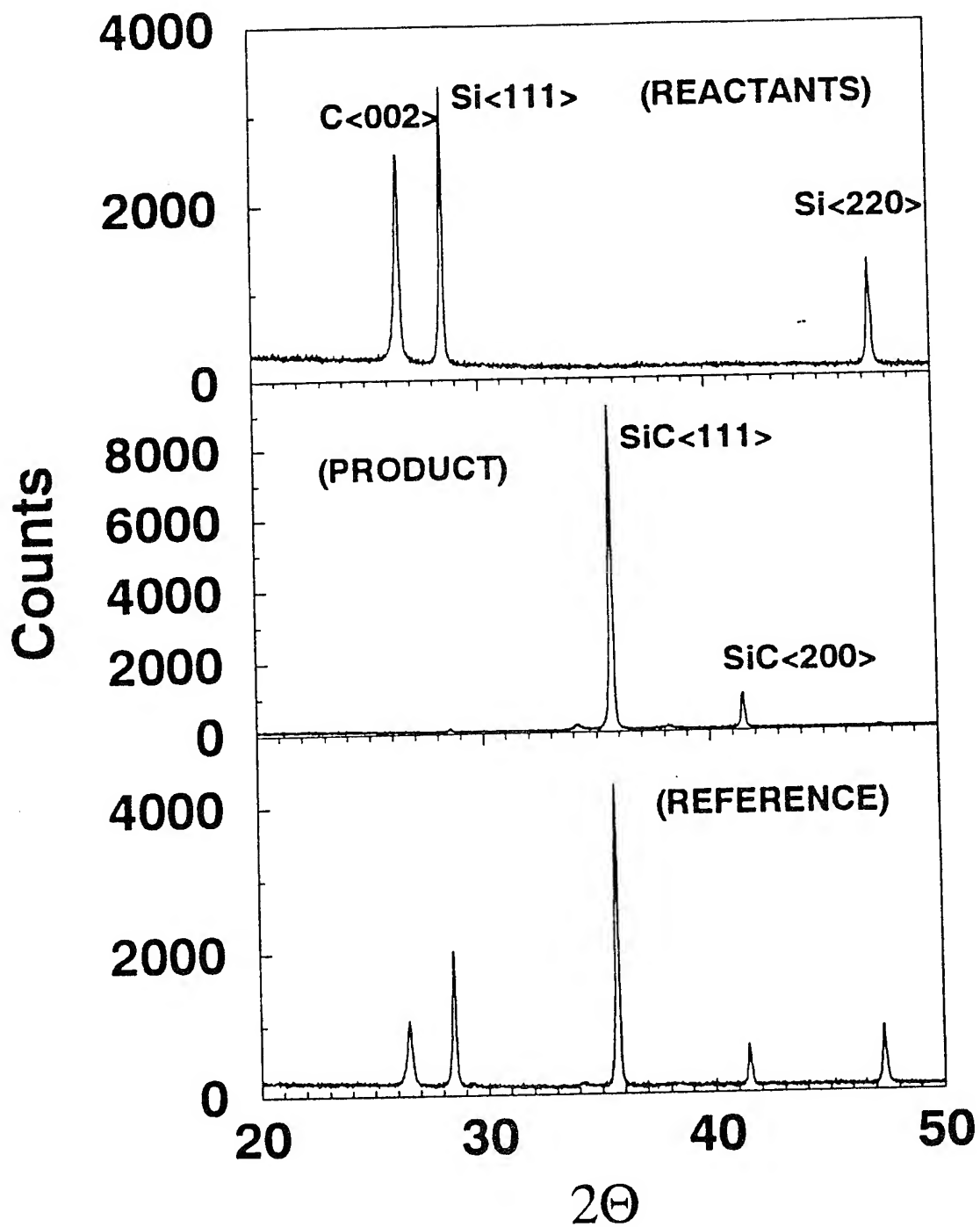
(b)







10KV 2.00KX 5.00μ 0000

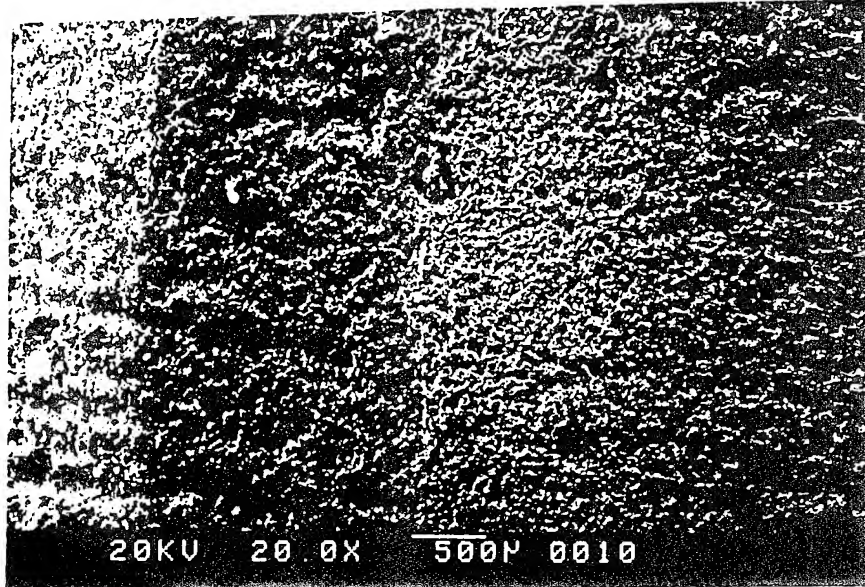


Zone I

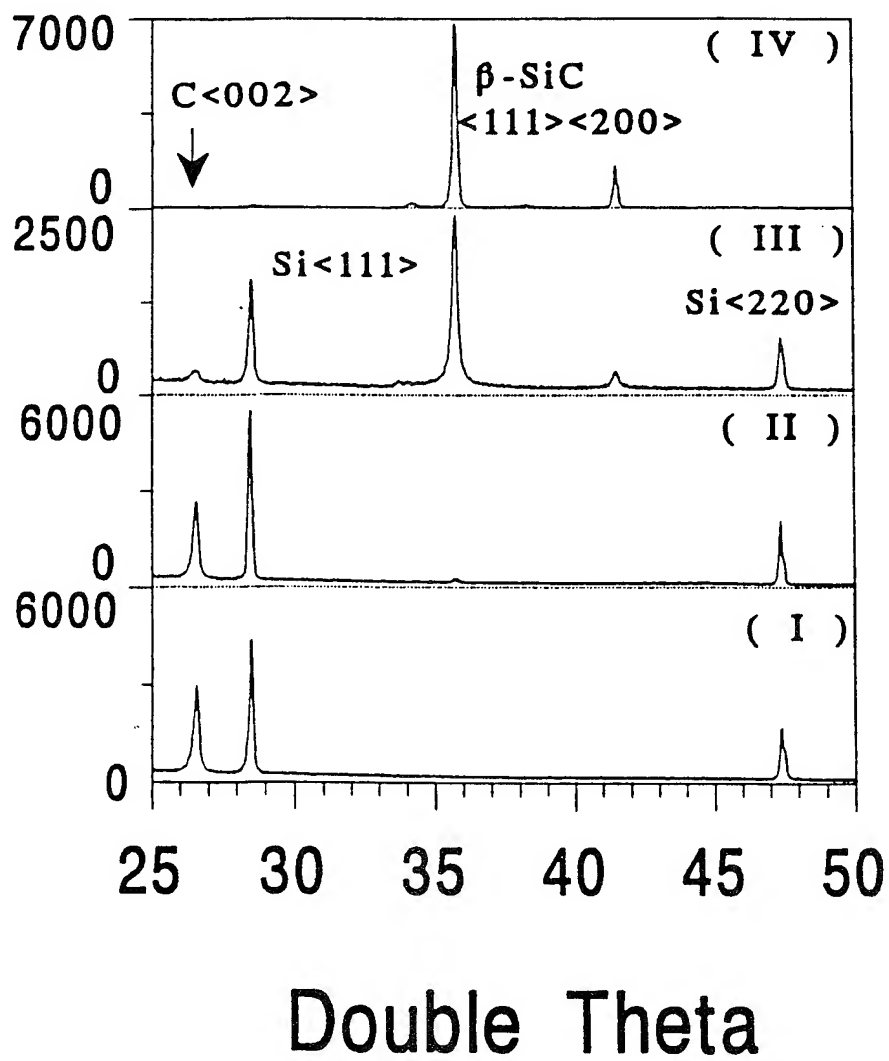
Zone II

Zone III

Zone IV



Counts



$$C_p \frac{\partial T}{\partial t} = \frac{\partial}{\partial x} \left(\kappa \frac{\partial T}{\partial x} \right) + \frac{\partial}{\partial y} \left(\kappa \frac{\partial T}{\partial y} \right) + H_c \frac{\partial \gamma_3}{\partial t} + \sigma \left[\frac{\partial^2 \psi}{\partial x^2} + \frac{\partial^2 \psi}{\partial y^2} \right]$$

$$\frac{\partial \gamma_1}{\partial t} = -K \frac{\gamma_1 \gamma_2}{\gamma_1 + \gamma_2} \exp (-E_a / RT)$$

$$\frac{\partial \gamma_2}{\partial t} = -K \frac{\gamma_1 \gamma_2}{\gamma_1 + \gamma_2} \exp (-E_a / RT)$$

$$\frac{\partial}{\partial x} \left(\sigma \frac{\partial}{\partial x} \psi \right) + \frac{\partial}{\partial y} \left(\sigma \frac{\partial}{\partial y} \psi \right) = 0$$

$$C_p = C_p (T, \gamma_1, \gamma_2, \gamma_3)$$

$$\kappa = \kappa (T, \gamma_1, \gamma_2, \gamma_3)$$

$$\sigma = \sigma (T, \gamma_1, \gamma_2, \gamma_3)$$

$$C_p \rho \frac{dT}{dt} = K \frac{d^2T}{dx^2} + QP \frac{dn}{dt} + \sigma E^2$$

$\text{Si} + \text{C} \rightarrow \beta\text{-SiC}$
Combustion Synthesis Modeling

Parameters:

SAMPLE SIZE:

$L=2.0 \text{ cm}$, $H=1.4 \text{ cm}$, $W=0.67 \text{ cm}$

SAMPLE DENSITY:

1.47 g/cm

Si/C MIXTURE RATIO:

1:1

REACTION HEAT:

$H=16 \text{ kcal/mole}$

ACTIVATION ENERGY:

$E = 40 \text{ kcal/mole}$

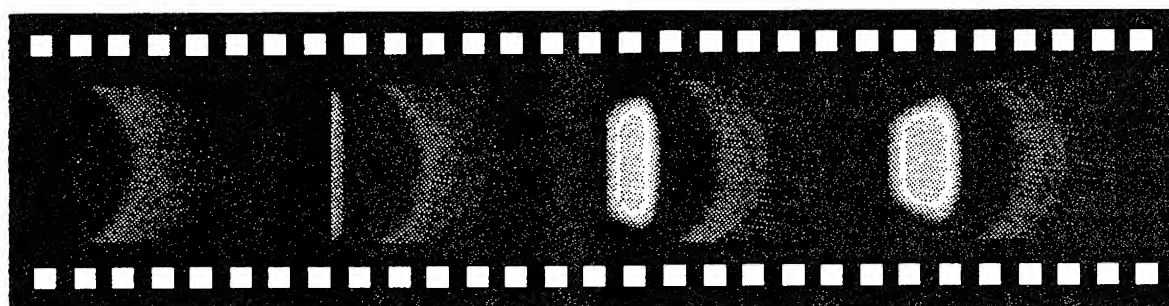
REACTION RATE:

$K=10 \text{ (1/ms)}$

Applied Voltage: 20 v

$\text{Si} + \text{C} \rightarrow \beta\text{-SiC}$
Combustion Synthesis Modeling

Temperature Scale (K)

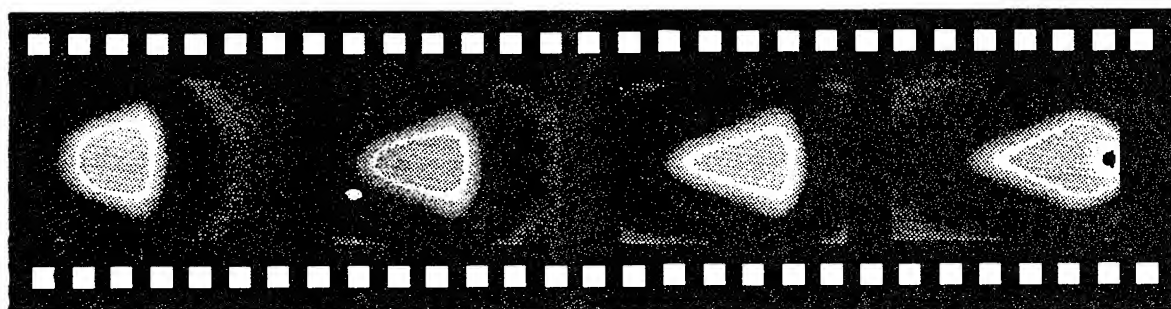


T=1 S

T=1.35 S

T=1.5 S

T=2 S



T=2.5 S

T=3 S

T=3.5 S

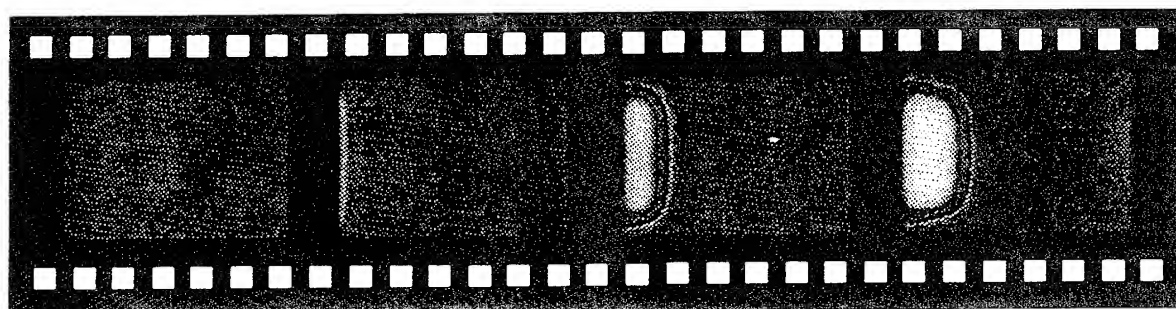
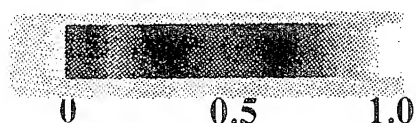
T=4 S

(Applied Voltage=20 v)

$\text{Si} + \text{C} \rightarrow \beta\text{-SiC}$
Combustion Synthesis Modeling

Conversion Profile

Conversion Scale

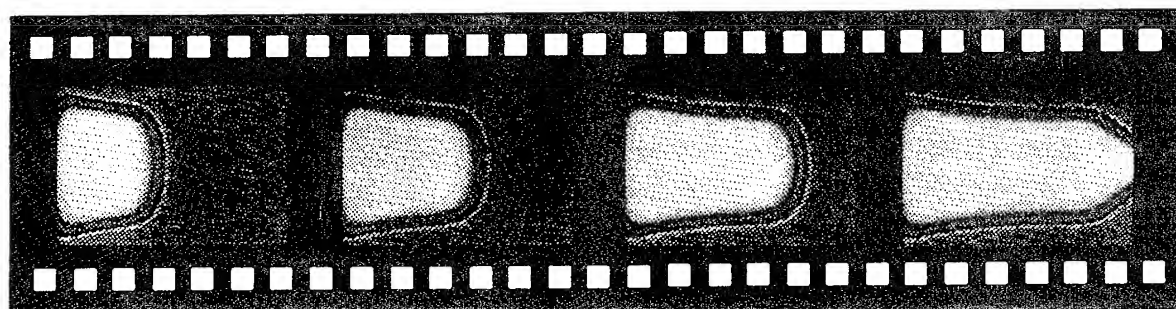


T=1 S

T=1.35 S

T=1.5 S

T=2 S



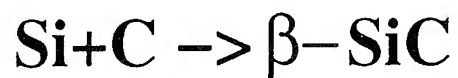
T=2.5 S

T=3 S

T=3.5 S

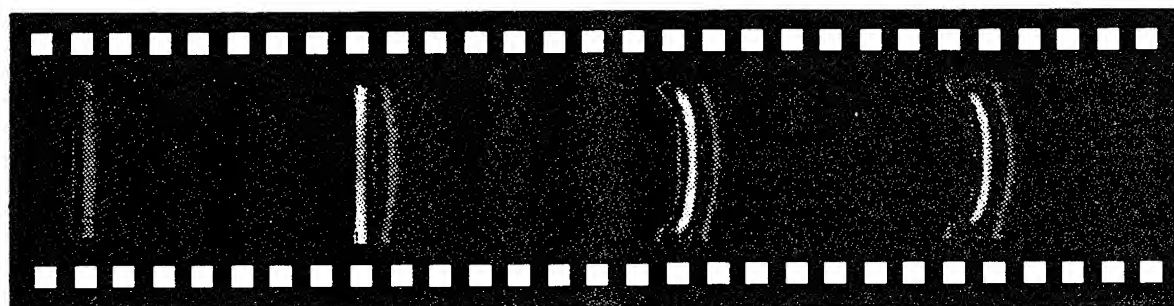
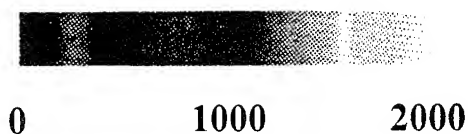
T=4 S

(Applied Voltage=20 v)



CURRENT PROFILE

Current density scale
(A/cm^2)

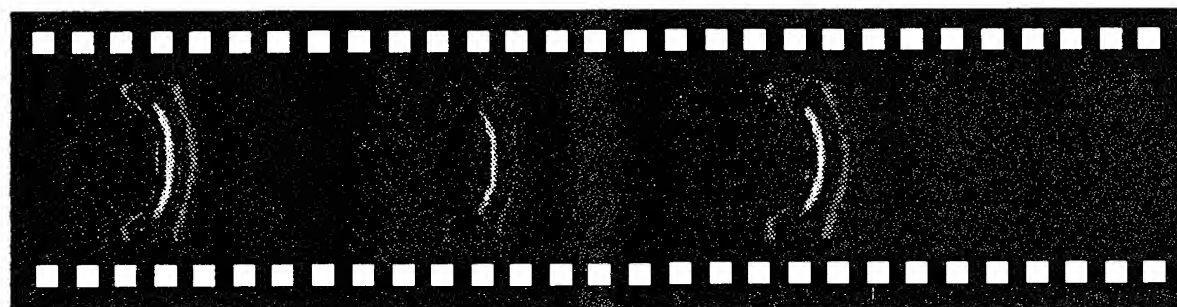


T=1 S

T=1.35 S

T=1.5 S

T=2 S



T=2.5 S

T=3 S

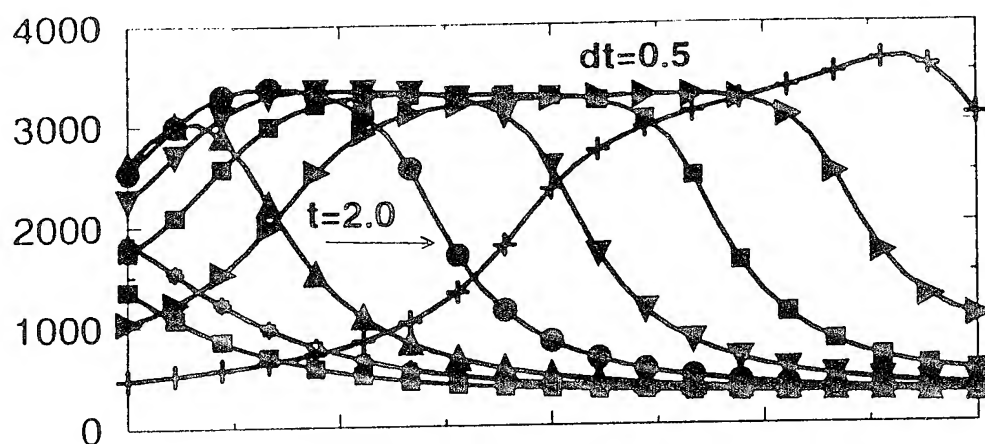
T=3.5 S

T=4 S

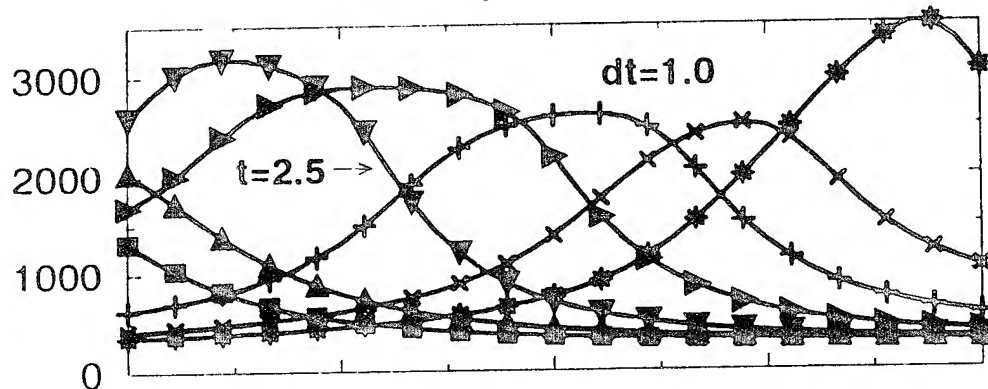
(Applied Voltage=20 v)

Temperature (K)

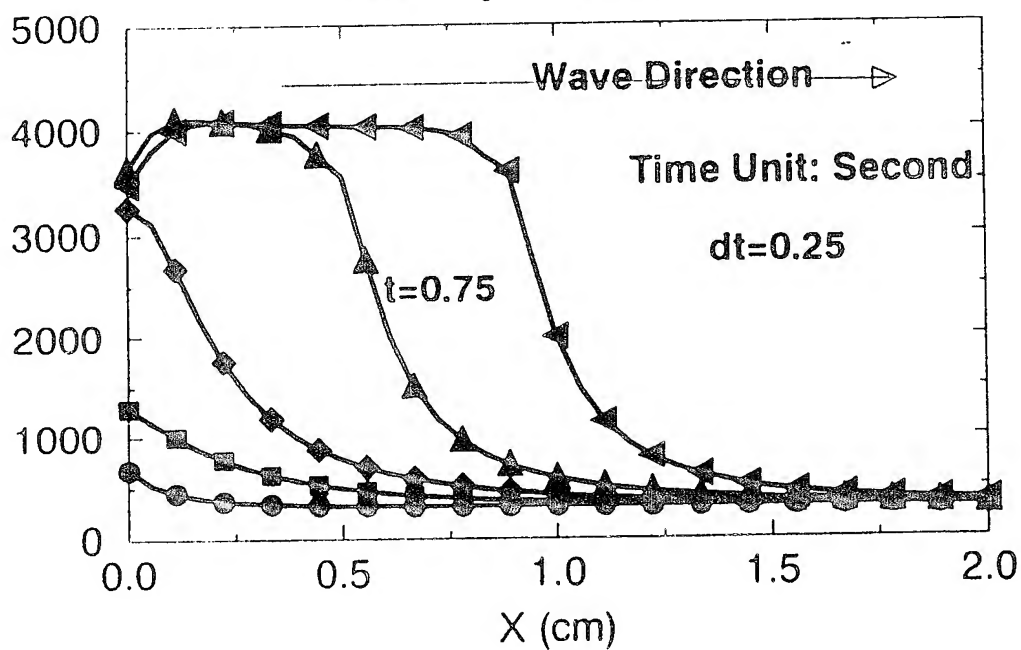
(a) $V_0=20$ volts

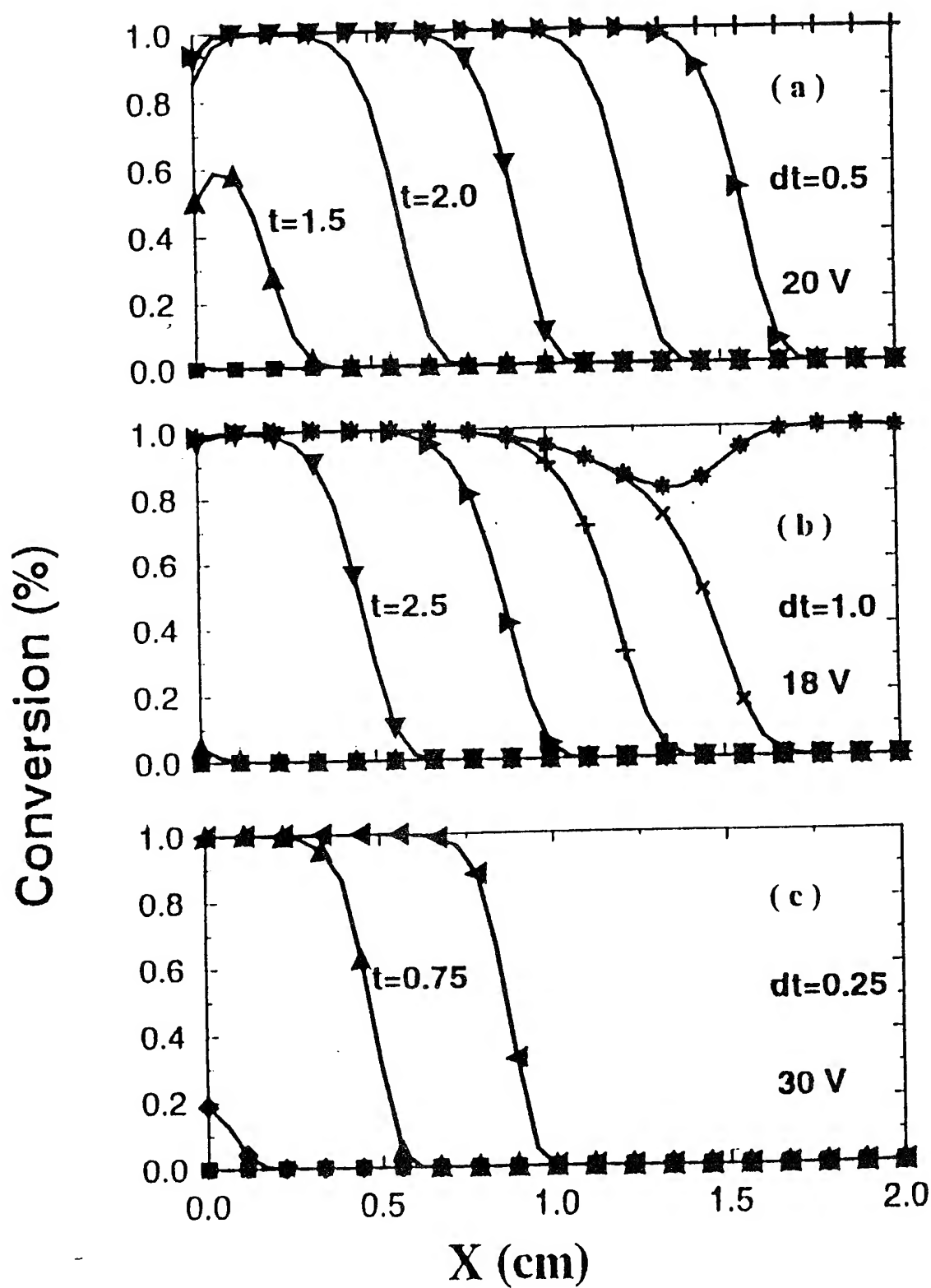


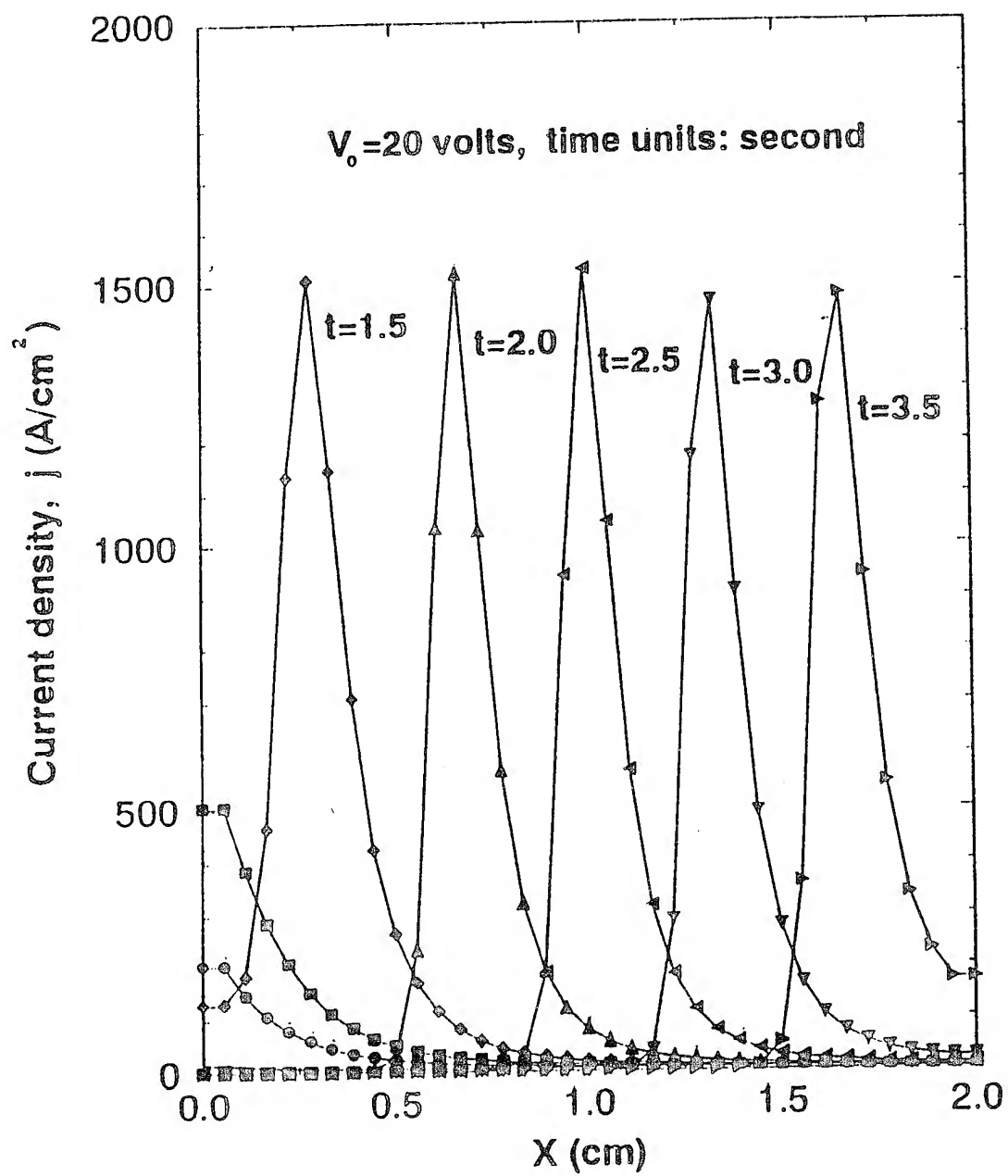
(b) $V_0=18$ volts

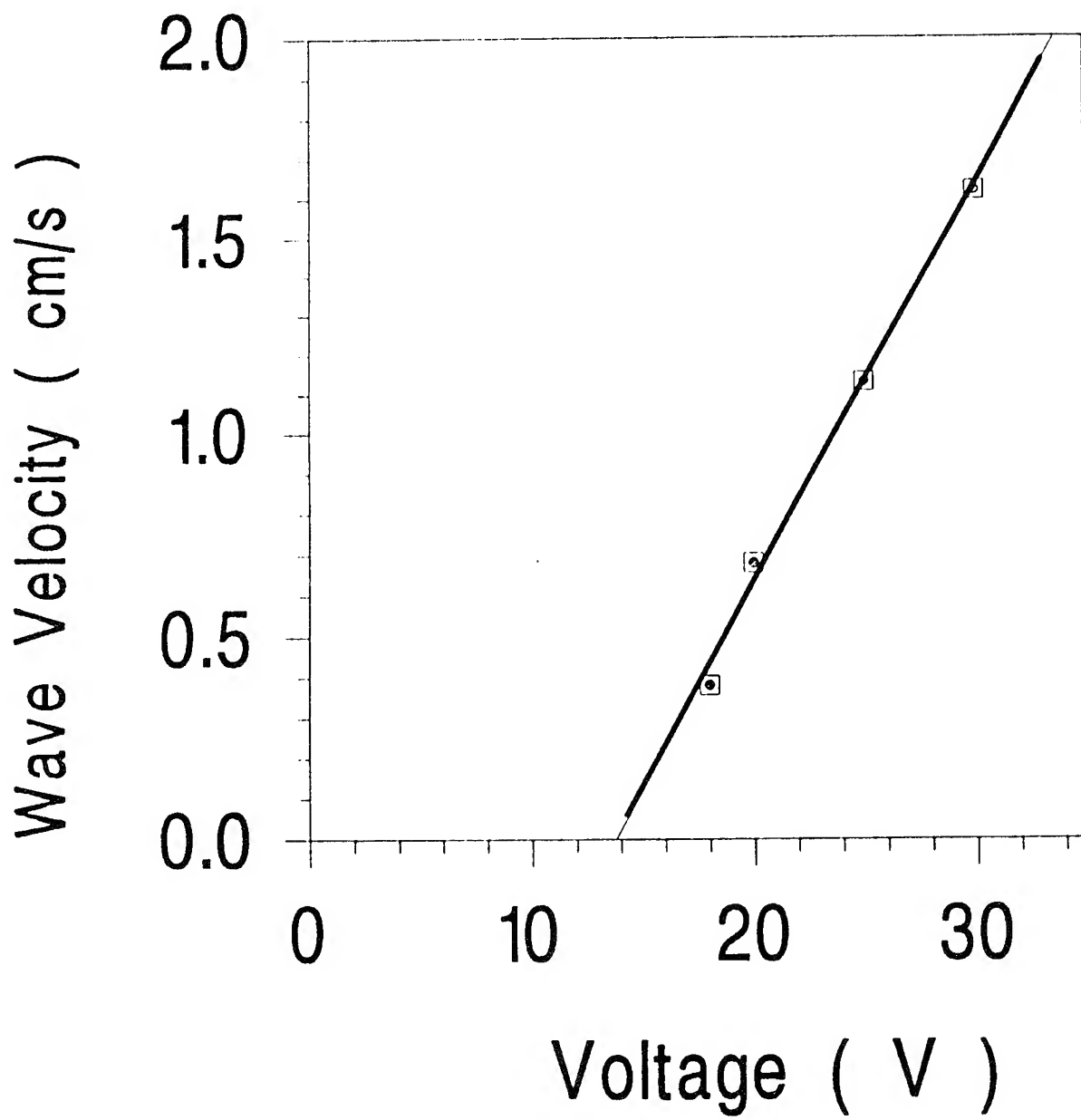


(c) $V_0=30$ volts









FIELD-ACTIVATED SYNTHESIS OF COMPOSITES

$\text{MoSi}_2 - x\text{SiC} : 0 \leq x \leq 1.0$

$y \text{ B}_4\text{C} - \text{TiB}_2 : 1.0 \leq y \leq 8.0$

$\text{MoSi}_2 - x\text{ZrO}_2 : 0.05 \leq x \leq 0.15$

$\text{MoSi}_2 - x\text{Nb} : 0.05 \leq x \leq 0.45$

Mixture: $(\text{Mo}+2\text{Si})/(\text{Si}+\text{C})=70/30$ Vol%

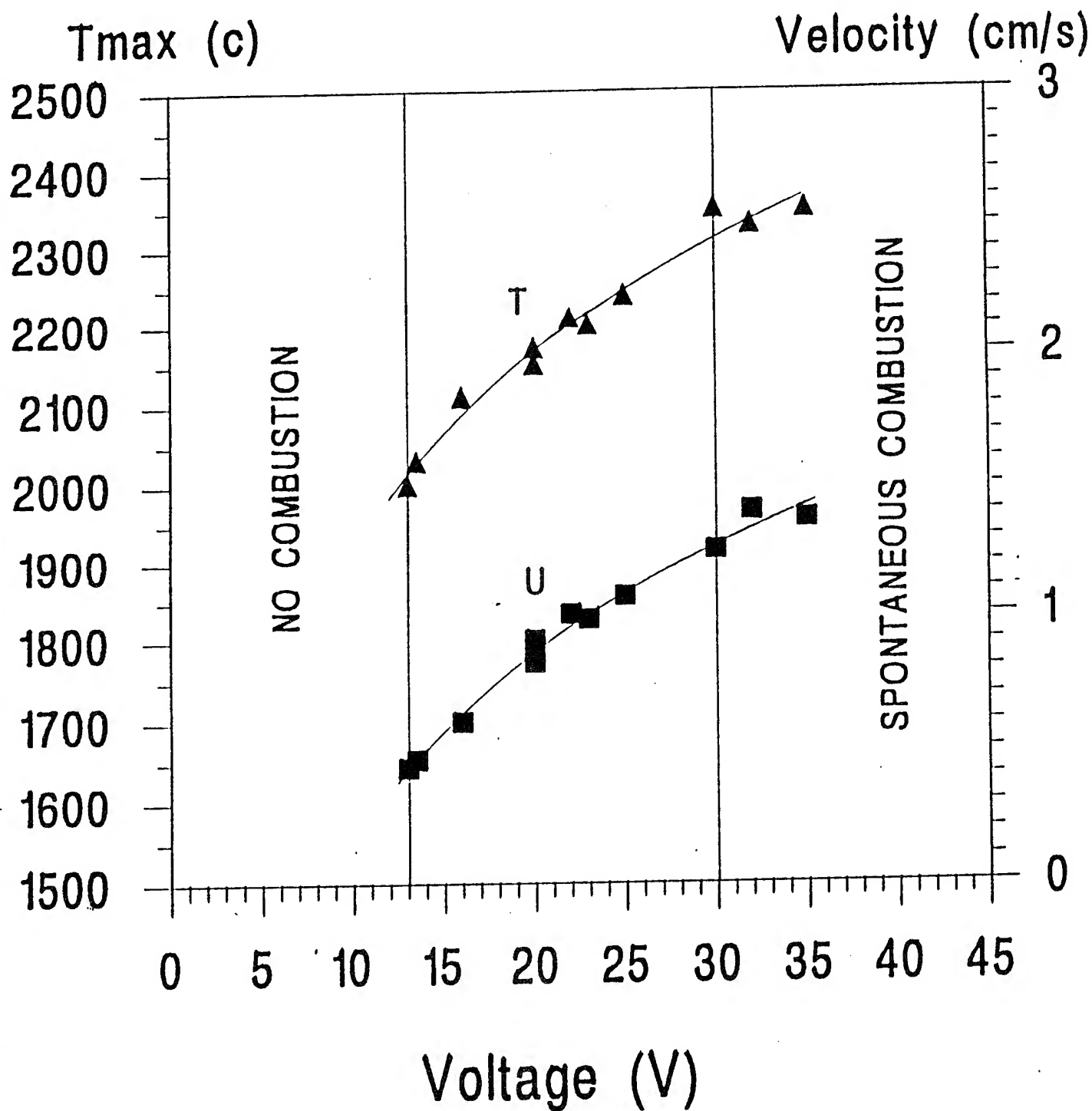
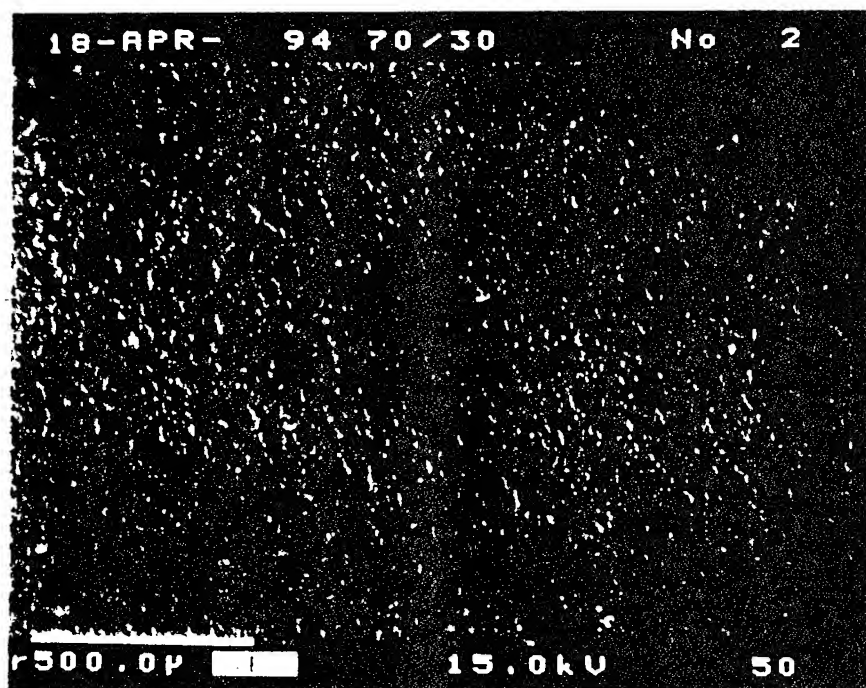
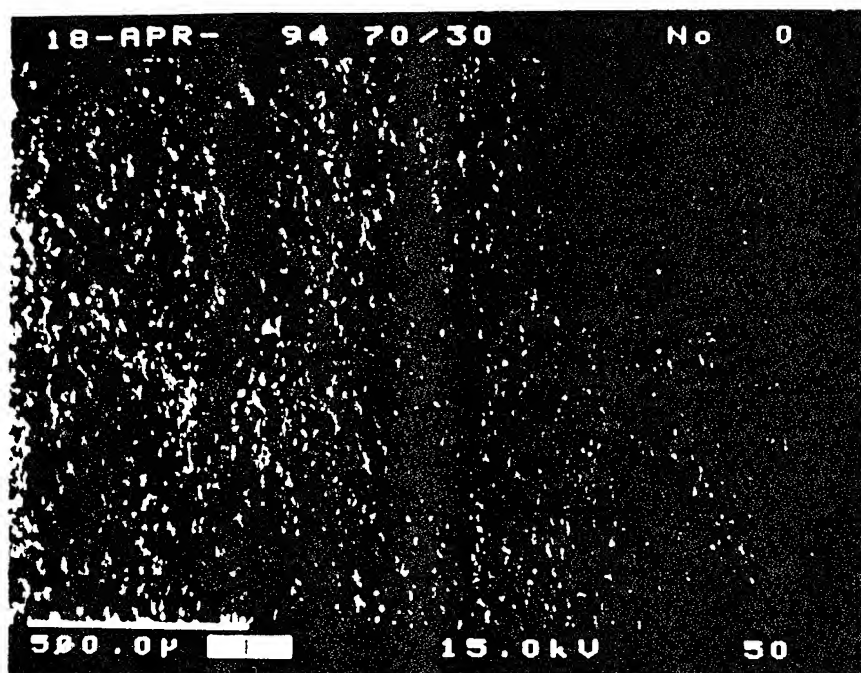


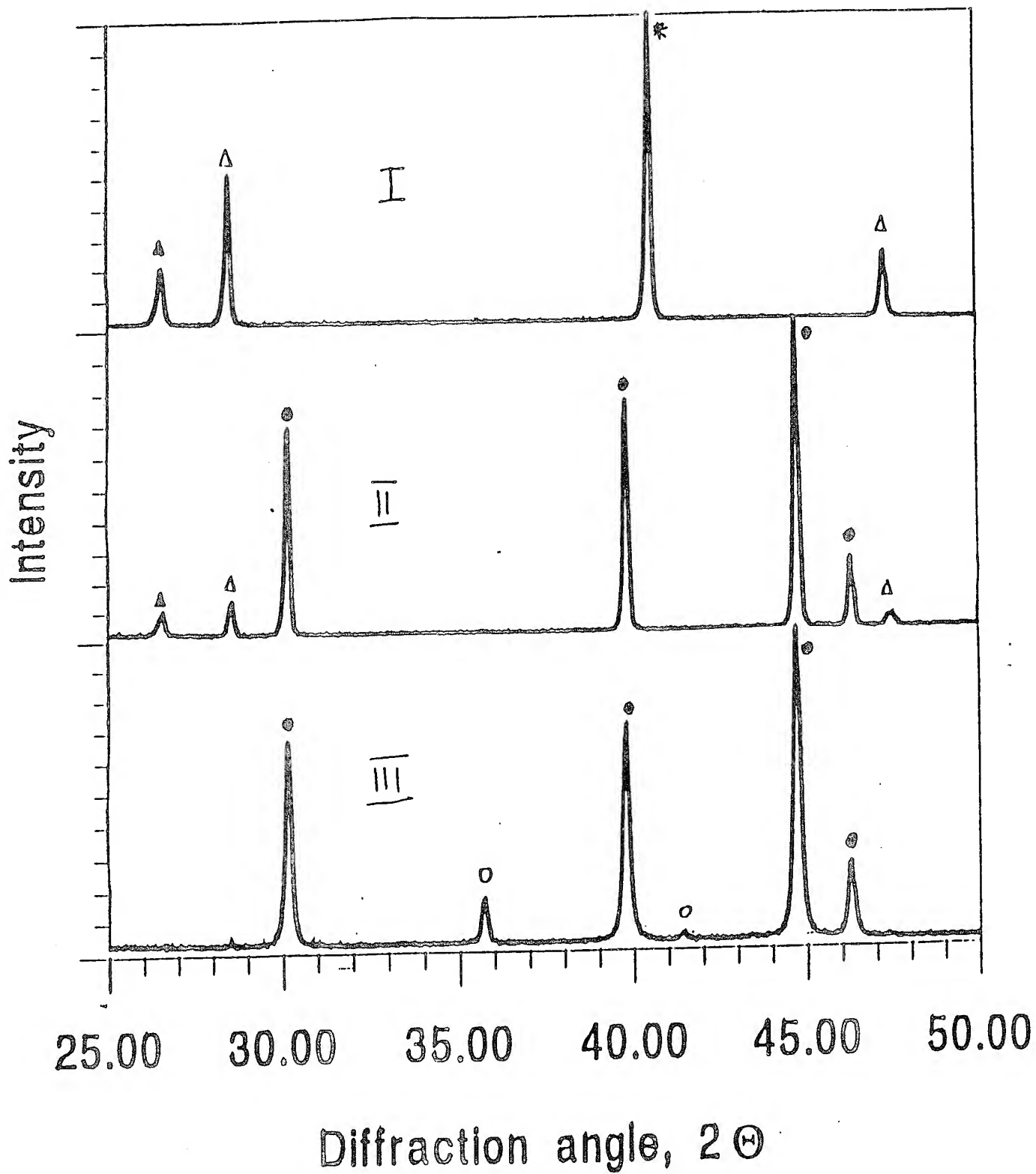
TABLE 1
Field-Assisted Self-Propagating Combustion of $\text{MoSi}_2\text{-xSiC}$ Composites

x	Applied Voltage (V) (Threshold)	T_a (K)	Product Phases (s)
0	0	1942	MoSi_2
0.18	0	1934	MoSi_2 , Si, C
0.26	44	1931	MoSi_2 , SiC
0.32	33	1929	MoSi_2 , SiC
0.45	13.5	1925	MoSi_2 , SiC
0.72	11.0	1918	MoSi_2 , SiC
0.85	13.0	1915	MoSi_2 , SiC
1.00	8.5	1912	SiC



I - starting mixture ($\text{Al}_2\text{O}_3, \text{Si}, \text{C}$)
 II - starting stage of conversion ($\text{Al}_2\text{O}_3, \text{Si}, \text{C}$)
 III - Final Product ($\text{Al}_2\text{O}_3/\text{Si}$)

} see X-ray diff. 1



* - Mg

• - $MgSi_2$

I - Starting mixture

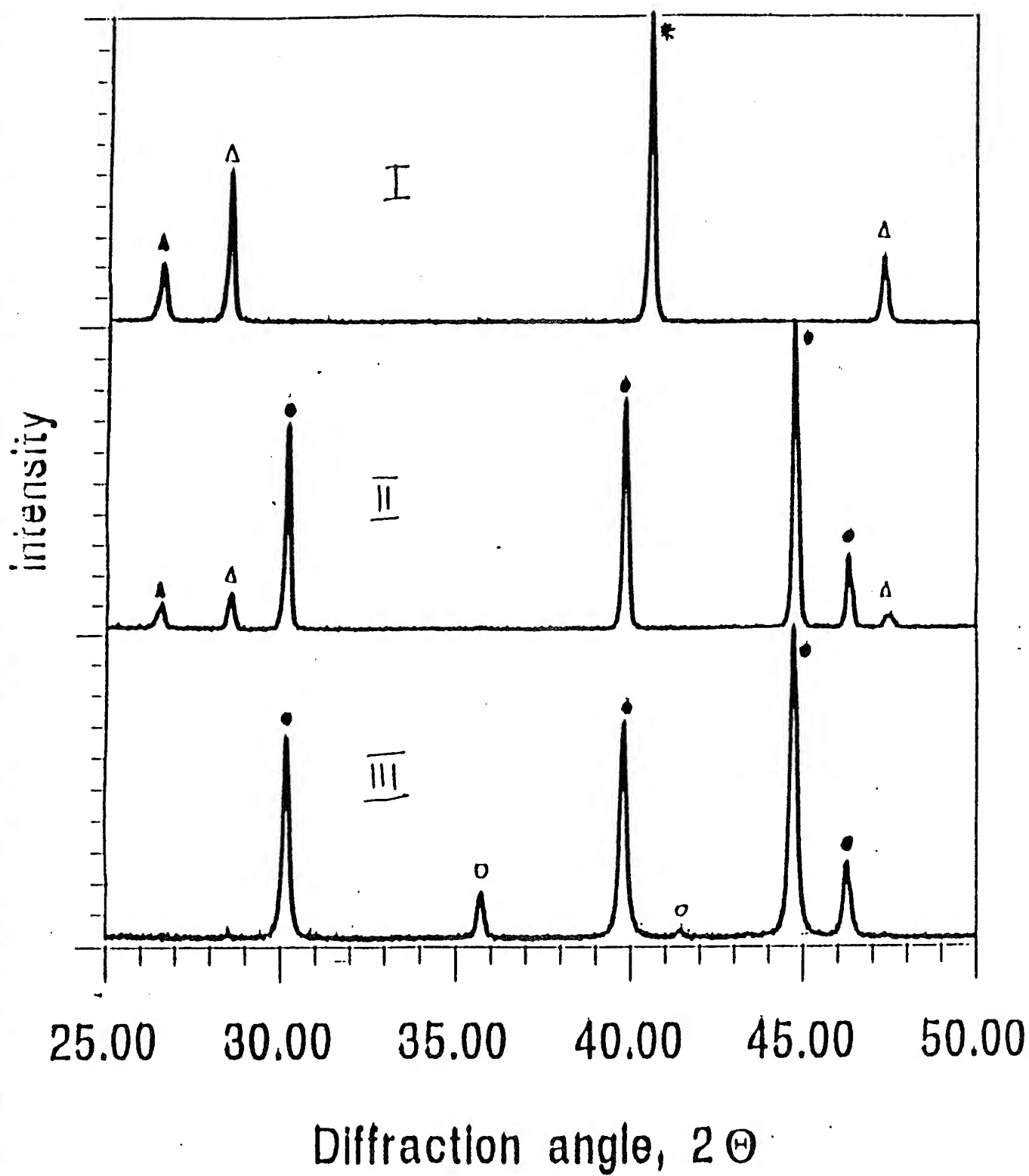
Δ - Si

○ - SiC

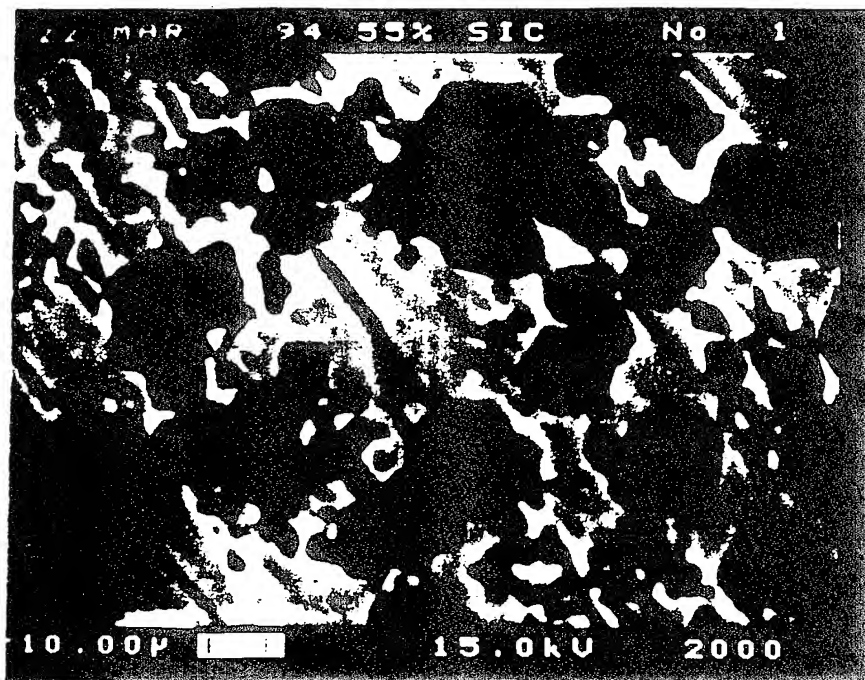
II - Starting stage of conversion

▴ - C

III - Final product

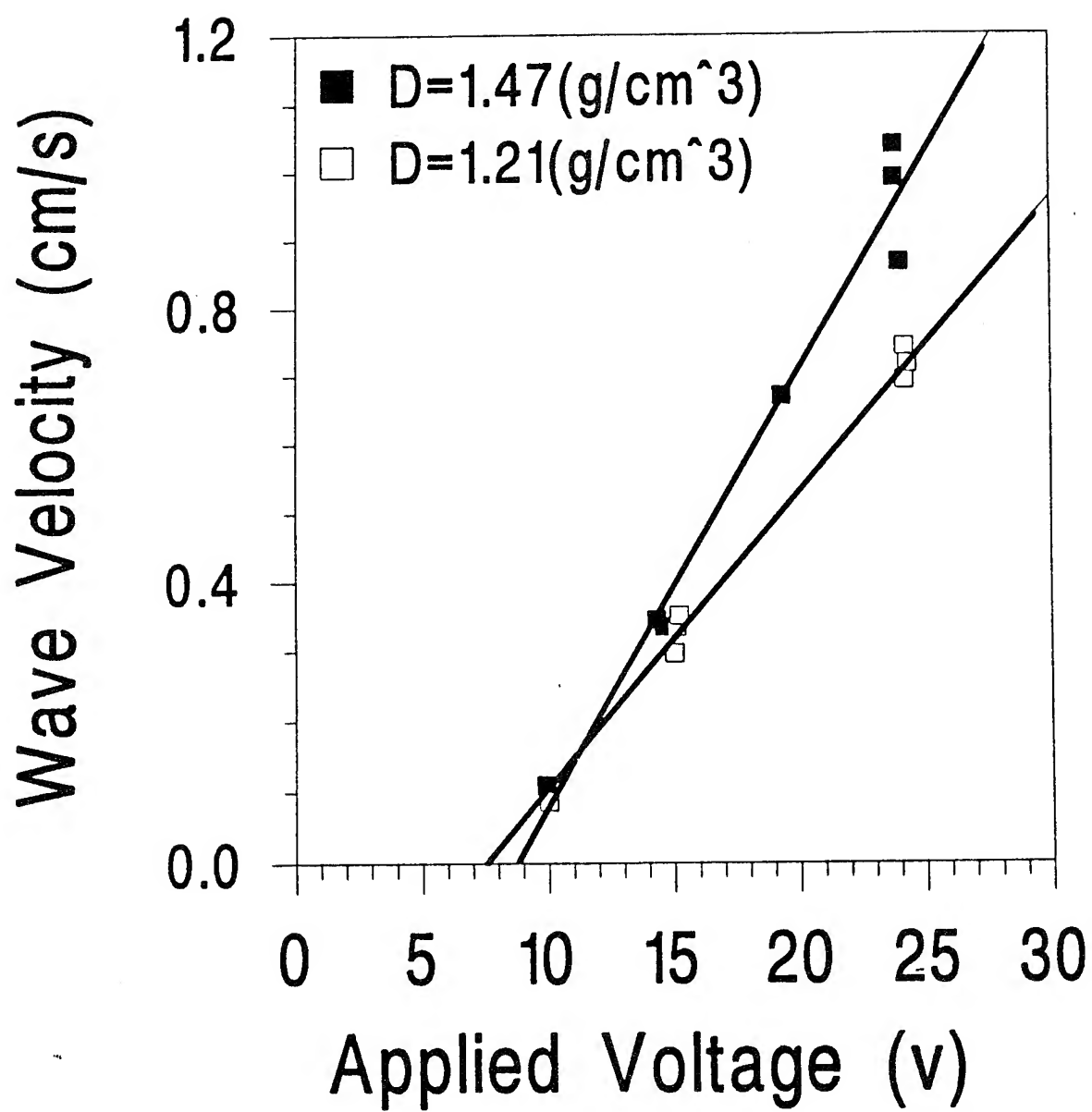


- | | | |
|-----------------|-------------------|-----------------------------------|
| * - Mo | ● - MoSi | I - Starting mixture |
| Δ - Si | ○ - SiC | II - Starting stage of conversion |
| ▲ - C | | III - Final product |

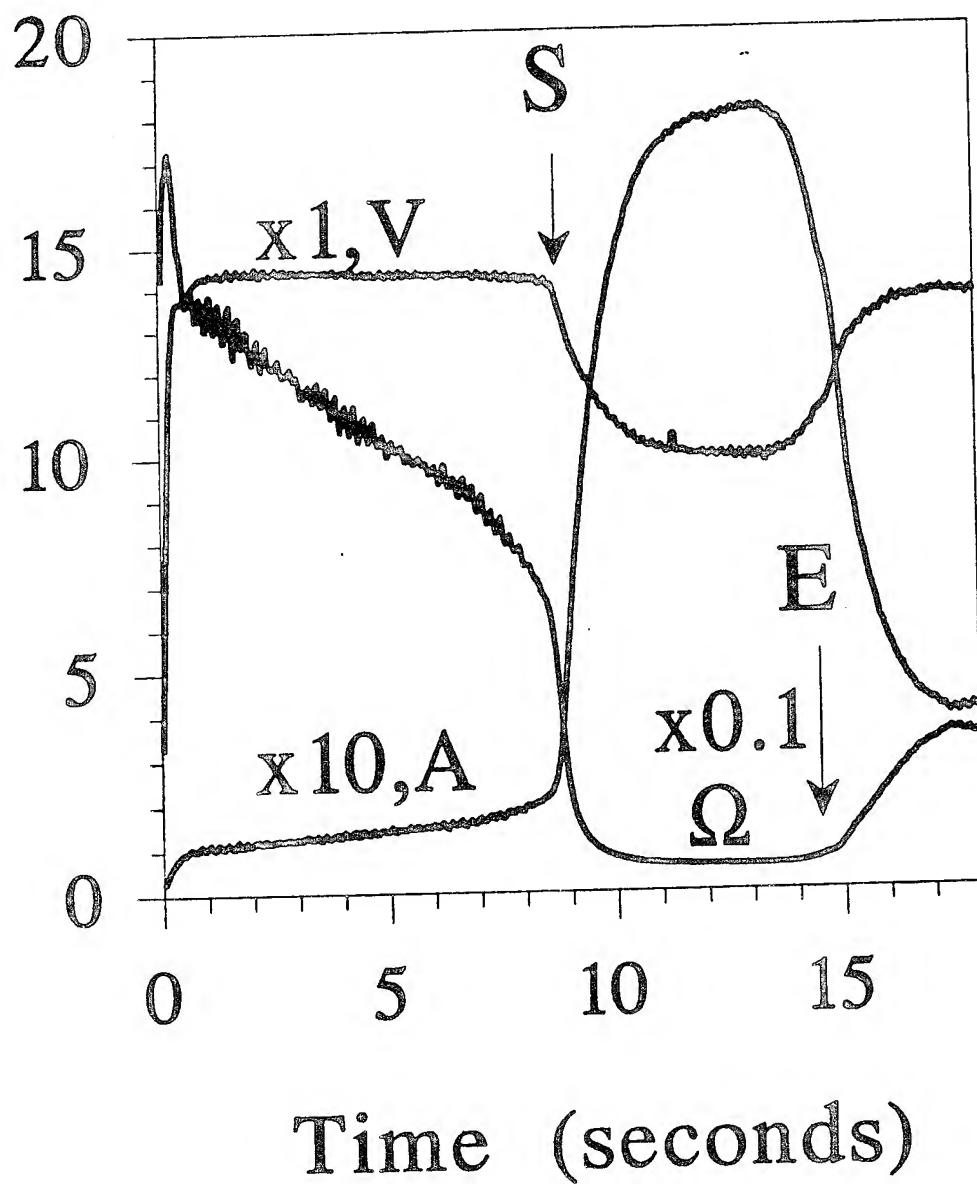


Black - Si
White - Al₂O₃

$$\text{Al}_2\text{O}_3 / \text{SiC} = 45 / 55 \text{ vol } \%$$



I, V and R



Chemistry at Static High Pressure:
Some General Principles and Recent Developments*

M. Nicol, S.M. Gibson, and D. Reifschneider

Department of Chemistry and Biochemistry
University of California Los Angeles, CA 90024-1569

We describe some classes of chemical change at high pressures and how they are detected. Many of the examples, taken largely from our laboratory, involve molecular solids which are more susceptible to pressure because of low initial densities and high compressibilities. The driving force, $P\Delta V$, lowers the free energy of denser configurations; corresponding volume of activations influence the kinetics of changes. The simplest transformations rearrange molecular packing. At 0.7 GPa, competition between inter- and intra- molecular F-F repulsions converts Teflon from a helical to a planar zig-zag structure.¹ Although CO and N₂ have essentially identical low pressure phases, CO polymerizes irreversibly above 5 GPa;^{2,3} and N₂ is diatomic to above 100 GPa. The high pressure chemistries of oxygen and sulfur show similar contrasts. O₂ remains diatomic in all high pressure phases, although spectra indicate unusual bonding and electronic structures.⁴⁻⁷ α -S₈ undergoes many structural and photochemical transformations, involving other molecular forms, to 10 GPa, although efforts to confirm reported phases and extend the diagram uncover discrepancies among studies using the same techniques, and contradictory results between techniques--even at ambient temperature.⁸⁻¹³

Naphthalene photochemistry¹⁴ led us to argue that unsaturated C=C and C=X bonds are unstable to polymerization above 10 GPa;¹⁵ and we discovered polymers forming from solid HCN¹⁶ and C₂N₂¹⁷ between 1.3 and 10 GPa. The HCN product is an azulmic acid,^{18,19} a ladder polymer produced by base-catalyzed anionic polymerization of HCN, electric discharges through CH₄-NH₃, or ⁶⁰Co irradiation of aqueous cyanide. The black product recovered from C₂N₂ at 10 GPa is a similar ladder polymer. The mechanisms of these reactions at high pressures are not established.

Raman and inelastic neutron spectra (INS) of TATB at high pressures show that the nitro substituents are perturbed by hydrogen bonds to amine groups.²⁰ The coupling between lattice phonon modes and higher energy vibrational modes, promoted by hydrogen bonding, has been suggested as a mechanism for depositing the mechanical energy of a shock wave in a detonation.²¹ Exactly how this is accomplished is not known. We have compared TATB with o-nitroaniline (ONA) and p-nitroaniline (PNA) to define the sources of the perturbations. Raman and INS studies of ONA, PNA, and the ring or amine perdeuterated isotopomers (ONA-d₄, ONA-Nd₂, PNA-d₄, and PNA-Nd₂) at high pressures also detect phase changes and variations of the mode coupling between phases. IR spectra at ambient pressure of the nitroanilines in Ar at 20 K or thin films at ambient to 20 K aid in interpreting the high pressure spectra.²² The lack of good normal-mode bases is a problem in interpreting the spectra. The ring, nitro, and amine modes are so strongly mixed that symmetry modes of benzene derivatives are not a good basis.^{23,24} We have assigned the IR spectra of ONA and PNA in Ar matrices and PNA films at 20 K or INS spectra at 15 K by computing optimal geometries for isolated molecules with an *ab initio* routine and then calculating the normal modes and their approximate vibrational

frequencies for this geometry. PNA is especially interesting. Spectra of isolated molecules are fit better by assuming a C_s symmetry, but C_{2v} symmetry is better assignments for the solid at low temperatures or high pressures. Under ambient conditions, the PNA crystals are layered, with molecules aligned head-to-tail in layered chains and the rings tipped slightly out of the layers.²⁵ At lower temperatures,²⁶ the rings appear to flatten into the layers, improving intra-layer hydrogen bonding. The structure of ONA is not so layered; and the IR spectra of ONA in Ar can be easily correlated with spectra of ONA crystals.

Raman spectra of PNA at high pressures correspond to changes at low temperatures attributed to alignment of the rings in the layers²⁷ and, between 3.0 and 4.6 GPa, a phase transition established by Block and Piermarini.²⁶ At higher pressures, PNA undergoes further chemical or phase changes. Raman spectra collected at pressures as low as 0.8 GPa from PNA samples that had been subjected to pressures above 10 GPa differ qualitatively from spectra of PNA samples that had not been so highly pressurized, suggesting that a different form of PNA or reaction product formed at higher pressure. The conditions where this species forms are not well established; however, the process is not photochemical. The material has not yet been recovered at ambient pressure.

* Support provided by NSF grant DMR90-11076, IGPP-LANL, and the UCLA Research Committee and assistance from M. Chun, W. Karney, A. Martin, and M. Morgano are gratefully acknowledged.

1. M.F. Nicol, J.M. Wiget, and C.K. Wu, *J. Poly. Sci.: Poly. Phys. Ed.* **18** (1980) 1087-1102.
2. A.I. Katz, D. Schiferl, and R.L. Mills, *J. Phys. Chem.* **88** (1984) 3176.
3. C.S. Yoo, *Ph. D. Dissertation* (University of California, Los Angeles, 1987).
4. M. Nicol and K. Syassen, *Phys. Rev.* **B28** (1983) 1201-1206.
5. S.F. Agnew, B.L. Swanson, and L.H. Jones, *J. Chem. Phys.* **86** (1987) 5239-52.
6. S. Desgrenies, Y.K. Vohra, and A.L. Ruoff, *J. Phys. Chem.* **94** (1990) 1117.
7. S.W. Johnson, M. Nicol, and D. Schiferl, *J. Appl. Cryst.* **26** (1993) 320-326.
8. G. Vezzoli, F. Datchile, and R. Roy, *Science* **166** (1969) 218.
9. K. Nagata, et al., *Jpn. J. Appl. Phys.* **31** (1992) 1078-1084.
10. P. Wolf et al., Cynn, in P. Pucci and G. Piccitto, eds., *Molecular Systems Under High Pressure* (North-Holland, Amsterdam, 1991), 263-271.
11. Y. Akahama, M. Kobayashi, and H. Kawamura, *Bull. Amer. Phys. Soc.* **38** (1993) 1598.
12. H. Luo and A.L. Ruoff, *Bull. Amer. Phys. Soc.* **38** (1993) 1570.
13. B. Eckert, et al., in H.D. Hochheimer and R.D. Etters, eds., *Frontiers of High-Pressure Research* (Plenum, New York, 1991), 143.
14. G.Z. Yin and M. Nicol, *J. Phys. Chem.* **89** (1985) 1171.
15. M. Nicol and G.Z. Yin, *J. de Physique* **45** (1984) C8-163.
16. K. Aoki, B.J. Baer, H.C. Cynn, and M. Nicol, *Phys. Rev.* **42** (1990) 4298.
17. C.S. Yoo, and M. Nicol, *J. Phys. Chem.* **90** (1986) 6726; **90** (1986) 6732.
18. K. Aoki and M. Sakashitani (private communication).
19. C.N. Matthews, *Origins of Life and Evolution of the Biosphere* **21** (1992) 421-434.
20. S.K. Satija, B.I. Swanson, J. Eckert, and J.A. Goldstone, *J. Phys. Chem.* **95** (1991) 10103.
21. D. Dlott and M. Fayer, *J. Chem. Phys.* **92** (1990) 3798.
22. M. Nicol et al., in M. Kamo, H. Kanda, Y. Matsui, and T. Sekine, eds., *Advanced Materials '94* (Intl. Communications Specialists, Tokyo, 1994) pp 205-210.
23. See, for example, D. Kumar et al., *Vibrational Spectros.* **4** (1992) 39.
24. E.W. Schmid et al., *Z. Elektrochemie* **64** (1960) 940.
25. K. Trueblood, *Acta Cryst.* **14** (1961) 1009.
26. S. Block and G.J. Piermarini, *SPIE Proceedings* **878** (1988) 21.
27. G.S.R. Krishna Murti, *Indian J. Phys.* **31** (1957) 353.

Chemistry at Static High Pressure:
Some General Principles and Recent Developments

Malcolm Nicol, Suzanna M. Gibson,
and Diane Reifschneider

The driving force of high pressure chemistry, $P\Delta V$

The simplest changes: molecular packing of Teflon,
 N_2 , O_2

Unstability unsaturated $C=C$ and $C=X$ bonds yield
New Polymers (CO , HCN , C_2N_2) and Photoproducts
(Naphthalene, $\alpha-S_8$)

Nitroanilines and the chemistry of TATB

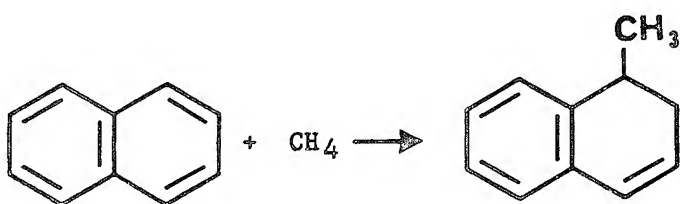
Support provided by NSF grant DMR90-11076,
IGPP-LANL, and the UCLA Research Committee
and assistance from M. Chun, W. Karney, A. Martin,
and M. Morgano are gratefully acknowledged.

The driving force of high pressure chemistry:

The chemical potential: $\Delta\mu = \Delta H - T\Delta S + P\Delta V$

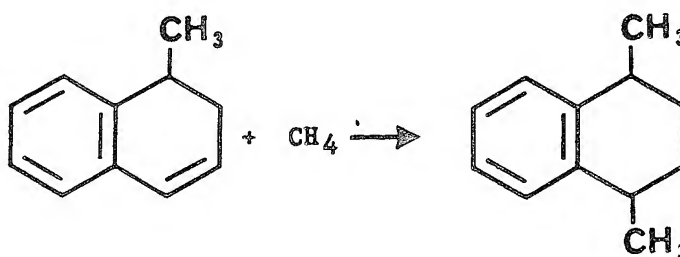
$$1 \text{ GPa cm}^3 \text{ mol}^{-1} = 10^9 \text{ N m}^2 \cdot 10^{-6} \text{ m}^3 \text{ mol}^{-1} \\ = 10^3 \text{ N m mol}^{-1} = 1 \text{ KJ mol}^{-1}$$

$\Delta V/(\text{cm}^3 \text{ mol}^{-1})$	$P/(\text{GPa})$	$\Delta\mu/(\text{KJ mol}^{-1})$
-1.00	1	-1.00
-1.00	10	-10.0
-10.00	10.0	-100



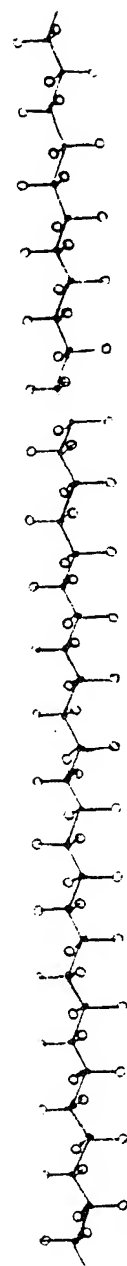
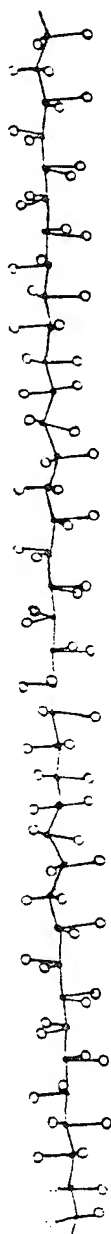
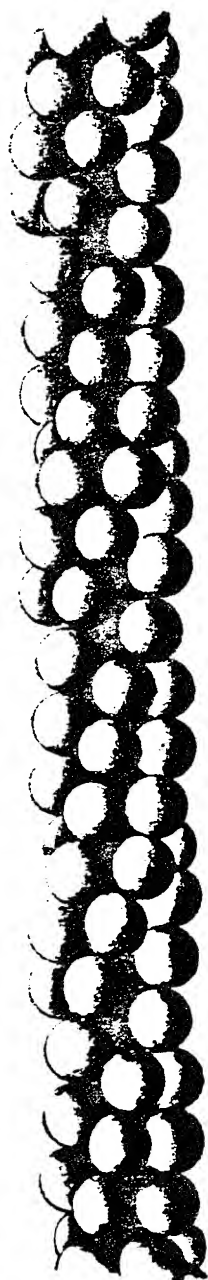
$$\Delta H^\circ \sim + 100 \text{ kJ/mol}$$

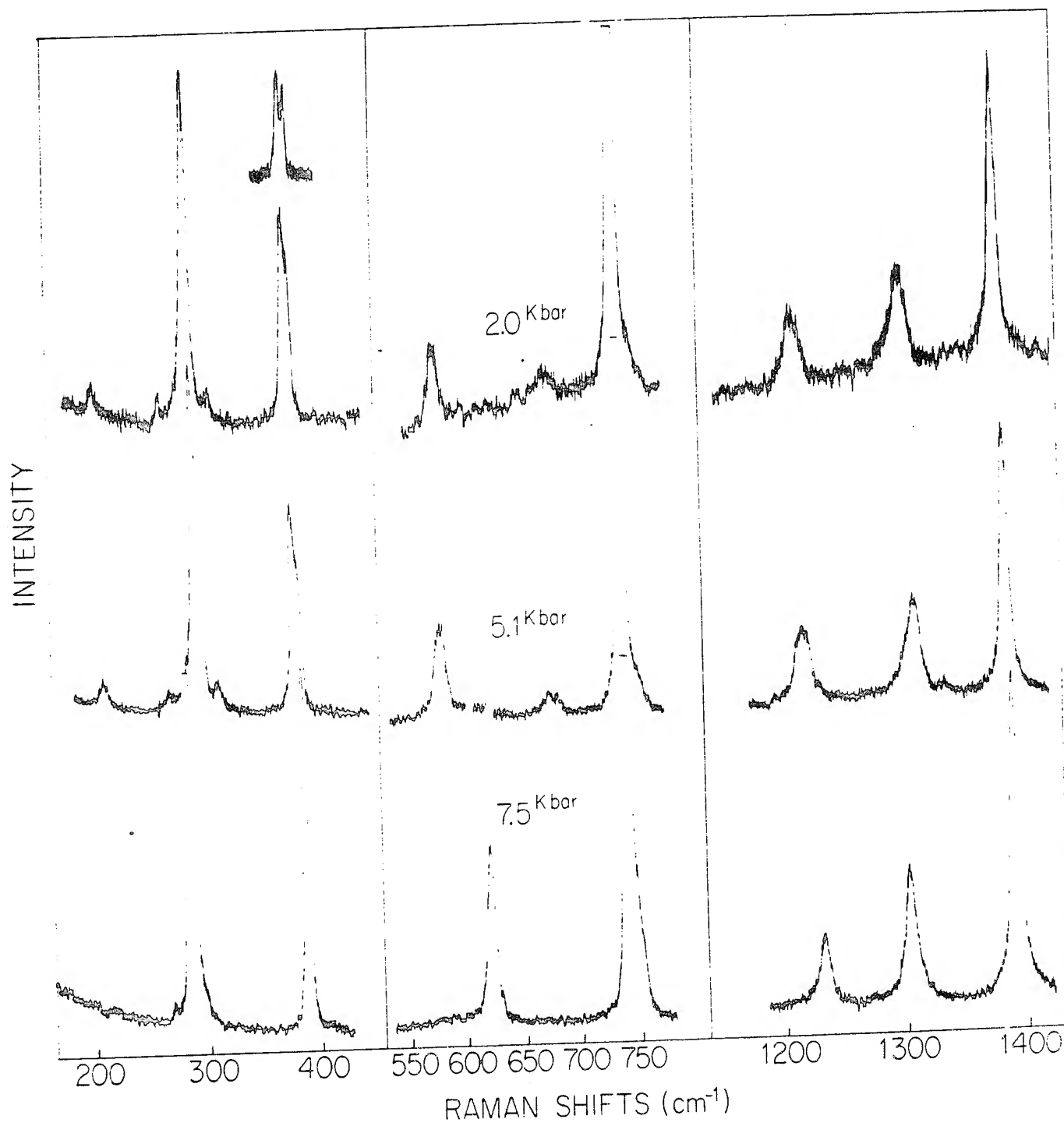
$$\Delta V^\circ \sim - 10 \text{ to } -20 \text{ cm}^3/\text{mol}$$

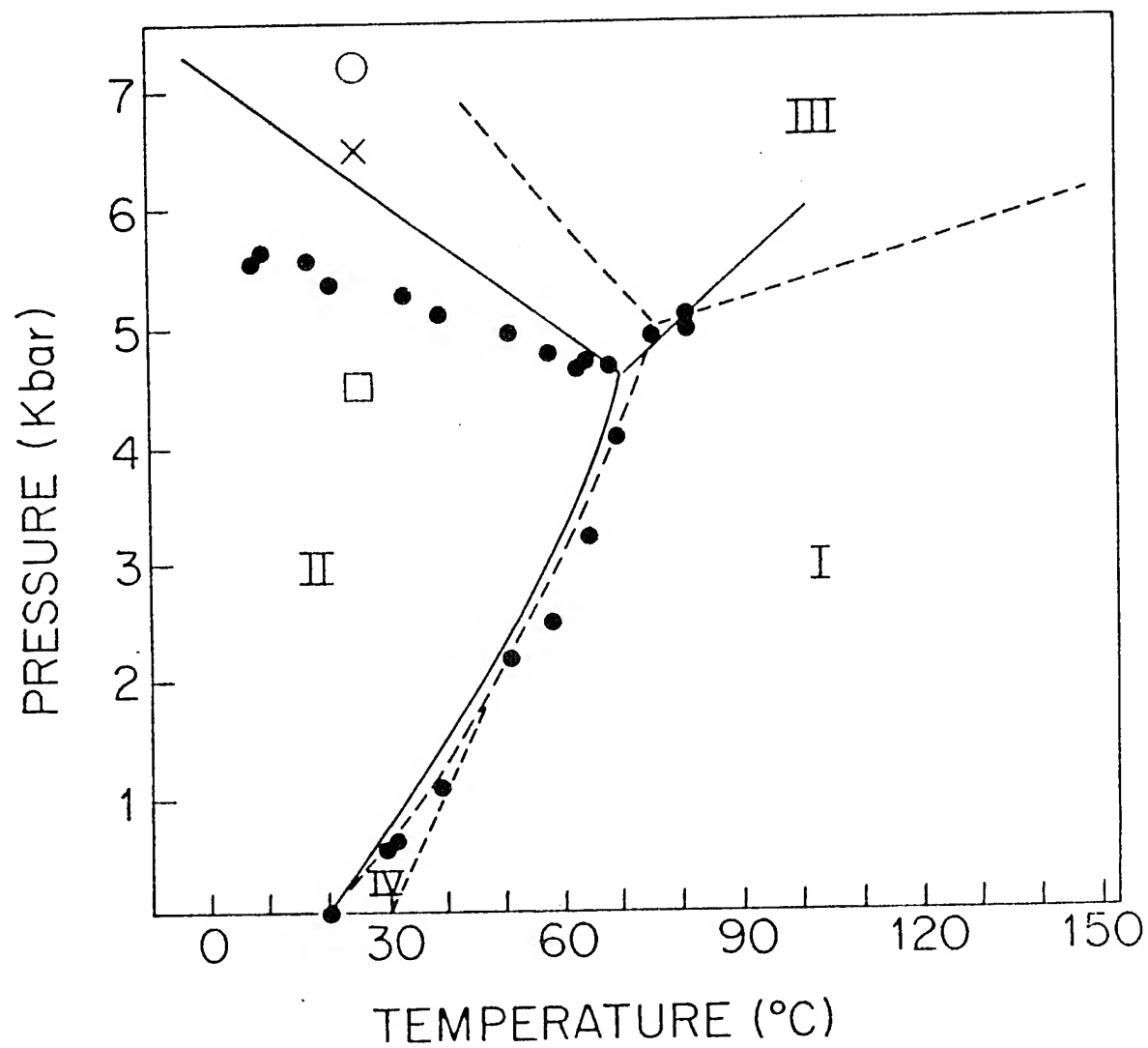


$$\Delta H^\circ \sim - 130 \text{ kJ/mol}$$

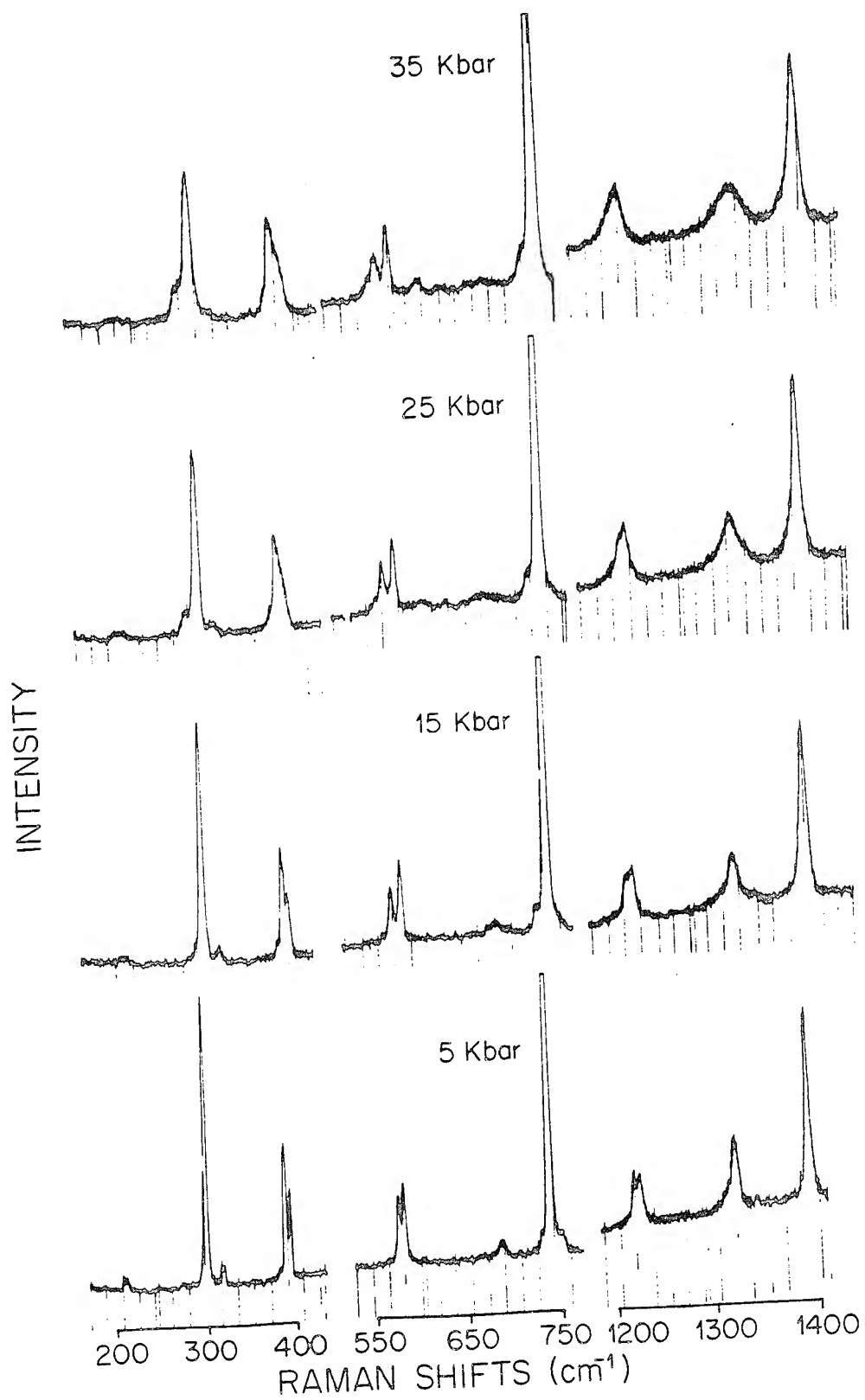
$$\Delta V^\circ \sim - 10 \text{ to } -20 \text{ cm}^3/\text{mol}$$



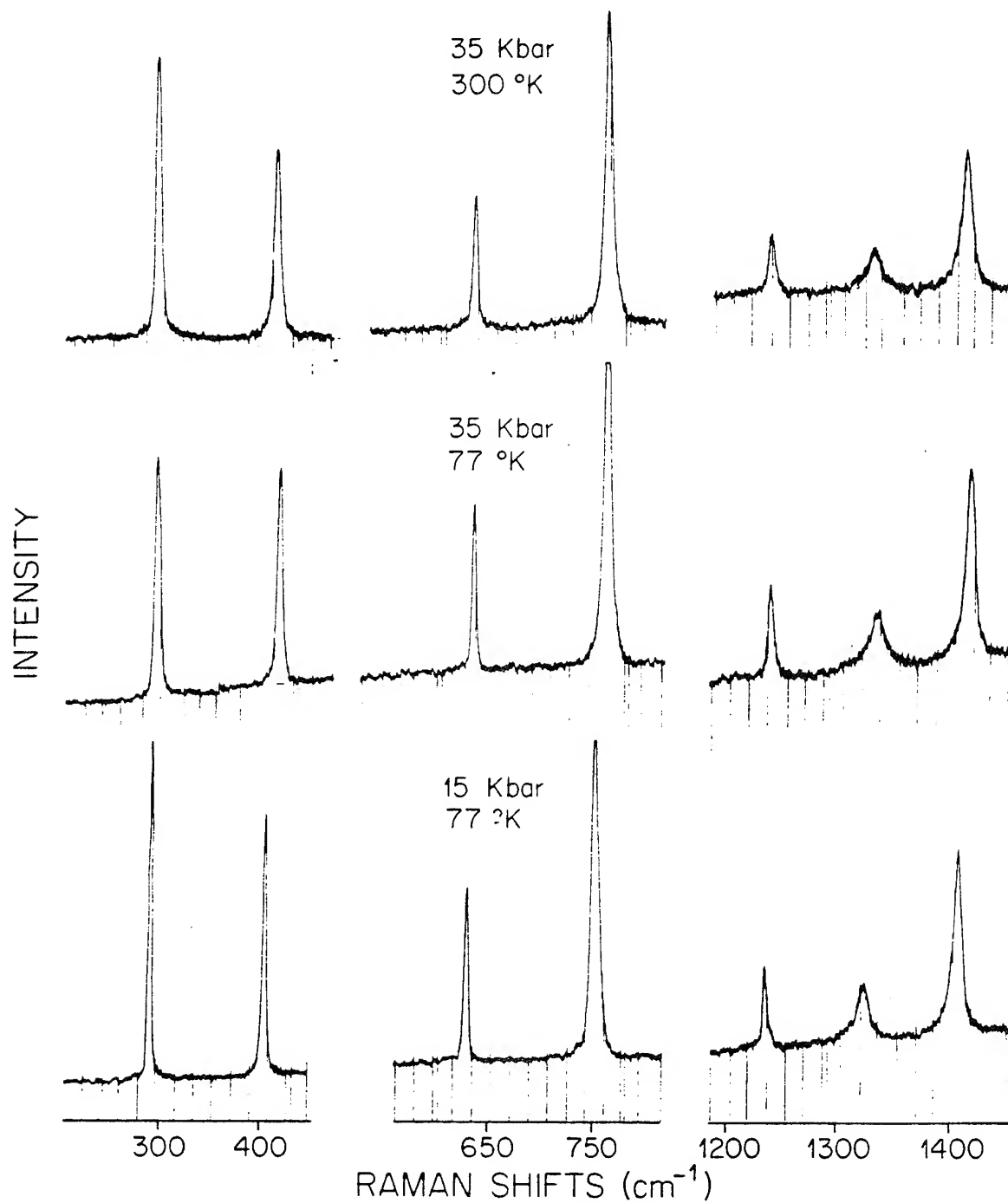




COMPRESS AT 77 K



CCCL AT HIGH P AND RELEASE AT 77K.



$$x(t) = \frac{I_2(t)}{I_2(t) + I_3(t)}$$

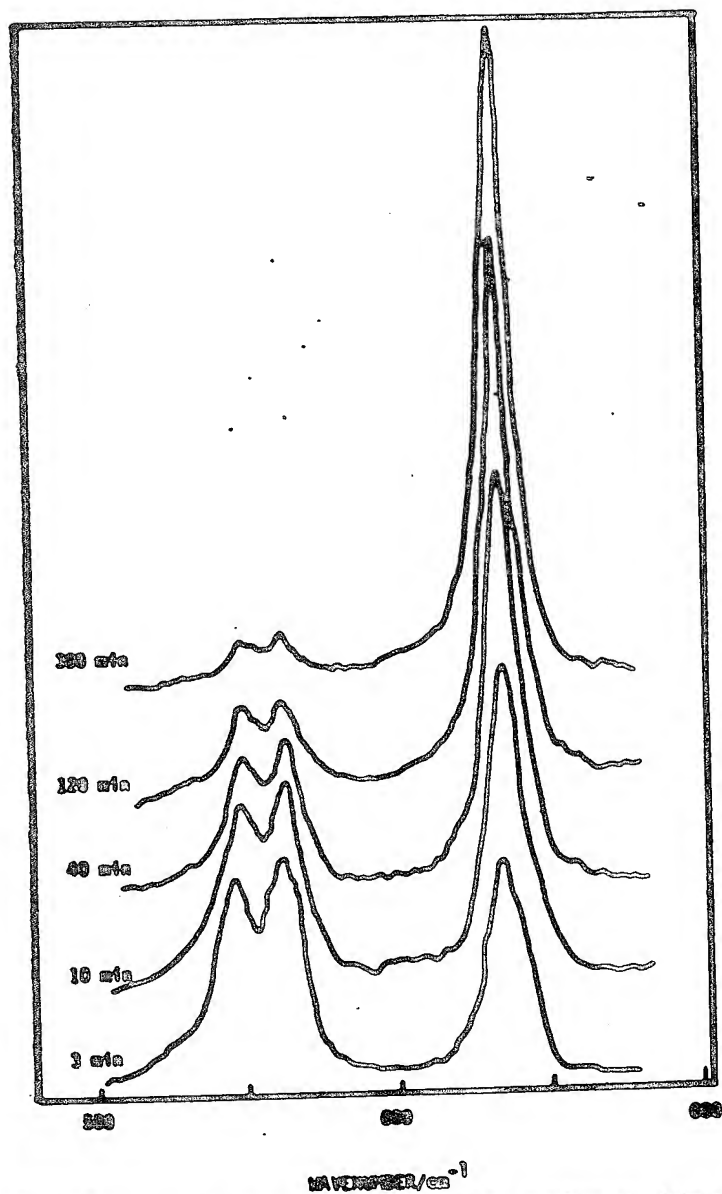


Fig. 3. Raman spectra of the 575 and 690 cm⁻¹ lines as a function of time.

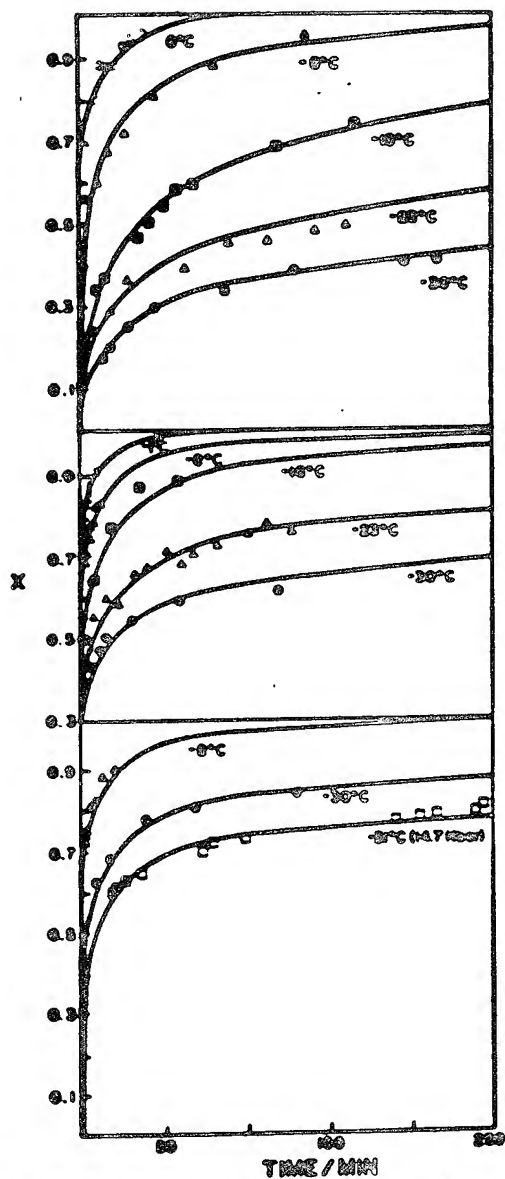


Fig. 4. Kinetic data for the PTFE II-III transformation at several pressures and temperatures: upper: 10 kbar at 0, -8, -15, -23, and -30°C; middle: 12 kbar at -1, -8, -16, and -30°C; lower: 14 kbar at -6 and -30°C and 14.7 kbar at -31°C. In each plot, the data for the highest temperature are the uppermost to the left.

PLOTS OF $\ln k$ vs T^{-1} AND P

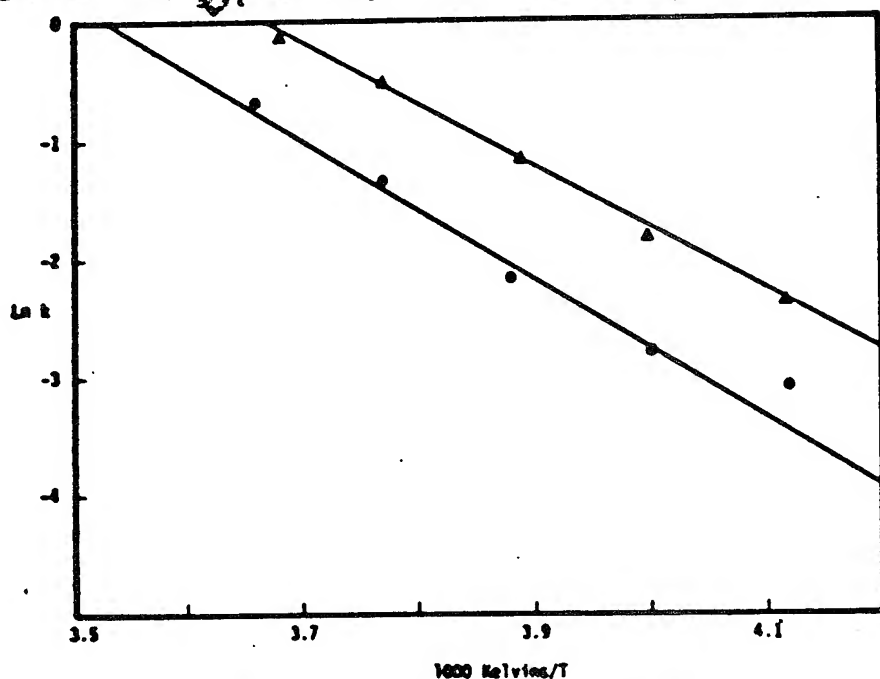


Fig. 9. Plot of $\ln k$ vs. $1/T$ for (●) 10 and (▲) 12 kbar.

TABLE II
Avrami Rate Constants for an Exponent of 0.5

Temperature (°C)	Pressure (kbar)			
	9	10	12	14
0		0.51	0.87	
-8		0.26	0.59	0.69
-15		0.11	0.30	
-23		0.060	0.16	
-30	0.009	0.045	0.09	0.16
-31				0.13 (14.7 kbar)

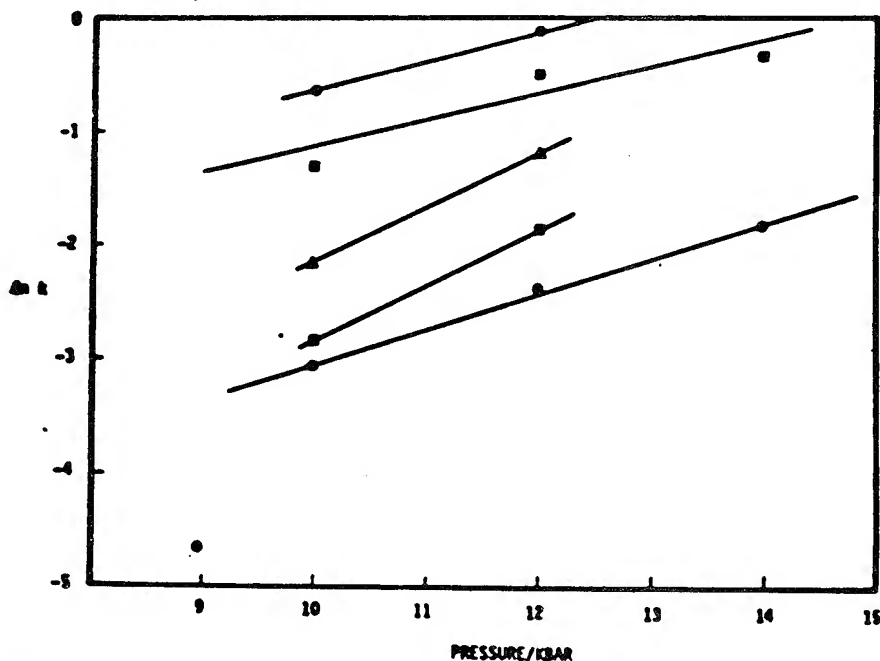


Fig. 10. Plots of $\ln k$ vs. P for (○) 0°C, (■) -8°C, (▲) -15°C, (□) -23°C, (■) -30°C.

ENTHALPY OF
ACTIVATION

$$\Delta H^\ddagger \approx 11 \text{ kcal/mole CF}_2$$

VERY LARGE

VOLUME OF
ACTIVATION

$$\Delta V^\ddagger \approx -7 \text{ cm}^3/\text{mole CF}_2$$

ABOUT $\frac{1}{3}$ OF
POLAR VOLUME.

TWO POSSIBLE INTERPRETATIONS

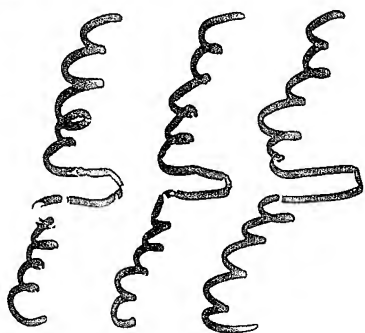
PHASE II HAS "TWIST" REVERSAL POINTS:



- REVERSAL POINT WHICH MUST "UNWIND"

EITHER REVERSAL POINT IS "BULKY", THAT IS, "LARGE", AND CAN UNWIND ONLY BY "PUSHING" BACK NEIGHBORS (LARGE ΔV^\ddagger , ΔH^\ddagger ON ONE MOLECULE).

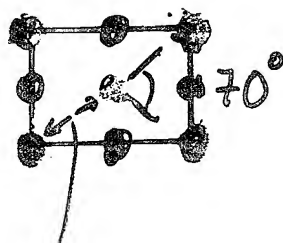
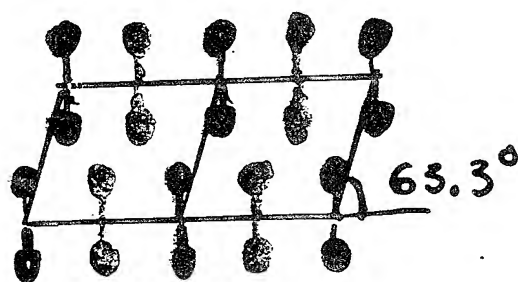
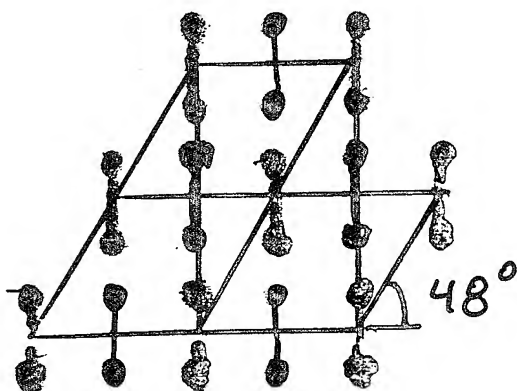
OR REVERSAL POINTS ON SEVERAL MOLECULES "CONDENSE" IN ONE PLANE



MANY MOLECULES TRANSFORM TOGETHER

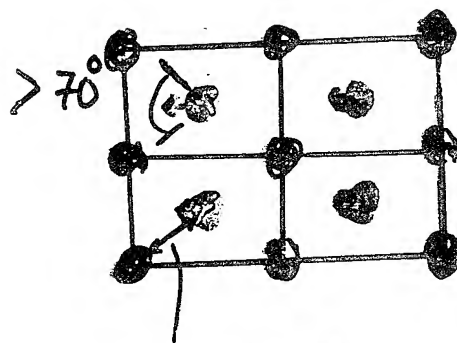
(SMALL ΔV^\ddagger , ΔH^\ddagger / MOLECULE) X MANY MOLECULES
= LARGE ΔV^\ddagger , ΔH^\ddagger

[illegible]



2.57 Å

9.6 GPa

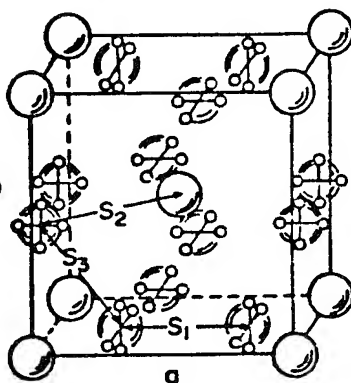


< 2.36 Å

19.6 GPa

PHASE DIAGRAM OF N_2

IN HIGH PRESSURE
 N_2 PHASE, MOLECULES
REORIENT RAPIDLY!



ONE 100
MILLION
ATMOSPHERES

PRESSURE (GPa)

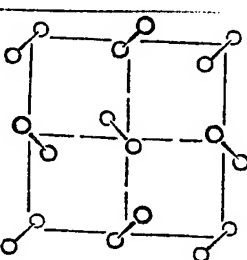
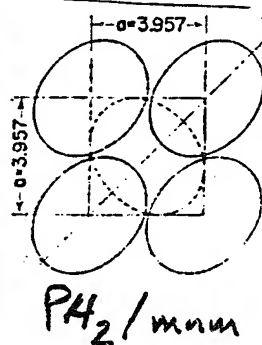
"Pm3n"

$P4_2/mnm$

$P6_3/mmc$

FLUID
 N_2

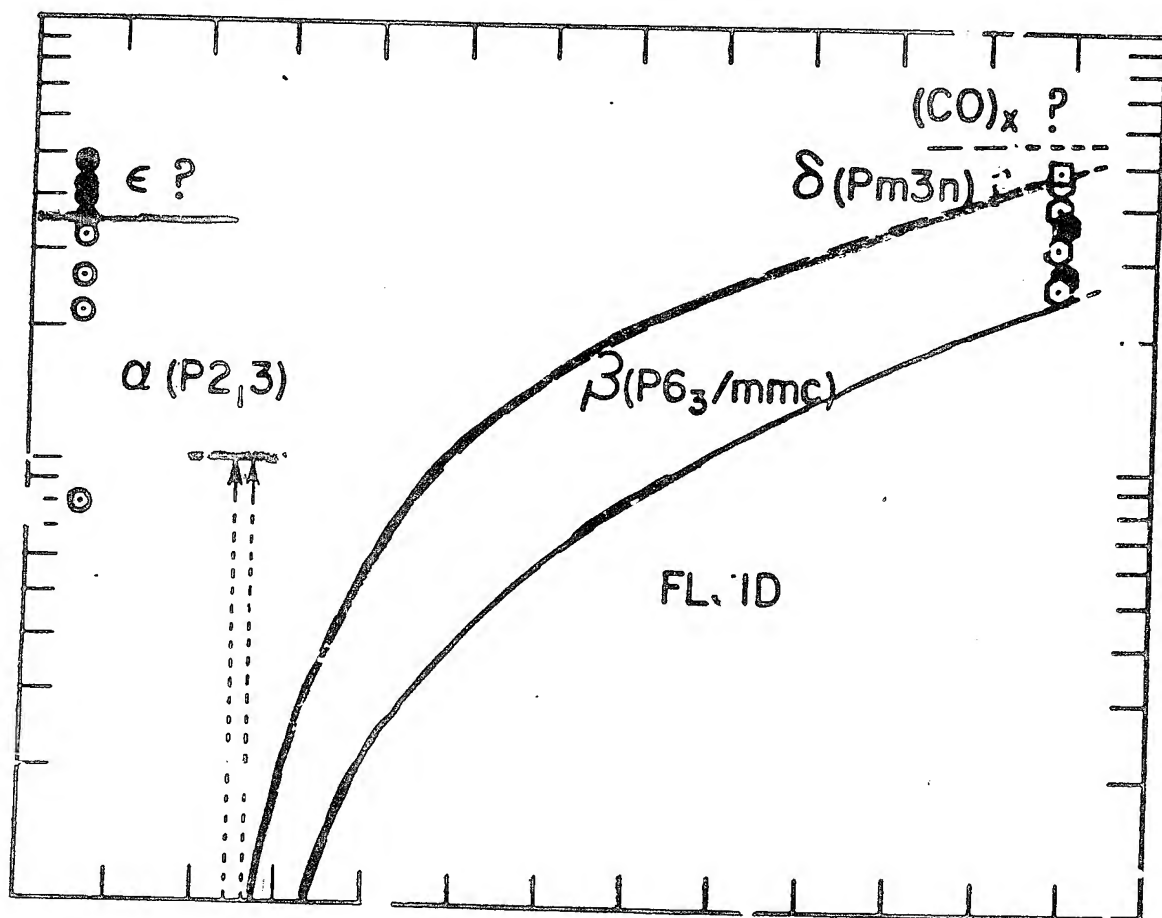
$Pa3$



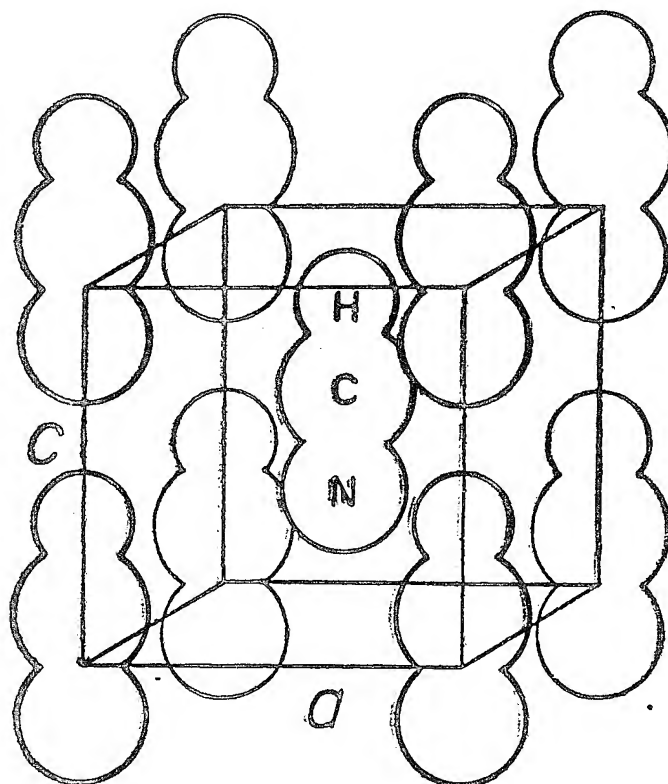
$Pa3$

TEMPERATURE (K)

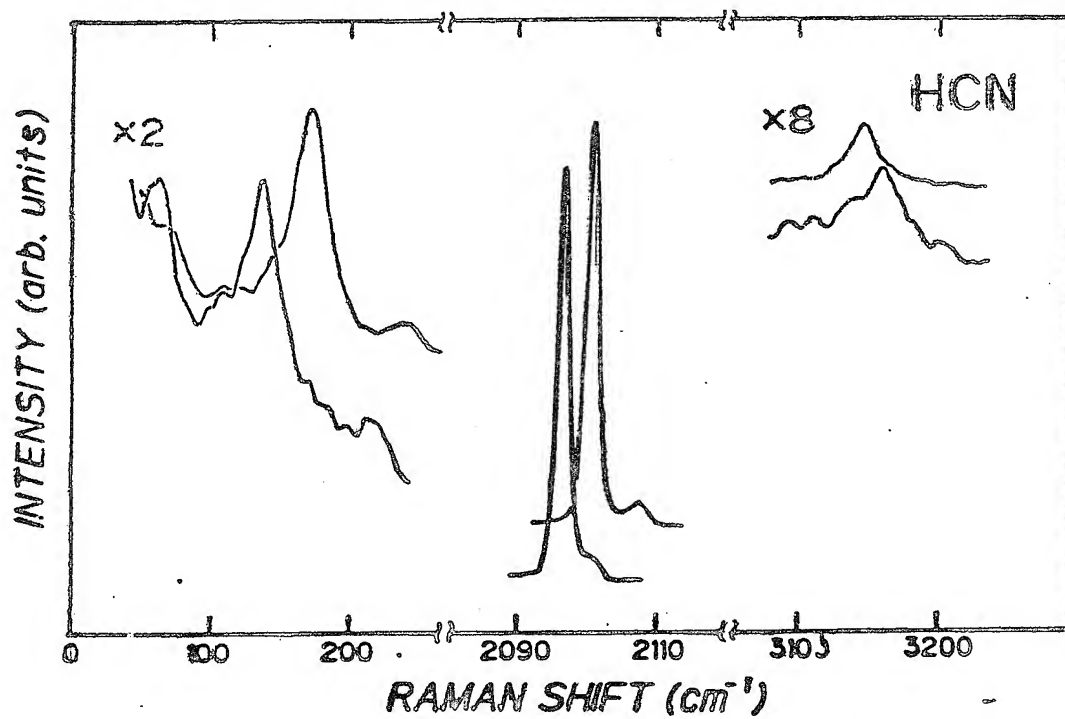
STRUCTURES OF $P4_2/mnm$
AND $Pa3$ PHASES ARE
DETERMINED BY G-G
INTERACTION.



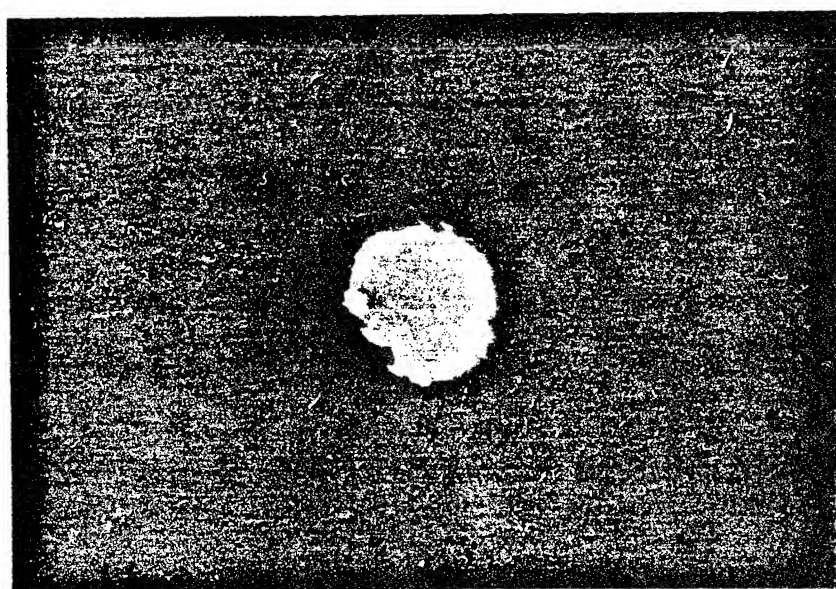
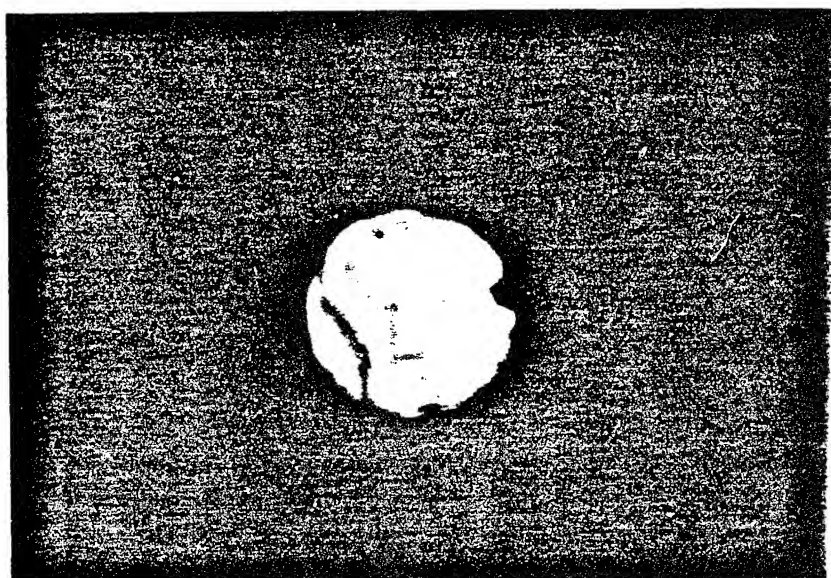
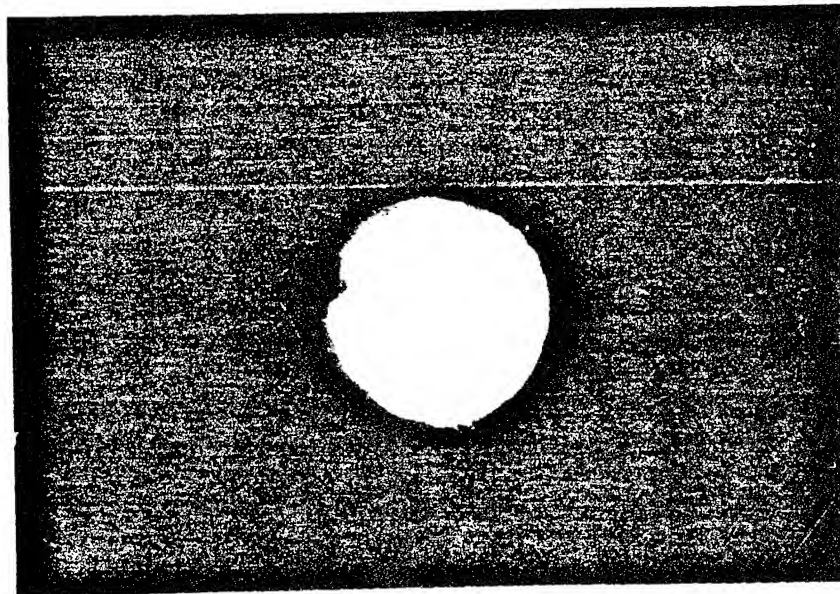


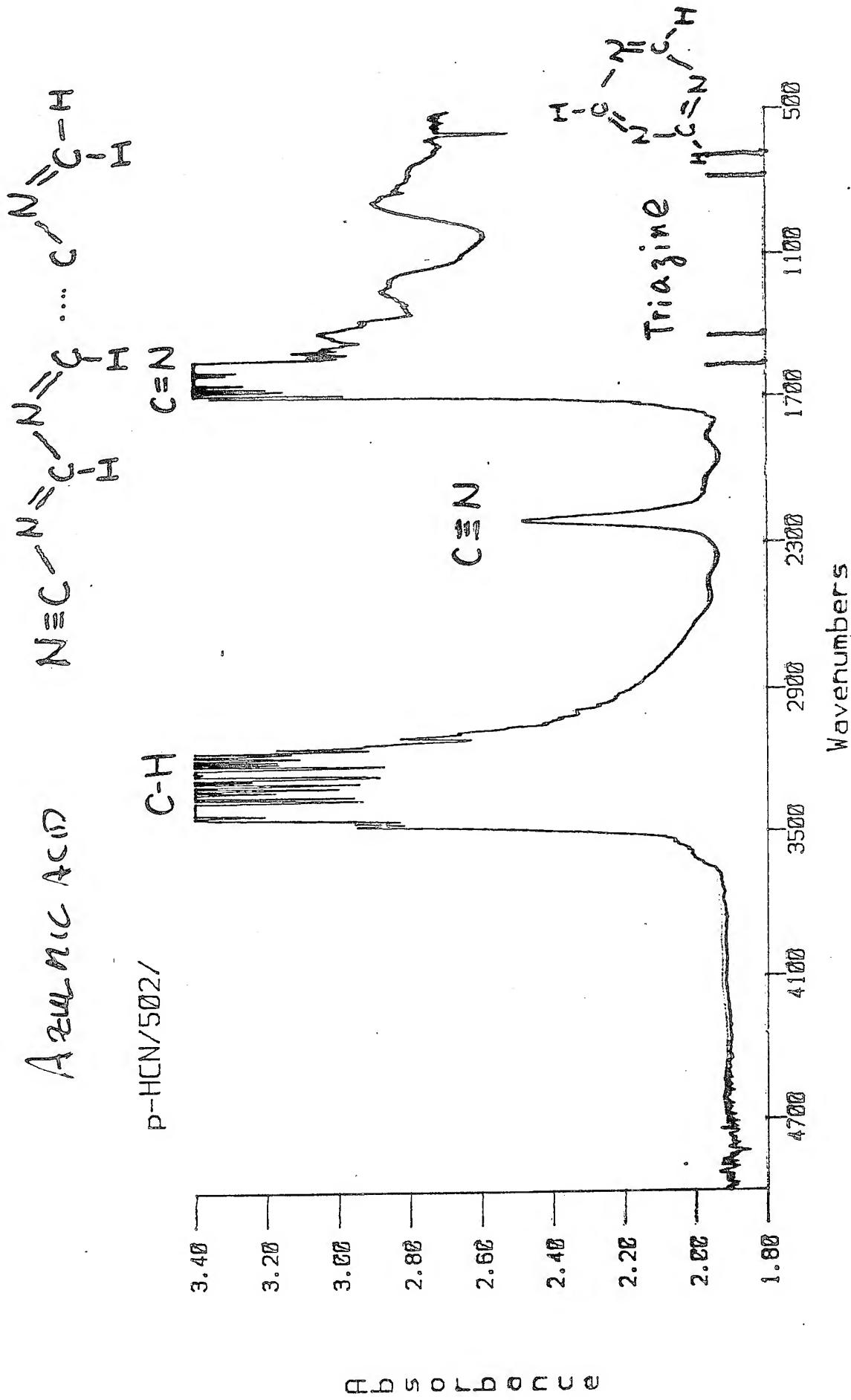


The crystal structure of body-centered tetragonal HCN



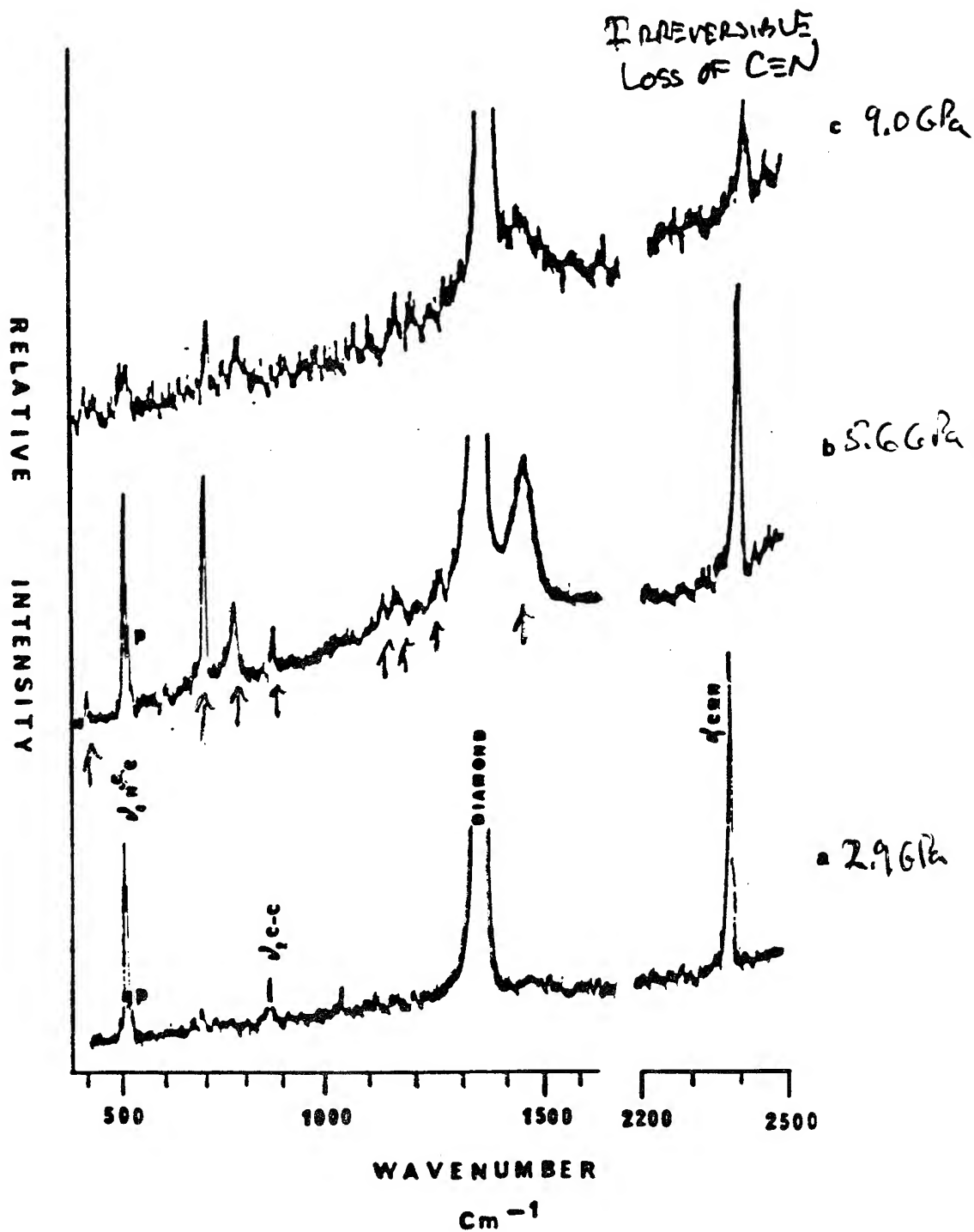
Raman Spectra of BCT (lower) and Orthorhombic (Lower) HCN



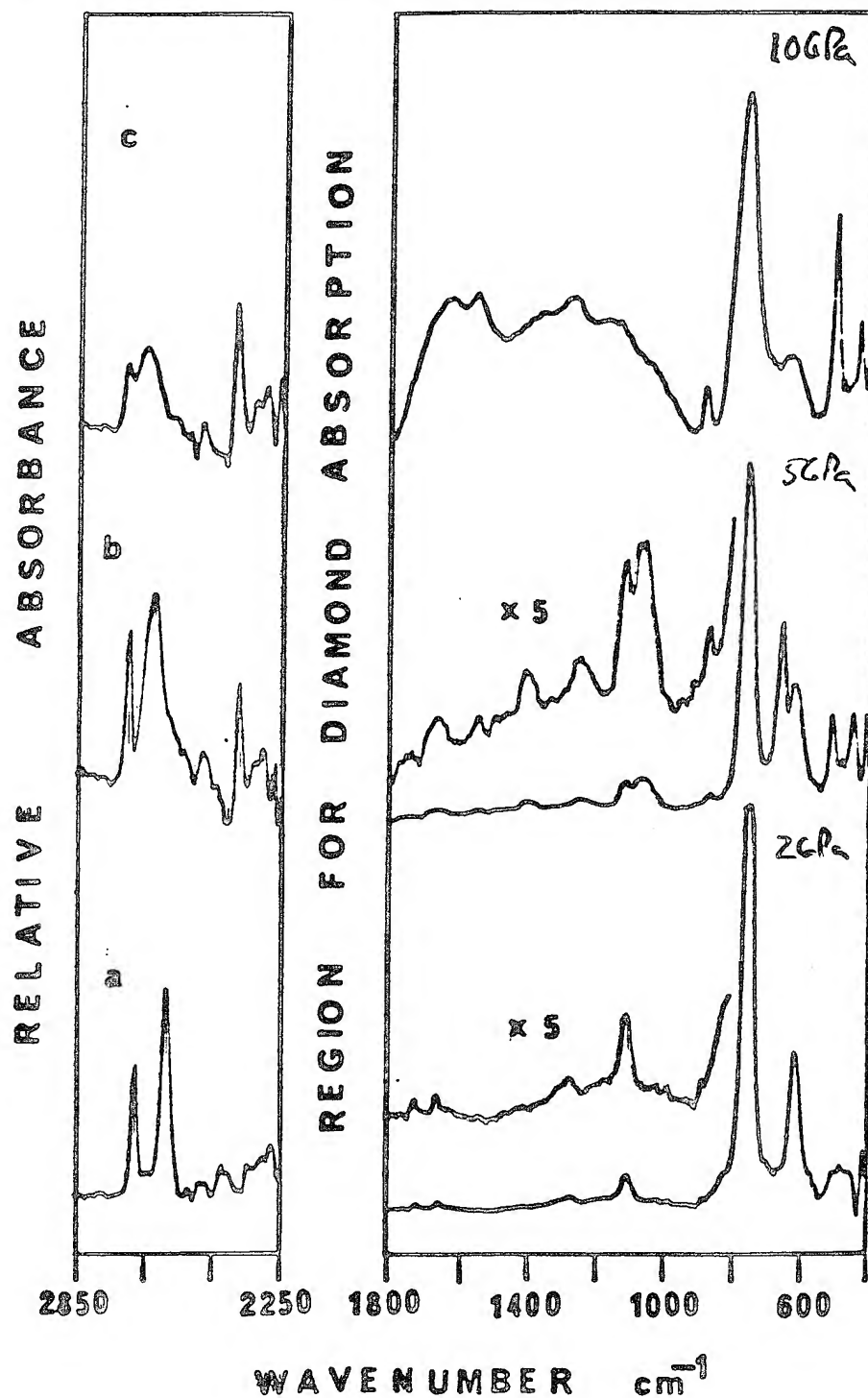


pHCN502.abs

RAMAN SPECTRA OF C_2N_2

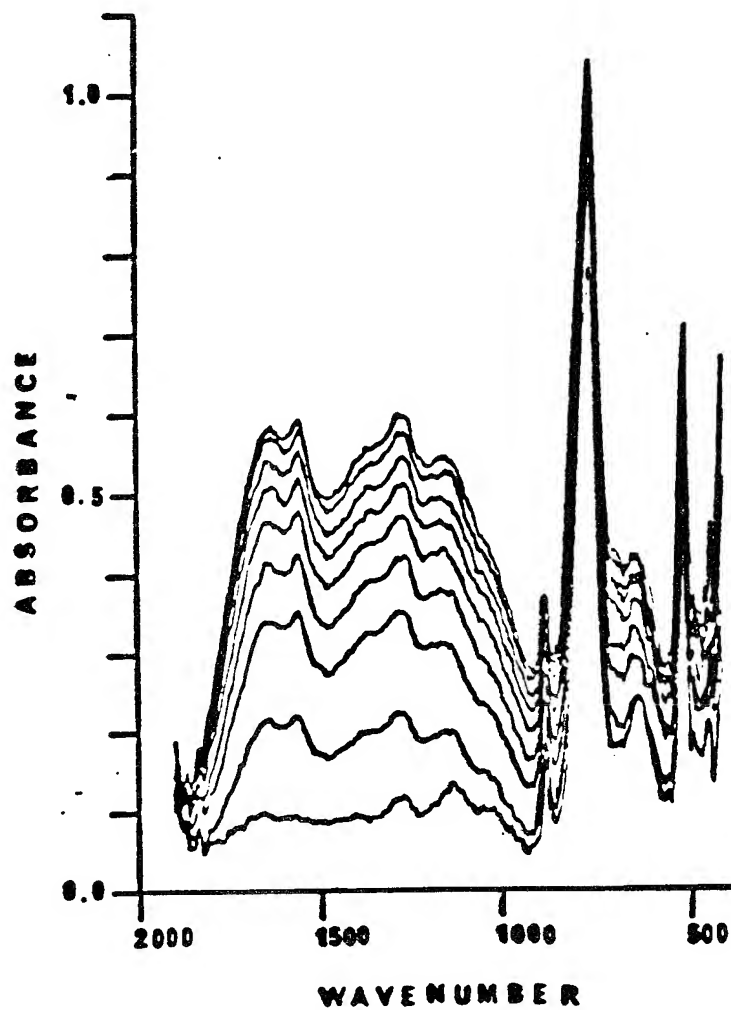


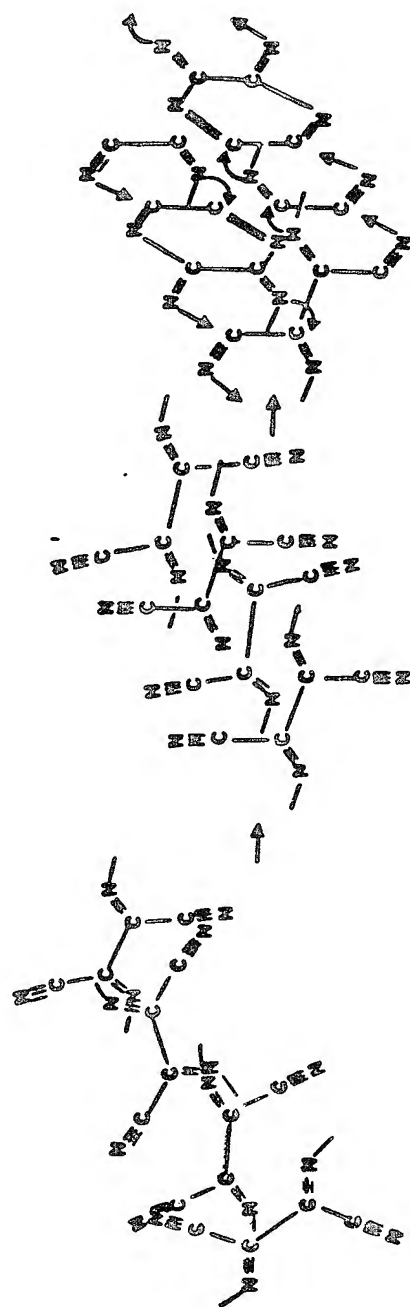
COMPARABLE CHANCES OF FIVE SPECTRA OF C_2N_2
 MANY NEW FEATURES ARE NEAR FEATURES
 OF RAMAN SPECTRA AT THE SAME P.

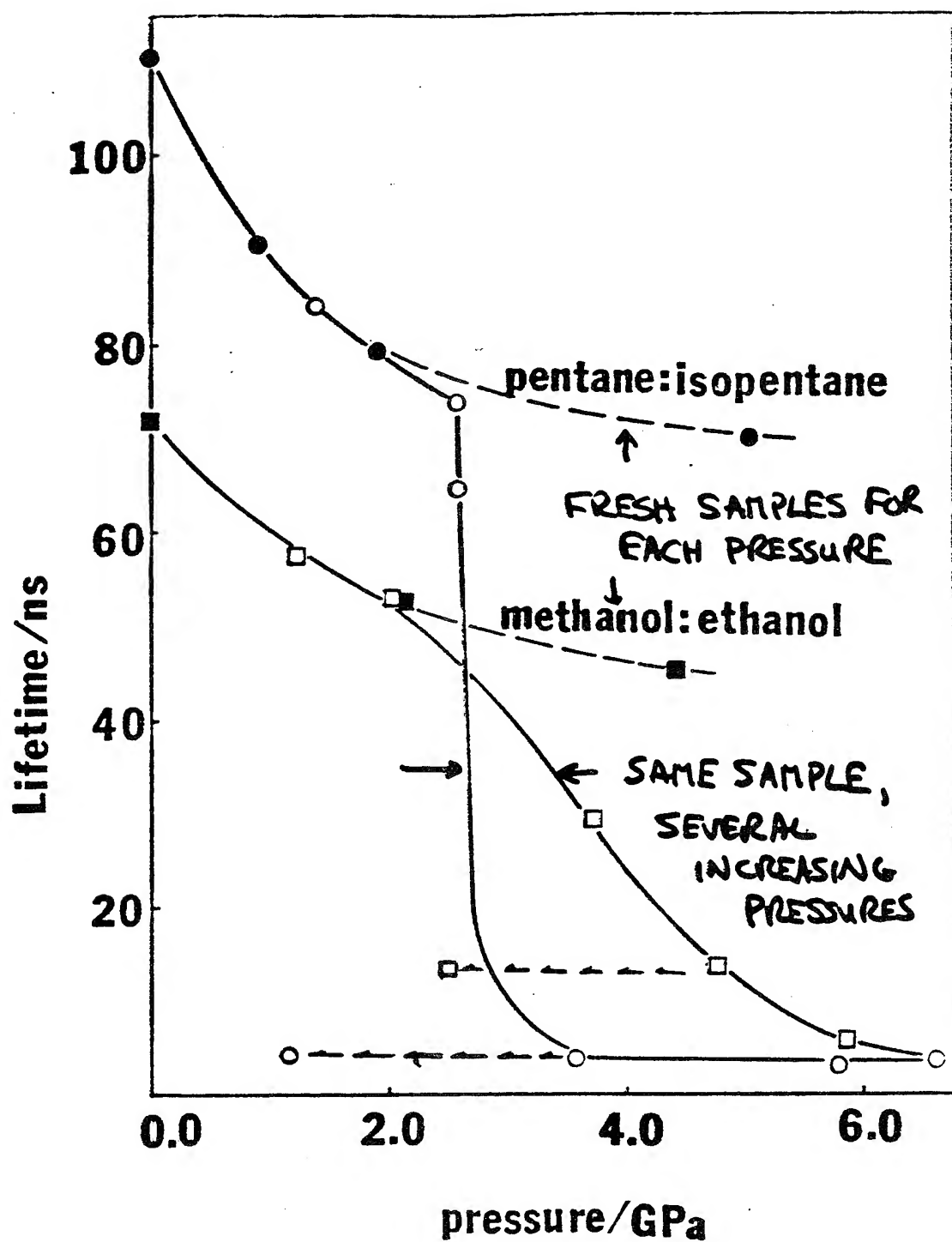


PRESSURE JUMP FTIR EXPERIMENTS WITH P-DISN

116Pa

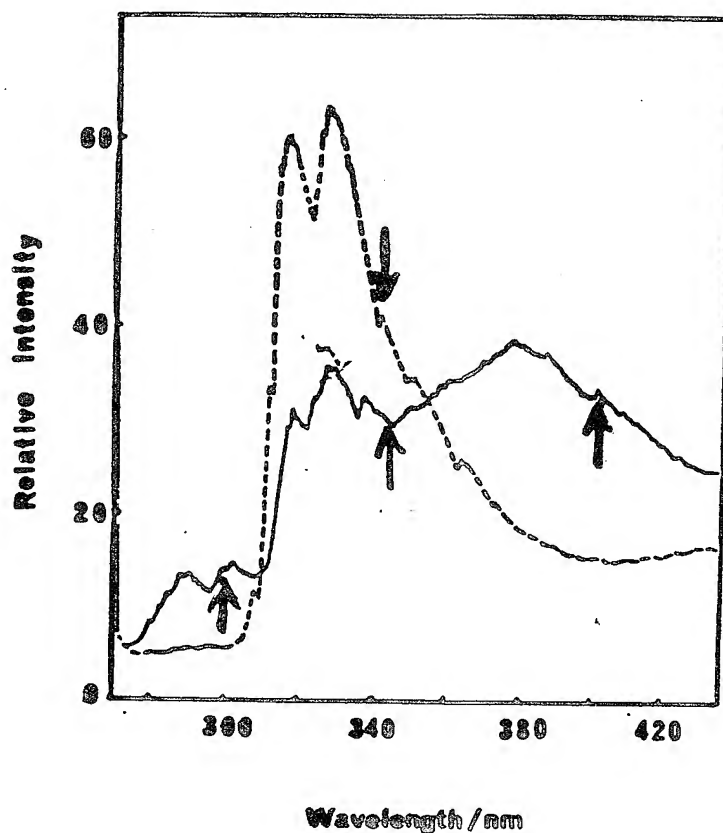






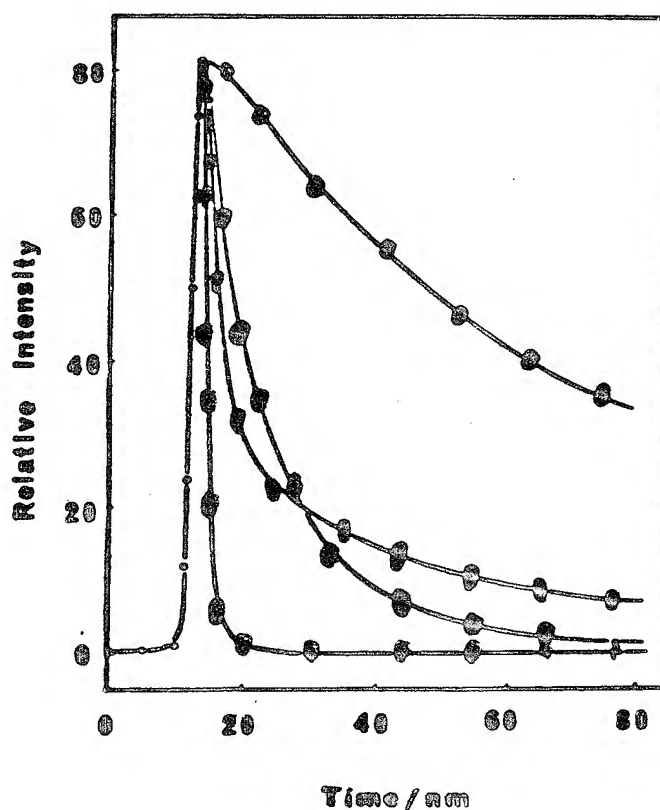
UV exposure and pressure dependence of naphthalene fluorescence lifetime τ_s in both alkane (P:I, 1:1) and alcohol (M:E, 4:1) solution.

Fluorescence (excitation: 270 nm) of 5×10^{-2} M naphthalene in 1:1 pentane:isopentane at 5 GPa before (dashed curve) and after (solid curve) 26-hours irradiation at 290 nm.



Fluorescence kinetics of 5×10^{-2} M naphthalene at 5 GPa in methanol:ethanol:

Excitation: 270 nm
 Observed:
 Before irradiation
 at 340 nm ●
 After irradiation
 at 340 nm ●
 400 nm ●
 298 nm ●



SHOCK CHEMISTRY MECHANISMS, KINETICS, AND APPLICATIONS

A.N. Dremín

Head of High Dynamic Pressure Department
Institute of Chemical Physics (Chernogolovka)
Russian Academy of Sciences Moscow Region
Chernogolovka 142432, Russia

Investigations of different relaxation phenomena, chemical reaction, polymorphic transformations, change of electrical, and optical properties, loss of strength of condensed matter under shock wave effects is the main area of investigation in our department. Characteristic times of these phenomena are often comparable with the shock loading time.

New successful applications of explosion energy includes metal treatments (welding, strengthening, stamping, ...), super-hard materials synthesis, and studies of shock wave effects such as polarization and anisotropy of brittle materials, and electro-conductivity. In the very beginning of the investigations, the intent was to reveal the mechanism of ideal condensed explosives detonation decomposition phenomenon and the mechanism of polymorphic transformation under the shock wave effect as well. In the latter case the transformation shock wave rate was the most striking. As for the explosives detonation decomposition mechanism, the problem amounted to finding out the causes of weak dependence of the detonation time on detonation pressure and the nature of the following contradiction. It had been experimentally revealed that, on the one hand, the time did not depend on the explosives charge structure (particles size; nature of fillers in pores, ...) and state (liquid or solid) and, on the other hand, the regularities of the Shock-to-Detonation Transition (SDT) process were strongly governed by the structure and state.

It was well known that shock discontinuity zone (SDZ) is extremely narrow ($< 100\text{\AA}$), that is the rate of substance loading inside the SDZ is extremely large. Naturally the question arises -whether the processes generated by shock wave effect would follow the regularities of the processes at static conditions. Real-time experiments and recovered samples investigations were performed concurrently. As regards to the shock effect specific features and primarily tremendous rate of particles acceleration inside the SDZ it makes sense to discuss separately the response to the shock effect of molecular crystals (and liquids) where each molecule can be considered in great part free and crystals with ionic and atomic bonds where properties of the crystal as a whole have to be taken into account.

Organic Materials. The polarization phenomenon was investigated in detail for organic substances. For substances consisting of dipole molecules the Hauver polarization model of dipole turn by shock wave front was proved. It was revealed that for polymer materials polarization signals were also related to molecular uncompensated dipoles turn in the front. However, it turned out that the dipoles motion in the front were not associated with their orientation in the direction of inertia forces effect; macromolecule and its separate parts seem to experience some conformation change during the acceleration process. It was found out that all organic substances investigated at shock pressures till up to 20 GPa were divided into two groups. Substances of the first group do not decompose under the shock wave effect; their compressibility changes gradually in the pressure interval; their electro-conductivity is ionic and changes gradually with pressure; they are transparent at shock-compressed state. And visa versa shock compressibility and electro-conductivity of the other group substances change at some property for each substance pressure sharply, the substances losing irreversibly their transparency. Different reaction of organic molecules (substitution,

addition, isomerization, polymerization,...) were observed under the shockwave effect, it turned out that aromatic thermally stable compounds decompose (with benzene ring breakage) easier than thermally relatively weak aliphatic ones.

For ideal explosive substances consisting of complex poly atomic organic molecules some qualitative physical model of their detonation wave front was elaborated in accordance with experimental data obtained. It had been found out that for each explosive charge there existed some proper shock pressure P (it is small than Chapman-Jouguet pressure and close to critical pressure to initiate detonation in homogeneous state), so that at pressure smaller than the P the explosive charge reaction origin and progress are strongly influenced by the charge structure, and on the contrary at pressures larger than the P , the explosive charge structure and state have nothing to do with the explosive decomposition regularities; the regularities become the explosive molecules property. At detonation due to extremely large rate of substance loading inside the wave SDZ it is brought into very non-equilibrium state; the substance molecules excitation and active particles (ions, radicals, fragments of molecules) origin taking place during the state of equilibration, in the shock wave front, so that behind the front the active particles and excited molecules reactions processed with speed since the reactions activation energy is low.

Inorganic Materials. Many results previously obtained by other investigators had been validated. These are the following: different defects (point and lengthy) are formed in crystalline lattice of solids and as a consequence enhancement of the solids chemical activity and sinterability; destruction, synthesis, and polymorphic transformations occurs. In addition it had been found out that shock wave effect sometimes was of an extremum in nature. The finding was interpreted in terms of the shock residual temperatures opposite effect. In the course of the investigations some new results (later verified by other scientific groups) such as intermetallic compound (Cu, Al) synthesis from the components powders mixture inside the shock wave front and the production of homogeneous alloy of metals absolutely impossible to be mixed at normal conditions (w/Mn). Some systems of rare earth oxides with titanium oxide have been investigated in the Department with many metastable compounds being produced. The compounds single crystals of 0,1-0,2 mm size have been obtained by shock synthesis from the oxides mixtures. They believe that the crystals originate from evercooled eutectic melt nearby residual temperature. The data testify in favour of the melt and compounds simultaneous origin inside the shock waves front. The foregoing intermetallic compound synthesis and the alloy production are also believed to proceed through eutectic melts originating due to strong dissipative processes which take place during powders mixtures compression inside shock wave front. The conclusion seems to be reasonable for strong effect when shock intensity exceeds considerably the material strength. For low and moderate intensities the problem is often open. To answer the question one needs continuous observation of the material change from the very beginning of its loading inside the shock wave front and at least during some seconds to be sure that nothing has happened with the material in the recovering device during the dead time between the shock passage through the sample and its subsequent analysis by conventional methods. The technique for such observation has been developed in the Department. It was shown by real-time electrical measurements that some changes with sample under investigation took place in fact in some ms or even later after the shock passage through the sample.

Tremendous rate of substance loading inside the SDZ makes the shock wave effect unique. For organic materials consisting of complex poly atomic molecules it leads, depending on the shock intensity, to defect formation non-equilibrium thermal excitation of the molecules, different reactions and destruction. For inorganic solids - depending on the shock intensity, it leads to defects formation, polymorphic transformation and destruction; for the powders mixtures of

materials - it leads to grinding, mixing, melting and sometimes to compound formation inside the shock wave front. The findings have been revealed by experimental techniques largely of mks resolution power. However the investigation have lead to the realization of the fact that at present the problem of the shock physics and chemistry needs experimental and theoretical investigations on the shock wave front time-space level (ps and tens of A). It becomes obvious that the problem goes from mesolevel to microlevel. One could think that explosion science and explosion energy use for mining, building, etc as the problem of macrolevel. It is characterized by time-space level largely of ms,s and m.The mesolevel problem results in many new applications of explosion energy (metal treatment, superhard materials production, etc). The investigation of the problem on the microlevel promises to open new horizons in the business of shock compression science.

REFERENCES THE LATEST PUBLICATIONS

1. Kurto A.P., Antipenko A.G., and Yakushev V.V. "Investigation of polymers shock polarization origin mechanism" All-Union seminar "Shock Wave Physics Fundamental Problems" Chernogolovka, 1987, N 1, part 1, pp.123-125
2. Nabatov S.S., Shubitidze S.O., and Yakushev V.V. "Self-conductor EMF phenomenon use for exothermic processes study in recovery device" Fiz.Gorenija i Vzriva (russ) 1990, N 6, pp.114-116.
3. Kurto A.P., Antipenko A.G., and Yakushev V.V. "Investigation of polymers shock polarization process relaxation" All-Union Meeting "Dielectric materials in extreme conditions", Suzdal, 1990, V II, pp.264-273.
4. Dremin A.N. "Shock discontinuity zone effect: the main factor in the explosive decomposition detonation process" Phil.Trans.R.Soc.Lond. A (1992), 339, 355-364.
5. Nabatov S.S. "Measurements of (KClO + Al) system electroconductivity at shock compression in recovery device" in Proc. of X Symp. on Combustion and Explosion. Section-Detonation. Chernogolovka, 1992, pp.124-126.
6. Dremin A.N., Breusov O.N. "Dynamic Synthesis of Superhard Materials" in Shock Wave in Materials Science. Ed.by A.B.Sawaoka, 1993, pp.17-34.
7. Nabatov S.S. "Thermoelectrical signals at shock wave compression of self-conductor in flat recovery device". Chemical Physics (russ), 1993, V 12, N 2, pp.167-169.
8. Metreveli A.A., Kolesnikov A.V. "Investigation of phase-formation in Nb-Ni system under shock wave effect". 5th All-Union Conference on Detonation. Krasnoyarsk, 1991, V 1, pp.200-202.

Shock discontinuity zone effect: the main factor in the explosive decomposition detonation process

BY A. N. DREMIN

Dynamic Pressure Department, Institute of Chemical Physics (Chernogolovka), Russian Academy of Sciences, Moscow Region, Chernogolovka 142432, Russia

A qualitative conception of the detonation mechanism in condensed explosives has been developed on the basis of experimental and numerical modelling data. According to the conception the mechanism consists of two stages: non-equilibrium and equilibrium. The mechanism regularities are explosive characteristics and they do not depend on explosive charge structure (particle size, nature of filler in the explosive state, liquid or solid, and so on). The tremendous rate of loading at the detonation wave shock discontinuity zone (ca. 10^{-13} s) is responsible for the beginning of the non-equilibrium stage. For this reason, the kinetic part of the shock compression energy is initially absorbed only by the translational degrees of freedom of the explosive molecules. It involves the appearance of extremely high translational temperatures for the polyatomic molecules. In the course of the translational-rotational relaxation processes (that is, during the first non-equilibrium stage of 10^{-10} s time duration) the most rapidly excited vibrational degrees of freedom accumulate surplus energy, and the corresponding bonds decompose faster than at the front at the equilibrium stage. In addition to this process, the explosive molecules become electronically excited and thermal ionization becomes possible at the translational temperature overheat zone. The molecules thermal decomposition as well as their electronic excitation and thermal ionization result in active particles (radicals, ions) being created. The active particles and excited molecules govern the explosive detonation decomposition process behind the shock front during the second equilibrium stage. The activation energy is usually low, so that during this stage the decomposition proceeds extremely rapidly. Therefore the experimentally observed dependence of the detonation decomposition time for condensed explosives is rather weak.

1. Introduction

The condensed explosives detonation decomposition mechanism problem is still to be investigated in the theory of detonation. Lately the problem has again attracted the attention of many scientists (Eyring 1975; Eyring & Leu 1975; Karo 1977; Owens & Sharma 1979; Coffey & Toton 1981; Delpuech *et al.* 1981; Zerilli 1983; Schmidt *et al.* 1983; Peyrard *et al.* 1984; Trott & Renlund 1985; Waino & Tsai 1985; Dufort & Delpuech 1985; Schmidt *et al.* 1986*a, b*; Moore *et al.* 1986; Peyrard *et al.* 1986; Odier *et al.* 1986; Eloy & Delpuech 1987; Walker 1988; Renlund & Trott 1988; Lambrakos *et al.* 1988; Tarver & Calef 1988; Diott & Fayer 1989; Trott & Renlund 1989; Delpuech 1989; Moore & Schmidt 1989; Gilman 1989;

Odier 1979). However, it should be noted that the instability is not a general property of all explosives. As far as powerful explosives are concerned, the mechanism has been investigated (Dremin 1983). It has been shown experimentally that the surface of the reaction front surface in liquid explosives reflects light like a mirror (Dremin & Savrov 1966). It means that the width of the reaction front is of the order of the wavelength of the light. However, the width of the detonation wave is considerably smaller than the width of the reaction front in the experiments.

The second result of our investigations of the mechanism of the detonation wave decomposition of condensed explosives is directly related to the first one. In the present paper, it has been found that the detonation reaction time t_{cs} (the duration of the chemical spike) does not in practice depend on the initial features of the explosive charge (on explosive particle size, on the size of the filler in the pores, on the explosive state, liquid or solid, and so on; see, e.g. Koldunov 1972). The reaction time t_{cs} turned out to be a characteristic of the explosive itself. It should be pointed out that the time depends only on the detonation wave pressure, the dependence being very weak. For example, t_{cs} for the detonation of TNT changes from ca. 1.5 μ s to ca. 2.2 μ s while the detonation wave pressure changes from 5 GPa to ca. 20 GPa. It is obvious that the temperature of the explosive changes considerably in this same pressure interval. If the shock decomposition mechanism were the same as the mechanism under ambient conditions, the change in t_{cs} would be much greater. However, experiment has shown that the dependence of t_{cs} on pressure is really weak. Searching for an explanation for the weak dependence of $t_{cs}(p)$, we surmise on the possible break-up of explosive molecules during the process of explosive compression within the detonation wave shock front. It has been assumed after the detonation theory founders that detonation reactions proceed in a similar way to thermal explosions. (The considerations proposed below are also valid for explosion regularities.) It is known that during the explosion induction period (the activation-stage time), which is the main part of the entire reaction time, only a small portion of the explosive decomposes but, the reaction later becomes of an explosive nature. It follows also from the theory that the activation-stage time of the explosive is a strong function of the chemical state and, on the contrary, the time for the final stages depends only weakly on the initial chemical state (Frank-Kamenetsky 1957). Logically the surmise whether the reaction tail is only registered at the end of the explosion - is based on understanding various features of the explosion, which are that only a small part of the explosive decomposes during the explosion activation-stage, and that the final stage of the explosion only depends weakly on the initial chemical state. If this is so, it means that the process activation stage does not take place during the explosive's compression within the shock front. In essence it means the following. Events which occur during the induction period of a thermal explosion take up most of the time of explosion. However, in a detonation the events proceed an order of magnitude faster within the extremely narrow shock front zone. The final stages of both processes proceed rapidly with times which depend only weakly on the initial state of the explosive.

It should be mentioned that it has since become clear that some experimental results testify in favour of the surmise. The point is that an induction period for detonation has not yet been observed in any of the explosives investigated. One has always registered a very sharp decrease of pressure (or particle velocity) within the chemical spike (Dremin *et al.* 1970; Seits *et al.* 1989; Green *et al.* 1989). It corresponds to the maximum reaction behind the detonation wave shock front. Therefore, one

could infer that the progress of the reaction had been conditioned by some preparatory process inside the shock front which is still beyond the reach of observation by present techniques. However, the possibility of the destruction of complex polyatomic molecules inside the shock front has been substantiated by special experiments in which samples of aromatic compounds (benzene, naphthalene, anthracene) have been recovered and investigated after shocks of 1.1–1.5 GPa (100–200 °C) intensity. It was found that the compounds partly decomposed (ca. 1%); the destruction corresponding to the rupture of bonds of the benzene ring (see Dremin & Babare 1982 and references therein). It should be noted that at the same static pressure and temperature the compounds investigated never decomposed entirely (Block *et al.* 1970). At normal pressure and high temperature they decompose without breaking the benzene ring. Chemical ring condensation and hydrogen elimination happen during the process. Complete graphitization occurs when the temperature reaches ca. 2000 °C (Magaril 1970). Taking the above facts into account, one can assume that the data testify in favour of the specific action of the shock wave front, that is, the shock front effect is responsible for the unusual destruction products of the aromatic compounds observed in the experiments.

Many explosives are complex organic compounds. Therefore, the decomposition of the explosives molecules inside the shock wave front seem to be a highly probable process. The portion decomposed is not known at present. Obviously it is some function of the wave intensity and can be significant at the detonation of powerful explosives in which the chemical spike pressure amounts to ten or more giga Pascals.

2. Results and Discussion

Naturally the question arises: What is the mechanism of the intrafront destruction of complex explosive molecules? Some of our papers have been devoted to this problem (Dremin 1973; Dremin & Shvedov 1976; Klimenko & Dremin 1980; Dremin 1987; Dremin *et al.* 1989). The 'accumulation mechanism' has been introduced for polyatomic molecules (Klimenko & Dremin 1980). The gist of the accumulation mechanism is as follows. Because of a tremendous rate of material loading inside the shock discontinuity zone (ca. 10^{-13} s), an excessively high translational temperature (overheat) appears at the beginning, and it is followed by the other-excitation of certain bonds. The overheat effect means a higher temperature level than the equilibrium one behind the front. The over-equilibrium translational temperature arises due to the fact that the kinetic part of the shock compression energy, which behind the shock front, is equally distributed among all the translational, vibrational and rotational degrees of freedom of the polyatomic molecules, is absorbed only by the translational degrees of freedom within the shock discontinuity zone. The maximum translational temperature overheat value is $T_{oh} = 2(n-1)(T-T_0)$, where n is the number of atoms in a molecule, and T_0 and T are equilibrium temperatures in front of and behind the shock wave front. It is obvious that due to the translational-vibrational relaxation process the energy of the translational degrees of freedom is redistributed to the vibrational degrees of freedom. At first, the energy flow will be directed towards those vibrational degrees of freedom which are most easily excited. If the energy flow towards these degrees of freedom exceeds the flow owing to the vibrational-vibrational relaxation process, they will over-excite and decompose faster in the shock front than behind it, where the state is one of equilibrium.

Phil. Trans. R. Soc. Lond. A (1992)

300

T/K 1500

0

Figure 1. Trajectory of the shock front

The considerations have been verified by calculations of the destruction of molecules inside the shock front along a one-dimensional system calculated by the model of Klimenko & Dremin (1980) for the system (see figure 1).

with parameters $\epsilon = 1.5$, $\gamma = 1.5$, and $\alpha = 1.5$. The interaction of the shock front with the system generated by the shock front with velocity 1000 m s⁻¹. The maximum potential

was used to describe the potential parameter corresponding to the corresponding bonds of the vibrational temperature calculated for two cases:

- (a) $r_e = 0.11$ nm; $\epsilon = 1.5$; and
- (b) $r_e = 0.11$ nm; $\epsilon = 1.5$; and

One can see from the calculations that the results predicted by Klimenko & Dremin (1980) for the first excited state of the first excited state is quite probable (see figure 1).

Phil. Trans. R. Soc. Lond. A (1992)

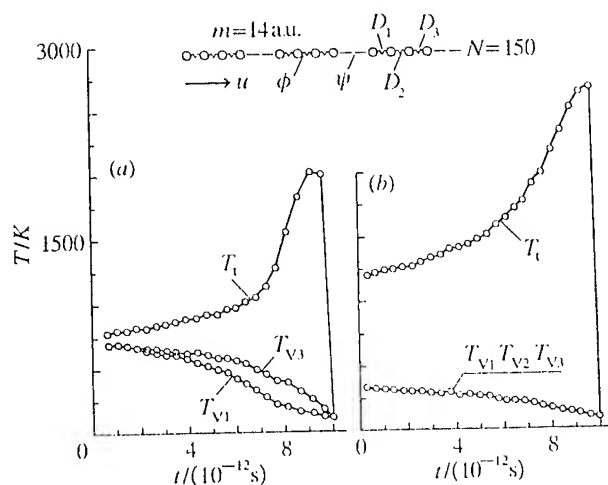


Figure 1. Translational temperature overhead for two sets of Morse potential parameter values, (a) and (b).

The considerations presented above are phenomenological. However, they have been verified by direct simulation of the process of excitation of polyatomic molecules inside the shock front (Dremin *et al.* 1989). The passage of the shock wave through a one-dimensional system consisting of tetratomic molecules has been simulated by the non-equilibrium molecule dynamic method developed in the HDPD (Klimenko & Dremin 1978; Dremin & Klimenko 1981). There were 150 molecules in the system (see figure 1). The exponential 6 potential

$$\psi(r) = \epsilon \left\{ \frac{6}{\alpha - 6} \exp \left[\alpha \left(-\frac{r}{\sigma} \right) \right] - \frac{\alpha}{\alpha - 6} \left(\frac{\sigma}{r} \right)^6 \right\},$$

with parameters $\epsilon = 50 \text{ K}$, $\alpha = 13.0$ and $\sigma = 0.385 \text{ nm}$, was used to describe the interaction of the various atoms in different molecules. The 'shock wave' was generated by the forced motion of the boundary molecule with a velocity of 900 m s^{-1} . The motion, in essence, is the shock wave particle velocity U . The Morse potential

$$\phi(r) = D \{ 1 - \exp [-\zeta((r/r_e) - 1)] \}^2,$$

was used to describe the interaction of neighbouring atoms inside the molecules. The potential parameters were varied to change the characteristic frequencies of the corresponding bonds. The translational temperature T_i as well as the profiles of the vibrational temperatures T_{v1} , T_{v2} and T_{v3} of the three bonds in the molecule have been calculated for two sets of Morse potential parameters values:

a) $r_e = 0.11 \text{ nm}$; $D_1 = 5.10^4 \text{ K}$, $\zeta_1 = 2.5$; $D_2 = 7.10^4 \text{ K}$, $\zeta_2 = 2.5$; $D_3 = 1.5 \cdot 10^4 \text{ K}$, $\zeta_3 = 1.5$; and

b) $r_e = 0.11 \text{ nm}$; $D_1 = D_2 = D_3 = 3.10^4 \text{ K}$, $\zeta_1 = \zeta_2 = \zeta_3 = 2.5$.

As can be seen from the figure that the translational temperature overhead (which was predicted by Klimenko & Dremin (1980)) takes place in both cases. As to overhead of the first excited mode, it has not been observed in this numerical experiment. It is quite probable that the fact that the model is only one-dimensional is responsible

for the negative result. However, this does not exclude the phenomenon for other complex molecules.

The origin of the translational temperature overhear is of great significance for understanding the mechanisms of the shock compression of complex molecules. The translational temperature overhear for molecules consisting of tens of atoms can be tens of thousands of degrees for shock wave intensities characteristic of the detonation of powerful explosives. At such temperatures the process of electronic excitation (activation energy 2–5 eV (Barltrop & Coyle 1975)) and even the thermal ionization process (activation energy 6–10 eV (Kondratiev 1974)) become possible inside the overhear zone.

Thus the non-equilibrium dissociation of polyatomic molecules inside the detonation wave shock front can proceed in three ways: through the accumulation mechanism, through electronic excitation as well as by thermal ionization. The accumulation mechanism has been developed before (Klimenko & Dremin 1980; Dremin *et al.* 1981; Dremin 1987). The decomposition mechanism through thermal ionization has not been investigated so far. As far as decomposition by electronic excitation is concerned, there are some experimental data supporting the mechanism. For example, hexogen (RDX, cyclotrimethylene trinitramine) samples recovered in special ampoules after the effect of shocks of 2.0–4.0 GPa have been investigated by X-ray photoelectron spectroscopy and paramagnetic resonance methods (Owens & Sharma 1979). It has been found that shock decomposition products of hexogen differ from those of its thermal decomposition, and are identical to those of the photochemical decomposition. The data testify in favour of decomposition by electronic excitation under the shock, because it is well known that the photochemical decomposition proceeds through the electronic excitation. It is interesting to note that the bonds in the hexogen molecule whose destruction is the origin of the recovered products, are identical to those excited bonds observed with high-speed Raman spectrometry in the shock-compressed state of hexogen (Delpuech *et al.* 1981; Dufort & Delpuech 1985; Delpuech 1989). The investigation has shown that approximately 100 ns behind the shock front of 10 GPa intensity the excited bonds are the bonds of the nitro-groups with the nitrogen of the ring.

Besides the aforesaid, the significant assumption of some preliminary electronic excitation of the molecules, introduced to explain the experimentally observed correlation between the electron structure of the molecules and their detonation ability should also be noted (Odier *et al.* 1986). However, the assumption has been introduced without any reliable and convincing interpretation of the excitation. But from the results obtained by us it follows that it is just the high-energy molecular collisions inside the translational temperature overhear zone that are responsible for the excitation.

It is obvious that owing to the three aforementioned ways in which polyatomic molecules can be destroyed inside the detonation wave shock front, some active particle (radicals, ions and so on) will originate. The particles behave as if they have been injected into the compressed and heated explosive. Naturally, they influence the subsequent decomposition of the explosive. The explosive detonation decomposition proceeds behind the shock front (that is, during the second afterfront stage) in a state of chemical and thermodynamic equilibrium when the translational temperature overhear and overexcitation of certain bonds disappear. The interaction of the explosive molecules with the active particles originating inside the front (that is, during the first intrafront stage) is the main process behind the front. As a rule

the activation energy for (1971). Because of the low, extremely fast and is also

Thus, in accordance with the mechanism of condensed explosive 'spot' mechanism. The most rapid decomposition process depends on the state (solid or liquid) of the explosive. The principal stage is the first in the sequence for the most slowly excited bonds (ca. 10^{-10} s). The time duration (Klimenko & Dremin 1980) and non-equilibrium decomposition of the first stage and it leads to the formation of detonation products during the first stage has not been investigated. This mechanism has been developed by French scientists (see Schmidt *et al.* 1980) for shock processes. However, the present still insufficient resolution of about 1 ns has hampered the study of the problem. The time scale is smaller. Therefore, one of the main methods of at least picosecond resolution of studying the chemical pathway control.

In spite of the fact that the experiments presented above advance a certain hypothesis for the explosive, the electronic excitation that it favours the explosion which molecule bonds excite the problem needs some further investigation. The chemical pathways of molecular decomposition from the very beginning of the process.

Professor W. Byers Brown, *Phil. Trans. R. Soc. Lond. A* (1992) manuscript.

Barltrop, J. A. & Coyle, J. H. 1975. The decomposition of anthracene at high pressure. *J. chem. Phys.* **63**, 1000.
Coyle, C. S. & Toton, E. T. 1975. The decomposition of solid explosives. *J. chem. Phys.* **63**, 1000.
Delpuech, A. E. & Cherville, J. 1989. *Phil. Trans. R. Soc. Lond. A* (1992)

phenomenon for other activation energy for this interaction is low (5-15 kcal mol⁻¹) (Kondratiev 1974). Because of the low value of the activation energy the decomposition proceeds extremely fast and is almost independent of the temperature change.

3. Conclusions

Thus, in accordance with our conception of the detonation decomposition mechanism of condensed explosives reaction is homogeneous rather than by the 'hot spot' mechanism. The mechanism regularities are the explosives characteristics. The decomposition process does not depend on the initial physical state (powder, pressed, or liquid) of the explosive charge. The process consists of two stages. The principal stage is the first intrafront stage. Its duration is equal to the time necessary for the most slowly excited bonds of complex polyatomic explosive molecules to be excited (ca. 10⁻¹⁰ s). The stage begins with the shock discontinuity zone of ca. 10⁻¹³ s duration (Klimenko & Dremin 1978; Klimenko & Dremin 1980). The activation mechanism through thermal non-equilibrium destruction of some explosive molecules takes place during the first stage and it leads to the fast transformation of the explosive into the final detonation products during the second stage. So, the first stage largely governs the detonation decomposition regularities of condensed explosives. Unfortunately this stage has not been investigated yet. Some Raman spectroscopy techniques have been developed by French (see Delpuech 1989 and references therein) and American scientists (see Schmidt *et al.* 1986*a, b* and references therein) for the investigation of the decomposition by shock processes. However, the spectral and time resolution of the techniques is for the present still insufficient. Indeed the spectral resolution of 10-20% and the time resolution of about 1 ns have been achieved. It is evidently too low a resolution for the study of the problem discussed since the entire time of the intrafront stage is even less than 1 ns. Therefore, one now needs elaboration of theoretical and experimental methods of at least picosecond resolving power. In that case one will have the possibility of studying the stage in detail. Obviously, until the problem is solved the chemical pathway controlling explosive energy release will be unknown. In spite of the fact that the detonation decomposition mechanism of condensed explosives presented above is still mostly qualitative, it is possible even now to advance a certain hypothesis: the highest detonation ability corresponds to the explosive, the electronic structure of which changes at compression in such a way that it favours the explosive molecules electron excitation, as well as explosives in which molecule bonds excitation times differ considerably from each other. However, the problem needs some further investigation. Probably it will be solved when the chemical pathways of molecules inside the detonation wave shock front are studied from the very beginning of explosive loading.

in which polyatomic front, some active behave as if they had ally, they influence the detonation decomposition second afterfront when the translational energy. The interaction inside the front (that is, the front. As a rule,

Professor W. Byers Brown and Dr J. E. Field are thanked for their editorial work on the manuscript.

References

- Atrop, J. A. & Coyle, J. D. 1975 *Excited states in organic chemistry*. London: John Wiley.
- Bai, S., Weir, C. E. & Piermarini, P. J. 1970 Polymorphism in benzene, naphthalene and anthracene at high pressure. *Science, Wash.* **169**, 586-587.
- Lee, C. S. & Toton, E. T. 1981 A microscopic theory of compressive wave-induced reactions in explosives. *J. chem. Phys.* **76**, 949-954.
- Delpuech, A. E. & Cherville, J. & Michaud, C. 1981 Molecular electronic structure and initiation. *Trans. R. Soc. Lond. A* (1992)

- of secondary explosives. In *Proc. Seventh Symp. (Int.) on Detonation* (ed. J. M. Short), pp. 65-74. Naval Surface Weapon Center, U.S.A.
- Delpuech, A. E. 1989 The use of time-resolved spectrometries in the study of initiation of explosives at molecular level. In *Proc. Ninth Symp. (Int.) on Detonation*, pp. 172-179. Office of Naval Research, U.S.A.
- Dlott, D. D. & Fayer, M. D. 1989 Shocked molecular solids: vibrational up pumping, defect to spot formation, and the onset of chemistry. *J. Chem. Phys.* **92**, 3798-3812.
- Dremin, A. N. 1983 Pulsating detonation front. *Fiz. Gorenia i Vzriva* **4**, 159-169.
- Dremin, A. N. & Savrov, S. D. 1966 On liquid explosives detonation front stability. *Fiz. Gorenia i Vzriva* **1**, 36-46.
- Dremin, A. N., Savrov, S. A., Trofimov, V. S. & Shvedov, K. K. 1970 *Detonation waves in condensed explosives*. Moscow: Nauka.
- Dremin, A. N. & Shvedov, K. K. 1976 On shock wave explosives decomposition. In *Proc. Sixth Symp. (Int.) on Detonation* (ed. D. J. Edwards), pp. 29-35. Office of Naval Research, U.S.A.
- Dremin, A. N. & Klimenko, V. Yu. 1981 On the effect of shock wave front on the reaction origin. *Progr. Astronaut. Aeronaut.* **75**, 253-268.
- Dremin, A. N. & Babare, L. V. 1982 The shock wave chemistry of organic substances. In *Shock waves in condensed matter* (ed. W. J. Nellis, L. Seaman & R. A. Graham), pp. 363-381. New York: American Institute of Physics.
- Dremin, A. N., Klimenko, V. Yu., Mikhailyuk, R. M. & Trofimov, V. S. 1981 On decomposition reaction kinetics in shock wave front. In *Proc. Seventh Symp. (Int.) on Detonation* (ed. J. M. Short), pp. 789-794. Naval Surface Weapon Center, U.S.A.
- Dremin, A. N., Klimenko, V. Yu. & Kosireva, J. J. 1985 On the mechanism of the reaction hot spot origin at liquid explosives detonation. In *Proc. Eighth Symp. (Int.) on Detonation* (ed. J. M. Short), pp. 678-687. Naval Surface Weapon Center, U.S.A.
- Dremin, A. N. 1987 On the physical model of condensed explosives detonation wave. In *Proc. Int. Symp. on Pyrotechnics and Explosives* (ed. D. Jing), pp. 497-505. Beijing: China Academic Publishers.
- Dremin, A. N., Klimenko, V. Yu., Davidova, O. N. & Zoludeva, T. A. 1989 Multiprocess detonation model. In *Proc. Ninth Symp. (Int.) on Detonation*, pp. 725-728. Office of Naval Research, U.S.A.
- Dufort, S. & Delpuech, A. E. 1985 A molecular mechanism for the initiation of secondary explosives. Influence of a shock light coming. In *Proc. Eighth Symp. (Int.) on Detonation* (ed. J. M. Short), pp. 847-854. Naval Surface Weapon Center, U.S.A.
- Eloy, J. F. & Delpuech, A. E. 1988 Experimental study of phonon-phonon interaction in explosives by laser probe mass spectroscopy. In *Shock waves in condensed matter* (ed. S. C. Schmidt & N. C. Holmes), pp. 557-560. Amsterdam: North-Holland.
- Eyring, H. 1975 Slow vibrationally activated reactions at high temperatures. *Chem. Engng News* **53**, 27-31.
- Eyring, H. & Lau, A. 1975 Fall-off from extrapolated values of all chemical reactions at very high temperatures. *Proc. natn. Acad. Sci. U.S.A.* **72**, 1717-1719.
- Frank-Kamenevsky, D. A. 1987 *Diffusion and heat transfer in chemical kinetics*. Moscow: Nauka.
- Gilman, J. J. 1989 Dynamic at detonation fronts in solids. In *Shock waves in condensed matter* (ed. S. C. Schmidt, Y. N. Johnson & L. W. Davison), pp. 267-270. Amsterdam: North-Holland.
- Green, L. G., Tarver, C. M. & Erscine, D. J. 1989 Reaction zone structure in supra compressed detonating explosives. In *Proc. Ninth Symp. (Int.) on Detonation*, pp. 670-682. Office of Naval Research, U.S.A.
- Karo, A. M., Hardy, J. R. & Walker, F. E. 1977 Theoretical studies of shock-initiated detonation. *Acta astronaut.* **5**, 1041-1050.
- Kim, H. & Dlott, D. D. 1990 Theory of ultra hot molecular solids: vibrational cooling and shock induced multi phonon up pumping in crystalline naphthalene. *J. chem. Phys.* **93**, 1695-1709.
- Klimenko, V. Yu. & Dremin, A. N. 1978 The structure of the shock wave front in liquids. I. *Detonation, critical phenomena, physico-chemical transformation in shock waves* (ed. O. S. Breusov), pp. 79-84. Chernogolovka: Nauka.
- Klimenko, V. Yu. & Dremin, A. N. 1981 *Detonation waves in condensed explosives*. Moscow: Nauka.
- Klimenko, V. Yu. & Dremin, A. N. 1983 *Detonation waves in condensed explosives*. Moscow: Nauka.
- Klimenko, V. Yu. & Dremin, A. N. 1985 *Detonation waves in condensed explosives*. Moscow: Nauka.
- Klimenko, V. Yu. & Dremin, A. N. 1987 *Detonation waves in condensed explosives*. Moscow: Nauka.
- Klimenko, V. Yu. & Dremin, A. N. 1989 *Detonation waves in condensed explosives*. Moscow: Nauka.
- Klimenko, V. Yu. & Dremin, A. N. 1991 *Detonation waves in condensed explosives*. Moscow: Nauka.
- Klimenko, V. Yu. & Dremin, A. N. 1993 *Detonation waves in condensed explosives*. Moscow: Nauka.
- Klimenko, V. Yu. & Dremin, A. N. 1995 *Detonation waves in condensed explosives*. Moscow: Nauka.
- Klimenko, V. Yu. & Dremin, A. N. 1997 *Detonation waves in condensed explosives*. Moscow: Nauka.
- Klimenko, V. Yu. & Dremin, A. N. 1999 *Detonation waves in condensed explosives*. Moscow: Nauka.
- Klimenko, V. Yu. & Dremin, A. N. 2001 *Detonation waves in condensed explosives*. Moscow: Nauka.
- Klimenko, V. Yu. & Dremin, A. N. 2003 *Detonation waves in condensed explosives*. Moscow: Nauka.
- Klimenko, V. Yu. & Dremin, A. N. 2005 *Detonation waves in condensed explosives*. Moscow: Nauka.
- Klimenko, V. Yu. & Dremin, A. N. 2007 *Detonation waves in condensed explosives*. Moscow: Nauka.
- Klimenko, V. Yu. & Dremin, A. N. 2009 *Detonation waves in condensed explosives*. Moscow: Nauka.
- Klimenko, V. Yu. & Dremin, A. N. 2011 *Detonation waves in condensed explosives*. Moscow: Nauka.
- Klimenko, V. Yu. & Dremin, A. N. 2013 *Detonation waves in condensed explosives*. Moscow: Nauka.
- Klimenko, V. Yu. & Dremin, A. N. 2015 *Detonation waves in condensed explosives*. Moscow: Nauka.
- Klimenko, V. Yu. & Dremin, A. N. 2017 *Detonation waves in condensed explosives*. Moscow: Nauka.
- Klimenko, V. Yu. & Dremin, A. N. 2019 *Detonation waves in condensed explosives*. Moscow: Nauka.
- Klimenko, V. Yu. & Dremin, A. N. 2021 *Detonation waves in condensed explosives*. Moscow: Nauka.
- Klimenko, V. Yu. & Dremin, A. N. 2023 *Detonation waves in condensed explosives*. Moscow: Nauka.
- Klimenko, V. Yu. & Dremin, A. N. 2025 *Detonation waves in condensed explosives*. Moscow: Nauka.

- J. M. Short), pp. 63-74.
- The study of initiation of detonation waves, pp. 172-179. Office of Naval Research, U.S.A.
- Shock-induced pumping, defect formation, pp. 812-819.
- Shock wave front stability. *Fiz. Gorenia*, 1970, 159-169.
- Detonation waves in condensed matter. In *Proc. Ninth Symp. (Int) on Detonation* (ed. J. M. Short), pp. 363-381. Office of Naval Research, U.S.A.
- Mechanism of the reaction between organic substances. In *Shock Waves in Condensed Matter* (ed. S. C. Schmidt & N. C. Holms), pp. 363-381. North-Holland.
- On decomposition of nitromethane. In *Proc. Ninth Symp. (Int) on Detonation* (ed. J. M. Short), pp. 382-391. Office of Naval Research, U.S.A.
- Mechanism of the reaction between organic substances. In *Shock Waves in Condensed Matter* (ed. S. C. Schmidt & N. C. Holms), pp. 363-381. North-Holland.
- Initiation of secondary detonations. In *Proc. Ninth Symp. (Int) on Detonation* (ed. J. M. Short), pp. 392-399. Office of Naval Research, U.S.A.
- Phonon interaction in condensed matter (ed. S. C. Schmidt & N. C. Holms), pp. 400-407. North-Holland.
- Chemical reactions at very high pressures. *Chem. Engng News*, 1981, 15-22.
- Kinetics. Moscow: Nauka, 1981.
- Shock-induced detonations in energetic solids. In *Shock waves in condensed matter* (ed. S. C. Schmidt & N. C. Holms), pp. 408-415. Amsterdam: North-Holland.
- Shock wave induced detonation in energetic molecular crystals. *Int. J. Quantum Chem.* 29, 1635-1634.
- Fundamental physics and chemistry behind molecular crystal detonation at a microscopic level. In *Chemistry and physics of energetic materials* (ed. S. N. Bulusu), pp. 79-130. The Netherlands: Kluwer Academic.
- X-ray photo electron spectroscopy and paramagnetic resonance evidence for shock-induced intramolecular bond breaking in some energetic solids. *J. appl. Phys.* 61, 1491-1497.
- Molecular model for cooperative propagation of shock-induced detonations in energetic solids and application to nitromethane. *J. appl. Phys.* 57, 2626-2636.
- Microscope model for propagation of shock-induced detonation in energetic solids. *Phys. Rev. B* 33, 2350-2363.
- Spectroscopic studies of shocked and detonating explosives. In *Shock waves in condensed matter* (ed. S. C. Schmidt & N. C. Holms), pp. 547-552. Amsterdam: North-Holland.
- Turbulence at detonation. *Fiz. Gorenia i Vzriva* 1, 29-35.
- Backward stimulated raman scattering in shock compressed benzene. *Phys. Rev. Lett.* 50, 664-664.
- Raman spectroscopies in shock-compressed materials. In *Shock wave in condensed matter* (ed. J. R. Asay, R. A. Graham & G. K. Straub), pp. 303-302. Amsterdam: North-Holland.
- Coherent anti-Stokes raman scattering in benzene and nitromethane shock-compressed to 10 GPa. *Physics* 1-3, 139-140.
- Coherent and spontaneous raman spectroscopy in shocked and unshocked liquids. In *Advances in chemical reaction dynamics* (ed. R. M. Rentzepis & C. G. S. Jones), pp. 425-454. New York: D. Reidel.
- Detonation reaction-rate structure for PBX 9502. In *Proc. Ninth Symp. (Int) on Detonation*, pp. 657-669. Office of Naval Research, U.S.A.
- TNT physical state and charge structure influence on its
- Phil Trans. R. Soc. Lond. A* (1992)

- detonation decomposition time. In *Combustion and explosions* (ed. L. N. Stesik), pp. 439-49. Moscow: Nauka.
- Sokolie, A. S. 1960 *Self-ignition, flame and detonation in gases*. Moscow: Academic Press.
- Tarver, C. & Calef, D. 1988 The detonation of high explosives. In *Energy and technology review High explosives* (ed. R. D. Lear & R. McGuire), pp. 1-8. Livermore, U.S.A.: HLNL.
- Trevino, S. F. & Tsai, D. H. 1985 Simulation of the initiation of detonation in an energetic molecular crystal: the overdriven case. In *Proc. Eighth Symp. (Int) on Detonation* (ed. J. R. Short), pp. 870-877. Naval Surface Weapon Center, U.S.A.
- Trofimov, V. S. & Dremin, A. N. 1966 On detonation velocity choice rule substitution. *Fiz. Goreni i Vzryv* 3, 19-30.
- Tsai, D. H. & Trevino, S. F. 1984 Simulation of the initiation of detonation in an energetic molecular crystal. *J. chem. Phys.* 81, 5636-5637.
- Trott, W. M. & Renlund, A. M. 1985 Single-pulse raman scattering studies of heterogeneous explosive materials. *Appl. Optics* 24, 1520-1528.
- Trott, W. M. & Renlund, A. M. 1989 Pulsed-laser-excited raman spectra of shock-compressed triaminotrinitrobenzene. In *Proc. Ninth Symp. (Int) on Detonation*, pp. 153-161. Office of the Chief of Naval Research, U.S.A.
- Walker, F. E. 1988 Physical kinetics. *J. appl. Phys.* 63, 5548-5551.
- Walker, F. E. 1990a Calculation of detonation velocities from hugoniot data. *Propellants Explosives Pyrotechnics* 15, 157-160.
- Walker, F. E. 1990a Correlation between reaction dynamics experiments and the detonation of explosives. *Propellants Explosives Pyrotechnics* 15, 190-193.
- Zerilli, F. J. & Totoni, E. T. 1983 Shock-induced molecular excitation in solids. *Phys. Rev. B* 28, 5891-5902.

The thermochemistry of energetic materials

*Combustion Research Institute
California*

The chemical processes involved in the decomposition of energetic materials have been investigated to determine the thermochemical properties of these materials. Corrected Moller-Plesset fourth-order perturbation theory has been used to determine heats of formation of decomposition and combustion products, to determine reaction pathways for calculating solvation energy at high pressure and the condensed phase decomposition, ignition and reaction of nitromethane and methane. Differences in decomposition energies for condensed and gas phase are discussed. In addition, the initial stages of condensed phase decomposition energies for nitro-triazoles are

The decomposition of energetic materials at high temperatures and pressures has been experimentally studied to study the reaction conditions, these processes are investigated and detailed chemical kinetic studies requires a knowledge of the thermochemical properties of the compound as well as those of the reaction process. From the thermochemical dissociation energies of various intermediates. By using these data to determine reaction pathways from reactants to products.

In this paper, we review the Corrected Moller-Plesset fourth-order perturbation theory procedure (Mellius 1990a) to determine the thermochemical properties of nitromethane and nitramines (nitroethane and nitropropane) to accurate gas-phase thermochemical properties and high-pressure reaction

Modeling Shock-Compression of Porous Composite Materials and Correlation with Observed Behavior*

M. R. Baer, M.U. Anderson and R. A. Graham
Sandia National Laboratories, Albuquerque, NM

The dynamic response of granular energetic materials involves a complex interaction of thermal, mechanical, and chemical processes associated with dispersive waves. Continuum mixture theory provides a foundation for theoretical description of combustion behavior and a key element to this approach is the treatment of volume fraction as independent kinematic variables¹. Thus, compressibility of all phases is modeled without any compromise on compaction behavior. Extensive modeling at a variety of loading conditions and porous states has shown that dispersive compaction waves trigger complex thermal, mechanical, and chemical behavior. For example, the combustion leading to the onset of deflagration-to-detonation transition (DDT) in granular explosives is known to involve complex combustion processes near compaction and shock fronts and numerical simulations of low-velocity impact, using a multiphase model, have provided detailed insights to the complicated nature of combustion and the wave mechanics. The incorporation of this model into multi-material hydrocode analysis are discussed to address the effects of confinement and its influence on accelerated combustion behavior.

In extending this modeling to composite blends of inert and reactive powders, continuum mixture theory has been formulated to treat multicomponent blends of powders in which more than two materials coexist at every point. The resulting sets of balance laws describe the continuum nature of the individual materials and the interactions between all components. Sets of interaction laws are suggested from the constraints from the Second Law and multiple rate dependent laws are derived to describe dynamic compaction. With this complex framework, combined theoretical and experimental studies is essential to explore the nature of the microscale processes of consolidation, deformation and reaction which are the key features of shock response of porous materials.

The experimental studies focus on the use of PVDF piezoelectric polymer stress-rate gauge to precisely measure the input and propagating shock stress response of porous materials. In addition to single constituent porous materials, such as granular HMX, resolved shock waves in porous composite intermetallic powders has confirmed the dispersive wave nature which is highly morphologically and material dependent.

¹ Baer, M. R. and Nunziato, J. W., "A Two-Phase Mixture Theory for the Deflagration-to-Detonation Transition (DDT) in Reactive Granular Materials", *Inter. Journal of Multiphase Flow*, V12, no. 6, 1986.

* This work was preformed at Sandia National Laboratories, supported by the US Dept. of Energy, under contract DE-AC04-76DP00789

A model for the shock behavior in a blend of $2\text{Al} + \text{Fe}_2\text{O}_3$ powders has been formulated whereby a three phase system is considered and relative flow effects are ignored. Shock loading conditions are considered in which no chemistry is induced. Numerical solution of the resulting field equations demonstrates that dispersive waves are produced which are not in thermodynamic equilibrium. Furthermore, numerical solutions also demonstrate that much of the deformation at the granular level takes place in the Fe_2O_3 material consistent with recovery observations. This preliminary study suggests that the multiphase nonequilibrium mixture model well describes the shock-induced behavior of composite materials. Future work will include chemistry and examine shock loading conditions with energy release induced during the dynamic compaction of the mixed powders.

Additional references:

M. R. Baer, J. W. Nunziatio, P. F. Embid, "Deflagration-to-Detonation in Reactive Granular Materials", *Numerical Approaches to Combustion Modeling*, Progress in Astronautics and Aeronautics, 1991, Vol. 135, Chapter 19.

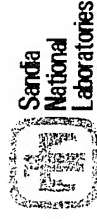
M. R. Baer, J. W. Nunziato, "Compressive Combustion of Granular Materials Induced by Low-Velocity Impact", *Ninth Symposium (International) on Detonation*, Vol I, OCNR 113291-7, pp 293-305.

M. R. Baer, "Numerical Studies of Dynamic Compaction of Inert and Energetic Granular Materials", *J. of Applied Mechanics*, Vol 55, 1988, pp 36-43.

P. F. Embid and Baer, M. R., "Mathematical Analysis of a Two-Phase Continuum Mixture Theory", *Continuum Mechanics and Thermodynamics*, 4, 1992, pp 279-312.

Modeling Shock-Compression of Porous Composite Materials and Correlation with Observed Behavior

M. R. Baer, M. U. Anderson and R. A. Graham

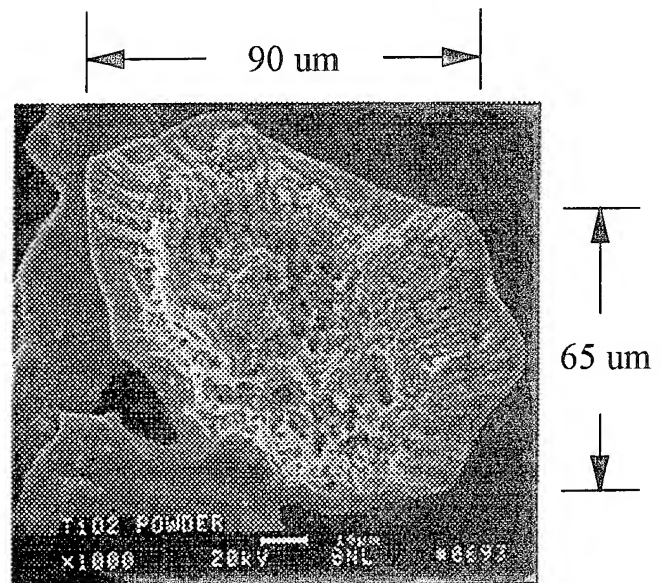


Presentation at ARO workshop on "Shock Synthesis of Materials"
at Georgia Institute of Technology

TIME RESOLUTION

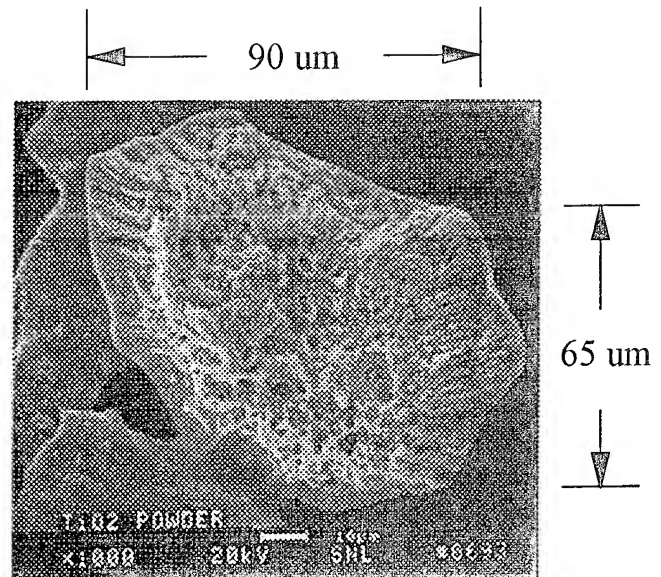
Particle equilibrium

round trip = 20 nanoseconds



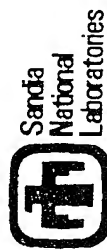
Deformation equilibrium

~ 100 nanoseconds

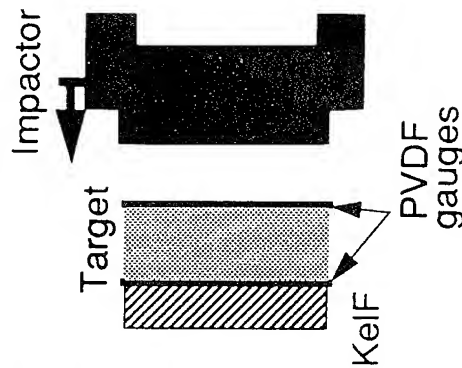
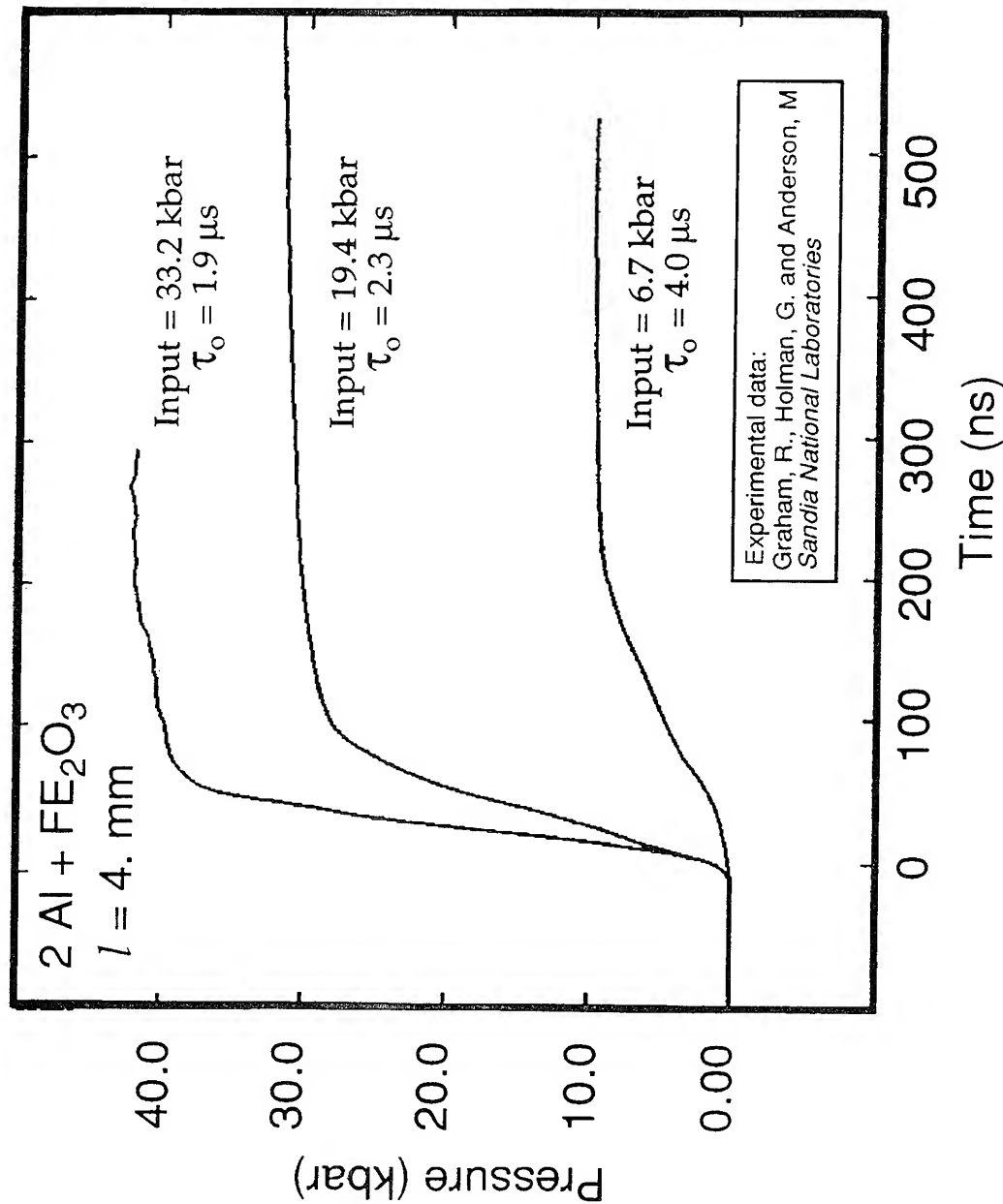


- few nanosecond resolution required to describe process

PVDF gauge records for shocked porous composite metal powders



Engineering Sciences Center



Scientific and Technical Issues



Engineering Sciences Center

Shock loading of distended materials (at low and high densities) involves a complex interaction of gas dynamics and solid dynamics -- much remains to be understood regarding this complex interaction

Deformation features emerge as dispersive waves in porous materials -- internal boundary effects have a profound influence on wave behavior

Theoretical Foundation:

Continuum mixture theory has been successfully applied to describe the shock response of high density granular materials -- extended application to low density materials

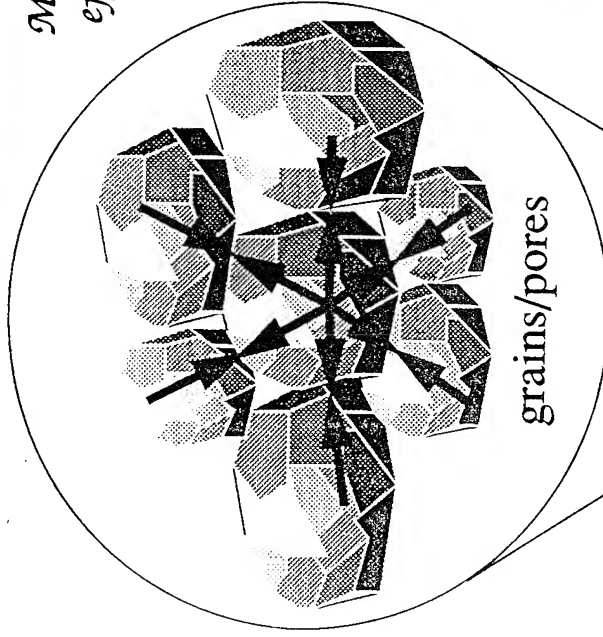
Continuum Mixture Theory

Engineering Sciences Center



Sandia
National
Laboratories

Microscale effects at internal boundaries have a profound effect on macroscale mechanical/chemical/thermal response



Theoretical foundation

- Balance laws
(Truesdell and Noll, Truesdell and Toupin)
- Internal Constraints
- Entropy Inequality
- Constitutive Principles
 - I. Phase Separation
 - II. Local Action
 - III. Frame-Indifference
 - IV. Dissipation

Continuum point

Continuum Mixture Theory



Engineering Sciences Center

* Nonequilibrium description

- conservation principles
- independent thermal-mechanical fields

* Volume fraction treated as independent kinematic variables

$$\psi_a = f(\rho_a, e_a, \bar{v}_a, \Pi_a, \dots, \phi_a)$$

* Interactions at internal boundaries

- constraints
- thermodynamics (2nd Law)



Thermodynamically -admissible constitutive laws



* Experimental quantification / guidance

Multicomponent Mixture Theory



Engineering Sciences Center

Conservation of Mass:

$$\dot{\rho}_a = -\rho_a \nabla \cdot \dot{\mathbf{v}}_a + c_a^\dagger$$

Conservation of Momentum:

$$\rho_a \ddot{\mathbf{v}}_a = \nabla \cdot \underline{\underline{\sigma}}_a + \rho_a \ddot{\mathbf{b}}_a + \dot{\mathbf{m}}_a^\dagger - c_a^\dagger \dot{\mathbf{v}}_a$$

Conservation of Energy:

$$\rho_a \dot{e}_a = \underline{\underline{\sigma}}_a : \dot{\nabla} \dot{\mathbf{v}}_a + \rho_a r_a + e_a^\dagger - (\dot{\mathbf{m}}_a^\dagger - c_a^\dagger \dot{\mathbf{v}}_a) \cdot \dot{\mathbf{v}}_a + c_a^\dagger \left(e_a + \frac{\dot{\mathbf{v}}_a \cdot \dot{\mathbf{v}}_a}{2} \right)$$

Constraints:

$$\sum_a c_a^\dagger = 0, \quad \sum_a \dot{\mathbf{m}}_a^\dagger = 0, \quad \sum_a e_a^\dagger = 0$$

Second Law:

$$\sum_a \frac{1}{T_a} \left(e_a^\dagger - \dot{\mathbf{m}}_a^\dagger \cdot \dot{\mathbf{v}}_a - c_a^\dagger \left(\psi_a + \frac{\phi_a p_a}{\rho_a} - \frac{1}{2} v_a^2 \right) - (\beta_a - p_a) \dot{\phi}_a - \frac{\dot{\mathbf{q}}_a \cdot \nabla T_a}{T_a} \right) \geq 0$$

Multiphase Characteristics Theory



Sandia
National
Laboratories

Engineering Sciences Center

1-D coupled PDE's:

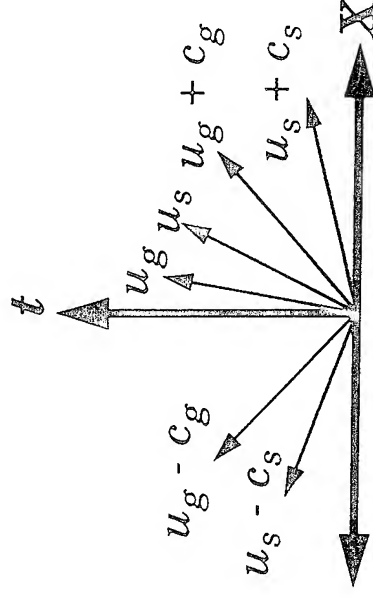
$$\frac{\partial \vec{U}}{\partial t} + \underline{A}(\vec{U}) \frac{\partial \vec{U}}{\partial x} = \vec{S}(\vec{U})$$

$$\vec{U} = (\rho_g, v_g, \eta_g, \phi_g, \rho_s, v_s, \eta_s)^T$$

Characteristics

$$\det(\underline{A}(\vec{U}) - \lambda \underline{I}) = 0 \quad \rightarrow$$

● Continuum description is hyperbolic



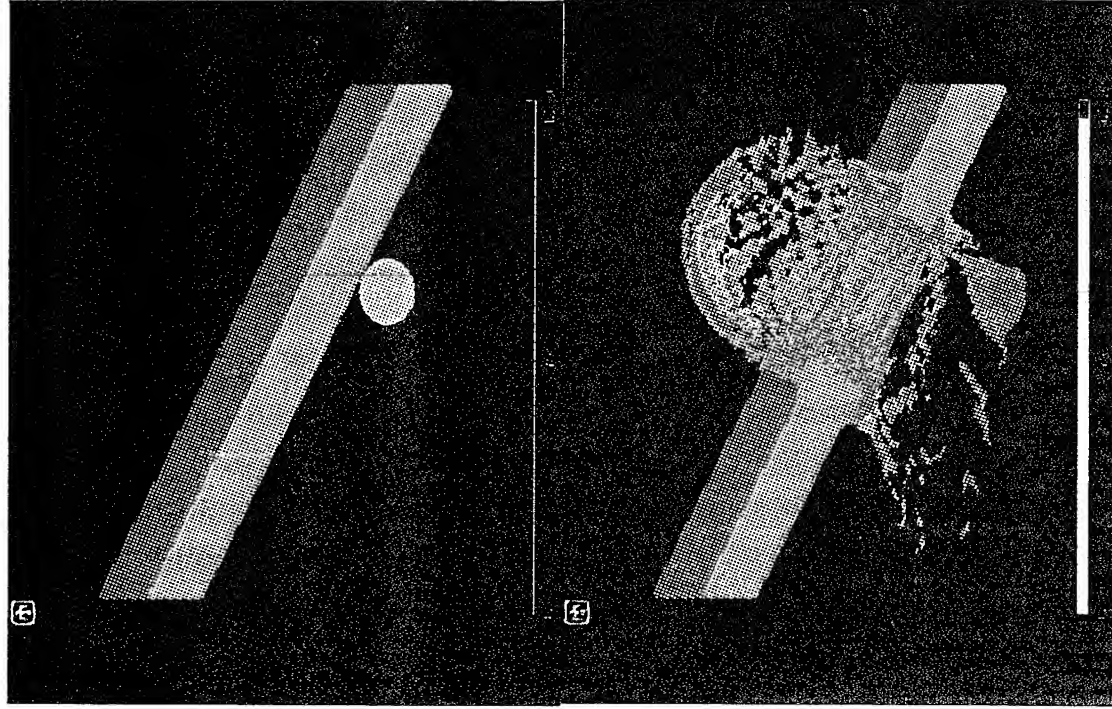
● Characteristics consistent with single phase theory

● u_s is a double characteristic

CTH - 3D Eulerian Shock Physics Code



Engineering Sciences Center



Phenomena:

Shock Wave Physics

Solid, liquid, vapor and mixed phases

Multimaterial

Elastic / Viscoplastic

Fracture / fragmentation

High Explosives

2nd order numerics

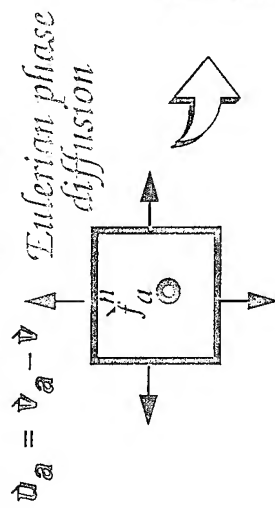
NEW ADDITION

Multiphase model based on
continuum mixture theory

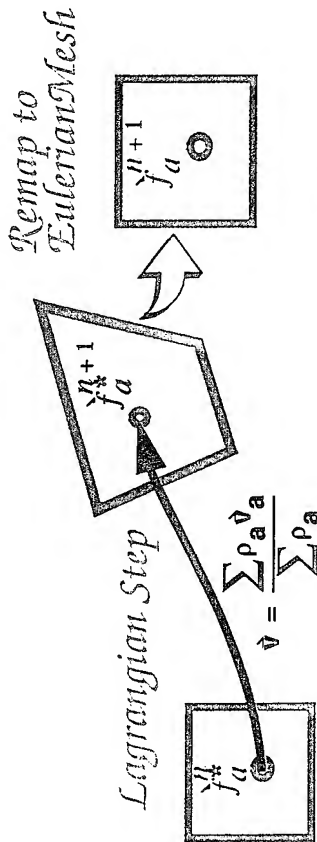
CTH Multiphase Mixture Model

Mixture and Phase variables: $\vec{Y} = (\rho, \rho \vec{v}, \rho E, \rho_a \rho_a \vec{v}_a \rho_a E_a \phi_a s_a \dots)^T$

Numerical Method:



(FCT / VCE solver)



(Stiff solver + interface tracker)

Finite Volume formulation:

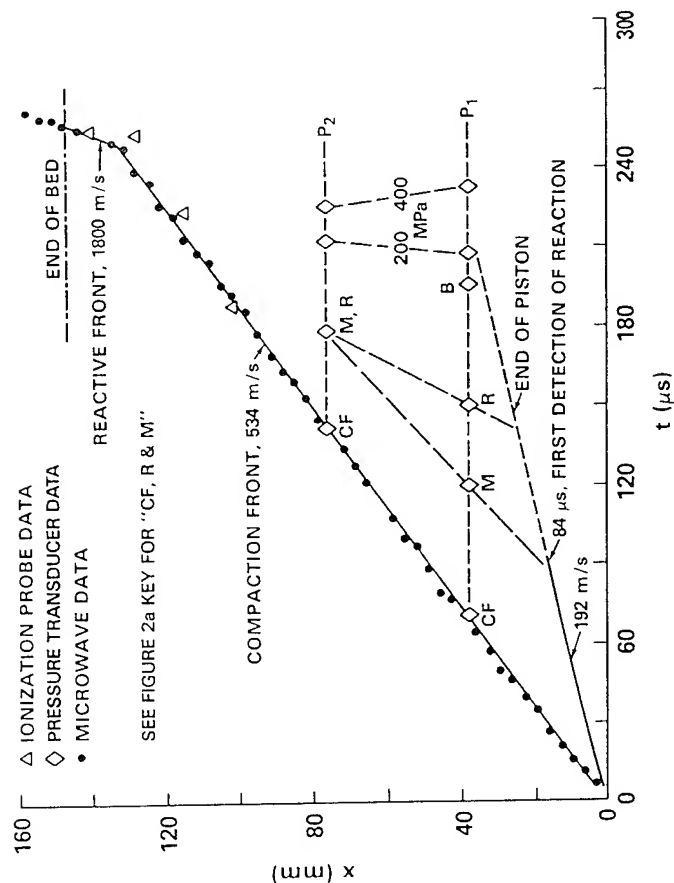
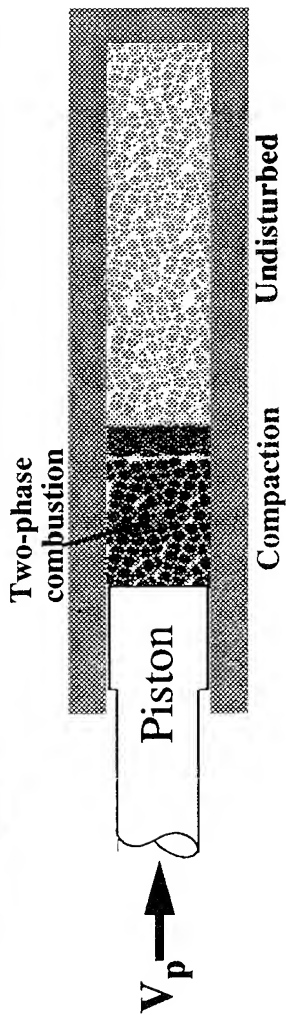
$$\frac{d}{dt} \int_{\beta} f_a dV = - \oint_{\partial \beta} (F_a \cdot n) dS - \oint_{\partial \beta} f_a (u_a \cdot n) dS = L_c(f_a)$$

$$\frac{d}{dt} \int_{\beta} f_a dV = \int_{\beta} R_a dV = L_P(f_a)$$

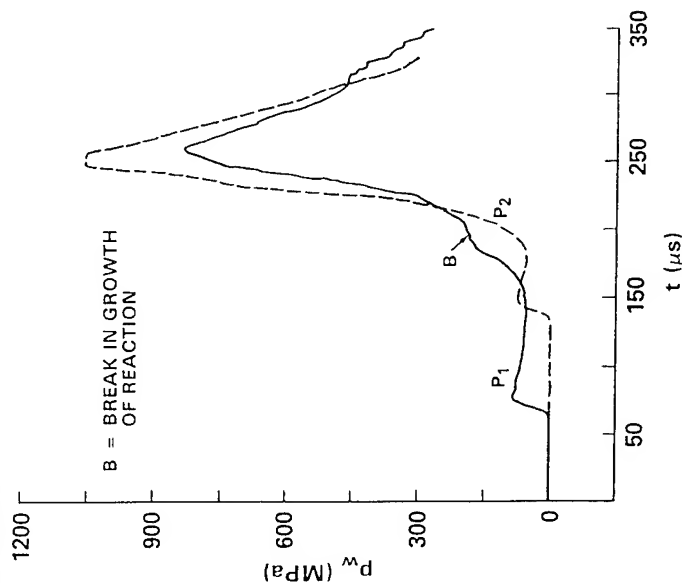
Low Velocity Impact on NC propellant bed



Engineering Sciences Center



Wave Trajectories



Pressure Histories

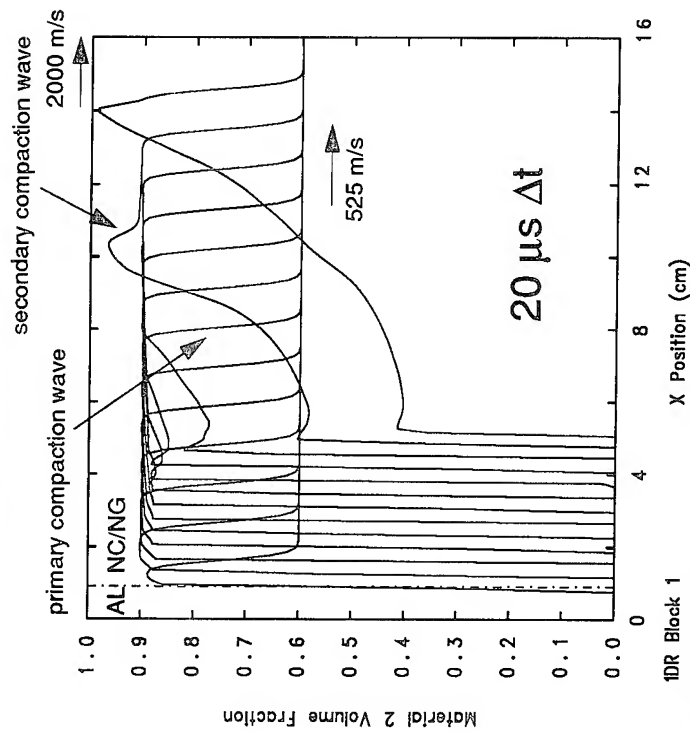
CTH Calculation of 190 m/s impact 60% TMD TS3659 NC/NG Ball propellant

Reactive Compaction Waves

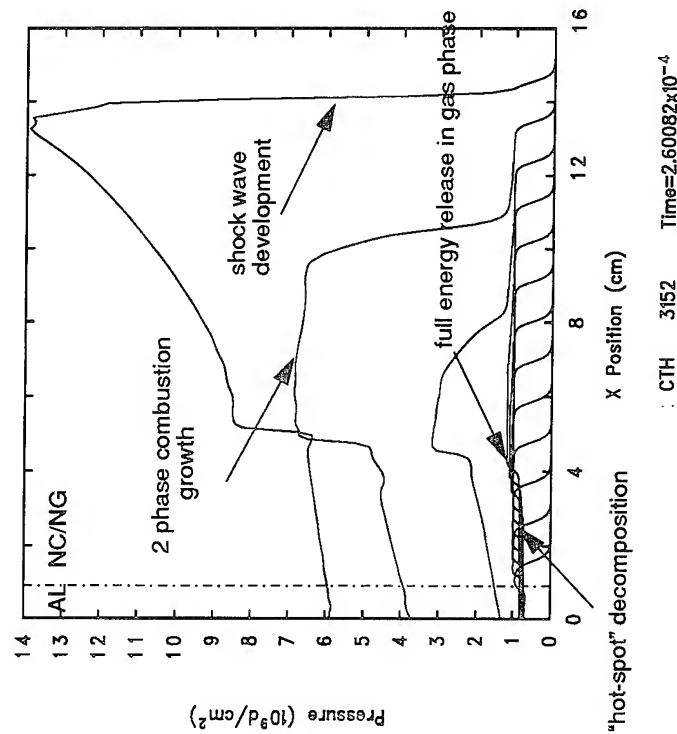


Engineering Sciences Center

Solid Volume Fraction



Mixture Pressure



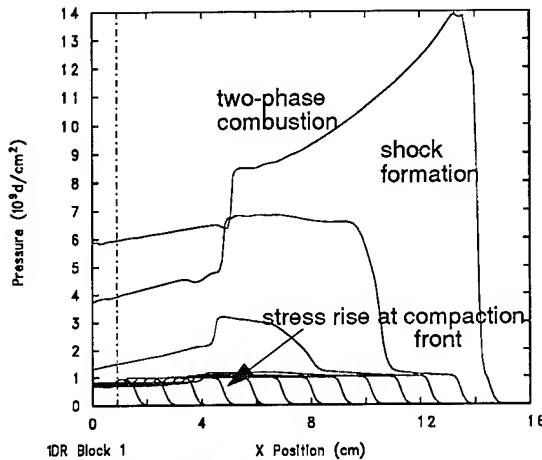
CTH Calculation Including Compaction-Induced Chemistry



Engineering Sciences Center

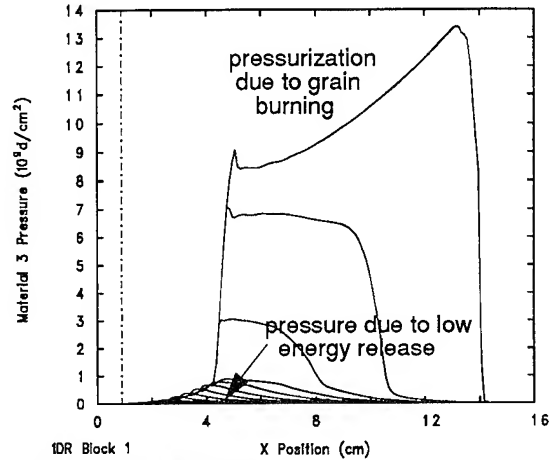
Mechanical Nonequilibrium between phases

Mixture Pressure



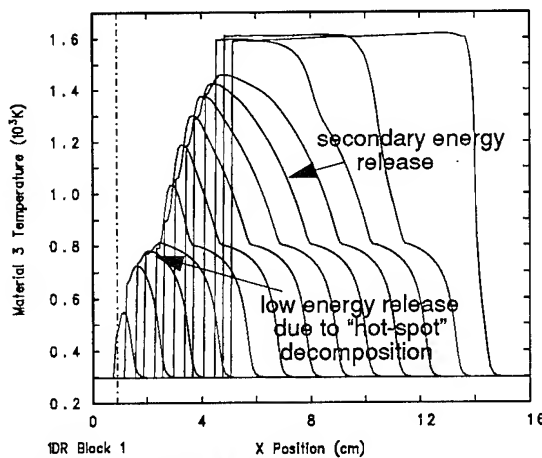
1-D Porous Impact Test Problem
DGJALO 4/07/94 10:55:32 CTH 3152 Time=2.60082x10⁻⁴

Gas Phase Pressure



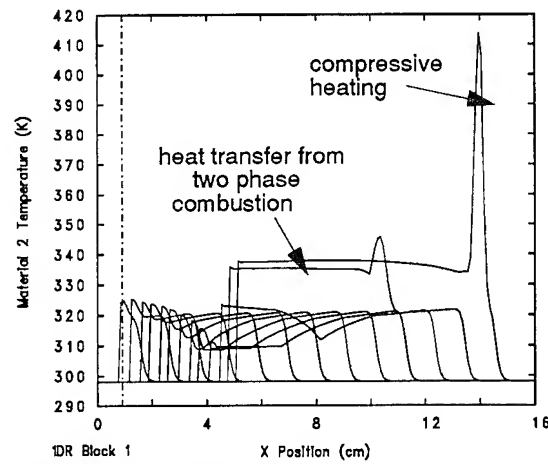
1-D Porous Impact Test Problem
DGJALO 4/07/94 10:55:32 CTH 3152 Time=2.60082x10⁻⁴

Gas Phase Temperature



1-D Porous Impact Test Problem
DGJALO 4/07/94 10:55:32 CTH 3152 Time=2.60082x10⁻⁴

Solid Phase Temperature



1-D Porous Impact Test Problem
DGJALO 4/07/94 10:55:32 CTH 3152 Time=2.60082x10⁻⁴

Thermal Nonequilibrium between phases

4/7/94

/u5/mrbaer/frame/rcth1.vg

3 Component Admissible Interaction Laws



Engineering Sciences Center

$$m_1^+ = -m_2^+ - m_3^+$$

$$m_2^+ - \frac{1}{2}c_2^+ (p_2 + p_1) - p_1 \nabla \phi_2 = \delta_{1,2} (p_1 - p_2) + \delta_{3,2} (p_3 - p_2)$$

$$m_3^+ - \frac{1}{2}c_3^+ (p_3 + p_1) - p_1 \nabla \phi_3 = \delta_{1,3} (p_1 - p_3) + \delta_{2,3} (p_2 - p_3)$$

$$e_1^+ = -e_2^+ - e_3^+$$

$$e_2^+ - (m_2^+ - c_2^+ p_2) \cdot p_2 + c_2^+ \left(e_2 + \frac{p_2 \cdot p_2}{2} \right) - (\beta_2 - p_2) \left(\dot{\phi}_2 - \frac{c_2^+}{\gamma_2} \right) = H_{1,2} (T_1 - T_2) + H_{3,2} (T_3 - T_2)$$

$$e_3^+ - (m_3^+ - c_3^+ p_3) \cdot p_3 + c_3^+ \left(e_3 + \frac{p_3 \cdot p_3}{2} \right) - (\beta_3 - p_3) \left(\dot{\phi}_3 - \frac{c_3^+}{\gamma_3} \right) = H_{1,3} (T_1 - T_3) + H_{2,3} (T_2 - T_3)$$

$$\dot{\phi}_2 - \frac{c_2^+}{\gamma_2} = \tau_{1,2} (p_2 - \beta_2 - p_1 + \beta_1) + \tau_{3,2} (p_2 - \beta_2 - p_3 + \beta_3)$$

$$\dot{\phi}_3 - \frac{c_3^+}{\gamma_3} = \tau_{1,3} (p_3 - \beta_3 - p_1 + \beta_1) + \tau_{2,3} (p_3 - \beta_3 - p_2 + \beta_2)$$

$$b_{i,j} = b_{j,i} \geq 0 \quad ; \quad b \in (\delta, H, \tau)$$

AL / Fe_2O_3 Experiment (6 Kb input)

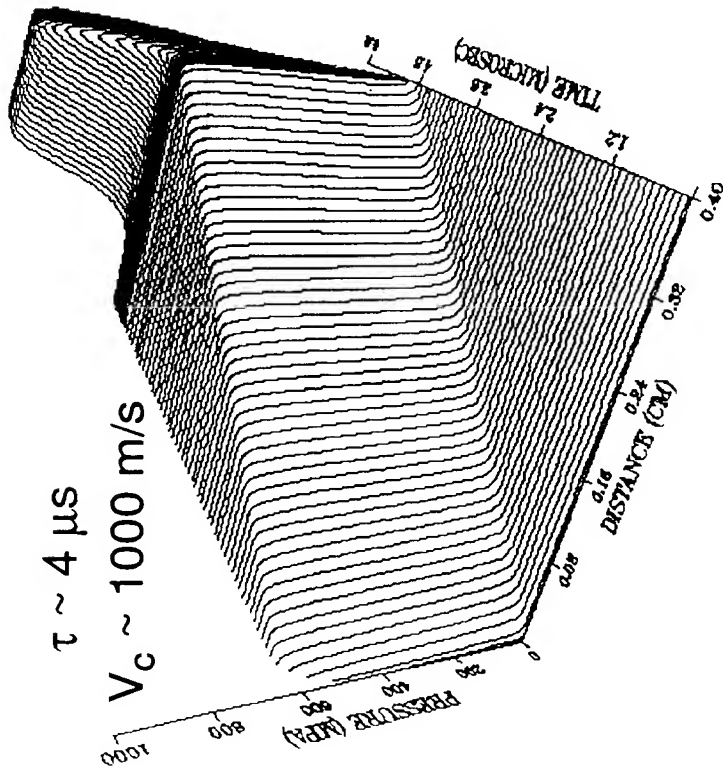


Engineering Sciences Center

Al

$\tau \sim 4 \mu\text{s}$

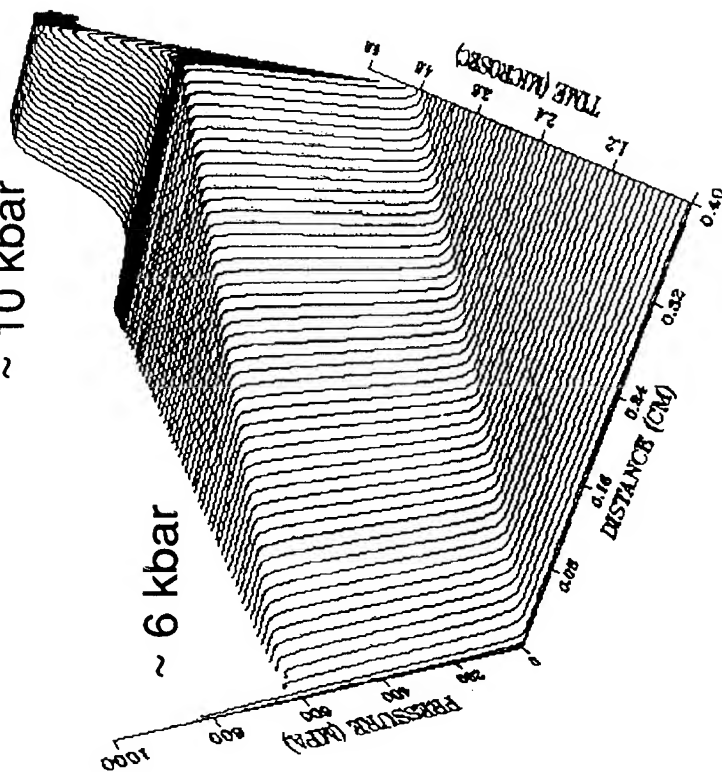
$V_c \sim 1000 \text{ m/s}$



Fe_2O_3

$\sim 10 \text{ kbar}$

$\sim 6 \text{ kbar}$



Pressure Fields

3 Component Approximation



Engineering Sciences Center

Initial Porous Mixture:

Void + A (Al) + B (Fe_2O_3)
 (1) (2) (3)

$$\phi_2^\circ = 0.22$$

$$\phi_3^\circ = 0.33$$

$$p_1, \beta_1 \sim 0.0$$

p_2, p_3 Mie-Gruneisen form

β_2, β_3 Konopicky eqns.

(Al - Wang and Zaidi, Powder Tech, 66, (1991)

Fe_2O_3 - Prasad and Varma, Indian J Tech, 18, (1980))

$$\delta_{1,2}, \delta_{1,3}, \delta_{2,3} \rightarrow \infty$$

Neglect phase diffusion

$$H_{1,2}, H_{1,3} \rightarrow 0$$

$H_{2,3}$ microlayer conduction model

No reactions

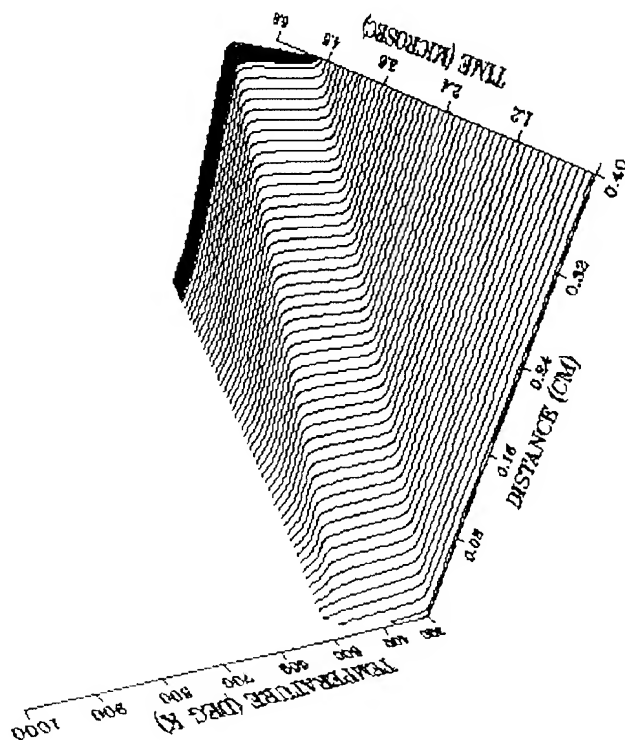
$$\tau_{i,j} \sim \frac{\phi_i \phi_j}{\gamma_{cs} d_p}$$

AL / Fe_2O_3 Experiment (6 Kb input)

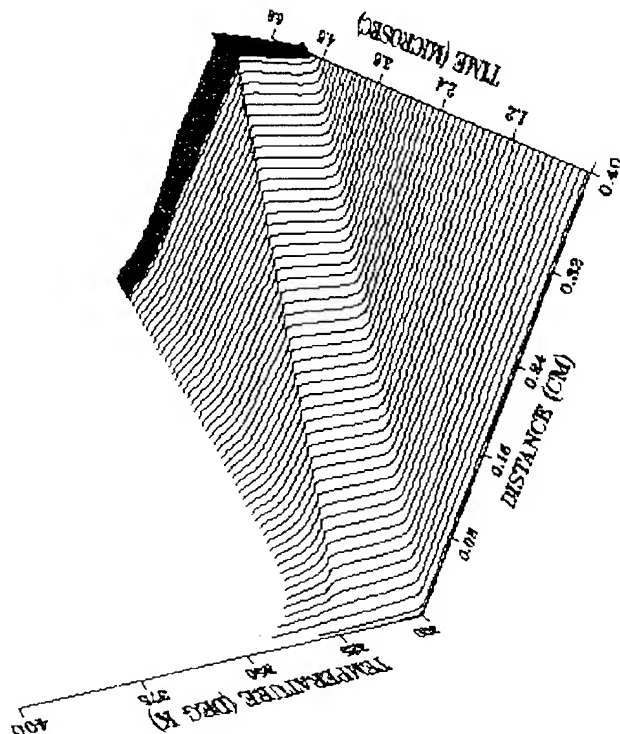


Engineering Sciences Center

Al



Fe_2O_3



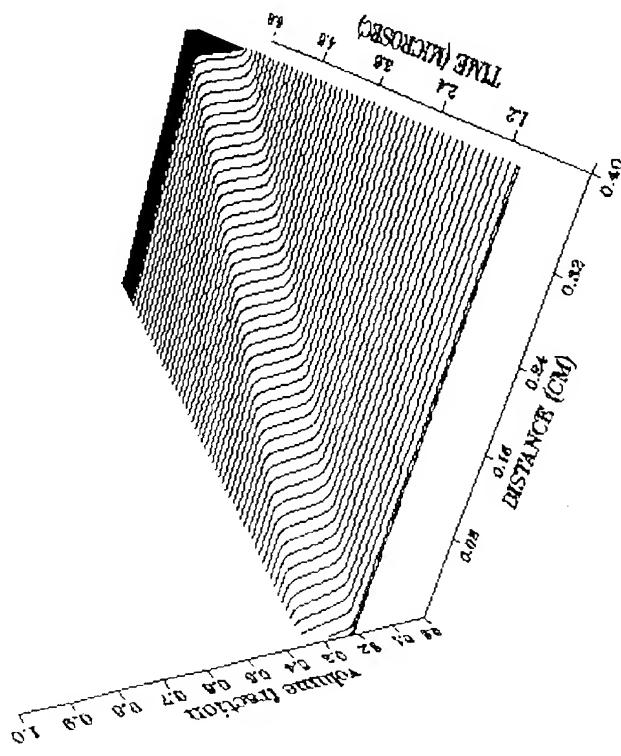
Temperature Fields

AL / Fe_2O_3 Experiment (6 Kb input)

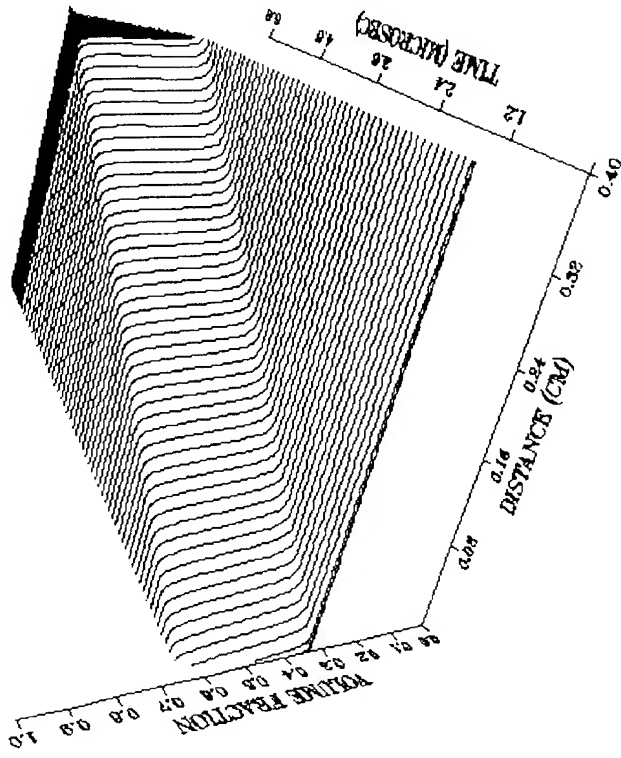


Engineering Sciences Center

Al



Fe_2O_3



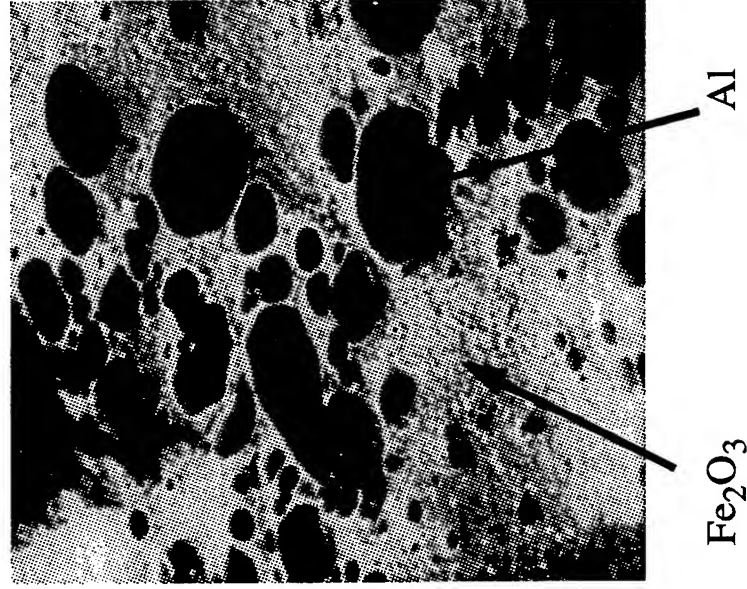
Volume Fraction Fields

Recovery Observations of Shocked 2 Al + Fe₂O₃



Engineering Sciences Center

20 μm



Initial mixture:

$$\phi_{\text{Al}}^0 = 0.22 ; \quad \phi_{\text{Fe}_2\text{O}_3}^0 = 0.33$$

$$\phi^0 = 0.55$$

Input Shock: 6.7 Kbar

Summary



Engineering Sciences Center

Problem of multiple scales

more insights into:

- *dispersive nature of multiphase waves*
- *localized mechanics*
- *nature and quantified "hotspots"*
- *chemical paths vs. thermal paths*
- *mixed phase behavior*

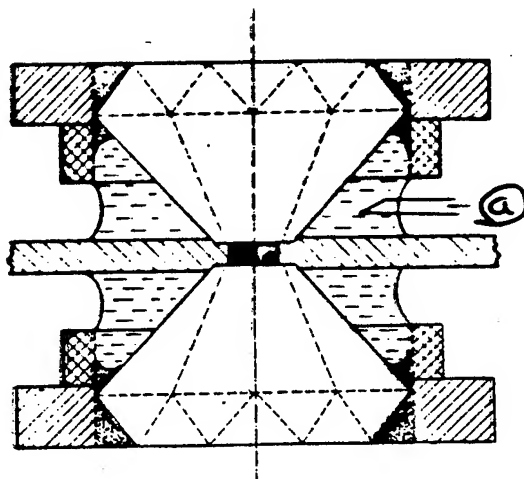
Experimental diagnostics to the granular level

Mixture theory offers a promising approach to describe composite reactive wave behavior

Micromechanical modeling

YINS SAMPLE RECOVERY TECHNIQUE

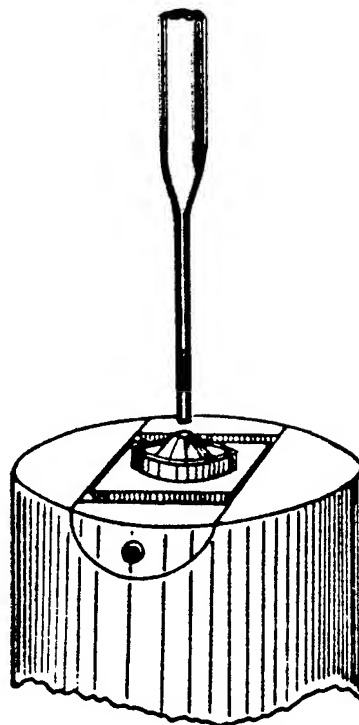
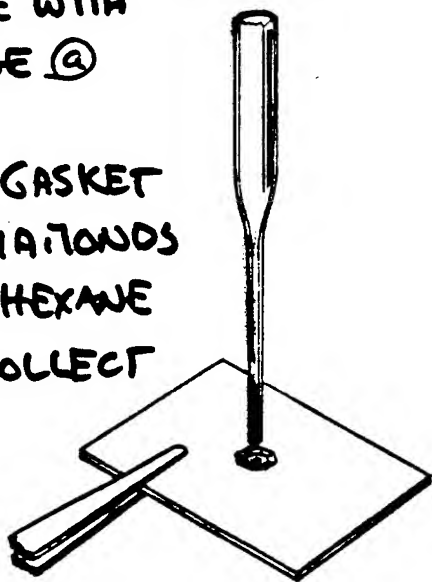
- ① SURROUND COMPRESSED CELL WITH HEXANE



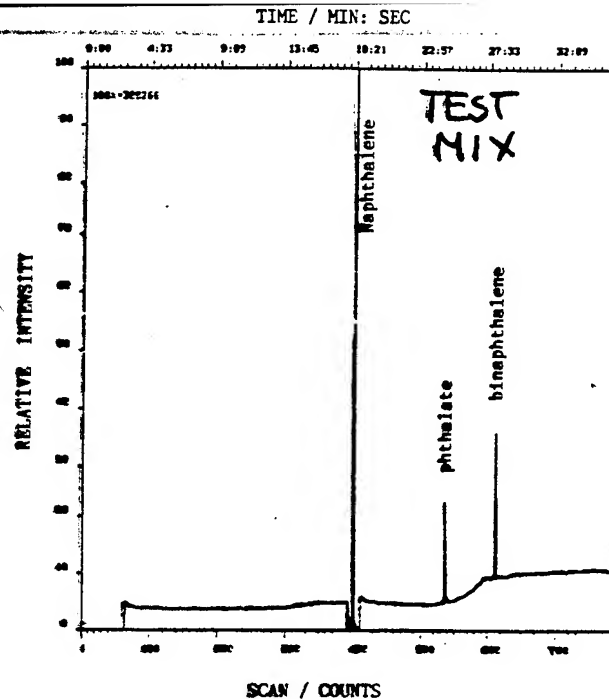
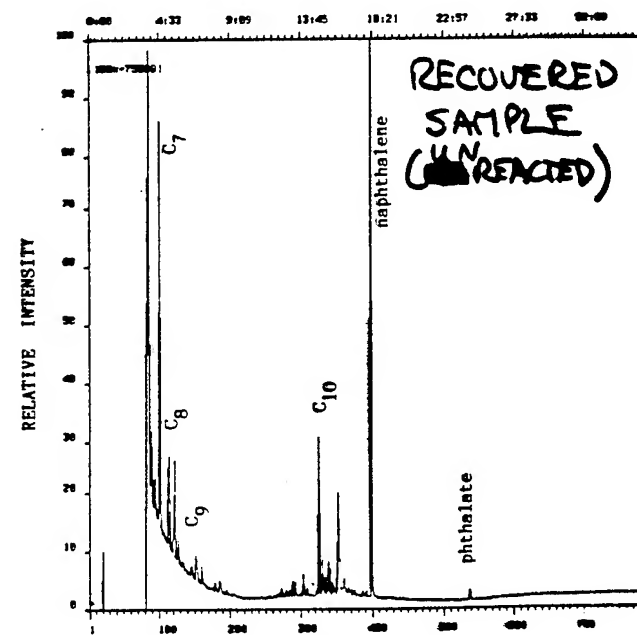
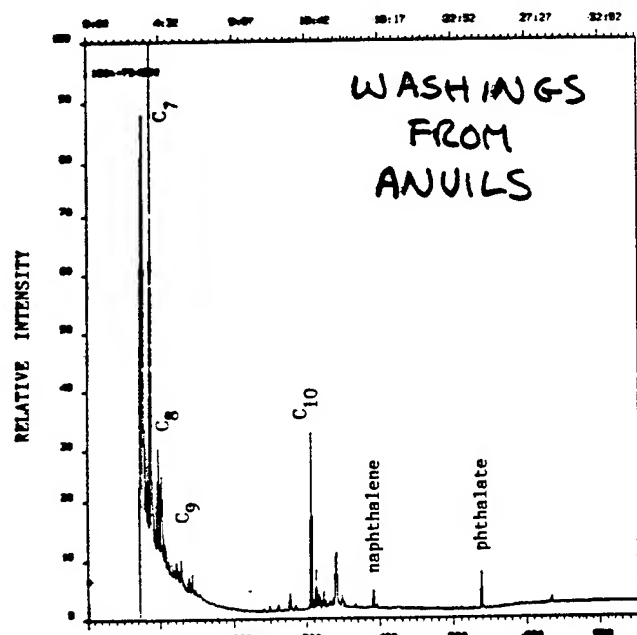
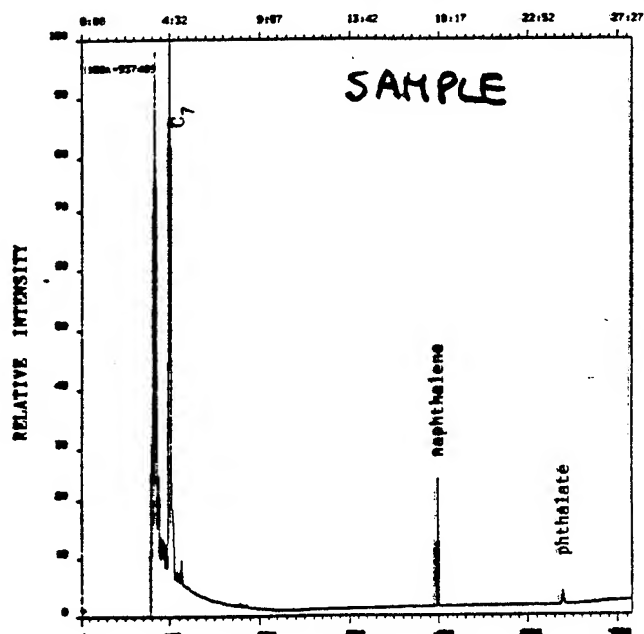
SAMPLE
 $V \approx 14 \times 10^{-9} \text{ l}$
 $m_N \approx 50-100 \text{ ng}$

- ② OPEN CELL AND REMOVE SAMPLE WITH SYRINGE a

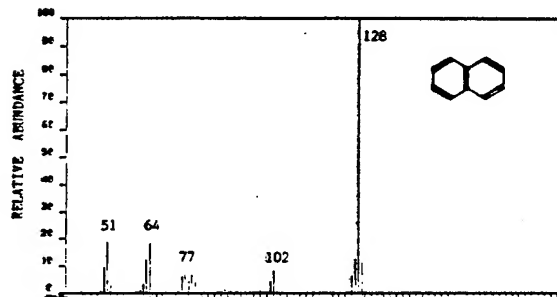
- ③ WASH GASKET AND DIAMONDS WITH HEXANE AND COLLECT WASH.



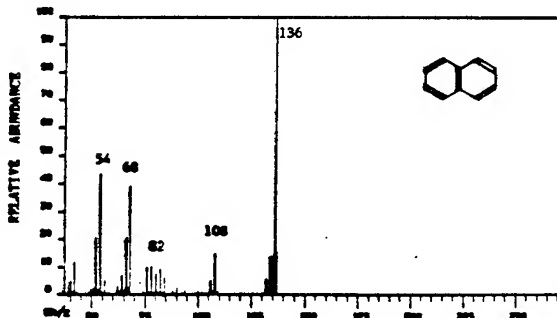
TIME / MIN: SEC



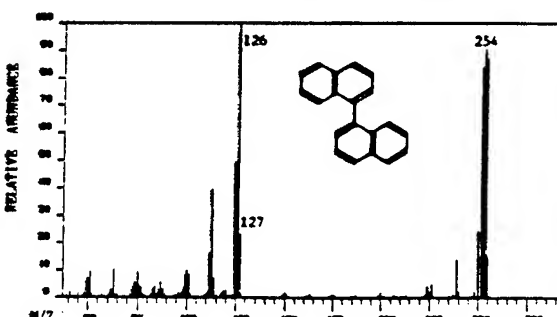
b. MASS INTENSITY REPORT: 00367-412 (TIC-00342, 000-0000)
00054-411 (TIC-00370, 000-0000)



c. MASS INTENSITY REPORT: 00370-20 (TIC-00410, 000-0000)
00370-275 (TIC-00442, 000-0000)



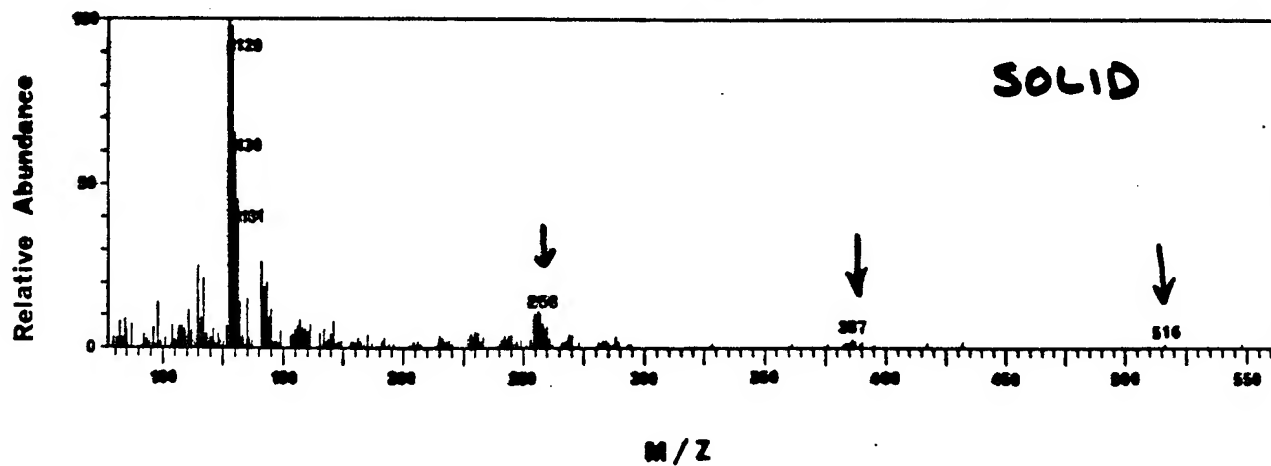
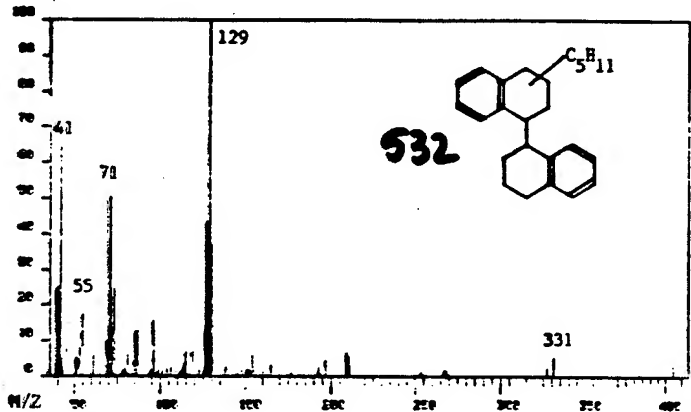
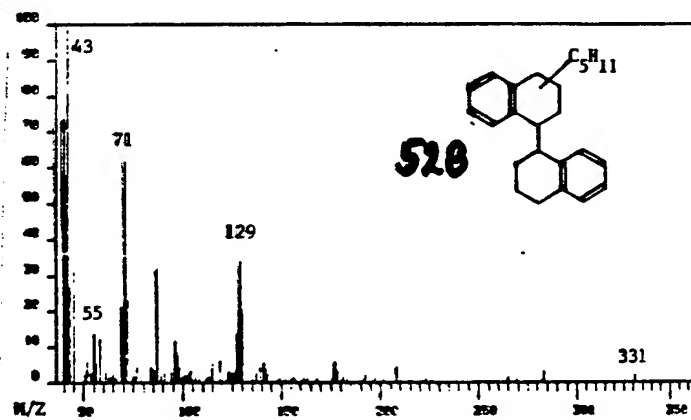
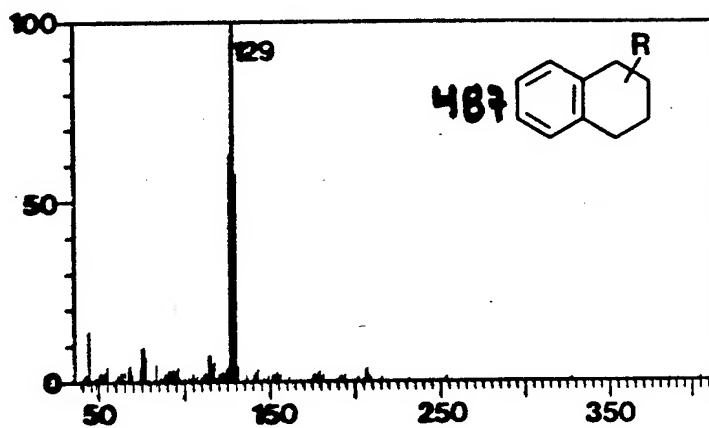
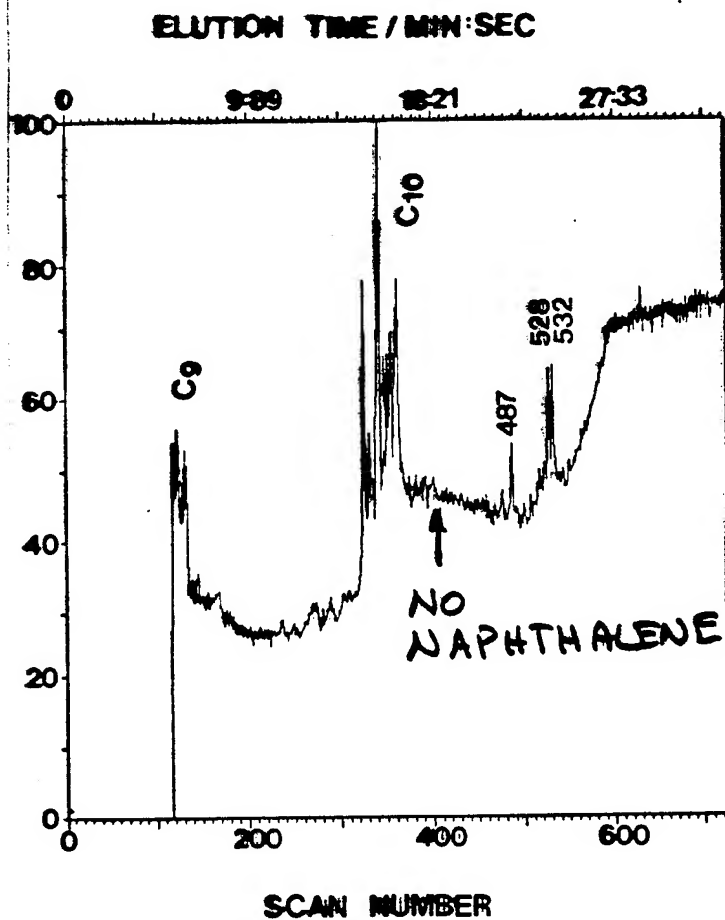
d. MASS INTENSITY REPORT: 00046-000 (TIC-00000, 000-0000)
00046-000 (TIC-00000, 000-0000)



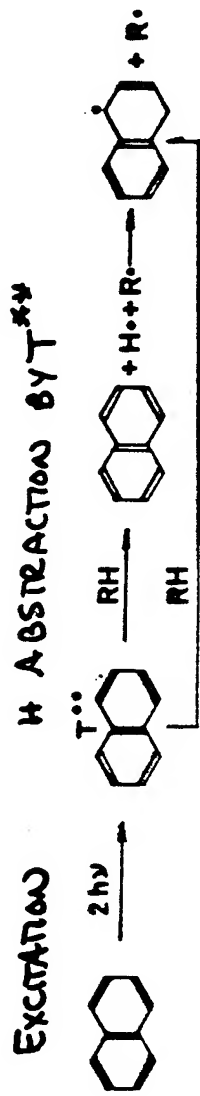
GC/MS SPECTRA (SELECTED) OF ~~REAGENTS~~ REAGENTS

GC-MS Elution Pattern of Photoproducts (Collected with Methanol)
 from 5×10^{-2} Naphthalene in 1:1 Pentane:Isopentane at 3.5 GPa and
 Mass Spectra of the Precipitate and GC Peaks 487, 528, and 532.

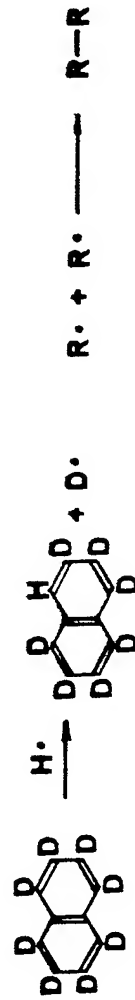
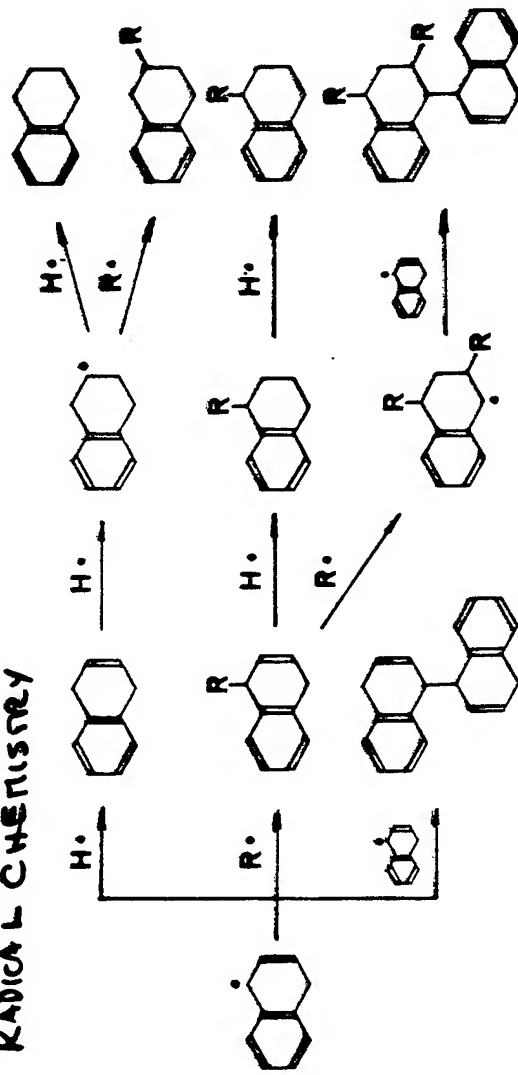
NOTE: No naphthalene was detected!



SOME PROBABLE MECHANISTIC STEPS



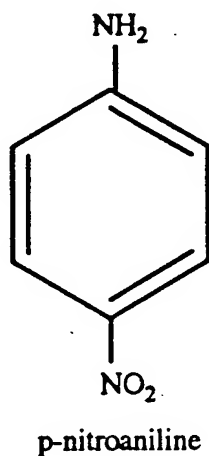
RADICAL CHEMISTRY



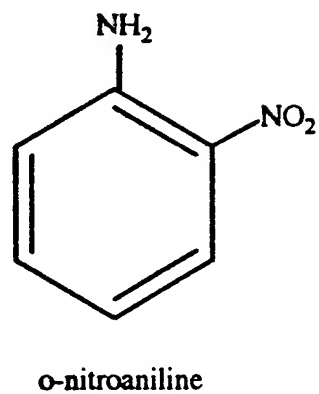
DEUTERATED NAPHTHALENE AND PROTONATED

SOLVENT YIELD SIGNIFICANT C₁₀D₇H

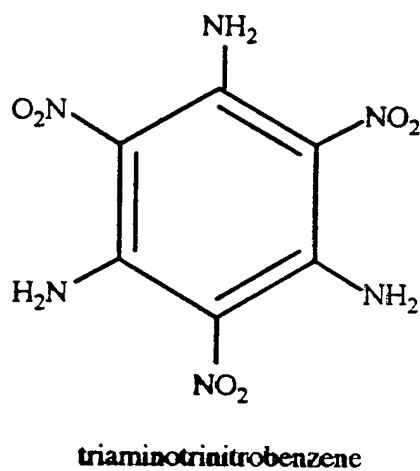
AT EARLY STAGE OF R_x



PNA

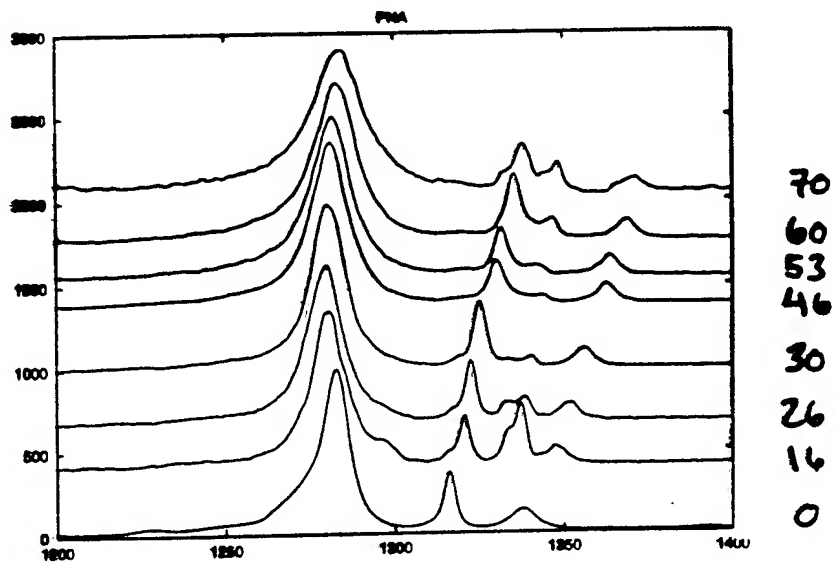
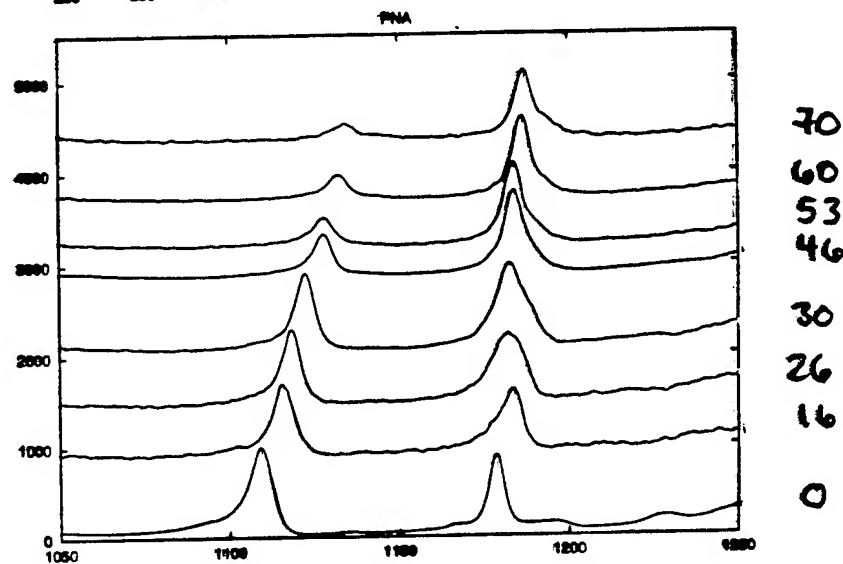
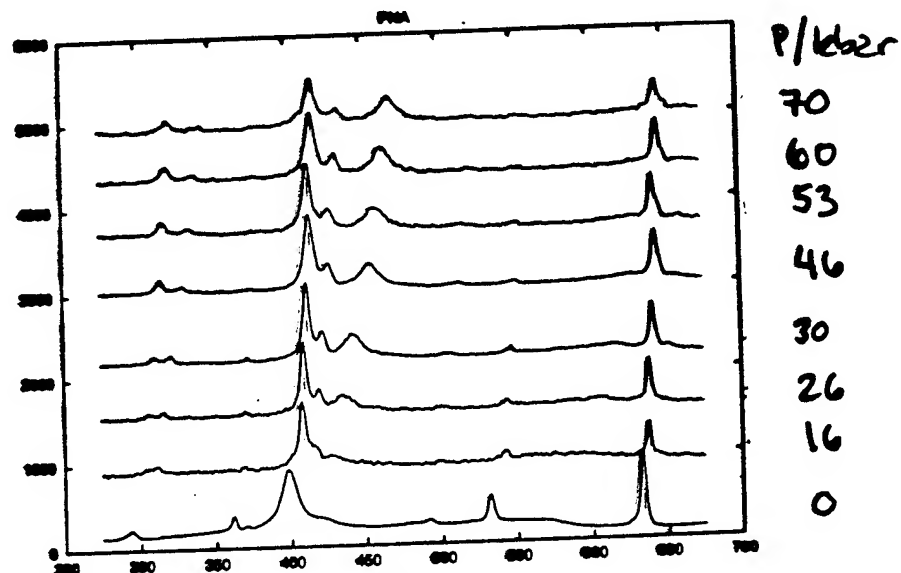


ONA



TATB

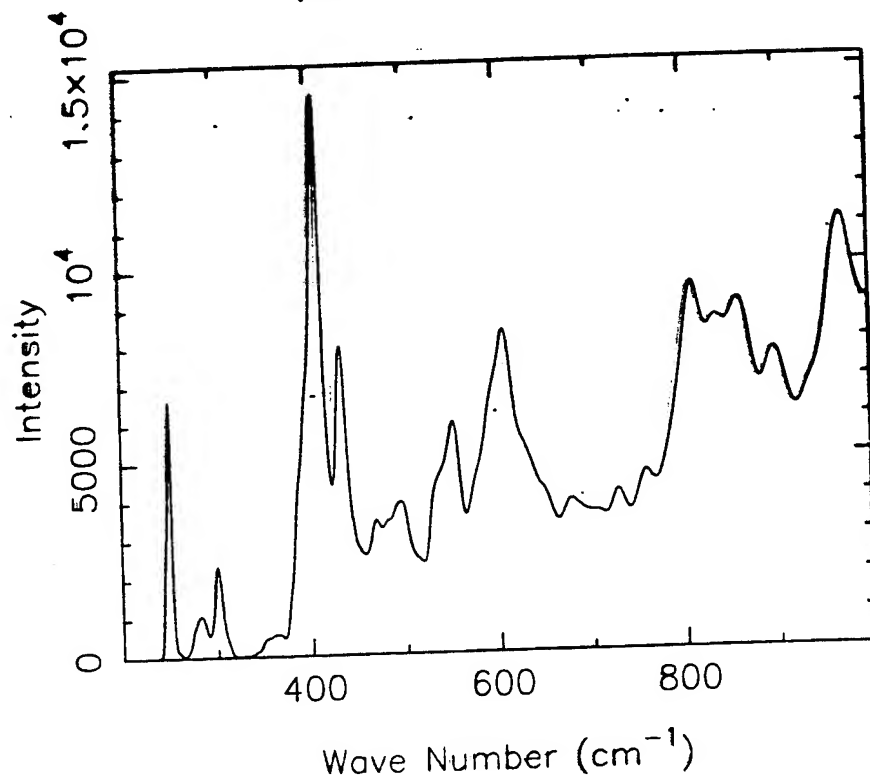
EFFECT OF PRESSURE ON THE RAMAN SPECTRUM OF PNA



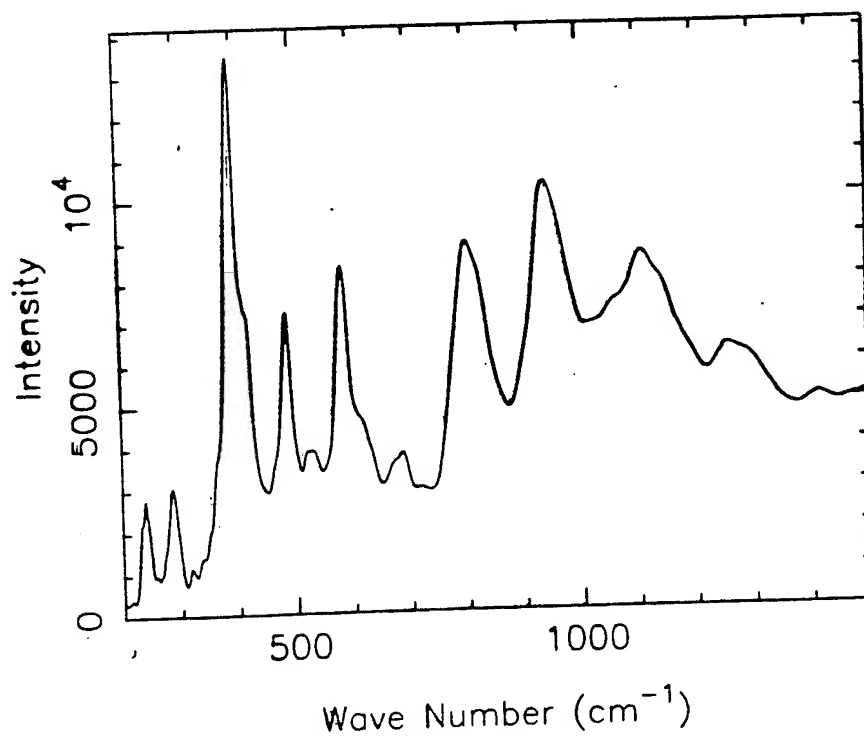
Raman shift /cm⁻¹

INELASTIC NEUTRON SCATTERING SPECTRUM OF PNA

pNA 1.5GPa 15K me1

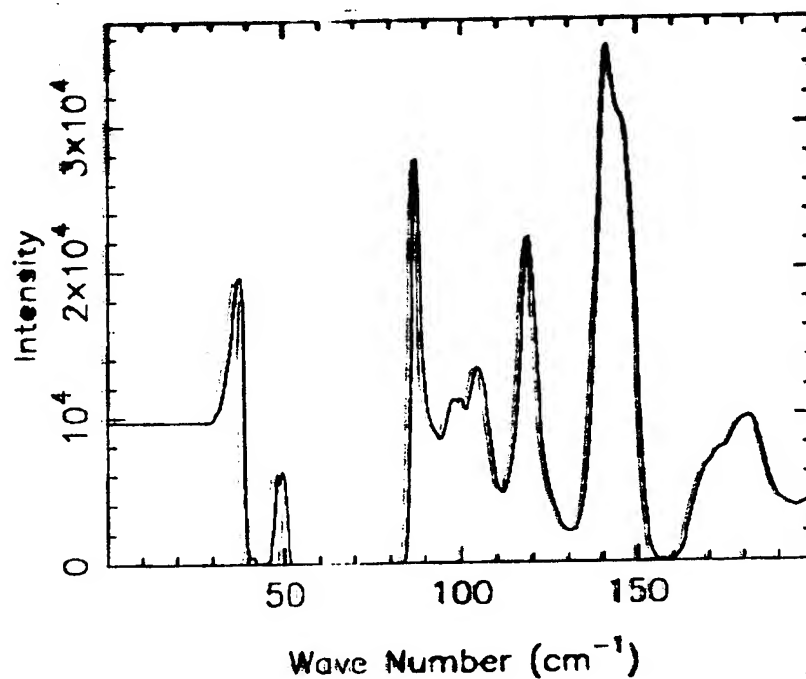


pNA

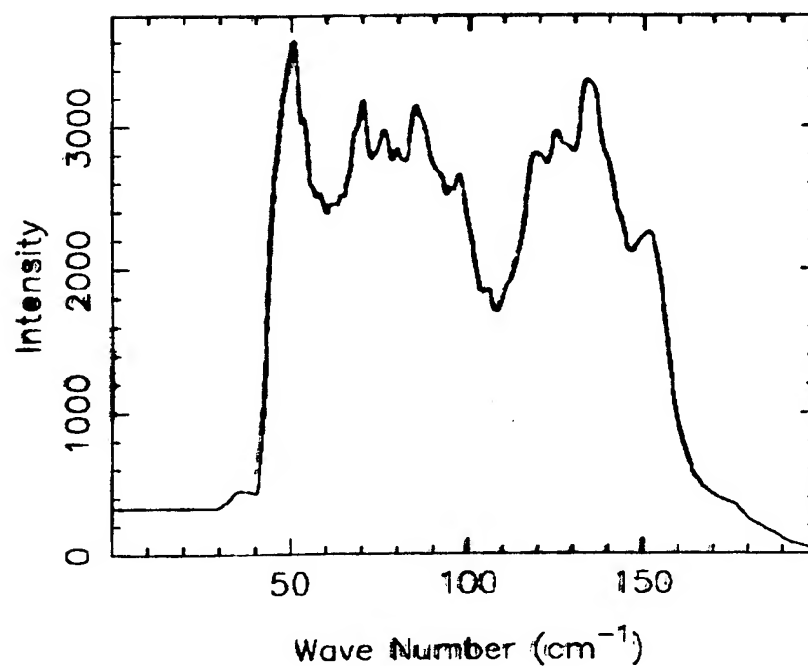


INELASTIC NEUTRON SCATTERING SPECTRUM OF PNA

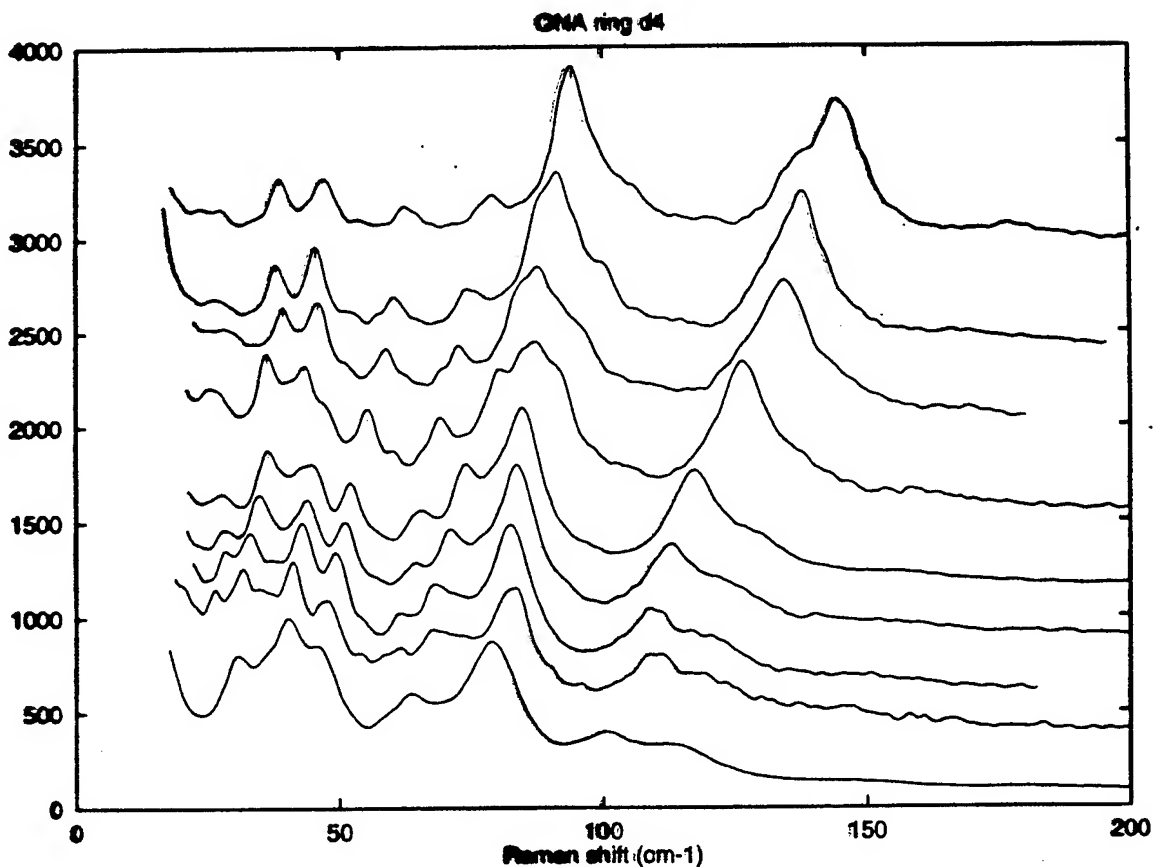
PNA 15K 10kbar (me01)



PNA low temp, amb press ME01



LATTICE MODE REGION FOR ONA: A LOW PRESSURE PHASE TRANSITION

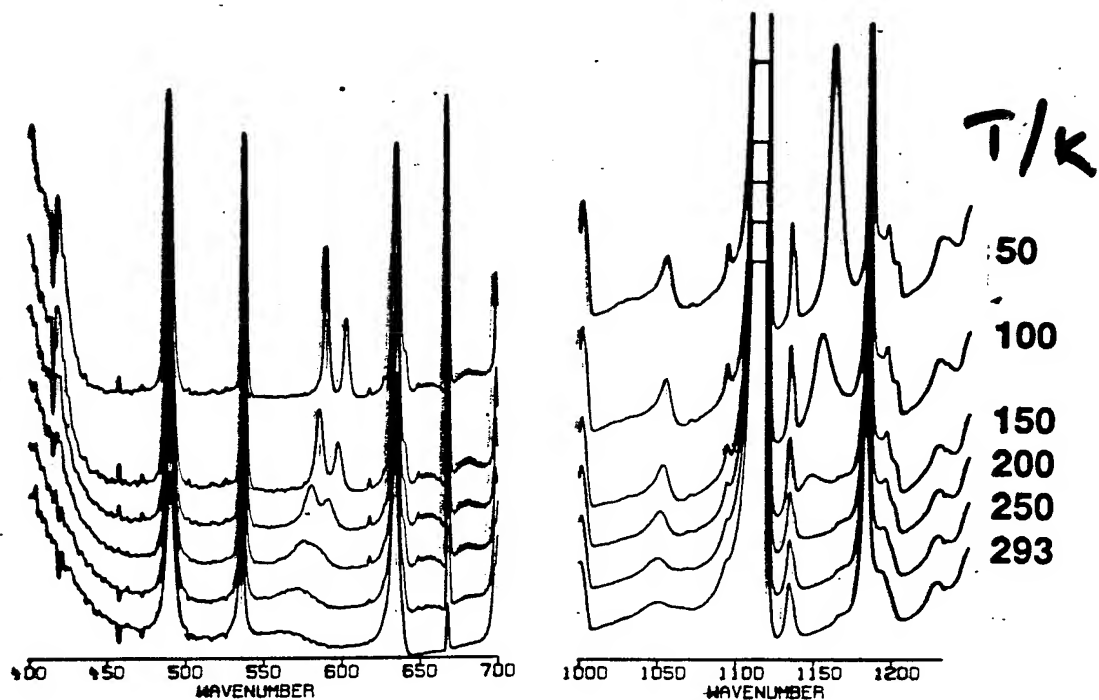


P/kbar
21
17
15
11 ←
7
4
3
2 ←
0

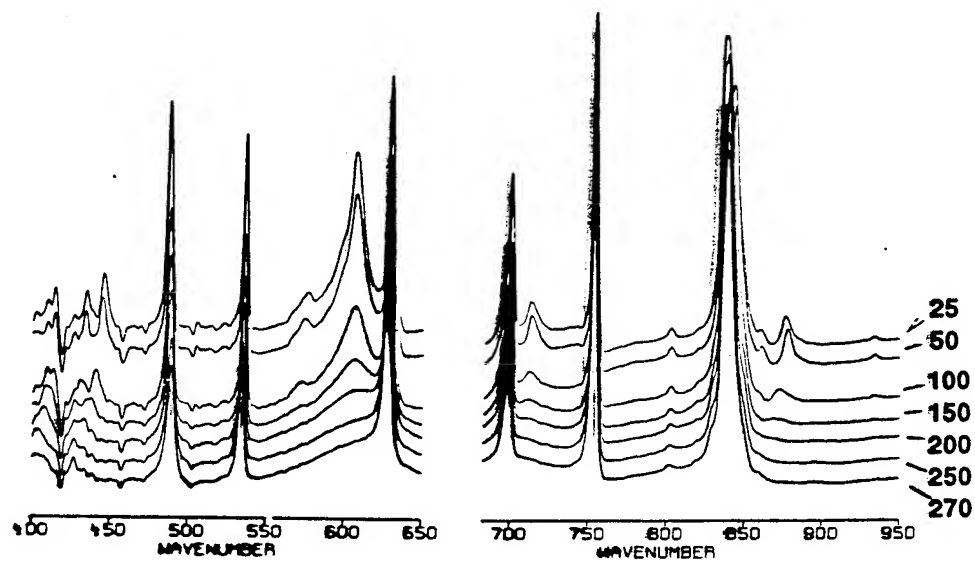
COOLING STUDY

1Ea

PNA



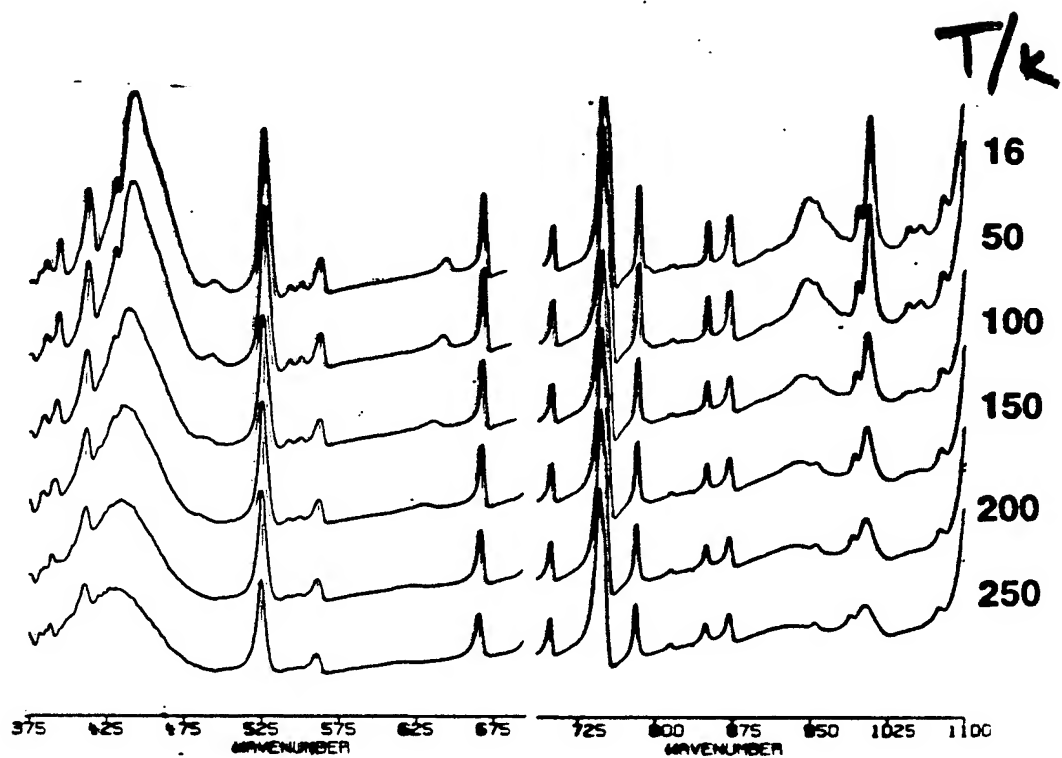
PNA
ND₂



COOLING STUDY

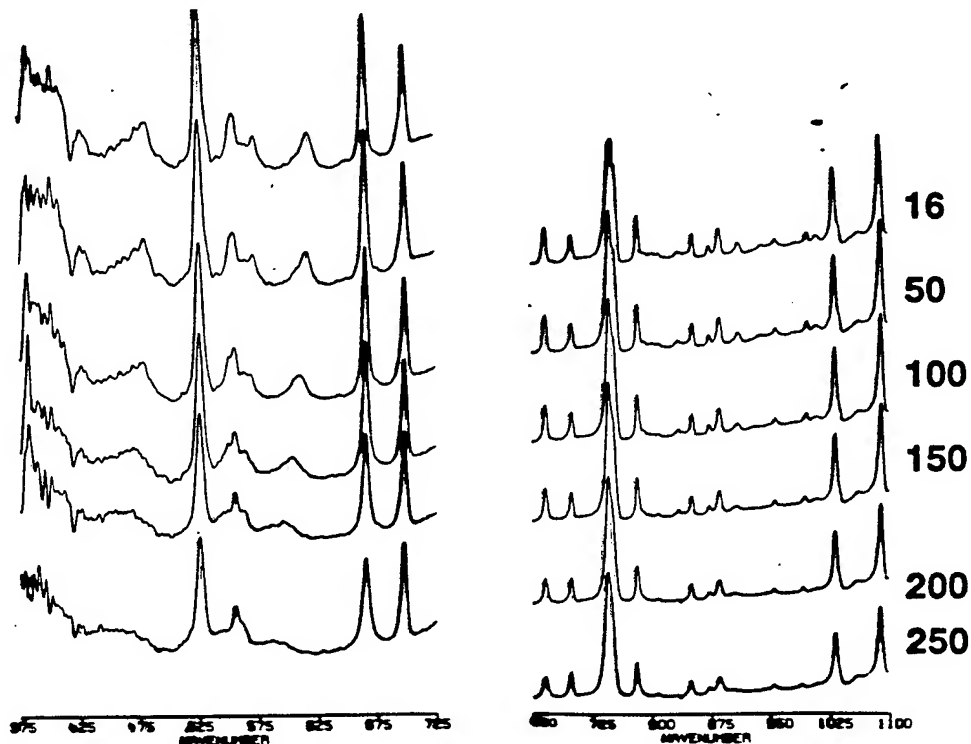
186

ONA



ONA

ND₂



MECHANISM OF SHOCK-INDUCED MECHANOCHEMISTRY

John J. Gilman
Department of Materials Science and Engineering
University of California at Los Angeles
Los Angeles, California, 90024

Mechanochemistry means chemical reactions driven by large mechanical strains. It was first reported by Bridgman in 1935, and since then studied extensively by Enikolopyan and by Boldyrev in Russia as well as Sohma in Japan. It is athermal; that is, independent of temperature, although it may sometimes be assisted by temperature. The mechanical strains affect the electronic structures of solids (or rapidly loaded liquids). If the overall strain tensor is compressive, shear strains are particularly important because they bend covalent bonds, thereby tending to close the LUMO-HOMO energy gaps.

Closure of a LUMO-HOMO gap causes metallization. That is, it allows the bonding electrons to become delocalized, and thereby to rearrange as needed to carry out a chemical reaction. Since the process is electronic, it can proceed at a very high rate. Thus this mechanism can keep up with sharp shock fronts.

If the overall strain tensor is tensile, a potential is developed which causes bonding electrons to tunnel across the LUMO-HOMO gap into anti-bonding states. That is, dissociation occurs. But this process will not be discussed further here since it does not lead to chemical reactions.

Evidence of LUMO-HOMO gap closure is provided by the monomolecular reactions that occur in covalent solids when they are subjected to compression; either in high-pressure cells, or during the formation of indentation hardness impressions. Eight cases are known in which cubic covalent semiconductors change their structures from the diamond-type to the beta-tin-type, and simultaneously become metallic. Evidence is also present under shock conditions where large increases in electrical conductivity have been observed just behind shock fronts by the Russian group of Zeldovich, by Melvin Cook, and by others. Also, optical opacity has been observed at detonation fronts. This indicates a high level of electrical conductivity at the front.

Further evidence that closure of the LUMO-HOMO gap plays an important role in mechanochemical reactions is provided by the fact that the stabilities of aminated trinitrobenzenes correlate linearly with their gaps. In the series: trinitro-benzene, monoamino-trinitro-benzene, diamino-trinitro-benzene, and triamino-trinitro-benzene; the LUMO-HOMO gap increases as does the stability. That is, TB is a very sensitive explosive, whereas TATB is quite insensitive.

The state of strain at a shock front is uniaxial compression. This is a combination of shear and isotropic compression. Behind the front the shear strains may, or may not, be relaxed through plastic flow or other processes, but initially the front imposes both shear and isotropic compression on the material. Since electronic processes are at least 10X as fast as acoustic processes this means that any changes that might be induced by the shear strains will have adequate time to occur. It also means that the material cannot escape being severely sheared as a high amplitude shock passes through it. This is emphasized here because much of the literature on shock-induced processes ignores shear effects.

Shear effects are expected to be more important in most cases than the effects of isotropic compression for the following reasons: a. they cause the major part of the heating if the material is porous; b. covalent bonds having smaller bending force constants than compression force constants; c. shear strains cause larger changes in the electronic structures of materials than isotropic compressions do because they reduce the symmetry of the molecular structure; and d. shear strains cause shape changes and this is consistent with the molecular shape changes that occur during chemical reactions.

A specific example of a shock induced reaction is the polymerization of benzene. This has been analyzed by Gilman and Armstrong. Its molecules are known to polymerize under quasi-static conditions at imposed pressures above 4 GPa. with temperatures above 600°C. It was suggested that the polymerization process starts with the combination of two benzene molecules to form one biphenyl molecule followed by further carbon additions and hydrogen subtractions to build up polyphenylenes; and other polymers. Normally flat benzene molecules buckle under compression applied parallel to their planes into the chair configuration. This deformation largely destroys the π -bonding, raising the energy level of the HOMO level, and lowering the LUMO level, thereby eliminating the HOMO-LUMO gap. Thus the bonding electrons are delocalized, allowing polymerization to proceed. The critical strain for this is estimated from molecular

mechanics. The bond lengths do not change, while the bond angles change from 120° to 109.5° . The compressive strain is about -4.3%; assuming that the molecules contract laterally by -5.7%. The volume change is about -5%. The carbon molecular orbitals change from the sp^2 trigonal type of benzene, to the sp^3 tetrahedral type of methane and diamond.

According to ultraviolet spectroscopy, the magnitude of the LUMO-HOMO gap is 3.65 eV. The molecular volume is 127 \AA^3 , so the excitation energy density (in mechanical units) is 4.6 GPa. Both static, and dynamic, studies of compressed benzene indicate that polymerization occurs when the macroscopic compression reaches about 0.5 at pressures in the range: 10-20 GPa. Electrical conduction at both low and high frequencies is also observed as expected from the present model.

Shock impact data provide the clearest benchmark for the onset of polymerization. It occurs at about 15 GPa., and a macroscopic uniaxial compression of 0.5, yielding a work of compression of about 7.5 GPa. But only part of this can be associated with shear strains. Multiplying by 3/5ths (the average ratio of the shear to the bulk modulus) gives 4.5 GPa. which is remarkably close to the necessary excitation energy-density given above.

Now turn to the azides. They explode through decomposition of the azide ion, yielding nitrogen gas. This consists of three nitrogen atoms (usually in a linear array) bound together by a σ -orbital and two π -orbitals. If the ion is bent, the π -orbitals must be substantially disturbed, thereby raising the bonding level (HOMO) and lowering the antibonding level (LUMO).

Initially the energy gap in $\text{Pb}(\text{N}_3)_2$ is 1.64 eV. (the first exciton level is 1.26 eV.) Bending a linear triad shortens its length. If the bend angle is δ , the longitudinal strain is $(1 - \cos \delta)/2$. The work of bending is about $(k_\delta \delta^2)/2$ where k_δ is the bending force constant = 4.63 eV/rad. Thus the work equals the initial gap when $\delta = 0.84 \text{ rad.}$, or the critical longitudinal strain = 0.17. Since the compressive strains at detonation fronts in lead azide are observed to be as much as 0.5, this is a very reasonable estimate.

Next, consider the ammonium ion. In this case strain has two effects because the ion is not centrosymmetric. One is reduction of the HOMO-LUMO gap through bond-bending; and the other is polarization of the ion through internal charge displacement. An unstrained ammonium ion which has the form of a tetrahedron with hydrogen nuclei at the corners. Each corner is a bond length, b away from the central nitrogen nucleus. The molecule has four each of two principle symmetry axes: one is two-fold, the other three-fold. Thus there are two principle deformation modes. Compression along the two-fold axis increases two of the bond angles, while compression along the three-fold axis second increases three of the bond angles; and in addition (at constant bond length), brings the central N-atom closer to the plane of three H-atoms that lies perpendicular to the compression axis than to the H-atom at the apex. This causes a net charge displacement. That is, to a piezoelectrically induced internal electric fields. If ϵ_{33} is the compressive strains, and the bond length is b , then the electrostatic energy change is about $(3q^2/4b)\epsilon_{33}$ where q = one electronic charge. If the strain is 0.2, since $b = 1.1 \text{ \AA}$, the change in energy is about 2 eV; and the local electric field is very high, about $2.4 \times 10^{10} \text{ V/m}$.

The nitrate ion and PETN have been discussed in one of the references.

The resonance binding energy per π -electron correlates quite well with the HOMO-LUMO energy gap for a large number of aromatic molecules. Thus the chemical "hardnesses" of molecules largely determine their sensitivities to shock-induced chemical reactions.

Related references by the author:

- "Metallization at Microindentations", Mat. Res. Soc. Symp. Proc., 276, 191 (1992).
- "Shear-induced Metallization", Phil. Mag. B, 67, 207 (1993).
- "Metallization and Insulization During Impact", Int. Jour. Impact Eng., 14, 291 (1993).
- "Shear-induced Polymerization of Benzene", with R. W. Armstrong, to be publ. in Shock Compression of Condensed Matter - 1993, Proc. APS Topical Meeting (1994).
- "Strain-induced Chemical Reactions at Detonation Fronts", *ibid.*

MECHANISM OF SHOCK-INDUCED MECHANOCHEMISTRY

John J. Gilman
Department of Materials Science and Engineering
University of California at Los Angeles
Los Angeles, California 90024

INTRODUCTION

In about 1843, James Joule demonstrated that mechanical work and thermal energy are equivalent. Therefore, since thermal energy affects chemical reactions, mechanical strain energy might be expected to affect them under appropriate conditions. Thus mechano-chemistry would stand alongside thermo-chemistry, photo-chemistry, electro-chemistry, radio-chemistry, and others. This mechanical/chemical alliance has little importance for the traditional phases of chemistry, gases and liquids, because they do not sustain shear deformations; but it is of great importance for solids.

The usual approach is the view that strain energy can assist thermal energy to enable reactions. In this approach, the mechanical work done to reach an activated state is subtracted from the activation energy. However, at temperatures below the Debye temperature of a solid, the strain energy density at the beginning of a reaction is often large compared with the thermal energy density. Thus, it alone can cause reactions. In this regime, therefore, it is more appropriate to say that thermal energy can assist strain energy to enable a reaction rather than the inverse.

During chemical reactions the primary geometric changes are those of shape. Changes of volume secondary. Typical reactions do not change the sums of the atomic volumes (to a first approximation). But reactions do change the arrangements of the atoms, so the shapes of the products of a reaction are often quite different from the shapes of the reactants. Therefore, shear deformations gain their importance through LeChatelier's principle. This is aided by the fact that the force constants for bond-bending are 4-5 times smaller than those for bond-stretching/compressing.

Shear deformations affect chemical reactions principally by causing changes in the electronic structures of molecules, or of crystals. The most important of these are changes in the energy differences between the highest bonding orbitals (HOMO-usually occupied by a pair of electrons in the ground-state), and the lowest anti-bonding orbitals (LUMO-usually unoccupied in the ground-state).

Viewgraph 1 - Effect of bond bending on LUMO-HOMO gap

Large shear strains cause the HOMO-LUMO gap to close making it easier for the bonding electrons to enter the anti-bonding states where they become delocalized, and able to move freely from one location to another; that is, to

execute a chemical reaction.

Shear has a much larger effect on the electronic structure of a collection of atoms than does a change of volume. The reason is that it reduces the symmetry of the atomic array while a volume change does not. The effects may belong to one of two modes. In the first mode, shear strain rearranges the electrons without moving the center of negative charge away from the center of positive charge. This is the homopolar mode. In the second, the heteropolar mode, the initial symmetry of the array is not centrosymmetric. Therefore, in this mode, shear strain separates the centers of negative and positive charge, thereby creating an electrostatic dipole. The local electric field of this dipole affects the LUMO-HOMO gap.

EXAMPLES

A striking example of the effect of shear strain is the effect it has on crystals with the diamond (or the closely related zincblende) structure. Some specific cases being silicon, germanium, and indium antimonide. When these are compressed along the four-fold axes of their structures, they cease being semiconductors to become metals, and they acquire the crystallographic structure of β -tin (the "white" tin-can kind). The chemical bond lengths change very little during this transformation, but the angles between the bonds become

markedly sheared:

Viewgraph 2 - Change of diamond to beta-Sn structure.

Viewgraph 3 - Another view of the diamond/beta-Sn structure change; emphasizing the shear strain.

Evidence that the shear strain is the important factor is provided by the fact that, at the critical strain, the work done in bending the bonds to reach the new structure is approximately equal to the LUMO-HOMO energy gap:

Viewgraph 4 - Correlation between work of bond-bending and energy gaps.

The relative importance of the shear strain can also be seen by comparing the fractional changes in the structural parameters that occur during the diamond/beta-Sn transformation:

Viewgraph 5 - For the eight known cases, the average fractional bond length changes compared with the fractional amounts of bond-bending during the transformation of the diamond structure into the beta-Sn structure.

It is concluded from these facts that bond-bending in compressed covalently bonded specimens has more effect on the electronic structure than increasing or decreasing the lengths of covalent bonds.

On the other hand, if the material is put into simple tension, the gap does not close; and at high enough tensions the material fractures. At low temperatures, this is clearly an athermal, mechanically-induced phenomenon, but it will not be discussed further here.

Estimates have been made of the strains needed to close the LUMO-HOMO gaps in some chemical species, and then compared with what is known about their reactivities. The first case to be discussed is that of the polymerization of benzene under shock conditions. This case has been discussed previously by Armstrong and Gilman. They considered the possibility that when initially flat benzene molecules are compressed along an axis lying in the planes of the molecules they buckle into the chair configuration:

Viewgraph 6 - Buckling of a benzene molecule.

This would change their C-C bond angles from 120° to 109.5° and close their LUMO-HOMO energy gaps:

Viewgraph 7 - Correlation diagram for benzene molecule.

The stress required to do this was estimated from the known vibrational force constants. It was found to be consistent with transformation data from shock experiments.

Also, using a molecular mechanics approach, Gilman studied what the effects of strain might be in the decomposition of some energetic molecules: azide ions, ammonium ions, nitrate ions, and PETN molecules. The objective was to estimate how much shear strain is needed to close their LUMO-HOMO gaps, thereby allowing them to decompose. The estimated critical strains are:

Viewgraph 8 - Critical Strains for Gap Closures

Species	Estimated Critical Strain
-----	-----
Azide ion	0.17
Ammonium ion	0.20
Nitrate ion	0.21
PETN	0.21

Note that the critical strains are similar for the various molecular species. However, since the force constants vary, the critical stresses are quite different. For the non-centrosymmetric nitrate ion (triangular) there is a piezoelectric

effect in addition to the bond-bending effect:

Viewgraph 9 - Nitrate ion.

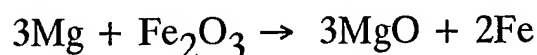
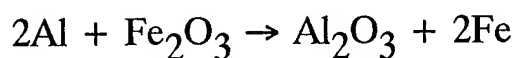
However, the energy change associated with the piezoelectric effect for a given strain is smaller than the change associated with the work of bond bending, so the latter is the most important effect. This was shown by writing an expression for the two terms as functions of the strain. Then the sum of these was equated to the LUMO-HOMO gap, yielding a quadratic equation in the strain. This was solved for the critical strain. Finally, the solution was substituted back into the quadratic equation to evaluate the two terms; showing that the bond-bending term is the largest:

Viewgraph 10 - Critical Strain for the Nitrate Ion

The effects of large mechanical strains can be dramatic. As long as 1935, Bridgman reported that several of the specimens he studied exploded when the anvils he used were compressed and twisted. In more recent years, Enikolopyan and his co-workers studied these fast reactions in considerable detail. The reaction types included decompositions, substitutions, additions,

and polymerizations; both endo- and exo-thermic. The components were both organic and inorganic substances. Among the many reactions were those of the highly exothermic "thermite" type:

Viewgraph 10 - Two "thermite" reactions.



When pellets of the reactants were compressed between Bridgman anvils to 5-15 kbar. they often exploded without gas generation, and without any observable temperature rise. The reaction times were less than 10^{-7} sec. Thus, since the reacting particles were as large as 1 mm., the detonation front velocities could be as large as 10^6 cm/sec. The energy release is much larger than the initial elastic strain energy which acts only in an initiation role. Enikolopyan concludes: "we observed the formation and propagation of a powerful detonation wave in solid substances at room temperature without the formation of gaseous substances. This indicates unambiguously that in solid substances there is a mechanism of direct conversion of chemical energy into mechanical energy without a gas phase".

A likely mechanism is that the electronic structure is changed by finite

bending of one or more covalent bonds. By analogy with the metallization that this causes in semiconductors, this causes delocalization of the bonding electrons. Thus a very dense plasma is created which allows fast chemical reactions.

Enikolopyan has pointed out that his observations imply very fast diffusion of the atomic components; a few orders of magnitude faster than the diffusion rates observed in liquids. This is consistent with the idea that one is dealing with a plasma where the limiting diffusion rate is about 5×10^{-3} cm²/sec., according to the Einstein-Smoluchowski equation.

METALS

So far what I have discussed refers to covalently bonded solids in which the sp³ hybrid orbitals are most important. But similar mechanisms apply for the transition metals where spd hybrid orbitals are responsible for most of the bonding.

PROPOSED METHODS FOR VERIFICATION OF THE MECHANISMS

Although many practical phenomena involve mechanochemistry, systematic studies of the underlying phenomena are rare. Some of the mechanochemical phenomena are:

1. The types observed by Bridgman and Enikolopyan between compressed and twisted anvils, such as: Mg plus SiO_2 yielding Si and MgO; explosion of hydrated cupric sulfate to yield Cu metal; decomposition of PbO yielding Pb; cross-linking of polymers; the thermite reaction; and many more.
2. The effects of mechanical strain on the photochemical reactions studied by McBride and coworkers.
3. The ultra-fast reactions at detonation fronts.
4. Decomposition reactions in polymer systems at low temperatures as studied by Boldyrev and Sohma.
5. Mechanical alloying.
6. Shock synthesis.
7. Friction and wear.
8. Cutting processes.
9. Biological systems.

SHEAR STRAINS AT SHOCK FRONTS

In the case of solids, the hydrodynamic approximation is an over-simplification; especially for transition metals and covalently bonded substances. One reason is that relaxation of the shear strains is a very slow process compared with the rates of many electronic processes. Furthermore, on the molecular

scale, the large shear strains can never be completely relaxed:

Viewgraph 11 - Large shear strains in both unrelaxed and relaxed shock fronts.

SOME GENERAL IMPLICATIONS

Some general implications should be mentioned of the fact that the energies of most substances are affected by microscopic shear strains. The first of these is that the shear part of the strain energy tensor cannot be neglected when the thermodynamic functions of solids are being calculated, nor can the transverse vibrational frequencies of a solid. All too often only the isotropic strains are considered. Most textbooks ignore the shears.

Furthermore, the surface energy should not be treated as a scalar, or as a vector quantity. It behaves like a second order tensor with less symmetry than that of the bulk solid. This implies, in turn, that the surface of a solid has a finite thickness.

MICROSCOPIC STUDIES

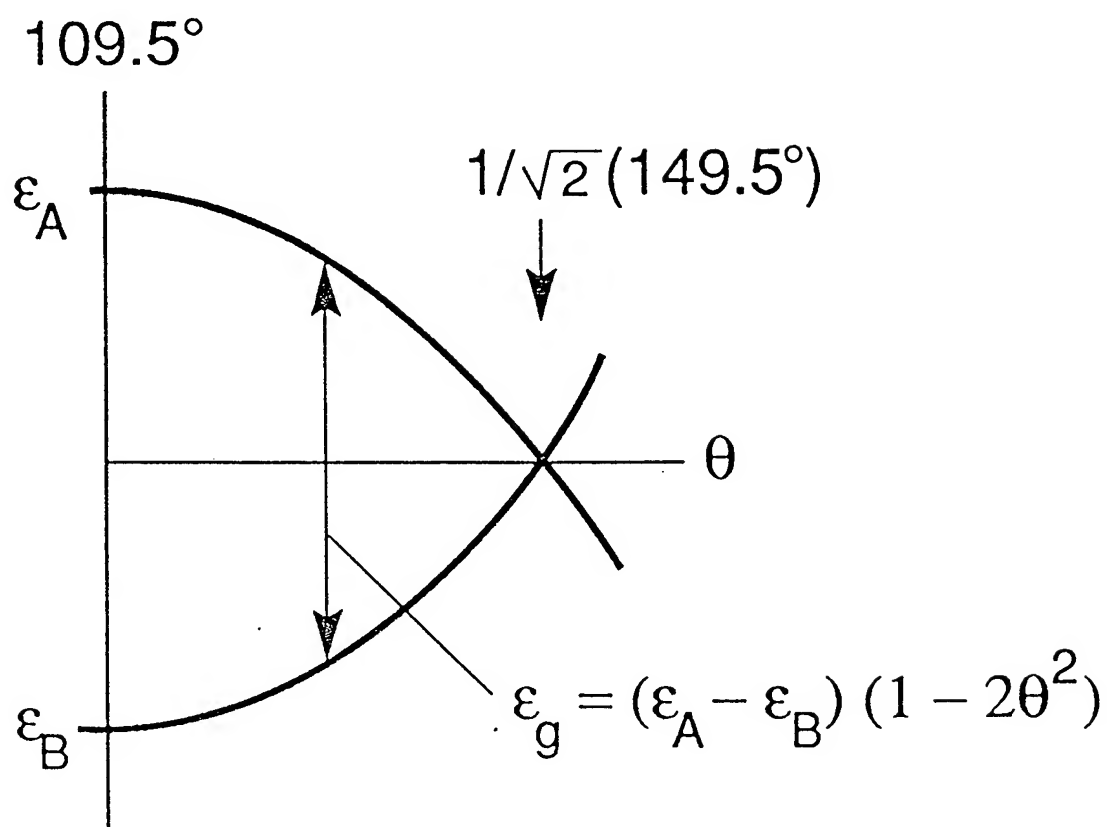
Most of the studies to date of mechanochemical effects have been phenomenological. Spin-resonance for detecting free radicals is an exception.

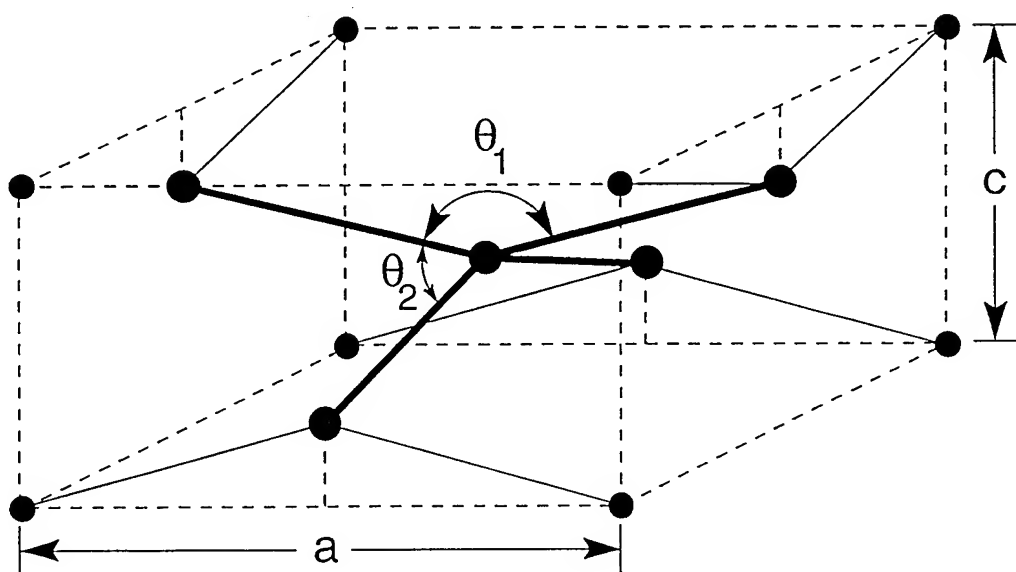
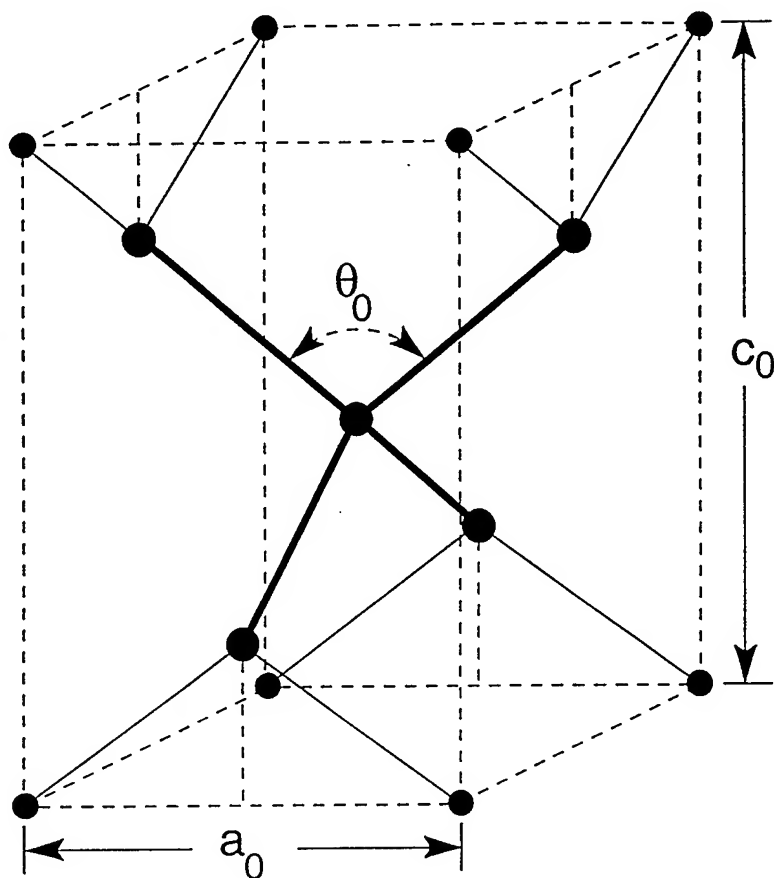
However, other techniques could be used:

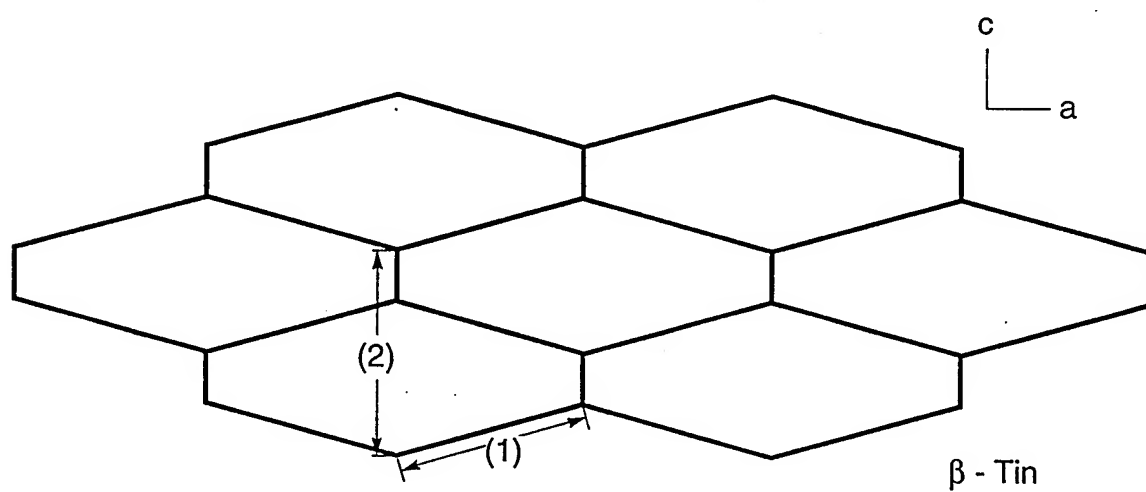
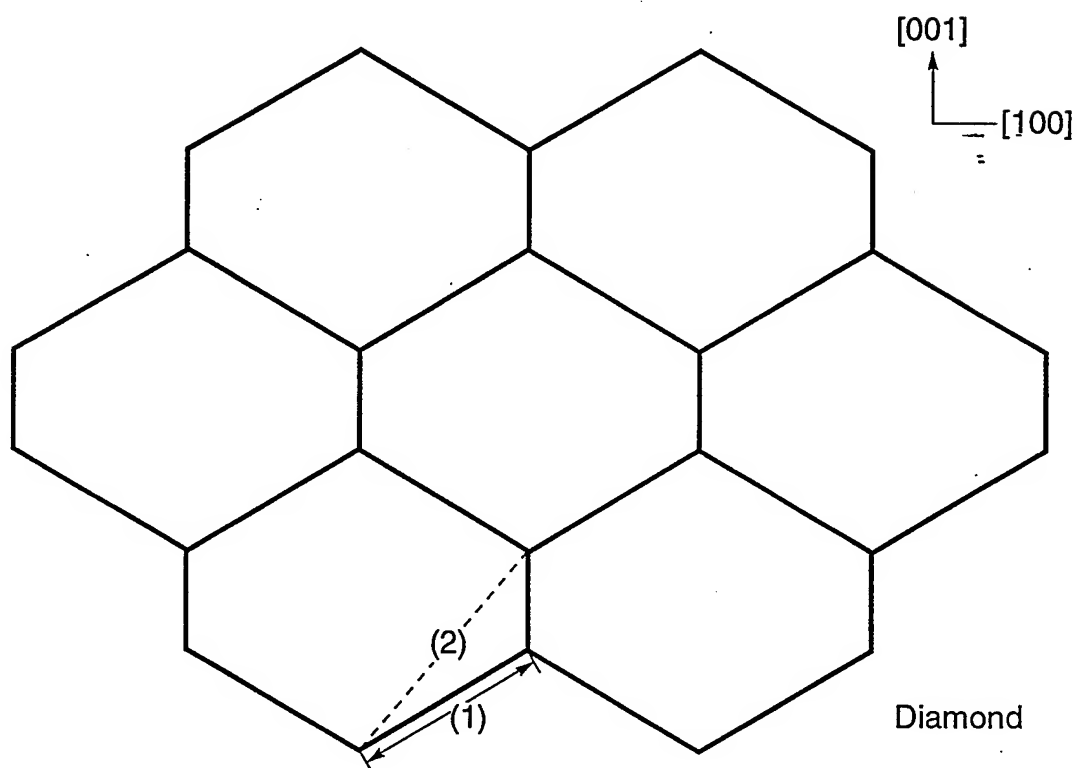
1. Optical absorption to follow the effect of strain on LUMO-HOMO gaps.
2. Surface generation of second-harmonic optical beams to see the effects of anisotropy and electron delocalization (increased polarizability) as gap closure is approached.
3. Examine changes in charge density waves when large strains are applied to appropriate solids.
4. Chemical probes may also be used. At surfaces changes in rates of adsorption, or reaction-rate, caused by large strains could be examined.
5. Sensitive molecules (small LUMO-HOMO gaps) might be isolated within a matrix of insensitive molecules, and then studied with optical probes.

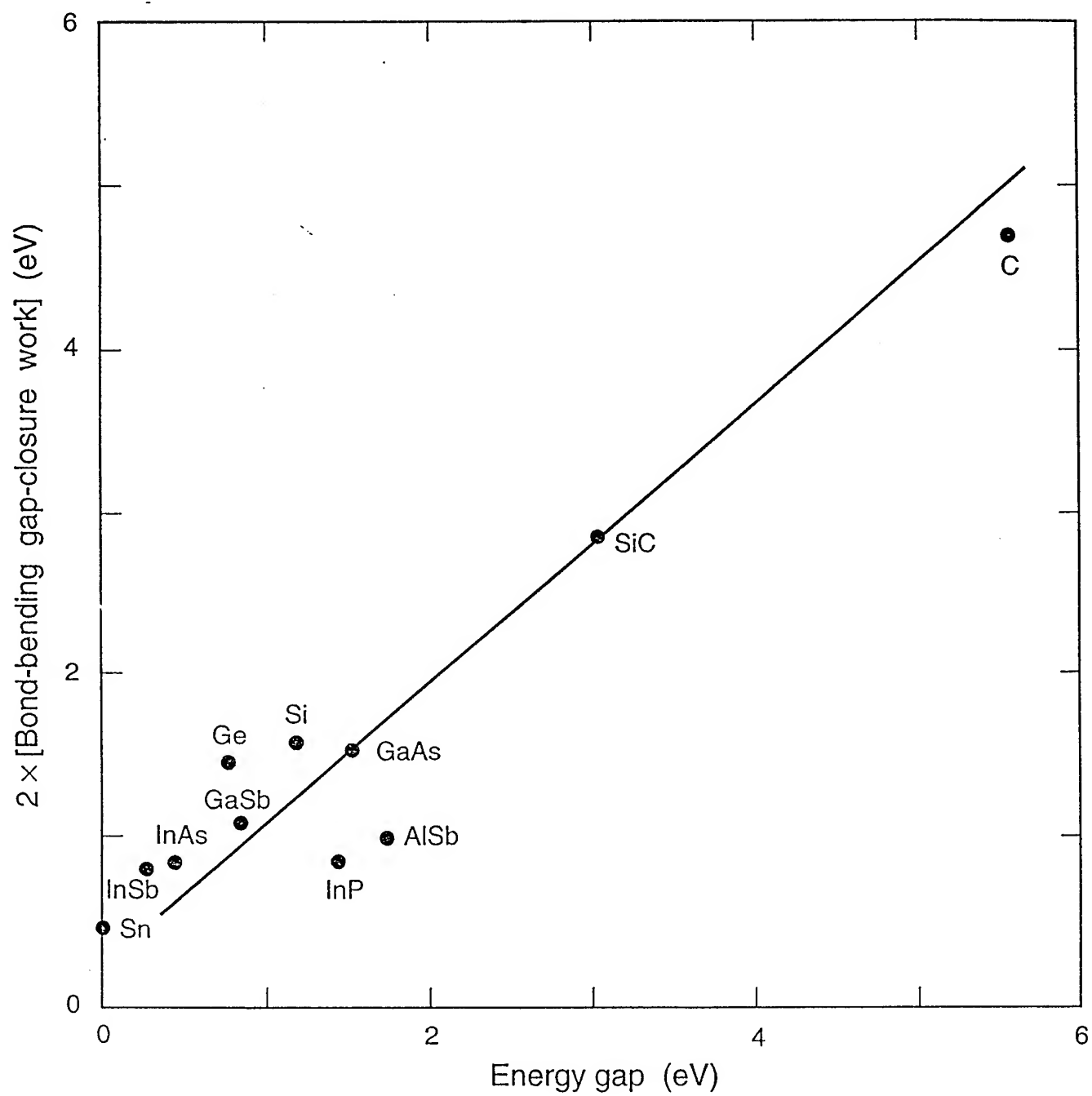
CONCLUSION

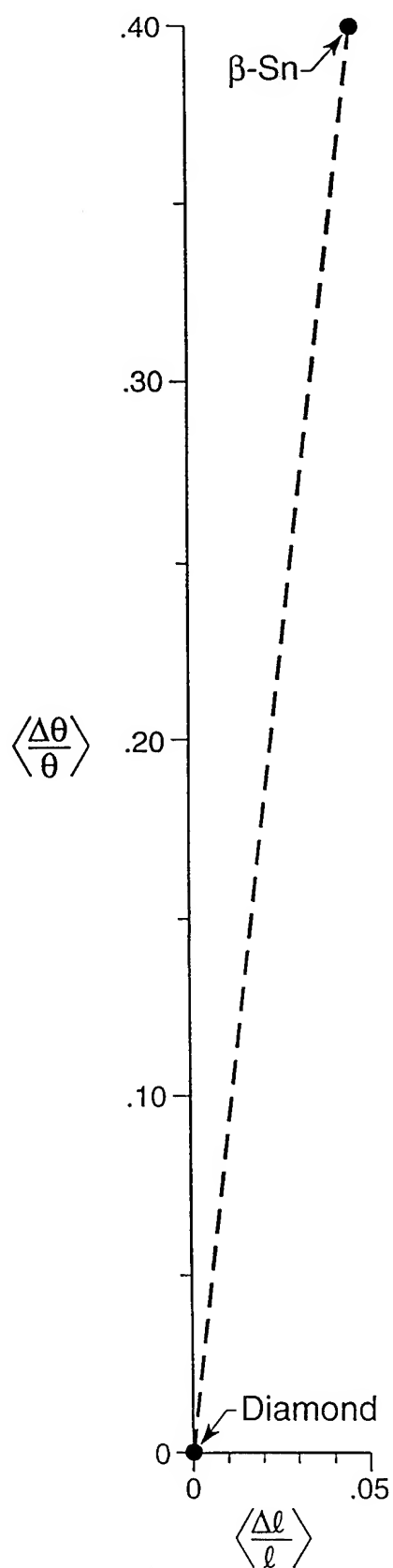
Numerous solid-state chemical reactions can be induced by mechanical driving potentials with or without the assistance of temperature. For covalently bonded solids, strained in compression, these reactions occur because the strain causes finite amounts of bond-bending which reduces, or closes, the LUMO-HOMO gaps of the reactants, thereby delocalizing the bonding electrons and allowing a reaction to proceed.

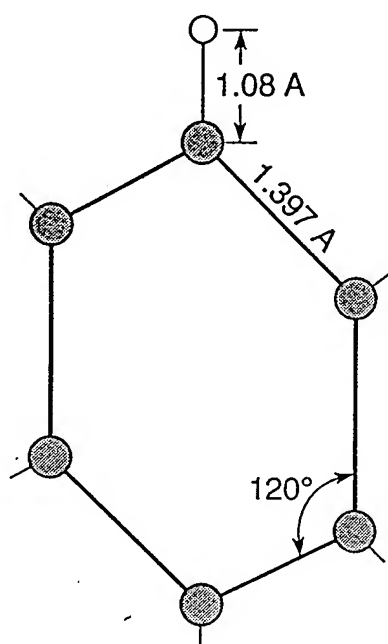




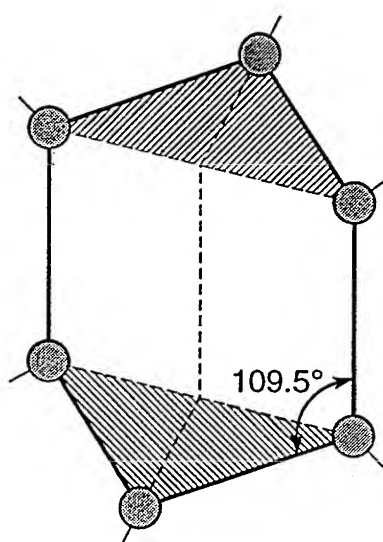




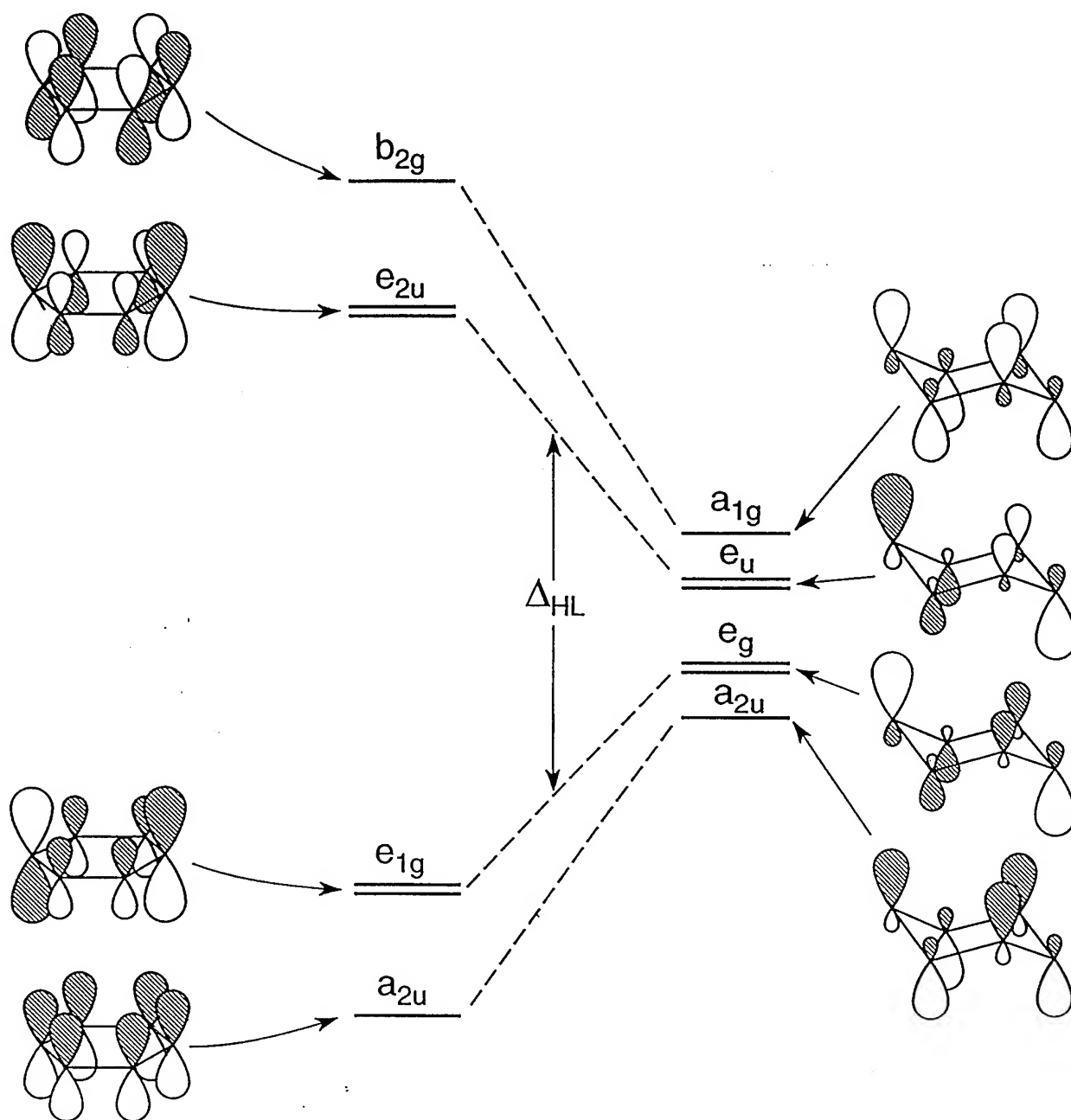




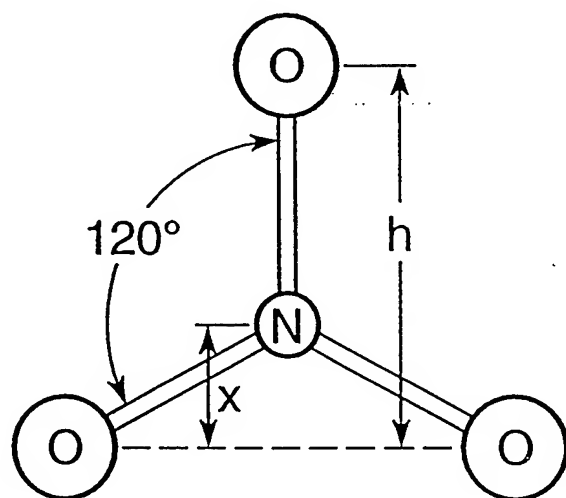
Planar



Buckled



Species	Estimated Critical Strain
Azide ion	0.17
Ammonium ion	0.20
Nitrate ion	0.21
PETN	0.21



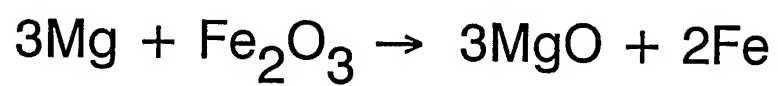
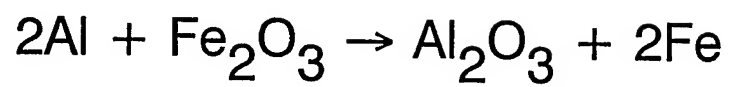
NITRATE ION (compressed along one bond):

$$\text{Piezoelectric energy} \approx 1.5(q^2/b)\epsilon$$

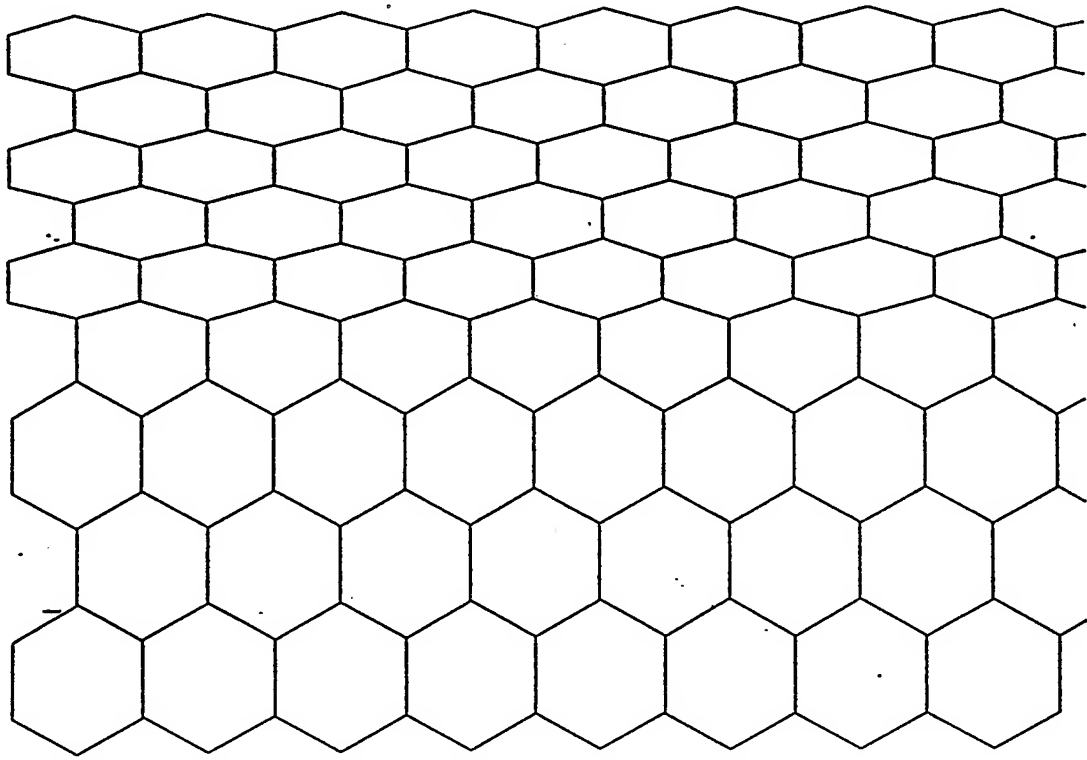
$$\text{Work of bond-bending} \approx 5.2k_\delta\epsilon^2$$

$$\text{Gap} \approx 4.9 \text{ eV.} = 8.6\epsilon + 69.7\epsilon^2$$

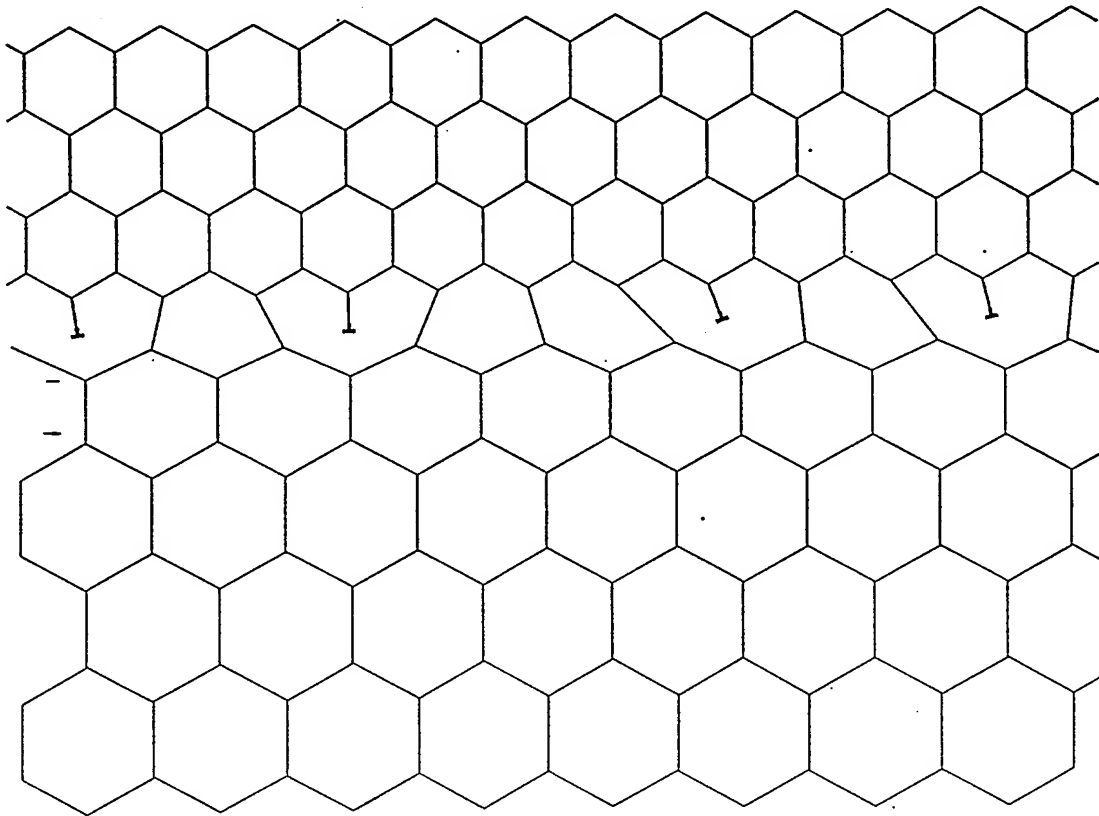
$$\text{Critical strain} = \epsilon^* \approx 0.21$$



[s]



[d]

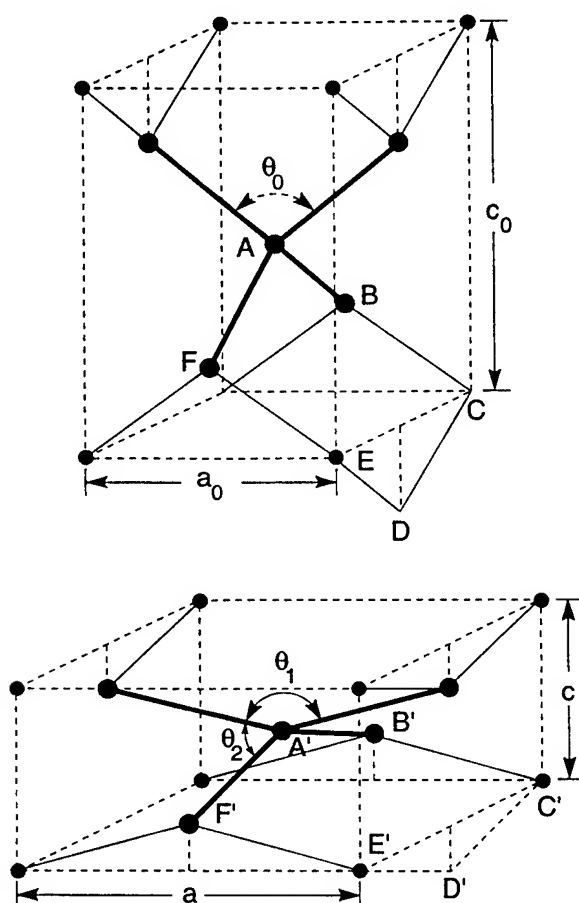


One pertinent fact is that uniaxial compression (a combination of isotropic compressive and shear strains) induces the transition to the metallic state at much lower stresses than those required for isotropic compression. This has been noted in passing but largely ignored. In the case of silicon the difference can be 40% or more; so the effect is not small (Gupta and Ruoff 1980). Further evidence of the importance of shear is provided by the crystallographic data that will be presented here.

A prototype transformation for semiconductors occurs when the diamond-framework, tetrahedrally bonded crystals (IV, III-V and II-VI types) are compressed. For eight known cases the cubic diamond framework becomes the tetragonal β -tin framework. In the latter structure, the crystals are metallic (for tin itself the resistivity is not isotropic, being different parallel and perpendicular to the tetragonal axis).

As Musgrave and Pople (1962) have pointed out, the β -tin framework can be reached by compressing the diamond framework along its cube edge while allowing it to expand laterally (fig. 1). The elementary deformation consists of compressing a tetrahedral bonding unit along an axis that passes through its centre and bisects the opposite edges, plus the topological constraint that 'bond rings' such as ABCDEF

Fig. 1



Schematic relationships between the diamond and β -tin frameworks. For tin, $\theta_c = 109.5^\circ$, $\theta_1 = 149.5^\circ$ and $\theta_2 = 94^\circ$. Note that the 'boat ring' ABCDEF which has equal sides and equal angles in the diamond framework becomes the ring A'B'C'D'E'F' which has equal sides but two sets of three angles in the β -tin structure. Also note that the next-nearest-neighbour distance c in the β -tin structure is 3.18 \AA , compared with 3.01 \AA for the nearest-neighbour bond length.

Table 1. Crystallographic parameters of the transformation of the diamond to the β -tin framework (group IV elements).

	Lattice parameter (\AA), tetragonal cells			Bond length d (\AA)	Bond angle θ (degrees)	Cell volume V (\AA^3)	Reference
	a	c					
α -tin	4.568	6.460		2.79	109.5	134.8	Landolt-Bornstein (1982)
β -tin	5.820	3.175		3.01	149.5; 94	107.5	Landolt-Bornstein (1982)
Percentage change	+27.4	-50.9		+7.9	+37; -14	-20.3	
α -germanium	4.001	5.658		2.45	109.5	90.6	Landolt-Bornstein (1982)
β -germanium	4.894	2.692		2.53	149.2; 94	64.5	Landolt-Bornstein (1982)
Percentage change	+22.3	-52.4		+3.2	+35; -14	-28.8	
α -silicon	3.840	5.430		2.35	109.5	80.1	Landolt-Bornstein (1982)
β -silicon	4.686	2.585		2.43	149.2; 94	56.8	Landolt-Bornstein (1982)
Percentage change	+22.0	-52.4		+3.4	+36; -14	29.1	
α -carbon†	2.522	3.567		1.54	109.5	22.7	Nielson (1986)
β -carbon†	(3.07)	(1.72)		(1.59)	(149; 94)	(16.2)	Nielson (1986)
Percentage change	(+22)	(-51.9)		(+3.2)	(+36)(-14)	(28.6)	

† Estimate of uniaxial transformation strain.

Table 2. Crystallographic parameters of the transformation of the diamond to the β -tin framework (group III-V compounds).

	Lattice parameter (\AA), tetragonal cells			Bond length d (\AA)	Bond angle θ (degrees)	Cell volume V (\AA^3)	Reference
	a	c					
α -InSb	4.581	6.479		2.81	109.5	136.0	Hanneman, Banus and Gatos (1964) Hanneman <i>et al.</i> (1964)
β -InSb	5.79	3.15		3.00	150.0; 94	105.6	
Percentage change	+20.9	-51		+6.8	+37; -14	-22	
α -GaSb	4.310	6.096		2.64	109.5	113.2	Yu, Spain and Skelton (1978) Yu <i>et al.</i> (1978)
β -GaSb	5.348	2.937		2.77	149.4; 94	84.0	
Percentage change	+24.1	-51.8		+4.9	+36; -14	-25.8	
α -AlSb	4.339	6.136		2.66	109.5	115.5	Baublitz and Ruoff (1982) Baublitz and Ruoff (1982)
β -AlSb	5.375	2.892		2.78	149.9; 94	83.6	
Percentage change	+24.1	-52.8		+4.5	+37; -14	-27.6	
α -InAs	4.284	6.059		2.62	109.5	111.2	Jamieson (1963) Jamieson (1963)
β -InAs	5.226	2.608		2.69	152.0; 93	71.2	
Percentage change	+22.0	-57.0		+2.7	+39; -15	-36	
α -GaP	3.854	5.451		2.36	109.5	80.96	Ruoff and Baublitz (1981) Ruoff and Baublitz (1981)
β -GaP	4.720	2.468		2.44	150.7; 94	54.98	
Percentage change	+22.5; -22	-54.7		+3.4	+38; -14	-32.1	

which becomes A'B'C'D'E'F' are conserved, that is they remain closed. In order for them to close while the nearest-neighbour bond lengths remain equal, the ring symmetry must change from three fold to two fold. This occurs more readily than symmetry-preserving isotropic compression because the bending force constants are substantially smaller than the stretching constants.

The crystallographic data (tables 1 and 2) show that the observed shear deformations $\Delta\theta/\theta$ of the bonds are numerically much larger than the bond compressions $-\Delta l/l$. Thus the bond-angle changes are much larger than the bond-length changes. The angle changes reduce the symmetry from cubic to tetragonal.

For tin itself, the crystallographic parameters are given at the top of table 1. Since the contraction of the *c* axis is nearly twice the expansion of the *a* axes, the volume change is modest. The fractional bond-angle changes are much larger (five to ten times) the bond-length changes. Thus both the crystallography and the mechanics indicate that shear predominantly induces the transition and not isotropic compression. An objective of this paper is to show that this is also consistent with the theory of chemical bonds.

The crystallographic facts indicate that, although these transitions are commonly said to be 'pressure induced', in reality the whole deformation tensor governs them, and not just the compression scalar. Thus they are 'deformation induced', or perhaps shear alone induces them.

Several of the other III-V, as well as II-VI, compounds transform to the rocksalt, instead of the β -tin, structure. This can also happen through shearing but will not be discussed here because the geometry is not as straightforward as for the β -tin case.

Note that the first-nearest-neighbour distance in the β -tin structure is 3.01 Å, while the second-nearest-neighbour distance is 3.18 Å. So the difference is only 5.6%. This has led many workers to assert that the coordination number is six, rather than 4, in β -Sn. However, conservation of the orbital rings (such as ABCDEF) requires that it be four as suggested by fig. 1.

It has become commonplace to discuss these semiconductor transitions in terms of diagrams of energy against density (Yin and Cohen 1980), but fig. 1 and the text above indicates that this obscures the nature of the change. The change is primarily one of shape, and only secondarily of specific volume. The same comment applies to other substances, for example the transformations in silicates and phosphates which also involve covalent bonds. In such cases, volume change is not an adequate descriptor of either the structural or the energetic factors.

Although it is questionable, if the assumption is made that bond lengths and angles affect the energy independently, then the energy can be taken to be a function of bond-length changes plus a function of bond-angle changes, and energy surfaces can be plotted. For small changes this approximation does not introduce large errors, but it is unreliable for changes as large as 37%. Also, for large strains, different paths from the initial to the final state are unlikely to be equivalent. This is a point that should be studied experimentally, although it has been largely ignored to date. It seems likely that the free energy is not a linear combination of functions of bond lengths and bond angles; so the free-energy surface needs to be determined point by point. This is, of course, easier said than done experimentally.

Data for the other homopolar diamond-framework crystals are also given in table 1. The data for carbon are estimates from theory and it is assumed that the β -tin structure is the transformation product. The congruence of the data among the four (or three) homopolar elements is striking.

Specifically, the fractional contractions of the c axes are nearly all equal, as well as the bond angles in the β -tin phase. This further suggests that shape rather than volume is the important factor. Heteropolar diamond-framework crystals behave similarly (Jamieson 1963), provided that their ionicity is less than the Phillips (1973) limit. Data for those that transform to the β -tin structure is given in table 2.

The data for InSb are quite congruent with those for its isoelectronic mate, tin (table 1). Less-congruent data for InSb has been reported by other workers, for example Jamieson. This illustrates the point that, because of the large shape change associated with the transformation, very precise crystallographic data are needed to distinguish among possible transformation products. These have not, in general, been available in this field.

Tables 1 and 2 indicate that changes in bond angles for this transformation are nearly invariant, again confirming the importance of shear strains.

Little is known experimentally about the state of deformation at the start of the transformation. Typically, only the 'pressure' is reported and/or the 'volume', but it is not clear whether the material still has cubic symmetry, and to what level of precision. Nor is it clear to what extent bond-angle changes are reversible in perfect, relatively unconstrained crystals. Thus the 'order' of the transition may depend on the loading conditions as well as the temperature.

A simple criterion for shear metallization can be derived from Pauling's original (approximate) theory of the chemical bond (Glasstone 1944). In the most simple version of this theory, the form of the wave function for a hybrid sp^3 orbital is (angular dependence only; the radial part is assumed to be unchanged by hybridization)

$$\psi_h = \frac{1}{2}(1 + 3 \cos \theta),$$

where θ is the angle with respect to the direction of the bond. The first term represents the s part of the orbital while the second represents the p part. The bond energy is proportional to the square of this, or

$$\psi_h^2 = \frac{1}{4}(1 + 6 \cos \theta + 9 \cos^2 \theta) = 4 \text{ (when } \theta = 0\text{)}.$$

The antibonding orbital has a similar form except that its energy decreases with increasing bond angle. The energy difference, or gap, between the bonding and antibonding energies is four when $\theta = 0$, but it decreases towards zero as the bond angle increases from its initial value (109.5°). The gap becomes zero when the bonding energy level has increased by half the gap. That is, the bonding energy has decreased from four to two; so the term in parentheses above becomes $9 \cos^2 \theta + 6 \cos \theta - 7 = 0$ at constant bond length. Solution of this for the positive root yields $\cos \theta = 0.78$, or $\theta = 39^\circ$. This plus 109.5° yields 148.5° , which is close to the 149.5° observed for tin and the other substances after the transformation. The excellent agreement may be fortuitous, but the calculation illustrates the principle that there is a strong dependence of bond energy on bond angle, and that there is a critical angle at which the bonding becomes metallic. Numerical band-theory calculations are consistent with this (Chelikowsky 1987).

The existence of a critical angle at which a phase transition occurs is consistent with the separation of the angular and radial dependences of wavefunctions. Further support can be given to this geometric criterion by showing that it yields the correct energy condition, that is by showing that the work done in changing the bond angle equals the energy needed to close the energy gap.

Imagine a bond of length b that is held in place at one end and acted on by a tangential force f at the other end. The force tends to change the bond angle θ and is

resisted by a bond-bending force constant k_θ (d cm). For a small change in the angle, the incremental work dW done by the force is $fb d\theta = k_\theta d\theta$. Integration yields $W = k_\theta(\Delta\theta)^2/2$ and, since the observed value of $\Delta\theta$ is 0.7 rad, $W = k_\theta/4$. The force constant k_θ has been defined in various ways, but most convenient is Harrison's (1980) definition $k_\theta = (3b^3/8)(C_{11} - C_{12})$ which relates it to the standard elastic constants C_{ij} .

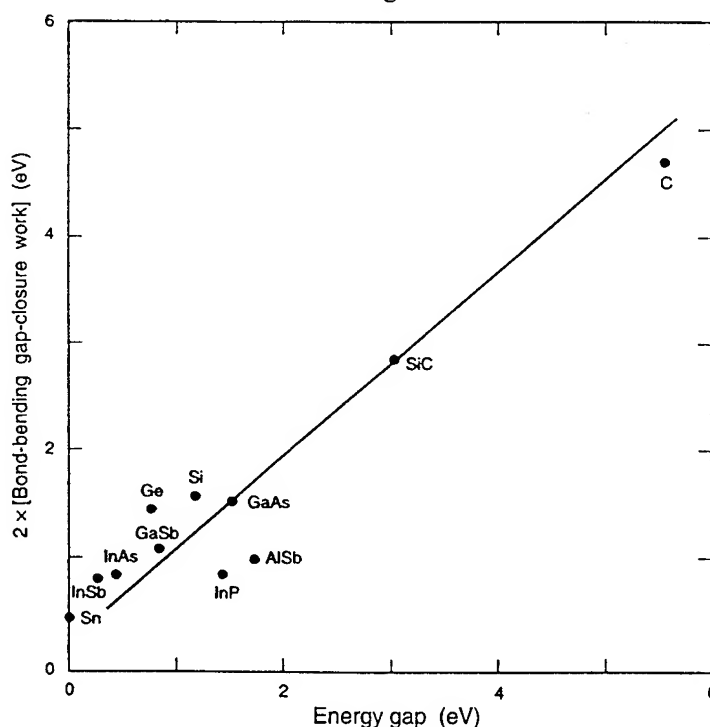
The energy needed to close the gap is $E_g/2$. Equating this with W yields $2W = E_g$ which is plotted in fig. 2. The data indicate that the relationship is approximately confirmed, although the fact that the correlation line does not pass through the origin indicates that the bond-bending work has been overestimated. The relationship shows that, as the gap increases, so does the force constant; therefore the angle change needed to close the gap remains approximately constant as is observed.

II–VI compounds have not been included in fig. 2 because their high ionicities make the simple bond-bending model inappropriate for them. However, shear deformations may play a key role in their transformations.

For states of uniaxial compression such as those experienced in the inertial confinement of strong shock waves, or in the confined static compression of indentations, bond-angle changes are accompanied by bond-length decreases, and metallization is induced by the combination. However, since the stretching force constants are much larger than the bending force constants (by a factor of about four) they provide most of the resistance to the loading, and bending accommodates most of the deformation. This may account for the efficacy of the Herzfeld theory in describing the transformations induced at indentations (Gilman 1992).

It is natural to wonder why so many diamond-framework crystals transform to the β -tin structure. There is a long-form answer based on numerical calculations, but a

Fig. 2



Approximate equality of twice the work of bond bending up to the critical gap-closure angle, and the energy gap for various elements and compounds. The work is calculated using Harrison's force constant for bond bending. The correlation line does not pass through the origin, suggesting that the work is somewhat overestimated. The elastic shear constants for InP and AlSb may be in error.

simple answer is based on the elementary static stability of localized bonds. For arrays in which the forces between the atoms are directed along lines between them, and the coordination number is four, there are two, and only two, ways to arrange the lines such that the forces acting along them are all of equal magnitude at static equilibrium. These are the cubic and tetragonal configurations in fig. 1. Note that, if the atoms are oppositely charged (as in ZnS, for example), other possibilities arise, such as the NaCl structure.

If it is accepted that shear can induce metallization, there are implications for many situations that do not appear to have been appreciated in the past. These include point-contact diodes and transistors (Clarke *et al.* 1988), various allotropic transformations including those involving the d-shell bonding in metals, chemical reactivity by facilitating electron transfers, the core structures of dislocations and dislocation dipoles, the mechanisms of machining and grinding, mode-III crack propagation, reversible compression-induced transitions in silicate-like frameworks, impacts and shock fronts, and indentations.

For tensile states of strain, metallization is not expected, but the 'insulization' of metals is. It is to be expected that insulization will be deformation dependent (i.e. dependent on both isotropic expansion and shear). This would change the metallic bonding from a delocalized mode to a localized mode. Therefore it might well play a role in such phenomena as crack propagation in which large tensile strains exist near crack tips. It might also account for why the spalling of metals that is associated with strong shock waves is often very localized, and it may account in part for the weakening effects of large concentrations of dislocations, as well as the hardening effects of dilatational dislocation dipoles in metals. Localization of the bonding would be expected to have a strong influence on the microscopic mechanisms of these various phenomena. For moderate tensile strains (about 0.1–0.5), not much localization of the s-like electrons would be expected, but the p-like and especially the d-like electrons would localize significantly.

REFERENCES

- BAUBLITZ, M. A., and RUOFF, A. L., 1982, *J. appl. Phys.*, **53**, 6179.
 CHELIKOWSKY, J. R., 1987, *Phys. Rev. B*, **35**, 1174.
 CLARKE, D. R., KROLL, M. C., KIRCHNER, P. D., COOK, R. F., and HOCKEY, B. J., 1988, *Phys. Rev. Lett.*, **60**, 2156.
 COTTRELL, A. H., 1988, *Introduction to the Modern Theory of Metals*, (London: Institute of Metals), chap. 1.
 EDWARDS, P. P., and SIENKO, M. J., 1983, *Int. Rev. Phys. Chem.*, **3**, 83.
 GILMAN, J. J., 1992, *J. Mater. Res.*, **7**, 535.
 GLASSTONE, S., 1944, *Theoretical Chemistry* (New York: Van Nostrand), pp. 97ff.
 GUPTA, M. C., and RUOFF, A. L., 1980, *J. appl. Phys.*, **51**, 1072.
 HANNEMAN, R. E., BANUS, M. D., and GATES, H. C., 1964, *J. Phys. Chem. Solids*, **25**, 293.
 HARRISON, W. A., 1980, *Electronic Structure and the Properties of Solids*, (San Francisco, California: W. H. Freeman), pp. 193ff.
 HERZFELD, K. F., 1927, *Phys. Rev.*, **29**, 701.
 JAMIESON, J. C., 1963, *Science*, **139**, 845.
 LANDOLT-BORNSTEIN, New series, 1982, Group III, Vol. 17a, Ed. by O. Madelung, Springer-Verlag, Berlin.
 MOTT, N. F., 1949, *Proc. Phys. Soc. A*, **62**, 416.
 MUSGRAVE, M. P. J., and POPL, J. A., 1962, *J. Phys. Chem. Solids*, **23**, 321.
 NIELSON, O., 1986, *Phys. Rev. B*, **34**, 5808.
 PHILLIPS, J. C., 1973, *Bonds and Bands in Semiconductors* (New York: Academic Press).
 RUOFF, A. L., and BAUBLITZ, M. A., 1981, *Physics of Solids at High Pressure*, edited by Schilling and Shelton (Amsterdam: North-Holland), p. 81.
 YIN, M. T., and COHEN, M. L., 1980, *Phys. Rev. Lett.*, **45**, 1004.
 YU, C., SPAIN, I. L., and SHELTON, E. F., 1978, *Solid St. Commun.*, **25**, 49.

SESSION - IV

**SHOCK SYNTHESIS APPLICATIONS
AND PROCESS MECHANISMS**

SESSION IV: SHOCK SYNTHESIS APPLICATIONS AND PROCESS MECHANISMS

Robert Young: SESSION CHAIR COMMENTS

Five talks were given in this session by: Toshimori Sekine of National Institute for Research in Inorganic Materials, Vladimir F. Nesterenko of Lavrentyev Institute of Hydrodynamics, Masatake Yoshida of National Institute of Materials and Chemicals Research, Yasuhiko Syono of the Institute for Materials Research at Tohoku University, and Naresh Thadhani of Georgia Institute of Technology. A common theme emerging from these talks is the influence of, and lack of knowledge about, reaction paths and associated rarefaction stability. The main points that each speaker made in their presentation will be considered next.

Sekine's talk, entitled "Synthesis of Inorganic and Organic Materials", contained results from shock-compression experiments on boron nitride and organic material systems. Sekine used boron nitride as a model material to demonstrate that diffusion-controlled nucleation and growth was necessary to stabilize a high-pressure phase. Based on this he inferred that martensitic phase transformations that were not followed by a diffusion process may quickly result in reversal to the original phase upon sample unloading. Converting graphite to the rhombohedral phase, thought to be a diffusionless transformation, was cited as an example where the rhombohedral phase is known to exist at high pressure but is not obtained from shock recovery experiments. Sekine contrasted the graphite system with the boron nitride system to show that the rhombohedral to cubic transformation is stable and obtainable through shock-recovery experiments. Its previously speculated reaction path, the rhombohedral to cubic transformation, is shown not to be martensitic, but diffusion dependent with the reaction path proceeding from rhombohedral, to a combination of hexagonal and turbostratic state, through a martensitic transformation, and finally to cubic phase through diffusion-controlled nucleation and growth. Furthermore, the total yield of cubic boron nitride is correlated with the total amount of diffusion that occurs at high pressure. His thesis is that a material which undergoes a true martensitic transformation, i.e., a transformation whose reaction path does not involve diffusion or change in chemical composition, is not retainable during rarefaction, and some time-dependent-reaction-path mechanism needs to be present in order to "quench" the phase with the rarefaction wave.

Sekine also discussed his work on synthesis of the theoretically predicted superhard C_3N_4 material from low-pressure shock recovery experiments on three organic materials. Experimental results indicate possible synthesis of slight traces of this material, but did not indicate that the material had been fully synthesized. The inference is the material probably exists, but the correct experimental approach has not been identified with the appropriate reaction path enabling recovery of C_3N_4 .

Nesterenko's talk entitled "Shock Synthesis of Non-Equilibrium Materials" was general in nature, and not focused to convey a deep understanding of any particular mechanism or material

response. However, his main theme dealt with the uncertainties associated with shock synthesis resulting from the lack of specific knowledge concerning how individual materials behave at a granular level. Nesterenko's work is focused on understanding how the shock-wave energy is localized and partitioned in particulate systems, and reveals the wide variation in conditions that are experienced. Evidence was shown of how energy-localization at shear-bands increased the yield of certain products, and the lack of those products in regions of the matrix where energy-localization did not occur. Nesterenko discussed the importance of energy-localization at the material surfaces to nucleate reactions or bonding between materials. The mechanics of pore deformation and collapse was shown to involve a high degree of energy-localization and is cited as the reason that they are relatively important in shock recovery experiments. However, he contends that the lack of fundamental knowledge concerning these mechanisms inhibits our ability to control the experiment, and the wide ranges in processing conditions that individual particulate constituents are exposed to in the experiment are left to chance. This processing variability creates a wide range of observed responses, and the lack of correlation between the observed response with localized processing histories.

Yoshida's talk entitled "Shock Synthesis of Diamond and C-B-N Materials" focused specifically on how different mechanisms in the reaction path influence the rarefaction stability and associated yield of certain material phases. His experiments indicate that shocked graphite transforms directly into hexagonal diamond through a diffusionless process, that fully converts back to graphite upon rarefaction. His experiments also indicate that experimental heterogeneities induce a diffusively-controlled transformation from hexagonal diamond to cubic diamond caused in part by adiabatic pore compression forming hot-spots. The thesis is that diffusion is time dependent within the domain of shock experiments, and only small relative amounts of diffusion can take place upon rarefaction, with respect to the amount of diffusion that takes place during pressurization. The inability for diffusion to take place during rarefaction inhibits the cubic diamond's ability to transform back to graphite, and as such is retained due to lowered diffusional rates associated with the reduced rarefaction temperatures. This thesis was supported by conducting experiments with copper powders of differing morphology mixed with graphite. The effect of copper powder of varying morphologies is to modify the thermal characteristic of the hot-spots, such that small irregular morphologies yield a more uniform temperature profile and associated gradients when contrasted to a large spherical morphology. In theory, more diffusion would take place in hexagonal diamond at higher temperature, thus for the same shock duration a higher cubic diamond yield is expected when large spherical copper powder morphology is employed in comparison with small irregular morphology. This is precisely what their experimental results indicated. A remarkable insight into the process. Further confirmations to their theory were obtained using the boron nitride system.

Syono's talk, entitled "Shock-Induced Transformations in Oxides", continued with the theme that diffusionless transformations are not "quenchable" during rarefaction, and added the further insight that changes in bonding can induce rarefaction stability enabling the altered phase to be recovered. Syono contrasted the rutile-to-fluorite transition to the zircon-to-scheelite transition in order to make this point. He presented theoretical and experimental evidence suggesting that rutile, upon shock, transforms by a displacive mechanism to a fluorite structure which is not retained upon rarefaction. However, zircon transforms to a scheelite type phase and has been successfully recovered from shock experiments. Syono presented evidence suggesting that the

only difference between these two transformations is a coherent rotation of the SiO_4 tetrahedra in zircon, and concluded that changes in the bond structure can also prevent back transitioning during rarefaction. Syono further pointed out that a reconstructive phase transition is necessary but not a sufficient condition to ensure recovery of the secondary phase, an example being the olivine-spinel transformation. His thesis is that this transformation is not diffusionless, because diffusionless transformations can be identified by deviations in the Hugoniot. He claimed that the lack of this observation is evidence that this transformation must be reconstructive in nature, and that reconstruction is inhibited by the experimental time domain.

Thadhani's talk, entitled "Materials Synthesis by Shock-Induced and Shock Assisted Solid-State Chemical Reactions", provided the best organized overview. His talk should have been the first one given in the conference, for examples presented would have saved time and effort in bringing everyone attending the conference to a common level. He subdivides the field of shock-chemistry into two areas: shock-induced reactions and shock-assisted reactions. Shock-induced reactions are those that take place in the high-pressure state before rarefaction, and shock assisted reactions take place after rarefaction. In combining time resolved and recovery experimental results, Thadhani was able to provide evidence that shock-induced solid-state reactions exist, a point contested before his talk. He methodically presented how to interpret results of recovery experiments by distinguishing between characteristics that occur uniformly within the bulk sample, with those characteristics known to proceed through time dependent mechanisms such as nucleation and growth. Examples were shown of morphology influence on both particulate deformation and initiation of chemical reactions. Many material synthesis examples were given and correlated with experimental processing conditions.

GENERAL DISCUSSIONS: The discussion associated with this session focused on identifying unique shock-chemistry attributes that could be exploited for material synthesis. The discussion was broken into two parts: the first identified unique attributes of shock-processing, and the second identified unique material induced attributes. The identified attributes include:

Unique Shock-Processing Attributes

- High Strain Rates
- Introduction of High Defect Populations
- Large Volume Processing
- High Hydrostatic Pressure
- High Deviatoric Pressure
- High Quench Rates
- High Temperatures
- Mechanical Energy Localization
- Short-Time Duration
- Localized Mixing of Constituents
- Obtainment of Non-Equilibrium States

Unique Material-Science Attributes

- Metastable Materials
- Non-Equilibrium Phases
- Near-Net-Shape
- Shock Modified Materials
- Joining of Metastable Materials
- Atomic Mixing of Incompatible Materials

This session ended without obtaining a consensus concerning defining the application for which

future shock synthesis research should be focused on. The assembled personnel consisted of very good problem solvers, but not good problem definers. Given a goal, the researchers are very competent in establishing objectives and plans to achieve the goal. This is accomplished because researchers are highly versed in technical knowledge. However, asking them to establish the goal is a different matter entirely. To establish the goal requires knowledge concerning the needs, which could be in terms of industrial, governmental, or consumer needs. The problem is the assembled group of scientists collectively possessed a large body of technical knowledge, and only a small amount of knowledge concerning a diverse cadre of specialized niche needs for this technology. In reality, the scientists are looking for the same information that the sponsors of this conference are: where is the future need for this technology?

To summarize the applications session from a technical standpoint, the discussions were not focused on developing materials for a specific applications, but were focused on understanding how to obtain unique materials by the use of shock-induced reactions. In general, the Japanese are orienting their research towards identifying the mechanisms that enable rarefaction stability for the formation of super-hard materials. Other research presented focused on identifying new compounds and associated properties. The two new pieces of knowledge presented at this session are; that time dependent mechanisms such as nucleation and growth or changes in chemical bonds enables material formed under the shock condition to be retained upon release, and that techniques are being established to differentiate between those materials formed in the shock-wave from those that are formed post-shock due to elevated temperatures and modifications that the shock-wave induces into the constituent's solid-state structures.

OVERALL IMPRESSIONS: The forte of the shock wave includes sudden alteration in material geometry, usually accompanied by alterations in solid-state properties and induction of chaotic intra and inter particle turbulence. The question is: where can this technology be applied most beneficially? In the session chair's opinion, from a business perspective, the focus for future research should be in developing novel electronic materials. This business sector is growing, is high-value added, uses relatively small amounts of material, and shock processing can impart unique electronic properties through solid-state alteration in terms of huge defect populations. It is well known that defects alter electronic properties, and most sensor applications utilize defects as the operational mechanism.

The question is, can the different types of defects generated in the material bulk by shock-waves be tailored to provide unique electronic properties that can be exploited? Furthermore, can unique electronic properties be obtained by certain combination of materials possessing huge defect populations? There are several reasons for focusing in this direction. The electronic business is still in its expansion cycle, which usually means the market is receptive to adapting new unique materials. This also implies that problems have been identified for which solutions are being actively sought. In general, electronic components are miniature in scale which means that small amounts of material synthesized under a controlled shock experiment could be useful to industry.

With respect to the current usefulness of the so-commonly-performed shock-recovery experiments, it seems that this is a good tool to survey the response of materials for a wide

variety of processing histories, in particular conditions of extreme pressure. An experiment has not been devised to yield a uniform process, and thus to generate uniform effects, throughout the material bulk. As such, current recovery experiments exhibit the results of different processing histories spatially. To develop a standard well characterized experiment for which process histories could be spatially correlated would be valuable. The lack of generally available real-time diagnostics with spatial resolution on the order of a micrometer and temporal resolution on the order of a nanosecond inhibits our ability to understand the mechanisms involved in shock-induced chemistry. Focusing experimentalists on developing a standardized capability would be very valuable.

Incredible insight into defining the controlling mechanisms in shock-induced chemistry seems to be coming from the Russian modeling effort. Specifically, the localization of energy in terms of intraparticle dynamics and particle deformation is leading to the understanding of where and how chemical reactions can nucleate. It is also providing some hints concerning what inhibits the reactions from going to completion. Focusing future modeling efforts on identifying the mechanisms that control intraparticle turbulence and particle deformation, and using these mechanistic models to develop experiments for confirmation could prove very useful.

At the beginning of this workshop many of the participants were highly skeptic about the ability to obtain a solid-state reaction in a shock wave. The workshop has gone a long way to dispel this disbelief. However, the critical experiment in this area has not been conducted. It would be very beneficial to assemble a subset of researchers tasked with specifying a definitive experiment. Not only would it serve to verify that shock-induced chemistry is possible, it would require the group to hypothesize in detail what the mechanisms are, and pre-think the meaning of different experimental result scenarios. Furthermore, no matter what the mechanism may be for shock-induced reactions, solid- or liquid-state, the question is, how can the mechanisms be best utilized to develop processes that yield useful and technologically interesting material characteristics?

In conclusion, I thought that many positive things came out of this workshop. More importantly, there seems to be a possible usefulness for this technology in the area of electronic materials. It was a real pleasure to be associated with this workshop, and I would be delighted to be involved in future discussions.

Shear-induced metallization

By JOHN J. GILMAN

Lawrence Berkeley Laboratory, Berkeley,
California 94720, USA

[Received 1 June 1992† and accepted 3 August 1992]

ABSTRACT

It is well known that compression causes insulators and semiconductors to become metallic when the concentration of the matrix atoms (or of impurity atoms) reaches a critical value given by the theories of Herzfeld, Mott, Hubbard, Edwards and Sienko, and others. It is argued here, based on the observed transitions in diamond-framework semiconductors, that microscopic shear strains are sometimes more important than dilatations. The simple theory of hybridized covalent bonds indicates that the energy gaps in these materials should vanish when compression causes the tetrahedral bond angle (109.5°) to increase to 148.2° . This is close to the average observed transformation angle of 149.2° (homopolar crystals). Implications for various phenomena are outlined.

It is well known that insulators become metallic if they are compressed a critical amount (Cottrell 1988). Volumetric compression criteria for this transition have been proposed by various workers, starting with Herzfeld (1927), then by Mott (1949) and further developed by Edwards and Sienko (1983). The proposed criteria, well corroborated by experiments, are based on changes in the overlapping of atomic wavefunctions as compression occurs, that is on changes in bond lengths. However, in the case of semiconductors, there is substantial experimental evidence that bond-angle changes are more important than length changes. In open structures, either bond-length or bond-angle changes can cause the overall volume changes that have been reported as experimental results.

The most straightforward case is that of covalent bonding. It leads to open crystal structures (the diamond structure is the prototype), and chemical bonds with distinct lengths and bond angles. Changing the lengths or the angles causes increases in the energies of the bonding orbitals, and decreases in the energies of the antibonding orbitals. In the language of solid-state physics, the valence-band edge increases in energy, while the conduction-band edge decreases. Thus the energy gap decreases for large strains (in some cases it increases for small strains). When it vanishes, the electrons at the top of the valence band become delocalized, and the material is said to have metallized.

In general, both isotropic compression and shearing are asymmetric. Lengthening a bond is clearly not the same as shortening a bond. Shearing may be symmetric, but often it is not. For example, increasing a right-angle to make it obtuse is not the same as making it acute by decreasing it. On the other hand increasing, or decreasing, a 180° angle is symmetric. Thus, depending on the sense of a particular deformation, the electrons may become either more, or less, localized.

†Received in final form 14 July 1992.

Synthesis of Inorganic and Organic Materials

Toshimori Sekine

National Institute for Research in Inorganic Materials

1-1 Namiki, Tsukuba 305, Japan

1. Introduction

New Materials characterized by noble mechanical, electronic, optical, and magnetic properties are receiving increasing attention in the modern science and technology. Shock compression provides us an unique environment for material synthesis in terms of pressure, temperature, density, and their rapid changing rates. Material synthesis can be developed not only in the thermodynamically stable field of a given phase and also in the metastable region as long as the synthetic pass is not prohibited kinetically. One of the most typical examples is CVD diamond grown below one atmosphere.

Many phase transformations of solids have been observed by shock compressions and static pressures. The phase transformation induced by shock compression must be fast reactive because of experimentally limited availability of time(roughly 1 microsecond).

Using a propellant gun with a 30 mm bore, we accelerate projectiles(mass of 40-100 gram) to a impact velocity of 2 km/s. Sample space is up to about 0.5 cm³. In most cases samples were mixed with massive copper powders to increase shock pressure and to quench efficiently.

2. Transformation in Boron Nitride

Boron nitride(BN) has been recognized as a similar material to carbon structurally and mechanically. Boron nitride displays five low pressure phases(hexagonal, rhombohedral, turbostratic, pyrolytic, and amorphous) and two high pressure phases(wurtzite-type and zincblend-type). Carbon has the phases corresponding to the BN phases, but the preparation of each single phase is not so easy as in BN. For example, rhombohedral graphite is known, but the synthesis of its single phase is not practical. Since transformation in shock synthesis has to occur in an extreme short period, the structural factor of the starting material such as crystallinity, orientation, and perfectness plays an important role. The initial, preshock condition also may have a critical effect as well as shock conditions.

In this paper we present two experimental results indicating that diffusion-controlled nucleation-growth mechanism, rather than martensitic mechanism, appears to be significant in some shock-induced transformations. The first is the rhombohedral BN to cubic BN transformation, which has been considered to occur in martensitic way[1]. Our recent results under relatively weak shock conditions revealed that the first products from the rhombohedral BN are both hexagonal and turbostratic BN and

that the products convert into cubic BN progressively over a threshold temperature[2]. The second is the turbostratic BN to cubic BN transformation[3]. This transformation needs diffusional process. It does not appear that the process is assisted by the presence of vapor or liquid since the shock condition is relatively weak.

It also should be noted that C60 crystalline powders convert into diamond by shock pressures of 20-50 GPa[4]. This is another example of diffusional transformation induced by shock compression.

3.Experiments of Organic Materials

Recently carbon nitride(C_xN_y) becomes an interesting material after the prediction of C_3N_4 theoretically to exhibit superhardness[5]. Hardness can be represented in fact by the bulk modulus. Empirical and some theoretical calculations have indicated that a large bulk modulus requires short, tetrahedral covalent bonds within a solid.

We tried to produce carbon nitride solids through shock recovery experiments of some organic materials such as 1,3,5-triazine($C_3H_3N_3$), hexamethylenetetramine($C_6H_{12}N_4$), and tetracyanoethylene (C_6N_4). It was difficult to recover samples after shock compression because of gas production from the decomposition of hydrocarbons. Some samples weakly shocked were recovered successfully, and X-ray diffraction indicated the presence of poorly crystallized solids. The greatest, broad diffraction peaks corresponding to the graphite (002) index shifted towards higher angles(shorter interlayer distance). This implies that some nitrogen is present in the graphitic solids.

In addition, we could obtain graphitic carbon nitride[6] through pyrolysis experiment of tetracyanoethylene under static high pressure and temperature condition. Preliminary investigation in the system C-N-H by diamond anvil cell coupled with laser heating system indicated a transformation of triazine and tetracyanoethylene to transparent materials with smaller volume at pressures of 30-40 GPa[7].

4.References

- [1] Sato, T., Ishii, T., and Setaka, N. (1982), J. Am. Cer. Soc., 65, c-162.
- [2] Sekine, T. and Sato, T.(1993), J. Appl. Phys., 74, 2440-2444.
- [3] Sato, T. and Sekine, T.(1994), Abstract in Symposium on Shock Waves, Japan '94, p 223-226(in Japanese).
- [4] Sekine, T.(1992), Proc. Jap. Acad., 68, ser.B, 95-99.
- [5] Liu, A.M. and Cohen, M.L.(1989), Science, 245, 841-842.
- [6] Sekine, T. Kanda, H., Bando, Y., Yokoyama, M., and Hojou, K.(1990), J. Mat. Sci. Lett., 9, 1386-1378.
- [7] Yagi, T., Aoki, T., Sekine, T., and Kanda, H.(1990), Abstract in 31st High Press. Conf. Japan. p.208-209(in Japanese).

Shock-induced mechanisms of phase transformation from rhombohedral BN to cubic BN

Toshimori Sekine and Tadao Sato

National Institute for Research in Inorganic Materials, Namiki, Tsukuba 305, Japan

(Received 4 January 1993; accepted for publication 8 May 1993)

Rhombohedral forms of layered boron nitride (*r*-BN) as mixtures with copper powders were shock compressed and quenched from pressures in the range 8–50 GPa. Recovered specimens were investigated by x-ray diffraction and electron microscopy. The graphite-like BN (*h*-BN) and turbostratic BN (*t*-BN) phases are observed in the pressure range 8–22 GPa and wurtzite-type BN (*w*-BN) in the range 17–39 GPa. The zincblende-type BN (*c*-BN) phase is identified from specimens subjected to high shock temperatures and consists of very fine grains mostly less than 10 nm. The mechanism of phase transformation of *r*-BN to *c*-BN is proposed to occur through two paths: (i) direct conversion by relatively strong shocks and (ii) indirect, kinetically controlled conversion via intermediate phases by shock loadings generating relatively weak pressures (< 50 GPa). The possible intermediate phases are *h*-BN, *t*-BN, and *w*-BN.

INTRODUCTION

Boron nitride has a very close similarity to carbon in terms of physical, mechanical, and chemical properties and structural relations. Intensive investigations of shock syntheses and polymorphic transformations in BN^{1–3} and carbon⁴ have been carried out. Although the rhombohedral form of graphite is known, a significant amount of rhombohedral graphite has not been obtained for detailed investigations. In our Institute, the rhombohedral BN (*r*-BN) whiskers and powders have been synthesized^{5,6} and investigated to understand the phase transformation mechanism through shock-recovery experiments at pressures of about 50 GPa.⁷ The previous results from shock-recovery experiments^{1,7,8} indicate that graphite-like BN (*h*-BN) transforms entirely to wurtzite-type BN (*w*-BN) and that *r*-BN converts directly to zincblende-type BN (*c*-BN). Static compressions of *h*-BN and *r*-BN produce *w*-BN at low temperatures and *c*-BN at high temperatures.^{2,9} Recent static, *in situ* high-pressure observations revealed that highly crystalline *r*-BN converts to *c*-BN through *w*-BN,¹⁰ but that poorly crystallized *r*-BN converts directly to *c*-BN at room temperature and at pressures of about 20 GPa.¹¹

According to the Hugoniot data obtained on *h*-BN,^{3,12} the threshold shock pressure to initiate the phase transition is estimated to be about 10 GPa, which is consistent to shock recovery results on highly crystalline *h*-BN.¹³ If we assume similar shock behaviors for *r*-BN since there are no Hugoniot data for *r*-BN, we can expect a similar threshold pressure for the *r*-BN to *c*-BN transformation. Therefore, there is a need to investigate the polymorphic transformation from *r*-BN to *c*-BN at relatively weak shock conditions in order to understand the shock-induced mechanism and process for phase transition in this material.

EXPERIMENTAL PROCEDURE

Powders of *h*-BN and *r*-BN were mixed with copper powders. The *h*-BN powder was the same as that used in previous studies.¹³ The *r*-BN powder was obtained through the chemical reaction of sodium tetrahydroborate

(NaBH₄) and ammonium chloride (NH₄Cl) in a N₂ atmosphere⁶ and contains very small amounts of *h*-BN. Two kinds of *r*-BN powders, referred to here as *r*-BN(L) and *r*-BN(H), were investigated and they are slightly different in *h*-BN content and in crystallinity, as indicated by x-ray diffraction patterns (Figs. 2 and 3). According to transmission electron microscopy (TEM), the ranges of the starting BN particle size are 0.2–5 μ m for the *h*-BN powder and 0.03–0.4 μ m for *r*-BNs. The 4 wt. % BN-96 wt. % Cu powder mixtures were pressed into stainless-steel containers to form disks. The sample thickness of the pressed disks was fixed at 1.5–2.0 mm for *r*-BN and a second Cu pressed disk, about 3 mm thick, was situated behind the sample to absorb the reflected shocks from the back of the container; the *h*-BN sample disks were about 4.5 mm in thickness and may be affected by reflected shocks. The bulk density of the pressed disk was estimated, within an error of about $\pm 3\%$, in order to calculate the first shocked state of pressure and temperature. The container was mounted in a holder and subjected to the impact of a flyer plate glued on the front surface of the projectile. The projectile was accelerated by a propellant gun.¹⁴ The impact velocity was measured in order to determine shock pressure and temperature. The duration of shock compression is proportional to the thickness of the flyer plate.

The recovered containers were cut open and specimens taken from the disks were immersed in a mixed acid of HNO₃ and HCl (1:3 by volume) to dissolve the copper matrix. Both powder x-ray diffraction and electron microscopy were employed to examine the recovered BN specimens.

The Hugoniot for the mixtures can be calculated by calculating the Hugoniot for a mixture of constituents with known Hugoniots and with the assumption of equal pressure and temperature of both constituents. As there is no significant difference of the bulk densities between copper powder and the Cu mixture pressed under the same load, the shock temperature for the pressed mixture is approximated by that for the copper pressed to the same load if one can assume the thermal equilibrium within the mixture

TABLE I. Shock-recovery conditions for mixtures of 4 wt. % BN-96 wt. % Cu.

Run ^a	Flyer thickness ^b (mm)	Impact velocity (km/s)	Bulk density ^d (g/cm ³)	Pressure ^c (GPa)		Temperature (°C)
				P_i	P_f	
31G	SUS/2	1.24	5.97	15	26.9	1500
42G	SUS/2	1.75	7.17	29	40.6	1450
64G	SUS/2	1.98	7.40	37	47.3	1550
267L	Al/3	1.15	7.81	11	14.0	350
255L	SUS/2	1.07	7.78	17	22.7	550
254L	SUS/2	1.49	7.90	27	33.4	850
283H	Al/3	0.920	7.88	8.5	10.8	250
269H	SUS/2	1.29	7.88	22	28.2	700
270H	SUS/2	2.06	8.28	43	49.7	1000
273H	SUS/12	1.7 ^c	8.14	33	39	850
275H	SUS/2	1.52	5.53	17	34.3	1800

^aStarting material; G=graphite-like BN, L=r-BN (L) as shown in Fig. 2, and H=r-BN (H) shown in Fig. 3. L and H contain small amounts of h-BN, some 8% and 2%, respectively.

^bSUS=stainless steel 304 and Al=Al alloy.

^cImpact velocity was estimated based on propellant mass.

^dEstimated errors are about $\pm 3\%$.

^ePressures P_i and P_f are the first shock pressure and the pressure equilibrated with the container, respectively.

during shock compression. Shock pressures were calculated based on the impedance match method using measured impact velocities.

RESULTS

Experimental conditions are summarized for h-BN and r-BN in Table I. The first shock pressure within the sample ranges between 8.5 and 43 GPa. Figure 1 depicts a series of x-ray powder diffractions of specimens for virgin h-BN and shocked h-BN. The shocked h-BN specimens contain

w-BN with the percentage of w-BN increasing with increasing pressure. c-BN was not observed in the shocked h-BN specimens. This is consistent with previous results.¹ A small amount of h-BN remained in the run product of #64, subjected to the maximum shock pressure in the present study, although Fig. 2 does not indicate that clearly.

Figure 2 shows a series of x-ray powder diffractions of specimens for virgin r-BN(L) and shocked r-BN(L). We adopted the index (hkl) as the hexagonal system for the rhombohedral BN instead of (hki) for simplicity, where $i = -(h+k)$. The starting r-BN contains about 8% h-BN that is greater than that of r-BN(H) (Fig. 3) as based on the diffraction pattern (Fig. 2). The product of run #267,

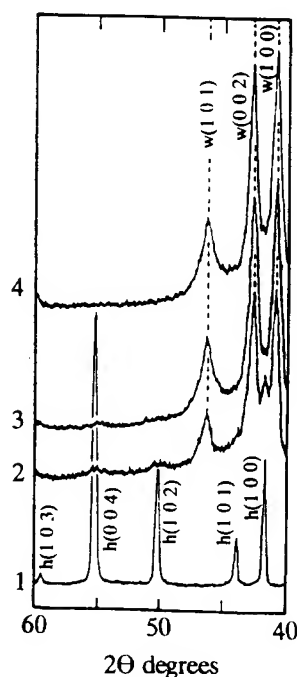


FIG. 1. X-ray diffraction patterns of the starting h-BN (1) and the specimens recovered from various shock pressures (2=#31G at 15 GPa, 3=#42G at 29 GPa, and 4=#64G at 37 GPa).

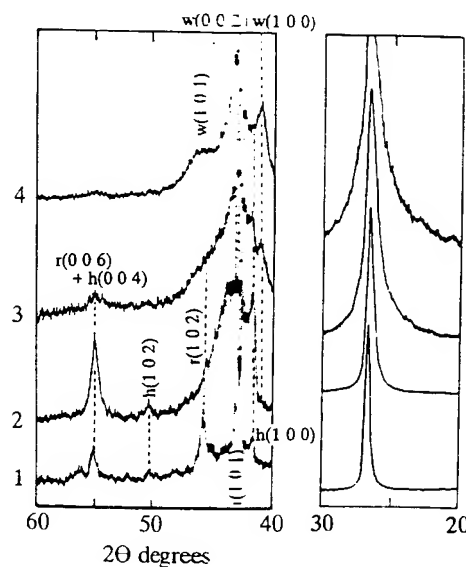


FIG. 2. X-ray diffraction patterns of the starting r-BN(L) (1) and the specimens recovered from various shock pressures (2=#267L at 11 GPa, 3=#255L at 17 GPa, and 4=#254L at 27 GPa).

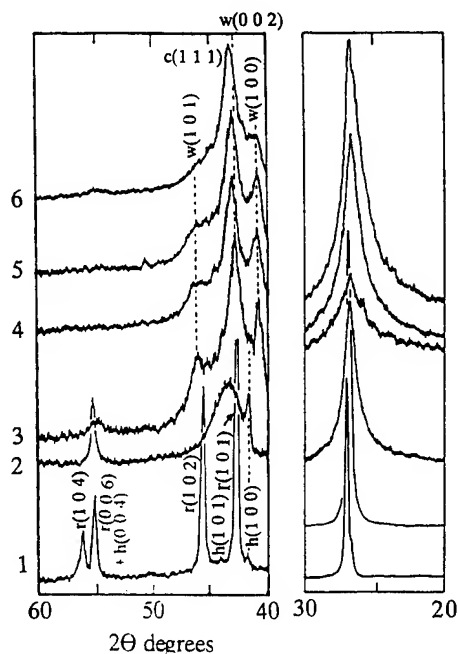


FIG. 3. X-ray diffraction patterns of the starting r -BN(H) (1) and the specimens recovered from various shock pressures (2=#283H at 8.5 GPa, 3=#269H at 22 GPa, 4=#270H at 43 GPa), with a longer shock duration (5=#273H) and with a higher shock temperature (6=#275H).

subjected to the 11 GPa shock compression, indicates remarkable intensities of h -BN diffraction peaks of (100) and (004) and a broad peak around 43° to 44° corresponding to the presence of t -BN.¹⁵ With increasing shock pressure, the diffraction peaks corresponding to w -BN (100) and (002) appeared very distinct. However, the peak position corresponding to the w -BN (002) shifted toward the higher diffraction angle and the peak corresponding to h -BN (100) decreased with increasing pressure. By comparison of the w -BN phases formed from h -BN and r -BN powders, it is noteworthy that the (101) peak of w -BN formed from r -BN diffuses considerably relative to the peaks (100) and (002) and that the relative intensity of (100) to (002) differs greatly. The latter may be due to the formation of t -BN from r -BN.

X-ray diffraction patterns of the starting and shocked specimens for r -BN(H) are shown in Fig. 3. The effect of different r -BN is not significant. The results of run #283, subjected to the weakest shock, display the increased intensities of h -BN (100) and (004), diminished r -BN peaks at (102), (104), and (105), and two broad peaks at approximately 43 – 44° and 82 – 83° in 2θ degrees. These diffraction patterns indicate the formation of h -BN and t -BN. The results of run #270, subjected to the maximum shock pressure, do not appear to indicate that peak pressure is important at least up to 43 GPa. In run #273, the shock duration was about six times longer than the other experiments, but the x-ray diffraction pattern does not change significantly. The starting mixture of No. 275 was less dense than the others in order to increase the shock temperature. The x-ray diffraction pattern for this run reveals

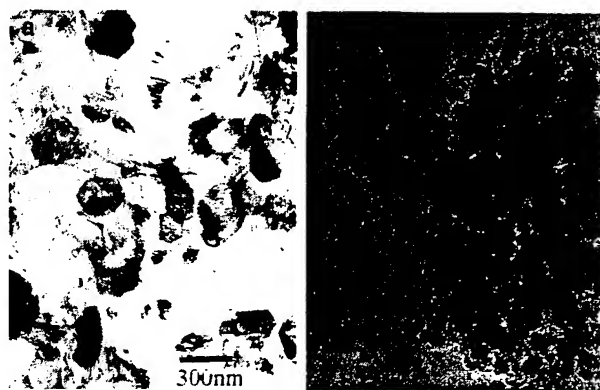


FIG. 4. Microphotographs of transmission electron microscopy of the typical grains of (a) the starting r -BN(L) and (b) c -BN grains in the run product #275H.

that the w -BN (100) peak starts to diffuse and that the peak position corresponding to w -BN (002) is identical to c -BN (111). This indicates that the major high-pressure phase is c -BN in the results of that run. The interplanar value corresponding to w -BN (002) is determined to be $0.2114 (\pm 0.0003)$ nm for runs No. 31, 42, 64, and 255, 0.2108 nm for run No. 269, 0.2103 nm for run No. 254, 0.2100 nm for runs #270 and #273, and 0.2088 nm for run No. 275. These interplanar distances correspond to the values for w -BN (002) and c -BN (111).

Figure 4 gives electron microphotographs of typical grains of starting r -BN(L) and shocked grains in #275 where grain sizes are very fine (mostly less than 10 nm) and electron diffraction patterns are identical to c -BN.

DISCUSSION

The present shock-recovery experiments at pressures of 8–50 GPa indicate that h -BN converts only to w -BN and that r -BN transforms to h -BN, t -BN, w -BN, and c -BN. The transformations of r -BN to h -BN and t -BN are observed at pressures below about 25 GPa. The amounts of w -BN and c -BN increase with increasing shock pressure and the relative amount of c -BN to w -BN increases with increasing shock temperature at a given pressure.

Sato *et al.*⁷ described the direct phase transformation of r -BN to c -BN by using strong shock compressions. Their shocked r -BN converted almost completely to c -BN with a small amount of unidentified phase which might be E -BN.¹⁶ The presence of the unidentified phase suggests that the specimen was subjected to intensive shock loading.^{8,16} The shock condition corresponds to the one extrapolated from the present experiments to stronger shocks. Therefore, there is no inconsistency between the present and previous results.

In the present study, the formation of h -BN from r -BN at weak shock pressures implies that slipping and rotation between layers proceed very fast and extremely easy at pressure. However, the r -BN hardly converts to h -BN with temperature.⁹ Static high-pressure experiments on r -BN^{9,10} also indicate the formation of h -BN from r -BN at pressures

below 8 GPa. If we assume that the shift of the diffraction peak corresponding to the *w*-BN (002) is caused by the coexistence of various amounts of *c*-BN, then the threshold pressure for the formation of *c*-BN is estimated to be about 25 GPa at relatively low shock temperatures and for pressures below 17 GPa at high shock temperatures. This implies that the phase transition is dominated by kinetics. These threshold pressures are greater than the one for the *h*-BN to *w*-BN transition.

The structural difference between *h*-BN and *r*-BN is only the number of the layered sequence since *h*-BN is thermodynamically stable. The phase *h*-BN converts immediately to *w*-BN under shock loading and never to *c*-BN. The *c*-BN phase favors high-temperature and high-pressure conditions, as indicated in the present results and previously observed in static experiments.⁹ This is consistent to the assumption that the mechanism for the phase transition of *r*-BN to *c*-BN is diffusional rather than diffusionless, i.e., martensitic. If intermediate phases are involved in the formation process of *c*-BN, then *h*-BN, *t*-BN, and *w*-BN are the most probable candidates as identified in runs for relatively weak shock loadings. It has been known that intensively shocked *w*-BN converts partially to *c*-BN.^{8,16} On the other hand, experiments with longer shock durations on *h*-BN have indicated no formation of *c*-BN under relatively weak shock loadings,¹³ while shock loading of preheated *h*-BN results in the conversion to *c*-BN, although the yield is very low.^{13,17} We have no firm evidence to indicate any difference between the *w*-BN phases formed from *h*-BN and *r*-BN, although the shift of the diffraction peak corresponding to *w*-BN (002) may be related to an intermediate phase such as the compressed wurtzite phase analogous to compressed *h*-BN.² We cannot exclude the possibility that *c*-BN is converted directly from *r*-BN. It is not possible to identify the shock-induced high-pressure phase of BN from the Hugoniot data alone because of the very small density and compressibility differences between the *w*-BN and *c*-BN phases.³ Flash x-ray diffraction investigations of BN during shock compression¹⁸ should be performed in order to determine *in situ* shock-induced high-pressure phase.

Onodera *et al.*⁹ pointed out that there are three possible formation paths of *c*-BN from *r*-BN under static compressions: (i) *r*-BN → *c*-BN, (ii) *r*-BN → *h*-BN → *c*-BN, and (iii) *r*-BN → *w*-BN → *c*-BN. The paths (i) and (iii) occur at higher pressures and the path (ii) at lower pressures. Under dynamic conditions only path (i) has been previously observed.⁷ From the present study other paths (iv) *r*-BN → *h*-BN → *w*-BN → *c*-BN and (v) *r*-BN → *t*-BN → *c*-BN can be realized at relatively weak shock conditions. The first step of path (iv) requires the change of a three-layered sequence to a two-layered sequence, which is followed by the slipping and 60° rotation between the layers. The second step is readily achieved at shock pressures of about 10 GPa. The final step requires a diffusional process to reconstruct the bonding in the zincblende structure, and in general this process controls the kinetics of the transition. To enhance the final step, high-temperature conditions are necessary. For path (v), our recent investigations of post-

shock *t*-BN²⁰ indicate formation of *c*-BN, but no *w*-BN, under similar shock conditions.

Ueno *et al.*¹¹ have shown the occurrence of the direct *r*-BN to *c*-BN transformation in a diamond anvil cell at room temperature. The transition starts at about 8 GPa, followed by a structural change of *r*-BN and finishes at about 25 GPa. Their *r*-BN sample was prepared from the CVD method and was not crystallized as well as ours, based on a comparison of the x-ray diffraction patterns. With a decreasing degree of crystallinity and layered sequence regularity, the formation area of *w*-BN appears to be reduced under both static and dynamic compressions.^{16,19} It should be pointed out that the crystallinity of the starting material is one of the most important parameters to influence the phase transformation, not only under static pressure but also under shock compression.

The transformation mechanism for the graphite to diamond transition has been suggested to be martensitic through recent VISAR measurements.⁴ Structurally, the hexagonal diamond phase, instead of the cubic diamond phase, is preferably shock induced from graphite by a martensitic mechanism.²¹ The major component of recovered diamond, however, consists of the cubic form. This is due to the requirement for heating to at least 1000 °C (Ref. 22) and to quenching the shock-induced hexagonal diamond to ambient condition. Since the rhombohedral phase of graphite has not been investigated, we cannot directly compare the transformation characteristics between the rhombohedral graphite and BN. The present results on rhombohedral BN may give a guide for the rhombohedral phase of graphite to cubic diamond transformation.

ACKNOWLEDGMENTS

We are grateful to O. Shimomura and T. Taniguchi for their helpful discussions during the preparation of the draft.

¹ T. Soma, A. Sawaoka, and S. Saito, *Mater. Res. Bull.* **9**, 755 (1976).

² F. R. Corrigan and F. P. Bundy, *J. Chem. Phys.* **63**, 3812 (1975).

³ W. H. Gust and D. A. Young, *Phys. Rev. B* **15**, 5012 (1977).

⁴ P. S. De Carli and J. C. Jamieson, *Science* **133**, 1821 (1961); D. G. Morris, *J. Appl. Phys.* **51**, 2059 (1980); W. H. Gust, *Phys. Rev. B* **22**, 4744 (1980); D. J. Erskine and W. J. Nellis, *Nature* **349**, 317 (1991) and *J. Appl. Phys.* **71**, 4882 (1992).

⁵ T. Ishii, T. Sato, Y. Sekikawa, and M. Iwata, *J. Cryst. Growth* **52**, 285 (1981).

⁶ T. Sato, *Proc. Jpn. Acad.* **61B**, 459 (1985).

⁷ T. Sato, T. Ishii, and N. Setaka, *J. Am. Cer. Soc.* **65**, c-162 (1982).

⁸ T. Akashi, A. Sawaoka, S. Saito, and M. Araki, *Jpn. J. Appl. Phys.* **15**, 891 (1976).

⁹ A. Onodera, K. Inoue, H. Yoshihara, H. Nakae, T. Matsuda, and T. Hirai, *J. Mater. Sci.* **25**, 4279 (1990).

¹⁰ T. Taniguchi, O. Shimomura, T. Sato, T. Oosawa, S. Yamaoka, W. Utsumi, M. Yamakata, and T. Kikegawa, in *Abst. 32nd High Press. Conf. Jap.* p. 260, 1991 (in Japanese).

¹¹ M. Ueno, K. Hasegawa, R. Oshima, A. Onodera, O. Shimomura, K. Takemura, H. Nakae, T. Matsuda, and T. Hirai, *Phys. Rev. B* **54**, 10226 (1992).

¹² S. P. Marsh, ed, *LASL Shock Hugoniot Data* (University of California, Berkeley, 1980), p. 324.

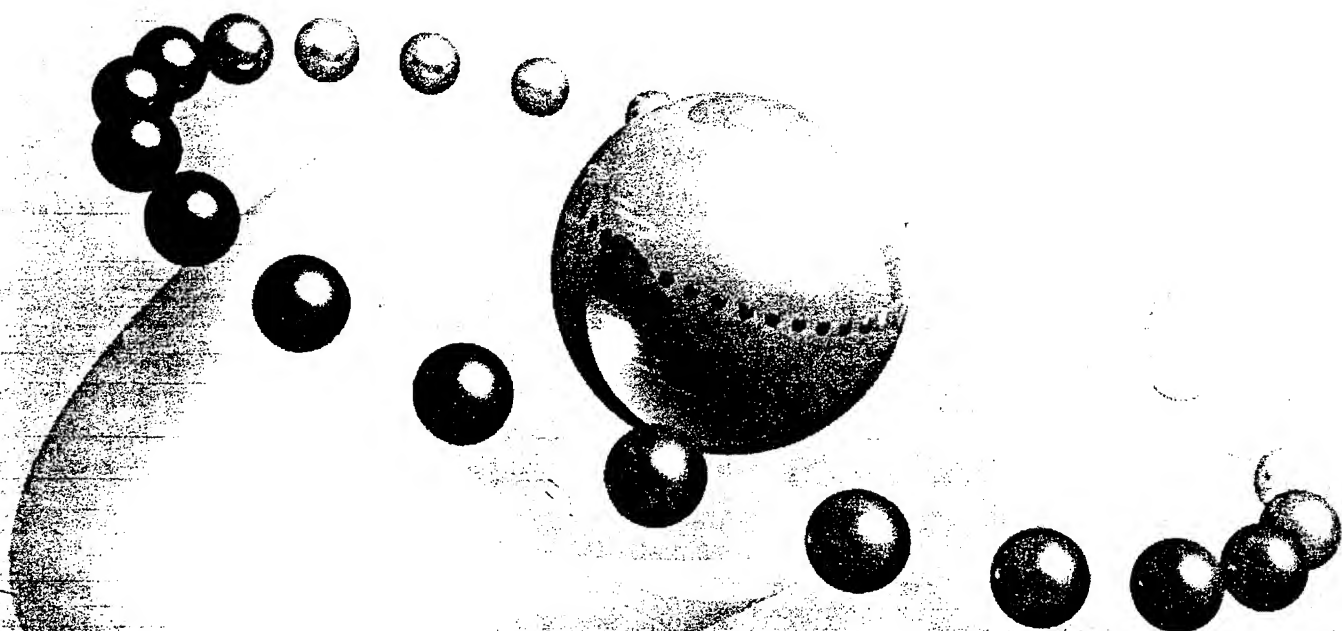
¹³ T. Sekine, in *Shock Compression of Condensed Matter*, edited by S. C. Schmidt, J. N. Johnson, and L. W. Davison (Elsevier, New York, 1990), p. 511.

- ¹⁴T. Sekine, M. Akaishi, N. Setaka, and K. Kondo, *J. Mater. Sci.* **22**, 3615 (1987).
- ¹⁵J. Thomas, Jr., N. E. Weston, and T. E. O'Connor, *J. Am. Chem. Soc.* **84**, 4619 (1963).
- ¹⁶T. Akashi, H. Pak, and A. B. Sawaoka, *J. Mater. Sci.* **21**, 4060 (1986).
- ¹⁷A. V. Kurdyumov, N. F. Ostrovskaya, V. A. Pilipenko, A. N. Pilyankevich, G. I. Savvakina, and V. I. Trefilov, *Sov. Phys. Dokl.* **26**, 487 (1979).
- ¹⁸Q. Johnson and A. C. Mitchell, *Phys. Rev. Lett.* **29**, 1369 (1972).
- ¹⁹H. Sumiya, T. Iseki, and A. Onodera, *Mater. Res. Bull.* **18**, 1203 (1983); I. S. Gladkaya, G. N. Kremkova, and V. N. Slesarev, *J. Less-Common Met.* **117**, 241 (1986).
- ²⁰T. Sekine and T. Sato (unpublished results).
- ²¹A. M. Podurets, A. I. Barenboym, Zh. N. Yelfimova, V. V. Pul', and R. F. Trunin, *Izves. Earth Phys.* **27**, 78 (1991).
- ²²F. P. Bundy and J. S. Kasper, *J. Chem. Phys.* **46**, 3437 (1967).

NIRIM COE RESEARCH PROGRAM

— Striving to Be a COE in Advanced Materials Research —

Advanced Materials Research Utilizing Extreme Conditions



Science and Technology Agency of Japan
National Institute for Research in Inorganic Materials

NIRIM Expands its Capabilities with COE to Promote the

What is COE?

COE stands for Center of Excellence (COE), which is composed of excellent research facilities and a complete research support system under the supervision of distinguished leaders. The COE program began in FY 1993, funded with Special Coordination Funds for Promoting Science and Technology, to make the national research institutes generate new fundamental research results. The National Institute for Research in Inorganic Materials (NIRIM) was selected as one of the initial COE organizations.

NIRIM selected three areas, "Ultra-High Pressure," "Ultra-High Temperature," and "Ultimate Analysis," as the COE program topics. It intends to systematically coordinate these extreme conditions to make the Institute the most advanced in the world, unsurpassed in internationality, openness, and dissemination capabilities.

COE



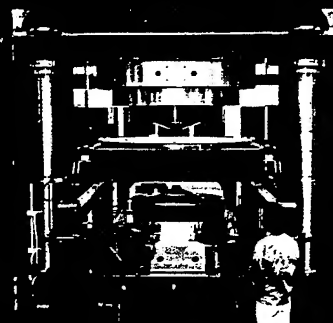
Next-Generation of Advanced Materials for Mankind

COE Subject Areas

**Advanced Materials Research
Utilizing Extreme Conditions.**

Ultra-High Pressure Techniques

Development of Ultra-High
Pressure Techniques in
Sub-Terapascal Region



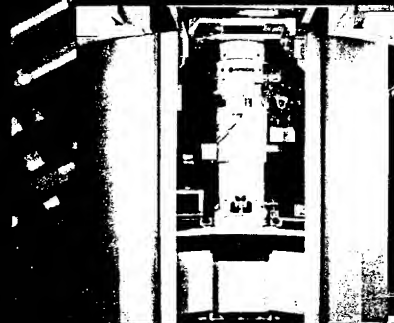
Ultra-High Temperature Techniques

Development of Ultra-High
Temperature Technique to
Produce "Superdiamond"



Ultimate Analytical Techniques

Development of the Advanced
Analytical Techniques at the
Nano-scale Regions, such as
Surfaces, Interfaces, and
Grain Boundaries



Development of the Advanced Materials



Generating ultra-high pressure equivalent
to that at the Earth's center to seek and
create high-density materials exceeding
diamond in hardness



Semiconducting Materials Used in Extreme
Conditions and Optical Materials for Short-
Wave Length

Ultra-High Pressure

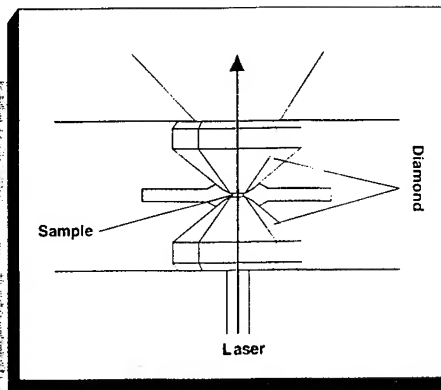
Ultra-high pressure techniques in sub-terapascal region (1 to 10 million atmosphere) will be developed simultaneously with temperatures of 10 thousand degrees to seek and create new ultra-high density materials. A high pressure apparatus with a large sample volume which can generate an ultra-high pressure of 20 GPa will also be developed to produce the ultra-high density materials.

1. Development of Sub-Terapascal-Level Ultra-High Pressure Technique

a. Diamond Anvil Cell

A diamond anvil cell consists of two pieces of single crystal diamond and is used to apply pressure to a sample placed between the two pieces. Ultra-high temperature is generated in the pressurized sample by irradiating it with a laser beam through the transparent diamond.

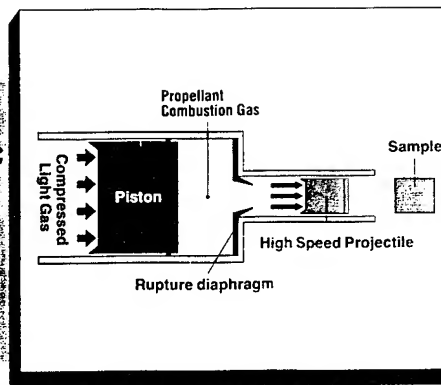
Generated Pressures: Up to 500 GPa
Generated Temperatures: Up to 4,000°C
Pressurized Volume: 10^{-6} ml
Duration: Several minutes at high-temperatures



b. Two-Stage Light Gas Gun Shock Compression Apparatus

Dynamic compression method utilizing the shock wave generated by the impact of ultra-high speed (up to 8 km/sec) projectiles. Material synthesis and characterization are possible through recovery experiments and in-situ observations.

Generated Pressures: Up to 1,000 GPa
Generated Temperatures: Up to 10,000°C
Pressurized Volume: 0.5 ml
Duration: 10^{-6} sec

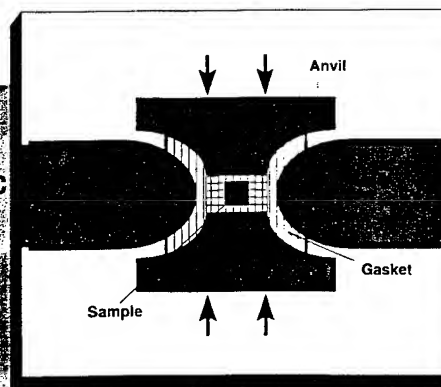


2. Development of Large Volume Ultra-High Pressure Apparatus

Belt-Type Ultra-High Pressure Apparatus

Apparatus to apply pressure to the sample located at the center of a cylinder with an upper and lower anvils. It generates ultra-high pressure over a large volume. It can synthesize and produce single crystals and sintered bodies of new high-density materials.

Generated Pressures: 5 to 20 GPa
Generated Temperatures: Ambient Temperature to 3,000°C
Pressurized Volume: 1,000 to 10 ml
Duration: Several Minutes to one Week



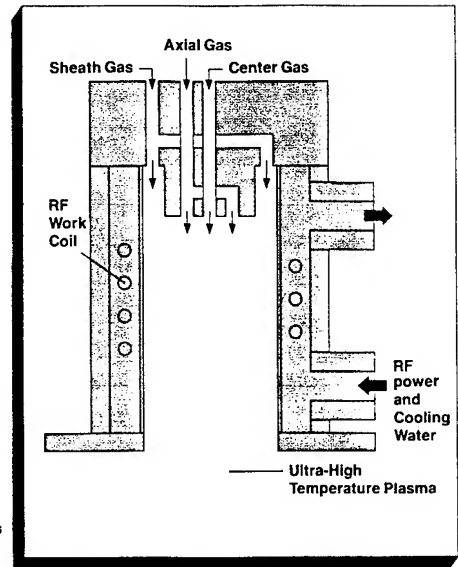
Ultra-High Temperature

Ultra-high temperature techniques will be developed to stably generate highly active plasmas and excited beams to create the next-generation of semiconductor materials, superdiamonds (cubic boron nitride and single crystal diamond films). Film synthesis techniques controlled at atomic or molecular levels will also be developed.

1. Ultra-High Temperature Techniques

Ultra-high temperature techniques will be developed to produce various processing plasmas at pressures lower than 1 atm using direct current, radio frequency, or microwave discharge.

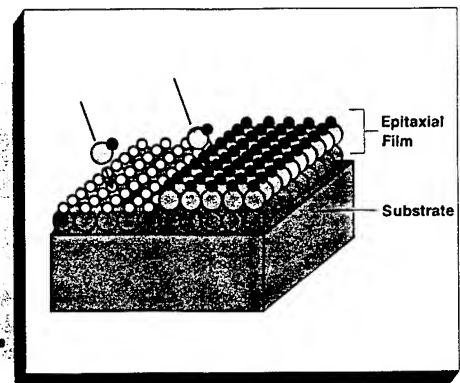
A plasma torch to produce ultra-high temperature plasmas at pressures of 0.1 to 1 atm.



2. Development of Film Fabrication Techniques

High-quality films are necessary to utilize the excellent properties of "super diamond". For this purpose, film preparation techniques, such as laser-assisted plasma chemical vapor deposition (CVD), ion beam synthesis, and radical beam epitaxy processes, will be developed.

A single-crystal film with an oriented axis is produced on a substrate by epitaxial growth techniques.



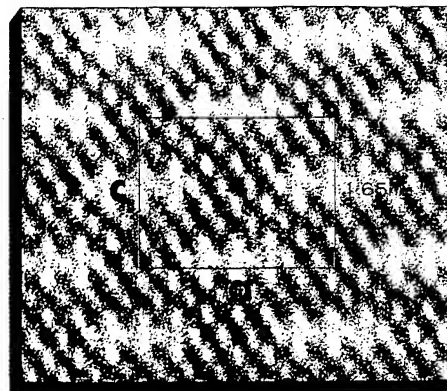
Ultimate Analysis

Analysis techniques will be developed to analyze very accurately the structure, composition, and bonding nature in the angstrom region of the surfaces, interfaces, and grain boundaries of the advanced materials using the advanced beam techniques of electron and ion beams.

1. Development of Local Structure Analysis Techniques

Observation techniques will be developed to dynamically view the local structure directly to identify micro deficiencies in the advanced materials. Image processing techniques will be introduced using an ultra-high voltage electron microscope with the highest resolution in the world.

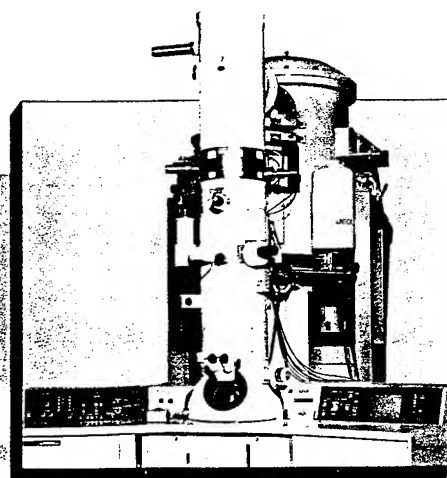
Lattice Image of $\text{TiBa}_2\text{Ca}_2(\text{CO}_3)_x\text{O}_y$ Superconducting Material. The carbonate bases which partially replace copper can be seen in light contrast (white).



2. Development of Local Composition Analysis Techniques

Analysis techniques will be promoted to investigate the local compositions of grain boundaries and interfaces of the advanced materials with high sensitivity and accuracy using an analytical electron microscope and a secondary ion mass spectrometer with the highest sensitivity in the world.

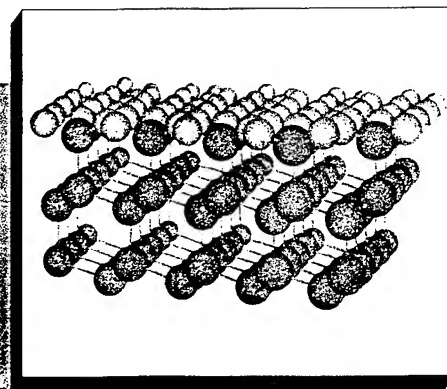
Advanced nano-structure elemental analysis can be conducted with extremely high sensitivity using a 300kV field-emission-type electron microscope and an ultra-small electron probe of 0.4 nano-meters.

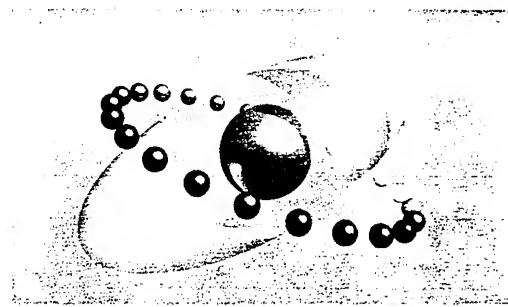


3. Development of Advanced Techniques of Surface Analysis

Surface analysis techniques will be developed to enable highly accurate analysis of the atomic structure, lattice vibration, and electron states of surfaces using an ion scattering spectrometer and a high-resolution electron energy loss spectrometer (HREELS).

The Atomic Structure of Vapor Phase Grown Diamond Revealed by EELS





Research Support System for the CEO Program

Open to Outside Researchers

- Outstanding researchers from all sections of the Institute will contribute as well as outside researchers.
- Reputable personnel from Japan and overseas will be invited.
- Visiting researchers.
- Short-term overseas researchers.

Complete Research Assessment

- The Advisory Committee composed of reputable domestic and overseas researchers has been established to assess and advise the COE programs.

Dissemination of Research Accomplishments

- The NIRM International Symposium on the Advanced Material will be held every year.
- The first symposium will be held in March 1994 in Tsukuba City.

Institute's Past Research Accomplishments

1989:

Succeeded in synthesizing translucent, polycrystalline cubic boron nitride without use of sintering agent.



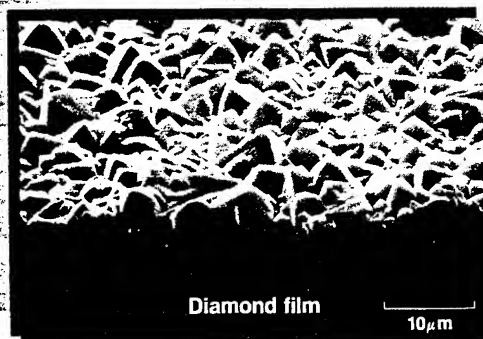
1990:

First in the world to succeed in synthesizing diamond using inorganic compound catalysts, such as carbonates, sulphates, and hydroxides.



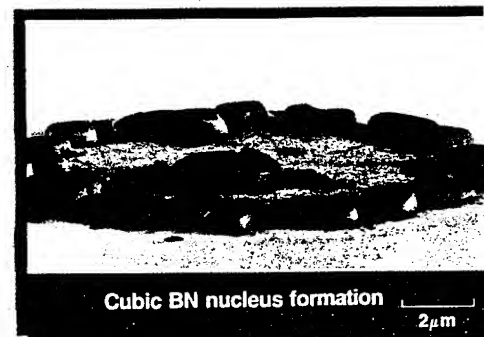
1981:

First in the world to succeed in vapor phase deposition of diamond films.



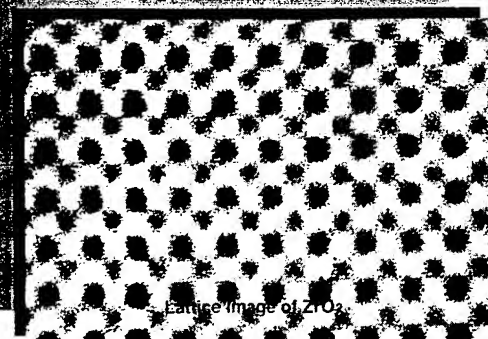
1991:

First in the world to succeed in cubic BN nucleus formation.



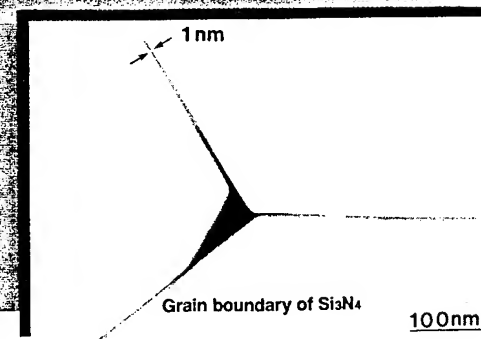
1990:

Developed an ultra-high voltage high resolution electron microscope with world's highest resolution. It became possible to identify oxygen atomic columns.



1993:

Developed a field-emission-type analytical transmission electron microscope with the highest sensitivity in the world. It can analyze the composition of one nano-meter wide grain boundary.



SHOCK SYNTHESIS OF NON-EQUILIBRIUM MATERIALS

V. F. NESTERENKO *

(INSTITUTE FOR MECHANICS AND MATERIALS, UCSD, LA JOLLA)

***On leave from Lavrentyev Institute of Hydrodynamics, Russian
Academy of Sciences, NOVOSIBIRSK, 630090, RUSSIA**

CONTENTS

1. Introduction

2. Micromechanics of porous condensed materials under intense dynamic loading

- 2.1 Experiments on dynamic behavior of powders on mesolevel of structure with thermoelectric method
- 2.2 Kinetics of pore collapse in the frame of Carroll-Holt model, comparison with experiments
- 2.3 Modified Carroll-Holt model, microcynetic energy
- 2.4 The front width of strong shocks in granular materials
- 2.5 Quasistatic and dynamic deformation of powders at shock loading, *powders and laminars. Fibers in powder.*
- 2.7 The "cold" boundary layer on the powder-monolith interface
- 2.8 Separation of components in mixtures under dynamic loading
- 2.6 Behavior of oxide films on the surfaces of granules under dynamic loading, *"metallization" of dielectric powders*
- 2.9 Shear instability of pore collapse in real materials; spall in powders - *out of today models*

3. Non-equilibrium heating of powders under dynamic loading

- 3.1 Experimental results on heterogeneous heat release at shock loading of powders
- 3.2 Analysis of thermodynamic models for heterogeneous heating
- 3.3 Skin model and processes of thermal relaxation in shocked powders
- 3.4 Behavior of porous powder mixtures

4. Advanced materials treatment

- 4.1 Criteria for strong compacts under dynamic loading
- 4.2 Preservation of amorphous state under dynamic loading
- 4.4 Shear localization in porous materials - *new tool for chemical reaction*
- 4.5 Low-temperature heat treatment of explosive compacts *(at high $\dot{\epsilon}$)*
- 4.6 Qualitative change of morphology and microstructure of *submicronic nanocrystalline ceramic ($ZrO_2-Y_2O_3$).*
- 4.3 Obtaining of super cooled states with shock wave loading *submicronic nanocrystalline ceramic ($ZrO_2-Y_2O_3$)*

5. Conclusions

SHOCK SYNTHESIS OF NON-EQUILIBRIUM MATERIALS

V. F. NESTERENKO *

(INSTITUTE FOR MECHANICS AND MATERIALS, UCSD, LA JOLLA, CA)

High dynamic pressures look like very promising tool for obtaining and treatment of metastable materials because involve local high temperatures and deformations during the short time with relatively low equilibrium temperature. Impulse loading is successfully used for such technological application like "explosive welding", which has its own window in industrial composite material production. Despite of the activity of researchers in former Soviet Union, USA, JAPAN and others countries explosive treatment of powdered materials did not provide the appropriate place in industrial applications. There are only some successful examples, including metal-ceramic-metal tubes for electroisolation parts in electrical furnaces and for hanging system in nickel melting furnaces, as coating of inner surface of stainless steel tubes with BN-Ni-Cr alloy mixture for gas-turbine engines and amorphous powder (ribbon) consolidation. The reason for these modest success, according to author opinion, is in the complexity and poor understanding of shock wave processes in such heterogeneous materials, like granular and powder materials.

The main efforts were connected with Hugoniot measurements, which do not represent processes on mesolevels (scale of grains diameters, or regions of localized plastic deformation on grains interfaces, etc.). But just these processes are responsible for the compact quality. That is why the micromechanics of granular material behavior at dynamic loading is very important. The kinetic of porous materials densification at dynamic loading on the base of experimental research and on "single cell" model approach will be considered.

*On leave from Lavrentyev Institute of Hydrodynamics, Russian Academy of Sciences, NOVOSIBIRSK, 630090, RUSSIA

The MESOLEVEL phenomena ("cold " boundary layer on the powder-monolith interface ,different regimes of particle deformations in shock waves in granular materials, component separation in mixtures , non-equilibrium thermodynamics ,including the rapid solidification by pressure drop) and criteria for strong bonding for porous materials after dynamic loading, as ceramic fiber behavior at porous matrix at impulse action will be discussed. The physical phenomena on this structural levels determine also the conditions for chemical reactions.

The examples of metastable materials treatment will be presented for the powders and ribbons of the amorphous metallic alloys, rapidly solidified granules of chromium steel of ferrite-martensit type and intermetallic Ti-AL alloy, nanocrystalline submicronic zirconia (t-modification) and high- T_c ceramics, as the properties of the joints of last one with metals.

REFERENCES

1. V.F.Nesterenko, High-rate deformation of heterogeneous materials (monograph), 1992, Nauka, Novosibirsk, 200 p.
2. V.F.Nesterenko, A.N.Lazaridi, Regimes of shock-wave compaction of granular materials // Proc. 12 AIRAPT and 27 EMPRG Intern. Conf. "High Pressure Science and Technology".-N. Y.; Melbourne: Gourdon and Breach Science Publ., 1990.-P. 835
- 3.A.V.Molotkov, A.B.Notkin, D.V.Elagin, V.F.Nesterenko, A.N.Lazaridi, The peculiarities of microstructure of explosive compacts from rapidly solidified titanium alloys after heat treatment, Fizika gorenij i vzryva, 1991,27,3 ,P.11
4. M.P.Bondar, V.F.Nesterenko, Contact deformation and bonding criteria under impulse loading, Fizika gorenij i vzryva,1991,27,3, P.103
5. V.F.Nesterenko, Shock treatment of high- T_c ceramics //Shock wave and high-strain -rate phenomena in materials, Ed. M.A.Meyers, L.E.Murr, K.P.Staudhammer, Marcel Dekker, Inc., 1992, P.809
6. V.F.Nesterenko, Treatment of advanced materials by high dynamic pressures// Proc. 13 AIRAPT Int. Conf., 1992, P.651
7. S.N.Kulkov, V.F.Nesterenko, M.P.Bondar, V.A.Simonov , A.G.Melnikov, P.V.Korolev , Explosive activation of rapidly solidified nanocrystalline ceramic powders $ZrO_2 - Y_2O_3$, Fizika gorenij i vzryva,29, 6, 1993, P.66

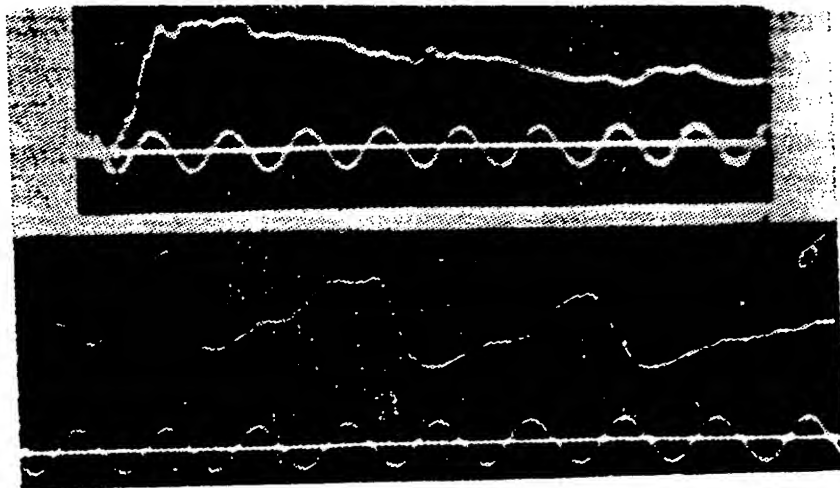


Рис. 2.7. Зависимость массовой скорости от времени в порошке фракции 1,5—2,0 мм (а) и в СМ с $\delta = 2,9$ мм (б) при одинаковых средних плотностях и условиях нагружения. Частота синусоиды 1 МГц, амплитуда сигнала в порошке 300 мВ, чувствительности измерительных трактов одинаковы.

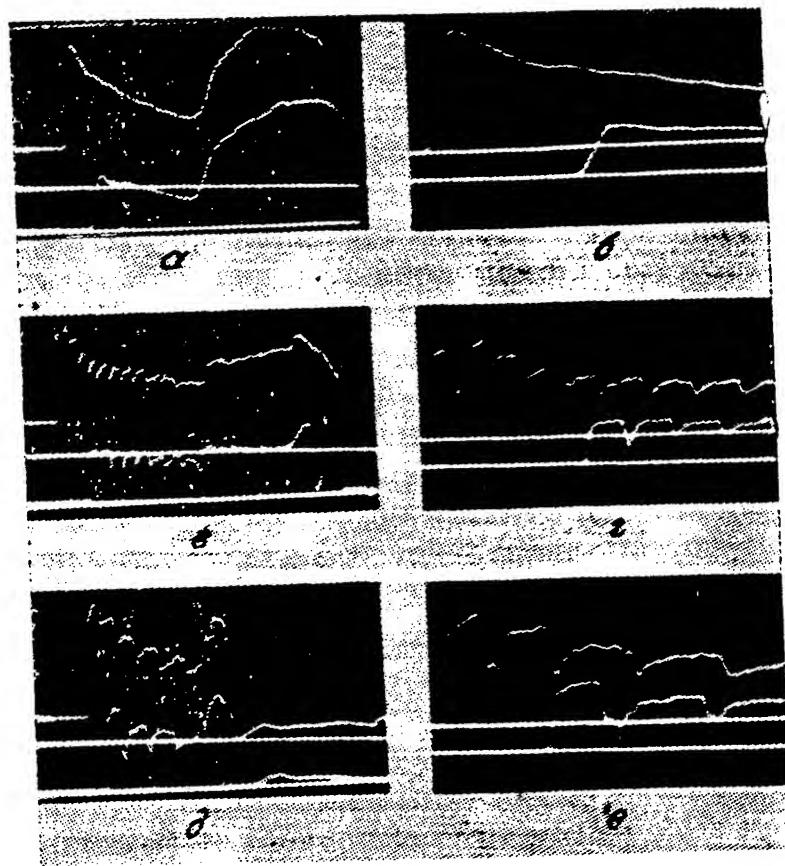


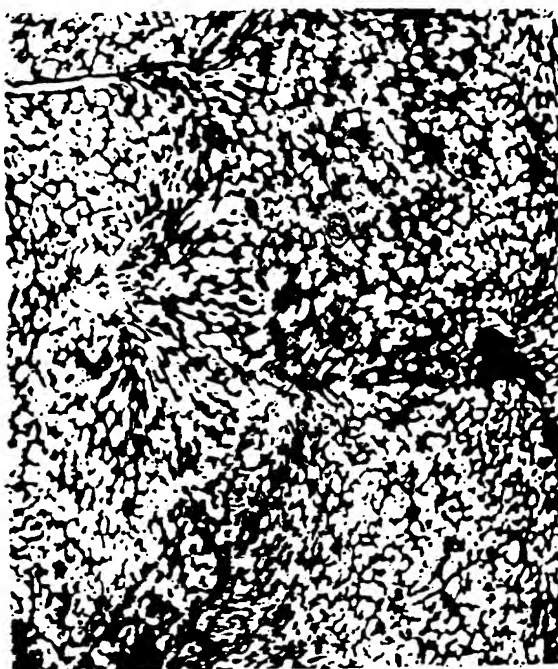
Рис. 2.8. Профили массовой скорости в порошке стекла и его слоистой модели для разных значений L и δ .

а, б — порошок стекла, $L_1 = 0$ мм, $L_2 = 15$ мм; в, г — СМ, $\delta = 1,45 + 1,45$ мм, $L_1 = 1,45$ мм, $L_2 = 16$ мм; д, е — СМ, $\delta = 2,9 - 2,9$ мм, $L_1 = 2,9$ мм, $L_2 = 14,5$ мм. По горизонтали: а, в, д — вся развертка 100 мкс, б, г, е — 30 мкс.

литудам массовых скоростей u и соответствующие им давления в голове каждого импульса нагружения в этих системах приведены в табл. 3.3. В скобках приведены значения давлений, соответствующие удару пластины со скоростью u по ближайшей по-



a



b



c



d

Fig. 1. Examples of quasistatic (c - $\times 250$; d - $\times 100$) and dynamic deformation regimes (a - $\times 250$; b - $\times 500$), a, c - copper granules, b, d - steel granules

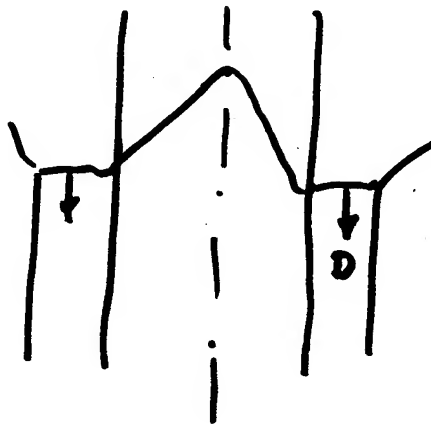
$$E_d/E \leq k$$

$k = 0.5$ - Dynamic regime of particle deformation.

($d_0 = 1.6$) $k \approx K_v/3 \Rightarrow P \geq K_v$ ($P \geq 3K$)

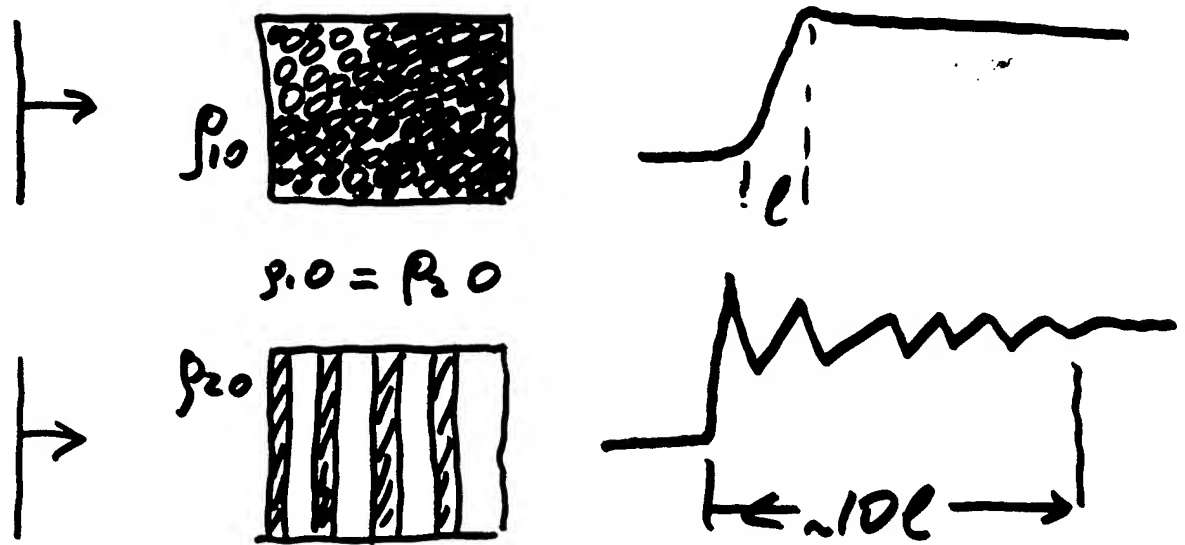
No dependence on initial particle size!

R. Prümmer, $P_D \approx K_v$
to produce uniform density
without Mach step.



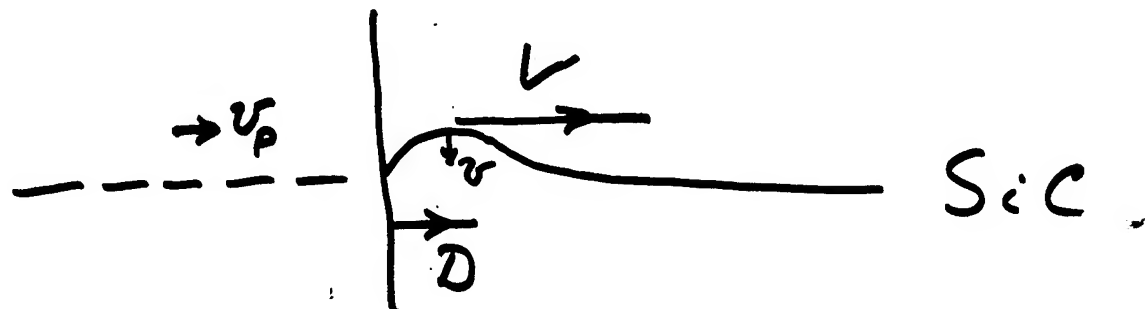
Conclusion: It's impossible to use
cylindrical scheme for strap compacts.

The change of initial mesostructure can qualitatively change the transition way:



The „Pore“ is the transformer of macrokinetic energy to mesoscopic level (particle interfaces) and is responsible for introducing the new mesoscopic parameter - microkinetic energy.

Ceramic fibers stability
at shock wave densification.



$$c_e(\text{SiC}) \approx 12 \text{ km/sec}$$

$$V = \left(\frac{c_e \cdot v_{\max}}{2} \right)^{1/2} ; D = \frac{d_0 v_p}{(d_0 - 1)}$$

The condition of stability (to remove
transverse vibration before shock front):

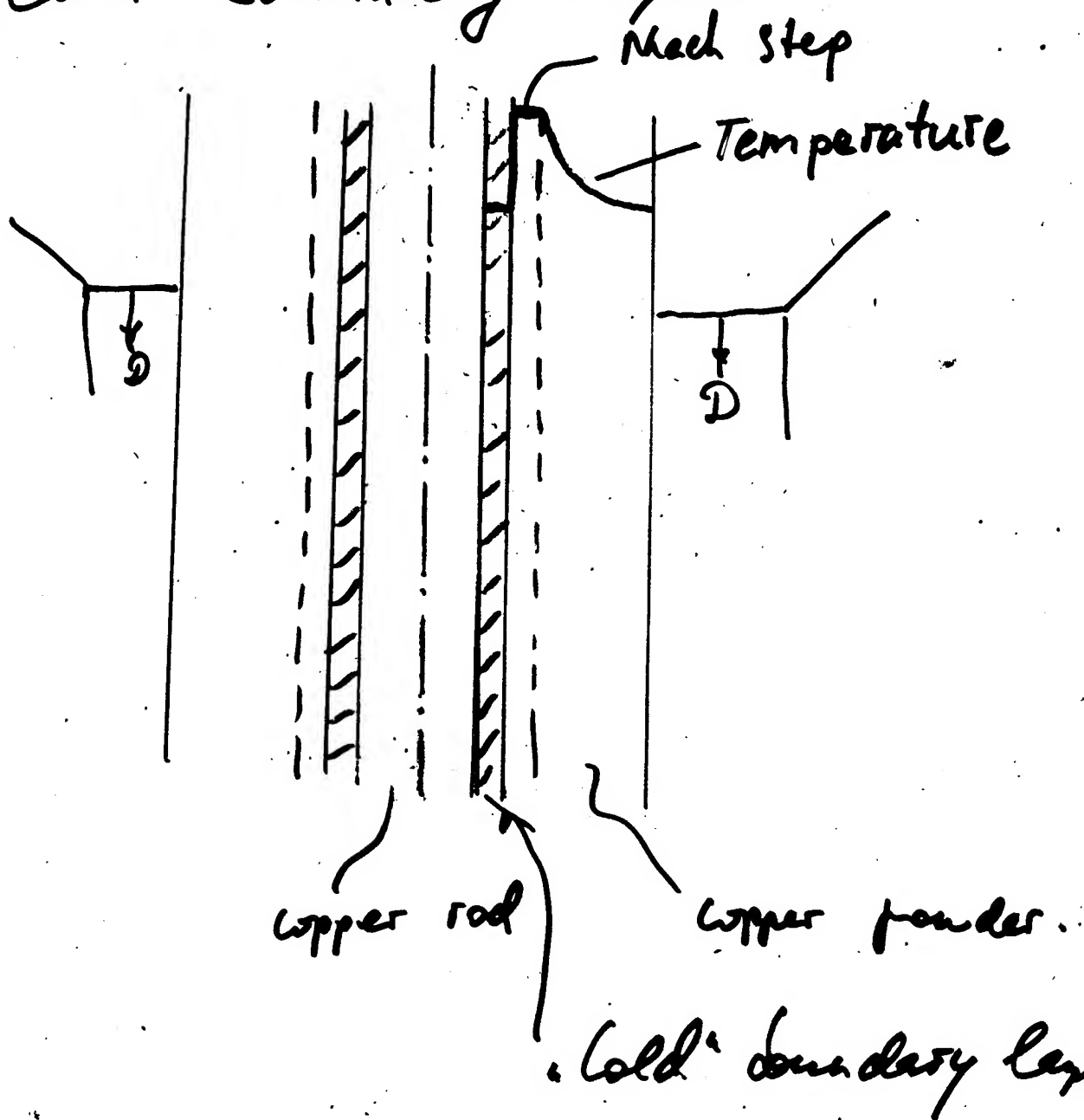
$$D > V$$

$$\text{If } v_{\max} \approx v_p \Rightarrow D > \frac{c_e}{2} \frac{(d_0 - 1)}{d_0}$$

$$d_0 \approx 3 \rightarrow D > 4 \text{ km/sec (melting of Al)}$$

$$d_0 \approx 1.8 \rightarrow D > 2.7 \text{ km/sec}$$

"Cold" boundary layer.



Mechanisms:

1. Non-stationary shock-wave interaction with interface
2. Deformation in rod propagates faster than shock wave in powder.

But: no plastic deformation of rod nearby interface.

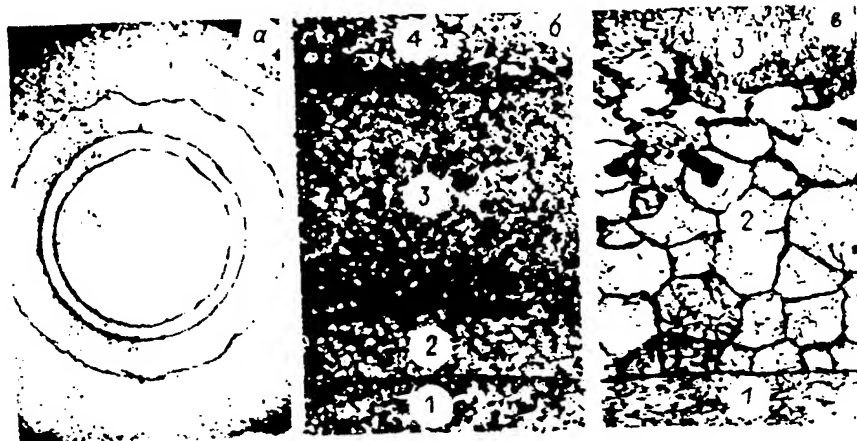


Fig. 5. "Cold" boundary layer at $D=3600$ m/sec (a - $\times 3.3$; b - $\times 50$; c - $\times 250$)

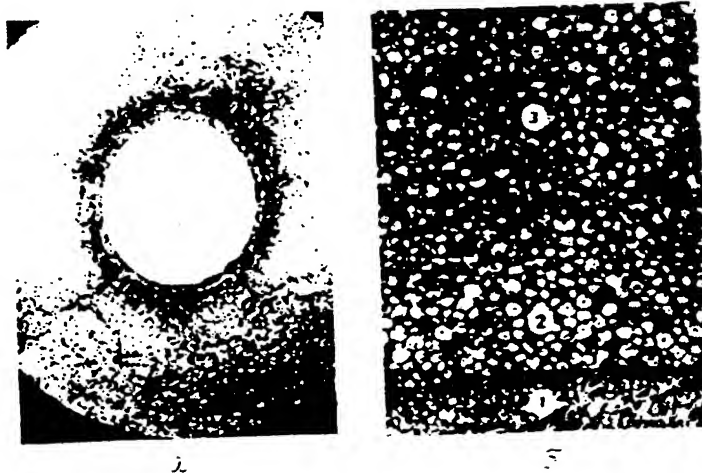


Fig. 6. "Cold" boundary layer at $D=2400$ m/sec (a - $\times 3.3$; b - $\times 50$).

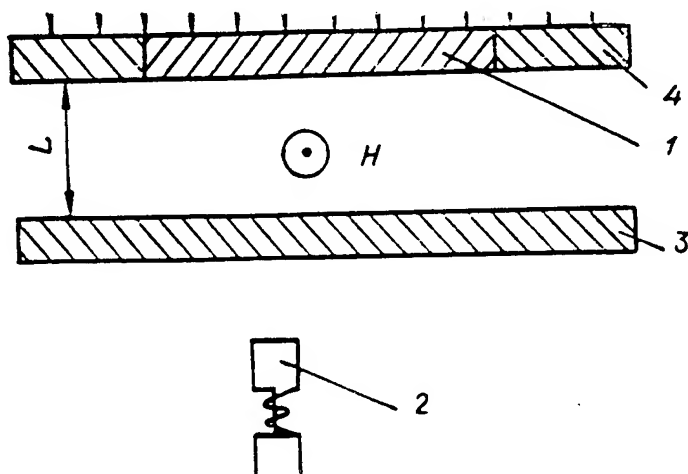


Рис. 1.10. Схема измерения параметров перехода диэлектрик — металл.

1 — порошок; 2 — измерительный контур; 3 — стеклянная пластина-преграда; 4 — медное кольцо; L — база измерения скорости свободной поверхности; стрелками показано направление распространения фронта ударной волны; H — магнитное поле.

Пусть в первоначально непроводящей среде имеется непрерывный профиль массовой скорости и в некоторой её точке среда приобретает металлическую проводимость. Тогда в нашей схеме возникнет электрический сигнал, связанный с появлением переменного поля, вызванного движением проводящей среды. Амплитуда этого сигнала будет определяться массовой скоростью в точке перехода диэлектрик — металл и в ее ближайшей окрестности. Изменение сигнала за счет движения задних слоев будет экранироваться областью вблизи этой точки с характерным размером $x \sim \kappa/D$, где κ — коэффициент магнитной диффузии, D — скорость ударной волны. Для меди $\kappa \approx 10^2 \text{ см}^2/\text{с}$. Значение скорости D в наших экспериментах составляло 3 мм/мкс. Отсюда $x \approx 10^{-3} \text{ см} = 10 \text{ мкм}$ — это оценка снизу из-за предположения, что медь характеризуется стандартным значением своей проводимости.

На рис. 1.11 приведены осциллограммы опытов с крупной и мелкой фракцией. Геометрия опытов была одинаковой. На этом рисунке t_0 соответствует моменту входа ударной волны в порошок, t_1 — моменту прихода ударной волны на свободную поверхность, t_2 — моменту торможения порошка о преграду. Все особенности сигналов хорошо воспроизводятся из опыта к опыту. Сравнение рис. 1.11, а и б показывает практически полное совпадение временных параметров и характерную разницу, примерно в 2 раза, амплитуд сигналов в момент t_0 . Важно также выделить рост сигнала

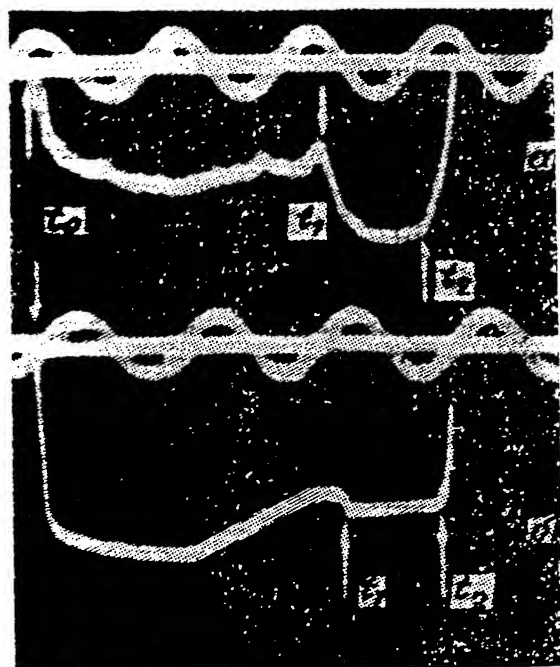
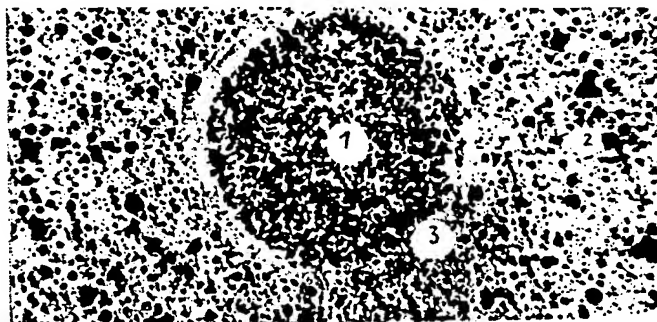


Рис. 1.11. Примеры типичных осциллограмм.

а — крупная фракция 0.1—0.5 мм; б — мелкая фракция $(1-20) \cdot 10^{-3} \text{ мм}$. Частота синусоиды 1 МГц.



Separation of components in the vicinity of tangential jump of partial velocity in porous mixture Cu-BN

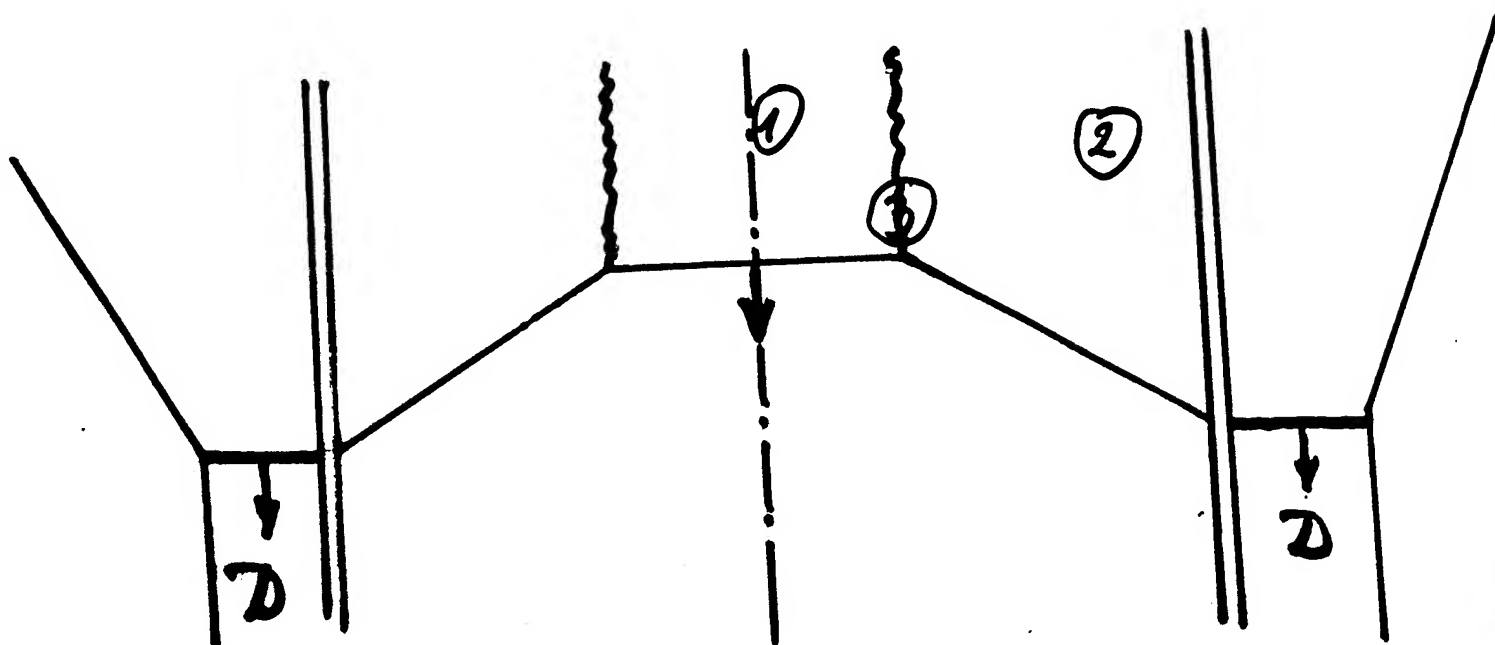






Fig. 2. Behavior of oxide films at the boundaries of copper granules in dynamic compaction regime ($\times 250$).

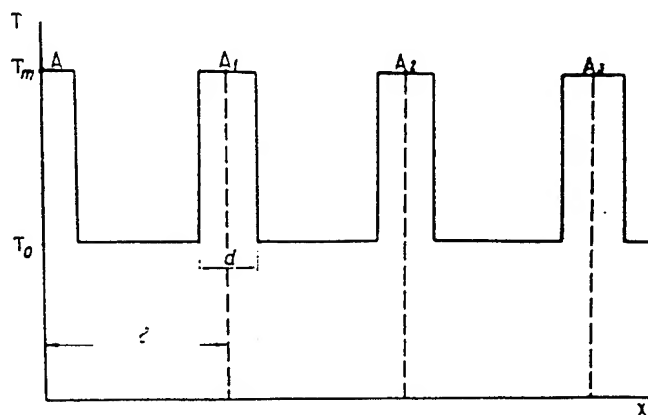
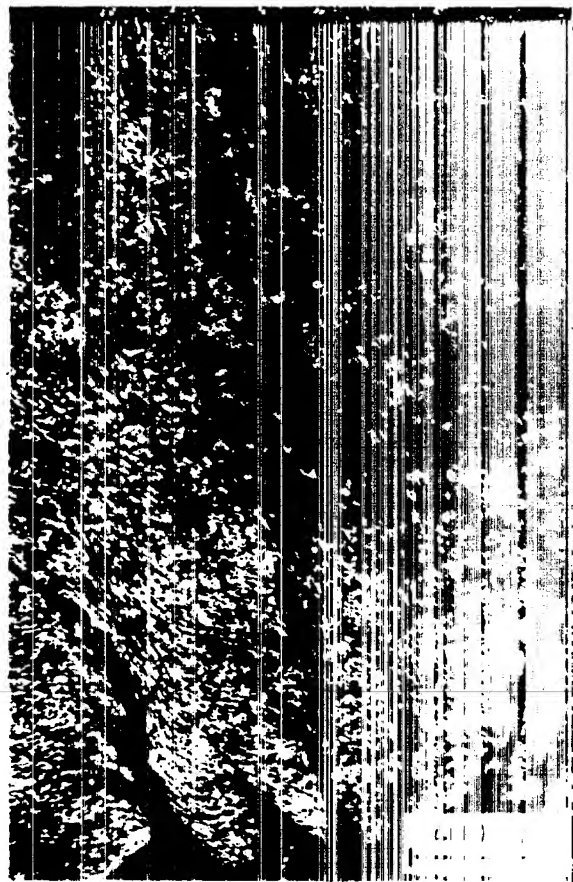


Fig. 3. Initial temperature distribution in shock-compressed material (d - the width of contact zone heated up to T_m ; l - the size of compacted powder particles, T_0 - the temperature of particle volume, equal to initial one)

Cu, $d = 100 \mu$

200μ





a



b



c



Fig. 1. The cracks develop in the center of the specimen (a) and in the adjacent region (b) in the case of a favorable mechanism of fracture of the steel; $\sigma = 100 \text{ MPa}$; $\epsilon = 100\%$; $D_0 = 100 \text{ mm}$.



Gr. $\alpha = 30^\circ$

20m

$$E_d/\bar{E} \leq K$$

Strong compact $K=0,25$

$$P \geq 2Kv \quad (P \geq 65)$$

Can be rewritten as

$$D > 6\sigma_{un}$$

Material	$\gamma, \text{ GPa}$	P_s
W	3,5	21
Al_2O_3	6	36
TiB_2	15	90
B_4C	18	108

$$\underline{EC + K\bar{T}}$$



Fig. 10. Deformation localization under explosive loading of amorphous foils.



Fig. 11. Localization band in laminated system of alternating layers of amorphous and copper foils.

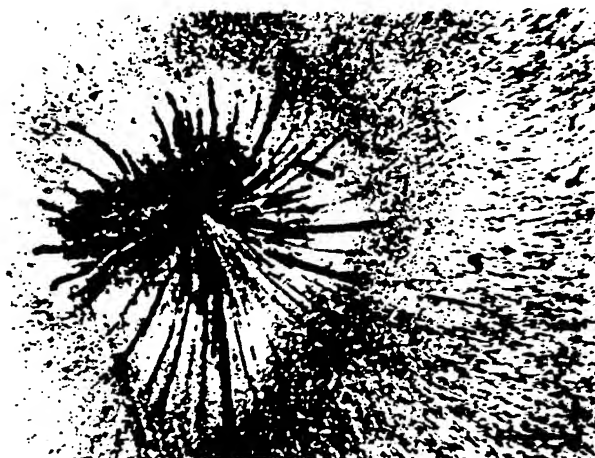


Fig. 12. Deformation localization in copper at collapse of copper cylinder, scale 200 μm .

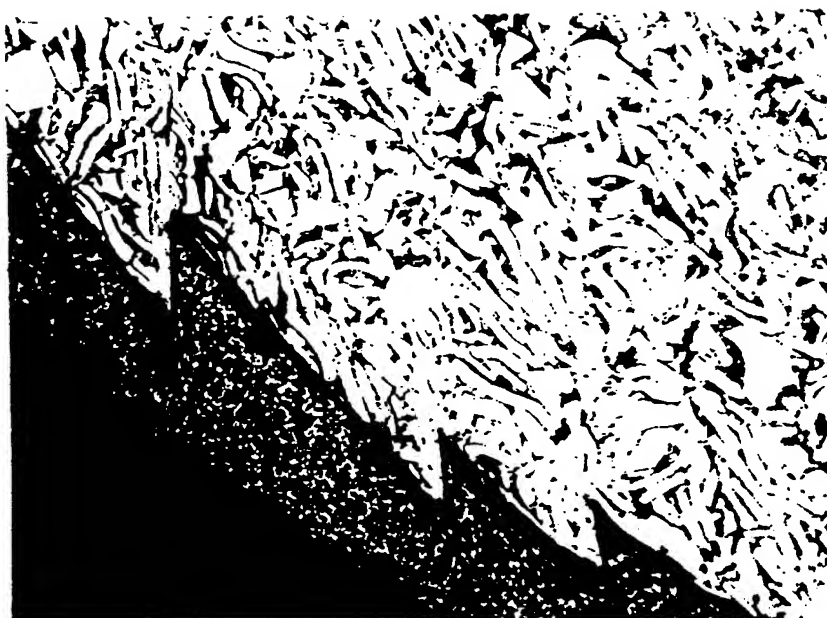
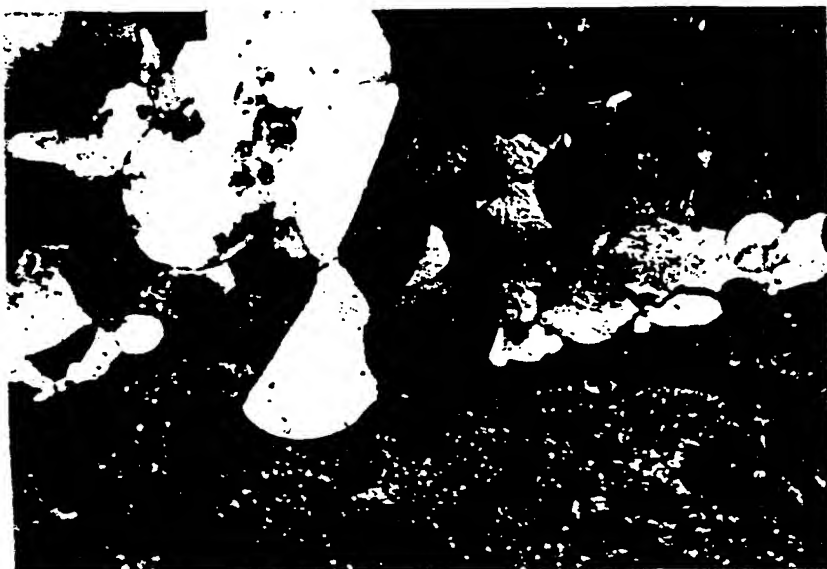


Fig. 7. Transparent particle localized shear:
a) 'Alniko', $\times 200$; b) 'ViknsR', $\times 50$.



Fig. 8. Localized shear deformation in mixture 71KNSR+40% copper.

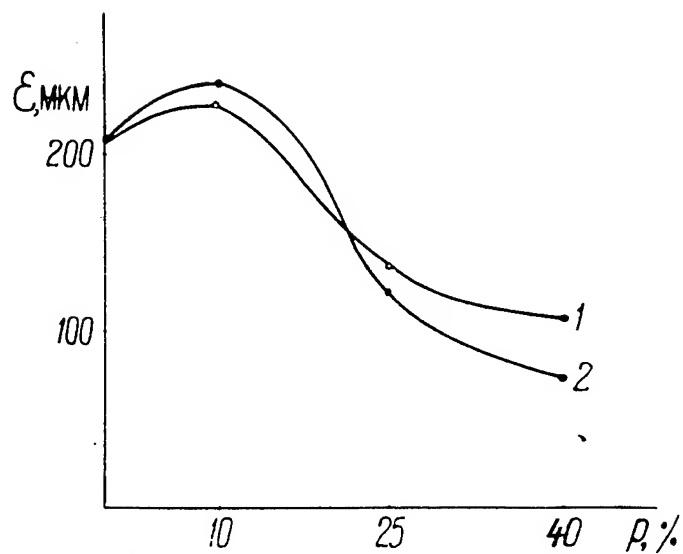
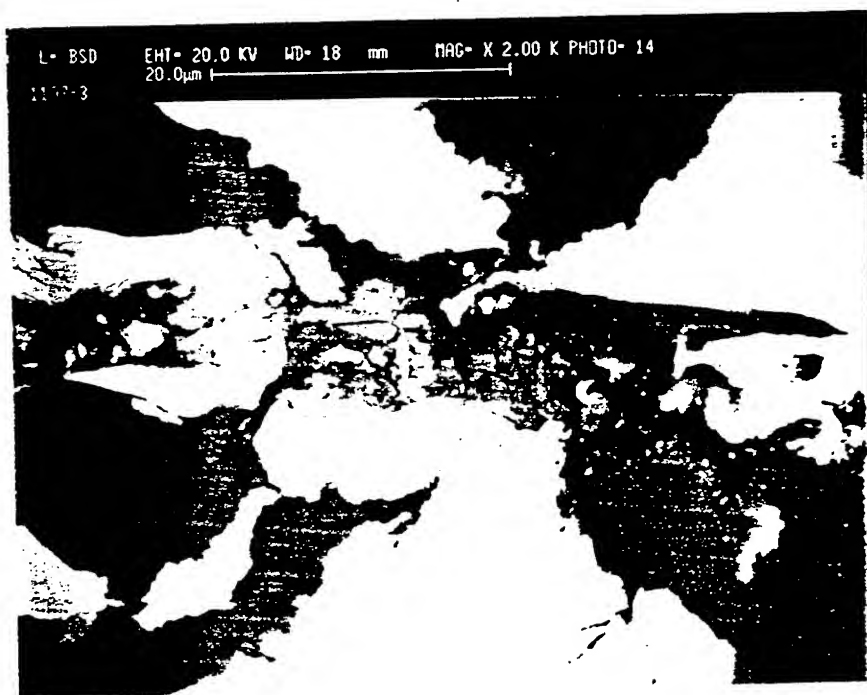
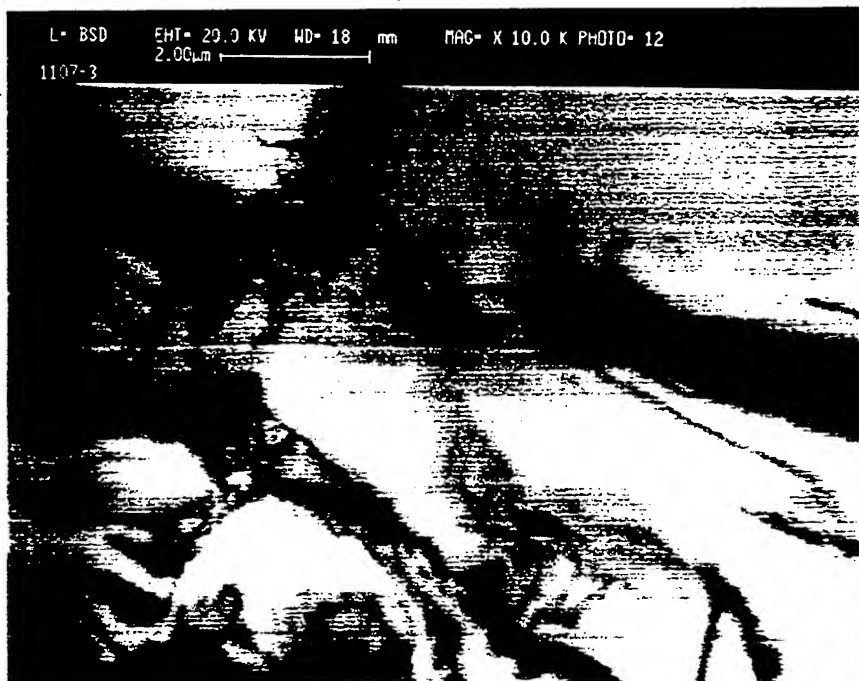


Fig. 9. Dependence ϵ on the content of Ni (1) and copper (2) in mixture with 2NSR under the same loading conditions.



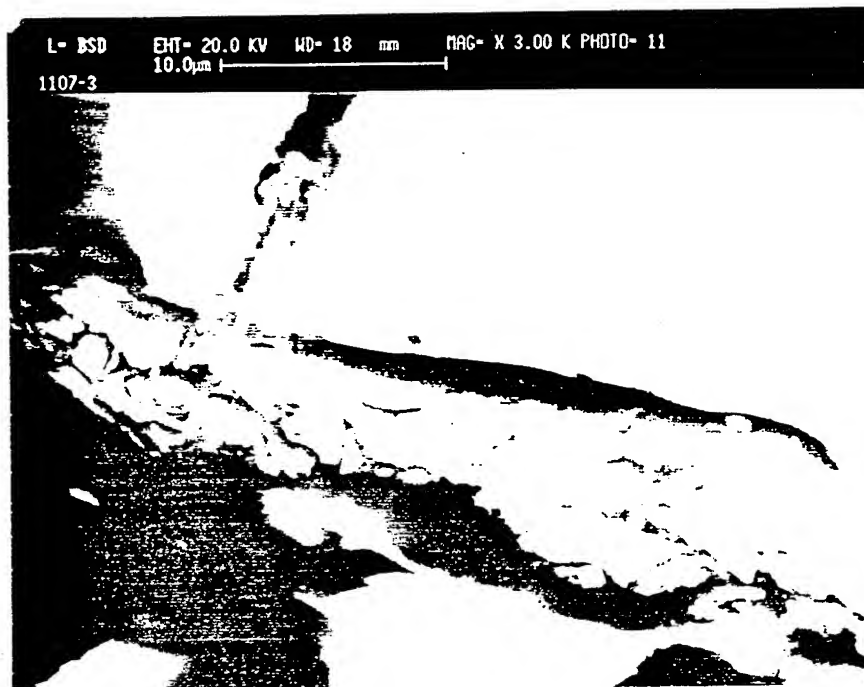
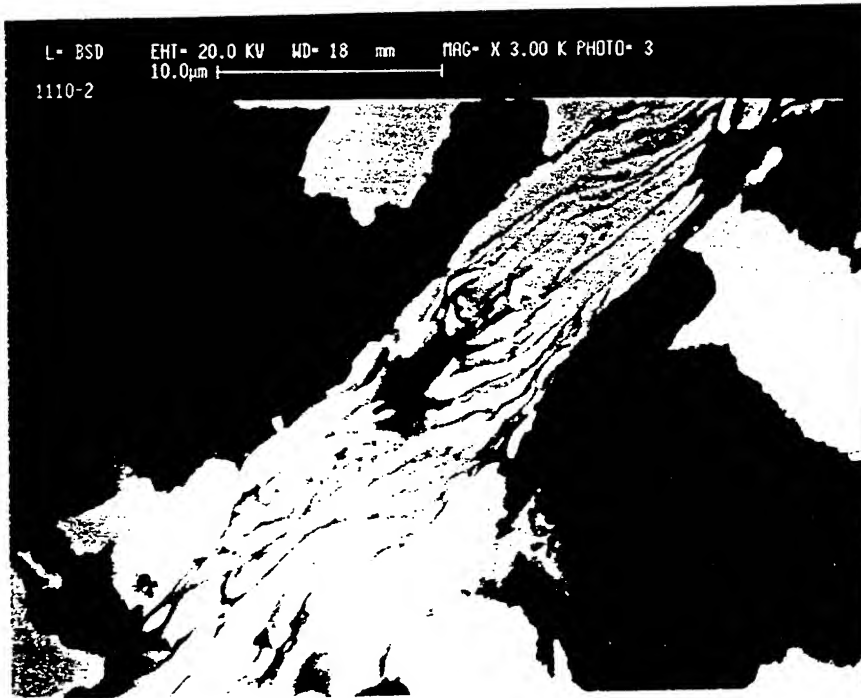
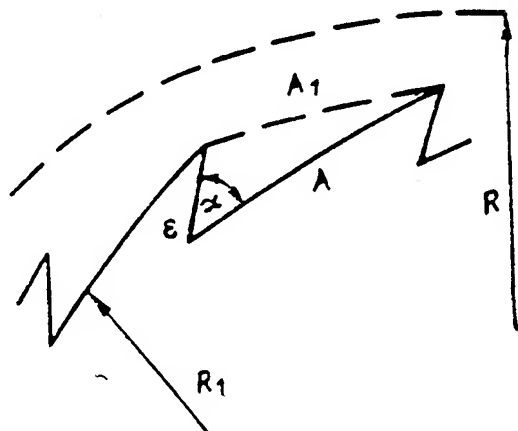


Рис. 5.4. Изменение геометрии внешнего контура образца при наличии локализованной деформации сдвига.



и учесть, что $\pi/N \ll 1$, $\epsilon \ll 2\pi R/N$, то можно положить $A = 2\pi R/N$, а $A_1 = 2\pi R_1/N$. Тогда связь между радиусами R и R_1 такова:

$$R_1 = R \sqrt{1 - \frac{N\epsilon}{\pi R} \cos \alpha}. \quad (5.12)$$

Учитывая, что конечная плотность образца ρ_K для практически важных режимов компактирования близка к теоретической (ρ_M), имеем $R^2 \cdot K = R_1^2$ (где $K = \rho_0 \rho_M + \frac{r^2}{R^2} (1 - \rho_0 \rho_M)$, ρ_0 — плотность намотки фольги) и с учетом (5.12) получаем

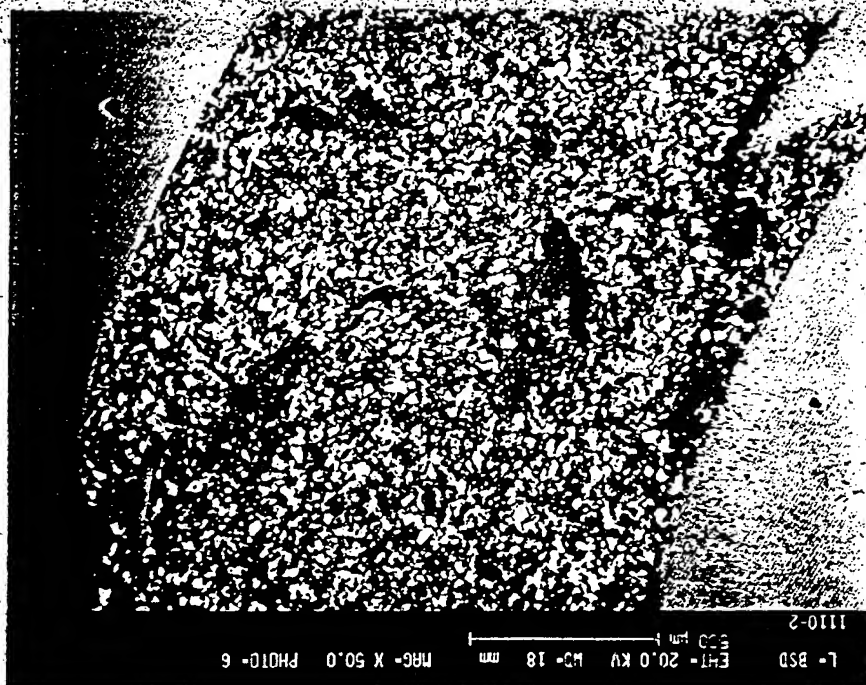
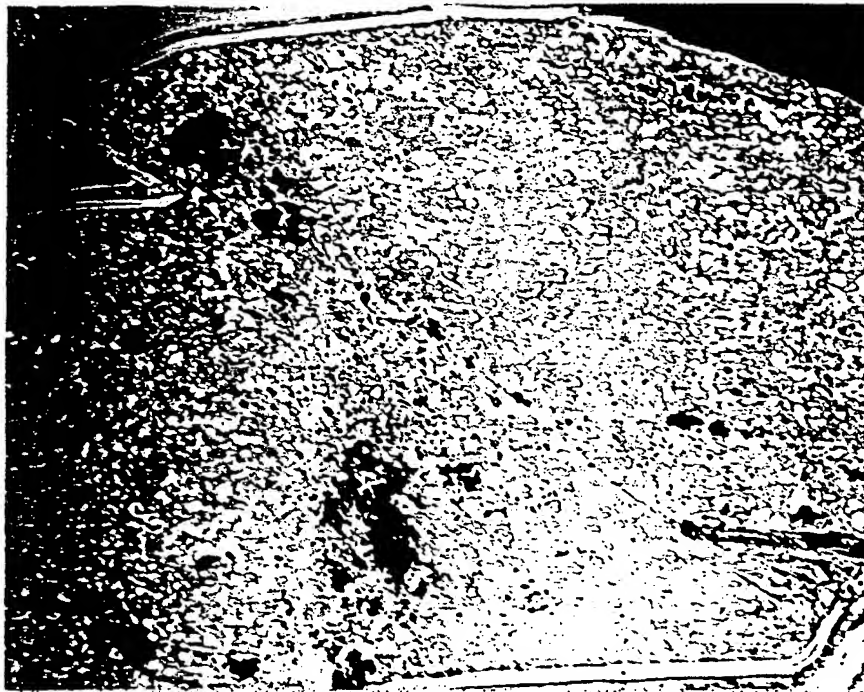
$$\rho_0 \rho_M + \frac{r^2}{R^2} (1 - \rho_0 \rho_M) = 1 - \frac{N \cdot \epsilon}{\pi \cdot R} \cdot \cos \alpha. \quad (5.13)$$

Выразив r через начальную толщину слоя фольги t ($r = R - t$), формулу (5.13) запишем в виде

$$t(2 - t/R)(1 - \rho_0 \rho_M) = \frac{N \cdot \epsilon}{\pi} \cos \alpha. \quad (5.14)$$

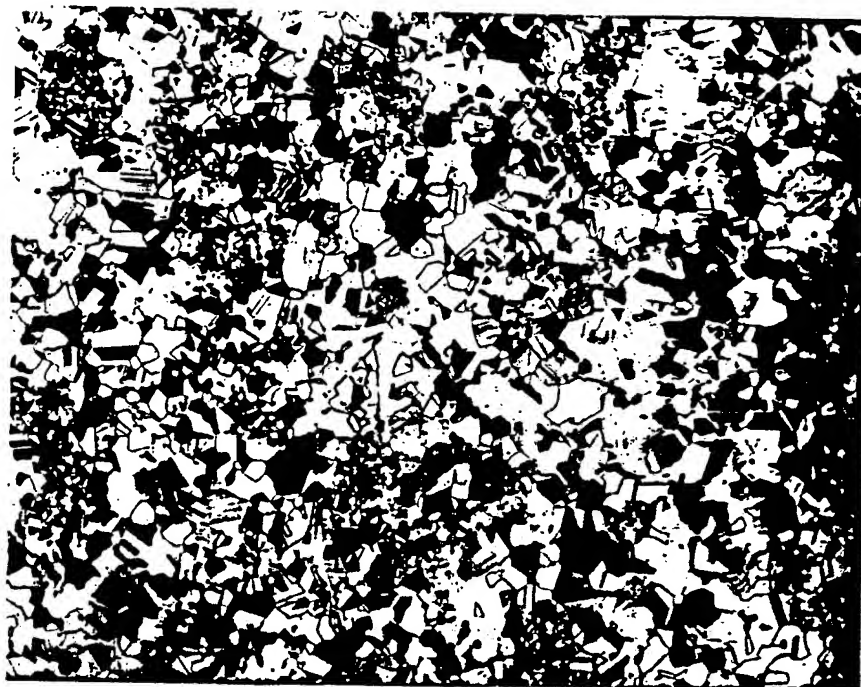
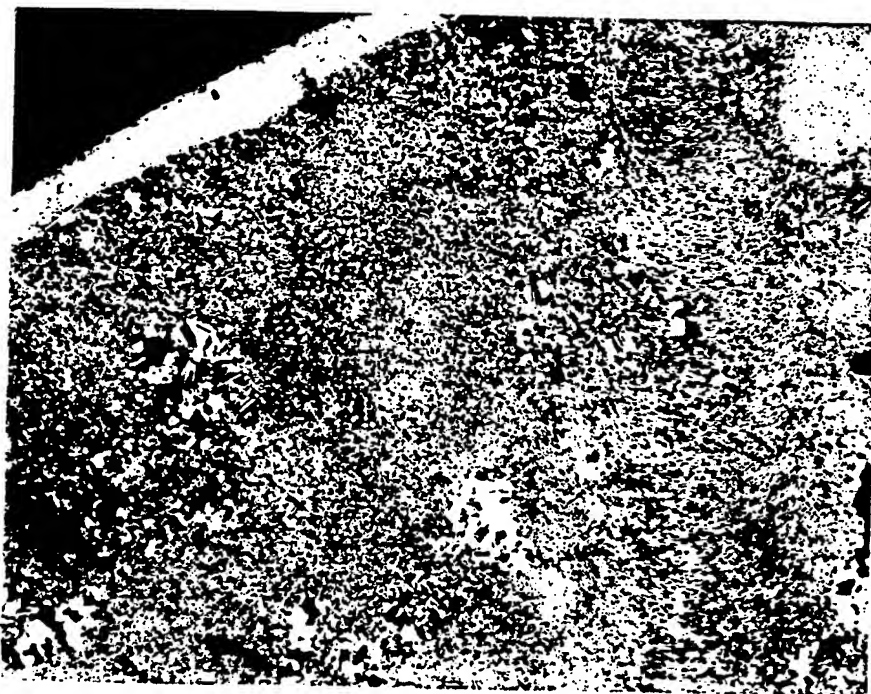
Функция слева в (5.14) возрастает от нуля при $t = 0$ до максимума при $t = R$, что согласуется с [276], где для порошков показано, что величина ϵ растет с увеличением отношения t/R . Это говорит в пользу единого механизма образования и развития локализованного сдвига при динамическом компактировании порошков и фольг.

Расчет $N \cdot \epsilon$ по формуле (5.14) (при $\rho_0/\rho_M = 0.50$ и 0.75 , $t = 0.5$ см, $t/R = 0.5$) дает значения в 1,1–1,3 раза больше экспериментальных в исследуемых диапазонах геометрии и режима нагружения. Это связано с приближенным характером рассмотрения изменений геометрии внешнего контура, в частности с неучетом его волнообразности, обусловленной неустойчивостью движения, а также отличием конечной плотности компакта ρ_K от теоретической. Если ввести зависимость ρ_K от режима компактирования, то формула (5.14) может описывать поведение величины ϵ в зависимости от параметров нагружения при замене ρ_M на ρ_K . Отметим, что $\alpha \approx 45^\circ$, поэтому можно считать, что $\cos \alpha \approx 0.7$.



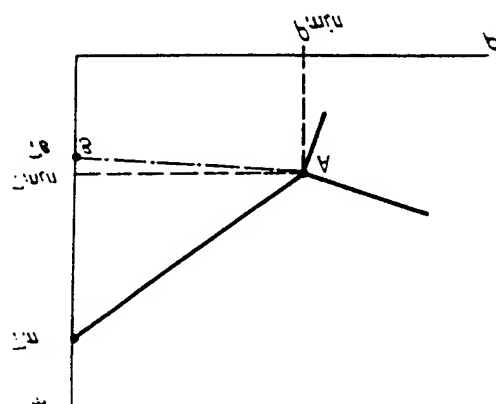
ПОСЛЕ ЛОБНОГО ЛАЗОСТАТИЧЕСКОГО ПРОССОВАННЯ*

ИЗМЕНЕНИЕ СТРУКТУРЫ ПРОССОВАННОГО ВЗРЫВОМ СУЛФА



dependence of melting temperature on pressure.

Fig. 4. Example of phase diagram for materials with anomalies



Phase transition in Zirconia under shock compression

Plasmachemical synthesis \Rightarrow t zirconia ($3\text{mol}\% \text{Y}_2\text{O}_3$)

1) particles - hollow spheres with
diameter $\approx 0.3 \mu\text{m}$

2) nanocrystalline structure

Questions:

1. Is it possible to crush submicron powders ($a \approx 0.3 \mu\text{m}$) by explosive methods, below the limit of traditional mechanical methods ($\sim 0.5 \mu\text{m}$)?
2. Is it possible to modify and activate liquid?
3. If 1,2 are available, will it result in acceleration of sintering process?

The condition of t-phase stability, critical grain size

$$G_t + y_t S_t + W_t < G_m + y_m S_m + W_m$$

G - Free energy of monocrystal

S - specific surface

y - Free surface energy

w - deformation energy

$$S = \frac{6}{\rho D}, \quad D - \text{grain size}$$

$$D < D_{cr} = \frac{6}{[(G_t - G_m) + (W_t - W_m)] \left(\frac{y_m}{\rho_m} - \frac{y_t}{\rho_t} \right)}$$

$$\langle \epsilon^2 \rangle^{1/2} \approx 0,032$$



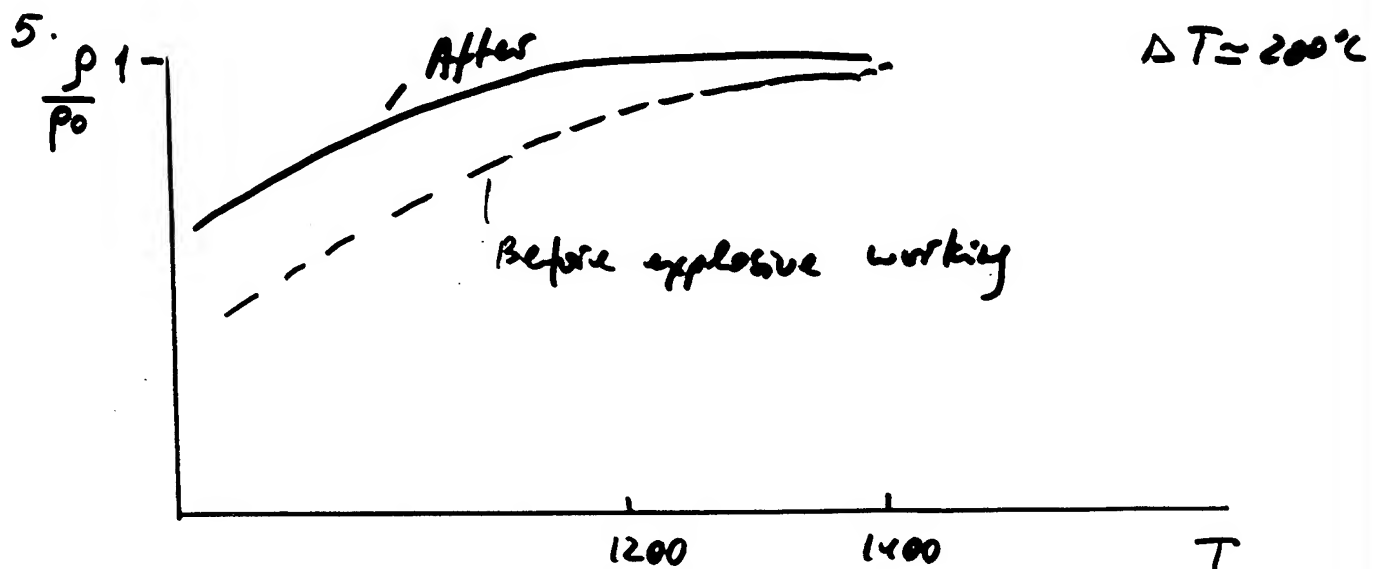
$$D_{cr} \approx 3 \mu\text{m} \quad D_0 \approx 10 \mu\text{m}$$



tetragonal phase is unstable after explosive working

Behaviour at subsequent heat treatment:

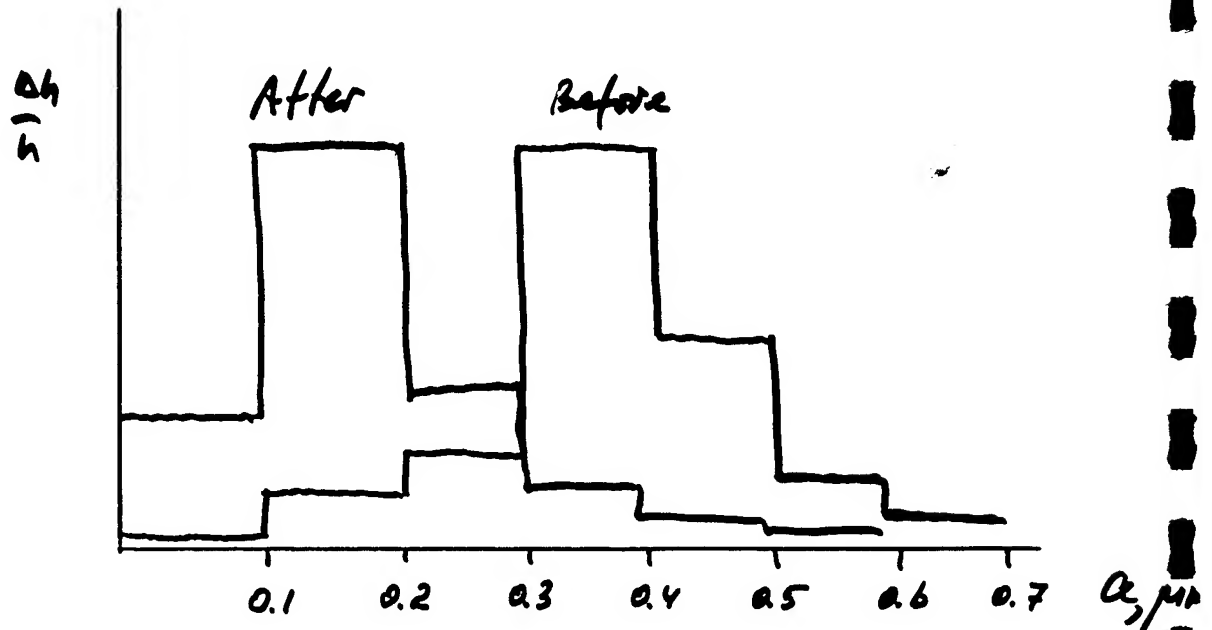
1. Decreasing of m-phase content at 1000°C to C
2. Decreasing of x-ray width to initial value at the same temperature 1000°C
3. $q/c \rightarrow 1.025$ after $T > 600^{\circ}\text{C}$
4. No grain size growth at $T < 1000^{\circ}\text{C}$



After explosive loading:

1. 100% t-phase \Rightarrow 58% t-phase + m-phase

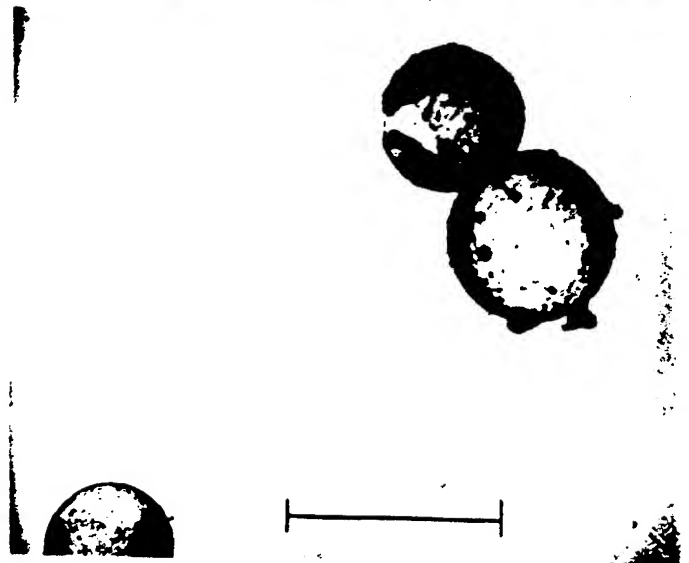
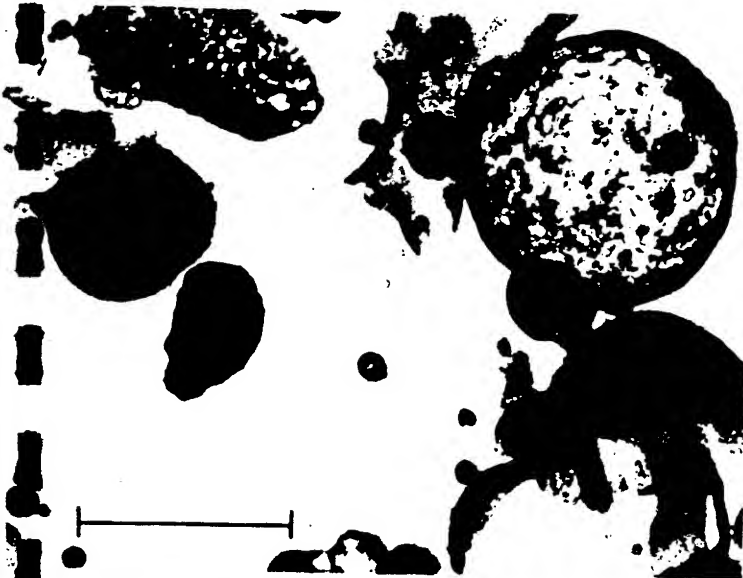
2.

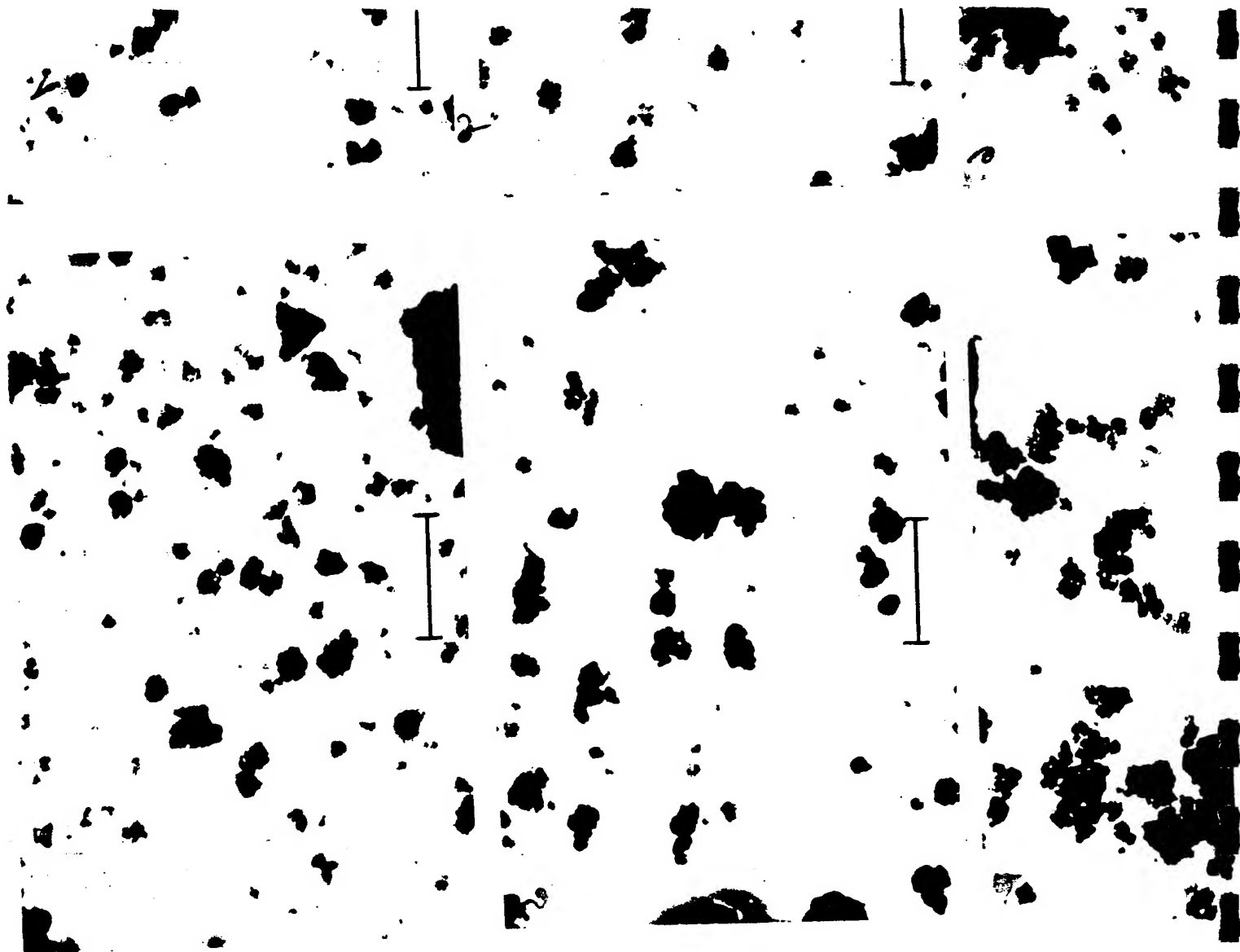


3. No change in grain size

4. Essential spreading of x-ray lines

5. Parameter of tetragonality $c/a \approx 1.06$





What can be used for chemical reactions:

1. Strong shock width $T/\ell \sim \bar{A}T/\ell \sim T/a$,
a - particle size
2. Some repeatable (P) phenomena can be used for testing of computer models ($\bar{T}_s(a)$), "old" boundary layer, shock width ...
3. Pore models, tested on shock wave width, can be put into kinetic of chemical reactions
4. Variation of energy pump into different phases in porous mixture by changing the relative particle sizes.
5. M1 + reactant dielectrics - M2 + dielectric products can be used for determination of chemical kinetics on time scale beginning from 10^{-7} sec
6. Controlled shear localization in porous mixtures - new tool for investigation and triggering reaction as in single band as in the volume at high strain rate ($\dot{\epsilon} \sim 10^6 \text{ sec}^{-1}$, $\epsilon \sim 10$).

Conclusion

There is very important class of mesoscale phenomena in granular materials which determine the initial condition for chemical reactions, as for shock wave material treatment

The variation of initial mesostructural parameters (at the same macro) can allow to control the transition phenomena at dynamic loading.

The probable ways for application for advanced materials:

I Need to be part of device (not just a piece of material):

- a) Thick coating on inner surface of thick-walled cylinders with large L/D
- b) Densification of metastable materials with subsequent optimized heat treatment
- c) metal - ceramic joints, better metal - ceramic - metal type

"Shock Synthesis of Diamond and C-B-N Materials"

M. YOSHIDA and S. FUJIWARA

National Institute of Materials and Chemical Research
Tsukuba, Ibaraki 305, JAPAN

Recent studies of shock syntheses of diamond, cubic boron nitride and solid solutions of diamond and cubic boron nitride conducted at National Institute of Materials and Chemical Research have been summarized.

Martensitic transformation from graphite to diamond: Pure graphite with approximately 90% of the crystal density was employed to study the mechanism of shock induced transformation from graphite to diamond. Measured pressure profiles in the graphite revealed that the employed graphite starts transformation at about 20 GPa. Sound velocity deduced from the catch-up time of the rarefaction wave increased with incident shock pressure from that of graphite at about 20 GPa to that of diamond at 30-35 GPa. Some pressure records clearly indicated double wave structure. The rise-up time of the second pressure jump, which corresponds to time duration of transformation process, was less than the resolution limit of the pressure gage; about 20 ns.

Recovery experiments were also carried for the same pure graphite. Maximum pressure and temperature in the sample were controlled independently. Pressure and temperature ranged from 20 to 100 GPa and 600 to 1800 K, respectively. Although many experiments were conducted above the mixture region, the yield of diamond was always less than 34%, indicating that almost whole diamond transformed back to graphite either under or after pressure unloading. Recovered graphite was analyzed by x-ray diffraction and it was observed that recovered graphite had the same microstructures as the starting material in spite of its transformation histories between graphite and diamond.

These experimental results clearly indicate that the main mechanism of shock induced transformation from graphite to diamond is not diffusive but diffusionless. Graphite is considered to undergo martensitic transformation to hexagonal diamond under shock compression and, when pressure is unloaded, hexagonal diamond goes back to original graphite phase by the same martensitic mechanism. This explains why the recovered graphite had the same microstructures as the starting material. Recovered cubic diamond may be synthesized because of heterogeneous nature of shock compression. As the samples had 10% porosity, shock wave produces heterogeneous states at the shock front and creates hot spots, forming cubic diamond by diffusive mechanism.

Shock synthesis with spherical copper powders: The yield of diamond is known to increase when graphite is mixed with copper powders. The increase of yield is more pronounced when spherical copper powders are employed. Graphite was mixed with 90 to 95 wt. % spherical copper powder of 100 μ m average diameter. Yield of diamond increased to more than 70%. This method was also effective in the syntheses of cubic boron nitride (cBN) from hexagonal BN (hBN) and solid solutions of cubic diamond and cubic boron nitride from hexagonal C-B-N compounds.

The spherical copper powder has less specific surface area than other morphologies. As the energy of compression is considered to be deposited on the surface first and then heat conduction relaxes to temperature equilibrium, smaller specific surface area will generate larger initial temperature rise and larger temperature quench rate. This mechanism is considered to be the main reason of high yields of diamond and other materials.

Microscopic observations of shock compression in powders: Temperature profiles in shocked copper powders were observed to estimate maximum temperature and temperature quench rate in spherical copper powders. As a preliminary experiments, pure copper powders were employed and nothing was mixed. The recording system employed a camera-lens and objective-lens combination (maximum approximately ten times of magnification), an electronic streak camera, and a liquid-nitrogen cooled CCD camera. The best spatial and temporal resolutions were 3 to 4 ns and 3 to 5 μm , respectively. The optical sensitivity of the system was calibrated using shocked argon plasmas of known spectral characteristics. It was observed that coarse spherical powders yield very high temperature and very rapid cooling rate. For a spherical copper powder with diameter of 100 μm , maximum brightness temperature and temperature cooling rate of 10000 K and 10 K/s, respectively, were observed.

Conclusions: From all the above experiments we conclude that the kink observed in the Hugoniot of graphite is attributed to martensitic phase transformation to hexagonal diamond which under unloading transforms back to the original phase by the same mechanism. Shock syntheses of cubic diamond should employ some heterogeneous hot spot formation which promote conversion of graphite to cubic diamond, possibly through the liquid phase. The same mechanisms are considered to be dominant in the shock syntheses of cBN and cubic C-B-N materials.

Better understanding of the mechanism and the kinetics of the transformations require not only better resolutions but also {it in situ} material identification by spectroscopic method, for example by Raman scattering spectroscopy.

1. M. Yoshida and N.N. Thadhani, in "Shock Compression of Condensed Matter 1991", S.C. Schmidt, R.D. Dick, J.W. Forbes, and D.G. Tasker eds., Elsevier Science Publishers B.V., p. 585 (1992).
2. S. Fujihara, K. Narita, Y. Saito, K. Tatsumoto, S. Fujiwara, M. Yoshida, K. Aoki, Y. Kakudate, S. Usuba, and H. Yamawaki, in "Shock Waves", K. Takayama ed., Springer-Verlag, Berlin, p. 367 (1992).
3. M. Yoshida, S. Fujiwara, and S. Fujihara, New Diamond, 30 (1993).
4. Y. Kakudate, M. Yoshida, S. Usuba, H. Yokoi, S. Fujiwara, M. Kawaguchi, K. Sako, and T. Sawai, in "Proceedings of Third IUMRS Int. Conf. Adv. Mater.", in press.
5. Y. Nakayama, M. Yoshida, Y. Kakudate, S. Usuba, H. Yamawaki, K. Aoki, K. Tanaka, and S. Fujiwara, in "Proceedings of International Workshop on Strong Shock Waves", p. 77 (1991).
6. M. Yoshida, in "Advanced Materials '94", M. Kamo, H. Kanda, Y. Matsui and T. Sekine eds., National Institute for Research in Inorganic Materials, p. 85 (1994).

STUDY OF SHOCK INDUCED SOLID STATE REACTIONS BY RECOVERY EXPERIMENTS AND MEASUREMENTS OF HUGONIOT AND SOUND VELOCITY

M. YOSHIDA, National Chemical Laboratory for Industry, Tsukuba, Ibaraki 305, Japan and
N. N. THADHANI, CETR, New Mexico Tech, Socorro, NM 87801.

Shock induced phase transition of graphite to diamond and shock induced chemical reaction in powder mixtures of niobium and silicon have been studied through recovery experiments and measurements of Hugoniot and sound velocity. Manganin-gage records were analysed to obtain Hugoniot and sound velocity in mixed phase region of graphite and diamond. These results clearly showed that samples fully converted into diamond. Analysis of recovery experiments showed that yield of diamond was less than 3 %, indicating regraphitization after or during pressure unloading. In the case of Nb-Si mixture, light emission from shocked powders was recorded by a streak camera. Arrivals of shock and rarefaction waves at the interface between the sample powder and a glass window were clearly recorded. Mechanism of shock induced chemical reaction is discussed using these results together with SEM/EDX observations of recovered samples.

1 INTRODUCTION

After it was realized that phase transitions can be induced by shock waves within a time scale of a fraction of a microsecond or less [1], many research works have been directed toward understanding of material behaviors, such as structural and chemical changes, under extreme dynamic conditions [2,3,4,5].

Experimental methods employed in these works can be divided into two classes; dynamic observations and post-shock analysis. Dynamic observations can directly observe phenomena that take place under dynamic loading. However, experimental capabilities are still limited to resolve phenomena with sufficiently high spatial and temporal resolutions, and in many cases, quantities to be measured do not allow dynamic observations with technologies currently available. On the contrary, post-shock analysis can incorporate numerous characterization methods. Thus many research works in shock induced chemistry have used this experimental method to understand the phenomenon. However, post-shock analysis inherently possesses a shortcoming that measured quantities or observed phenomena are not necessarily attributed to shock compressions because recovered materials have seen both shock and post-shock effects and

distinction of these effects is often very difficult.

Indeed, one of the issues in shock induced chemistry that has remained controversial is to what extent the material was synthesized under shock compression. In the case of pressure induced transitions, if the recovered high pressure phase is not a high temperature phase, then the material recovered is certainly synthesized under compression, but a part of the high pressure phase may then disappear by reverse transition to the original phase due to high residual temperature. Shock syntheses of compounds by chemical reactions in component elements, have different situations as, in many cases, compounds have negative heat of formation. It is possible that reaction can proceed during shock compression or by residual temperature. Thus it is very difficult to know whether or not, and to what extent, the products were formed under compression alone.

Hence, dynamic observations are required to distinguish the effects occurring under compression and after unloading. Batsanov [6] observed a kink in his measured Hugoniot of powder mixture of tin and sulfur, and concluded that the kink is due to the heat generated by a reaction between the two elements. However a kink in the Hugoniot may sometimes be attributed to phase changes of one or more reactants and does not necessar-

ily indicate evidence of chemical reactions. Furthermore, detection of reaction by Hugoniot measurement requires that reactions take place at the shock front or its vicinity. If reactions take place considerably far away from the shock front it becomes impossible for reactions to impart their occurrence to the Hugoniot even if it actually took place when material is still under compression.

Measurements of the sound velocity by observing the rarefaction catch-up at two or more gage locations reflect the extent of reactions between these locations and can be used to detect occurrence of reactions behind the shock front. It should be noted that in applying this method to reacting powder mixtures, all the sound velocity data for both reactant elements and product compounds, as a function of pressure and temperature, should be known. Furthermore, this method requires that the sound velocity of reactants and that of products be appreciably different.

In this study, recovery experiments together with measurements of Hugoniot and sound velocity were performed for two cases; shock induced phase transition from graphite to diamond and shock induced chemical reactions in niobium/silicon powder mixtures. As will be described in the following sections, analyses for the former case were relatively simple because equations of state can be well defined and the difference of sound velocities between the reactant and the product is significant. In the latter case, we do not have enough knowledge on equations of state of both reactant elements and products compounds. Still it will be shown that measured Hugoniot and sound velocity can indicate events that cannot be resolved by recovery analyses.

2 EXPERIMENTS AND RESULTS

2.1 Phase Transition from Graphite to Diamond

Many models have been proposed to describe shock induced phase transition of graphite to diamond. DeCarli [7] has concluded that diamond is mainly formed

at "hot spots", whereas Morris [8] questions this hypothesis. Possible existence of regraphitization of diamond due to high residual temperature makes it difficult to conclusively infer degree of transition under shock compression from recovery experiments. Experiments of diamond crystals [9] suggest that residual temperature where regraphitization becomes significant is ≈ 1800 K. X-ray diffraction of shock loaded diamond powders [10] indicated that graphitization can occur even at residual temperature of about 1100 K.

In this study, pure and crystallized graphite made from coal pitch was employed as a starting material. The initial density was 2.05 g/cm^3 .

2.1.1 Recovery Experiments

Several recovery systems were employed to control pressure and temperature independently. The calculated maximum pressure and maximum bulk temperature in the graphite sample are shown in Fig.1

Recovered samples were ground to powder and were oxidized in a plasma reactor to remove graphite. Oxy-

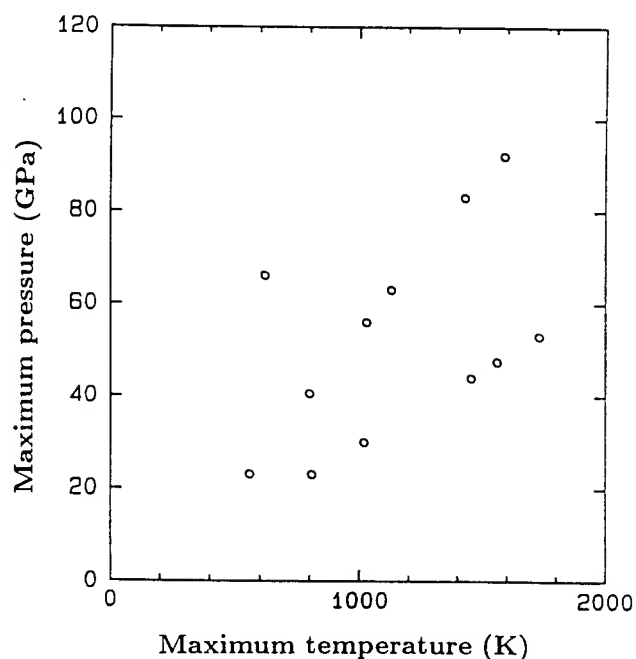


FIGURE 1

Maximum pressure and temperature in the graphite sample. Phase transition was not taken into consideration.

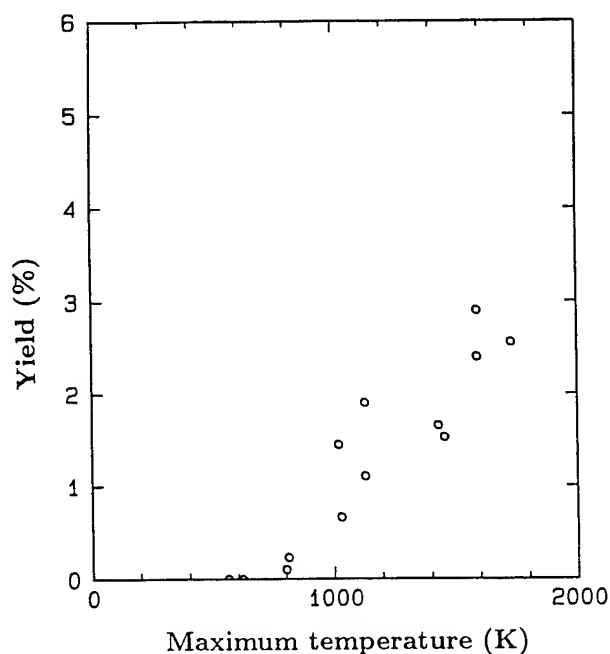


FIGURE 2

Recovered diamond yield plotted against maximum temperature in graphite.

gen, with 0.5 to 0.7 Torr of pressure in a quartz chamber, excited by an rf generator of 13.56 MHz and 200 W, effectively removed the graphite. Weight reduction of shock synthesized diamond under the condition mentioned above was much less than 0.1 % per hour and for most cases oxidation of 10 to 20 hours removed the graphite completely. X-ray diffraction patterns of oxidized samples were identified to be those of cubic diamond. Hexagonal diamond was not detected by X-ray diffraction.

Obtained yield of diamond did not show dependence on pressure but exhibited dependence on temperature. Yields plotted against the maximum temperature of the sample are shown in Fig.2. Shock compressions along the a- and c-axes did not show distinct differences in terms of diamond yield and they were not distinguished in Fig.2.

2.1.2 Hugoniot and Sound Velocity

Embedded manganin gages were used to measure Hugoniot and sound velocity of the shocked graphite. The thickness of the sample was nominally 2.5 mm.

Manganin gages (Dynasen Inc.) of ≈ 0.28 mm thickness were inserted between the driver/sample and sample/sample interfaces. In all the experiments, graphite was compressed along the c-axis. The average pressure value and shock wave velocity derived from the difference of shock arrival times generates one Hugoniot point. Sound velocity(C) was calculated by

$$C = \frac{\rho_0 X_L}{\rho \Delta t}, \quad (1)$$

where X_L and Δt are the thickness of the graphite sample and the time difference of rarefaction wave arrival at two surfaces of a sample slab, respectively. Δt was evaluated from arrival times at gauge locations by correcting the transit time of the rarefaction wave through the gage insulator.

Figure 3 shows the U_s-u_p Hugoniot of the graphite. Calculated Hugonits of graphite and diamond both with initial density of 2.05 g/cm^3 are also shown for comparison. A kink is observed at a shock velocity of about 6.5 km/s, and indicates the start of phase transition to the dense diamond phase. Pressure at the kink is about 25 GPa. McQueen [11] observed kinks for various graphite samples at shock velocity of about 6.0 km/s. The difference in the shock velocities may partly be due to flow perturbation by insertion of the gages in our case. Analysis of a pressure waveform at the second gage location suggests that the transition pressure is 20 GPa.

Figure 4 shows dependence of sound velocity on shock pressure. Calculated bulk sound velocities for graphite and diamond of the same initial loading density (2.05 g/cm^3) are also shown. This figure indicates that graphite-to-diamond transition starts at about 20 GPa and is complete at about 30 to 35 GPa. If the beginning of the transition is at 20 GPa, then the end point, above which single wave structure can be observed, is calculated to be 33 GPa which agrees well with the experimental results.

2.1.3 Discussion for Graphite to Diamond Transition

In the recovery experiments on graphite along the c- and a-axes with initial loading density of 2.05 g/cm^3 ,

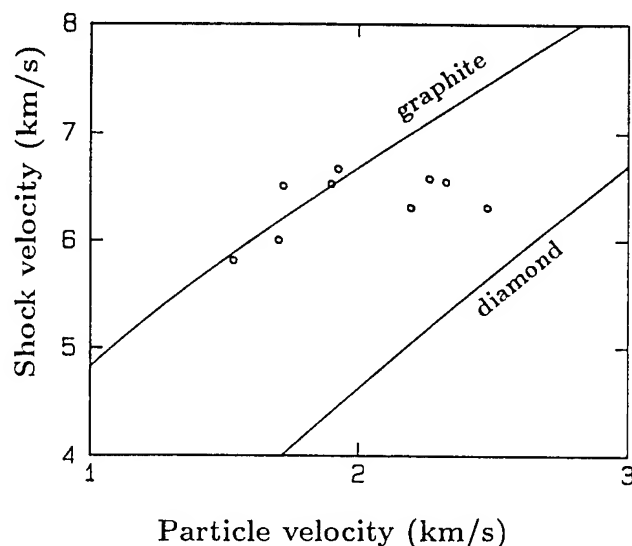


FIGURE 3
 $U_s - u_p$ Hugoniot of graphite.

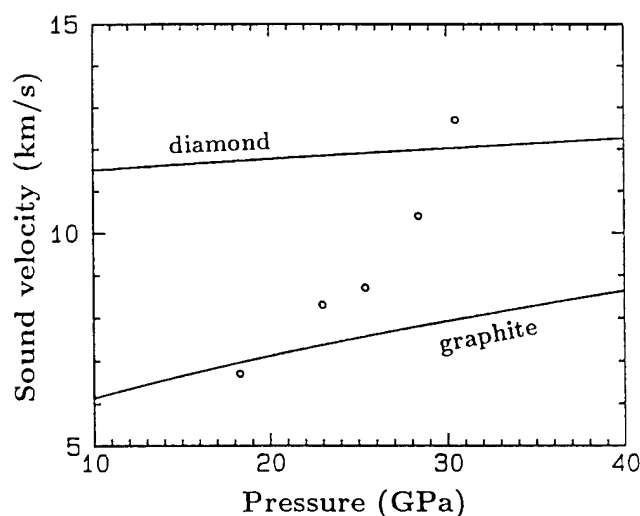


FIGURE 4
Sound velocity obtained from rarefaction catch-up plotted against the shock pressure.

only cubic diamond was recovered and the yield of diamond was dependent on the temperature alone. The yield increased with increasing shock temperature and the observed highest yield was about 3 % at about 1800 K. However, the Hugoniot and sound velocity measured for the same graphite under shock compression along the c-axis clearly indicated that this material starts a transition to the dense diamond phase at about 20 GPa and

the transition is complete at about 30 to 35 GPa. Thus it was shown that some of our recovery experiments involved complete transition to the diamond phase. One reason for the observed low yield data of diamond in recovery experiments could be the high temperature rise induced by large pV work done as a result of the phase transition to the dense phase. The maximum temperature calculated in Figs. 1 and 2 should be increased by several hundreds of K for complete transition to the diamond phase.

Another possible reason is that the mechanism of the phase transition is martensitic rather than diffusive [12]. Graphite possibly transforms to hexagonal diamond very rapidly and hexagonal diamond, upon release of the pressure, transforms back to the original phase. The cubic diamond may have been formed by a diffusive mechanism at local hot spots. The dependence of the yield of diamond on maximum temperature can then be explained as a dependence of the yield on the initial shock pressure because temperature rise is most prominent at the initial shock rise and the initial shock will play the most important role in the formation of local hot spots.

2.2 Shock Induced Reactions in Nb/Si Powder Mixtures

Recovery experiments were first conducted on Nb/Si powder mixtures and the recovered samples were observed by scanning electron microscope (SEM) with EDX elemental analysis. X-ray diffraction (XRD) analysis was also employed to identify bulk reaction products. Hugoniot and sound velocity measurements were then conducted to clarify events taking place under shock compression.

2.2.1 Recovery Experiments

The mixture of niobium and silicon with 1:1 atomic ratio, was hand packed in a 304 stainless steel capsule. Packed samples had thickness of 2 mm and diameter of 12 mm. Loading density was nominally 55 % of the solid mixture. The recovery assembly employed a plane wave generator, a high explosive, and momentum traps. A 100 mm diameter plane wave generator [13,14] was employed



FIGURE 5

An SEM photo of a sample shocked to 40 GPa.

in both direct contact and flyer plate impact experiments. Recovered sample capsules were axially cut into two pieces to reveal the cross-section for microstructural characterization.

Although several shots have been done at different pressure levels, only one recovery result will be presented in this report and other results will be summarized elsewhere [15].

An SEM photograph of a sample shocked to a peak pressure of approximately 40 GPa is shown in Fig.5, which was taken at a point one third radius off the center.

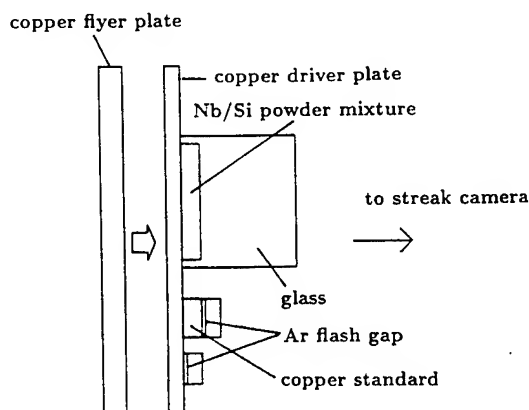


FIGURE 7

An experimental arrangement for recording light emission from the sample powder.

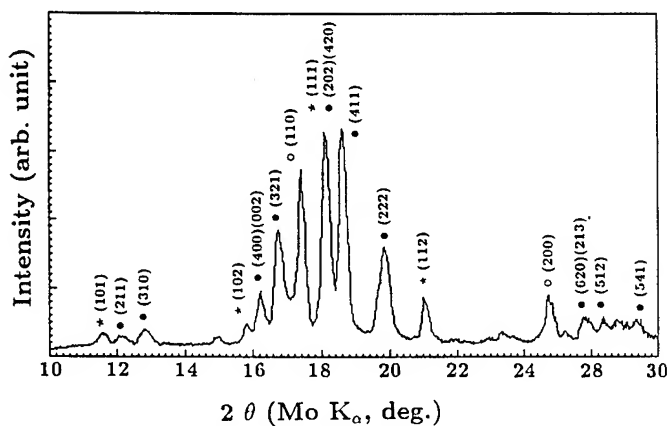


FIGURE 6

X-ray diffraction patterns. ★-NbSi₂, ●-Nb₅Si₃, ○-Nb.

EDX analyses in this area revealed that the light part contained only niobium and the dark part only silicon. No particle boundaries were found in the silicon region, which clearly indicates that silicon was once molten. Elemental compositions observed at the light gray and dark gray parts corresponded approximately to Nb₅Si₃ and NbSi₂ respectively. X-ray diffraction analysis was made using Mo K_α radiation and a collimator of ≈ 0.3 mm effective diameter. An XRD pattern taken at an area of Fig.5 is shown in Fig.6. All the peaks were assigned, as indicated in the figure, to those of either cubic niobium, hexagonal NbSi₂, or tetragonal Nb₅Si₃, indicating partial reactions.

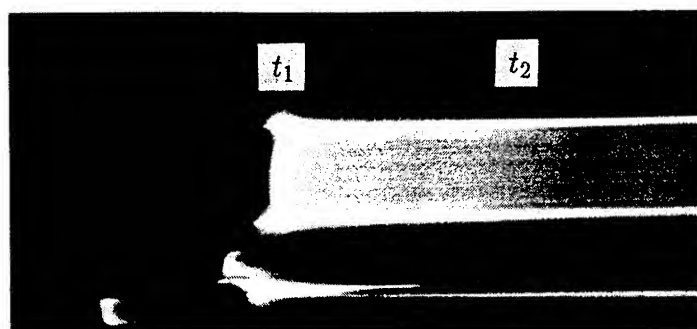


FIGURE 8

A streak record of light emitted from the sample. For explanations, see text.

2.2.2 Hugoniot and Sound Velocity

An experimental assembly used for Hugoniot and sound velocity measurements of Nb/Si powder mixtures is shown schematically in Fig.7. Copper was employed as both flyer and driver plates. Sample discs of dimension 20 mm diameter and 1 to 3 mm thickness were placed in contact with the driver plate and a transparent (fused quartz or pyrex) window.

A typical streak camera record of light emitted from the sample is shown in Fig.8. When a shock wave hits the interface of the sample powder and the window, very intense light, due to void collapse which generates high temperature, is observed (t_1). This intense light serves as an arrival time indicator of the shock at the powder/window interface. Shock velocity can then be obtained using this arrival time and the arrival time at the surface of the driver plate. Arrival time data at a surface of a standard material, copper, can be used to deduce compression data for the sample by the impedance mismatch method. The duration of the intense light is very short and constant light emission follows after this intense light until it starts to gradually attenuate the light intensity (t_2) due to the catch-up of the rarefaction wave which decreases the temperature of the sample. Again this arrival time of the rarefaction catch-up for a couple of sample thicknesses allows calculation of the rarefaction velocity in Lagrange co-ordinate, and the sound velocity behind the shock front can be obtained from Eq. (1).

Our experimental method is essentially the same as the one employed by McQueen *et al.*[16], except for the difference that, in the present case, the temperature of the shock compressed powder is extremely high and self luminous light of the sample material itself can be recorded directly instead of observing light emitted from an optical analyzer.

Measured Hugoniot and calculated powder Hugoniot of the 55 % dense Nb/Si mixture are presented in Fig.9. Our calculation assumed $p-T$ equilibrium and constant $\rho\gamma$, and employed Hugoniot data for Nb [17] and hydrostatic compression data for Si [18].

The measured Hugoniot of Nb/Si mixture showed two branches 'A' and 'B'. The branching is not due to exper-

imental errors but rather actual shock behavior. Often in different samples in the same shot, one sample datum fell on the lower branch and another on the higher. Sample thickness did not correlate to the branching effect. Branching may be due to small differences in experimental conditions, such as bulk density or inhomogeneity. Branch B exhibits higher compressibility than the calculated Hugoniot and seems to represent phase transformation(s) to dense phase(s). The phase diagram of silicon [19] has negative dp/dT between the solid and dense liquid phases. Additionally, the calculated Hugoniot for 55% initial density powder crosses the phase boundary at about 5 GPa. This point is indicated in Fig.9 and it looks like the deviation of branch B from the solid powder Hugoniot starts from this point. Thus it is believed that shock induced melting of silicon is the cause of the higher compressibility along branch B. Branch A with higher shock velocity possibly represents a Hugoniot without melting. Slightly higher U_s than the calculated Hugoniot suggests the existence of solid state reactions taking place within the rise time of the shock front.

The distance-time diagram for shock propagation and rarefaction catch-up is shown in Fig.10. Shock pressure

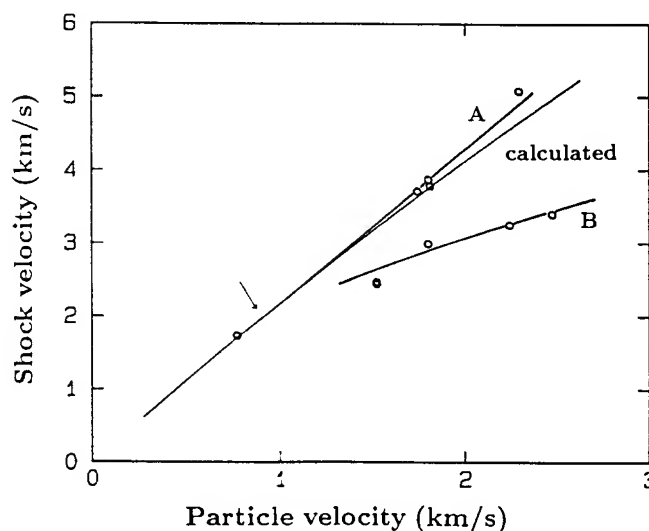


FIGURE 9

Hugoniot of Nb/Si powder mixture. Branches A and B are experimental. Calculated Hugoniot crosses the solid/liquid phase boundary of Si at a point indicated by an arrow.

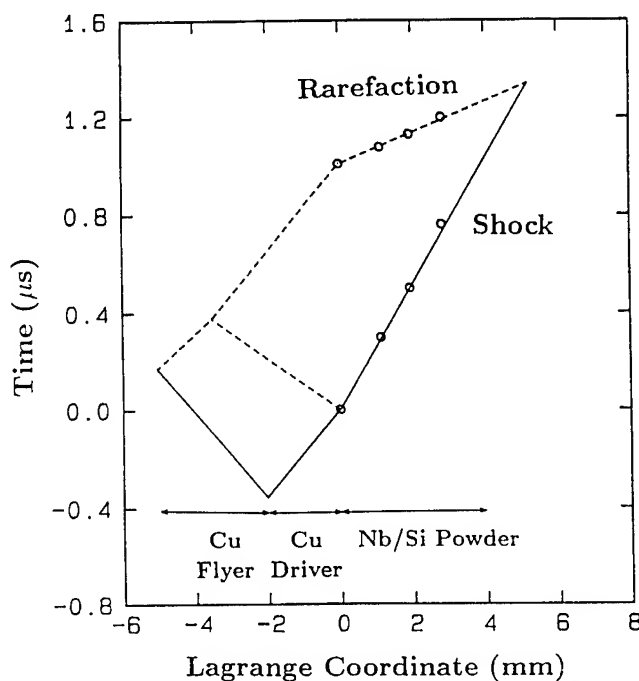


FIGURE 10

X-t diagram for shock and rarefaction trajectories. Shock pressure is approximately 20 GPa.

in the Nb/Si powder was ≈ 20 GPa. Trajectories in copper plates are calculated with a one-dimensional hydrodynamic code using published data for copper [20]. Elastic-plastic effects were neglected and copper was assumed to be perfectly plastic. Sound velocity deduced from the experimentally obtained rarefaction trajectory in the Nb/Si mixture was 8.3 km/s. As the calculated arrival point of the rarefaction wave at the interface between the copper and the Nb/Si mixture lies on an extrapolated rarefaction trajectory, the measured velocity will correspond to bulk sound velocity. Calculated bulk sound velocity of 55 % dense Nb/Si mixture under shock pressure of 20 GPa is 5.6 km/s. Measured sound velocity is about 50 % higher than the theoretical value. This experimental result is in favor of the existence of solid state reactions because intermetallic compounds generally have higher sound velocities.

2.2.3 Discussion for Nb/Si

Recovery experiments indicated clear evidence of bulk melting of silicon. Hugoniot measurements showed

branching into two $U_s - u_p$ curves. The lower U_s branch was attributed to the phase transition of Si into the dense liquid phase. The higher U_s branch was very close to the calculated powder Hugoniot of the solid phase. A result of sound velocity measurement done in the higher U_s branch indicates the existence of solid state reactions possibly occurring within the rise time of the shock front. However, even though materials reacted in the solid phase, the work done to the sample and the heat of reaction will eventually melt, at least a part of, the sample and will smear out any evidence of what took place under compression. Recovery experiments with higher initial loading density or with much lower initial temperature should be helpful in checking the possibility of solid state reactions for this powder mixture.

Measurements of EOS data for reactant and product materials are also necessary for interpreting results of Hugoniot and sound velocity measurements.

3 CONCLUDING REMARKS

In the study of shock induced transition from graphite to diamond, it is clearly demonstrated that measurements of Hugoniot and sound velocity play an important role in interpreting the results of recovery experiments. Hugoniot and sound velocity revealed that, for the graphite employed in this study, phase transition starts from ≈ 20 GPa and completes between 30 to 35 GPa. The yield of diamond is dependent on temperature only and the highest yield of the cubic diamond phase is less than 3% even for the cases where graphite transformed completely to diamond. It was suggested that the main mechanism of the pressure induced transition is martensitic. Obtained cubic diamond may be formed by a diffusive mechanism at local hot spots.

In the case of shock induced reactions of Nb/Si powder mixture, the Hugoniot exhibited two branches. The higher U_s branch was attributed to solid state reactions and the lower U_s branch to phase transition of Si into a dense liquid phase. The reason of branching is not clear but is possibly due to small differences in the experiments. It is obvious that more detailed EOS data are

needed for silicon, niobium and each product to get clear conclusions from measurements of Hugoniot and sound velocity. More detailed dynamic observations with different initial conditions will be useful for understanding complicated phenomena.

Acknowledgements

A part of this work was performed while one of the authors (NNT) was staying at National Chemical Laboratory for Industry with funding provided by the Science and Technology Agency of Japan. The authors would like to acknowledge the support of the members of the High Energy Density Section of NCL.

References

- [1] D.Bancroft, A.L.Peterson, and S.Minshall, *J. Appl. Phys.* 27 (1956) 291.
- [2] G.E.Duvall and R.A.Graham, *Rev. Mod. Phys.* 49 (1977) 523.
- [3] R.A.Graham, B.Morosin, E.L.Venturini, and M.J.Carr, *Ann. Rev. Mater. Sci.* 16 (1986) 315.
- [4] R.A.Graham, B.Morosin, Y.Horie, E.L.Venturini, M.Boslough, M.J.Carr, and D.L.Williamson, in: *Shock Waves in Condensed Matter*, ed. Y.M.Gupta (Plenum Press, New York, 1986) pp. 693-711.
- [5] N.N.Thadhani, in: *Shock Compression of Condensed Matter - 1989*, eds. S.C.Schmidt, J.N.Jhonson, and L.W.Davison (North-Holland, Amsterdam, 1990) pp. 503-510.
- [6] S.S.Batsanov, G.S.Doronin, S.V.Klochkov, and T.I.Teut, *Comb. Expl. Shock Waves* 22 (1986) 765.
- [7] P.S.DeCarli, in: *High Pressure Science and Technology, Vol. 1*, eds. K.D.Timmerhaus and M.S.Barber (Plenum Press, New York, 1979) pp. 940-943.
- [8] D.G.Morris, *J. Appl. Phys.* 51 (1980) 2059.
- [9] V.R.Howes, *Proc. Phys. Soc.* 80 (1962) 648.
T.Evans and P.F.James, *Proc. Roy. Soc. London A.* 277 (1964) 260.
- [10] M.Yoshida, *Shock Consolidation of Pure Diamond Powders* (CETR report A-05-86, Center for Explosive Technology Research, New Mexico Tech, 1986).
- [11] R.G.McQueen and S.P.Marsh, in: *Behavior of Dense Media under High Dynamic Pressures* (Gordon and Breach, New York, 1968) pp. 207-216.
- [12] D.J.Erskine and W.J.Nellis, *Nature* 349 (1991) 317.
- [13] S.Fujiwara and M.Kusakabe, *Jap. Patent* 78-29673 (1978).
- [14] K.Tanaka, S.Fujiwara, M.Kusakabe, and M.Yoshida, in: *Shock Waves in Condensed Matter*, ed. Y.M.Gupta (Plenum Press, New York, 1986) pp. 929-934.
- [15] N.N.Thadhani and M.Yoshida, to be published.
- [16] R.G.McQueen, J.W.Hopson, and J.N.Fritz, *Rev. Sci. Instrum.* 53 (1982) 245.
- [17] S.P.Marsh (ed.), *LASL Shock Hugoniot Data* (University of California Press, Berkeley, 1980) pp. 112.
- [18] C.S.Menoni, J.Z.Hu, and I.L.Spain, in: *High Pressure in Science and Technology, Part III*, eds. C.Homan, R.K.MacCrone, and E.Whalley (North-Holland, New York, 1984) pp.121-124.
- [19] F.P.Bundy, *J. Chem. Phys.* 41 (1964) 3809.
- [20] R.G.McQueen, S.P.Marsh, J.W.Taylor, J.N.Fritz, and W.J.Carter, in: *High-Velocity Impact Phenomena*, ed. R.Kinslow (Academic Press, New York, 1970) pp. 532.

Advanced Materials '94

**Proceedings
of
The NIRIM International Symposium on
Advanced Materials '94
Tsukuba, Japan, March 13 – 17, 1994**

**Edited by
*M. Kamo, H. Kanda, Y. Matsui and T. Sekine***

National Institute for Research in Inorganic Materials

Microscopic Observations of Shock Compression in Powders

M. Yoshida

High Energy Density Laboratory

National Institute of Materials and Chemical Research

Tsukuba, Ibaraki 305, Japan

Abstract

Spherical copper powders of different sizes were shock compressed and their shock-wave fronts were microscopically observed. The recording system employed an electronic streak camera and a liquid-nitrogen cooled CCD camera. Standardised shocked argon light source was first recorded to calibrate the optical sensitivity of the recording system and the brightness temperature profile of the event was deduced. It was observed that coarse spherical powders yield very high temperature and very rapid cooling rate at the shock front. For spherical copper powders with diameter of 500 μm , maximum brightness temperature and temperature cooling rate of approximately 2.0×10^4 K and 10^{12} K/s, respectively, were observed at 43 GPa bulk shock pressure.

1. Introduction

Shock compression is inherently accompanied by heterogeneous energy deposition, resulting in non-equilibrium state at the shock front followed by relaxation processes during, and in some cases even after, compression. The existence of heterogeneity in shock compression has long and widely been recognized through many studies such as detonation initiation of explosives [1], recovery analyses of powder materials [2, 3], shock induced chemical reactions in organic substances [4, 5], molecular dynamic simulations [6], and so on.

In shock syntheses of diamond, this heterogeneous nature of shock compression has been fully utilized to increase the yield of diamond [7]. Graphite or graphite-like carbon was mixed with spherical copper powders and was shock compressed to 30 to 40 GPa. The yield of diamond exceeded 70 %. The same method has been extended successfully to shock syntheses of cubic boron nitride [8] and cubic BN-C solid solutions [9].

These shock synthesis studies have promoted a microscopic investigation of heterogeneous processes in shock compression of powders. Here we report our first preliminary experimental results on copper powders. Graphite or any other material was not mixed and pure copper powders were shock compressed and their shock wave fronts were observed by a streak camera.

2. Experimental

Spherical copper powders with purity of 99.9% were hand-tapped into a cylinder of 20 mm in diameter and formed a disk of 2 ~ 3 mm in thickness. Irregular shape copper powder was also used for comparison purpose. Table 1 lists copper powders employed in this study. The initial loading density geometrically measured was approximately 65 % of the solid.

An explosive plane-wave generator with effective planar area of 100 mm in diameter initiated a liquid explosive, nitromethane, to accelerate a 2 mm thick aluminum-alloy (6061) flyer plate. Target plate was the same 2 mm thick 6061 Al plate on which a sample disk of copper powder was attached. The flyer plate velocity was 3.7 km/s. This shock system was maintained the same in all the powder compression experiments reported here.

Impact of the flyer plate generates 40 GPa shock pressure in a target plate. The shock pressure in the sample is estimated to be 43 GPa from impedance mismatch between 6061 Al and copper powder. When the shock wave reaches the interface between copper powder and the fused-quartz window, very strong light pulse can be observed followed by relatively weak light. The strong light is attributed to heterogeneous structure of the shock front in powders. The weak light is from equilibrated compressed state of the shocked powder and it endures until the rarefaction wave from the back surface of the flyer plate decreases the pressure and the temperature at the interface. The brightness of the weak light is usually two to three orders of magnitude smaller than the first strong light pulse and it is difficult to record both lights

simultaneously with sufficient accuracy. As the interest is in the heterogeneity at the shock front, only the strong light pulse is recorded by a recording system described in the followings.

An image converter camera (Imacon 700, Hadland Photonics Ltd.) with streak rate of 50 ns/mm resolved the events temporarily. The streak image on the phosphor screen of the streak camera was recorded by a liquid-nitrogen cooled CCD camera (Model 3200, Astromed Ltd.) with 1152×770 pixels and 16 bits resolution of photo-electrons in each pixel. Time resolution was typically $3 \sim 5$ ns.

Two lens systems were employed. For a low magnification case a lens of 600 mm focal length formed an image on a photocathode of the image converter camera with magnification ratio of approximately 0.22. For a high magnification case, an objective - camera lens combination with maximum 12 times magnification ratio formed an microscopic image of powders. Spatial resolution as good as 3 to 4 μm was attained in this case.

The evaluation of spatial and temporal profiles of brightness of the events requires a standard light source to calibrate the optical sensitivity of the recording system. As the sensitivity depends on the streak rate, the standard light source is to be recorded with the same streak rate as the experiments. This disables the usage of a black-body furnace or a standard lamp because their brightness is usually a couple of orders of magnitudes weaker than the events. We employed an argon plasma generated by shock compression as a standard light source. The argon plasma is considered to be a black-body light source. Calibration of spectral brightness of shocked argon has been described previously [10] and will not be detailed here. The temperature can be controlled accurately in a range between 12,000 and more than 20,000 K and with accuracy of ± 500 K by changing the shock wave velocity.

Before each shock compression observation, light emission of shock compressed argon plasma was recorded with a bandpass filter (420 ± 5 nm) and the same optical components. For the components to be replaced in each experiment, such as PMMA blast-proof window, mirror and fused-quartz, materials from the same lot are employed.

3. Results and Discussion

A typical record at 420 ± 5 nm wavelength for low magnification case is shown in Fig. 1. Two samples were shock loaded simultaneously. Peak intensity at each spatial point was deduced to temperature by assuming black-body radiation and comparing the photo-electron counts to the counts obtained for the standard argon plasma light source with known brightness. Table 2 summarizes the results for low magnification observations. A 25 μm camera slit limits the spatial resolution to approximately 110 μm at powder/fused-quartz interface. This resolution did not allow us to resolve events microscopically for powders of 100 $\mu\text{m}\phi$ or less. Obtained brightness temperatures for powders A and B are averaged over hot and cold areas as well. For the powder D, the spatial resolution is an order of magnitude smaller than the particle size, 1 mm ϕ , and reflects well-resolved temperature profile of the event. The observed temperature, $(1.7 \pm 0.1) \times 10^4$ K is approximately four times of the calculated temperature.

To obtain better spatial resolution, an objective-lens and a camera-lens combination was employed. The focal lengths of the objective and the camera lenses were 50 and 600 mm, respectively. This lens system magnified the image to maximum 12 times. Spatial resolution was 3 to 4 μm and a little worse than the theoretically calculated value due possibly to optical qualities of a blast-proof PMMA window and other optical components. Figure 2 shows an observed streak camera image for a 500 $\mu\text{m}\phi$ copper powder. The slit lies on a center of one copper powder. The maximum temperature was attained at the center of the powder and was $(2.0 \pm 0.2) \times 10^4$ K. Maximum quench rate was also at the center of the powder and was approximately 10^{12} K/s.

Although more experiments are required to extract a quantitative model for shock compression process in powders, there are two notable observations.

One is the rise time of the shock front. In many theoretical analyses [11, 12, 13, 14] of shock compression in powders, it is often assumed that the shock rise-up is rather smooth and the order of rise-up time is the shock transit time over the diameter length. The irregularity of the shock wave front roughly corresponds to the shock transit time over the diameter length. (Calculated transit time for 500 μm is 120 ns.) Fig. 2 exhibits that rise-up is approximately one third of the calculated value; light intensity reaches to the maximum in about a couple of tens of nanoseconds and then falls within time duration a little longer than the rise-up.

The other is the dependence of the maximum temperature value on powder diameter. As the specific internal and kinetic energies are independent to powder sizes and morphologies, the same amount of energy is to be deposited regardless to the size of the powder. If we assume that the energy deposition occurs mainly on the surface of the powders and the thickness of the layer of energy deposition does not depend on the size of the powder, the peak temperature should increase in proportion to the diameter of the powder because the specific surface area is inversely proportional to the diameter of the powder. However, this is inconsistent with observations. The observed maximum temperatures for 1 mm ϕ and 500 μ m ϕ spherical copper powders are essentially the same within the experimental error. If we take the result of 100 μ m ϕ powder as a maximum temperature and compare that with the result of 1 mm ϕ powder, the ratio of specific surface area of 10 produced only 1.7 times difference in temperature. The temperature difference will even be smaller as the result for 100 μ m is averaged over hot and cold areas.

4. Conclusions

Shock compression in spherical copper powders is microscopically observed. The best spatial and temporal resolutions were 3 to 4 μ m and 3 to 5 ns, respectively. Time resolved brightness temperature profiles were measured using standardized argon plasma light source at 420 nm. Maximum temperature between 1.2 and 2.0 $\times 10^4$ K were obtained for 100 μ m to 1 mm diameter copper powders. The experiments are still to be evolved to various powders to obtain detailed understandings of heterogeneous nature of shock compression in powders.

References

- [1] A.W.Campbell, W.C.Davis, J.B.Ramsay, and J.R.Travis, *Phys. Fluid* **4**, 498 (1961).
- [2] R.A.Graham, B.Morosin, E.L.Venturini, and M.J.Carr, *Ann. Rev. Mater. Sci.* **16**, 315 (1986).
- [3] N.N.Thadhani, *Progress in Materials Science* **37**, 117 (1993).
- [4] A.N.Dremin and L.V.Babare, in "Shock Waves in Condensed Matter — 1981", W.J.Nellis, L.Seaman, R.A.Graham eds., American Institute of Physics, p. 657 (1982).
- [5] D.D.Dlott and M.D.Fayer, *J. Chem. Phys.* **92**, 3798 (1990).
- [6] D.W.Brenner, in "Shock Compression of Condensed Matter 1991", S.C.Schmidt, R.D.Dick, J.W.Forbes, and D.G.Tasker eds., Elsevier Science Publishers B. V., Amsterdam, p. 115 (1992).
- [7] S.Fujihara, K.Narita, Y.Saito, K.Tatsumoto, S.Fujiwara, M.Yoshida, K.Aoki, Y.Kakudate, S.Usaba, and H.Yamawaki, in "Shock Waves", K.Takayama ed., Springer-Verlag, Berlin, p. 367 (1992).
- [8] M.Yoshida, S.Fujiwara, and S.Fujihara, *New Diamond* **30**, 30 (1993).
- [9] Y.Kakudate, M.Yoshida, S.Usaba, H.Yokoi, S.Fujiwara, M.Kawaguchi, K.Sako, and T.Sawai, in "Proceedings of Third IUMRS Int. Conf. Adv. Mater.", in press.
- [10] Y.Nakayama, M.Yoshida, Y.Kakudate, S.Usaba, H.Yamawaki, K.Aoki, K.Tanaka, and S.Fujiwara, in "Proceedings of International Workshop on Strong Shock Waves", p. 77 (1991).
- [11] D.G.Morris, *Metal Sci.* **16**, 457 (1982).
- [12] W.H.Gourdin, *J. Appl. Phys.* **55**, 172 (1984).
- [13] R.B.Schwarz, P.Kasiraj, T.Vreeland Jr., and T.J.Ahrens, *Acta Metal.* **32**, 1243 (1984).
- [14] K.Kondo and S.Sawai, *J. Am. Ceram. Soc.* **73**, 1983 (1990).

Table 1
Copper powders

Powder	Diameter	Remarks
A	$< 100\mu\text{m}$	irregular
B	$100\mu\text{m}$	spherical
C	$500\mu\text{m}$	spherical
D	1 mm	spherical

Table 2
Results of peak temperature measurements
(at $420 \pm 5\text{ nm}$)

Powder	Temperature (10^3 K)
A ($< 100\mu\text{m}$, irregular)	7 ± 0.5
B ($100\mu\text{m}\phi$, spherical)	12 ± 0.3
D ($1\text{ mm}\phi$, spherical)	17 ± 1
(Calculated)	4.0

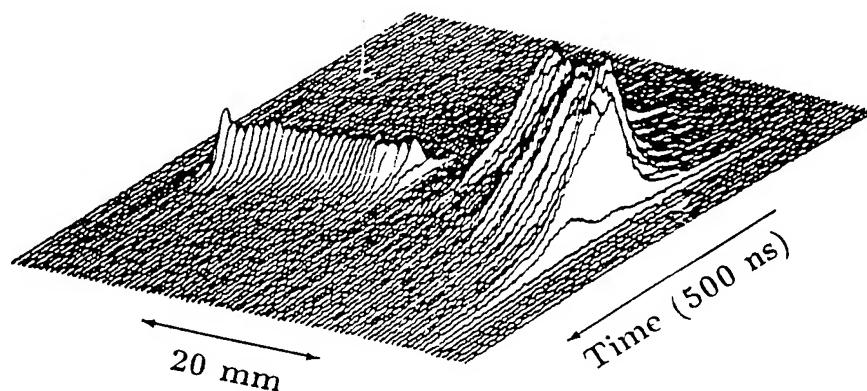


Fig. 1 A typical streak record of the shock wave front in $100\mu\text{m}\phi$ (left) and $1\text{ mm}\phi$ (right) powders.

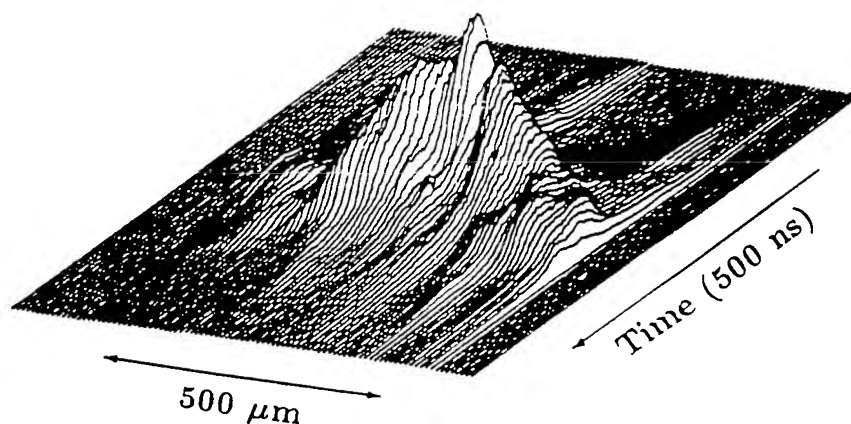


Fig. 2 A streak record of the shock front structure for a magnified $500\mu\text{m}\phi$ copper spherical particle.

SHOCK-INDUCED TRANSFORMATIONS IN OXIDES

Yasuhiko Syono

Institute for Materials Research, Tohoku University,
Katahira, Aoba-ku, Sendai 980-77, Japan

Phase transformations observed in shocked solids [1] have attracted interest of shock scientists from the first discovery α - ϵ transition of iron [2] and shock synthesis of diamond.[3] If they are considered to be used for material synthesis in shock process, understanding of their mechanism is indispensable. The phase transformations inducible under shock compression should be due to fast reaction kinetics, since the shock duration is limited within a microsecond time scale in laboratory experiments.[4-6] The high pressure phases are generally back-transformed in the pressure release process and unquenchable. However, some irreversible phase transformations provide important information for the mechanism in the shock process.

One of the most thoroughly studied cases is the rutile-fluorite- α - PbO_2 transition in the shock process. Hugoniot measurements of TiO_2 with the rutile form revealed a phase transformation with about 15 % volume decrease, suggesting a fluorite structure as a possible high pressure phase.[7] Strong anisotropy in the transition pressures was also noted, i. e. lower transition pressures in the shock-loading perpendicular to the c-axis than that parallel to the c-axis. However, the recovered phase with the α - PbO_2 structure had a density only 2 % denser than rutile, indicating that it was not the high pressure phase and metastably formed in the shock release process.[8] Proposed displacive mechanism based on the topological relationship among the crystal structures of rutile, fluorite and α - PbO_2 successfully explained the observed anisotropy in the transition pressures. Direct evidence to support the proposed mechanism was obtained by TEM observation of lamellae consisting of rutile and α - PbO_2 in the shock-recovered products; Orientation relationship between coexisting rutile and α - PbO_2 was found to be exactly as expected from the proposed mechanism. Computer simulation of rutile-fluorite transition also revealed that the transition could occur within a picosecond time scale, much shorter than the typical rise time of the shock front, and only with the uniaxial compression perpendicular to the c-axis.[9] Later static high pressure study confirmed that the high pressure phase has a tetragonally distorted fluorite structure, corroborating the above model.[10]

Recently similar shock-induced phase transformations were found to occur in the rare earth sesquioxides with the A, B and C type structures in the decreasing order of density.[11,12] Direct transition from C-type to A-type was observed under both shock and static pressures with about 10 % volume decrease. However, shock recovered phase was found to be with the B-type structure, which was presumably formed during the pressure release process. Similarity among the crystal structures of the A, B and C type was pointed out, which makes the phase transformation due to displacive mechanism during shock process possible. Sequential phase transformations of C-A-B type rare earth sesquioxides in the shock process is quite analogous to those of rutile-fluorite- α - PbO_2 as mentioned above.

Complete retention of high pressure phases induced via displacive mechanism by shock loading seems to be rather difficult, since they are in general easily back-transformed during shock release process. Some blocking mechanism would be needed to stabilize the induced high pressure phase. The scheelite type ZrSiO_4 was successfully recovered from the shock loading of the zircon type ZrSiO_4 . [13] It has been noted that zircon to scheelite transition is very similar to the rutile-fluorite transition, as far as the cation arrangements are concerned.[14] Only difference is the coherent rotation of SiO_4 tetrahedra during the zircon-scheelite transition, which may play an important role in preventing back transition from shock-induced high pressure phase.

to the zircon phase during pressure release. A phase transformation due to similar block movement of atomic cluster was suggested in the case of shock formation of Cr_3Si (A15) type Nb_3Si from the Ti_3P type structure, although shock-yield of the high pressure phase was rather low.[15] The shock-induced A15 type Nb_3Si was found to have superconducting critical temperature of 18 K, instead of non-superconducting Ti_3P type Nb_3Si . [16] In this regard worthy mentioning is that wBN can be synthesized from hBN, [17] while hexagonal form of diamond formed by shock loading of graphite is unquenchable. [18,19] This marked contrast suggests importance of bonding between different elements of B and N in preventing back-transformation from shock-induced wBN.

There have been long arguments whether the olivine-spinel transformation is due to diffusion-controlled nucleation-growth mechanism or martensitic mechanism. From the viewpoint of shock compression experiments, no martensitic mechanism seems to work in the shock process, since no anomaly around the phase transition pressures determined by static high pressure-temperature studies was ever noticed in the Hugoniot measurements of forsterite. [20-22] This strongly suggests that the phase transformations of the reconstructive nature is hardly achieved during a short time interval of the shock process. Even an order-disorder phase transformation with cation rearrangements seems to be unfavorable under shock compression; The disordered rutile type FeTaO_4 was found to transform to the disordered $\alpha\text{-PbO}_2$ type, instead of the ordered NiWO_4 type structure obtainable by static high pressure experiments. [23]

The work was carried out in cooperation with M. Kikuchi, K. Kusaba, T. Atou and K. Fukuoka.

- References--- [1] G. E. Duvall and R. A. Graham, *Rev. Mod. Phys.*, 49 (1977) 523. [2] D. Bancroft, E. L. Peterson and S. Minshall, *J. Appl. Phys.*, 27 (1956) 291. [3] P. S. DeCarli and J. C. Jamieson, *Science*, 133 (1961) 1821. [4] Y. Syono, *High Pressure Explosive Processing of Ceramics*, R. A. Graham and A. B. Sawaoka (eds.), Transtech, Aedermansdorf (1986) p.377. [5] Y. Syono, *Shock-Waves in Condensed Matter-1987*, S. C. Schmidt and N. C. Holmes (eds.), North Holland, Amsterdam (1988) p.19. [6] Y. Syono, K. Kusaba, T. Atou and K. Fukuoka, *Shock Waves*, K. Takayama (ed.), Springer, Berlin (1992) vol.1, p.121. [7] Y. Syono, K. Kusaba, M. Kikuchi, K. Fukuoka and T. Goto, *High Pressure Research in Mineral Physics*, M. H. Manghnani and Y. Syono (eds.), Terra/AGU, Tokyo/Washington, D. C. (1987) p.385. [8] K. Kusaba, M. Kikuchi, K. Fukuoka and Y. Syono, *Phys. Chem. Miner.*, 15 (1988) 238. [9] K. Kusaba, Y. Syono and Y. Matsui, *Shock Waves in Condensed Matter-1989*, S. C. Schmidt, J. N. Johnson and L. W. Davison (eds.), North Holland, Amsterdam (1990) p.135. [10] H. Sato, S. Endo, M. Sugiyama, T. Kikegawa, O. Shimomura and K. Kusaba, *Science*, 251 (1990) 786. [11] T. Atou, K. Kusaba, K. Fukuoka, M. Kikuchi and Y. Syono, *J. Solid State Chem.*, 89 (1990) 378. [12] T. Atou, M. Kikuchi, K. Fukuoka, K. Kusaba and Y. Syono, *Proc. of the 1993 joint AIRAPT/APS Topical Conference on High Pressure Science and Technology*, Colorado Springs (1994), in press. [13] K. Kusaba, Y. Syono, M. Kikuchi, and K. Fukuoka, *Earth Planet. Sci. Lett.*, 72 (1985) 433. [14] K. Kusaba, T. Yagi, M. Kikuchi and Y. Syono, *J. Phys. Chem. Solids*, 47 (1986) 675. [15] B. Olinger, *Acta Cryst.*, A38 (1982) 151. [16] S. Ohshima, T. Wakiyama, T. Goto and Y. Syono, *Jpn. J. Appl. Phys.*, 22 (1983) 264. [17] T. Soma, A. Sawaoka and S. Saito, *Mater. Res. Bull.*, 9 (1974) 755. [18] D. J. Erskine and W. J. Nellis, *Nature*, 349 (1991) 317. [19] M. Yoshida and N. N. Thadhani, *Shock Compression of Condensed Matter 1991*, S. C. Schmidt et al. (eds.), North Holland, Amsterdam (1992) p.585. [20] I. Jackson and T. J. Ahrens, *J. Geophys. Res.*, 84 (1979) 3039. [21] Y. Syono, T. Goto, J. Sato and H. Takei, *J. Geophys. Res.*, 86 (1981) 6181. [22] J. M. Brown, M. D. Furnish and R. G. McQueen, *High Pressure Research in Mineral Physics*, M. H. Manghnani and Y. Syono (eds.), Terra/AGU, Tokyo/Washington, D. C. (1987) p.373. [23] K. Kusaba, K. Fukuoka and Y. Syono, *J. Phys. Chem. Solids*, 52 (1991) 845.

SHOCK-INDUCED PHASE TRANSITIONS IN SOLIDS: THEIR UNDERSTANDING AT ATOMISTIC LEVEL

Yasuhiko SYONO

Institute for Materials Research, Tohoku University, Katahira, Sendai 980, Japan

Investigations of shock-induced phase transitions in several oxides were made from a microscopic viewpoint to disclose their mechanism. Needs for both the in-situ measurements of shock-compressed states and residual effects examination of shock-recovered materials are pointed out. Two examples of phase transitions of Fe_2O_3 and LiNbO_3 as well as LiTaO_3 due to electronic origin are described in detail, by combining comparative studies at static high pressures using a diamond anvil cell. Displacive mechanism for a sequential rutile-fluorite- α - PbO_2 transition in TiO_2 under shock loading and unloading is discussed on the basis of both Hugoniot measurements and recovery experiments. Electron microscopy is shown to be most useful to obtain microscopic information of phase transitions under shock process, and two examples for TiO_2 and Nb_2O_5 are demonstrated.

1. INTRODUCTION

Shock-induced phase transitions in solids have been one of the central issues from the very beginning of the shock wave research.¹⁻⁵ The 13 GPa phase transition of iron was first observed under shock loading in precise measurements of pressure volume relation by electrical pin contactor method as early as in 1955,⁶ and the structure of the high pressure phase was determined to be hexagonally close packed one, only when the x-ray diffraction study became possible under static high pressures in 1964.⁷ Following the first artificial synthesis of diamond by catalytic reaction of metal at static high pressures using the belt-type apparatus,⁸ polycrystalline diamond powders were also synthesized by shock compression technique.⁹

Since these early demonstrable examples, a number of phase transformations have been observed either by in-situ measurements of shock compression curve or by shock synthesis experiments using recovery system. However, most of the research work has been done from the macroscopic viewpoint for the continuous body, although the measured data are becoming more and more precise and time-dependent analysis possible. Therefore, our knowledge of the mechanism of shock-induced phase transitions is still limited,

and a more microscopic approach based on the crystal and electronic structures of substances is indispensable for real understanding of the mechanism of phase transition under shock process at atomistic level.

In this article, several examples of shock-induced phase transitions studied in the author's laboratory for these ten years will be presented. The experimental approach for the microscopic study on the shock-induced phase transitions will be largely influenced by whether the shock-induced phases are quenchable at ambient conditions after shock release. If they are unquenchable as in the case of electronic and most of displacive transitions, the only information obtainable from shock experiments is by in-situ measurements, pressure-volume relation, for example. In these reversible phase transitions, direct comparison with static high pressure experiments using a diamond anvil cell is most effective, since these transitions are generally induced at static condition. Such examples are shown here for the case of pressure-induced phase transition in Fe_2O_3 and LiNbO_3 as well as LiTaO_3 .

If the shock-induced phases can be retained after the passage of shock waves, rich information on the phase transition mechanism will be

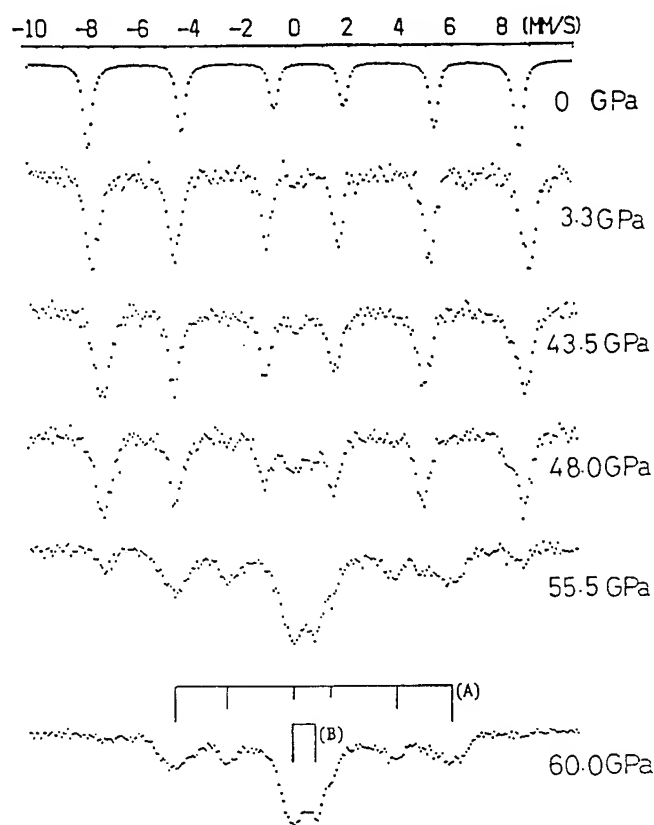


FIGURE 2

Pressure variation of Mössbauer spectra of Fe_2O_3 . The spectrum at 60 GPa was interpreted by superposition of sextet (A) and a doublet (B).¹⁵

plete conversion was attained above about 55 GPa. The spectrum of the high pressure phase measured at 60 GPa was analyzed to consist of a sextet and a doublet, indicating at least two kinds of iron ions with different electronic states. The paramagnetic doublet spectrum was explained by low spin state iron ions, accompanied by probable reduction in valence. Later Nasu et al. reported that the remaining sextet at 60 GPa gradually vanished with increasing pressure, suggesting the perfect low spin state above 80 GPa.¹⁶

2.2. LiNbO_3 and LiTaO_3

A phase transition in ferroelectric LiNbO_3 under shock loading was first suggested by Stanton and Graham.¹⁷ However, unusually high Hugoniot elastic limit apparently disturbed correct interpretation of the measured Hugoniot data. Thorough investigation on the high pres-

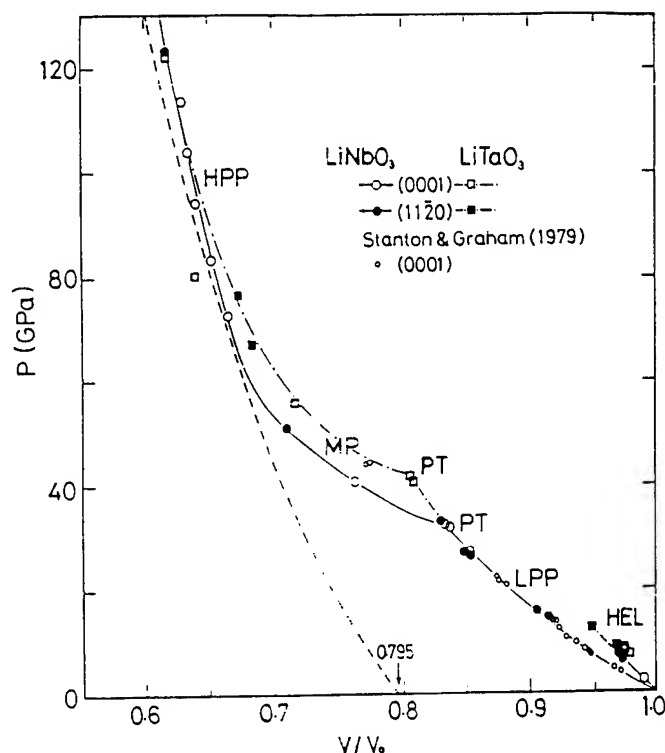


FIGURE 3

Shock compression curve of LiNbO_3 and LiTaO_3 .^{18, 19} Broken line indicates the isotherm of LiNbO_3 derived from Birch-Murnaghan fit. HEL: Hugoniot elastic limit, LPP: Low pressure phase, PT: Phase transition, MP: Mixed phase, HPP: High pressure phase

sure behavior of LiNbO_3 as well as LiTaO_3 at both dynamic and static condition was carried out. Figure 3 reproduces the shock compression curve of LiNbO_3 ¹⁸ and LiTaO_3 ¹⁹. In both substances, discontinuous decrease in volume was clearly observed at 32.6 and 40 GPa respectively, indicating onset of the phase transition. The volume change accompanied by the phase transition was estimated to be 20.5 and 20 % for LiNbO_3 and LiTaO_3 respectively.^{18, 19}

High pressure x-ray diffraction studies were carried out for LiNbO_3 ^{20, 21} and LiTaO_3 ²¹, using a diamond anvil cell. Results for pressure variation of d-spacings of the observed reflections are shown in Fig. 4.²¹ Abrupt change in x-ray diffraction patterns was observed at about 32 and 40 GPa for LiNbO_3 and LiTaO_3 , in good agreement with the observed phase transition pressure by shock compression technique.

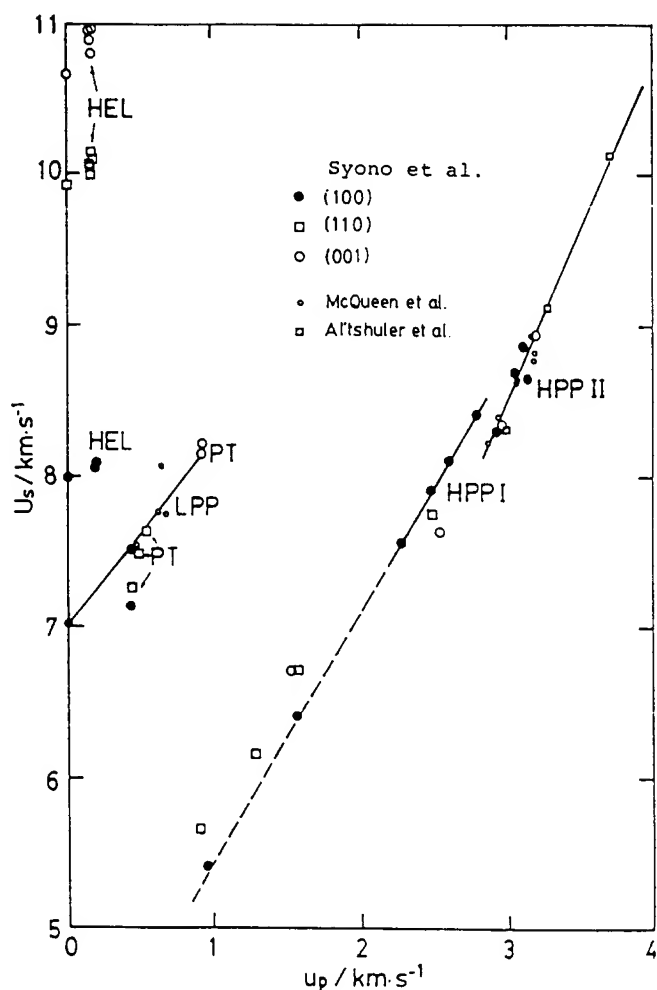


FIGURE 5

Hugoniot data in the shock velocity versus particle velocity plane of rutile single crystal.²⁶

adiabat measurements, as shown in Fig. 6, which revealed that HPP II is denser by about 30 % than rutile, again suggesting some change in the nature of chemical bond under such high compression.

The volume difference of 15 % between rutile and HPP I at zero pressure suggested that HPP I has a fluorite or its related structure.²⁸ However, shock recovery experiments revealed^{22,29} that only α - PbO_2 type phase, which is denser by only 2 % than rutile, was formed and its yield was strongly dependent on the shock propagation direction, i. e. much larger yield along [100] than [001].²⁷ The onset pressure where the α - PbO_2 type phase appeared was also found to coincide with the phase transition pressures observed

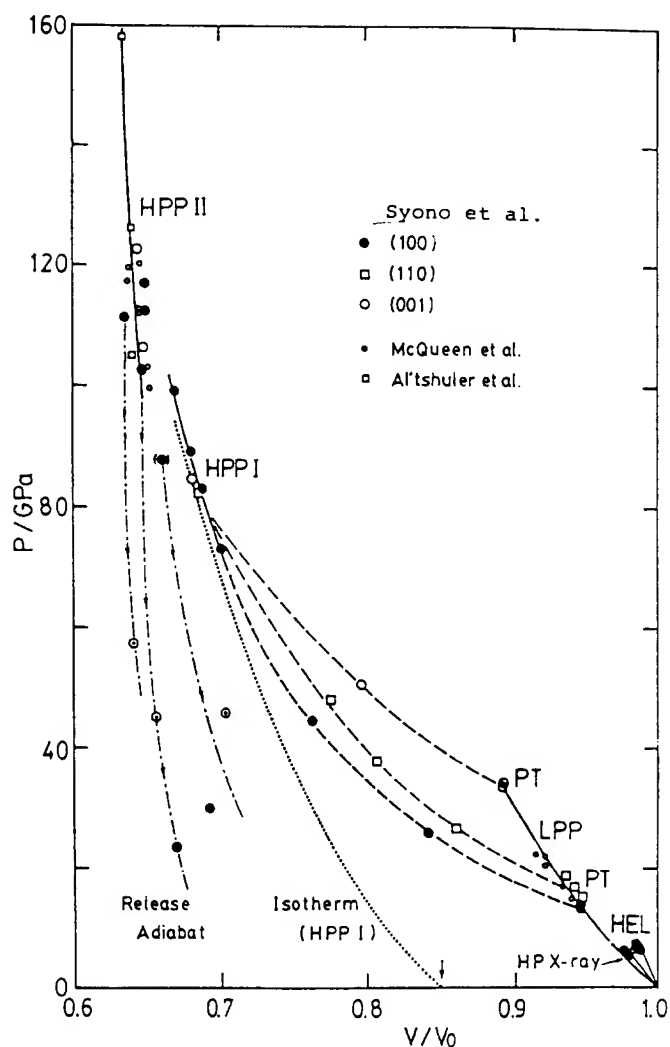


FIGURE 6

Shock compression curve of rutile single crystal.

by Hugoniot measurements.²⁶ These experimental results strongly suggest that the α - PbO_2 type phase is metastably formed from the unquenchable fluorite-like phase in the shock release process. Possibility of such sequential phase transformation of rutile-fluorite- α - PbO_2 series in MX_2 type compounds has already been proposed by Hyde et al.³⁰ More specific scenario for the phase transition in the shock process was presented by Kusaba et al. very recently.²⁷

Figure 7 schematically illustrates how the [100] shock loading of rutile leads to a fluorite-like arrangement without involvement of extensive atomic diffusion, where the original [010] and [001] directions of rutile should con-

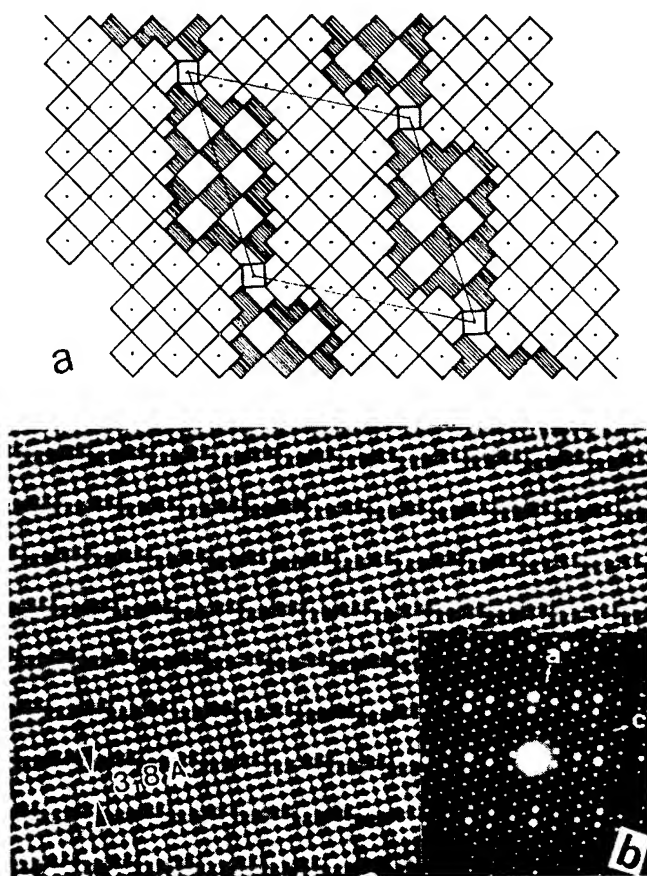


FIGURE 9

Crystal structure (a) and high resolution image (b) of $\text{H-Nb}_2\text{O}_5$ viewed along the monoclinic b axis parallel to the columnar block axis.

quench mechanism may be excluded, because melting temperature of Nb_2O_5 is well below the Hugoniot temperature. Noteworthy is that such formation mechanism of highly disordered structure might be closely related to that of diaplectic glass of feldspar and other tectosilicates.³⁸

4. CONCLUDING REMARKS

The work presented here clearly demonstrates that microscopic approach for the study of shock effects in solids is promising and particularly electron microscopy is very useful for the understanding of shock phenomena at atomistic level. Although the scope of the present article is limited to rather simple pressure effects of shock waves, similar approach will also be applied to more complex aspect of shock chemistry.

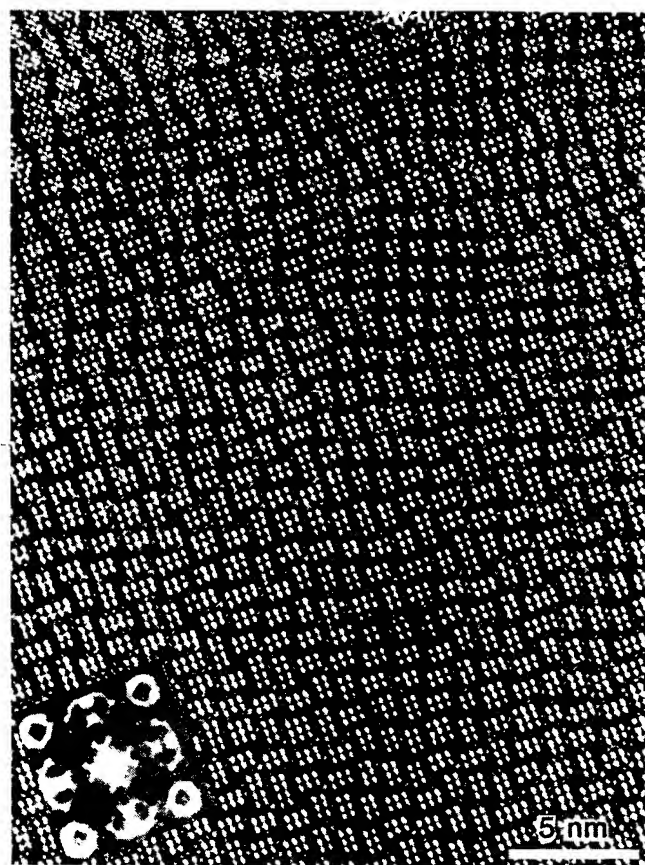


FIGURE 10

High resolution electron micrograph of the shock induced disordered phase taken with the incident beam parallel to the columnar axis.⁴⁷

ACKNOWLEDGEMENTS

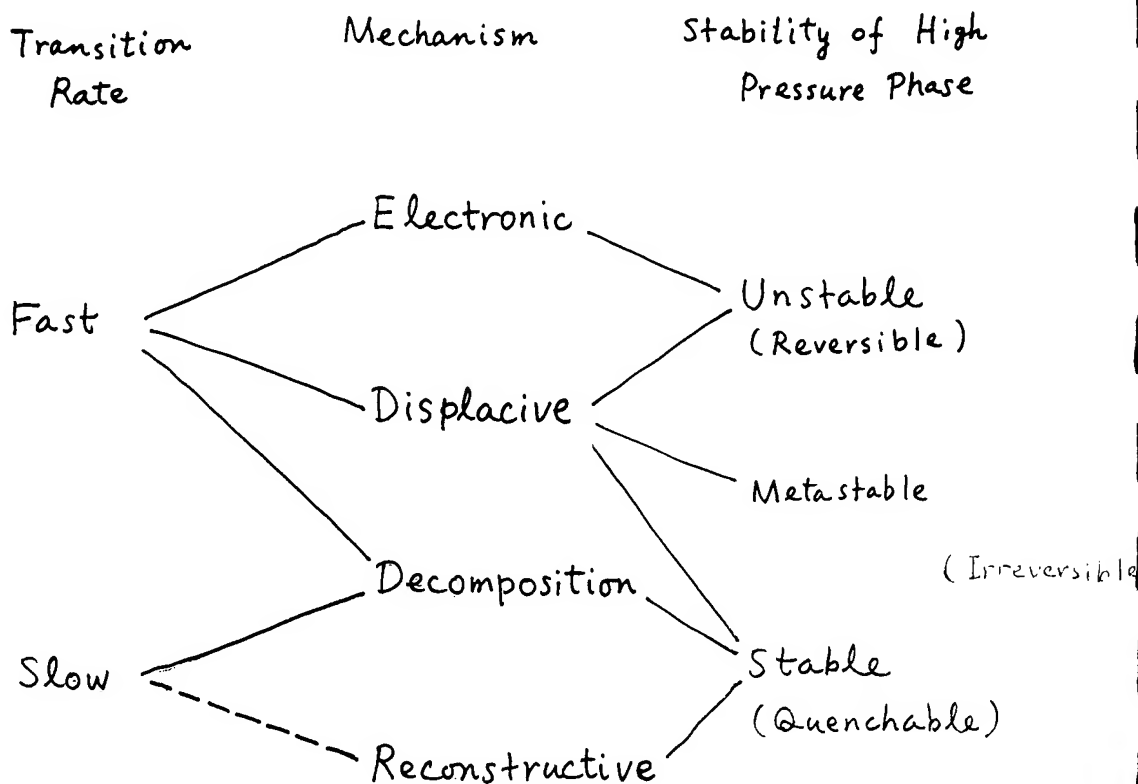
The author is particularly indebted to his colleagues, Dr. M. Kikuchi, Messrs. K. Kusaba and K. Fukuoka, for invaluable contribution. Special thanks are due to Dr. T. Goto, now with Institute for Solid State Physics, University of Tokyo, for collaboration in the early stage of this work. He wishes to express his thanks to Dr. K. Hiraga for electron microscopy, Drs. T. Yagi and T. Suzuki, Institute for Solid State Physics, University of Tokyo, for high pressure x-ray diffraction and Prof. A. Ito, Department of Physics, Ochanomizu University, for Mössbauer measurements. He is most grateful to Profs. Y. Nakagawa, M. Hirabayashi, and S. Akimoto of the Institute for Study of the Earth's Interior, Okayama University, for warm encouragements.

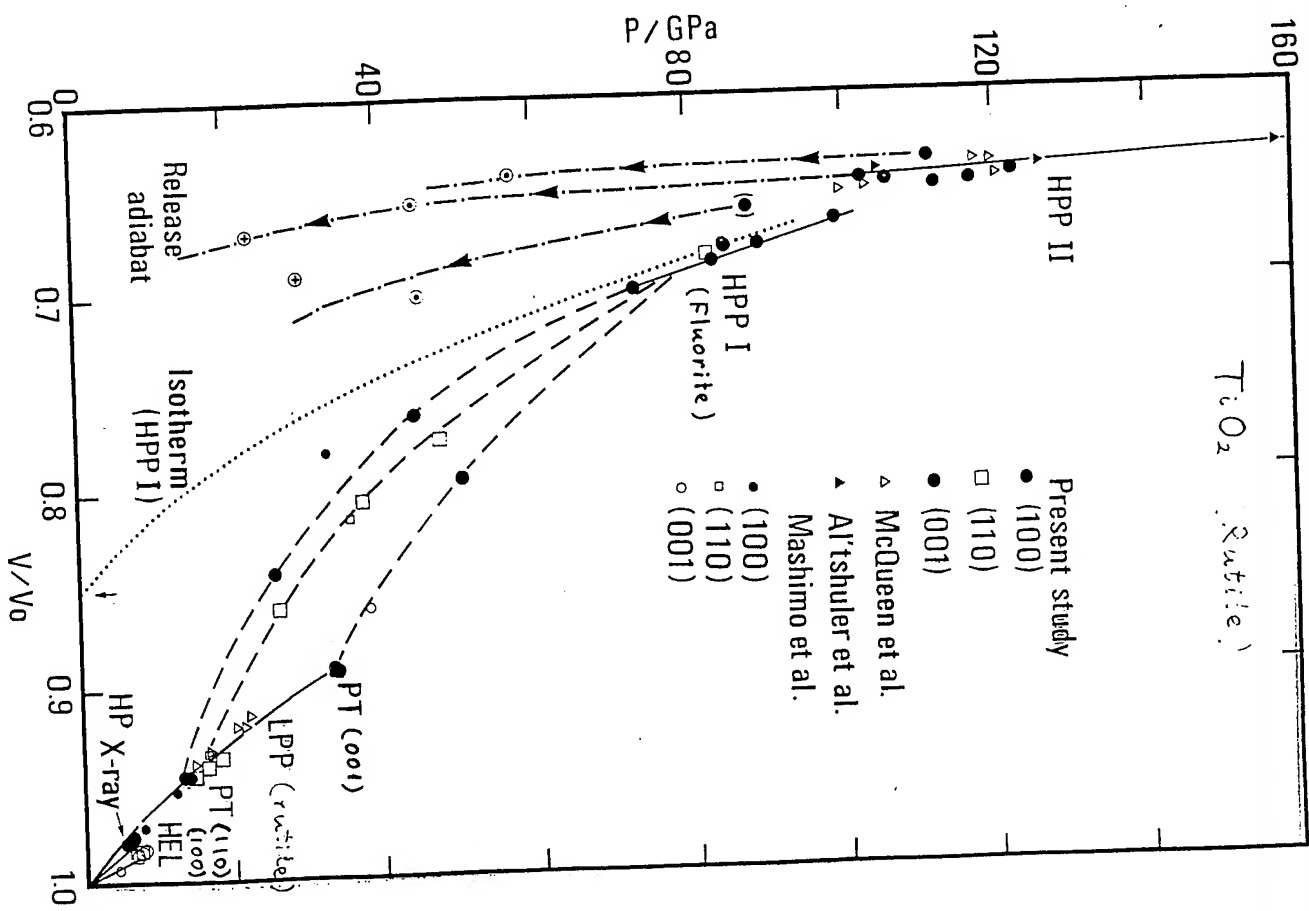
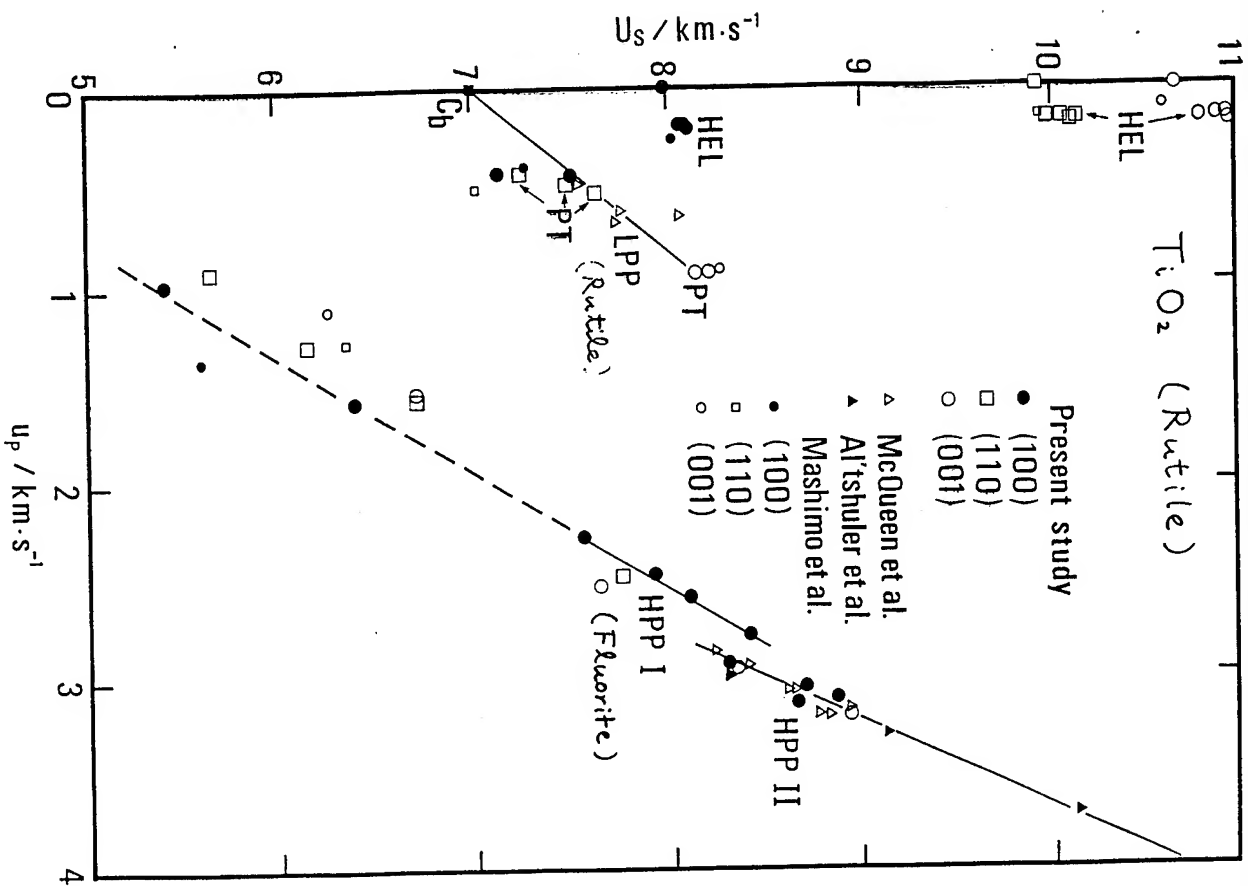
SHOCK-INDUCED TRANSFORMATION IN OXIDES

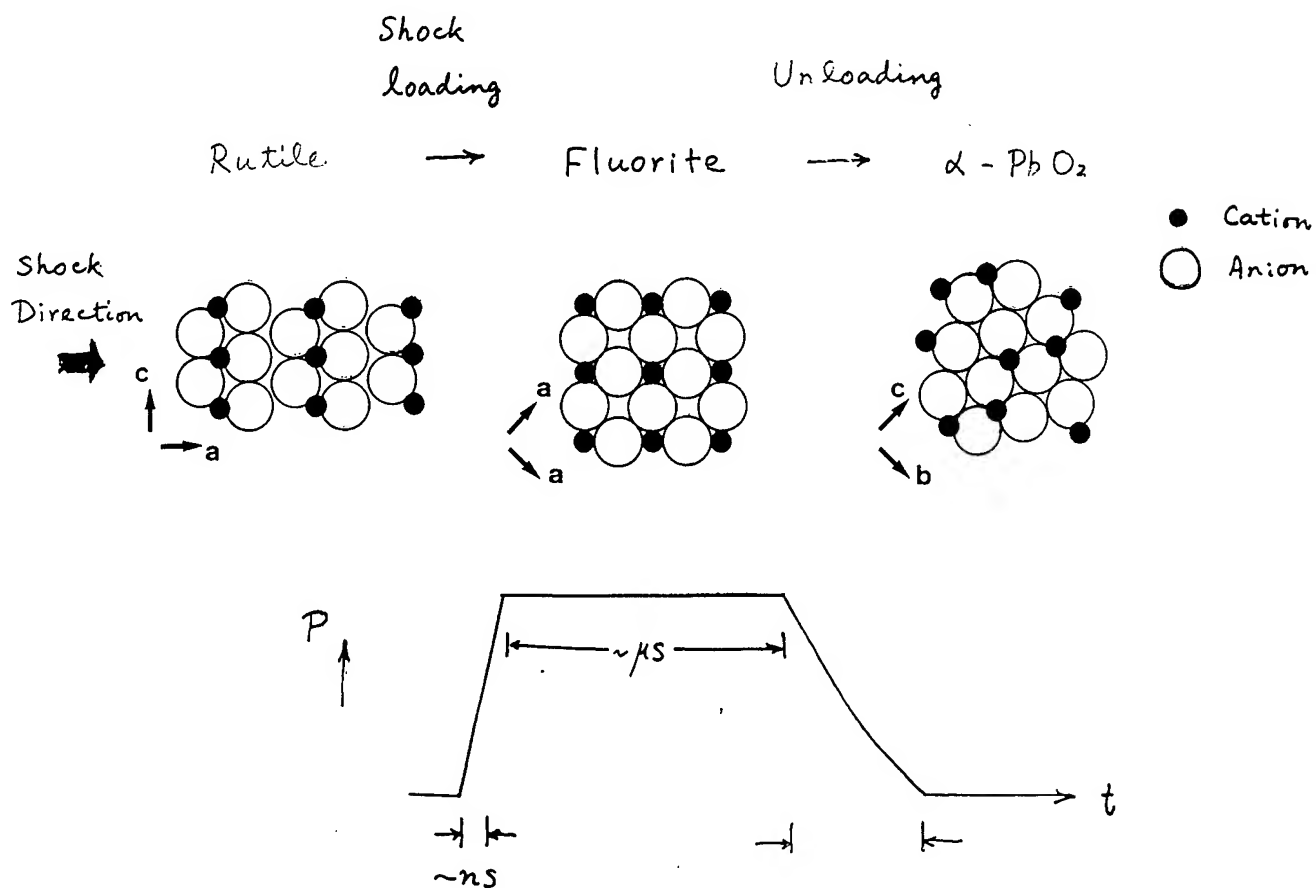
Yasuhiko Syono
Institute for Materials Research
Tohoku University

In Collaboration with
Toshiyuki Aton
Keiji Kusaba
Masae Kikuchi
Kiyoto Fukunaka

SHOCK-INDUCED PHASE CHANGES

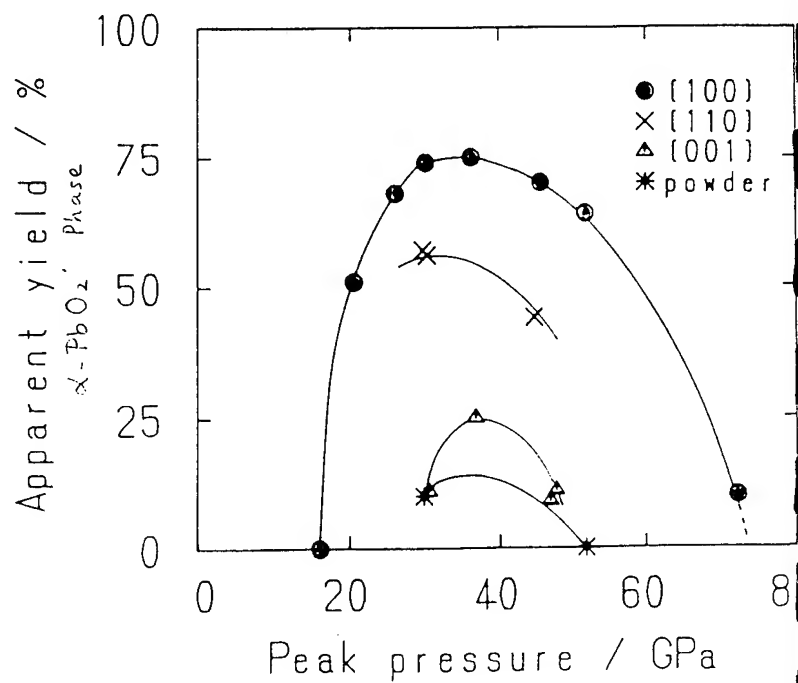
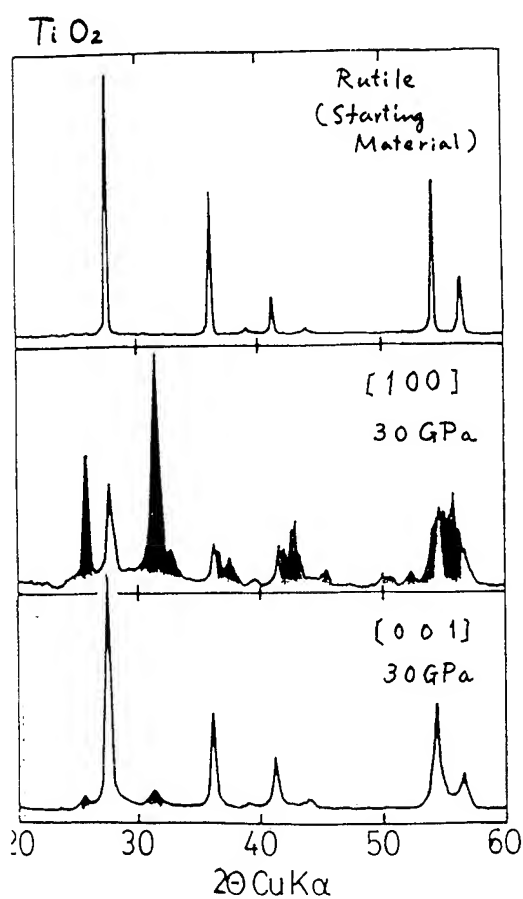


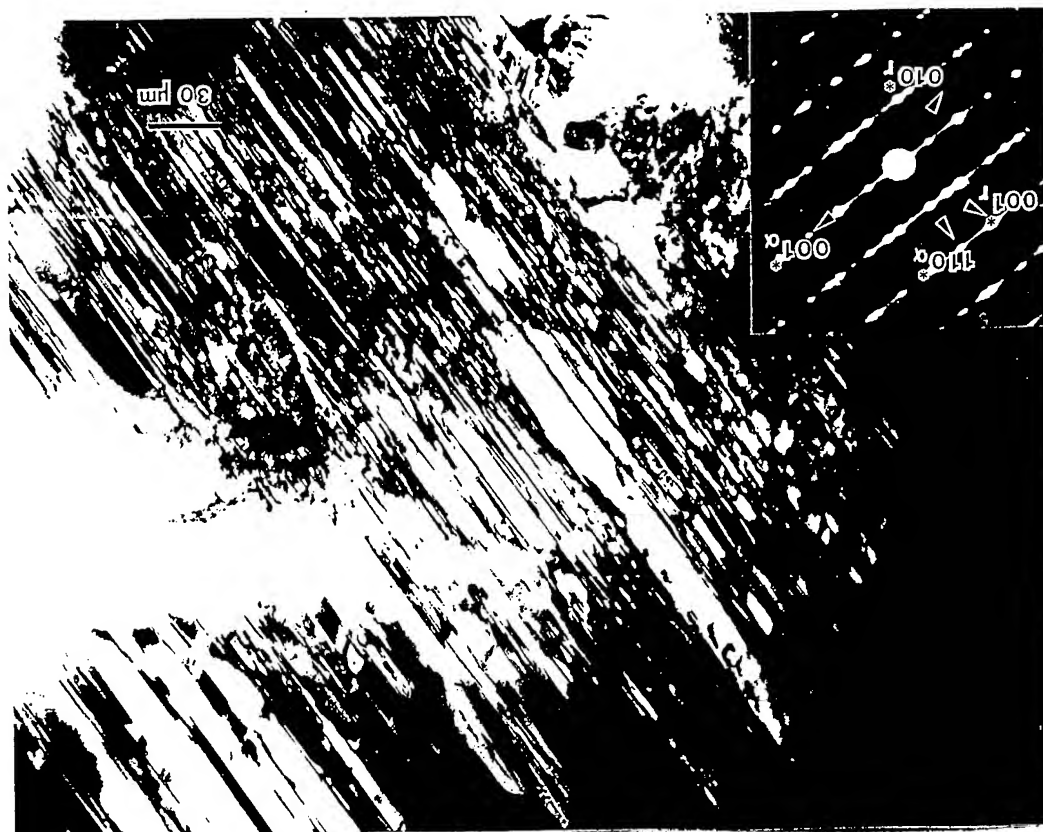
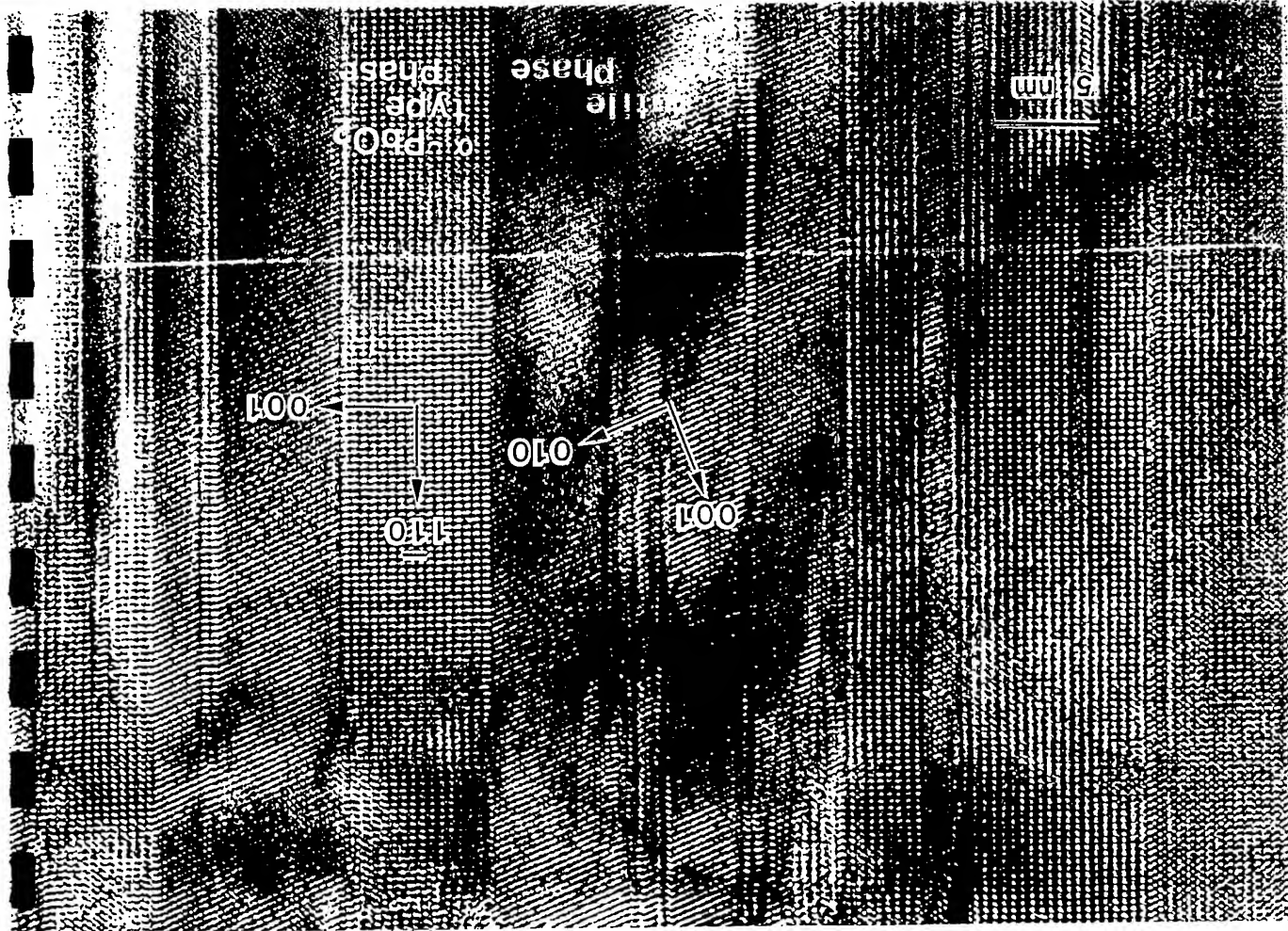




Kusaba et al.

Shock Recovery Experiments of Rutile (TiO₂) Single Crystals





incidence beam // $[100]$

Rutile - Fluorite Transition

Kusaba et al.

Rutile

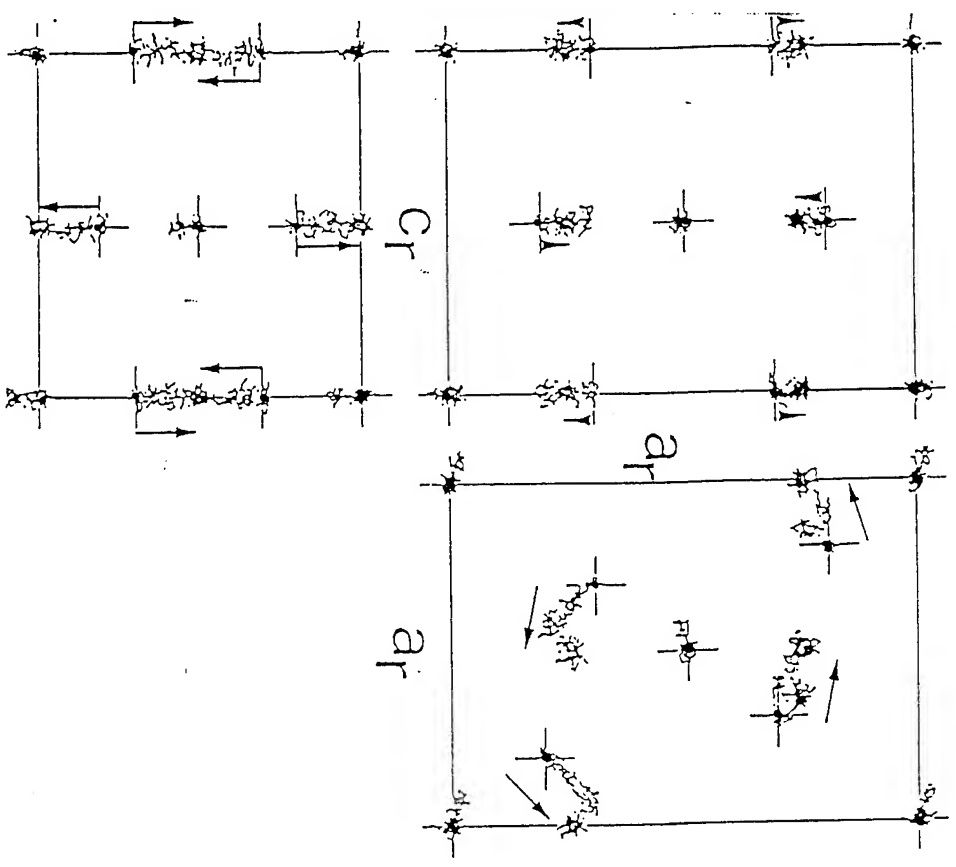
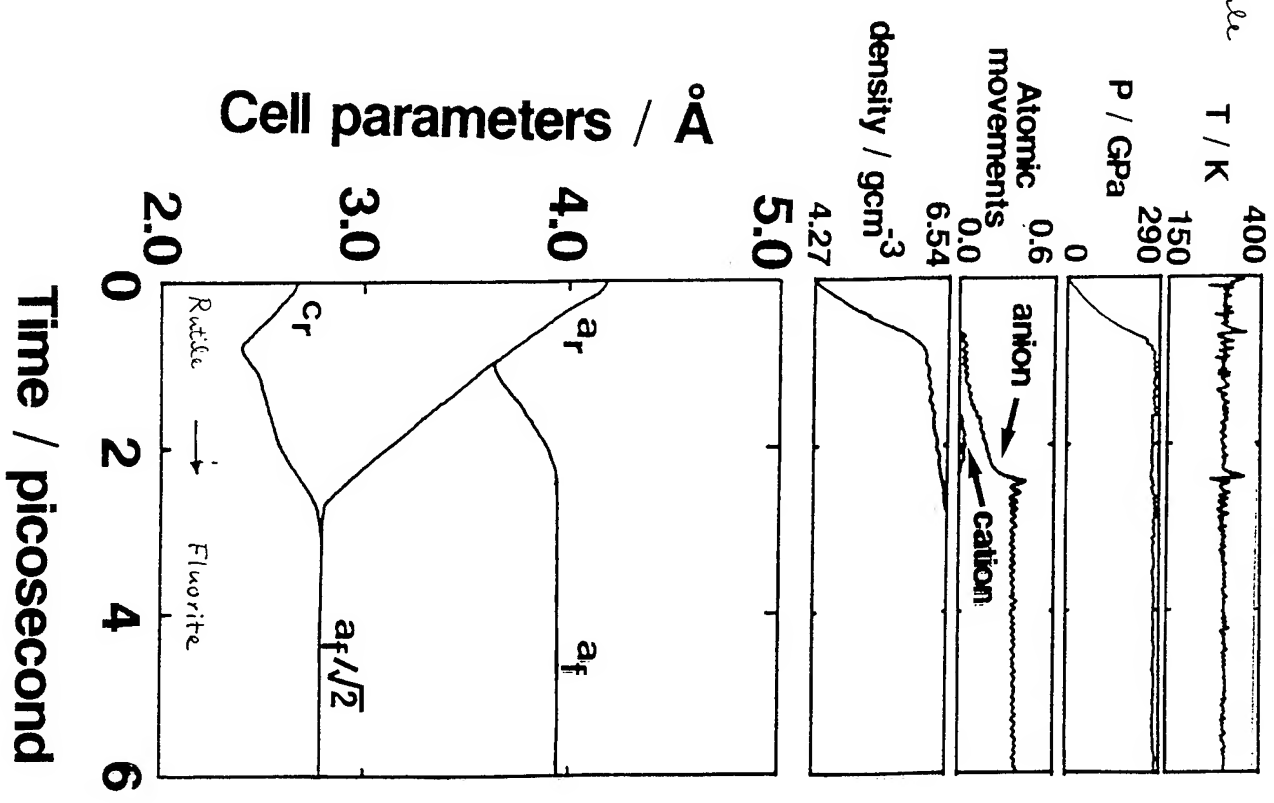
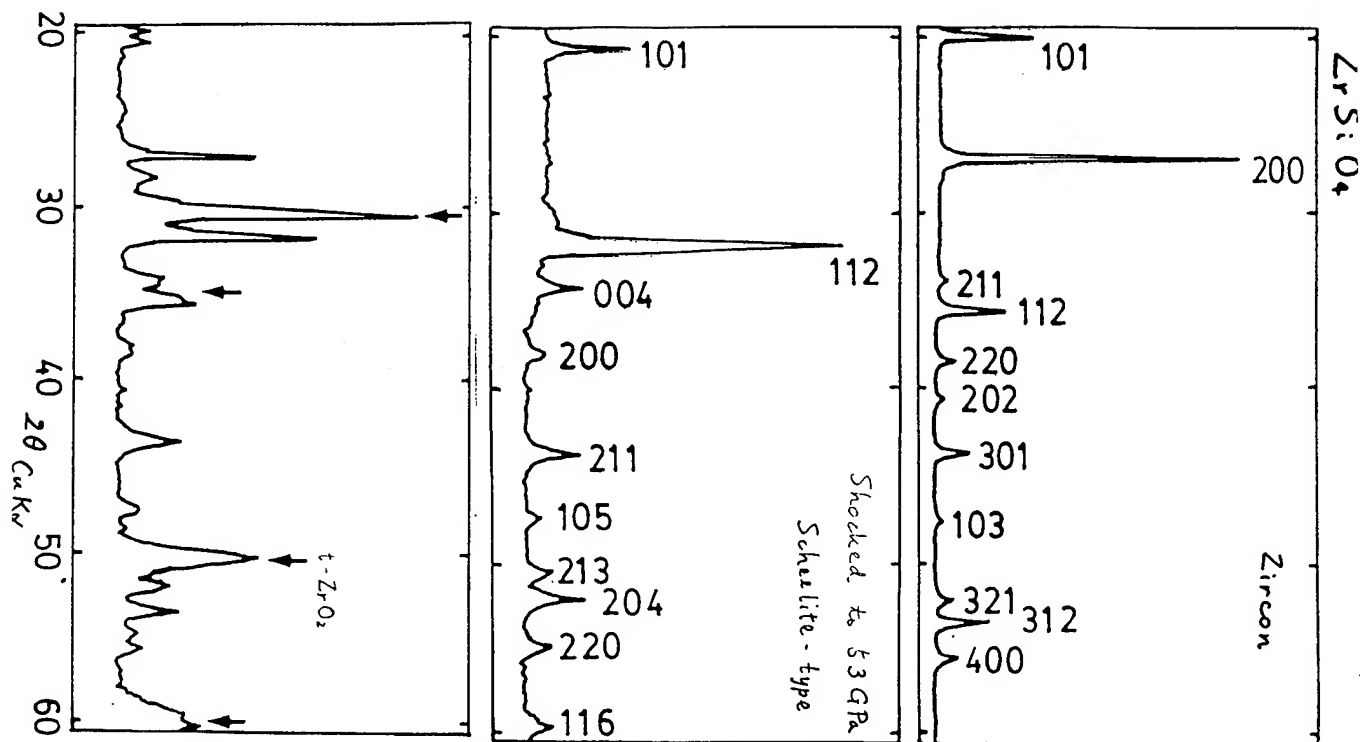


FIGURE 2

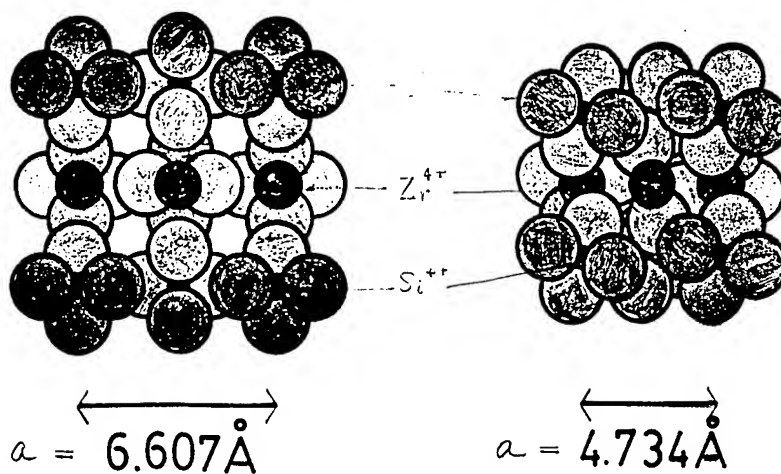
Atomic movements in phase transition from rutile to related-fluorite structure. Initial positions are indicated by cross points and arrows show atomic movements. Cations are in the center all the edges of the unit cell.



Kusaba et al.



c-projection Zircon type Scheelite type

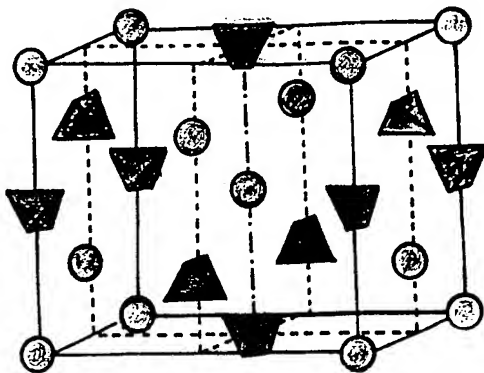


$14_1/amd$

$14_1/a$

$$\frac{\Delta V}{V_0} = -10\%$$

Zircon ($I 4_1/a m d$)



$$a = 6.607 \text{ \AA}$$

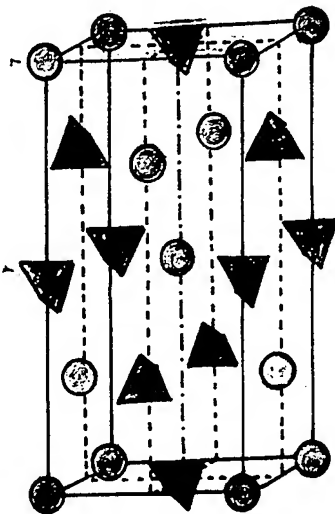
$$c = 5.981 \text{ \AA}$$

$$V = 261.1 \text{ \AA}^3$$

$$c/a = 0.905$$

$$\frac{\Delta V}{V_0} = -9.9\%$$

Scheelite ($I 4_1/a$)

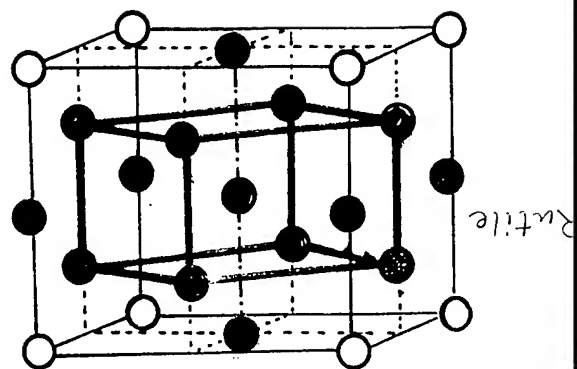
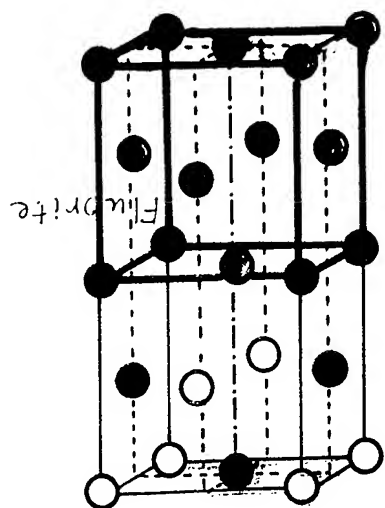


$$a = 4.734 \text{ \AA}$$

$$c = 10.51 \text{ \AA}$$

$$V = 235.5 \text{ \AA}^3$$

$$c/a = 2.219$$



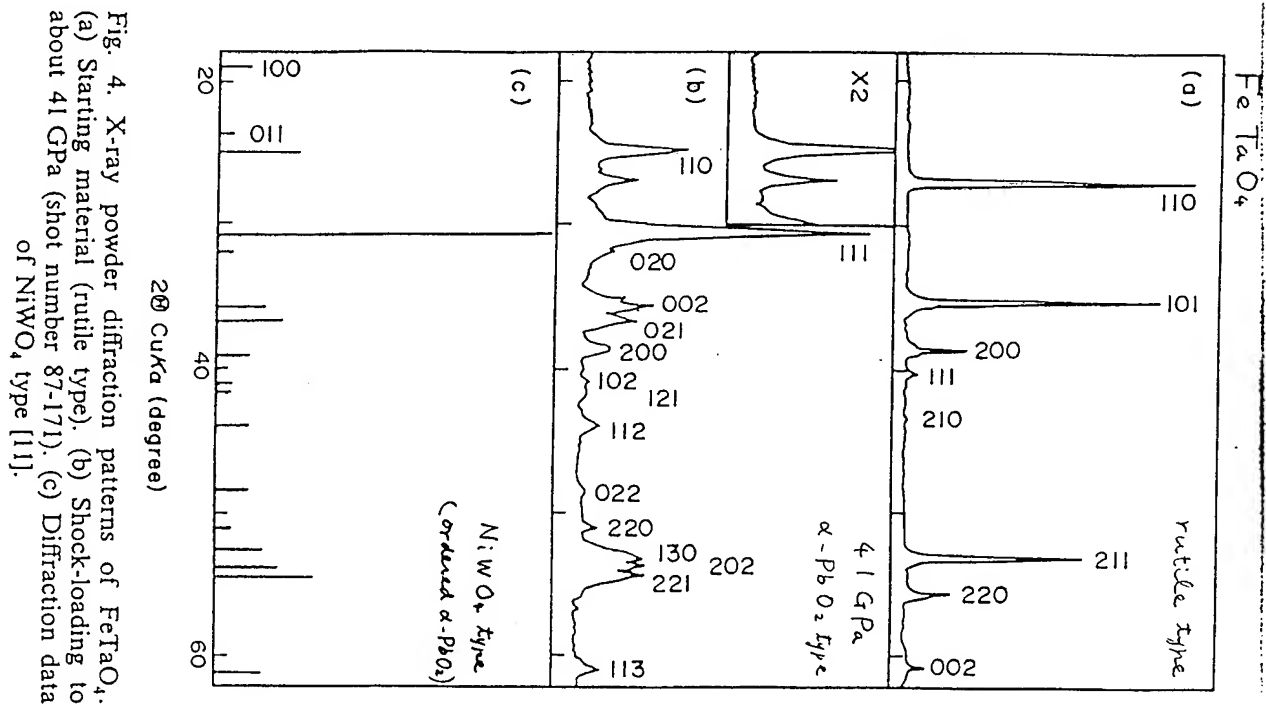
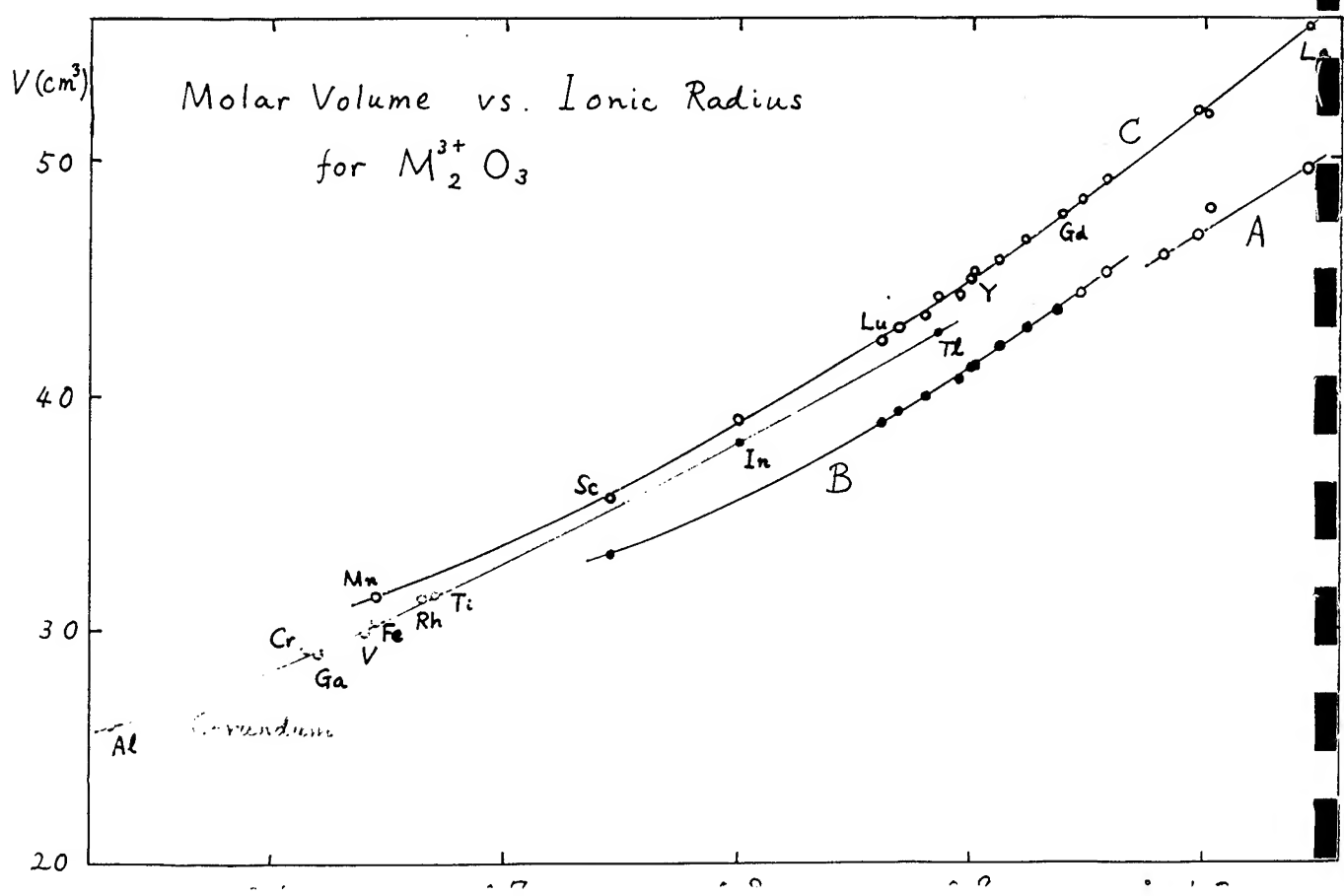
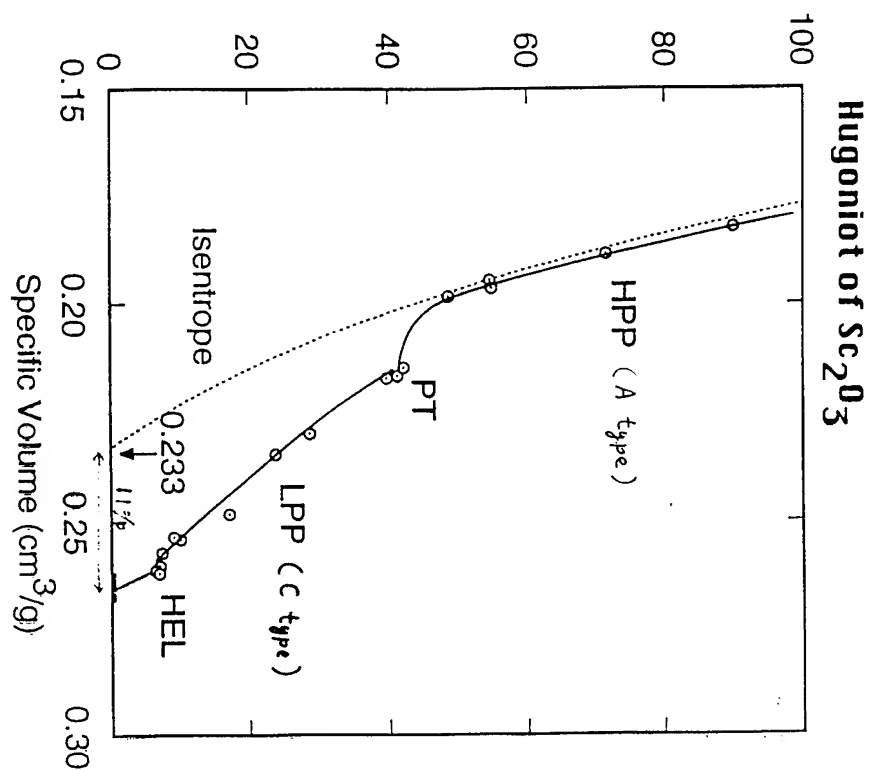
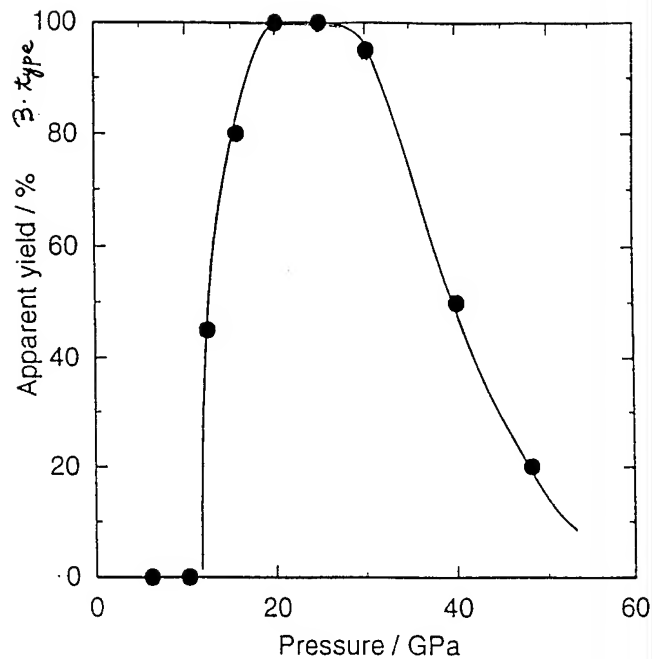
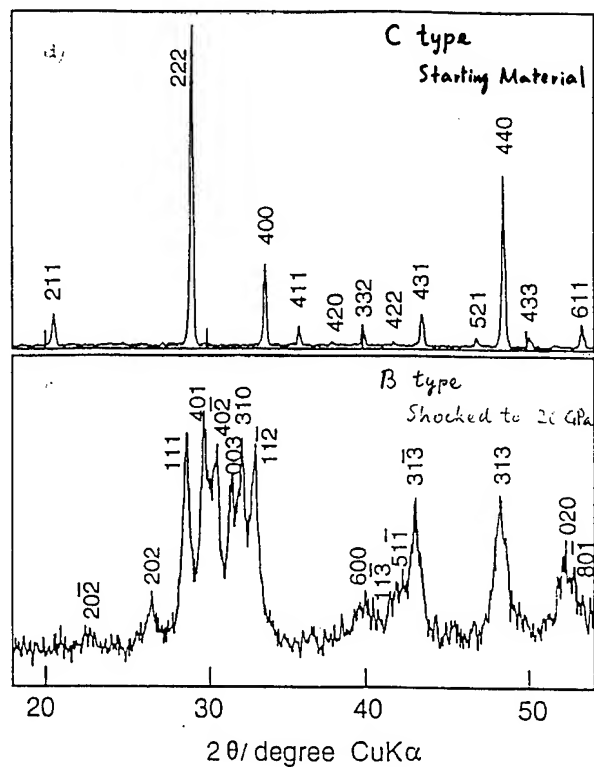
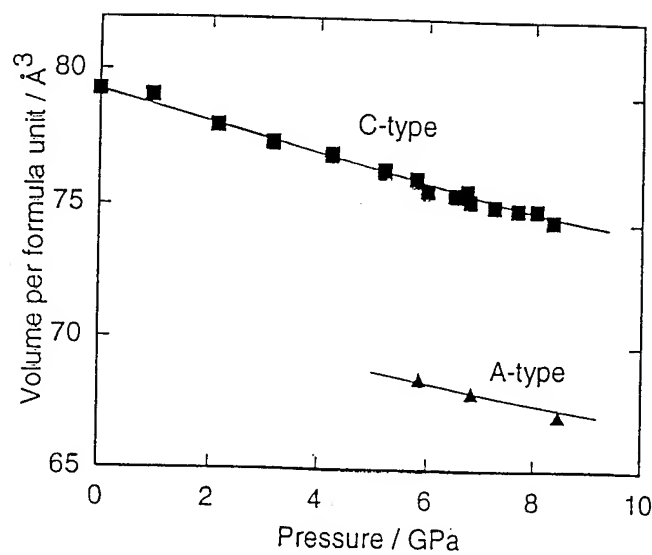
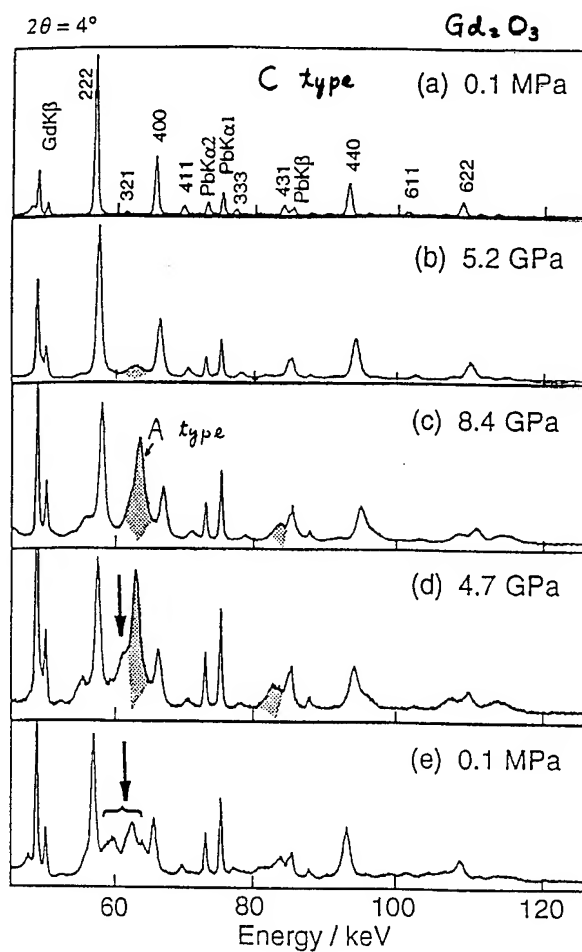


Fig. 4. X-ray powder diffraction patterns of FeTaO_4 . (a) Starting material (rutile type). (b) Shock-loading to about 41 GPa (shot number 87-171). (c) Diffraction data of NiWO_4 type [11].



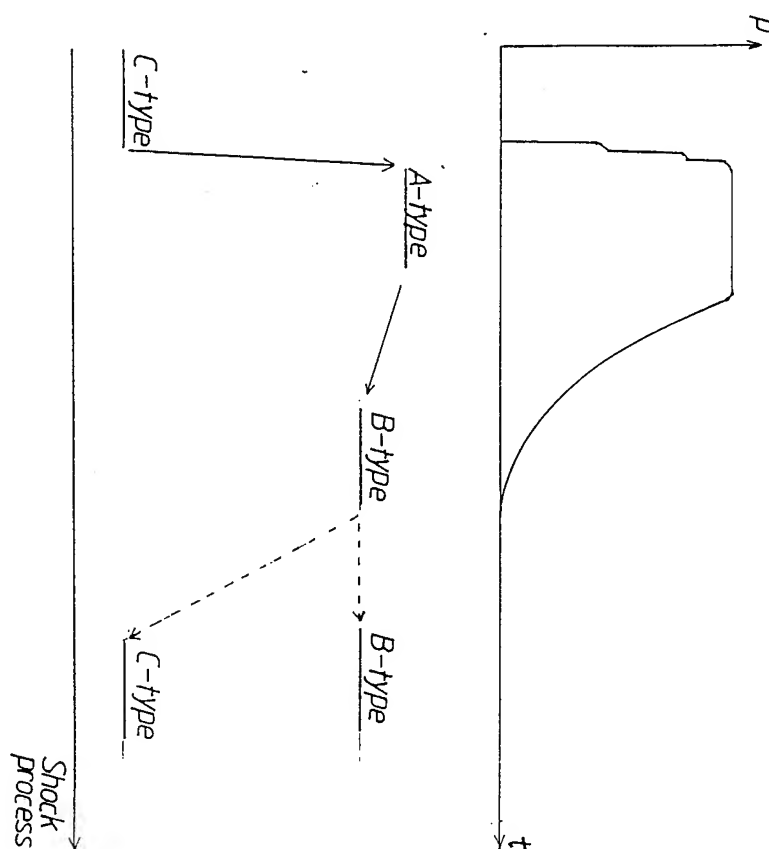


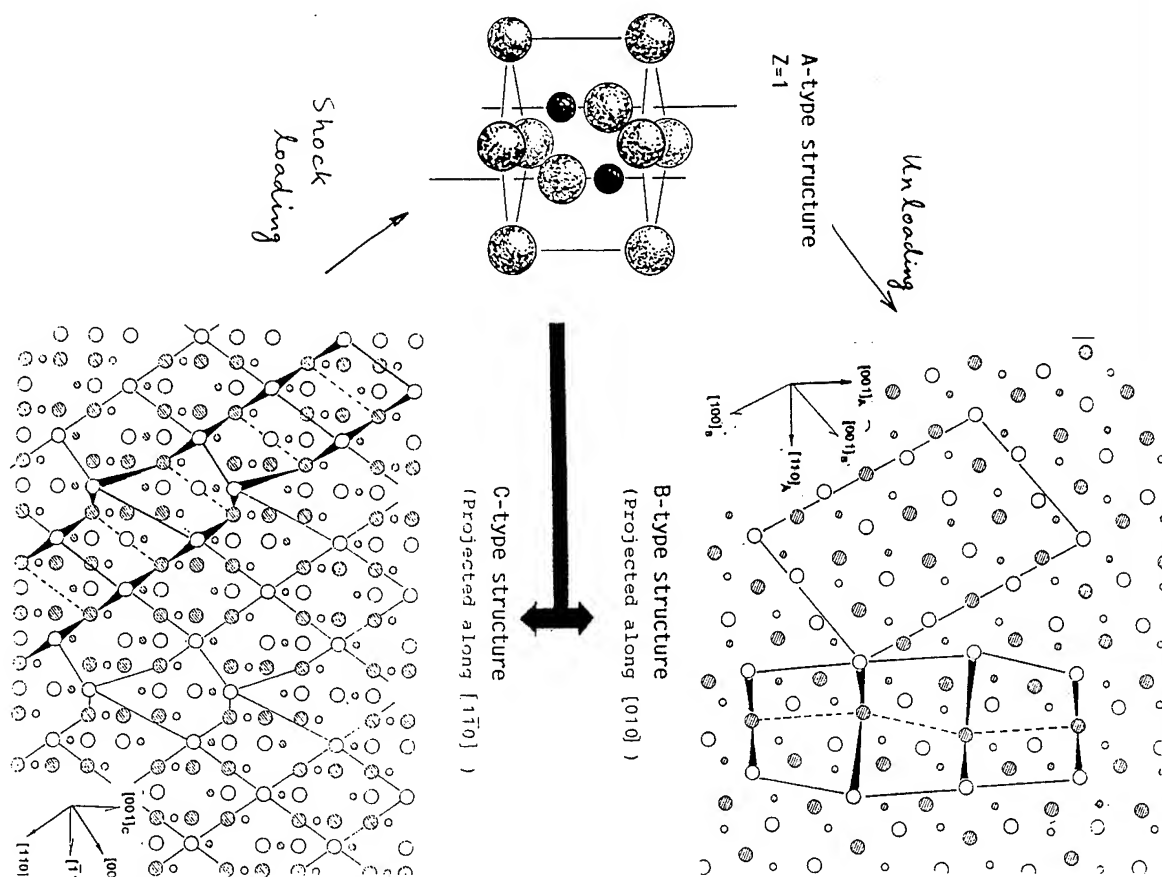
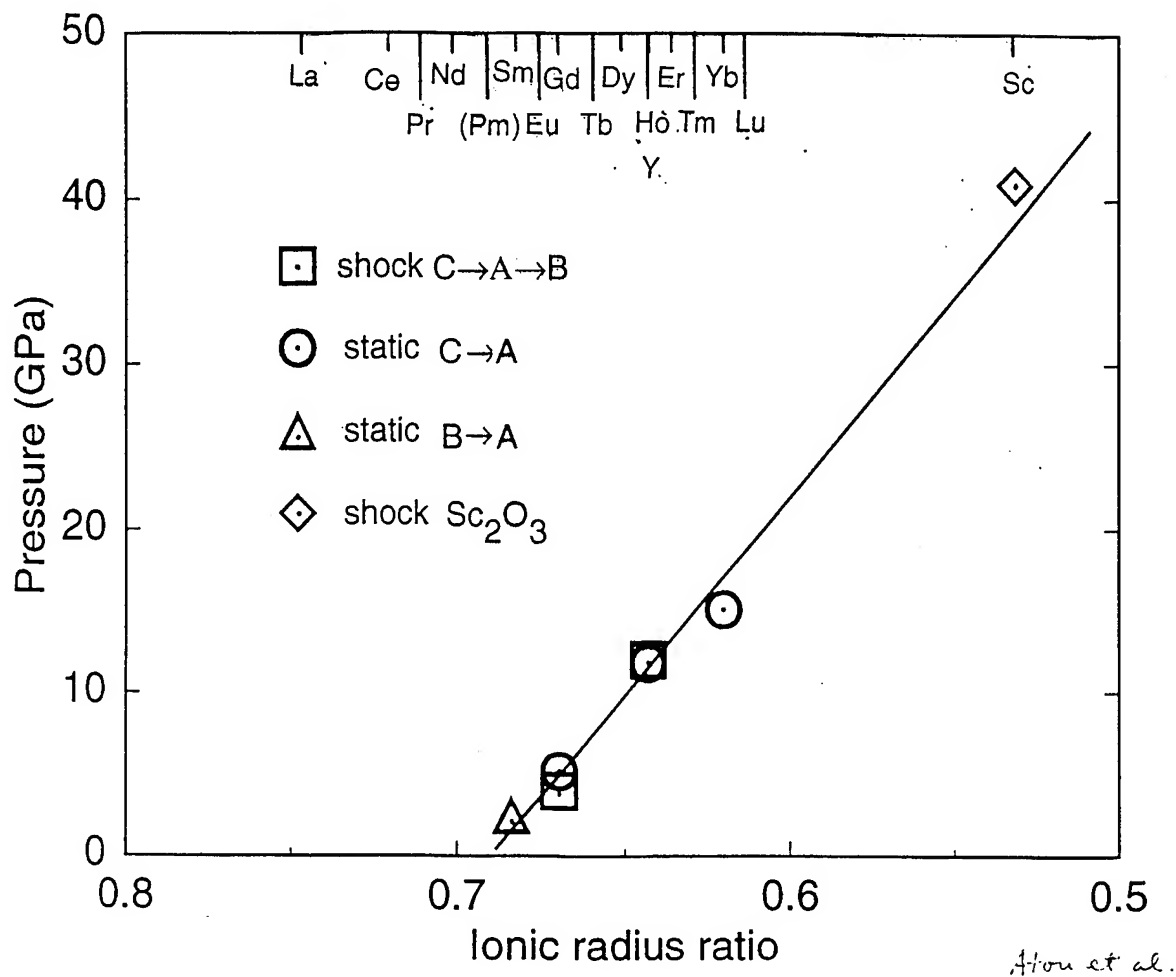


Hydrostatic Compression of Gd_2O_3

Hou et al.

Phase Transformation of Rare Earth Sesquioxides
in Shock Loading and Unloading





Shock Synthesis via Phase Transformation

Freezing of High Pressure Phase

w-BN

cf. hexagonal diamond

cf. c-BN & diamond

ZrSiO₄ (scaevite type)

cf. rutile

Nb₃Si (A15 type)

Metastable Phase Formation during Unloading

TiO₂ (α-PbO₂ type via fluorite)

Ln₂O₃ (B-type via A-type)

Factor Governing Reverse Reaction Kinetics

Chemical Bond

Rotation of Molecule

Impurity

Particle Size or Strain

Low Temperature

Short T-T bonds
linear chain

Non-stoichiometry allowed

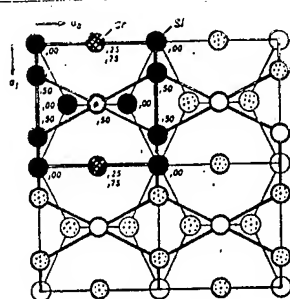
High T_c

Short T-X bonds

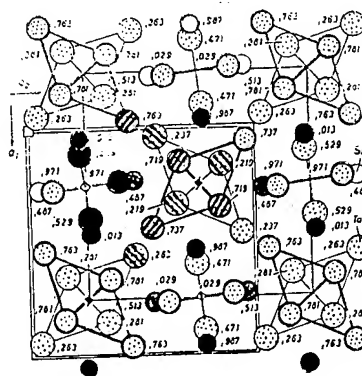
favored for electronegative elements
for X = Si, Ge, P, As, etc.

Stoichiometric

Low T_c



Nb₃Si (A15)



Ti₃P

Shock Transformation

in Nb₃Si

K. Takayama (Ed.)

Shock Waves

Proceedings
of the 18th International Symposium
on Shock Waves
Held at Sendai, Japan 21–26 July 1991

With 1268 Figures

Springer-Verlag
Berlin Heidelberg New York
London Paris Tokyo
Hong Kong Barcelona
Budapest

Professor Dr. Kazuyoshi Takayama

Shock Wave Research Center, Institute of Fluid Science,
2-1-1 Katahira, Aoba, Sendai 980, Japan

ISBN 3-540-55686-9 Springer-Verlag Berlin Heidelberg New York
ISBN 0-387-55686-9 Springer-Verlag New York Berlin Heidelberg

Library of Congress Cataloging-in-Publication Data. International Symposium on Shock Waves (18th : 1991 : Sendai-han, Japan) Shock waves : proceedings of the 18th International Symposium on Shock Waves, held at Sendai, Japan, 21-26 July 1991 / K. Takayama, ed. p. cm. Includes bibliographical references and index. ISBN 3-540-55686-9 (Berlin). – ISBN 0-387-55686-9 (New York) 1. Shock waves Congresses. 2. Shock waves—Industrial applications—Congresses. 3. Shock tubes—Congresses. 4. Fluid dynamics—Congresses. I. Takayama, K. (Kazuyoshi), 1940-. II. Title. QC168.85.S45I578 1991 531'.1133—dc20 92-29581

This work is subject to copyright. All rights are reserved, whether the whole or part of the material is concerned, specifically the rights of translation, reprinting, reuse of illustrations, recitation, broadcasting, reproduction on microfilms or in any other way, and storage in data banks. Duplication of this publication or parts thereof is permitted only under the provisions of the German Copyright Law of September 9, 1965, in its current version, and permission for use must always be obtained from Springer-Verlag. Violations are liable for prosecution under the German Copyright Law.

© Springer-Verlag Berlin Heidelberg 1992
Printed in Hong Kong

The use of general descriptive names, registered names, trademarks, etc. in this publication does not imply, even in the absence of a specific statement, that such names are exempt from the relevant protective laws and regulations and therefore free for general use.

Typesetting: Camera ready by author
55/3140 - 5 4 3 2 1 0 - Printed on acid-free paper

Phase changes in solids during shock loading and unloading

Y. Syono, K. Kusaba, T. Atou and K. Fukuoka

Institute for Materials Research, Tohoku University, Katahira, Aoba-ku, Sendai 980, JAPAN

Abstract. Polymorphic phase transformations have been found in many substances by shock compression. The transition pressures observed by dynamic and static compression are generally in good agreement, provided that the kinetics of phase changes, such as those which are displacive or electronic in origin, is sufficiently fast to be completed within the short time interval of a shock process. Molecular dynamical calculations of rutile under uniaxial stress showed that the phase transition to high pressure fluorite phase could be completed within a few picoseconds, much shorter than the shock rise time within the shock front. The fact that the phase transition pressures of rutile single crystals depends on the shock loading directions can also be explained, given the uniaxial nature of the plane shock loading within the shock front. On the other hand, there are also many examples in which the recovered materials cannot be considered as due to the shock-induced high pressure phase itself, but metastably formed during the unloading process. To apply the shock wave technique for materials synthesis, the importance of the knowledge on the shock-induced phase transformations as well as pressure-temperature history of shock process is mentioned.

Key words: Shock in condensed matter, Phase change

1. Introduction

Shock wave research on solid materials now celebrates its own history of almost half a century (Rice et al. 1958, Duvall and Fowles 1963) and has now established a unique world, compatible with that of the static high pressure experiments. The shock compression technique has been widely used for precise determination of the pressure-volume relation of various solids, and applied for the equation-of-state study at ultrahigh pressures. In the analysis of shock compression experiments in solids, the hydrodynamic approximation is adopted, since the shear stress in the compressed solids can be neglected when the shock strength exceeds the maximum shear strength. Agreement between the compression data obtained by dynamic and static means is sufficiently good, and provides the basis for using the shock compression data as a pressure standard for static high pressure measurements.

However, shock response of solids shows significant discrepancy with that of fluid. Firstly, a low diffusion rate limits the equilibrium to be attained within the very short time interval of the shock process. Furthermore lower compressibility, hence higher shock impedance, of condensed matter than that of gas induces a smaller increase in temperature by shock compression. Secondly, solids show a finite shear strength, which is particularly enhanced at low stress level, as exemplified in the Hugoniot elastic limit. The finite shear strength also causes the formation of shear bands upon shock loading, and heterogeneous yielding in brittle solids (Grady 1977). Although this is an important aspect in the discussion of shock effects in solids, here, only the case where hydrostatic and uniform pressures are approximately realized in shock compressed solids, will be dealt with.

2. Shock-induced phase transformations in solids

Phase transformations induced by shock waves have been known in many substances and are a central issue of shock wave research in solids (Duvall and Graham 1977; Syono 1986, 1988). For example, the 13 GPa transition in iron was first discovered in an elaborate shock loading experiment with a pin-contact method by Bancroft et al. (1956) as early as in 1955, and later confirmed by static high pressure experiments using X-ray diffraction (Takahashi and Bassett

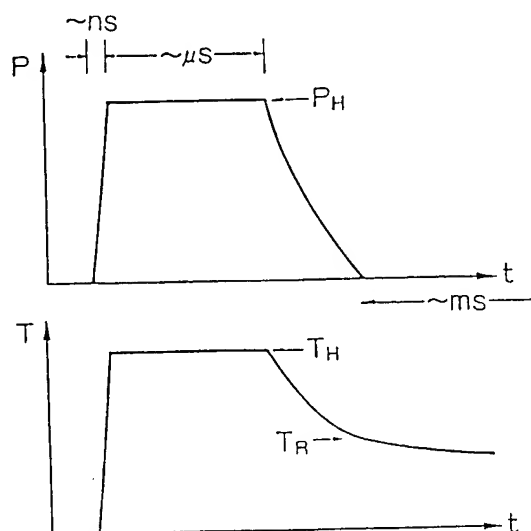


Fig. 1. Schematic illustration of pressure and temperature profile of shock wave. Suffix H or R means Hugoniot or residual respectively

1964). Soon after the first synthesis of diamond using a belt-type apparatus (Bundy et al. 1955), polycrystalline diamond powders were synthesized by shock processing (DeCarli and Jamieson 1961). More recently significant development in the diamond anvil technique has extended the range of static high pressures up to Megabars and allowed such comparisons at much higher stress level. Simultaneous detections of the B1-B2 transition in CaO at about 70 GPa (Jeanloz et al. 1979) and also the spin-pairing transition in Fe_2O_3 (Goto et al. 1982; Syono et al. 1984) in both dynamic and static experiments were typical examples.

In the phase transitions to be induced in a short time interval of shock loading, reaction kinetics should be most important (Horie and Duvall 1968; Hayes 1974). If the phase change is of a reconstructive nature governed by atomic diffusion, it may hardly be achieved by shock loading (Syono et al. 1981). The phase transition which can be realized in the shock process should be due to electron or displacive mechanisms. However, agreement between the phase transition pressures by dynamic and static pressures gives an impression that phase transitions proceed during the hydrostatic regime of the shock process.

The shock itself rises to full amplitude within a few nanoseconds, bringing the compressed substance into a thermodynamic state which subsists for about a microsecond in laboratory experiments (Fig. 1). Since the kinetics of most of these phase transitions is much faster than imagined, the reaction within a shock rising process may become important. If this is the case, structural rearrangements in the phase changes are considered to occur mostly within a shock front and some non-equilibrium effects such as anisotropy in the phase transition pressures could be explained.

Another important aspect of such fast transitions is easy reversion during the shock release process. Such fast transitions can be easily back-transformed to the ambient phase, or metastable phase on the rarefaction process. In that sense, reaction mechanisms occurring during both shock rise and release processes are most important for the understanding of the shock-induced phase transition. In the present article, phase changes under the shock process will be discussed in terms of mechanisms at the atomic level, putting focus on the phenomena within a shock front of steep rise time and also the rarefaction stage of the shock process.

3. Phase transitions during shock rise time within a shock front

Polymorphic phase transformations have been found in many substances by shock compression (Duvall and Graham 1977). The transition pressures observed by dynamic and static compression are also in good agreement (Jones and Graham 1971; Syono 1986), provided that the kinetics of the phase transformations is sufficiently fast to be completed within a short time interval of

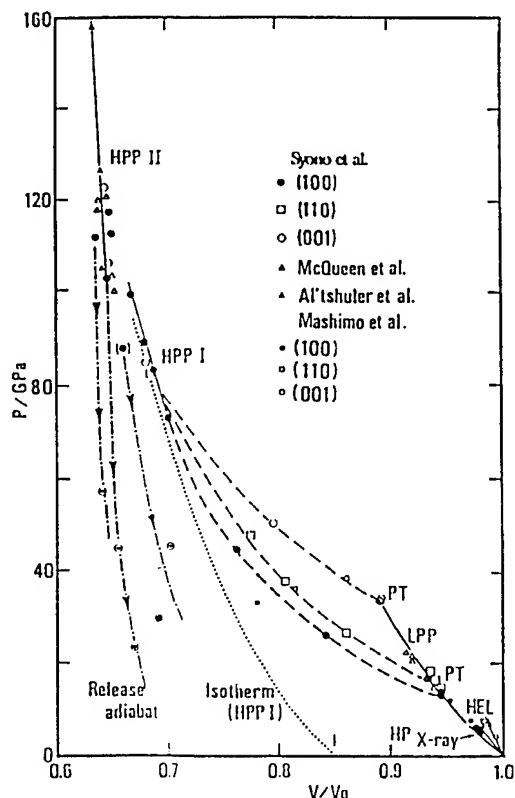


Fig. 2. Shock compression curve of rutile (TiO_2) single crystal (Syono et al. 1987). HEL, PT, LPP and HPP are Hugoniot elastic limit, phase transition, low pressure phase and high pressure phase respectively

the shock process, such as in phase transitions due to displacive or electronic origin. These fast phase transformations are generally induced by static high pressures and at room temperature, suggesting that a thermal activation process is not involved. However, phase transition pressures were reported to show remarkable dependence on the shock loading direction with respect to the crystallographic orientations (Fritz et al. 1971, Syono et al. 1987, Earskin and Nellis 1991). Such anisotropy in the phase transition pressure could be explained by considering the uniaxial nature of plane shock loading within the shock front. As a typical example, anisotropic phase transition in shocked rutile (TiO_2) single crystals will be elucidated here in detail.

Figure 2 shows the shock compression curve of rutile single crystals for various shock loading directions (Syono et al. 1987). The phase transition pressure was conspicuously lower for shock loading perpendicular to the tetragonal c axis, i.e. $[100]$ and $[110]$, than parallel to the c axis, $[001]$. From the estimated volume change of about 15 percent at zero pressure, the shock-induced high pressure phase was considered to have a fluorite-related structure, which was recently confirmed by static high pressure experiments (Sato et al. 1991). The anisotropic yield observed in the shock recovery experiments (Fig.3) was quite consistent with shock compression measurements, although the recovered phase had an $\alpha\text{-PbO}_2$ type structure which was presumably formed during shock unloading, as will be discussed in the next section (Kusaba et al. 1988).

A displacive mechanism which was compatible with that by Hyde et al. (1972) was proposed to explain the rutile-fluorite transition in the shock loading process, as illustrated in Fig.4 (Kusaba et al. 1988), and simulated by molecular dynamical calculations (Kusaba et al. 1990). Figure 5 shows how the rutile structure converts to the fluorite structure by the $[100]$ uniaxial compression. As the pressure increased to about 280 GPa within a picosecond, unit cell dimensions of both a and c axis of the rutile structure linearly decreased. In the next stage between 1-3 picoseconds, complete conversion to the fluorite structure was demonstrated. One of the a axis of the rutile structure continuously decreased, while the other a axis and c axis increased. Cubic fluorite structure was completely stabilized after 3 picoseconds. Contrary to the $[100]$ compression, $[001]$ compression

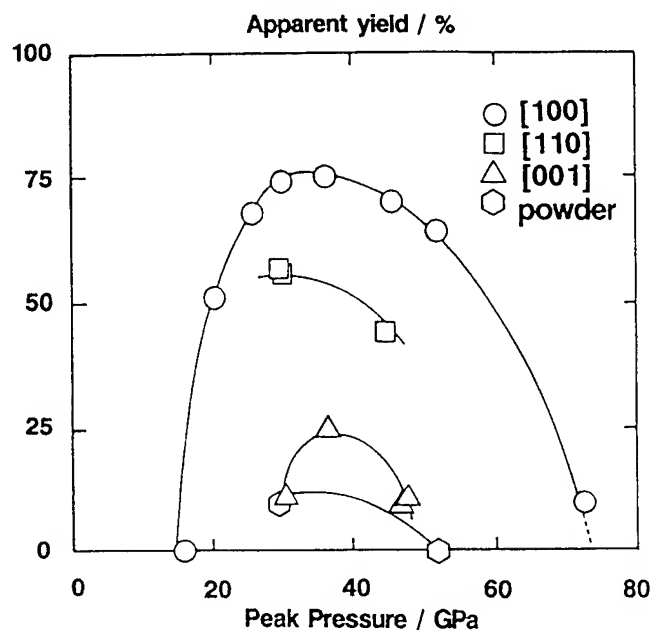


Fig. 3. Recovery yield of α -PbO₂ phase of TiO₂ versus shock pressure (Kusaba et al. 1988)

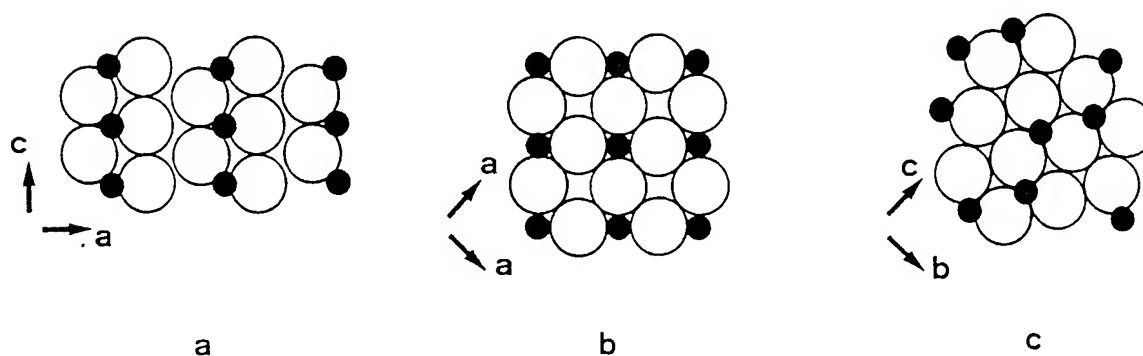


Fig. 4. Topological relationship between rutile (a), fluorite (b) and α -PbO₂ (c) structures. Large open circles and small solid circles are anion (O) and cation (Ti) ions respectively. Note the correspondence between uniaxially compressed rutile along the [100] direction and fluorite

did not lead to the formation of the fluorite structure, but to CaCl₂ type structure which was expected to have similar density of the rutile or α -PbO₂ type structure. The calculation clearly indicated that the phase transformation was completed within a few picoseconds which is far shorter than the rise time of the shock loading process, and the observed anisotropy was closely related to the crystal structure.

4. Formation of metastable phase in shock unloading

On the other hand, there are many examples in which the recovered materials could not be considered as the shock-induced high-pressure phase itself, but metastably formed during the unloading process. These metastable phases do not show high density as expected from Hugoniot measurements but show some structural relevance to the shock-induced high pressure phase. Formation of α -PbO₂ phase in TiO₂ and SnO₂ (Kusaba et al. 1988 1991) and the B-type rare earth oxide phase in T₂O₃ and Gd₂O₃ (Atou et al. 1990) are typical examples.

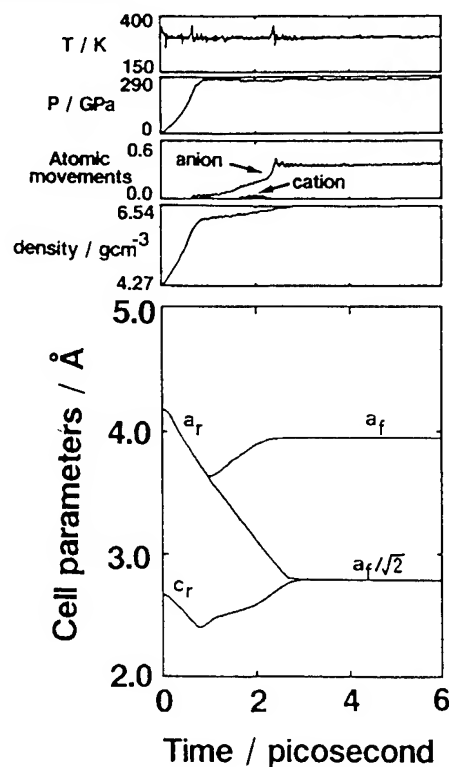


Fig. 5. Computer simulation of rutile-fluorite phase transition induced by [100] compression of rutile (Kusaba et al. 1990). Suffix r or f means rutile or fluorite, respectively

As has been discussed in the previous section, the α - PbO_2 phase of TiO_2 was metastably formed during the shock unloading process, since the α - PbO_2 phase was only denser by 2 % than rutile and could not be assigned as the observed high pressure phase which was at least 15 % denser than rutile (Syono et al. 1987). The instantaneous nature of fluorite- α - PbO_2 type phase transition was suggested by Seifert (1968) and also simulated by molecular dynamical calculations (Matsui and Kawamura 1987). Since the rutile-fluorite and fluorite- α - PbO_2 type phase transitions were shown to occur during shock loading and unloading process respectively in quite an orderly fashion within a very short time interval, a certain relation between relative orientations of each structure is expected. This was actually confirmed by electron microscopic observation of lamellae consisting of rutile and α - PbO_2 type phases which was found in the products recovered from the mixed phase region.

It is interesting to note that the shock-induced high pressure phase of ZrSiO_4 with the scheelite structure was retained after the shock pressure was released (Kusaba et al. 1985). Since the cationic arrangements in zircon and scheelite are considered to correspond to rutile and fluorite respectively, the combination of different cations with different coordination would play a role for the blocking mechanism which prevents the back transition. The fact that the zircon-scheelite transition was induced only at high temperatures and not at room temperature suggests involvement of a thermal activation process, in contrast to the rutile-fluorite transition which was induced at room temperature under static high pressure (Sato et al. 1991).

Shock-induced phase change analogous to the rutile-fluorite- α - PbO_2 type transition was recently found in the C-A-B phase transition in Y_2O_3 and Gd_2O_3 (Atou et al. 1990). The shock-induced phase was shown to have the B-type structure of rare earth oxides and the pressure dependence of its yield is shown in Fig. 6. However, the onset pressure of the B-type phase was found to be close to the stabilization pressure of the A-type phase of rare earth oxides rather than the B-type phase, as shown in a systematics between the transition pressure versus cationic radii in Fig. 7. Considering the close similarity between the A-type and B-type structures, it is natural

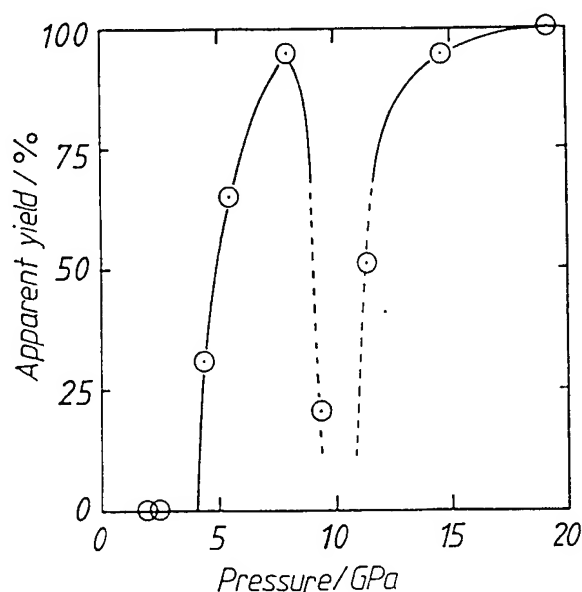


Fig. 6. Recovery yield of B-type Gd_2O_3 versus shock pressure (Atou et al. 1990)

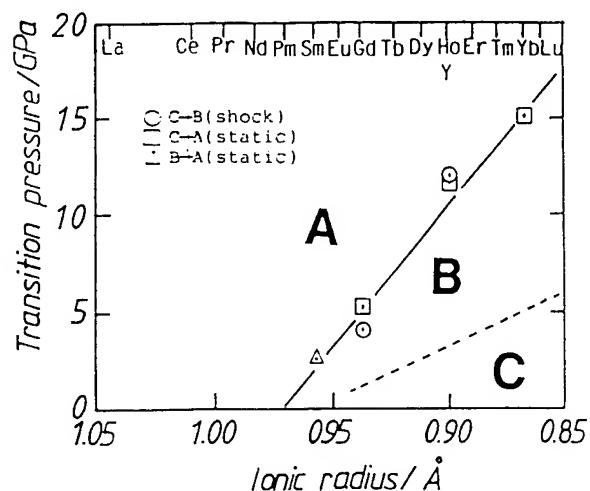


Fig. 7. Transition pressure of C-B-A phase change of rare earth sesquioxides versus cation radii (Atou et al. 1990)

to conclude that the recovered B-type phase was metastably formed during shock unloading from the shock-induced high pressure phase with the A-type structure.

The anomalous feature of shock yield for the B-type phase of Gd_2O_3 also provides important information about the effects of residual temperature. Decrease in the yield for 8 - 10 GPa was interpreted due to enhancement of back transition to the C-type phase by the increase in residual temperature with shock pressure. The reappearance of the B-type phase above 11 GPa could be explained by a residual temperature above about 1200 C which was sufficiently high to anneal out the induced A-type phase and to stabilize the B-type structure at ambient pressure.

Formation of metastable phases during the shock unloading process is not necessarily of crystalline phases but amorphous ones. Many tectosilicate minerals such as quartz or feldspar are known to transform to so-called diaplectic glass, which is denser than the corresponding fused glass and shows microcrystalline nature, indicating glass formation due to solid-solid transition (Arndt 1984, Okuno et al. 1985).

Completely different kinds of phase change inducible in the shock unloading process occurs in the decomposition reaction accompanied by degassing. Evidence for decomposition reactions during shock unloading was suggested by compressing vanadium hydride above 100 GPa (Syono et al. 1984). Similar decomposition reactions such as dehydration or devolatilization by shock loading have been reported, although their mechanism has not been clarified yet (Boslough et al. 1982, Lange et al. 1985).

5. Concluding remarks

Phase transformations under shock loading have been utilized for synthesis of new materials with high pressure phases. Several successful cases including graphite-diamond conversion by shock processing have been reported so far. However, yield of the high pressure phases critically depends on the kinetics of the phase changes and the stability of the induced phases. Furthermore, compared with static high pressure synthesis, synthesis via shock processing suffers from the serious drawback of residual temperature; Shock temperature is not subdued to the starting value after the release of shock pressure and the residual temperature exponentially increases in accordance with the increase of the shock pressure and porosity of the starting materials. Therefore high pressure phases once formed by shock loading are susceptible to be annealed out

to the starting low pressure phase in the post-shock process. In that sense information on the phase change mechanism under shock processing as well as knowledge of the pressure-temperature history of the shock process is needed to apply the shock wave technique for materials synthesis or processing, and promote the efficiency of the synthesis yield.

Acknowledgements

The authors wish to thank Y. Matsui, Institute for Study of the Earth's Interior, Okayama University, T. Goto, Institute for Solid State Physics, University of Tokyo, and M. Kikuchi, IMR, Tohoku University, for their invaluable contributions to this work. The work was partly supported by a Grant-in-Aid for Scientific Research of Priority Areas, Shock Wave Research, supported by Ministry of Education, Science and Culture of Japan.

References

- Al'tshuler LV, Podurets MA, Simakov GV, Trunin RF (1973) High-density forms of fluorite and rutile. *Sov Phys Solid State* 15:969-971
- Arndt J (1984) Shock isotropization of minerals. In: Asay JR, Graham RA, Straub GK (eds) *Shock waves in condensed matter-1983*, North Holland, Amsterdam, pp 473-480
- Atou T, Kusaba K, Fukuoka K, Kikuchi M, Syono Y (1990) Shock-induced phase transition of M_2O_3 ($M = \text{Sc, Y, Sm, Gd and In}$)-type compounds. *J Solid State Chem* 89:378-384
- Bancroft D, Peterson EL, Minshall S (1956) Polymorphism of iron at high pressure. *J Appl Phys* 27:291-298
- Boslough MB, Ahrens TJ, Vizgirda J, Becker RH, Epstein S (1982) Shock-induced devolatilization of calcite. *Earth Planet Sci Lett* 61:166-170
- Bundy FP, Hall HT, Strong HM, Wentorf RH Jr (1955) *Nature* 176:51
- DeCaril PS, Jamieson JC (1961) Formation of diamond by explosive shock. *Science* 133:1821-1822
- Duvall GE, Fowles GR (1963) Shock waves. In: Bradley RS (ed) *High pressure physics and chemistry* 2:209-291
- Duvall GE, Graham RA (1977) Phase transitions under shock wave loading. *Rev Mod Phys* 49:523-579
- Earskin DJ, Nellis WJ (1991) Shock-induced martensitic phase transformation of oriented graphite to diamond. *Nature* 349:317-319
- Fritz JN, Marsh SP, Carter WJ, McQueen RG (1971) The Hugoniot equation of state of sodium chloride in the sodium chloride structure. In: *Accurate Characterization of the High Pressure Environment*, US National Bureau of Standards, Special Publication 326:201-208
- Goto T, Sato J, Syono Y (1982) Shock-induced spin-pairing transition in Fe_2O_3 due to the pressure effect on the crystal field. In: Akimoto S, Manghnani H (eds) *High-pressure research in geophysics*, Terra Sci Publ, Tokyo, pp 595-609
- Grady DE (1977) Processes occurring in shock wave compression of rocks and minerals. In: Manghnani MH, Akimoto S (eds) *High pressure research: applications in geophysics*, Academic Press, New York, pp 389-438
- Hayes (1974) Polymorphic phase transformation rates in shock-loaded potassium chloride. *J Appl Phys* 45:1208-1217
- Horie Y, Duvall GE (1968) Shock waves and kinetics of solid-solid transitions. In: *Proc of Army Symposium on Solid Mechanics*, John Hopkins University, Maryland
- Hyde BG, Bursill LA, O'Keeffe M, Anderson S (1987) Continuous topological variation in coordination in crystals. *Nature Phys Sci* 237:35-38
- Jeanloz R, Ahrens TJ, Mao HK, Bell PM (1979) B1-B2 transition in calcium oxide from shock wave and diamond-cell experiments. *Science* 206:829-830

- Jones DE, Graham RA (1971) Shear strength effects on phase transition "pressure" determined from shock compression experiments. In: *Accurate Characterization of the High Pressure Environment*, US National Bureau of Standards, Special Publication 326:229-242
- Kusaba K, Syono Y, Kikuchi M, Fukuoka K (1985) Shock behavior of zircon: phase transition to scheelite structure and decomposition. *Earth Planet Sci Lett* 72:433-439
- Kusaba K, Kikuchi M, Fukuoka K, Syono Y (1988) Anisotropic phase transition of rutile under shock compression. *Phys Chem Miner* 15:238-245
- Kusaba K, Syono Y, Matsui Y (1990) Molecular dynamics calculation of rutile-fluorite phase transition induced by uniaxial compression. In: *Shock Waves in Condensed Matter-1989*, Eds Schmidt SC, Johnson JN, Davison LW, North Holland, Amsterdam: 135-138
- Lange MA, Lambert P, Ahrens TJ (1985) Shock effects on hydrous minerals and implications for carbonaceous meteorites. *Geochim Cosmochim Acta* 49:1715-1726
- Mashimo T, Nagayama K, Sawaoka A (1983) Anisotropic elastic limits and phase transitions of rutile phase TiO_2 under shock compression. *Appl Phys* 54:5043-5048
- Matsui Y, Kawamura K (1987) Computer experimental synthesis of silica with the $\alpha\text{-PbO}_2$ structure. In: Mangnani MH, Syono Y (eds) *High-pressure research in mineral physics*, Terra/AGU, Tokyo/Washington DC, pp 305-311
- McQueen RG, Jamieson JC, Marsh SP (1967) Shock-wave compression and X-ray studies of titanium dioxide. *Science* 155:1401-1404
- Okuno M, Marumo F, Syono Y (1985) The structure of a shock-induced anorthite glass. *Mineral J (Japan)* 12:197-205
- Rice MH, McQueen MG, Walsh JM (1985) Compression of solids by strong shock waves. In: Seitz F, Turnbull D (eds) *Solid state physics*, Academic Press, New York, pp 1-60
- Sato H, Endo S, Sugiyama M, Kikegawa T, Shimomura O, Kusaba K (1990) Baddeleyite-type high-pressure phase of TiO_2 . *Science* 251:786-788
- Seifert KF (1968) Untersuchungen zur Druck-Kristallchemie der AX_2 -Verbindungen. *Fortschr Miner* 45:214-280
- Syono Y (1986) Mechanism of phase changes under the shock process. In: Graham RA, Sawaoka AB (eds) *High pressure explosive processing of ceramics*, Transtech, Aedermansdorf, pp 377-400
- Syono Y (1988) Shock-induced phase transitions in solids: Their understanding at atomistic level. In: Schmidt SC, Holmes NC (eds) *Shock waves in condensed matter-1987*, North Holland, Amsterdam, pp 19-26
- Syono Y, Goto T, Sato J, Takei H (1981) Shock compression measurements of single-crystal forsterite in the pressure range 15-93 GPa. *J Geophys Res* 86:6181-6186
- Syono Y, Ito A, Morimoto S, Suzuki T, Yagi T, Akimoto S (1984) Mössbauer study on the high pressure phase of Fe_2O_3 . *Solid State Commun* 50:97-100
- Syono Y, Kusaba K, Fukuoka K, Fukai Y, Watanabe K (1984) Shock compression of V_2H and V_2D and anomalous decompression behavior. *Phys Rev B* 29:6520-6524
- Syono Y, Kusaba K, Kikuchi M, Fukuoka K, Goto T (1987) Shock-induced phase transitions in rutile single crystal. In: Manghnani MH, Syono Y (eds) *High pressure research in mineral physics*, Terra/AGU, Tokyo/Washington DC, pp 385-392
- Takahashi T, Bassett WA (1964) High-pressure polymorph of iron. *Science* 145:483-486

MATERIALS SYNTHESIS BY SHOCK-INDUCED AND SHOCK-ASSISTED SOLID-STATE CHEMICAL REACTIONS

N.N. Thadhani

School of Materials Science and Engineering
Georgia Institute of Technology, Atlanta, GA 30332-0245

We are investigating the synthesis of materials by shock-compression of powder mixtures which lead to chemical reactions resulting in the formation of equilibrium and non-equilibrium phases, as well as compounds with radically modified microstructures. The reactions occur as manifestations of enhanced solid-state chemical reactivity of powders, caused by configurational changes and defect states introduced during shock-compression. Two types of reactions are possible: *shock-induced* chemical reactions occurring during the shock-compression state, in time scales of *pressure equilibrium*, and *shock-assisted* reactions occurring after unloading to ambient pressure, in time scales of *temperature equilibrium*.

Strong evidence exists, based on real-time measurement studies of various investigators, to believe that the occurrence of shock-induced chemical reaction in the microsecond duration is indeed possible. Post-shock microstructural analysis of recovered products also reveals characteristics which can be distinguished on the basis of whether the reactions have occurred by the "*shock-induced*" or "*shock-assisted*" mode.

Shock-assisted chemical reactions are initiated due to bulk shock temperature increases (in time scales of thermal equilibration) by processes involving defect-enhanced solid-state diffusion in an essentially shock-modified material. The rapid dissipation of the heat of the diffusion reaction, limits product formation only at localized regions. The microstructures produced are, thus, typical of those observed during solid-state diffusion couple experiments. *Shock-induced* reactions on the other hand, show products forming in bulk regions, with microstructural characteristics typical of self-sustained exothermic reactions, in which the reaction time is shorter than the time required for the dissipation of the heat of reaction. Shock-induced reactions, therefore, require mechanisms different from those involving conventional solid-state nucleation and growth processes from either the liquid or the solid phase. The complex nature of rate-dependent processes occurring during shock-compression of powders, evident from investigations of recovery and instrumented experiments and numerical modeling studies, have precluded the development of theories of actual reaction mechanisms.

In this presentation, mechanistic aspects that distinguish between *shock-induced* and *shock-assisted* chemical reactions will be described. Results of time-resolved pressure measurements performed on Ti-Si powder mixtures, coupled with recovery experiments on the same powder mixtures will be presented. The effects of configurational changes introduced as powder particles are deformed or fractured during shock compression, and the influence of material

properties (flow and fracture characteristics) and shock-loading conditions on such effects, will be analyzed to provide pointers for mechanisms of processes leading to chemical reaction initiation and compound formation. The utilization of both types of reaction processes for synthesis of intermetallic compounds and ceramics, containing refined microstructures, will also be discussed.

The work presented here has been performed in collaboration with R. A. Graham and his coworkers at Sandia National Laboratories, and graduate students E. Dunbar (NMT), H.A. Grebe (NMT), V. Joshi (NMT), J.H. Lee (GT) and T. Royal (GT). The research funding has been provided in part by ARO Grant No. DAAH04-93-G-0062, NSF Grant No. DMR-9396132 and Sandia National Laboratories Contract No. 42-5737.

REFERENCES

R.A. Graham, "Solids Under High Pressure Shock Compression: Mechanics, Physics, and Chemistry," Springer Verlag, 1993.

A.N. Dremin and O.N. Breusov, "Processes Occurring in Solids Under the Action of Powerful Shock Waves," Russian Chemical Reviews, 37 (5) (1968) 392.

R.A. Graham, B. Morosin, E.L. Venturini and M.J. Carr, "Materials Modification and Synthesis Under High Pressure Shock Compression," Ann. Rev. Mat. Sci., 16(1986)315.

N.N. Thadhani, "Shock-induced Chemical Reactions and Synthesis of Materials," Progress in Materials Science, Vol. 37, No. 2, (1993) pp. 117-226

N.N. Thadhani, "Shock-induced and Shock-assisted Solid-State Chemical Reactions," J. Appl. Phys., to be published in August 1994 (in press).

S.S. Batsanov, G.S. Doronin, S.V. Klochkov and A.I. Teut, "Synthesis Reactions Behind Shock Fronts," *Combustion, Explosion, and Shock Waves*, 22 (6), p. 134, 1986.

E. Dunbar, R. A. Graham, G.T. Holman, M.U. Anderson, and N.N. Thadhani, "Time-resolved Pressure Measurements in Chemically Reacting Powder Mixtures"; N.N. Thadhani, E. Dunbar, and R.A. Graham, "Characteristics of Shock Compressed Configuration of Ti and Si Powder Mixtures"; and G.T. Holman, R.A. Graham, and M.U. Anderson, "Shock Response of Porous $2\text{Al}+\text{Fe}_2\text{O}_3$ Mixtures," in Proc. of AIRAPT/APS High Pressure Science and Technology Conference, 28 June to 2 July, 1993, Colorado Springs, ed., S.C. Schmidt, in press.

I. Song and N.N. Thadhani, "Synthesis of Nickel-Aluminum Intermetallic Compounds by Shock-induced Chemical Reactions", J. Mater. Synthesis and Processing, Vol. 1, No. 5, 1993, p. 347.

MATERIALS SYNTHESIS BY SHOCK-INDUCED AND SHOCK-ASSISTED CHEMICAL REACTIONS

Naresh N. Thadhani

School of Material Science and Engineering
Georgia Institute of Technology, Atlanta, GA.

May 24-26, 1994

*ARO Sponsored Workshop on Shock
Synthesis of Materials*

OUTLINE

- General Objectives and Approach
- Shock-Compression Characteristics (Powders)
- Shock-Induced and Shock-Assisted Reactions
- Shock-Assisted Chemical Reactions
(mechanisms and microstructural characteristics)
- Shock-Induced Chemical Reactions
(evidence, mechanisms, characteristics)
- Materials Synthesis Applications
- Summary and Concluding Remarks

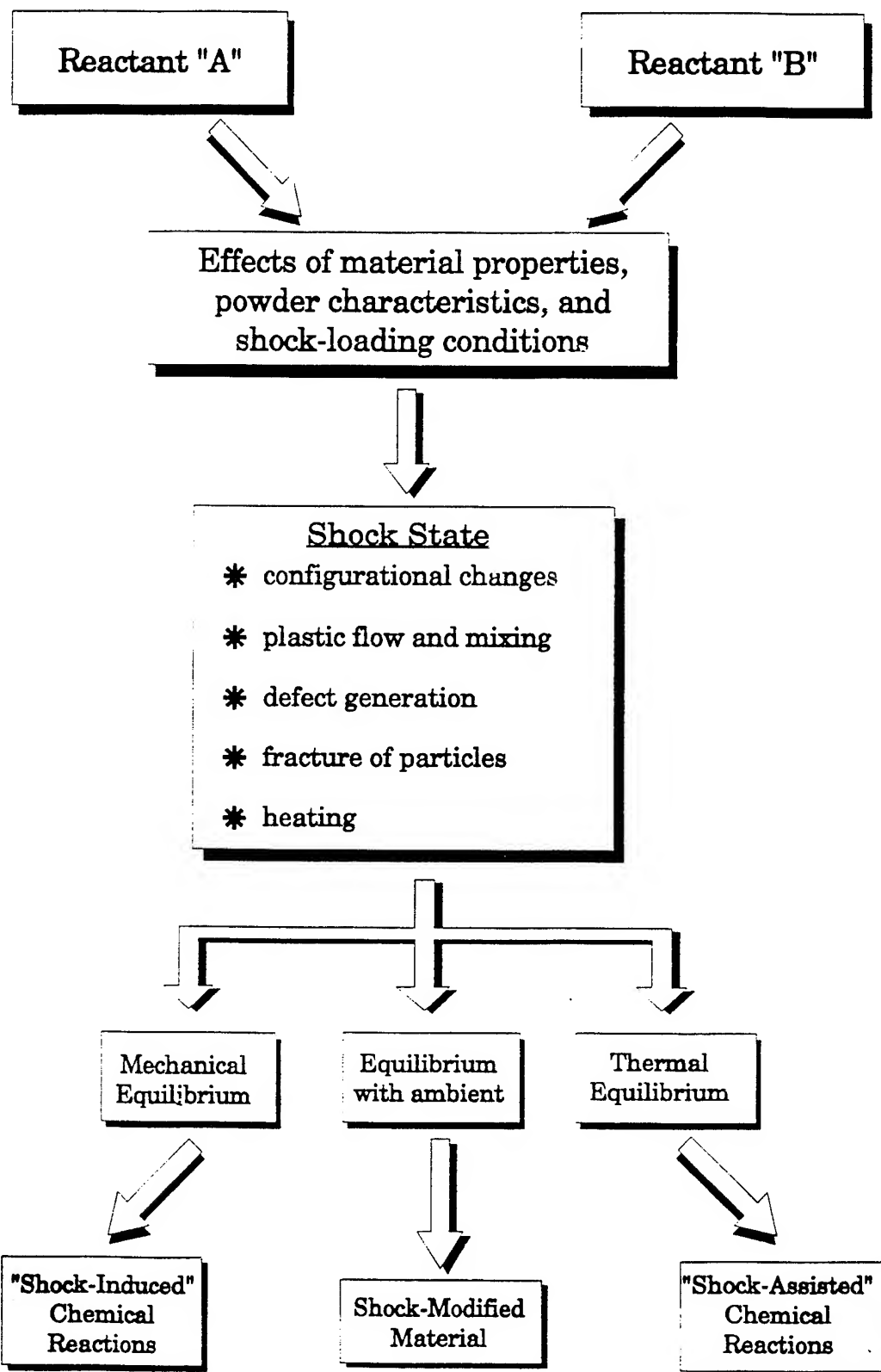
MATERIALS SYNTHESIS BY SHOCK CHEMISTRY

(OBJECTIVES)

To understand reaction mechanisms for control of microstructure and properties of synthesized materials.

- Mechanism**
- Solid-State (diffusional or diffusionless)
 - Liquid-State (dissolution / reprecipitation)
 - Exothermicity Effects

- Kinetics**
- During Shock State [Shock-Induced]
(pressure equilibrium, 1-2 μ s)
 - After Unloading [Shock-Assisted]
(temperature equilibrium, tens of μ s)
 - No Reaction [Shock-Modified]
(equilibrium with ambient)

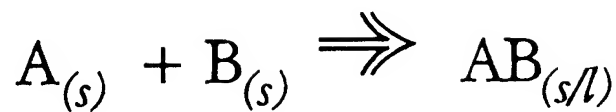


SHOCK-ASSISTED CHEMICAL REACTIONS

- * Mechanism involves defect-enhanced solid-state diffusion due to bulk temperature increases in time scales of temperature equilibration.
- * Reactions occur in localized interparticle regions (few μm)
- * Microstructure characterized by clean grains with no evidence of melting and solidification
- * "Shock-assisted" reactions used as a post-shock process in which reactant-mixture compacts are subsequently reaction sintered produce very fine grain sizes ($< \text{few } \mu\text{m}$)

SOLID-STATE DIFFUSION REACTIONS

(1-D diffusion couple)



$$\text{time} = t \cong \frac{p^2}{64D_v} \cong \frac{p^2}{64D_o \exp(-G/RT)}$$

(Defect-enhanced diffusion, Whittenberger, 1990)

$$\text{Replace } D_v \text{ by } D_d = f_L D_L + f_c D_c \cong D_v + 0.005 D_c$$

$$t \cong \frac{p^2}{64D_v} \cong \frac{p^2}{64 [D_o \exp(-G/RT) + 0.005 \{D_o \exp(-G/RT)\}]}$$

p = particle diameter = diffusion distance

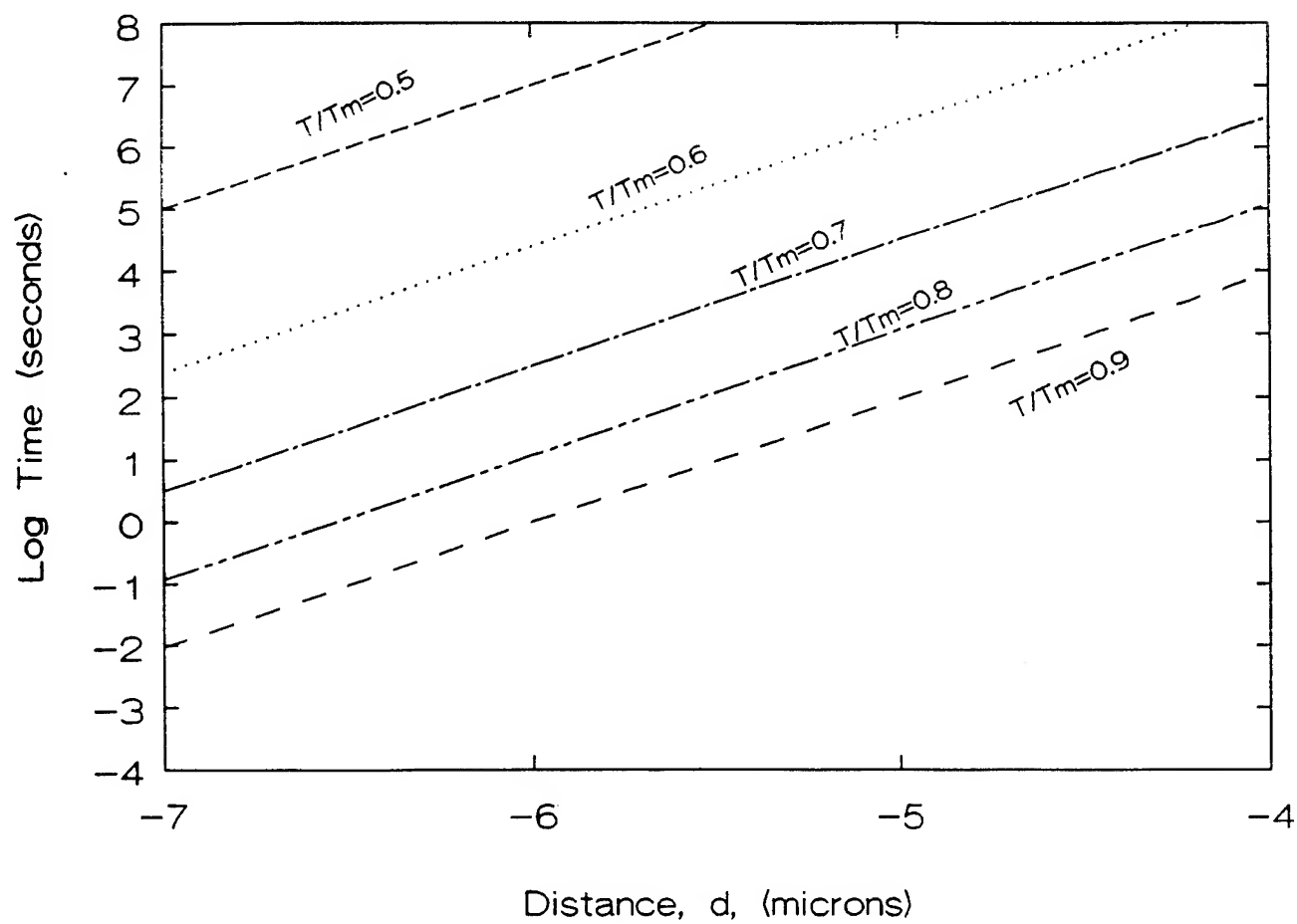
D_v = temperature dependent bulk diffusivity

D_o = diffusion constant ($10^{-5} \text{ m}^2/\text{s}$)

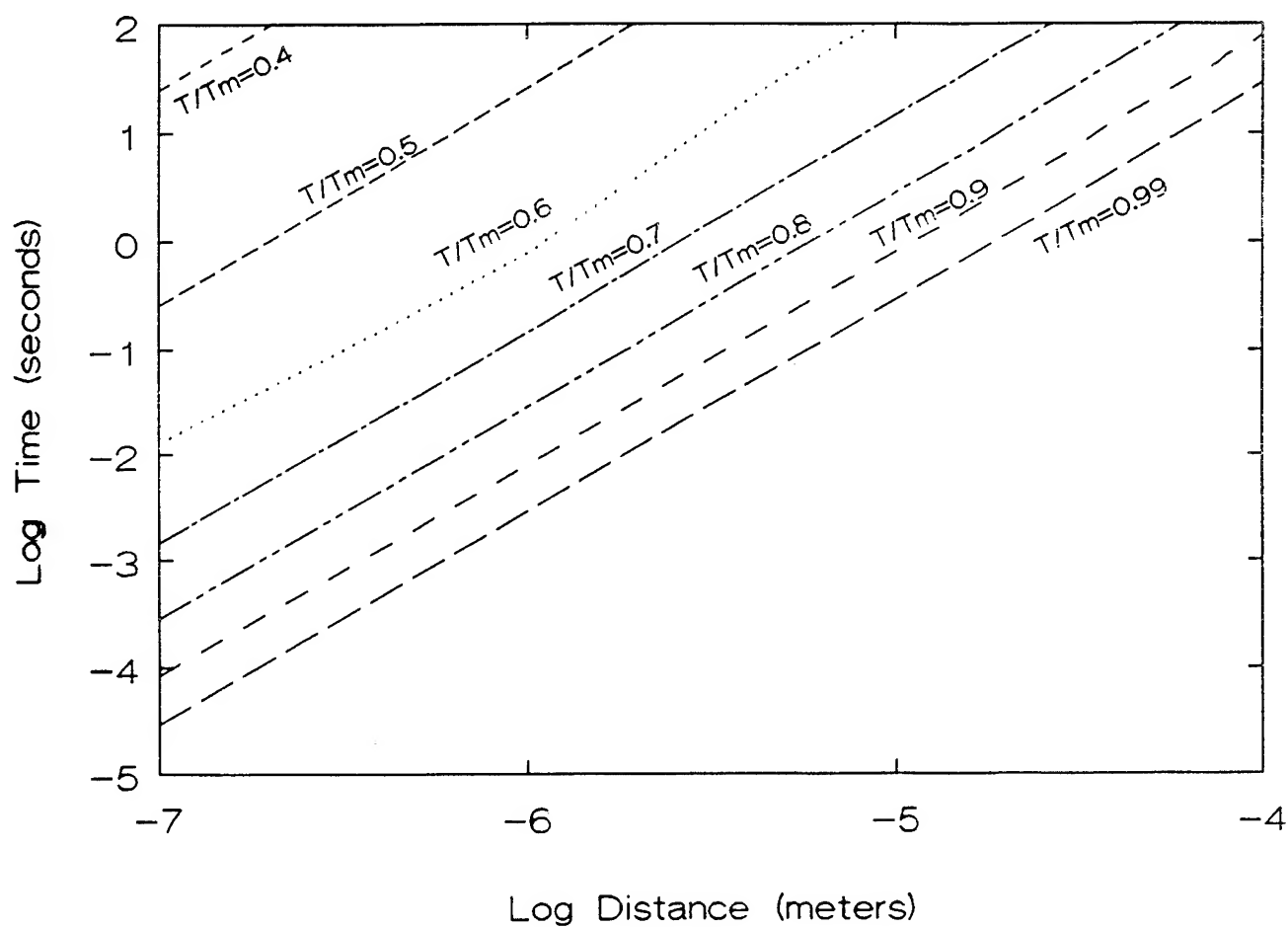
Q = activation energy ($\cong 151 T / T_m \text{ kJ/mol}$)

R = gas constant, and T = Temperature

SOLID-STATE DIFFUSION COUPLE



SOLID-STATE DIFFUSION COUPLE WITH DEFECT-ENHANCED DIFFUSION



Shock Compressed TiC Compact (88% dense) \Rightarrow Reaction Sintered at 20°C/min.



at 1600°C in Ar, 12 min. hold

SHOCK-INDUCED CHEMICAL REACTIONS

(Titanium-Silicon System)

Ti-Si SYSTEM

- highly exothermic ($\Delta H_R = -72.5 \text{ J/g.atom}$)
- combustion reaction mechanism dependent on powder morphology and heating rate
- Mechanical alloying forms amorphous state

PRESENT WORK

- Ti-Si powders of three different sizes
- time-resolved (PVDF gage) experiments
- shock-recovery experiments
 - ☆ determine reaction threshold
 - ☆ characterize unreacted configuration

Ti-Si POWDER MIXTURES

100μm



FINE

1-3 μm Ti

<5 μm Si



MEDIUM

10-45 μm Ti

10-45 μm Si

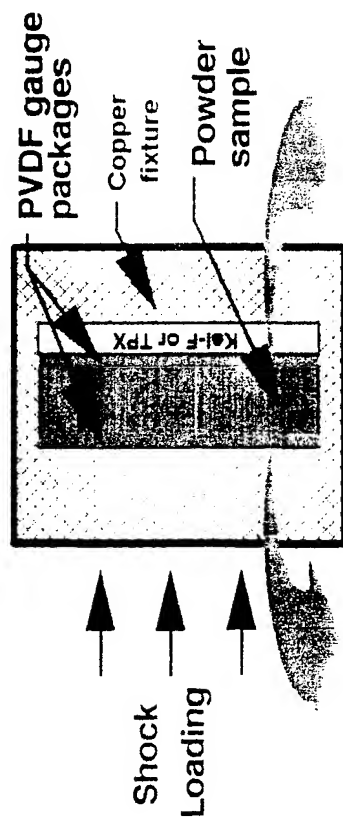


COARSE

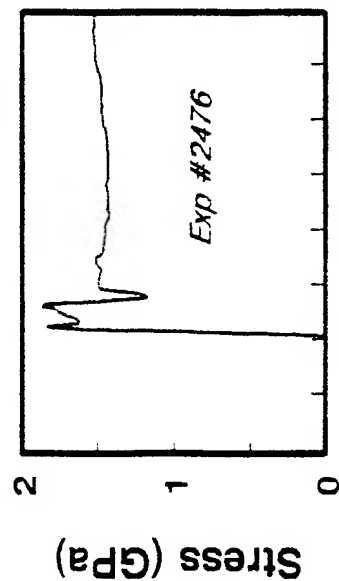
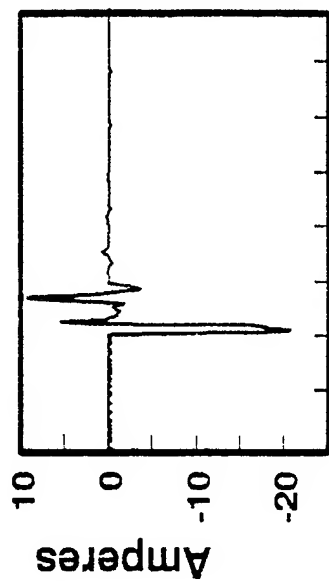
105-149 μm Ti

45-149 μm Si

Stress-Rate Dependent Measurements

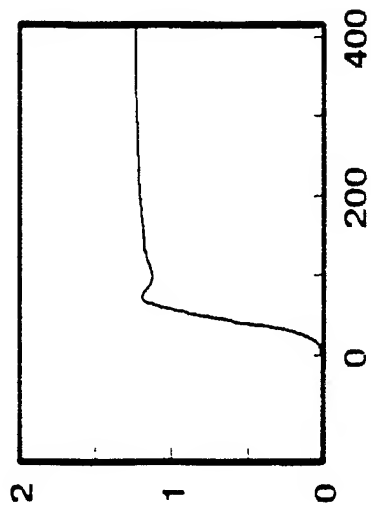
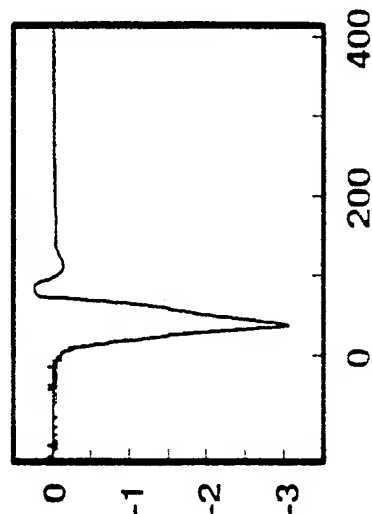


Input



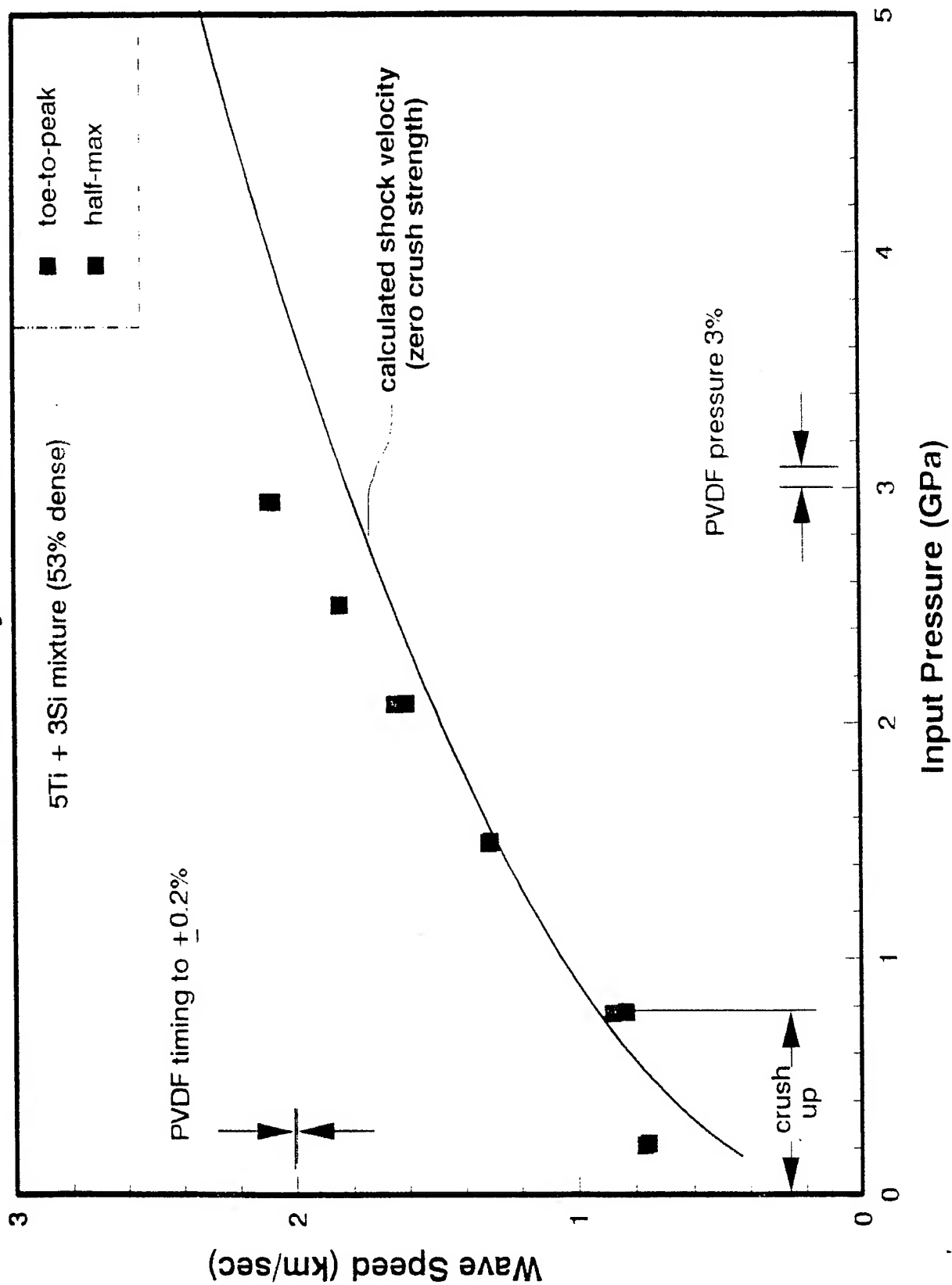
Time (nanoseconds)

Propagated Wave

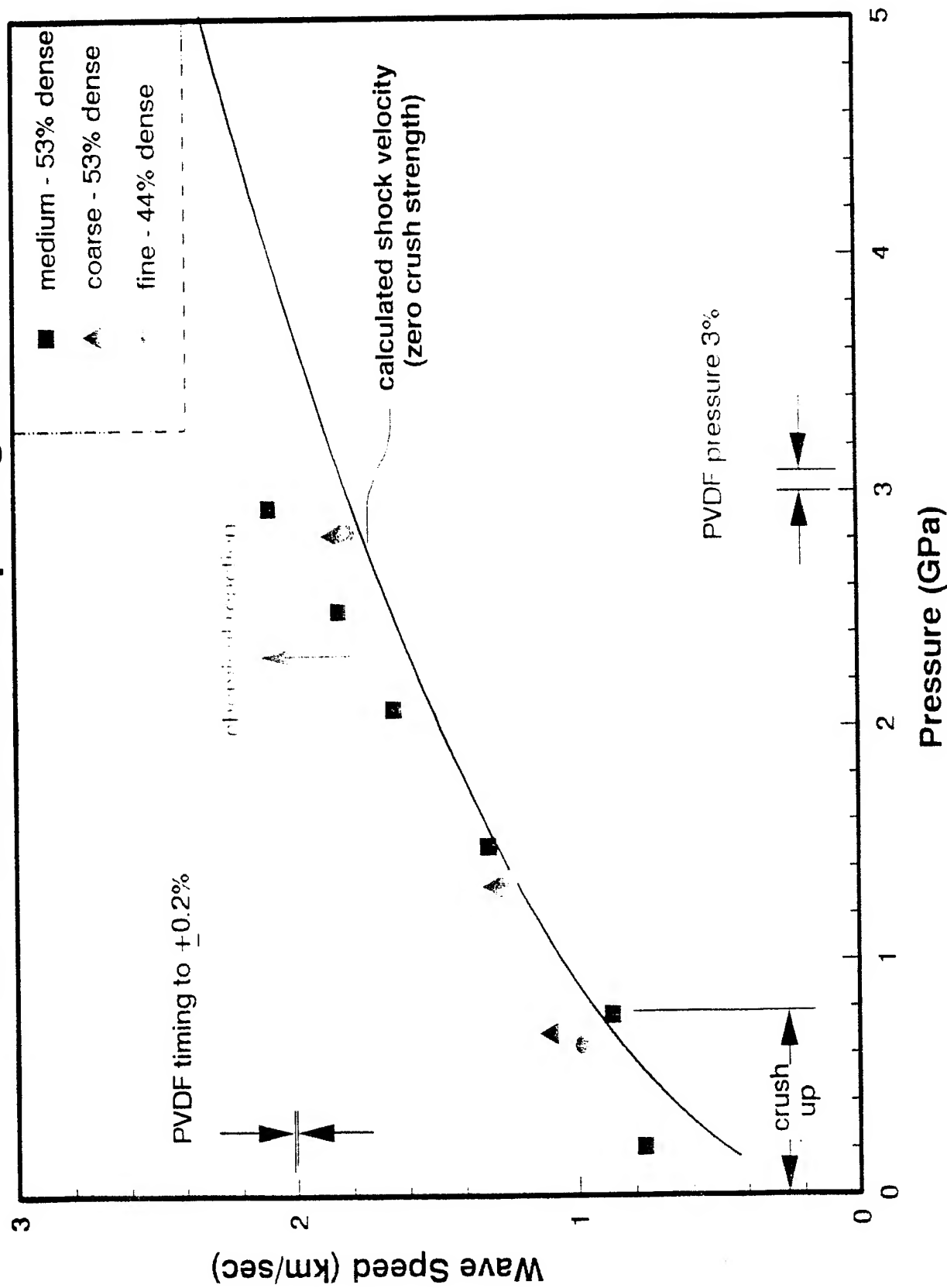


Time (nanoseconds)

Wave Velocity - Pressure



5Ti + 3Si various morphologies



BEAR FIXTURE SHOCK CONDITIONS

(based on 2D numerical simulations on 50% dense Rutile powder by Norwood, 1985)

Momma Bear - Comp B

(31.8 mm ϕ x 6.35 mm thick)

Momma Bear - Baratol

(31.8 mm ϕ x 6.35 mm thick)

Poppa Bear - Baratol

(45.7 mm ϕ x 6.35 mm thick)

Pressure:

Bulk - 18 GPa
Focus - 41 GPa

Bulk - 7.5 GPa
Focus - 27 GPa

Bulk - 5 GPa
Focus - 4.5 GPa

Mean Bulk Temperature (50% dense):

Bulk - 425°C
Edge - 550°C

Bulk - 22.5°C
Edge - 250

Bulk - 150°C
Edge - 75°C

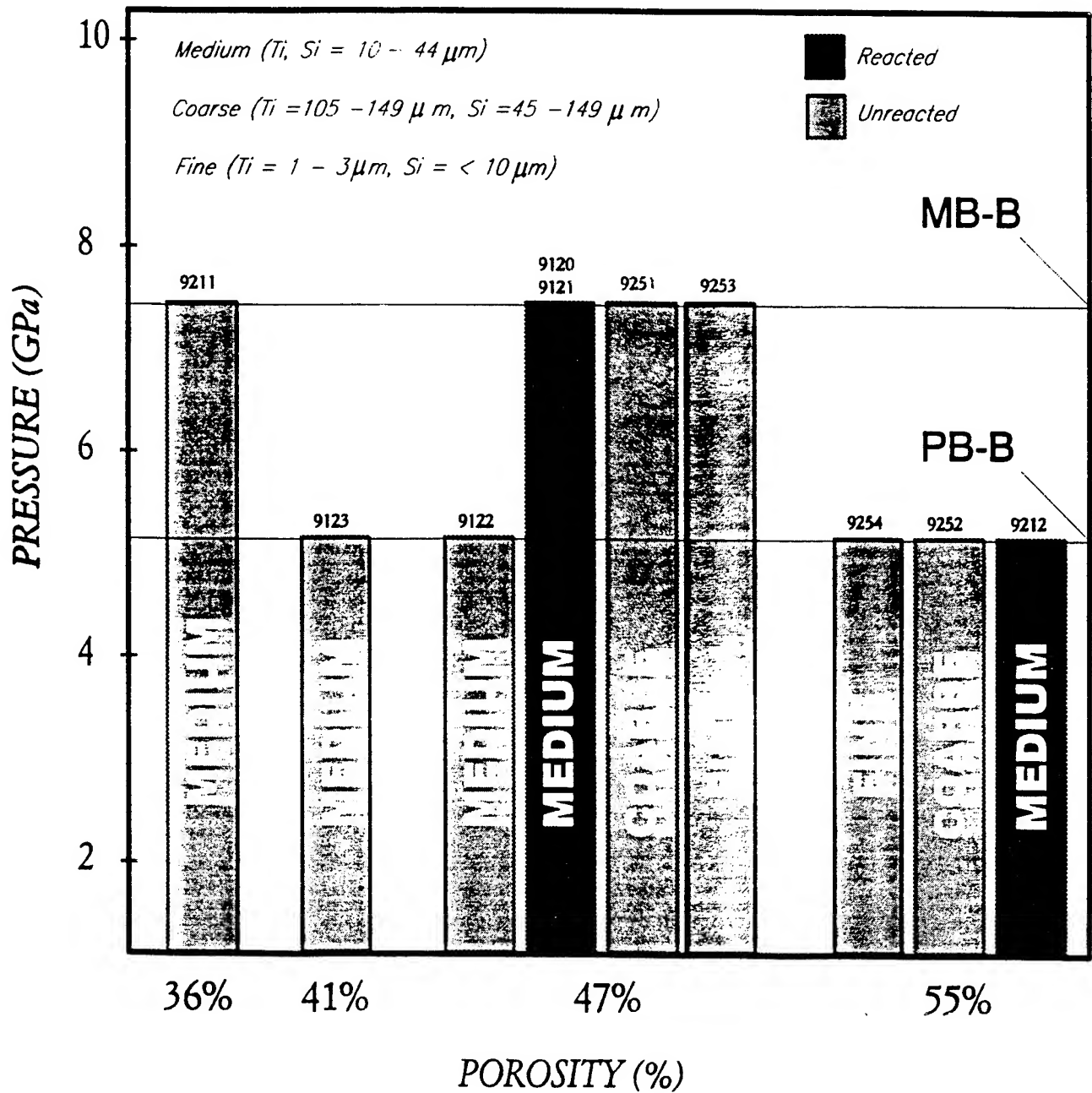
SHOCK-COMPRESSION EXPERIMENTS*

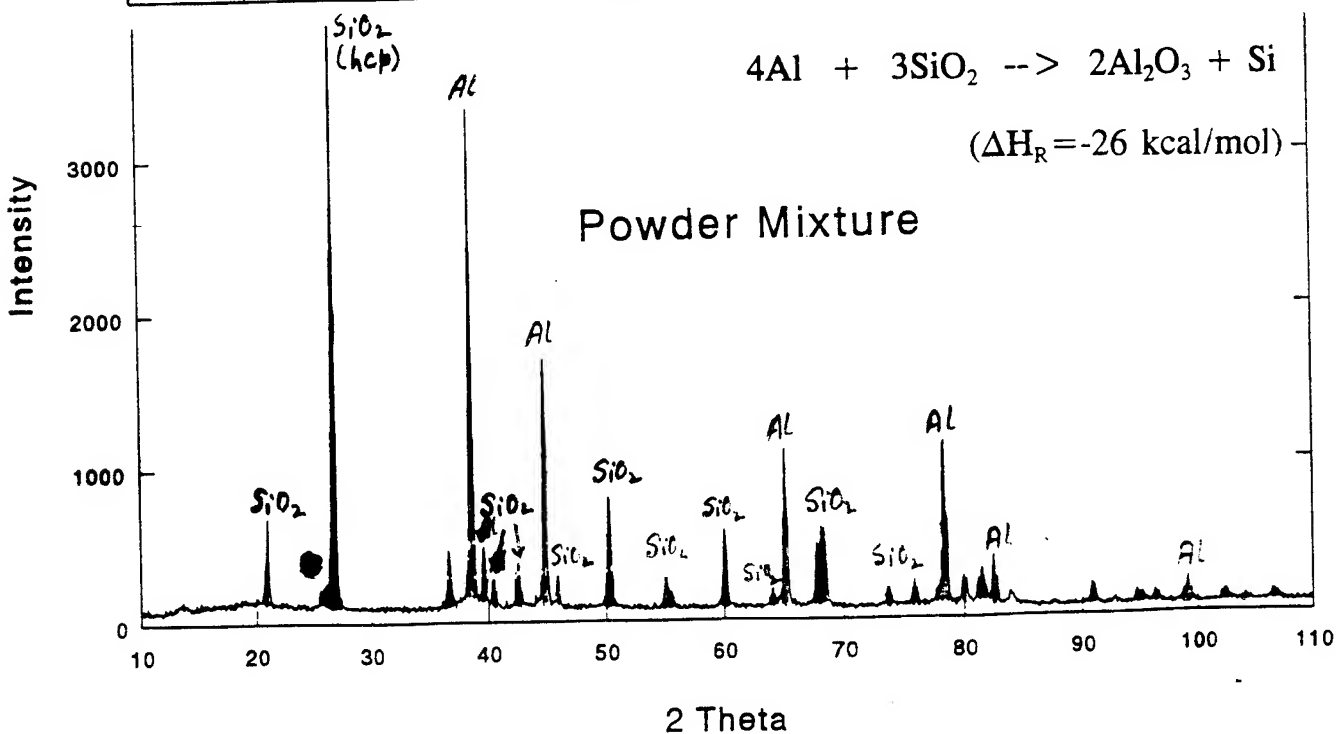
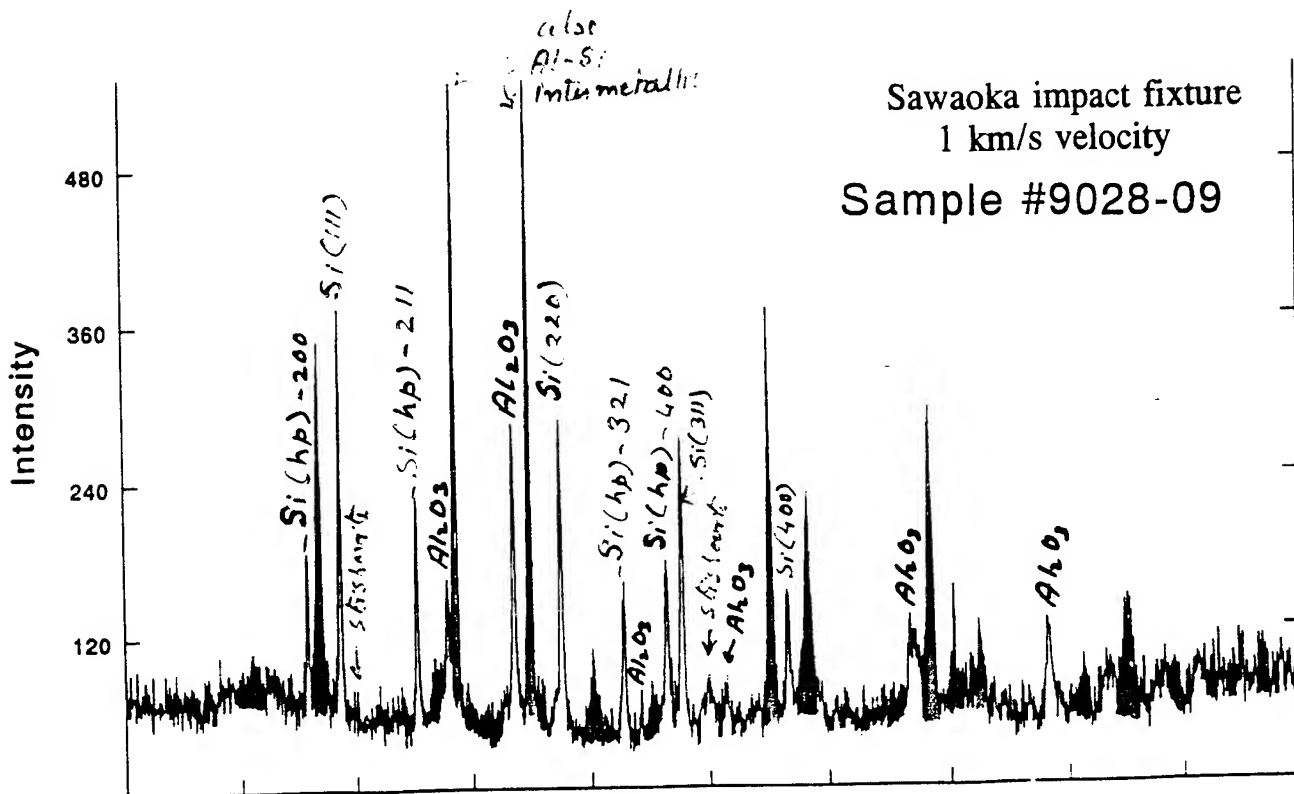
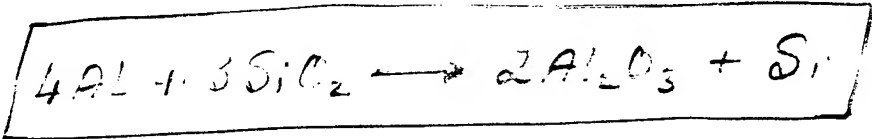
<i>Morphology</i>	<i>Shock fixture/Conditions</i>	<i>Packing Density</i>	<i>Porosity</i>
Medium	MB-B(7.5 ± 2.5 GPa)	64%	36%
	($31.8 \text{ mm } \phi \times 6.35 \text{ mm th.}$)	53%	47%
	PB-B (5.0 ± 1 GPa)	59%	41%
	($45.7 \text{ mm } \phi \times 6.35 \text{ mm th.}$)	53%	47%
		45%	55%
Coarse	MB-B(7.5 ± 2.5 GPa)	53%	47%
	PB-B (5.0 ± 1 GPa)	45%	55%
Fine	MB-B(7.5 ± 2.5 GPa)	53%	47%
	PB-B (5.0 ± 1 GPa)	45%	55%

* MEAN - BULK - TEMPERATURES MUCH BELOW
MELT TEMPERATURE OF Si.

REACTION MAP FOR 5Ti + 3Si

(Pressure versus Porosity)





SUMMARY AND REMARKS

- * Enhanced *solid-state* chemical reactivity caused by configurational changes in powder mixtures during shock-compression, lead to *shock-assisted* and *shock-induced* chemical reactions.
- * "Shock-assisted" reactions occur at localized interparticle regions, via *defect-enhanced* solid-state diffusion, after unloading to ambient conditions and in time scales of temperature equilibration.
- * "Shock-assisted" reactions can be used as a post-shock process in which bulk density reactant-mixture compacts are subsequently reaction sintered to produce materials with refined microstructures.
- * "Shock-induced" reactions occur during shock-compression in time scales of pressure (mechanical) equilibration.
- * PVDF gage stress-wave measurements on 5Ti+3Si powder mixtures up to 5 GPa, show (i) crush-up behavior dominated by powder morphology effects and (ii) wave velocity increases for medium morphology powders, indicating evidence of "shock-induced" chemical reactions.
- * Simultaneous deformation, flow, and mixing, of reactants is a necessary condition for "shock-induced" chemical reactions.
- * "Shock-induced" reactions can be used for possible synthesis of non-stoichiometric compounds or high-pressure phases.

"SHOCK-INDUCED" AND "SHOCK-ASSISTED" SOLID-STATE CHEMICAL REACTIONS IN POWDER MIXTURES

N.N. Thadhani

School of Materials Science and Engineering
Georgia Institute of Technology, Atlanta, GA 30332-0245

ABSTRACT

Shock-compression of powder mixtures can lead to chemical reactions, resulting in the formation of equilibrium as well as non-equilibrium compounds, and rapid increases in temperature. The reactions occur as manifestations of enhanced solid-state chemical reactivity of powders, caused by configurational changes and defect states introduced during shock-compression. Two types of reactions are possible and can be distinguished on the basis of their respective process mechanisms and kinetics. *Shock-induced* chemical reactions occur during the shock-compression state, before unloading to ambient pressure, and in time scales of *mechanical equilibrium*. In contrast, *shock-assisted* reactions occur after unloading to ambient pressure, in an essentially shock-modified material, in time scales of *temperature equilibration*. The mechanisms of *shock-assisted* reactions include solid-state defect-enhanced diffusional processes. *Shock-induced* reactions on the other hand, require mechanisms different from conventional solid-state nucleation and growth processes. The complex nature of deformation of powders has precluded a detailed understanding of the reaction mechanisms of such high-rate reaction processes. Results of controlled experiments, however, suggest that *shock-induced* chemical reactions involve non-diffusional processes giving rise to mechanochemical effects and solid-state structural rearrangements. In this paper, mechanistic concepts that distinguish between *shock-induced* and *shock-assisted* chemical reactions are described. The effects of configurational changes introduced during shock compression, and the influence of material properties and shock-loading characteristics on such effects, are analyzed to identify the mechanisms of complex processes leading to chemical reaction initiation and compound formation.

(To be published in Journal of Applied Physics)

1. INTRODUCTION

The combination of defect states and packing characteristics produced in powders due to dynamic void compression, plastic deformation, flow, and mixing, is possible singularly by shock-compression [1-5]. The enhancement in chemical reactivity resulting under such conditions, can cause powder mixtures to undergo **chemical reactions** during the microsecond duration shock state. Conclusive evidence exists, based on real-time measurement studies, to believe that the occurrence of chemical reaction in the microsecond duration is indeed possible during shock compression [6,7].

Highly activated states are also produced in shock compressed materials which can lead to accelerated mass transport during post-shock thermal treatments [8-10]. Consequently, chemical reactions can occur in "shock-modified" powder mixtures at temperatures substantially lower than, and at rates significantly faster than, similar self-sustaining combustion-type reactions [11-12]. Post-shock chemical reactions occurring as a result of shock compression simply assisting (activating or modifying) the powder mixture for subsequent thermal-initiation, can be classified as "*shock-assisted*" reactions. On the other hand, reactions initiated by shock-compression and occurring within the **pressure equilibrium** (microsecond duration) time scale, can be classified as "*shock-induced*" chemical reactions. In some cases, it may be difficult to infer if the so-called *shock-induced* chemical reactions in powder mixtures occurred during the high-pressure shock state before unloading, or if they occurred subsequent to loading and unloading to ambient conditions. It is possible that the bulk (residual) temperatures generated in the shock-compressed powders in time scales of **thermal equilibrium** (millisecond duration), can subsequently initiate reactions in the highly reactive configuration produced as a result of shock-modification effects. Such reactions occurring subsequent to unloading would again, in principle, be classed as *shock-assisted* and not *shock-induced* chemical reactions.

Mechanisms of *shock-assisted* chemical reactions, initiated by bulk shock temperatures in time scales of thermal equilibration, or by post-shock thermal treatments, can be understood on the basis of defect-enhanced solid-state diffusion processes in shock-modified materials. In contrast, *shock-induced* chemical reactions involve mechanisms that are different from those involving usual processes of nucleation and growth from either the **molten liquid** or by diffusion

in the **solid-state**. Manifestations of enhanced solid-state chemical reactivity leading to *shock-assisted* and *shock-induced* chemical reactions have brought forward a new class of energetic materials that are unique in their response to shock-compression. As a consequence, synthesis of compounds containing equilibrium and non-equilibrium phases, or radically modified microstructures is possible via these chemical reaction processes [5].

The objective of this paper is to describe mechanistic concepts that distinguish between "*shock-induced*" and "*shock-assisted*" chemical reactions occurring in shock-compressed powder mixtures. The two classes of reactions will be discussed on the basis of comparisons with other solid-state reaction processes. Analysis of configuration changes introduced during shock compression, and effects of materials characteristics on such configurational changes, deduced from a large number of experimental observations, will also be presented.

2. SHOCK-RESPONSE OF POWDERS

The response of powders to shock-compression effects is significantly different from that of solid-density materials. A large amount of energy is dissipated in plastic deformation and crushing of the powders in the process of void annihilation. Various void collapse models have been developed [13], based on rate-independent and rate-dependent, as well as perfectly-plastic and elastic-viscoplastic material considerations. Stress-wave measurements have also been performed [7], which reveal that crush-up of powders to solid density produces complex wave loading characteristics. The measured shock-wave rise times are observed to vary from a few tens to several hundreds of nanoseconds [7], depending on the magnitude of the shock. While, rapid-loading rates at high pressures make it necessary to incorporate rate-dependent considerations, long rise times at low pressures alter the otherwise prompt thermal effects and hydrodynamic considerations assumed in theoretical treatment of the shock state. A realistic analysis of shock-compression effects, therefore, becomes extremely complex.

Experimental measurements also show that the crush strength of powders is a function of their initial packing density and powder particle morphology [7]. Furthermore, in the case of mixtures of powders, e.g., Al+Fe₂O₃ [14], it has been shown that the crush-up behavior is

dominated, alternately, by the compression characteristics of the respective components [14]. Thus, the crush-up of the mixture is influenced initially by the compressibility of Al (at low pressures) and later by the compressibility of Fe_2O_3 (at higher pressures). Such characteristics of the deformation response of powders make it very difficult to formulate simple models that can explain the process mechanisms of phenomena occurring during shock compression in a wide range of temporal, spacial, and pressure scales.

Shock compression of powders and powder mixtures also results in various types of mechanical, physical, and chemical effects. A large number of defects are introduced in the powders due to the kinetic energy of the shock pulse. Extensive plastic deformation, fluid-like turbulent flow, heating, particle comminution, and mixing of constituents with fresh and cleansed surfaces is possible. These effects significantly alter the mechanical, physical, and chemical characteristics of powders, thereby influencing their solid-state reactivity.

The various processes occurring in powders during shock compression are best characterized in a mechanistic concept developed by Graham [15]. The overall concept is described as occurring in three stages: an initial configuration, transition zone, and final compressed configuration. The initial configuration strongly influences the overall process because of its control on energy localization, fluid-like flow, and mass mixing. The transition region lasting for a few to hundreds of nanoseconds corresponds to peak rise in pressure. Finally, the release zone accommodates the reduction in pressure, with release occurring along the solid shock-modified state. The transition zone is the most critical event, and forms the basis of a model defined by CONMAH (CONfiguration change, Mixing, Activation, and Heating) [15], which addresses processes occurring during shock-compression of powders and ultimately leading to either "*shock-induced*" or "*shock-assisted*" chemical reactions, or simply unreacted "*shock-modified*" state.

During shock compression, irreversible changes are caused in the starting **configuration**. The individual powder particles are substantially deformed to fill the voids, thereby producing a significantly altered final configuration. The degree of deformation of particles, and hence, the total configurational change, is influenced by differences in properties of constituent materials, volumetric distribution of constituents, powder morphology, starting porosity (or void

volume), and shape of voids. The defect substructure within the solid particulates is also substantially changed at the atomic and microscopic levels. **Mass mixing** during the transition zone occurs due to the turbulent flow of particles in and around the void space during the process of pore collapse. **Shock activation** occurs due to the extensive plastic deformation of individual particles and their relative flow past each other which results in generation of large defect densities, cleansing of particle surfaces as well as opening of fresh surfaces. Finally, localized and bulk **heating** provides a thermal environment, which can either facilitate reaction processes, or even anneal out defects and produce recrystallized microstructures. The various attributes of processes occurring during shock-compression, as described by CONMAH [15], can be summarized schematically in Figure 1. Thus, the overall scenario leading to *shock-induced* chemical reactions in times scales of **mechanical equilibrium**, or *shock-assisted* reactions in time scales of **thermal equilibrium**, or simply unreacted *shock-modified* states attained **upon equilibration with the ambient**, can be generalized in a phenomenological concept. The mechanisms of *shock-assisted* and *shock-induced* chemical reactions will be discussed in more detail next.

3. SHOCK-ASSISTED REACTIONS IN POWDER MIXTURES

It is well established that the defects generated due to shock-compression can significantly modify and enhance the solid-state reactivity of powders [1-5,8]. Brittle ceramics and even metals, such as silicon, undergo significant grain size reduction due to shock compression, via grain fracturing or by generation of sub-grain structures [16]. Increased mass transport rates are possible in shock-compressed materials due to introduction of defects and creation of new paths for motion of point defects along grain boundaries [17]. Such characteristics play a vital role in enhancing the solid-state chemical reactivity of powders and their mixtures, essentially by creating a *shock modified* material. Various attempts have been made to advantageously utilize the enhancement in reactivity of *shock-modified* materials by post-shock controlled-rate thermal treatments. Successful examples of these include sintering of difficult-to-consolidate oxide and non-oxide ceramics [16,17], improving catalytic activity of materials [8,18], and enhancing the kinetics of nucleation of precipitation-strengthening phases [19] or other types of metastable high-pressure phases [8].

Enhanced reactivity also leads to altered solid-state chemical reaction behavior of shock-modified powder mixtures. A brief description and typical examples of enhanced chemical reactivity evidenced by differential thermal analysis of shock-compressed intermetallic-forming powder mixtures will be presented next, followed by calculations of solid-state diffusion, to explain the mechanisms of *shock-assisted* chemical reactions.

3.1 Thermal Analysis of Shock-Modified Powder Mixtures

The post-shock thermally-initiated chemical reaction behavior of shock-compressed powders was first studied by Hammett et al [9] on Ni-Al mixtures. They used differential thermal analysis (DTA) and observed that mechanical mixtures of Ni-Al powders in unshocked condition showed a reaction exotherm at 650°C, corresponding to the occurrence of a self-sustaining reaction initiating with the melting (eutectic) of Al. The shocked mechanical mixtures revealed two reaction exotherms, the main exotherm at 650°C and another "pre-initiation" exotherm at $\approx 550^\circ\text{C}$ corresponding to a solid-state reaction.

In a similar but more detailed study, Dunbar et al [10] investigated Ni and Al powders of three different particle morphologies, all mixed in a volumetric distribution corresponding to the stoichiometric Ni_3Al compound and packed at the same density. Figure 2 shows the DTA traces of shock-compressed flaky, fine, and coarse/rounded morphology Ni-Al powder mixtures, all shocked under identical conditions. Mixtures of powders of all three morphologies exhibit the "pre-initiation" solid-state reaction exotherm at $\approx 550^\circ\text{C}$ prior to the main liquid-state reaction exotherm at 650°C, similar to Hammett et al's [9] observations. However, the relative magnitudes of the liquid-state and solid-state exotherms are strongly dependent on effects of powder morphology on shock-modification. Considering the magnitude of the exotherms to correspond to the extent of the reaction, it can be deduced that coarse/rounded morphology mixtures exhibit mostly a liquid-state reaction and a small amount of reaction in the solid-state. Fine morphology mixtures exhibit a significantly larger solid-state reaction and only limited liquid-state reaction. Flaky powder mixtures react completely in the solid-state at temperatures significantly below the melting of Al.

Microstructural analysis of the shock-compressed configuration of the three types of Ni-Al powder mixtures explains the effect of powder morphology on their chemical reaction behavior. The optical micrographs shown in Figure 3, reveal different levels of deformation and mixing of Ni and Al particles in the respective powder mixtures [10]. Flaky powder morphology mixtures show extensive deformation and flow of both components, resulting in more intimate mixing, and a greater surface area contact. Fine powders show particle agglomeration and lesser overall deformation, but greater surface area contacts. In the shock-compressed configurations resulting with flaky and fine powder morphologies (with particles compressed to $< 25 \mu\text{m}$), solid-state diffusion reactions are easily favored over distances of particle dimensions at temperatures much below the melting of Al and within the time frames of heating in the DTA. Thus, there remains little or no unreacted material available for subsequent liquid-state reaction. In contrast, coarse/rounded morphology powder mixtures (particle size $> 50 \mu\text{m}$) show plastic deformation only at Ni-Ni contacts and mixing only in areas of Al trapped in voids between Ni particles. The shock-modified coarse-morphology mixture, therefore, shows only limited reaction by solid-state diffusion, and bulk of the reaction occurs subsequently upon melting of Al. Similar results of enhanced solid-state chemical reaction behavior due to shock-compression effects have also been observed in other aluminide and silicide forming powder mixtures [20].

A shift in reaction mechanism from a liquid-state process (occurring with melting of one constituent) to a solid-state diffusion process at temperatures much below the melting of either constituent, has been reported in various thermal analysis studies of powder mixtures [21-23]. In general, it is observed that the liquid-state reaction is favored in mixtures packed at lower densities and at faster heating rates in the DTA, with enough time not being available for solid-state diffusion processes. Liquid state reactions are, however, inhibited and solid-state reactions favored, if solid-solid diffusivities of the powder mixture components are accelerated due to presence of defects, shorter diffusion distances, more intimate contacts at higher packing densities, and with the formation of fresh/cleansed contacts between surfaces of intimately mixed powder components, such as those created in mechanically modified powder mixtures during shock-compression [8-10] or ball milling [22,23].

3.2 Analytical Treatment of Solid-state Diffusion Reactions

Solid-state diffusion-controlled chemical reactions can be approximated by a one-dimensional infinite solid diffusion couple geometry with a concentration independent diffusion coefficient. The time (t) required for compound formation by solid-state diffusion can be expressed as:

$$t \approx \frac{p^2}{64 D_v} \approx \frac{p^2}{64 D_o \exp\left(-\frac{Q}{RT}\right)} \quad (1)$$

where, p is diameter of the powder particles (assuming spherical geometry) and also corresponds to the total diffusion distance, and D_v is temperature dependent rate of volume diffusion. For Ni-Al intermetallic forming mixtures, diffusion constant D_o is considered approximately equal to $10^{-5} \text{ m}^2/\text{s}$ [24], activation energy Q is estimated from the melt temperature ($\approx 151 T_m \text{ kJ/mol}$ [24]), R is universal gas constant, and T is absolute temperature. Thus, the total time for compound formation by solid-state diffusion in a Ni-Al powder mixture is calculated to be ≈ 2800 hours for spherical particles of $1 \mu\text{m}$ diameter, or $\approx 10^6$ hours for $25 \mu\text{m}$ diameter particles, at one-half the melt temperature of Al.

On the other hand, if defect-enhanced solid-state diffusion processes are considered, then a treatment similar to that adopted by Whittenberger [25] for formation of intermetallic compounds by ball milling, can be used. Equation (1) is then modified to replace the bulk diffusivity, D_v , by an enhanced-diffusion coefficient, D' , based on Hart's approximation [26]. Thus,

$$D' = f_L D_v + f_c D_c \quad (2)$$

where, f_L and f_c are the fractions of atoms associated with the lattice and dislocation core, respectively, (the sum of which is 1), and D_c is the diffusion coefficient along the dislocation core. Using Shewmon's [24] analysis and approximations for number of atoms per unit length in dislocation core ($n = 5$), dislocation density ($\approx 10^{16} \text{ lines/m}^2$), and number of atoms per unit area per unit length of dislocation ($1 \times 10^{19} \text{ atoms/m}^2 \text{ per unit length}$), D' is obtained as [25]:

$$D' \approx D_v + 0.005 D_c \quad (3)$$

For $T > 1/2 T_m$, diffusion along a dislocation can be assumed similar to atomic mobility in grain boundaries. Considering pre-exponentials for volume and grain boundary diffusion to be same and activation energy for grain boundary diffusion to be about half of that for volume diffusion [25], the total time for compound formation by defect-enhanced diffusion processes is:

$$t \approx \frac{p^2}{D_v} \approx \frac{p^2}{64 [D_o \exp(-\frac{Q}{RT}) + 0.005 (D_o \exp(-\frac{Q}{2RT}))]} \quad (4)$$

Using Eq. (4), the time for compound formation in Ni-Al powder mixtures of $\approx 25 \mu\text{m}$ average particle diameter (from Fig. 3) shock-modified at 22 GPa, is calculated to be ≈ 4.5 hours at temperatures of one-half the melt temperature of Al. Considering the reaction onset temperature of 500°C deduced from DTA traces in Fig. 2, the defect-enhanced solid-state diffusion time is calculated to be ≈ 31 seconds for reactions observed to occur in the DTA. Unshocked powder mixtures would still require ≈ 8 hours for complete diffusion, at the same 500°C reaction temperature. The considerably short reaction time in the case of shock-modified mixtures is consistent with the heating schedule achieved in the DTA at heating rates of $10^\circ\text{C}/\text{minute}$ (Fig. 2).

The analytical treatment for defect-enhanced solid-state diffusion can in fact be extended to *shock-assisted* chemical reactions occurring in powder mixtures subsequent to unloading from the shock pressure to the ambient state. Such reactions occur due to bulk temperature increases in time scales of thermal equilibration. Thus, if one considers Ni-Al powders of $25 \mu\text{m}$ diameter (from Fig. 3) and bulk shock temperatures approaching melting of Al ($\approx 0.95T_m$), the time for compound formation is calculated to be less than 100 milliseconds. Thermal equilibrium during shock-compression of powders is also attained in similar time scales. It can, therefore, be inferred that *shock-assisted* chemical reactions occur by **defect-enhanced solid-state diffusion** processes with bulk shock temperature increases in time scales of thermal equilibration. Such reactions may, however, occur only in localized areas. Progress of reaction to bulk regions may depend on diffusion through interfacial reacted region, and dissipation of heat of reaction.

4. SHOCK-INDUCED REACTIONS IN POWDER MIXTURES

Occurrence of *shock-induced* chemical reactions by mechanisms involving defect-enhanced solid-state diffusion processes is not possible during the microsecond scale duration of the shock-state. Is it then possible that these high-rate chemical reactions occur via solid-state diffusionless mechanisms involving non-conventional mechanically induced nucleation and growth processes? Can shock-compression induced plastic flow cause restructuring of atomic arrangements as well as alteration of nature of chemical bonding to induce such high-rate chemical reactions?

Shock-induced martensitic transformations in iron [27,28], as well as the *shock-induced* graphite-to-diamond transitions [29-31] are examples of solid-state structural changes occurring in materials at shock speeds. Evidence of *shock-induced* phase transitions has been provided by direct time-resolved *in situ* measurements of changes in bulk properties (Hugoniot characteristics) accompanying the transformation [27,28]. Real-time detection of such changes in bulk properties, or kinks in shock adiabats, are direct evidence of phenomena occurring at the shock-front or in its vicinity.

Shock-induced chemical reactions are generally accompanied by relatively small changes in bulk material properties. Thus, most conventional pressure and velocity measurement systems may fail to accurately respond to reaction rate measurements. Rapid temperature increases, which are commonly associated with such exothermic reactions, are the only direct property change accompanying the chemical reaction. However, it is difficult to distinguish the reaction temperature from the heterogeneous temperature increases associated with shock-compression of powders. Thus, attempts to measure the reaction temperature in real-time using, for example, radiation pyrometry techniques [32-33], have demonstrated conflicting results due to temperature increases from shock compression (void collapse) masking the temperatures produced due to chemical reaction. Time-resolved measurement studies which provide evidence for reactions occurring in the shock-compression state will be presented next, followed by discussions of various phenomenological concepts explaining mechanistic processes leading to *shock-induced* chemical reactions.

4.1 Evidence of Shock-induced Chemical Reactions from Time-Resolved Experiments

In spite of the many limitations of time-resolved techniques, various shock-compression experiments have been performed that have shown that the exothermic energy accompanying *shock-induced* chemical reactions can be released in reactive powder materials in time scales shorter than the duration of the shock state. Sheffield and Schwarz [34] performed time-resolved experiments and measured wave profiles in shocked titanium subhydride and potassium perchlorate mixtures. They observed possible evidence of reactions occurring in a microsecond time scale, and proposed that the reaction front moves through reactive material at shock wave velocity, similar to that in initiation of high explosives. Kovalenko and Ivanov [35] performed Hugoniot measurements as well as recovery experiments on lead nitrate and aluminum powder mixtures. They found that chemical reactions forming the observed products were also evident in the Hugoniot data, thus providing the evidence that chemical reactions occur at a rate commensurate with shock wave propagation.

Hugoniot measurements have also been performed by Batsanov *et al.* [6] to determine the extent of reaction as a function of shock pressure in stoichiometric mixtures of tin and sulfur. They used manganin pressure gages to obtain records of the shock profile, and observed that at pressures > 15 GPa the measured pressure points deviate towards the right (increased volume) of the Hugoniot curve calculated for the unreacted mixture. However, because of large uncertainties in the measured Hugoniots relative to the difference in pressure at a given specific volume, their determination of the reacted fraction was only an estimate.

The most revealing and comprehensive results providing evidence of *shock-induced* chemical reactions include PVDF gage [36] stress-wave measurements performed by Dunbar *et al.* [7], on Ti-Si powder mixtures of various powder particle morphologies, at shock pressures up to 5 GPa. The stress recorded by the input gage, and the shock velocity measured by timing the travel time of the wave between the input and backer gages (sandwiching the Ti-Si powder mixture sample) were used to obtain the pressure-volume compressibility characteristics. Crush up of the powders to solid-density was observed at 1 GPa pressure. With increasing pressure, the compressibility shifted to larger volumes and an increase in volume to as much as 20% was observed at 5 GPa pressure. The volume increase is attributed to the thermal expansion due to

sudden temperature increases caused by the chemical reaction. Higher magnitudes of stress were also recorded by the backer gage, and higher shock-wave velocities were measured for input stresses greater than 1 GPa. The combination of these results provide conclusive evidence of chemical reactions occurring during shock-compression and resulting in the formation of Ti-Si intermetallic compounds in time scales of mechanical equilibration [7]. The measurements also showed that the Ti-Si powder mixtures of different morphology have different crush strengths, and therefore, reveal different reaction thresholds, consistent with results of recovery experiments performed on the same powder mixtures [37].

In samples obtained from shock-compression recovery experiments, it is not possible to directly ascertain the kinetics or the mechanisms of processes leading to *shock-induced* chemical reactions. Post-shock microstructural characterization of the recovered materials reveals the final state of the product attained after equilibration with the environment. Furthermore, the large exothermicity of the reaction often results in melting of the products, leaving no evidence of how and when the reaction may have occurred. The final structure simply reveals characteristics typical of a melted and resolidified material. Figure 4 shows examples of typical microstructures of compounds formed via *shock-induced* chemical reactions in powder mixtures of Ni-Al, Ni-Si, and Ti-Si. A uniform contrast microstructure and presence of spherically-shaped voids (indicating possible gas escape or shrinkage) are typical of a fully reacted material. Microstructures showing shock-compressed unreacted powder mixture constituents (similar to Figure 3) provide significantly more information about the mechanistic characteristics of the powders and their configuration attained prior to the onset of reaction.

4.2 Conceptual Mechanisms of Shock-induced Chemical Reactions

Theoretical confirmation of *shock-induced* chemical reactions has been provided by the modeling scheme developed by Horie and coworkers [38,39], based on a family of constitutive models termed VIR. In principle, the VIR models characterize the macroscopic behavior of porous reactive mixtures from those of three ingredients: voids, inert species, and reactive species. However, these modeling schemes are based on an assumed kinetics, without consideration of initiation mechanisms and are therefore more useful in predicting the state of shock-compressed powder mixtures subsequent to reaction initiation. Mechanistic processes

occurring at the onset of reaction initiation and leading to reaction completion are not explained by these models. Several other mechanisms based on thermochemical, non-diffusional, mechanical/deformational, and mechanochemical concepts have also been documented in the literature, and will be discussed next.

4.2.1 Thermochemical Concepts

Mechanistic modeling of *shock-induced* chemical reactions was first attempted by Maiden and Nutt [40] using thermochemical analysis. They developed a heterogeneous model to calculate *shock-induced* reaction initiation thresholds by assuming that the reaction is ignited when the surface temperature of a pore meets a hot-spot ignition criterion. In essence, the reaction initiation process was assumed to be similar to that for high explosives. Russian researchers Enikolpyan *et al.* [41] have contradicted the hot-spot ignition criterion, based on the argument that the extremely rapid reactions for both strongly and weakly exothermic powder mixture systems are independent of the starting temperature. Thus, they proposed that the observed explosive-like reactions in powder mixtures, occur due to **unique chemical processes not requiring thermal activation**, but instead through **mechanical disintegration and mixing of the constituents** by the shock wave.

In recent studies on silicide forming powder mixtures, Yu and Meyers [42] proposed that if the energy generation due to the chemical reaction is greater than the energy dissipated by thermal conduction, a steady state reaction can start from local hot-spot areas and propagate into the interior of the particles. Accordingly, critical molten hot-spot regions were calculated, based on a shock energy threshold corresponding to the mean bulk temperature which must be above that required to initiate reactions at ambient pressure. However, the shock energy threshold criterion is based on time scales of **thermal equilibrium** corresponding to millisecond time duration. Thus, the energy threshold criterion and the hot-spot initiation mechanism may be applicable to *shock-assisted* chemical reactions occurring after unloading to ambient pressure, but not to *shock-induced* chemical reactions occurring during the shock-compression state in time scales of **mechanical equilibrium**.

4.2.2 Pressure-assisted Diffusional and Non-diffusional Concepts

Generation of high pressure and its effect on accelerated diffusional transport cannot account for the high rates of *shock-induced* chemical reactions. Analytical calculations described in Section 3.2 reveal accelerated diffusion due to shock-compression effects causing *shock-assisted* reactions to occur in not less than millisecond-scale time durations. High pressure can thermodynamically assist in nucleation by providing additional driving force, but it cannot alter the kinetics of processes involving diffusion dependent phenomenon. Dremin and Breusov [3] have discussed the role of shear stresses and argued that when combined with high pressures, the rates of chemical reaction and phase transformations become higher, and the processes go to completion during the application of shear stress. In general, shear deformation has also been shown to form phases which may otherwise not be observed in absence of shear.

Attempts to investigate "non-diffusional" processes for *shock-induced* chemical reactions, have evolved around atomic rearrangements similar to structural phase transitions. Formation of diamonds during meteoritic impact is believed [43,44] to occur by direct solid-state transformations under the action of shock waves. Altshuler [28] has proposed that the diamonds form by a process similar to martensitic transformations, with the large number of point, line, and planar defects, generated in the shock front at supercritical pressures, forming the crystal nucleation sites. The rapid transition of the parent lattice into the diamond phase is facilitated by non-diffusional martensitic rearrangements, based on the cooperative motion of many atoms to small distances. More recent Russian studies [45] have shown that graphite-to-diamond conversion occurs via a martensitic transformation to the lonsdaleite phase which then transforms to diamond via a diffusion-controlled process. On the other hand, transformations from amorphous carbon to diamond and similarly from amorphous analogues of boron nitride to cubic boron nitride have been proposed to occur via reconstructive phase transformation process [46].

Reaction mechanisms involving processes similar to martensitic transformations require structural rearrangements of reactant lattices and mixing of the constituents in a continuum, to yield the product compound and microstructure. The reaction may go through an intermediate non-crystalline compound before forming the final product lattice, or may directly transform to the product lattice state, with accompanying volume change and energy release. Probes to

monitor these paths in real time need to be developed, similar to in-situ x-ray diffraction techniques available to monitor phase changes in materials [47]. A necessary condition for transformations involving non-diffusional structural rearrangements, such as in martensitic transformations, may also include orientation dependence between the initial constituents and the final product states. Determination of such a criterion would be necessary if *shock-induced* chemical reactions are considered to occur via similar non-diffusional structural rearrangements.

4.2.3 Mechanochemical Concepts

Mechanisms of *shock-induced* chemical reactions in powder mixtures have also been explained on the basis of mechanochemical concepts. The "ROLLER" model proposed by Dremin and Breusov [3], and the "CONMAH" model proposed by Graham [15], are both based on mechanochemical concepts, and describe the possible mechanistic processes leading to *shock-induced* chemical reactions.

According to the "ROLLER" model [3], when two layers of a substance are displaced relative to one another, the nucleating phase located between them, can be regarded as a kind of a **roller** in which mixing and alloying of the constituents occurs. Since the time required for rearrangement of electron shells (10^{-13} to 10^{-14} s) is much shorter than the time required for contact between atoms (10^{-12} s), it implies that all atoms passing in the immediate vicinity of the nucleus have sufficient time to combine with it and form the new phase. Thus, in contrast to usual growth of the nucleating crystals, in which the atoms diffuse to the nucleation site via random walk, with the available thermal energy, formation of the new phase during shock-compression occurs via transport of the entire mass of initial phase by plastic flow, to the nucleation center. The required atoms then combine selectively with particles of the new alloy phase, thereby undergoing continuous growth. According to Dremin and Breusov's calculations [3], the new phase thus formed can have dimensions of $\approx 2.9 \times 10^4$ atoms (or $\approx 3 \mu\text{m}$).

The "ROLLER" model demonstrates a possible scenario of the reaction process, assuming that an ideal globally-mixed configuration has been attained. However, unlike the CONMAH model [15], it does not describe the processes leading to configuration changes prior to the inception of reaction. The mechanochemical nature of *shock-induced* chemical reactions

has been clearly illustrated in the different studies performed on intermetallic- and ceramic-forming elemental powder mixtures [reviewed in Refs. 4,5]. From these studies it is evident that plastic deformation, flow, and mixing of **both** (or all) constituents, is essential for the occurrence of *shock-induced* chemical reactions. If only parts of constituent particles, or only one constituent undergoes plastic deformation and flow, then *shock-induced* chemical reactions may not occur except only at localized interfacial regions due to *shock-assisted* rather than *shock-induced* processes. Examples of such a behavior are clearly observed [5] in mixtures of Nb with Si and Ni with Al, as shown in Figure 5. In the case of premature melting of either Si or Al (revealed by its cellular structure in Fig. 5 (a) and (b)), no deformation of the other metallic constituent (e.g., Nb or Ni, respectively) is observed leaving them with the same undeformed morphology in the recovered product. Melting may however, result in localized *shock-assisted* reaction (as shown in (Fig. 5 (a) and (b)), due to wetting of melted Si (or Al) at interfaces of Nb (or Ni) particles. Likewise, the virtually negligible deformation of Ni particles in an abundant matrix of the softer, more deformable Al (as shown in Fig. 5(c)), again limits mixing between the two metals resulting in a reduced propensity for subsequent *shock-induced* reaction initiation. Mechanochemical effects involving plastic deformation and flow of powders into and around voids (from the starting porosity), causing fluid-like flow, mass mixing, and dispersion of constituents, can therefore, be defined as an essential part of process leading to *shock-induced* chemical reactions.

5. CORRELATION OF CONCEPTS WITH EXPERIMENTAL OBSERVATIONS

Quantifying the relationships that include mechanisms of solid-state *shock-induced* chemical reactions, based on the mechanochemical concepts discussed above, still remains to be performed. On the other hand, what is available is conclusive evidence that chemical reactions in powder mixtures, leading to formation of compounds, occur during shock-compression in time scales of mechanical equilibrium. In addition, analysis of properties influencing the reaction behavior (initiation thresholds determined from controlled recovery experiments) and product formation characteristics (microstructure of reacted and unreacted states) is also available. Such characteristics of the reaction behavior and the microstructure, can be used to formulate and develop quantifiable models of reaction mechanisms. A careful review of experiments on *shock-*

induced chemical reactions also alludes to the very important but complex role of the intrinsic properties of reactant materials, in influencing the reaction behavior of powder mixtures during shock-compression, in addition to shock loading conditions and powder morphology characteristics. In particular, as discussed in the previous section, the **deformation response** of powders during shock compression, controlling the flow and mixing of reactants and introducing configurational changes, is the most important property influencing the **initiation** of *shock-induced* chemical reactions. Subsequently, the reaction behavior and product formation characteristics, may be influenced by thermodynamic properties of the reacting system.

In the case of metal-metal powder mixtures, the extent of plastic flow and mixing, the type and level of defects formed, and the packing configuration generated during the shock state, is controlled by the deformation characteristics of the mixture constituents, and extrinsic properties including particle morphology, void volume, and shock-compression conditions. In turn, the **deformation characteristics** are affected by the intrinsic high-strain-rate flow stress of the constituents. For example, metallic Si is typically brittle, however, depending on particle size and shock-conditions, it can either fracture, plastically deform, or even undergo melting (at pressures > 11 GPa [48]). Figure 6 (a) shows an SEM micrograph of Ti-Si powder mixtures revealing plastic deformation, flow, and inter-constituent mixing with small and medium sized Si powders ($< 40 \mu\text{m}$). On the other hand, extensive fracture and fragmentation is observed with coarse ($> 100 \mu\text{m}$) Si powders with limited deformation of Ti particles (as shown in Figure 6 (b)), under the same shock conditions. With increase in shock pressure, the same coarse Si powders undergo extensive plastic deformation and flow, as shown in Figure 6 (c).

It has also been observed, that the shock-compression response of Si, is different in mixtures with different metallic constituents. When mixed with Ni or Ti, Si powders show extensive fracture and fragmentation or even plastic deformation, while metallic constituents also undergo significant plastic deformation and flow. However, when Si powders are mixed with Nb, then at the same stress levels, Si alone undergoes fracture or plastic deformation, while the Nb particles remain undeformed and maintain the starting morphology. The different metal-silicon mixtures, therefore, require **different threshold conditions** for initiation of *shock-induced* chemical reaction: < 10 GPa for Ni-Si and Ti-Si systems, 20-40 GPa for Nb-Si system, and > 40 GPa for Mo-Si system, at the same 55% initial density [20,37]. The dissimilar shock-

compression response of Si with different metallic constituents further illustrates the mechanochemical nature of *shock-induced* chemical reactions, unlike processes in which thermochemical mechanisms dominate the threshold conditions.

Some of the physical, chemical, and mechanical property differences between Si and metallic constituents Ti, Nb, Ni, and Mo, are listed in Table I, along with product formation properties (including maximum heat of reaction (ΔH_R), volume change, cohesive energy (ΔH_C), and the ratio $H_R/\Delta H_C$) of Ti-Si, Nb-Si, Ni-Si, and Mo-Si compounds. Consistent with the results of reaction thresholds and the properties listed in the Table, the propensity for **initiation** of *shock-induced* chemical reactions made possible by appropriate changes in configuration, correlates best with differences in the **yield strength** of constituents. Once initiated, reaction **completion and product formation** characteristics, correlate best with the **heat of reaction** normalized with the **cohesive energy**. The normalization with cohesive energy is used to include the effects of binding energies between like and unlike atoms. Other properties of reactants have only minor indirect effects on the reaction behavior. Thus, although models with quantifiable relationships describing the reaction mechanisms are not available, domains correlating material properties with the reaction behavior may be obtained to better understand the mechanochemical processes leading to *shock-induced* chemical reactions.

5. SUMMARY

Manifestations of enhanced solid-state chemical reactivity caused by configuration changes introduced during shock-compression of powder mixtures, can lead to *shock-assisted* or *shock-induced* chemical reactions. *Shock-assisted* reactions occur via solid-state defect-enhanced diffusion after unloading to ambient pressure, in time scales of **temperature equilibration**. *Shock-induced* reactions, on the other hand, occur during shock-compression upon **mechanical equilibration** and before unloading to ambient pressure. Analysis of the effects of configuration changes introduced during shock compression, and the influence of material properties and shock-loading characteristics on such effects reveal that *shock-induced* chemical reactions occur via mechanisms involving non-diffusional processes giving rise to structural rearrangements and mechanochemical effects. Thus, processes that account for mechanisms

dominated by simultaneous mechanical deformation effects, determine the onset criterion and the extent of bulk reactions occurring during shock-compression of powders. Compound formation characteristics, are however, influenced by thermochemical properties. It is also evident that thermally activated processes cannot account for *shock-induced* chemical reactions, except in the case where shock-compression simply assists by creating conditions favorable for reaction to occur in time scales of thermal equilibration or by post-shock thermal initiation. Such *shock-assisted* reactions can be explained on the basis of thermally-activated defect-enhanced solid-state diffusion mechanisms. It can therefore, be concluded that *shock-induced* chemical reactions occur by mechanisms dominated by solid-state diffusionless mechanochemical processes, unlike the defect-enhanced solid-state diffusional mechanisms of *shock-assisted* chemical reactions.

ACKNOWLEDGEMENTS

Funding for the author's research has been provided in part by the National Science Foundation Grant No. DMR-9396132 and the Army Research Office Grant No. DAAH04-93-G-0062 at Georgia Institute of Technology, and by the Sandia National Laboratories Contract No. 42-5737 for work supported at New Mexico Tech. The author wishes to acknowledge the valuable discussions, and the continued motivation and encouragement provided Dr. Robert A. Graham, Sandia National Laboratories for this work. The contributions of past and present graduate students are also gratefully acknowledged.

REFERENCES

1. G. Duvall, Chairman, "Shock-Compression Chemistry in Materials Synthesis and Processing, NMAB Report No. 414, National Academy Press, Washington D.C., 1984.
2. R.A. Graham, "Solids Under High Pressure Shock Compression: Mechanics, Physics, and Chemistry," Springer Verlag, 1993.
3. A.N. Dremin and O.N. Breusov, "Processes Occurring in Solids Under the Action of Powerful Shock Waves," Russian Chemical Reviews, 37 (5) (1968) 392.
4. R.A. Graham, B. Morosin, E.L. Venturini and M.J. Carr, "Materials Modification and Synthesis Under High Pressure Shock Compression," Ann. Rev. Mat. Sci., 16(1986)315.
5. N.N. Thadhani, "Shock-induced Chemical Reactions and Synthesis of Materials," Progress in Materials Science, Vol. 37, No. 2, (1993) pp. 117-226
6. S.S. Batsanov, G.S. Doronin, S.V. Klochkov and A.I. Teut, "Synthesis Reactions Behind Shock Fronts," *Combustion, Explosion, and Shock Waves*, 22 (6), p. 134, 1986.
7. E. Dunbar, R. A. Graham, G.T. Holman, M.U. Anderson, and N.N. Thadhani, "Time-resolved Pressure Measurements in Chemically Reacting Powder Mixtures," in Proc. of AIRAPT/APS High Pressure Science and Technology Conference, 28 June to 2 July, 1993, Colorado Springs, ed., S.C. Schmidt, in press.
8. R.A. Graham and N.N. Thadhani, "Solid-State Reactivity of Shock-Processed Solids," in Shock Waves in Materials Science, ed., A.B. Sawaoka, SpringerVerlag, 1993, p. 35.
9. W.F. Hammett, R.A. Graham, B. Morosin, and Y. Horie, "Effects of Shock Modification Effects on Self-Propagating High Temperature Synthesis of Nickel Aluminides," in *Shock Waves in Condensed Matter*, eds., S.C. Schmidt and N.C. Holmes, Elsevier Science Publishers B.V., 1988, p. 431.

10. E. Dunbar, N.N. Thadhani, and R.A. Graham, "High Pressure Shock Activation and Mixing of Ni-Al Powder Mixtures," J. of Mater. Sci., Vol. 28, (1993) 2903.
11. Z.A. Munir and U. Anselmi-Tamburini, *Mater. Sci. Rep.*, **3** (7,8), 277 (1989).
12. V. Hlavacek, *Amer. Ceram. Soc. Bull.*, **70** (2), 240 (1991)
13. W.Tong and G. Ravichandran, "Dynamic Pore Collapse in Viscoplastic Materials," *J. Appl. Phys.*, in press.
14. G.T. Holman, R.A. Graham, and M.U. Anderson, "Shock Response of Porous 2Al+Fe₂O₃ Mixtures," in Proc. of AIRAPT/APS High Pressure Science and Technology Conference, 28 June to 2 July, 1993, Colorado Springs, ed., S.C. Schmidt, in press.
15. R.A. Graham, "Issues in shock-induced solid state chemistry," in Proc. of 3rd International Symposium on Dynamic Pressures, La Grande Motte, France, June 5-9, 1989.
16. O.R. Bergmann and J. Barrington, Effect of Explosive Shock Waves on Ceramic Powders," *J. Amer. Ceram. Soc.*, 49 (1966) 502.
17. E.K. Beauchamp, "Shock Activated Sintering," in High-Pressure Explosives Processing of Ceramics, eds., R.A. Graham & A.B. Sawaoka, Trans Tech Publ. 1987, p. 139.
18. J. Golden, F. Williams, B. Morosin, E.L. Venturini, R.A. Graham, in Shock Waves in Condensed Matter - 1981, edited by W.J. Nellis, L. Seaman, R.A. Graham, American Institute of Physics, pp. 72-76.
19. N.N. Thadhani, A.H. Mutz, and T. Vreeland, Jr., "Structure/Property Evaluation and Comparison Between Shock-Wave Consolidated and Hot-Isostatically Pressed Compacts of RSP Pyromet 718 Alloy Powders," *Acta Metall.*, Vol. 37 (3), (1989) pp. 897-908.

20. E. Dunbar, "Effect of Volumetric Distribution of Starting Powders on Shock-Induced Chemical Synthesis," M.S. Thesis, New Mexico Tech, 1992.
21. F. Bordeaux and A.R. Yavari, "Ultra Rapid Heating by Spontaneous Mixing Reactions in Metal-metal Multi-layer Composites," *J. Mater. Res.*, 5(8) (1990) 1656.
22. G.T. Hida and I.J. Lin, "Elementary Processes in SiO_2 -Al Thermite Reaction Activated or Induced by Mechanochemical Treatment," in *Combustion and Plasma Synthesis of High Temperature Materials*, eds., J.B. Holt and Z. A. Munir, VCH Publishers, (1990), p. 246.
23. S.C. Deevi, "Self-Propagating High-Temperature Synthesis of Molybdenum Disilicide," *J. Mater. Sci.*, 26 (1991) 3343.
24. P.G. Shewmon, Diffusion in Solids, McGraw-Hill Book Company, Inc., NY, 1963.
25. J.D. Whittenberger, "Solid State Processing for High Temperature Alloys and Composites, in Solid State Powder Processing, eds., A.H. Clauer and J.J. deBarbadillo, TMS publication, 1990, pp. 137-155.
26. E. Hart, "On the Role of Dislocations in Bulk Diffusion," *Acta Metall.*, 5 (1957) 597.
27. G.E. Duvall and R.A. Graham, "Phase Transitions Under Shock Wave Loading," Rev. Mod. Phys., 49, 523 (1977).
28. L.V. Al'tshuler, "Phase Transitions in Shock Waves (Review)," *Appl. Mech. Technical Phys.*, No. 4, pp. 93-103, (1978).
29. P.S. DeCarli, "Method of Making Diamond," U.S. Pat. No. 3,238,019, March 1, 1966.
30. P.S. DeCarli and J.C. Jamieson, "Formation of Diamond by Explosive Shock," Science, 133 (1961) 1821.

31. P.S. DeCarli and D.J. Milton, "Stishovite: Synthesis by Shock Wave," *Science*, **147** (1965) 144.
32. M.B. Boslough and R.A. Graham, "Submicrosecond Shock Induced Chemical Reactions in Solids: First Real Time Observations," *Chem. Phys. Letters*, **121** (1985) pp. 446-452.
33. M.B. Boslough, "Shock-Induced Solid-State Chemical Reactivity Studies Using Time Resolved Radiation Pyrometry," *Int. Journal of Imp. Eng.*, **Vol. 5** (1987) pp. 173-180.
34. S.A. Sheffield and A.C. Schwarz, in Proceedings of the Eighth International Pyrotechniques Symposium, edited by A.J. Tulis, (IIT Research Institute, Chicago, 1982) p. 972.
35. A.N. Kovalenko and G.V. Ivanov, Comb. Explo. and Shock Waves, **19**, 481 (1981).
36. R.A. Graham, M.U. Anderson, Y. Horie, S-K. You, and G.T. Holman, "Pressure Measurements in Chemical Reacting Powder Mixtures with the Bauer Piezoelectric Polymer Gage, Shock Waves, an International Journal, Vol. 3, No. 2, 1993.
37. N.N. Thadhani, E. Dunbar, and R.A. Graham, "Characteristics of Shock Compressed Configuration of Ti and Si Powder Mixtures," in Proc. of AIRAPT/APS High Pressure Science and Technology Conference, 28 June to 2 July, 1993, Colorado Springs, ed., S.C. Schmidt, in press.
38. M.D. Hwang, "Modelling of Shock-Induced Chemical Reactions in Powder Mixtures using the VIR Model," Ph.D. thesis, North Carolina State University, Raleigh, NC 1992.
39. Y. Horie and A.B. Sawaoka, Shock Compression Chemistry of Materials, KTK Scientific Publishers, Tokyo, 1993, p. 235.
40. D.E. Maiden and G.L. Nutt, in Proceedings of the Eleventh International Pyrotechnics Seminar, (Vail, Colorado, 1986), p. 813.

41. N.S. Enikolopyan, A.A. Khzardzhyan, E.E. Gasparyan, and V.B. Vol'eva, Academy Nauk, USSR, Procs. Phys. Chem., 294, 567 (1987).
42. L.H. Yu and M.A. Meyers, unpublished results, University of California at San Diego, La Jolla, California, 1992.
43. E. Anders, *Astrophys. J.*, 134, 1606 (1961).
44. M.E. Lipschutz and E. Anders, *Science*, 134, 2095 (1961).
45. H.H. Borimchuk and G. Kurdjumov, presented at Fifth All-Union Meeting on Detonation, Aug 5-10, 1991, Krasnoyarsk, Russia.
46. A.N. Dremin and O.N. Breusov, "Dynamic Synthesis of Superhard Materials," in Shock Waves in Materials Science, ed. A.B. Sawaoka, Springer-Verlag, 1993, pp. 17-34.
47. R.R. Whitlock, J.S. Wark, and G. Kiehn, "Streaked X-ray Diffraction From Laser-Shock Crystals, in Shock Compression of Condensed Matter - 1989, eds. S.C. Schmidt, J.N. Johnson, L.W. Davison, Elsevier Science Publishers B.V., 1990, p. 897 and 901.
48. F.P. Bundy, *J. Chem. Phys.*, 41 (1964) 3809.

TABLE I: PROPERTY DIFFERENCES BETWEEN SI-BASED BINARY SYSTEMS

PROPERTY	SYSTEMS AND CORRESPONDING VALUES (DIFFERENCE DECREASING LEFT-TO-RIGHT)				
Electronegativity	Ti - Si 1.5-1.8	Nb - Si 1.6-1.8	Ni - Si 1.8-1.8	Mo-Si 2.1-1.8	
Density (g/cm ³)	Mo - Si 10.2-2.33	Ni - Si 8.9-2.33	Nb - Si 8.6-2.33	Ti - Si 4.5-2.33	
Sound Velocity (km/s)	Nb - Si 4.44-7.99	Ni - Si 4.58-7.99	Mo-Si 5.12-7.99	Ti - Si 5.22-7.99	
Thermal Conductivity (W/cmK)	Mo-Si 1.38-1.49	Ni - Si .909-1.49	Nb - Si .537-1.49	Ti - Si .219-1.49	
Yield Strength (MPa)	Mo-Si 400-93	Nb - Si 207-93	Ti - Si 140-93	Ni - Si 59-93	
Heat of reaction, ΔH_R (kJ/mole)	Ti - Si -32.9	Mo-Si -17.5	Ni - Si -13.4	Nb-Si -8.8	
Volume Change (%)	Mo-Si -40.6%	Ti-Si -27.8%	Ni-Si -12.6%	Nb-Si -7.8	
Cohesive Energy*, ΔH_C (kJ/mole)	Ti-Si -58.9	Mo-Si -51.3	Nb-Si -42.5	Ni-Si -38.4	
$\Delta H_R / \Delta H_C$	Ni-Si 0.66	Ti-Si 0.56	Mo-Si 0.35	Nb-Si 0.21	

* $\Delta H_C = 1/2 (\Delta H_A + \Delta H_B) + \Delta H_R$ where, ΔH_A and ΔH_B are cohesive energies of solids A and B (from C. Kittel, Introduction to Solid-State Physics, Wiley, NY, 1976). Properties of products refer to those of compounds with maximum ΔH_R .

FIGURE CAPTIONS

- Fig. 1. Schematic illustrating the effects of shock-compression of powder mixtures and processes resulting from these effects.
- Fig. 2. DTA traces of shock-processed samples of 3Ni+1Al mixtures of coarse, flaky and fine morphology powders showing different reaction characteristics. While coarse morphology powders show mostly a liquid-state reaction exotherm following a minor solid-state reaction exotherm, the fine and flaky morphology powder mixtures show predominantly solid-state reaction with little or no reaction in the liquid state [10].
- Fig. 3. Micrographs of shock-compressed mixtures of (a) coarse/rounded, (b) fine, and (c) flaky morphology powders mixed in Ni₃Al stoichiometry ratio, packed at same initial density, showing different deformation characteristics (shock direction is left-to-right). The bright contrast particles are of Nickel, while Aluminum particles have a dark (grainy) contrast [10].
- Fig. 4. Micrographs showing examples of typical microstructures of compounds formed via *shock-induced* chemical reactions in powder mixtures of Ni-Al, Ni-Si, and Ti-Si. A uniform contrast microstructure and presence of spherically-shaped voids (indicating possible gas escape or shrinkage) are typical of a fully reacted microstructure.

Fig. 5. Photomicrographs showing shock-compressed configuration of mixtures of (a) Nb with silicon, equivolumetric, (b) Ni with Al, equivolumetric, and (c) Ni with volumetric abundance of Al. The premature melting of Si (dark cellular structure) in (a) and of Al (dark grainy structure) in (b), and the virtually negligible deformation of the harder Ni in an abundant matrix of the more deformable Al in (c), inhibits intimate mixing and thus reduces the propensity for subsequent *shock-induced* chemical reactions, except at localized regions where the molten metal wets the solid particles.

Fig. 6. SEM micrographs of unreacted configuration of Ti-Si powder mixtures (Ti bright, Si dark contrast), showing the effects of particle morphology and loading conditions on the shock-compression response of Si; (a) extensive fracture of medium morphology, $\approx 45 \mu\text{m}$ particles, at 5 GPa; (b) fracture and fragmentation of coarse morphology, $\approx 150 \mu\text{m}$ particles, at 5 GPa; and (c) extensive plastic deformation and flow of medium morphology, $\approx 45 \mu\text{m}$ particles, at 7.5 GPa [37].

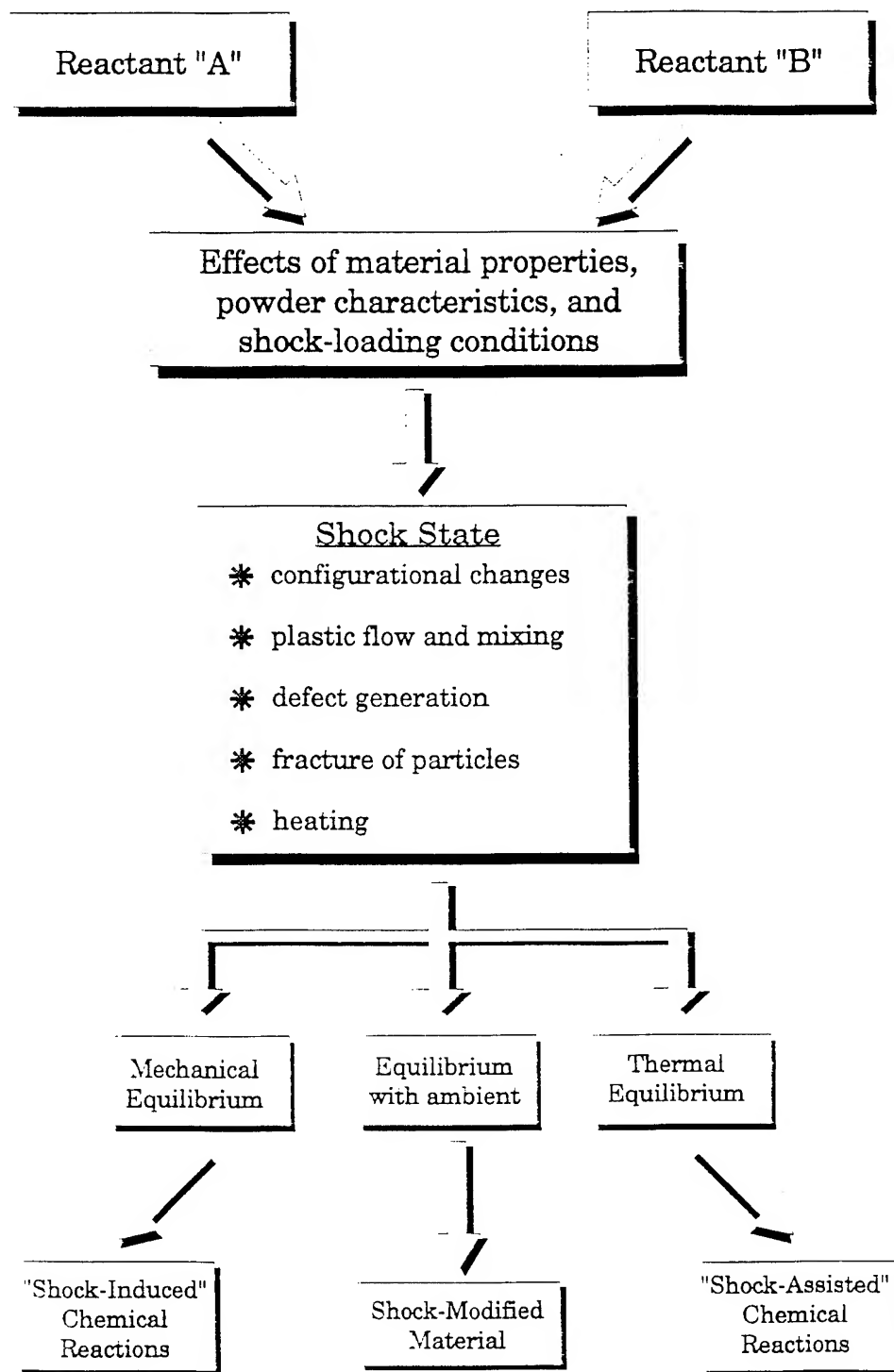


Fig.1. Schematic illustrating the effects of shock-compression of powder mixtures and processes resulting from these effects.

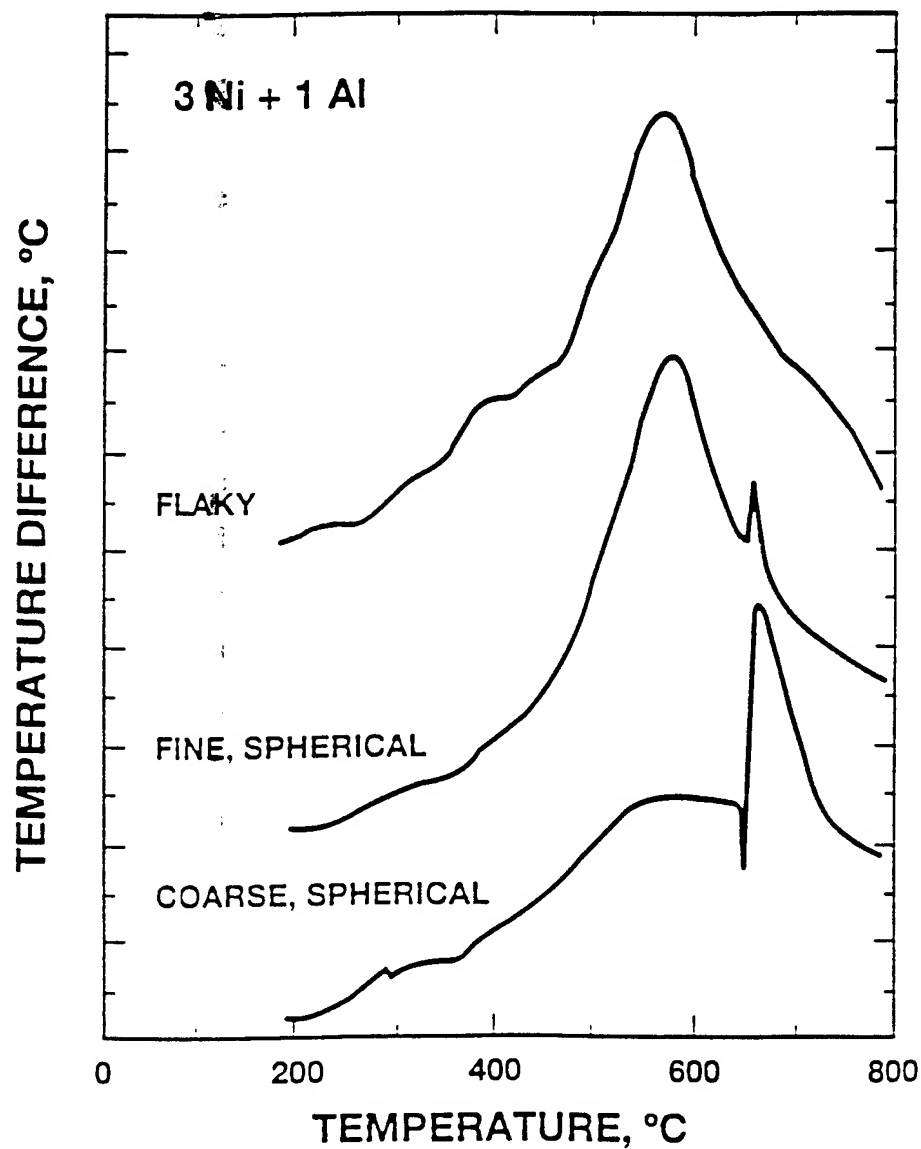
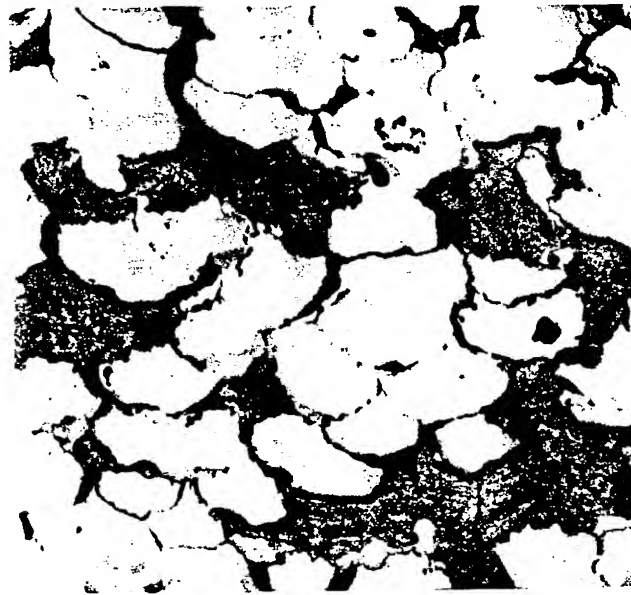


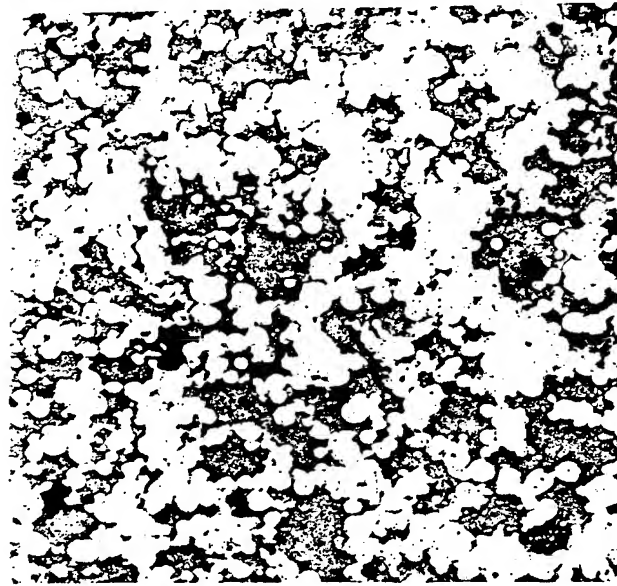
Fig. 2.

DTA traces of shock-processed samples of 3Ni+1Al mixtures of coarse, flaky and fine morphology powders showing different reaction characteristics. While coarse morphology powders show mostly a liquid-state reaction exotherm following a minor solid-state reaction exotherm, the fine and flaky morphology powder mixtures show predominantly solid-state reaction with little or no reaction in the liquid state [10].

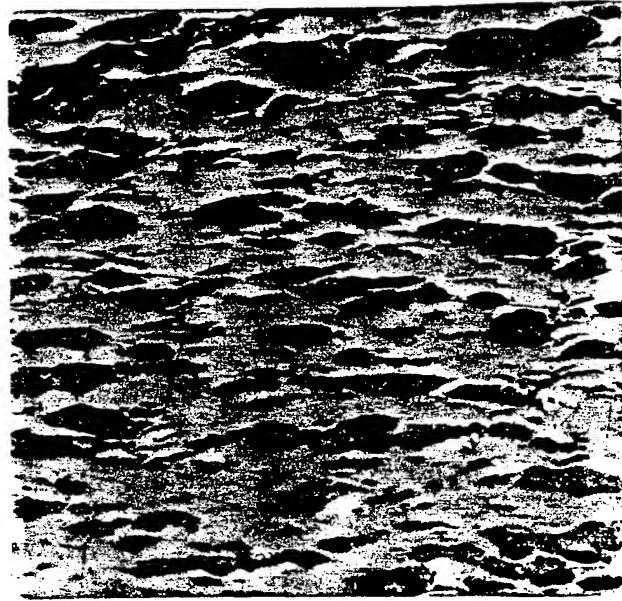
(a)



(b)



(c)



100 μm

Fig. 3. Micrographs of shock-compressed mixtures of (a) coarse/rounded, (b) fine, and (c) flaky morphology powders mixed in Ni_3Al stoichiometry ratio, packed at same initial density, showing different deformation characteristics (shock direction is left-to-right). The bright contrast particles are of Nickel, while Aluminum particles have a dark (grainy) contrast [10].

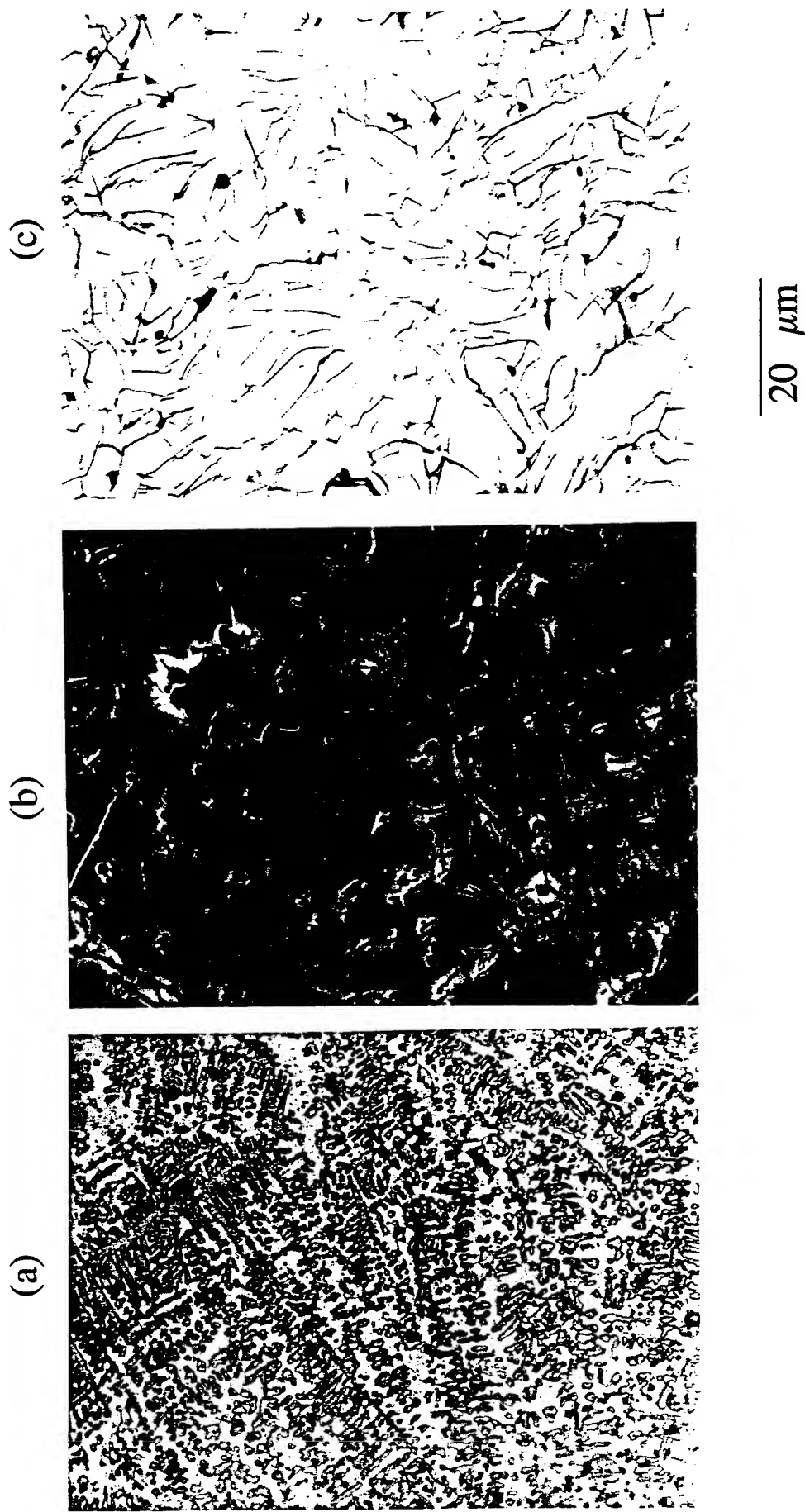


Fig. 4. Micrographs showing examples of typical microstructures of compounds formed via *shock-induced* chemical reactions in powder mixtures of Ni-Al, Ni-Si, and Ti-Si. A uniform contrast microstructure and presence of spherically-shaped voids (indicating possible gas escape or shrinkage) are typical of a fully reacted microstructure.

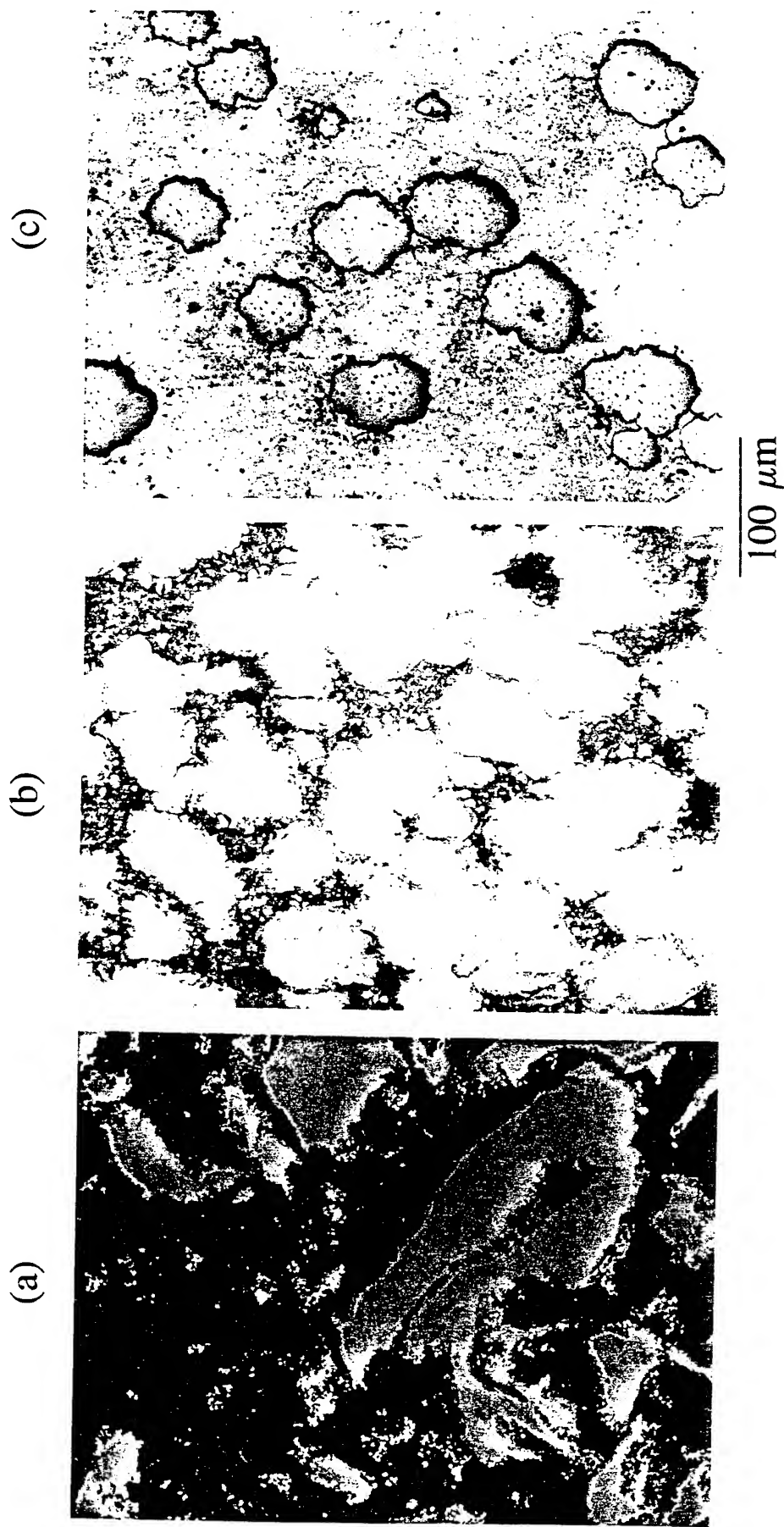


Fig. 5. Photomicrographs showing shock-compressed configuration of mixtures of (a) Nb with silicon, (b) Nb with Al, (c) Nb with volumetric abundance of Al. The premature melting of Si (dark cellular structure) in (a) and of Al (dark grainy structure) in (b), and the virtually negligible deformation of the harder Nb in an abundant matrix of the more deformable Al in (c), inhibits intimate mixing and thus reduces the propensity for subsequent *shock-induced* chemical reactions, except at localized regions where the molten metal wets the solid particles.

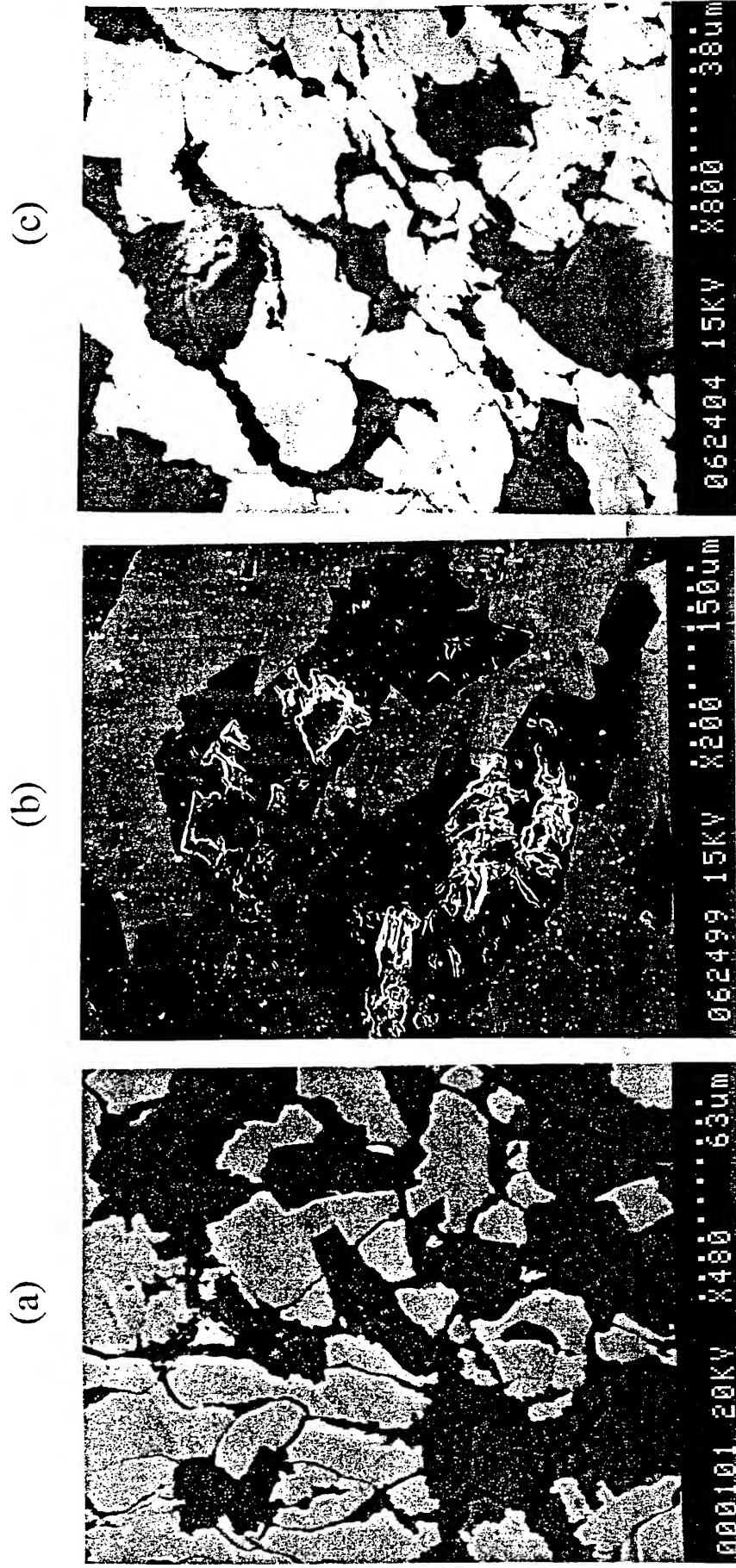


Fig. 6. SEM micrographs of unreacted configuration of Ti-Si powder mixtures (Ti bright, Si dark contrast), showing the effects of particle morphology and loading conditions on the shock-compression response of Si; (a) extensive fracture of medium morphology, $\approx 150 \mu\text{m}$ particles, at 5 GPa; (b) fracture and fragmentation of coarse morphology, $\approx 45 \mu\text{m}$ particles, at 5 GPa; and (c) extensive plastic deformation and flow of medium morphology, $\approx 150 \mu\text{m}$ particles, at 7.5 GPa [37].

WORKSHOP ON "SHOCK SYNTHESIS OF MATERIALS", MAY 23-24, 1994

**Sponsored by: U.S. Army Research Office, Research Triangle Park
U.S. Army Research Office, (AMC) Far East
U.S. Army Research, Development, & Standardization Group (UK)
(Hosted by Georgia Institute of Technology, Materials Science & Engineering)**

<u>NAME</u>	<u>AFFILIATION / PHONE-FAX</u>
Nail Akhmadeev*	Department of Civil Engineering, North Carolina State University, Box 7908, Raleigh, NC 27695, Tel: (919) 515-1340, Fax: (919) 515-7908. (Other address: Head, Laboratory of Explosion & Shock Processes, Institute of Mechanics, Russian Academy of Sciences, UFA Branch, Moscow Technology College, Moscow, Russia)
Mark Anderson*	Advanced Materials Physics Dept., Org. 1153, MS 0345, P.O. Box 5800, Sandia National Laboratories, Albuquerque, NM 87185-0345, Tel: (505) 844-5726, Fax: (505) 844-5459
Mel Baer*	Energetic Materials and Fluid Mechanics Dept., Org. 1512, MS 834, P.O. Box 5800, Sandia National Laboratories, Albuquerque, NM 87185-0834, Tel: (505) 844-5223, Fax: (505) 844-8251
S.S. Batsanov*	Dept. of AMES, R-011, University of California at San Diego, La Jolla, CA 92093, Tel: (619) 534-4719, Fax: (619) 534-7078
Sarit Bhaduri	Department of Metallurgy, University of Idaho, Moscow, Idaho 83843, Tel:
Mark Boslough*	MS 0821, Experimental Impact Physics, Sandia National Laboratories, P.O. Box 5800, Albuquerque, NM 87185-0821, Tel: (505) 845-8851, Fax: (505) 844-0918, e-mail: mbboslo@sandia.gov
Edward Chen*	Materials Science Division, U.S. Army Research Office, P.O. Box 12211, 4300 S. Miami Blvd., Research Triangle Park, NC 27709-2211, Tel: (919) 549-4325, Fax: (919) 549-4310
Rod Clifton	Division of Engineering, Brown University, Box "D", 182 Hope Street, Providence, RI 02912, Tel: (401) 863-2855, Fax: (401) 863-1157, e-mail: clifton@engin.brown.edu
Charlie Collins	Georgia Institute of Technology, School of Materials Science and Engineering, Atlanta, GA 30332-0245, Tel: (404) 894-2853, Fax: (404) 853-9140
Andrew Crowson	Materials Science Division, U.S. Army Research Office, P.O. Box 12211, 4300 S. Miami Blvd., Research Triangle Park, NC 27709-2211, Tel: (919) 549-4261, Fax: (919) 549-4310, e-mail: crowson@aro-emni.army.mil
D. P. Dandekar**	U.S. Army Research Laboratory, Materials Directorate, 405 Arsenal Street, Watertown, MA 02172-0001, Tel: (617) 923-5704, Fax: (617) 923-5065
Jeffrey Davis	Naval Surface Warfare Center, 10901 New Hampshire Avenue, Code - 9230, Silver Spring, MD 20903, Tel: (301) 394-2847, Fax: (301) 394-1590
A.N. Dremin*	Head of High Pressure Physics Dept., Institute of Chemical Physics, Russian Academy of Sciences, Chernogolovka, Moscow Region, Fax: 7-096-515-3588
Jerry Forbes	Code 920, Naval Surface Warfare Center, Silver Spring, MD 20903, Tel: (301) 394-1697, Fax: (301) 394-1590
J.J. Gilman*	5731 Boulter Hall, UCLA, Los Angeles, CA 90024, Tel: (310) 825-9608, Fax: (310) 206-7353

* Speaker, ** Session Chair

- Judah Goldwasser Office of Naval Research, Mechanics & Energy Conversion Division, Code 333, 800 North Quincy St., Room 507, Arlington, VA 22217-, Tel: (703) 696-2164, Fax: (703) 696-0934, e-mail: judah@onr-hq.navy.mil
- Y.M. Gupta* Washington State University, Shock Dynamics Center, Physical Science Building, Rm. 948, Pullman, WA 99164-2814, Tel: (509) 335-7217, Fax: (509) 335-6115, e-mail: tam@sd11.physics.wsu.edu
- Bill Holt Naval Surface Warfare Center, Code G22, Dahlgren, VA 22448, Tel: (703) 663-8687, Fax: (703) 663-8643
- Yuki Horie* Dept. of Civil Engineering, North Carolina State University, Box 7908, Raleigh, NC 27695, Tel: (919) 515-7696, Fax: (919) 515-7908, e-mail: horie@eos.ncsu.edu
- Kailasam Iyer** Research and Technology International Office, U.S. Army Research Office, P.O. Box 12211, Research Triangle Park, NC 27709-2211, Tel: (919) 549-4258, Fax: (919) 549-4248
- Ken-ichi Kondo Research Laboratory for Engineering Materials, Tokyo Institute of Technology, 4259 Nagatsuta, Midori-ku, Yokohama 227, JAPAN, Tel: 81-45-924-5342 Fax: 81-45-921-1015
- Kathryn Logan Georgia Institute of Technology, Office of Interdisciplinary Programs, Atlanta, GA 30332-0130, Tel: (404) 894-6902, Fax: (404) 894-7339, e-mail: kathryn.logan@oip.gatech.edu
- T. Mashimo High Energy Rate Laboratory, Kumamoto University, 2-39-1 Kurokami, Kumamoto City 860, JAPAN, Tel: 096-344-2111 ext. 3746, Fax: 096-345-1598
- Marc A. Meyers* Dept. of AMES, R-011, University of California at San Diego, La Jolla, CA 92093, Tel: (619) 534-4719, Fax: (619) 534-7078
- Zuhair A. Munir* Div. of Materials Science & Engineering, University of California, Davis, Davis, CA 95616-5294, Tel: (916) 752-6348, Fax: (916) 752-8240
- V. Nesterenko* Institute of Mechanical Materials, University of California at San Diego, La Jolla, CA 92093, Tel: (619) 534 4719, Fax: (619) 534-7078
- Malcolm Nicol* Department of Chemistry and Biochemistry, University of California, Los Angeles, CA 90024-1569, Tel: 310-825-2419, Fax: 310-206-6628, e-mail: mfn@chem.ucla.edu
- Andrus Niiler** U.S. Army Research Lab - WTD, Ballistic Research Laboratory, SLC-BR-TB-EP, Aberdeen Proving Ground, Aberdeen, MD 21005, Tel: (410) 278-4884, Fax: (410) 278-9969, e-mail: niiler@arl.army.mil
- Byungwoo Park Georgia Institute of Technology, School of Materials Science and Engineering, Atlanta, GA 30332-0245, Tel: (404) 894-2544, Fax: (404) 853-9140, e-mail: byungwoo.park@mse.gatech.edu
- Serguei Psakhie* Department of Civil Engineering, North Carolina State University, Box 7908, Raleigh, NC 27695, Tel: (919) 515-1340, Fax: (919) 515-7908, e-mail: spsakhie@eos.ncsu.edu, (Other address: Head, Dept. of Computer Simulation, Russian Materials Science Center, Tomsk State University, Tomsk, Russia)
- G. Ravichandran* California Institute of Technology, Dept. of Aeronautical Engineering, Mail Stop 105-50, Pasadena, CA 91125, Tel: (818) 395-4525, Fax: (818) 304-0175, e-mail: ravi@atlantis.caltech.edu
- Tyrus Royal Georgia Institute of Technology, School of Materials Science and Engineering, Atlanta, GA 30332-0245, Tel: (404) 894-1475, Fax: (404) 853-9140, e-mail: gt0860c@acme.gatech.edu

- Toshimori Sekine* National Institute for Research in Inorganic Materials, Namiki 1-1, Tsukuba, Ibaraki, 305 JAPAN, Tel: 81-298-51-3351, Fax: 81-298-52-7449 or 81-298-51-4005
- Don Shockey Poulter Laboratory, SRI-International, 333 Ravenswood Avenue, Menlo Park, CA 94025, Tel: (415) 859-2587, Fax: (415) 859-2260
- Greg Stangle NYS College of Ceramics, Alfred University, Alfred, NY 14802, Tel: (607) 871-2486, Fax: (607) 871-3469
- Yasuhiko Syono* Institute for Materials Research, Tohoku University, Katahira 2-1-1, Aoba-ku, Sendai 980-77, JAPAN, Tel: 81-22-227-6200 x2930, Fax: 81-22-215-2086
- Zhi-Ping Tang Dept. of Civil Engineering, North Carolina State University, Box 7908, Raleigh, NC 27695
- N.N. Thadhani* Georgia Institute of Technology, School of Materials Science and Engineering, Atlanta, GA 30332-0245, Tel: (404) 894-2651, Fax: (404) 853-9140, e-mail: naresh.thadhani@mse.gatech.edu
- Bonnie Turner Georgia Institute of Technology, School of Materials Science and Engineering, Atlanta, GA 30332-0245, Tel: (404) 894-2881, Fax: (404) 853-9140
- Kenneth Vecchio Dept. of AMES, MC-0411, University of California at San Diego, La Jolla, CA 92093, Tel: (619) 534-3510, Fax: (619) 534-7235, e-mail: kvecchio@ames.ucsd.edu
- Justin Wark* Physics Department, Clarendon Laboratory, Oxford University, Parks Road, Oxford OX13PN, ENGLAND, Tel: 011-44-865-272251, Fax: 011-44-865-272400, e-mail: jsw@vax.ox.ac.uk
- Diana Woody Naval Surface Warfare Center, 10901 New Hampshire Avenue, Code 920, Silver Spring, MD 20903, Tel: (301) 394-1396, Fax: (301) 394-4634
- M. Yoshida* High Energy Density Lab, National Institute of Materials and Chemical Research, 1-1 Higashi, Tsukuba, Ibaraki, 305, JAPAN, Tel: 81-298-54-4789, Fax: 81-298-54-4783, e-mail: yoshida@nime.go.jp
- Robert Young** Southwest Research Institute, San Antonio, TX 78228-0510, Tel: (210) 522-2408, Fax: (210) 522-5122

* Speaker, ** Session Chair

NOT ATTENDING

Iqbal Ahmad U.S. Army Research Office, AMC - Far East, Unit h5002, APO AP 96337 - 0007, Tel: 81-03-3423-1374, Fax: 81-03-3423-1832

R.W. Armstrong University of Maryland, Dept. of Mechanical Engineering, College Park, MD 20742, Tel: (301) 405-5291, Fax: (301) 314-9477

Tony Chu Army Research Laboratory, Watertown, MA 02172

M. Cowperthwaite Poulter Laboratory, SRI-International, 333 Ravenswood Avenue, Menlo Park, CA 94025, Tel: (415)

Steve Fishman Materials Division, Office of Naval Research, 800 North Quincy St., Arlington, VA 22217-5000, Tel: (703) 696-0285, Fax: (703) 696-0934

G.T.(Rusty) Gray MST-5, MS-G755, Los Alamos National Laboratory, Los Alamos, NM 87545, Tel: (505) 667-5452, Fax: (505) 667-8021

W.L. Johnson Materials Science and Applied Physics, Mail Code 138-78, California Inst. of Technology, Pasadena, CA 91125, Tel: (818) 395-4433, Fax: (818) 395-2940

Bruce Kramer Materials and Manufacturing, National Science Foundation, 4201 Wilson Boulevard, Arlington, VA 22230, Tel: (703) 306-1330, Fax: (703) 306-0298

Milt Linevsky Division of Materials Research, National Science Foundation, 4201 Wilson Boulevard, Arlington, VA 22230, Tel: (703) 306-1371, Fax: (703) 306-0319

Bruce MacDonald Division of Materials Research, National Science Foundation, 4201 Wilson Boulevard, Arlington, VA 22230, Tel: (703) 306-1835, Fax: (703) 306-0515

James McCauley Dean, NYS College of Ceramics, Alfred University, Alfred, NY 14802, Tel: (607) 871-2411, Fax: (607) 871-2344

R. Miller Energetics & Propulsion Mechanics Div., Office of Naval Research, Code 1132P, 800 North Quincy St., Room. 704, Arlington, VA 22217-5000, Tel: (703) 696-4404, Fax: (703) 696-0934

W. Nellis Lawrence Livermore National Lab, L-299, P. O. Box 808, Livermore, CA 94550, Tel: (510) 422-7200, Fax: (510) 422-2851

F. Owens ARDEC, Bldg. 3022, Picatinny, NJ 07806-5000, Tel: (201) 724-4625, Fax: (201) 724-2175

Wilbur Simmons Materials Science Division, U.S. Army Research Office, P.O. Box 12211, 4300 S. Miami Blvd., Research Triangle Park, NC 27709-2211, Tel: (919), Fax: (919)-549-4310

Phil Stanton MS 0821, Experimental Impact Physics, Sandia National Laboratories, P.O. Box 5800, Albuquerque, NM 87185-0821, Tel: (505) 845-8439, Fax: (505) 844-0918

Karl Steinbach European Research Office, U.S. ARD and SG - UK, Mail Box PCS 802 - Box 15, FPO - AE 09499-1500, Tel: 44-71-514-4933, Fax: 44-71-724-1433

Andrew Strutt Dept. of AMES, R-011, University of California at San Diego, La Jolla, CA 92093, Fax: (619) 534-7078

William Tao Lawrence Livermore National Lab, P. O. Box 808, L-282, Livermore, CA 94551, Tel: (510) 423-0499, Fax: (510) 422-2382

Robert Whitlock Naval Research Laboratory, Code 4680, 4555 Overlook Avenue, Washington, D.C. 20375, Tel: (202) 767-2154, Fax: (202) 767-4868

George Yoder Materials Division, Office of Naval Research, 800 North Quincy St., Room 704, Arlington, VA 22217-5000, Tel: (703) 696-0282, Fax: (703) 696-0934